Paleoceanography of the Eastern Tropical North Pacific on Millennial Timescales

Elsa Arellano-Torres

Thesis submitted for the degree of

Doctor of Philosophy

The University of Edinburgh

2010

I attest that:

All material presented in this document was compiled

and written by myself unless otherwise acknowledged.

Elsa Arellano-Torres, 2010

Contents

A mi familia y Mano

Dos monjes discutían sobre una bandera que ondeaba al viento.

Un monje dijo, "Es la bandera la que se mueve."

El otro dijo, "¡No! Es el viento quien la mueve."

Y seguían discutiendo sin parar

Hui-Neng, el sexto patriarca se encontro con ellos y les dijo:

"No es la bandera ni el viento, lo que se mueve es la mente."

(Platform Sutra)

Acknowledgements

Abstract

The occurrence of large scale and rapid climate shifts at millennial time-scales (sub-orbital) remains an enigma between records from high and low latitudes spanning the Late Quaternary. This thesis studies such variations in the eastern tropical North Pacific (ETNP) using marine sediment cores retrieved from Mexico and Nicaragua. The main goals are to understand the nature of millennial timescale climate-changes in the Pacific low latitudes, to identify the atmospheric and oceanic teleconnections involved, to document the impacts on the biogeochemical cycles of carbon, nitrogen and silicon, and their potential to regulate Greenhouse Gas (GHG) concentrations during the last two glacial cycles (the last 240,000 years before present).

In this thesis, we use a suite of multi-proxy records from the Core MD02-2519, which are compared to others records from adjoining regions to study the climatic history of the ETNP at millennial timescales. The Core MD02-2519, was retrieved from 955 mbsl off NW Mexico. It is strategically located within the North Pacific Intermediate Water (NPIW), underlying the coastal upwelling and denitrification zones of the ETNP. The paleoceanography of the region is studied using proxy records of productivity, denitrification, intermediate water circulation and radiocarbon activity, which are discussed in 5 separated chapters. In *Chapter 1*, we use records of organic carbon (%OC) and diffuse spectral reflectivity (DSRa*) to document changes in productivity, which are shown in phase with Northern Hemisphere (NH) timing at millennial scale, suggesting a direct atmospheric teleconnection with higher northern latitudes. In *Chapter 2*, reconstruction of nitrogen isotope records ($\delta^{15}N$) show that abrupt changes in denitrification are in phase with NH timing over the last glacial period; however, the advection of heavy nitrate from southern sources is also documented, possibly from the denitrification zone off Peru-Chile. Records of opal (%opal – *Chapter 3*) and carbon isotopes from benthic foraminifera ($\delta^{13}C$-*Uvigerina* – *Chapter 4*) support the inference of oceanic teleconnections between the ETNP and the South Pacific via subthermocline circulation. In *Chapter 4*, the $\delta^{13}C$ records also suggest that intermediate water circulation changed over glacial periods and terminations, being the result of intrusion of southern component waters. In *Chapter 5*, the reconstruction of radiocarbon activity ($\Delta^{14}C$) records from surface (planktonic foraminifera) and intermediate water (benthic foraminifera) suggest oceanic degassing of old-carbon from the deep ocean during

the last termination. In this way, the ETNP upwelling system could be an important locus of CO_2 release at millennial timescales.

$\circledast$

Introduction

Understanding rapid climate change has become one of the key focuses in earth sciences over the last two decades. This interest is driven by social concerns over anthropogenic effects on climate and a need to understand the climate system to improve our predictive capabilities. Over the last decades, paleoclimatologists have studied various climate archives such as rocks and soils, tree rings, icecaps, coral reefs and marine sediments (IPCC, 2001). These works highlight the complex interaction within the ocean-atmosphere system, the threshold behaviour and feedbacks, as well as the various modes and frequencies of climate change on different time scales (Alley et al., 1999; Clark et al., 1999a). However, the overarching goal of generating assertive prediction models depends upon pinpointing the leading mechanisms as well as the causes and consequences of these interactions.

The Late Quaternary (i.e. approximately the last 1 Ma) has witnessed dramatic climate variability in a wide range of temporal scales. On longer timescales, orbital parameters have acted as a pacemaker for climate at periods of $20 - 100$ ka (Hays et al., 1976), amplified by feedbacks within the earth climate system (e.g. Clark et al., 1999a). At the opposite end of the temporal spectrum, seasonal to inter-annual variability can be directly studied and forecasted (e.g. monsoons, cyclones and tropical storms), whereas the millennial to sub-millennial scales are less understood (Alley et al., 1999). Millennial scale variations in climate were first discovered in Greenland and the North Atlantic (Bond et al., 1999; Dansgaard et al., 1984; Dansgaard et al., 1993) but successive studies have documented their near global occurrence with an apparent periodicity of ~ 1500 years (Alley et al., 1999; Clark et al., 1999b; Hendy et al., 2002; Ono et al., 2005). This has generated a heated ongoing debate concerning the geographical initiation (high versus low latitudes), the modes of propagation (ocean versus atmosphere), and processes that amplify and sustain these climate oscillations. One of the enduring challenges of paleoclimate studies is the comparison between cores from different locations (e.g. high versus low latitudes), stemming from chronological uncertainties and the limited availability of high resolution records. These limitations have hampered concrete conclusions concerning lead-lags between records and pinpointing the provenance of the climatic signals.

In the North Pacific, previous studies have documented millennial scale variations equivalent to the temperature variations found in records from Greenland and the North

Atlantic (i.e. Dansgaard-Oeschger (D/O) and Heinrich (H) events). The retrieval of marine cores from California and Oregon has evidenced that such rapid environmental changes have a clear association to interstadial events *or* D/O over the last 60 ka (Behl and Kennett, 1996; Cannariato et al., 1999; Hendy and Kennett, 1999). Millennial-scale changes have been also found in tropical regions identified with changes in the tropical hydrological cycle (Altabet et al., 2002; Ivanochko et al., 2005; Peterson et al., 2000; Wang et al., 2001). In this way, the global documentation of these fluctuations is critical to determine the processes driving millennial scale climatic changes, understand the climatic mechanisms linking high and low latitudes and the teleconnections between distant regions. A way to address these issues is by means of multi-proxy studies tracking high and low latitude processes in the same core.

The principal aim of this contribution is to investigate sub-orbital variations in the eastern tropical North Pacific (ETNP) where previous studies have shown large environmental variability during the Late Quaternary (Ganeshram and Pedersen, 1998; Ganeshram et al., 2000). The overall objective is to unravel the nature of millennial climate variations, focussing in a marine sediment core collected off Mazatlan, NW Mexico (Figure I-A), by means of paleoceanographic reconstructions of upwelling and productivity, denitrification and water column oxygenation, subsurface and intermediate water circulation. Comparisons with other climatic records are done to specifically address the mode of propagation between high and lower latitudes in the Pacific; and whether they were propagated to the study site through the atmosphere (upwelling and productivity) or through the ocean (intermediate water circulation/ventilation). In this thesis, these issues are studied with a multy-proxy approach separated in 5 chapters, each of which has been written in the style and format of individual papers to facilitate their publication. This inevitably introduces redundancy in some sections, but it has been minimised whenever possible.

Northeastern Pacific records of millennial scale variability

Several studies in the NE Pacific have documented variability on millennial timescales using geochemical and micropaleontological proxy records, interpreted as rapid changes in intermediate water oxygenation (Behl and Kennett, 1996; Cannariato et al., 1999). Changes in oxygenation are often recorded as cyclical laminated/bioturbated sequences and in the remains of benthic organisms of marginal settings. Apparently, dramatic changes in the strength of the oxygen minimum zone (OMZ; Figure I-B) have occurred on this region in association with D/O cycles, shown by weakening and maybe

disappearance of the OMZ during cool episodes, but strengthening during warm periods (Behl and Kennett, 1996; Cannariato et al., 1999; Kennett and Ingram, 1995). This suggest that millennial scale variations can be transmitted from higher latitudes via intermediate water circulation (Keigwin, 2002; Stott et al., 2000). Despite the time constrain of the records collected from Santa Barbara Basin (SBB) (up to 60 ka), the magnitude and character of the oscillations are comparable to temperature changes recorded in Greenland, suggesting that synchronic climate responses between regions can be transmitted via the atmosphere (Hendy and Kennett, 1999). For instance, several studies document variations in biological productivity, upwelling and surface waters, driven by wind-forcing (Hendy et al., 2002; Ortiz et al., 2004). Thus the available evidence indicates two possible mechanisms and modes of climate propagation of millennial scale climatic changes in the NE Pacific: one controlled by productivity and another by intemediate circulation.

Changes in Marine Productivity

One hypothesis attributes variations in the surface water biological productivity to modifications in subtropical winds and upwelling as the primary cause of oxygenation changes at glacial-interglacial and millennial timescale in the NE Pacific (Ganeshram et al., 2002; Hendy et al., 2002). A reduction in coastal upwelling and biological productivity might reduce subsurface oxygen consumption due to decaying of organic matter (Ortiz et al., 2004) besides affecting denitrification (Ganeshram et al., 2000). This, in combination with enhanced bottom water renewal, could explain the oxygenated conditions during stadials in records from SBB (Hendy and Pedersen, 2005; Ivanochko et al., 2005). Thus the tropical regions might have played a major role in rapid climate changes. The coupled tropical ocean-atmosphere interactions could modulate global climate on interannual, decadal and probably at millennial timescale, for instance, by modulating the latitudinal position of the Intertropical Convergence Zone (ITCZ) (Ivanochko et al., 2005; Peterson et al., 2000; Wang et al., 2001). In particular, small temperatures variations in the equatorial Pacific can produce responses in trade winds strength, thermocline depths, rainfall regimes and productivity. Importantly, these changes are related to tropical mechanisms.

![Map and depth sections of the eastern tropical Pacific showing core site locations and water masses](image)

A. Map showing the eastern Pacific bathymetry with core sites. Labels: High, Low, ITCZ. Core sites: (705) PC08, MD02-2519, (450) MD02-2518, (420) NH15P, (712) MD02-2520, (863) MD02-2524.

B. OXYGEN [μMOL/KG] depth section. Water masses labeled: STMW, AAIW, SSW, NPIW, PDW.

C. SALINITY [PSS-78] depth section. Water masses labeled: STMW, AAIW, SSW, NPIW, PDW.

x

Figure I. Study site. The main Core MD02-2519 (black dot) was collected off Mazatlan, NW Mexico (lat. 22° 30.89'N; long. 106° 39.00'W; 955 m water depth). Other cores studied in this thesis are shown for reference (black stars) with depth shown in brackets (full details are provided in the corresponding chapter (see text)). (A) Bathymetry (Schlitzer, 2004) and main features of atmospheric circulation in the ETNP during boreal winter, when the Intertropical Convergence Zone (ITCZ) is located in its southernmost position. The development of pressure gradients between the continental Low-pressure over NW Mexico and the North Pacific High, create the perfect conditions to develop strong winds (white arrows) required to fuel and sustain the seasonal upwelling (Bakun and Nelson, 1991). (B) Oxygen concentration (µmol/kg) in the water column. The Oxygen Minimum Zone (OMZ) is seen in purple. (C) Salinity (PSS78 - Practical Salinity Scale 1978) (Key et al., 2004) along the GLODAP cruise-18 (see map inset in B). Intermediate waters are identified by its salinity minimum at ~ 34.5, i.e. North Pacific Intermediate Water (NPIW) and Antarctic Intermediate Water (AAIW). Other water masses are Subsurface Subtropical Water (SSW), Subtropical Mode Water (STMW) and Pacific Deep Water (PDW).

Changes in Intermediate Waters

A second hypothesis maintains that changes in bottom water ventilation are controlled by changes in the strength and location of the North Pacific Intermediate Water (NPIW) source (Crusius et al., 2004; Keigwin, 1998; Kennett and Ingram, 1995). Today, the Okhotsk and the Bering Sea in the NW Pacific, are the main formation and transformation regions of NPIW (Talley, 1999; You et al., 2000). In the modern ocean, this water mass is well recognized to be oxygen-deficient (Figure I-B), but in the past, changes in water ventilation have been documented. Studies in the Okhotsk Sea suggest that during the Last Glacial Maximum (LGM) the extent of NPIW formation could increase and spread out to the south (Keigwin, 1998). Thus a reinforcement of sea-ice generation and water mixing during the LGM may lead to an increase in the formation of NPIW (Ono et al., 2005).

Therefore, the expansion of NPIW could support the interpretation of more oxygen content in the source region during cold periods and stadial events (Ono et al., 2005), as well as the synchronous presence of oxygenated conditions in the downstream region of the NE Pacific (e.g. SBB) (Hendy and Kennett, 2003). However, records of carbon isotopes in benthic foraminifera from the Gulf of California document few evidence for ventilation changes during the LGM and the Younger Dryas (YD) (Keigwin, 2002). This represents the possibility that in the eastern tropical Pacific (ETP), past changes in oxygenation may be related to other sources of intermediate water ventilation, for example, the Southern Ocean (SO). The Antarctic Intermediate Water (AAIW) forms a fresh tongue circulating around the southern Subtropical Pacific gyre, extending near to the equator (~ 1.6°S) and flowing via

western boundary undercurrents before spreading back eastward into the tropics, sometimes detectable as far north as 6.5° in the Northern Hemisphere (NH) (Talley, 1999). Several studies suggest that AAIW could be much stronger in the past, crossing the equator and ventilating the North Pacific at times (Lund and Mix, 1998; Mix et al., 1999; Ninnemann and Charles, 1997; Ninnemann and Charles, 2002). Thus oxygenation changes in the ETP could be explained both by the expansion and contraction of NPIW, as well as penetration of southern component waters (Hendy and Kennett, 2003).

At present, a critical evaluation of these hypotheses is hampered by chronological uncertainties, mainly because the processes were separately reconstructed in different cores spread over the Pacific, and the uncertainty of the age models prevent comparison between records to assess timing, duration and intensity at millennial scales. In this thesis, every effort has been made to date the records used, as accurately as possible, with a variety of methods including detailed ^{14}C dating and correlation with well-dated records and tephra (ash) layers. We have avoided errors by reconstructing multiple proxy records in the Core MD02-2519 (Figure I), so the lead-lags are independent of any given chronology. For instance, if changes in the oxygen of bottom waters were controlled by local productivity then we would expect the corresponding records to be coeval. However, if they are driven by different mechanisms, we could determine the source by association with other records.

To evaluate these hypotheses, the productivity changes at millennial timescales are investigated in *Chapter 1*, based on records of organic carbon (%OC) and diffuse spectral reflectivity (DSRa*). An evaluation of the controlling mechanisms affecting denitrification are shown in *Chapter 2* using nitrogen isotope records (δ^{15}N). By reconstructing these processes in the same core, we attempt to eliminate chronological uncertainties and evaluate their phase relationship. Additionally, if past changes in productivity and denitrification relate to large-scale tropical reorganisations in climate, this should affect the biogeochemical cycles of nutrients, thus the changes should be spatially coherent. This is evaluated by comparing records of δ^{15}N (*Chapter 2*) and biogenic silica (%opal) (*Chapter 3*) to other records in the ETP. On the other hand, to evaluate whether the changes in oxygenation/ventilation are related to ageing (i.e. more carbon remineralisation) of intermediate waters or due to high latitude processes, we reconstruct subsurface to intermediate water circulation in *Chapter 4*, based on benthic foraminifera carbon isotope records (δ^{13}C$_b$). In *Chapter 3* and *Chapter 5*, we examine the role of the tropical ocean to

sequestrate carbon (CO_2) during glacial periods with opal and surface radiocarbon activity records ($\Delta^{14}C$ - planktonic foraminifera). Finally, the distribution and deglacial release of 'old carbon' from the deep ocean to the atmosphere is investigated in *Chapter 5* using records of radiocarbon activity ($\Delta^{14}C$ – planktonic and benthic foraminifera). The global implications of these findings, and comparisons with records from distant regions are always presented in the different chapters.

Descriptions of the lithology and sediment structures of the cores used in this study, retrieved during the MONA Cruise Expedition 2002, are included in the *Appendix A*. The collection of the geochemical data of the Core MD02-2519 is presented in the *Appendix B*. Finally, data sets of other cores investigated (see black stars in Figure I) are presented in the *Appendix C*, i.e. Cores MD02-2518 (*Chapter 1*) and NH15P (*Chapter 4*) collected off Mazatlan, Mexico from 450 mbsl and 420 mbsl, respectively; the Core MD02-2520 collected off Tehuantepec, Mexico from 712 mbsl (*Chapter 2* and *Chapter 3*); the Core PC08 collected off Southern Baja California, Mexico from 705 mbsl (*Chapter 4* and *Chapter 5*); and the Core MD02-2524 collected off Nicaragua from 863 mbsl (*Chapter 3*).

Temporal Framework

To aid in the evaluation of the chronology and correlation of the major climatic events discussed in this thesis, the temporal framework and boundaries of these events are described next, focusing on the Late Quaternary at two timescales: glacial-interglacial and millennial. The *Quaternary* spans the last 2.6 Ma of Earth history separated into two epochs: the *Pleistocene* (2.6 Ma to 12 ka BP) and the *Holocene* (12 ka to present).

The *glacial-interglacial* (G-IG) timescales are importantly related to variations in the Earth's orbit around the Sun and the amount of solar radiation received on the surface. Periodic components of the so called *Milankovitch cycles* occur every ~100 – 413 ka (known as *eccentricity*), ~ 41 ka (known as *obliquity*) and ~ 19 – 23 ka (known as *precession*) (Berger, 1984; Milankovitch, 1941). The periods of maxima (*interglacial*) and minima (*glacial*) peaks of solar radiation have been identified in marine records like alternating warm and cold intervals. Because they are deduced from oxygen isotope data ($\delta^{18}O$), it is common to refer to them by their *Marine Isotope Stage* (MIS) number. Commonly, the orbitally tuning SPECMAP $\delta^{18}O$ stack record (Imbrie et al., 1984) is the reference to define the ages of the MIS boundaries using the scale by Martinson *et al.* (1987). In this thesis, we

follow the MIS classification, although the boundaries are based on the modified scale of the LR04 $\delta^{18}O$ stack record (Lisiecki and Raymo, 2005). The LR04 ages of the MIS boundaries for the last two glacial cycles are: *MIS-1* ≈ 14 ka to present; *MIS-2* ≈ 29 to 14 ka; *MIS-3* ≈ 57 to 29 ka; *MIS-4* ≈ 71 to 57 ka; *MIS-5* ≈ 130 to 71 ka (where the peak *5e* ~ 123; *5d* ~ 109; *5c* ~ 96; *5b* ~ 97; *5a* ~ 82 ka); *MIS-6* ≈ 191 to 130 ka; *MIS-7* ≈ 243 to 191 ka (where the peak *7d* ~ 224, *7c* ~ 217, *7b* ~ 205, *7a* ~ 192 ka).

The last glacial period lasted about 60 ka (including MIS-4, MIS-3 and MIS-2) and it is characterised by two different types of climate changes, which occurred rapidly and repeatedly at millennial timescales, known as *Dansgaard-Oeschger* (D/O) and *Henrich* (H) events (Bond et al., 1993; Dansgaard et al., 1993; Heinrich, 1988). The D/O events were first documented in ice core records from Greenland as 25 warmer episodes called *interstadials*. The H events were first identified in marine records from the North Atlantic as 6 layers with large amount of coarse-grained sediments from land (Heinrich, 1988; McIntyre and Ruddiman, 1972). The H events are related to some of the coldest intervals between D/O events known as *stadials* (Bond et al., 1993). In this thesis, the age of the rapid climatic events of the last glacial cycle is based on the GISP2 $\delta^{18}O$ scale (Grootes and Stuiver, 1997) as described in *Chapter 1*.

During the last glacial period, an important climatic event occurred as part of the MIS-2: the *Last Glacial Maximum* (LGM). This event is conventionally defined from sea-level records like the most recent interval in Earth history when the global ice sheets reached their maximum integrated volume (Mix et al., 2001). Although there still remains an ongoing debate to precise its absolute age (e.g. Clark et al., 2009), here we characterise the LGM as the interval between 24 - 18 ka as suggested by the EPILOG project (Mix et al., 2001). The end of the last glacial period, also called the *last deglaciation* or *Termination I (TI)*, is defined as the transition between LGM and the Holocene (~17.8 – 11.5 ka) in which the CO_2 atmospheric levels increased by ~ 80 ppmv (Barnola et al., 1987; Monnin et al., 2001; Petit et al., 1999). The main features of the deglaciation include: the events Heinrich 1 (H1) ≈ 17.8 – 16 ka, Bølling/Allerød (B/A) ≈ 14.8 – 12.8 ka, and Younger Dryas (YD) ≈ 12.8 – 11.5 ka (Hemming, 2004; Monnin et al., 2001).

🌍

Chapter 1

Millennial timescale climate variability in the eastern tropical North Pacific over the last two glacial cycles

1.1   Introduction

Abrupt millennial timescale variations (i.e. greater than centennial but less than orbital) have been found in the Pacific Ocean over the last glacial period (71 - 14 ka before present) as indicative of abrupt climate changes. In the NE Pacific, millennial timescale variations were first reported as changes in intermediate water oxygenation (Kennett and Ingram, 1995). In Santa Barbara Basin (SBB), the sediments show 17 distinct laminated intervals that occurred frequently between 60 - 12 ka BP (Behl and Kennett, 1996). The timing of these laminated sequences created great interest due to their correspondence with warmer periods recorded in Greenland ice cores known as interstadial or Dansgaard/Oeschger events (Dansgaard et al., 1984); in contrast to colder periods or stadials which in some cases are accompanied by abrupt ice rafting in the North Atlantic (i.e. Heinrich events) (Bond et al., 1993; Dansgaard et al., 1993; Heinrich, 1988). The oxygen poor conditions in the North Pacific intermediate waters during interstadials were inferred from laminated sediments (Behl and Kennett, 1996), and corroborated by benthic-foraminifera assemblages typical of nearly anoxic conditions (Cannariato et al., 1999).

Studies in the NE Pacific (e.g. off Oregon, Santa Monica and Santa Barbara, the Baja California Peninsula and the Gulf of California) have identified millennial-scale variations recorded in oxygen isotopes of planktonic foraminifera (Hendy and Kennett, 1999; Hendy et al., 2004), sediment chemical composition (Hendy and Pedersen, 2005; Hendy et al., 2004) and nitrogen isotopes (Emmer and Thunell, 2000; Hendy and Pedersen, 2005). A range of environmental changes have been inferred from these records including: changes in the strength of the oxygen minimum zone (Cannariato et al., 1999), sea surface temperatures and thermocline depths (Hendy and Kennett, 1999), intermediate water masses (Stott et al., 2000), sediment redox conditions (Hendy and Pedersen, 2005; van Geen et al.,

2003), subsurface denitrification (Emmer and Thunell, 2000), upwelling and marine productivity (Ortiz et al., 2004).

The discovery of the near global expression of millennial-scale variations during the last glacial period (i.e. marine isotope stages (MIS) 2 - 4) denotes intimate teleconnections in the climate system between the ocean and the atmosphere, and between high and low latitudes. For instance, synchronous temperature rises over Greenland and the North Atlantic (e.g. Bond et al., 1993; Dansgaard et al., 1993; Keigwin and Jones, 1994) have been linked to the northern migration of the Intertropical Convergence Zone (ITCZ) and increased upwelling intensity in the NE Pacific (Hendy and Kennett, 1999; Hendy et al., 2002; Ortiz et al., 2004). Such intimate latitudinal teleconnection is also exemplified by the millennial scale variability of atmospheric greenhouse-gasses (GHG: H_2O_{vapour}, CH_4 and N_2O) trapped in ice core records (IPCC, 2001). For example, interstadial increases of CH_4 production derived from low latitude wetlands, show to be tied to the global water cycle with similar frequencies (Flückiger et al., 2004; Flückiger et al., 1999; Ivanochko et al., 2005). Whereas N_2O changes are thought to be modulated by the efficiency of the oceanic biological pump and oceanic denitrification (Flückiger et al., 2004; Pedersen et al., 2003).

Most of the Northern Hemisphere (NH) millennial time scale records do not extend beyond the penultimate interglacial period (i.e. MIS-5). In contrast with ice core temperature records from Antarctica which span several glacial-interglacial (G-IG) cycles (EPICA et al., 2004; Petit et al., 1999; Spahni et al., 2005), the Greenland temperature records do not extend older than 123 ka BP (Broecker, 1992; Curry and Oppo, 1997). Recently discovered in marine sediments from the North Atlantic mid-latitudes, sea surface temperature (SST) records have demonstrated the presence of millennial-scale variations, extending over 250 ka BP (Martrat et al., 2004) and up to 430 ka BP (Martrat et al., 2007). However, no such time equivalent records are available in the Pacific Ocean.

In this study, two marine sediment cores from the eastern tropical North Pacific (ETNP) are studied for the following purposes: (*i*) to document and understand the nature of the millennial timescale variations older than 120 ka BP; (*ii*) to investigate the relationship between low and high latitude records at these time scales; and (*iii*) to explore the relationship between millennial scale variability in the E Pacific and past changes in GHG.

To obtain a continuous record of climatic changes for the last two glacial cycles (~240 ka BP) we use the records of organic carbon (%OC) and the diffuse spectral reflectivity (DSRa*) property of the sediment. We demonstrate that the colour attribute a* (red/green) of the sediments has a striking similarity to the %OC record, as previously identified in the Magdalena margin of Baja California (Mexico) by Ortiz et al. (2004). The OC and DSRa* records are used to construct the age model of Core MD02-2519 and extend the chronology up to the penultimate glacial cycle (~ 240 ka BP). Futher, we evaluate the age differences between records from tropical and higher latitude regions like Greenland (Grootes and Stuiver, 1997) and the North Atlantic mid-latitudes (Martrat et al., 2004). Spectral and wavelets analyses are also applied to investigate the relationship and the pacing between records at millennial scales during MIS-2-4 and MIS-6, i.e. the last and penultimate glacial periods, respetively. Finally, a comparison of productivity records from the ETNP with CH_4 records from ice cores (i.e. GISP2 and Byrd-EPICA) ilustrate the potential of the ETNP to respond as a natural source of GHG at millennial timescales, linking changes in upwelling to the climatic pacing of the Northern Hemisphere.

1.2   Materials and Methods

The piston cores MD02-2518 and MD02-2519 were retrieved from the continental slope off Mazatlan, Mexico (Figure 1.1), during the IMAGES (*International Marine Global Past Change Studies*) oceanographic expedition MONA (Beaufort, 2002). The Core MD02-2518 was raised from 450 m depth and the Core MD02-2519 from 955 m depth, from the upper and the mid-continental slope, respectively. The total length of each core is 4000 and 3600 cm, respectively. The sediment sequences change from massive to laminated intervals. The laminations range from fine (0.5 - 2 mm) to thicker banding (5 – 20 mm), sometimes alternating with faintly bioturbated intervals. The extent of the bioturbated intervals does not exceed 10 cm, except in the Core MD02-2519 where moderate bioturbation covers up to 50 cm between 2000 - 2250 cm depth (*see information provided in the* Appendix A).
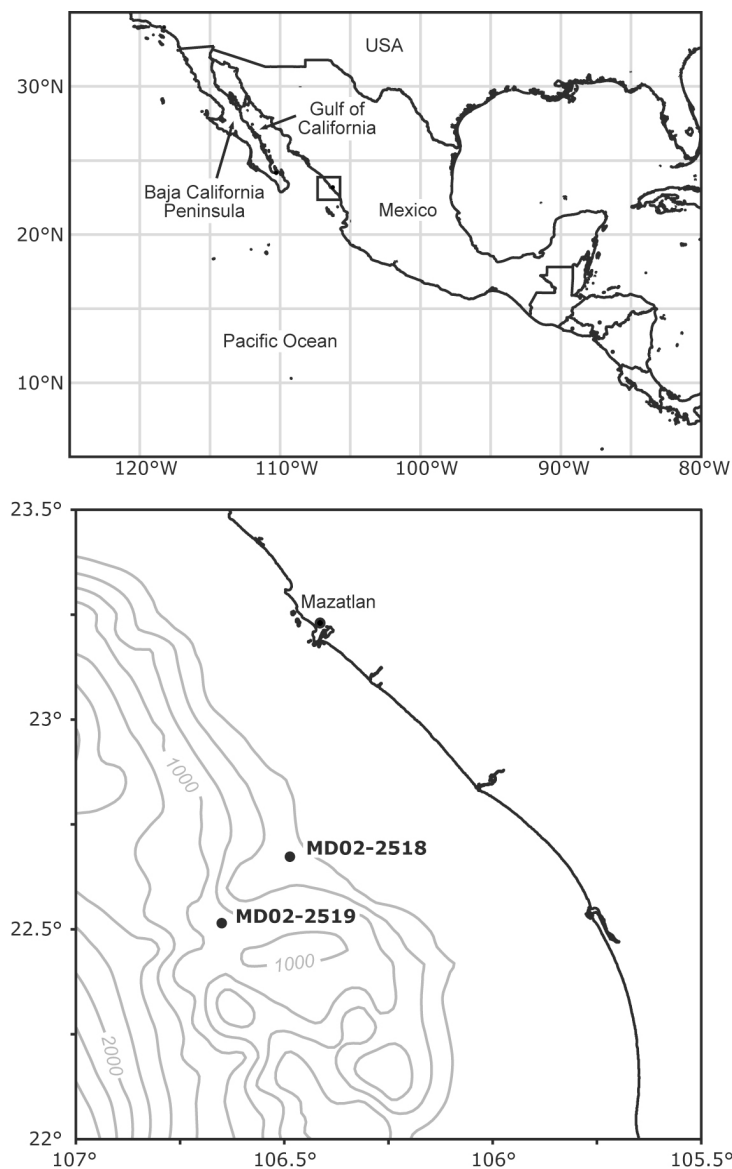
Figure 1-1 Map of the study area showing the location of the cores MD02-2518 (lat 22° 40.39'N; long 106° 29.19'W; 450 m water depth) and MD02-2519 (lat 22°30.89' N; long 106° 39.00W; 955 m water depth).

The cores sites are located in the ETNP, within an intense oxygen-minimum zone (OMZ) that extends from ~150 – 800 m depth with almost undetectable O_2 concentrations between 150 and 600 m water depth ($[O_2] < 10\,\mu$M) (Ganeshram et al., 1999). At the surface, the region experiences intense wind driven upwelling, high levels of biological productivity and elevated export production (Bakun and Nelson, 1991; Roden, 1962). The sediments reflect such conditions, being extremely rich in organic carbon (%OC > 7%) and other biogenic components (Ganeshram and Pedersen, 1998).

1.2.1   Paleoceanographic Proxies

Sample analyses of organic carbon (%OC) and oxygen isotopes of benthic foraminifera (δ^{18}O-BF) were performed in the Wolfson Laboratory, School of Geosciences, the University of Edinburgh. To perform the C-N analyses, the samples were selected every 1 - 2 cm (~ 80 – 250 yrs/sample) for the Core MD02-2518 and every 2 cm (~ 60 – 100 yrs/sample) for the Core MD02-2519. The sediments were freeze-dried, ground and homogenized in an agate mortar. To remove all traces of carbonates, the samples were acidified with HCl (5%) on a hot plate at 70°C. The %OC was determined using a C-N Elemental Analyser (CE Instruments NA2500) coupled to a CG PRISM II Mass Spectrometer.

Analyses of δ^{18}O in the Core MD02-2519 were performed in sediment samples chosen every 2 – 5 cm in the first half of the core (0 - 1800 cm) and every ~ 10 - 20 cm in the second half (1800 - 3600 cm), depending on the foraminifera abundances. All sediments samples were routinely washed with running water through a 65μm mesh size to eliminate the finer fraction. Approximately 10 organisms of benthic foraminifera *Uvigerina* spp. were carefully picked, rinsed and sonicated for few seconds in double-distilled water for isotopic analyses. The hand-picked carbonate sample was reacted with 100% orthophosphoric acid at 75°C in a "Kiel Carbonate III" preparation device. The resulting CO_2 was analysed on a *Thermo Electron Delta⁺ Advantage* stable isotope ratio mass spectrometer. The standard deviation for the analyses was ± 0.07‰ for δ^{18}O, based on a marble powder MAB2B run as a sample over the same period as the studied samples; values are quoted relative to PDB.

The diffuse spectral reflectivity (DSR) was measured on board the ship at every 2 cm with a Minolta-2022 spectrophotometer (Beaufort, 2002). The parameter *a** (the '*red/green*' attribute) was calculated automatically with the spectrophotometer. The DSR is a non-destructive technique used to obtain a rapid assessment of the geochemical composition (Ortiz et al., 1999) and provides a semi-quantitative assessment of the sediment components (Mix et al., 1992). The method has shown to be particularly suitable for organic rich-sediments in the NE Pacific margin, where different colour attributes have been successfully linked to %OC, %CaCO₃, terrigenous sediments and others (Ortiz et al., 1999; Ortiz et al., 2004). Following these studies, the parameter DSRa* (the '*red/green*' attribute) is used as a semi-quantitative indicator of %OC. This is further described in the following sections,

where we show the striking similarity between the DSRa* and the %OC records in the cores MD02-2518 and MD02-2519 between 0 - 120 ka (i.e. MIS-1 to MIS-5). On this basis, the DSRa* curve is used as a proxy of %OC in older intervals.
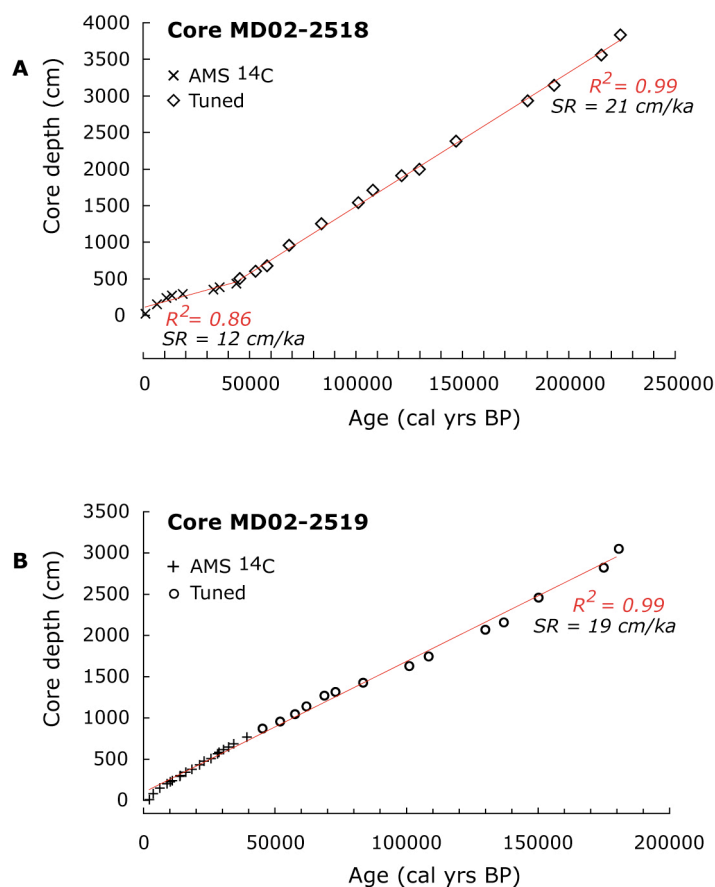
Figure 1-2 Age model of the sediment cores (A) MD02-2518 and (B) MD02-2519, including AMS ^{14}C and tuned ages. Symbols are age control points: crosses and plus signs from radiocarbon dates; diamonds and circles from estimated dates based on the GISP2 and ODP-977A scales (Grootes and Stuiver, 1997; Martrat et al., 2004). Red line is the average sedimentation rate (SR) (see Table 1.1 for details).

1.2.2   Age Model Construction

The age models of the cores MD02-2518 and MD02-2519 were constructed using various approaches (Figure 1.2 and Table 1.1). First, we constructed a radiocarbon-based chronology for the last 40 ka (Table 1.2), which will be described in detail in the following section (*page 10*). The independent chronology (Figure 1.3) shows coeval millennial scale timing between the cores MD02-2518, MD02-2519 and GISP2 over this period. This raises the possibility that after tuning the DSRa* or %OC records to Greenland, we might be able

to extend our chronology beyond the radiocarbon limits (Figure 1.4). To test this, we compared age models generated by ^{14}C dating to tuned age models based on GISP2, where both chronologies overlap. Listed in Table 1.3 is shown that the age differences are within the estimated uncertainties of the GISP2 scale (Grootes and Stuiver, 1997) and the radiocarbon error 1σ (Table 1.2). This evaluation is used to validate the tuning of the older intervals to the North Atlantic δ^{18}O record ODP-977A (Martrat et al., 2004) (Figure 1.5). Full details of these procedures are given the following sections. The result will be a composite chronology spanning ~ 240 ka for the Core MD02-2518 and ~ 200 ka for the Core MD02-2519 – which is the main chronology used in this thesis.

The tuned chronology of the Core MD02-2519 (based on the OC and DSRa* records) was additionally compared with the δ^{18}O-*Uvigerina* curve and the LR04 δ^{18}O stack. The δ^{18}O record was not used in the age model construction but to delimit the end of the core. The consistency between chronologies of the cores MD02-2518 and MD02-2519 was additionally verified by the identification of ash layers that are common to both records (Figure 1.5). Such corroboration was essential, particularly for the Core MD02-2518 of which the δ^{18}O record is not available. It should be emphasised that tuning the records may ignore subtle time leads/lags between cores, but still useful to understand the nature of the millennial-scale variability recorded in the ETNP beyond the last glacial period.

Radiocarbon dating

The radiocarbon controls of the cores MD02-2518 and MD02-2519 are based on 8 and 19 radiocarbon dates, respectively, spanning the last ~ 44 ka BP (Table 1.2). The accelerator mass spectrometry (AMS) ^{14}C dates were analysed at the NERC Radiocarbon Laboratory (RCL) in East Kilbride, UK, in samples based on organic carbon or mixed planktonic foraminifera species. The raw ^{14}C dates were calibrated with the online version for marine samples Calib 5.0.2 - Marine04 (Stuiver and Reimer, 1993), using a reservoir age correction (ΔR) of 203 ± 48 years, as reported by Reimer and Reimer (2001). Reservoir corrected ages older than ~ 22 ka, were transformed to calendar years before present using the polynomial equation (Bard et al., 2004):

Age (cal yr BP) = -2.5196 x 10^{-6} x [Age ^{14}C age yr BP] [2] + 1.237 x [Age ^{14}C yr BP] -175

Table 1.1

AGE MODEL: Core MD02-2518

Source	MD02-2518 depth (cm)	Age (Cal ka BP)	Source (*symbol*)
AMS ^{14}C	10	1.2	×
AMS ^{14}C	140	6.7	×
AMS ^{14}C	230	11.2	×
AMS ^{14}C	260	13.8	×
AMS ^{14}C	284	18.9	×
AMS ^{14}C	340	33.2	×
AMS ^{14}C	372	36.2	×
AMS ^{14}C	422	44.0	×
D/O 12	490	45.3	◇
D/O 14	590	51.9	◇
D/O 17	664	57.5	◇
D/O 19	954	68.4	◇
D/O 21	1250	83.6	◇
D/O 23	1534	101.0	◇
D/O 25	1712	108.1	◇
(MIS 5e) 26	1906	121.6	◇
(MIS 6.0) S1'	1990	130.0	◇
(MIS 6.4) S4'	2376	150.3	◇
(MIS 6.6) 9'	2930	180.8	◇
(MIS 7a) 11'	3146	193.4	◇
(MIS 7c) 12'	3560	215.5	◇
(MIS 7d) 13'	3836	224.5	◇

AGE MODEL: Core MD02-2519

Source	MD02-2519 depth (cm)	Age (Cal ka BP)	Source (*symbol*)
AMS ^{14}C	1	2.4	+
AMS ^{14}C	74	3.8	+
AMS ^{14}C	140	6.3	+
AMS ^{14}C	194	9.1	+
AMS ^{14}C	216	10.2	+
AMS ^{14}C	230	11.1	+
AMS ^{14}C	284	13.9	+
AMS ^{14}C	290	14.1	+
AMS ^{14}C	332	16.1	+
AMS ^{14}C	370	18.5	+
AMS ^{14}C	424	21.4	+
AMS ^{14}C	466	23.2	+
AMS ^{14}C	500	25.7	+
AMS ^{14}C	558	28.2	+
AMS ^{14}C	576	28.8	+
AMS ^{14}C	606	30.5	+
AMS ^{14}C	636	32.5	+
AMS ^{14}C	676	34.5	+
AMS ^{14}C	758	39.5	+
D/O 12	870	45.3	○
D/O 14	956	51.9	○
D/O 17	1044	57.5	○
D/O 18	1138	61.9	○
D/O 19	1272	68.4	○
D/O 20	1316	72.8	○
D/O 21	1428	83.6	○
D/O 23	1630	101.0	○
D/O 25	1744	108.1	○
(MIS 6.0) S1'	2070	130.0	○
(MIS 6.2) 1'	2156	137.0	○
(MIS 6.4) S4'	2458	151.3	○
(MIS 6.5) 8'	2824	175.1	○
(MIS 6.6) 9'	3040	180.8	○

Table 1-1 Age controls used to construct the age model of cores MD02-2518 and MD02-2519. AMS ^{14}C dates are detailed in Table 1.2 . Identified D/O events correspond to the classification of GISP2 (crosses and plus signs) and ODP-977A (diamond and circle symbols). D/O-Dansgaard/Oeschger, S-Stadial and MIS-Marine Isotope Stages are given for reference. Symbols on the right column are equivalent to those in Figure 1.2 .

Table 1.2

AMS ^{14}C dates: Core MD02-2518

Core depth (cm)	Raw ^{14}C Age (yr)	error +	Calibrated Age (yr BP)*	error 1σ -	error 1σ +	Notes: Material	Calib source
10	1891	35	1242	63	51	OC	1
140	6442	44	6689	77	85	OC	1
230	10413	72	11207	82	71	OC	1
260	12515	97	13768	115	125	OC	1
284	16204	162	18871	121	108	OC	1
340	28838	850	32881	1251	1251	OC	2
372	31772	1234	36621	1454	1454	OC	2
422	40188	3555	44035	3017	3017	OC	2

AMS ^{14}C dates: Core MD02-2519

Core depth (cm)	Raw ^{14}C Age (yr)	error +	Calibrated Age (yr BP)*	error 1σ -	error 1σ +	Notes: Material	Calib source
1	2865	73	2365	116	94	OC	1
74	4049	61	3802	79	93	OC	1
140	6050	61	6266	54	72	OC	1
194	8689	64	9114	79	101	OC	1
216	9555	73	10198	82	84	PF	1
230	10272	62	11082	134	94	PF	1
284	12664	53	13911	86	75	OC	1
290	12831	64	14084	84	76	PF	1
332	14173	65	16139	205	193	PF	1
370	15717	84	18475	184	296	OC	1
424	18667	109	21417	278	272	OC	1
466	20091	173	23191	316	346	OC	1
500	21920	153	25713	208	145	OC	1
558	24147	154	28226	399	399	OC	2
576	24690	169	28831	369	369	OC	2
606	26239	216	30548	364	364	OC	2
636	27987	281	32471	349	349	OC	2
676	29852	367	34507	342	342	OC	2
758	35012	749	39522	1015	1015	OC	2

* ΔR = 203 + 48
OC - organic carbon; PF - mixed planktonic foraminifera species
(1) Stuiver *et al.*, 2005; (2) Bard *et al.*, 2004

Table 1-2 List of AMS ^{14}C dates of cores MD02-2518 and MD02-2519.

Figure 1.3 shows OC records from cores MD02-2518 and MD02-2519 plotted against the age model derived from AMS ^{14}C calibrated dates, and contrasted to the Greenland temperature record δ^{18}O GISP2 to recognised the millennial scale events (shown with numbers). Overall, we identify a very good correspondence between stadial and interstadial events, as each datum falls within the maximum and minimum 1σ error of the radiocarbon age model (Table 1.2). The selection of particular events listed in Table 1.3 are used to compare the radiocarbon age model (Figure 1.3) with an alternative age model completely tuned to GISP2 (*annexed Figures 1a* and *1b*). The resulting age differences are about 110 - 880 yrs (Table 1.3), mostly within the age uncertainty of the GISP2 timescale (Grootes and Stuiver, 1997). Therefore, we found that the range of ages on both timescales is consistent; and demonstrate that the inflection point seen in Figure 1.2-A (i.e. Core MD02-2518) is not an artefact of changing the age model (see *annexed Figure 1b*). These results support the contention that the timing of the climatic events in our cores match the GISP2 scale. These observations are in agreement with previous studies showing synchronicity

between records from Greenland and the NE Pacific during Termination I (TI) and the Last Glacial Maximum (LGM) (Hendy and Kennett, 1999; Hendy et al., 2004).
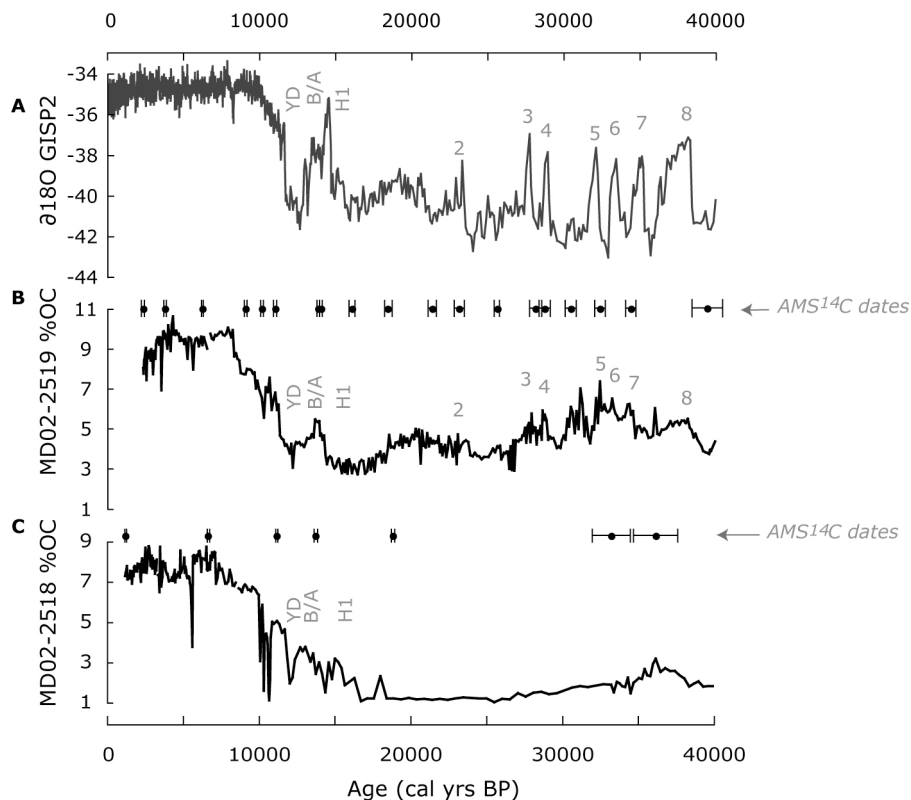
Figure 1-3 Radiocarbon based chronology of cores MD02-2519 and MD02-2518 over the last 40 ka. Dots with error bars are AMS ^{14}C dates. (A) δ^{18}O GISP2; (B) and (C) are OC records. Numbers are GISP2 interstadial (D/O) events. YD – Younger Dryas; B/A – Bølling Ållerød; H1 – Heinrich 1.

Tuning with GISP2

Beyond the radiocarbon limits (> 40 ka), the cores MD02-2518 and MD02-2519 were tuned to GISP2 δ^{18}O record (Grootes and Stuiver, 1997). Overall, the maxima values of OC and DSRa* match with the major δ^{18}O interstadial events or D/O (shown by the dotted lines in Figure 1.4). Therefore, the tuning to GISP2 provides a datum comparable to calendar years, where linear interpolation between control points can be applied for the last 120 ka.

Table 1.3

Event		Core MD02-2519 Depth (cm)	Age GISP2 (Cal yr BP)	AMS^{14}C (Cal yr BP)	Age difference (yrs) GISP2 - ^{14}C
YD		230	11500	11080	420
B/A		286	14530	13970	560
H1		320	16250	15550	700
D/O 2		466	23300	23190	110
D/O 3		558	27820	28230	410
D/O 4		576	28840	28830	110
H3		594	30100	29860	240
D/O 6		652	33460	33290	170
D/O 8	(A1)*	724	38320	37440	880
D/O 12	(A2)*	870	45283	-	-
D/O 14	(A3)*	956	51933	-	-
D/O 17	(A4)*	1044	57540	-	-
D/O 18		1138	61870	-	-
D/O 19	(A5)*	1272	68437	-	-
D/O 20	(A6)*	1316	72750	-	-
D/O 21	(A7)*	1428	83557	-	-
D/O 23		1630	101000	-	-

* Antarctica (A) warm events, analogues to interestadial events in GISP2 (Blunier and Brook, 2001).

Table 1-3 List of selected intervals from the Core MD02-2519 showing the age differences between two age models: one constructed by tuning to GISP2 timescale, and another based on AMS ^{14}C dates over the last 40 ka BP.

Tuning beyond GISP2

The age model of the cores MD02-2518 and MD02-2519 was extended beyond the GISP2 time limit (~120 ka) using the shipboard diffuse spectral reflectivity records (DSRa*) following the strategy described by Ortiz *et al*. (2004). In the cores MD02-2518 and MD02-2519, the DSRa* records bear a striking resemblance to the OC content, with obvious millennial timescales events between 120 – 240 ka BP (Figure 1.5). Hence, the DSRa* record is used as a proxy of OC in older intervals, which is tuned to the ODP-977A δ^{18}O record from the Iberian Margin, in the North Atlantic, to extend our records beyond the limit of Greenland GISP2. The chronology of the Core ODP-977A (36º 1.907' N; 1º 57.32 'W; 1984 mbsl) (Martrat et al., 2004) was originally constructed comparing δ^{18}O profiles of the planktonic foraminifera *Globigerina bulloides* with defined orbitally-tuned isotopic events, assuming constant sediment accumulation rates between tie-points. In Figure 1.5 we show the graphical tuning and the position of the tie-points used to construct the age models of cores MD02-2518 and MD02-2519, as well as the final chronology created by linear interpolation.
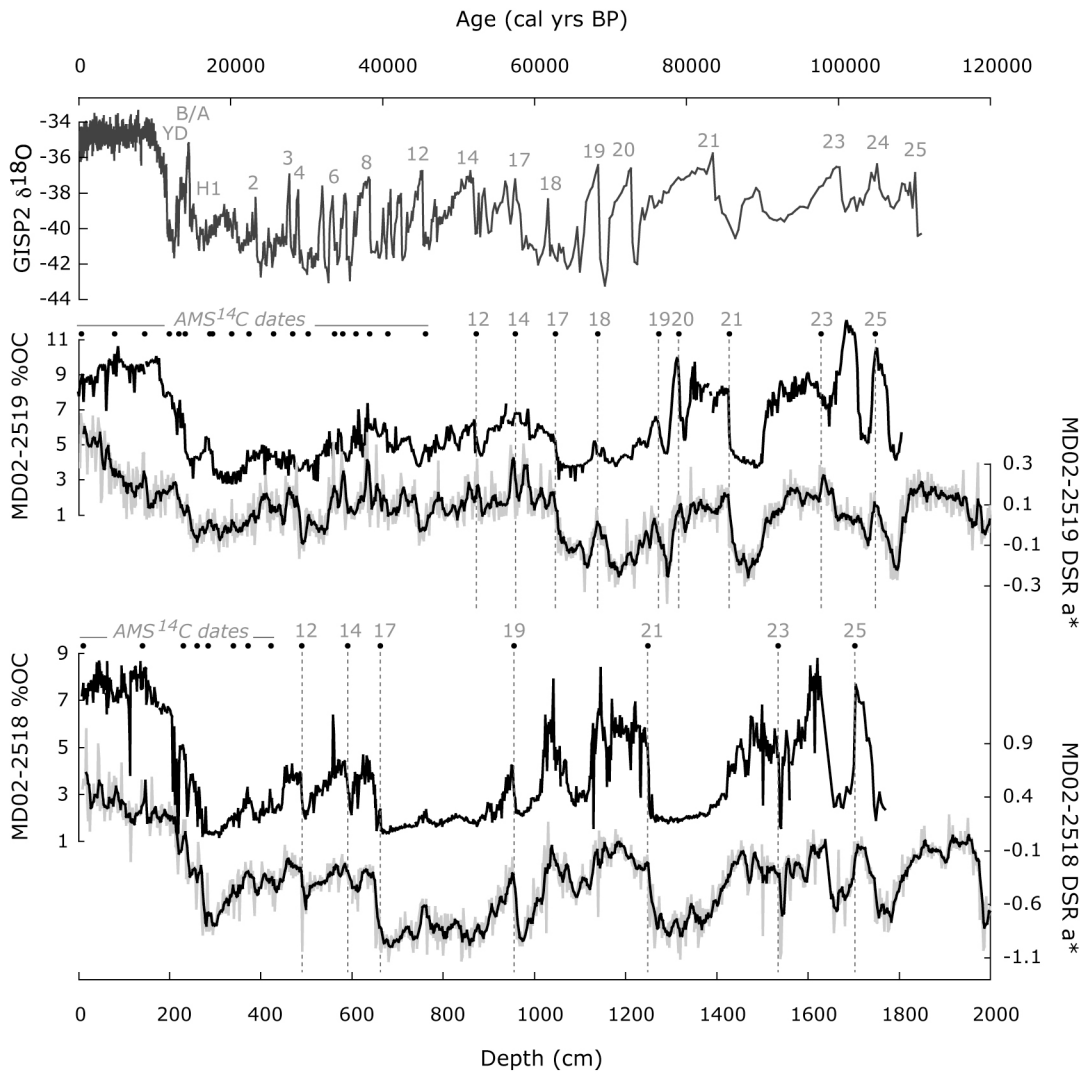
Figure 1-4 Records of organic carbon (%OC) and diffuse spectral reflectivity (DSRa*) of cores MD02-2519 and MD02-2518 correlated to the δ¹⁸O-GISP2 tuning target. Notice the scale differences on the x axis: OC and DSRa* vs. depth; δ¹⁸O vs. age.

Verification of the age model

To verify the resultant composite age model of Core MD02-2519 we compared the oxygen isotope record (δ¹⁸O-*Uvigerina*) with the LR04 δ¹⁸O-stack record (Lisiecki and Raymo, 2005), to see how the timing of the events corresponds between cores. As shown in Figure 1.6, the records show a good temporal agreement over the last 200 ka. In general, the time differences between isotopic events are shorter than 1500 yrs. In this way, the δ¹⁸O-BF curve confirms that the Core MD02-2519 does not extend beyond MIS-6, and validate the tuning to the Core ODP-977A on intervals older than 120 ka. The constructed chronologies

indicate that the cores MD02-2518 and MD02-2519 span ~ 240 ka and ~ 200 ka, respectively. Additionally, we used two approaches to verify the consistency between the age models. First, the clear graphic correspondences between DSRa* records. Second, the presence of two distinct ash layers at 2780 cm (MD02-2518) and 2855 cm (MD02-2519) (Figure 1.5), which the age model places naturally at the *interstadial-8*' (~ 175 ka) in both cores. One limitation, however, was the inability to detect additional ash layers common to both records. Analysis of physical and chemical properties of tephra layers are important targets for future investigations in these records. In spite of this, the final age models of the cores are consistent with the oxygen isotope curve, along with previous studies showing that it is possible to tune NE Pacific records with those from Greenland and the North Atlantic (e.g. Behl and Kennett, 1996; Hendy et al., 2002; Ortiz et al., 2004).

1.2.3   Spectral and Wavelets Analyses

Spectral analyses were performed using the software *Analyseries 2.0.4.2* (Paillard et al., 1996) to extract the major time frequencies present in the records. To further validate the results, they were independently extracted with *SPECTRUM 2.2* (Schulz and Stattegger, 1997). The results obtained by using the two different software packages were similar. Comparisons were made on the results of spectral analyses between cores from low and high latitudes, and between the last and the penultimate glacial periods.

Time series analyses were applied to the %OC (Core MD02-2519 only) and the DSRa* records (both cores). Two glacial periods were independently analysed to obtain specific periodicities. The first interval is centred between 15 – 70 cal ka BP (corresponding to MIS 2 – 4), and the second between 130 – 185 cal ka BP (corresponding to MIS-6). The spectral analyses performed with *Analyseries* followed two classical methods, Blackman Tukey (B-Tukey) and Maximum Entropy (MEM). The 'input' dataset for each spectral analysis was 're-sampled' to obtain an even time resolution (every 100 yrs) by applying cubic-spline simple-interpolation. The linear trend of the series was removed and 'default' pre-whitening was applied. The B-Tukey method (based on standard Fourier-transform) was used to obtain the linear power spectrum and to identify the main linear oscillations (*Tukey* window function with bandwidth of 0.23 cycles/ka, explaining 50% of series). In addition, the MEM method was applied to increase the resolution of the spectral peaks (explaining 30% of series). To determine the statistical significance of the frequencies obtained (i.e. not

noise signals), F-tests were performed using a MTM (Multi-Taper Method). Only frequencies with > 90% confidence level were accepted (i.e. F-test > 0.90 in the output frequencies between $5 \times 10^{-5} – 1 \times 10^{-3}$ cycles/ka) and compared with the SPECTRUM results.
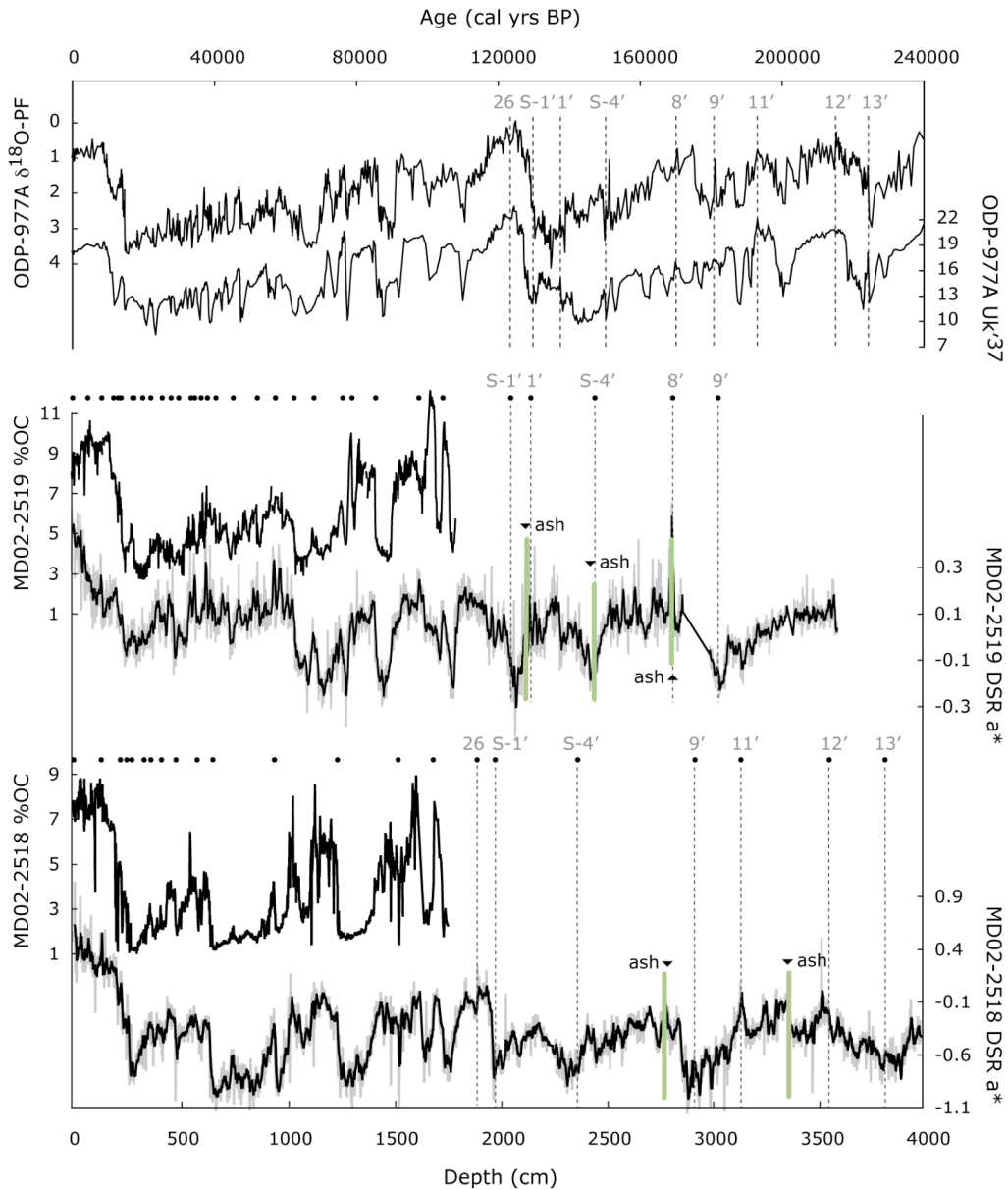
Figure 1-5 Records of organic carbon (%OC) and diffuse spectral reflectivity (DSRa*) of cores MD02-2519 and MD02-2518, correlated to the δ^{18}O ODP-977A tuning target (dotted lines). Green bands show the position of ash layers placed at 2780 and 3350 cm in Core MD02-2519; and at 2160, 2440 and 2855 cm depth in Core MD02-2518. Black dots are age control points. Notice the scale differences on x axis: OC and DSRa* vs. depth; δ^{18}O vs. age.
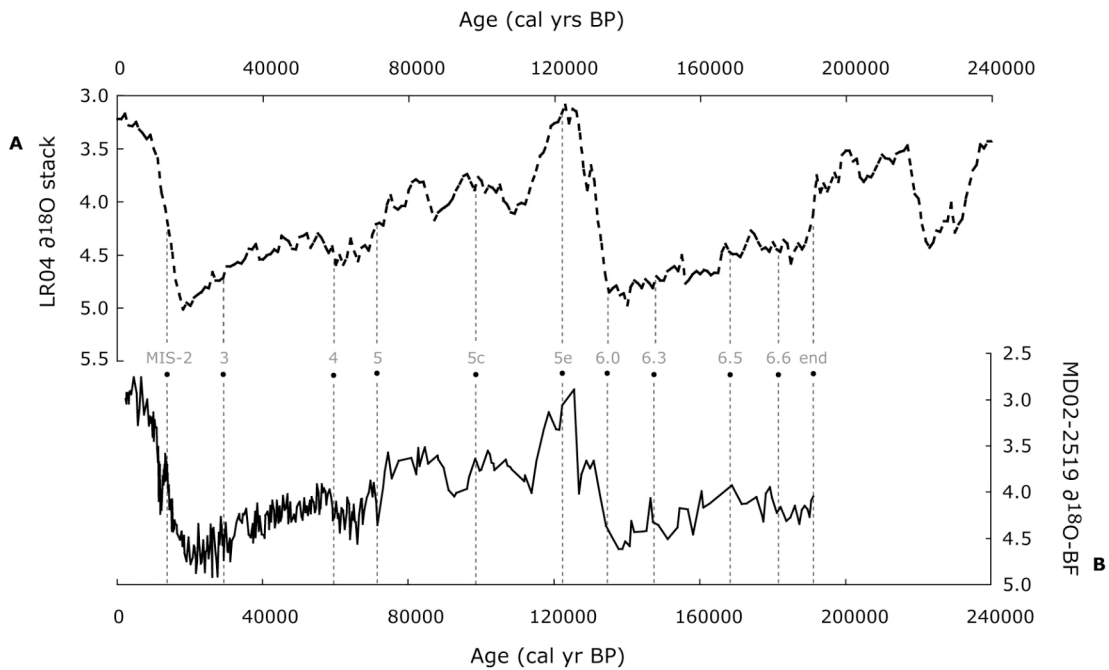
Figure 1-6 Comparison between oxygen isotope records: (A) LR04 δ¹⁸O stack record (Lisiecki and Raymo, 2005); (B) Core MD02-2519 δ¹⁸O record of the benthic foraminifera Uvigerina spp (plotted on the "radiocarbon – tuned" age model shown on Table 1.1). Numbered vertical dotted lines indicate identifiable Marine Isotope Stages (MIS).

The harmonic analyses performed with SPECTRUM (analogous to that of auto-spectral analysis) did not require re-sampled input data because the software has been designed for unevenly spaced time series (based on Lomb-Scargle Fourier transform and Welch-Overlapped-Segment-Averaging procedure (Schulz and Stattegger, 1997)). The default over-sampling factor (OFAC) and the highest frequency (HIFAC) were used in all analyses; they were tested for 2-3 harmonic components using a significance level of 0.05, the linear trend was removed. After we verified and selected the major spectral peaks of each time interval (15 – 70 ka and 130 – 185 ka), we cleaned the series with a band-pass Gaussian filter centred at the frequencies obtained with MEM. The combined sum of Gaussian filters (bandwidth = 0.2×10^{-4}) was used to identify the pacing and principal features of the series. Finally, the DSRa* and OC records were examined with *wavelets analysis* to determine the non-stationary periodicities of the time series. Such a property is identified by the change in the slope of the spectral curve, indicative of phase variations in the low frequencies and represent groups of stationary and non-stationary waves. The Morlet method was applied to the wavelets analysis as it is commonly used to locate variations of power within the time series. The Morlet method consists of a plane-wave modulated by a Gaussian function,

which decomposes the series into *time-frequency spaces* to determines both, the dominant modes of variability (phase changes) and how those modes change in time. We applied this method using the default settings of the online software developed by Torrence and Compo (1998). Only values inside the 90% cone of influence (COI) were considered significant.

1.3   Results and Discussion

1.3.1   Sedimentation rates and identification of millennial timescale events

The age models constructed for the cores MD02-2518 and MD02-2519, denote regular sedimentation rates (SR) and linear age vs. depth relationships ($R^2 = 0.86$ to 0.99) (Figure 1.2). Although an inflection point on the slope is identified at 50 ka BP in the Figure 1.2-A (i.e. Core MD02-2518), it cannot be explained as an artefact of the age model based on radiocarbon, but to a slight change in the sedimentation rate. This is demonstrated through the construction of an age model completely tuned to GISP2 (*annexed Figure 1b*), which shows a similar inflection point at this time. Furthermore, the average SR $\sim$ 12 - 20 cm/ka and $\sim$19 cm/ka of the cores MD02-2518 and MD02-2519 (respectively) largely agree to previous studies (Ganeshram and Pedersen, 1998). Based on the graphic correlations to Greenland and the North Atlantic, the age scales of the cores collected off Mazatlan show that the reflectivity record spans up to 200 ka (Core MD02-2519) and 240 ka (Core MD02-2518) (Figure 1.7). As confirmed by the δ^{18}O-*Uvigerina* record, the age of the Core MD02-2519 extends back to MIS-6.6 and the Core MD02-2518 up to MIS-7d.

The millennial scale events identified in the %OC and DSRa* records are numbered following the GISP2 and the ODP-977A terminology. The 26 events of the last climate cycle (0 – 130 ka BP) correspond to interstadial events Dansgaard/Oeschger (D/O 1 – 26) (Dansgaard et al., 1993) (Figures 1.8). The 15 events beyond D/O-26 correspond to interstadial events (I-1' to 15') during the penultimate glacial period (130 - 240 ka BP) (Martrat et al., 2004). In the course of MIS-2, MIS-4 and MIS-5b, some of the millennial-scale events are better resolved in the %OC record of Core MD02-2519 than in the Core MD02-2518 during D/O-2, 3, 4, 15, 17, 18 and 22, possibly aided by the higher sedimentation rates during glacial times. However, the colour reflectivity record of both cores is sensitive enough to reveal all D/O events, thus the DSRa* record can extends its timescale up to I-9' in the Core MD02-2519 and up to I-25' in the Core MD02-2518.
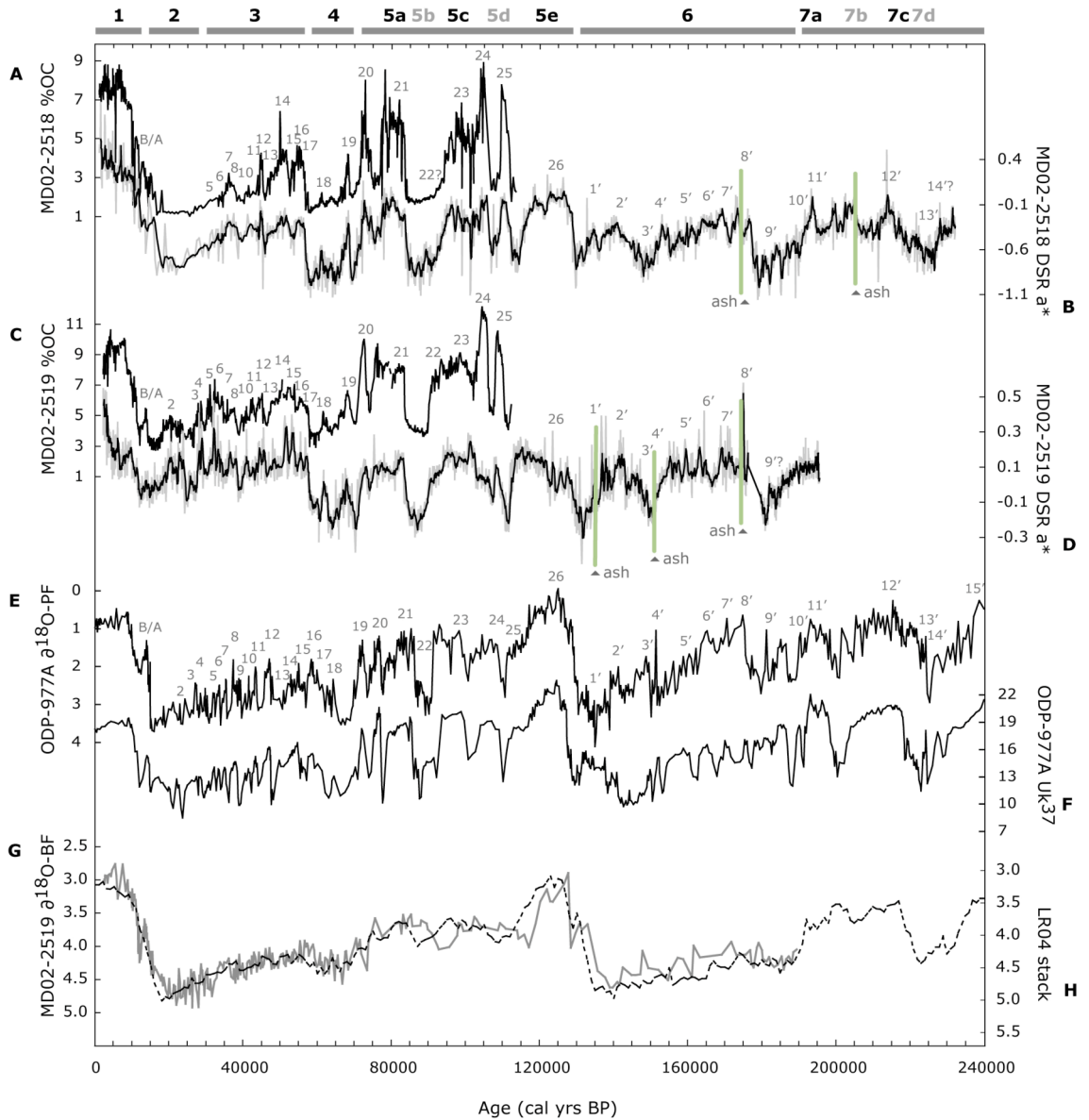
Figure 1-7 Records spanning the last two glacial cycles (0 - 240 ka). Band on top shows glacial-interglacial MIS 1 – 7d. (A) %OC and (B) DSRa* records of Core MD02-2518 (black line – 5 point moving average). The ash layers are placed at 173.4 and 205.0 ka BP. (C) %OC record and (D) DSRa* records of Core MD02-2519 (black line – 5 point moving average). The ash layers are placed at 137.0, 152.3 and 175.1 ka BP. (E) $\delta^{18}O$-Globigerina bulloides and (F) sea surface temperature (Uk'37) records of Core ODP-977A (Martrat et al., 2004). (G) $\delta^{18}O$-Uvigerina spp. record of Core MD02-2519. (H) LR04 $\delta^{18}O$ stack record (Lisiecki and Raymo, 2005). Numbers between 0 - 130 ka are referred to D/O events (1 – 26). Numbers between 130 - 240 ka are interstadials (1' – 15'), marked with a question mark (?) when doubtful.
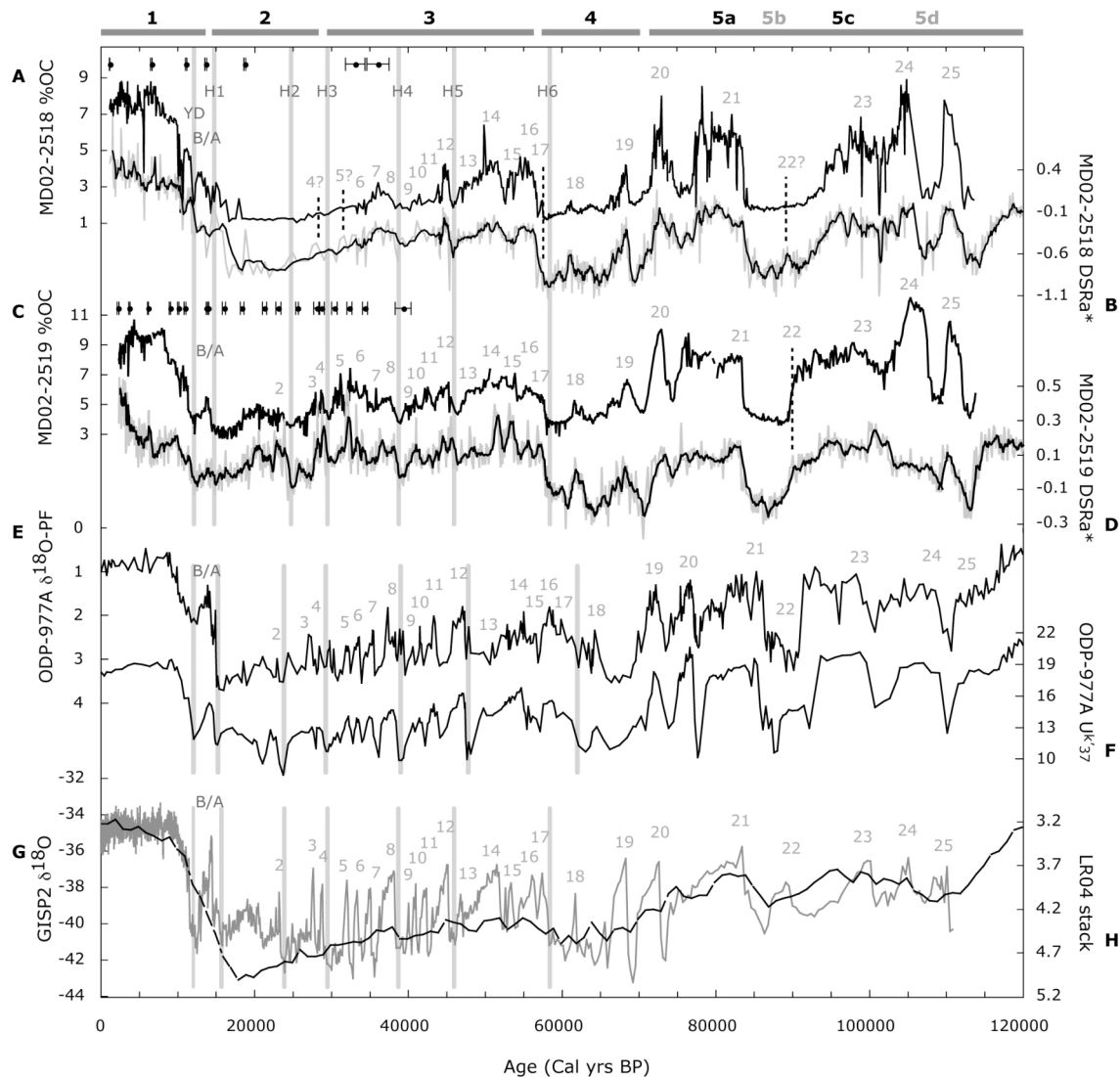
Figure 1-8 Comparison between records over the last glacial cycle (0 - 120 ka). Band on top shows MIS 1 – 5d. (A) %OC and (B) DSRa* records of Core MD02-2518 (black line – 5 point moving average); (C) %OC and (D) DSRa* records of Core MD02-2519 (black line – 5 point moving average); (E) $\delta^{18}O$ Globigerina bulloides and (F) SST Uk'37 records of Core ODP-977A; (G) GISP2 $\delta^{18}O$ record; (H) LR04 $\delta^{18}O$ stack record. Dots with error bars are AMS ^{14}C dates. Numbers are D/O 1-25; vertical grey lines are the YD and Heinrich events H1 - H6 (Bond et al., 1999).

1.3.2 High-resolution records of productivity in the ETNP

The marine sediment cores MD02-2518 and MD02-2519, display frequent and large shifts in %OC and DSRa* (Figures 1.7 and 1.8). The OC varies between 1 – 8.9% and 2.7 – 12% in each core, respectively. Higher values of organic carbon are seen during interstadials (i.e. warm periods), although 2 - 3 times lower values are seen during glacials and stadials,

including H-events (i.e. cold periods). Maximum values ($OC_{MD02-2518} > 6\%$; $OC_{MD02-2519} > 8\%$) in OC records are present during D/O-20, 21, 23, 24 and 25 and the Holocene. Both cores have the lowest values (< 2-3%) over MIS-2, 4 and 5b. The patterns of OC-MAR variation are similar to the %OC record given the linear sedimentation rates seen in Figure 1.2, thus not shown. The OC-MAR values average 138 mg/cm^2/ka in Core MD02-2518 (22–256 mg/cm^2/ka) and 418 mg/cm^2/ka in Core MD02-2519 (200–816 mg/cm^2/ka).

At present, the NE Pacific experiences high levels of primary productivity as cold but nutrient-rich water is brought to the surface by Ekman transport. Here, the upwelling is predominantly wind driven, thus coupled to prevailing atmospheric patterns and very sensitive to climate changes (Hendy et al., 2004; Ortiz et al., 2004). The sediments accumulating beneath the upwelling zones, which are rich in organic matter, can provide high resolution records of local responses linked to climate variability (Ganeshram and Pedersen, 1998). Off NW Mexico and California, previous studies (Ganeshram and Pedersen, 1998; Hendy and Pedersen, 2005; Hendy et al., 2004) have shown that the OC can be a consistent recorder of changes in paleo-productivity and upwelling as it shows patterns similar to other productivity proxies such as bio-barium, sedimentary trace elements, carbonate concentrations, planktonic foraminifera assemblages and occasionally carbon isotopes records. Under upwelling settings, high levels of organic matter are exported from the surface in the form of organic debris. This produces the intensification of the oxygen depleted conditions in the water column (i.e. organic carbon oxidation), the development of reducing conditions in sediments, as well as the preservation of sedimentary organic carbon (Ganeshram et al., 1999). The occurrence of high-resolution records of %OC (and DSRa*) in the cores collected off NW Mexico could then be interpreted as proxies of productivity linked to upwelling variations.

Productivity proxy records of the cores MD02-2518 and MD02-2519 show close similarities to Greenland and the North Atlantic temperature records (Figures 1.7 and 1.8). Off NW Mexico, the identified productivity events appear to be synchronous and equally sensitive to the climate changes recorded in higher latitudes at millennial timescales. As documented by previous studies in the NE Pacific (Hendy et al., 2002), this response suggests an intimate atmospheric relationship between regions of the Northern Hemisphere (NH), given the spatial and temporal intensity of these climatic signals. In the following sections, the low-latitude upwelling/productivity changes are compared with high-latitude

temperature records over the last and penultimate glacial cycles.

1.3.3 MIS 1 – MIS 5: patterns and periodicities

In the sediment Core ODP-977A from the North Atlantic mid-latitude, the changes in sea surface temperatures (SST) correspond with 26 warm phases (interstadials) and their complementary cold phases (stadials), as documented in ice core records from Greenland (Dansgaard et al., 1984) (Figure 1.8). Six cold events also correspond with punctual ice rafted debris or H-events (Bond et al., 1993; Heinrich, 1988). In the cores MD02-2518 and MD02-2519, however, the 26 interstadial events match with increases in productivity (high %OC and DSRa* values) whereas the corresponding stadials represent a decrease. Such a relationship reinforces that climatic teleconnections exist between distant regions of the NH. Although subtle differences are also evident between records:

(1) Patterns of rapid change.- The rapid temperature changes seen in Greenland and the North Atlantic records display "asymmetrical" patterns of very rapid warming followed by a more gradual cooling similar to a "saw-tooth" pattern (Figure 1.8-E – G). In contrast, the changes associated with productivity (%OC and DSRa* records) are more "symmetrical" (i.e. gradual increases and gradual decreases) (Figure 1.8 A–D). In the NW Mexican margin, although the productivity variations are controlled by atmospheric modifications in the wind-driven upwelling system, it seems that the rapid initiation into a new interstadial does not occur as abruptly as in Greenland or the North Atlantic. This could mean that the teleconnections between low and high latitudes are not exclusively controlled by the atmosphere, but also involve the ocean.

Although such a possibility will be explored in detail in the following chapters, we show in the *annexed Figure 1a,* the comparison between records from the ETNP and Antarctica, which illustrates that a mechanism to transmit climatic signatures between these regions could exist at millennial scales. Here, we used the age model of Core MD02-2519 which is entirely tuned to the GISP2 scale (*annexed Figures 1a* and *1b*) to estimate the age and pattern differences displayed by the productivity proxy, relative to the temperature proxy of the ice-core $\delta^{18}O$ records GISP2 and Byrd. Overall, the number of interstadial events found in the OC and DSRa* records over MIS-2 to 4 coincide more to Greenland timing, however, the pattern of each interstadial is more symmetrical and similar to the record from

Antarctica (e.g. A1, A2, A3) (see colour bands in *annexed Figure 1a*). The mechanistic relationship to explain this effect could suggest that during MIS-2 to 4, the millennial scale events recorded in the ETNP were not only controlled by the atmospheric circulation of the NH, but also influenced by the Southern Hemisphere (SH). On the other hand, this could be an indication of the role played by the tropics in the global manifestation of interstadial events. Evidence of the physical expression of the Antarctica timing has been also identified in Greenland records, suggesting that gradual climatic changes might potentially trigger abrupt climate transitions (Barker and Knorr, 2007). These findings document the gradual manifestations of the tropical climate at millennial timescales, highlighting the influence of the tropical regions to convey climatic signals between hemispheres. Although further comparisons with other tropical records would be useful to support this idea, this will be investigated in following chapters.

(2) Stadial events.- The comparison between marine records from high and low latitudes reveals specific differences in the H events. In marine records collected from the North Atlantic, the H events are coincident with the most prominent SST minima if compared with other stadial (cold) periods (Bond et al., 1993; Broecker, 2000; McManus et al., 1994). In the records collected off NW Mexico, this feature is not observed because the minima %OC and DSRa* values, coincident with H events, are not necessarily more pronounced than other stadials (*see* Figure 1.8). For instance, the stadials intervening D/O 6-7, 11-12, 19-20, 20-21 and 24-25 are as low as those related to H events. In addition, the minima events in %OC and DSRa* are more in agreement with atmospheric temperatures of the GISP2 $\delta^{18}O$ record than to sea surface temperatures (SST) (*not shown*), which show lower values during H events (e.g. McManus et al., 1994; van Kreveld, 2000). Such differences allow the identification of regional amplifications associated with millennial-scale cycles. This suggests that each pronounced cooling, evident in North Atlantic SST during H events, is a local amplification caused by massive freshwater discharges and ice-melting of the Laurentide Ice Sheet (Bond et al., 1993; Curry and Oppo, 1997). Therefore, the effects of the spatial temperature gradients over the North Atlantic during H events (i.e. coolings) are considered more pronounced in the very high latitudes (e.g. Core ODP-980, 55°N – *not shown*) than in the mid-latitudes (e.g. Core ODP-977A, 36°N).

Similarity, the temperature patterns of Greenland and the productivity off NW Mexico, points to a high – low latitude teleconnection that is unlikely to be explained only

by iceberg discharges. As suggested by past-ocean simulations (Ganopolski and Ramstorf, 2001), the North Atlantic could have three distinct states of circulation, each of which could be associated to a different pattern of atmospheric operation. Hence, the teleconnection between Greenland, the mid-latitudes (Martrat et al., 2004) and the tropics (e.g. the NW Mexican margin) had to be preferentially transmitted through NH atmospheric circulation, rather than oceanic changes directed by North Atlantic freshening and the meridional overturning circulation (MOC). Furthermore, these observations seem to be applicable to the stadial events of the penultimate glacial or MIS-6 (*see section* 1.3.4).

(3) *Time frequencies*.- A third difference between high and low latitudes is seen in the frequency of the millennial-scale events. In records from Greenland and the North Atlantic, the millennial timescale events evidence a dominant periodicity of 1 - 2 ka during glacials with asymmetrical shapes between the warm and the cold phases (Bond et al., 1999; Grootes and Stuiver, 1997; van Kreveld, 2000). It is thought that this "1-2 ka cycle" is modulated by the internal dynamics of the Greenland ice sheets and ultimately, the mediator of the D/O events (Bond et al., 1993; Bond et al., 1999; Dansgaard et al., 1993). In the records from NW Mexico, the spectral and wavelet analyses indicate similar periodicities, somehow expected considering that the records were tuned to the GISP2 chronology. However, some differences also emerge.

Although the "1-2 ka cycle" do exist in the cores MD02-2518 and MD02-2519 during the last glacial, the periodicities of 1.5 and 2.0 ka/cycle are not dominant. Instead, periodicities of ~ 5.3, 4.2 and 2.9 ka/cycle prevail in the spectral and wavelets analyses (Figure 1.9 *C - D* and Figure 1.10); and given the > 90% confidence associated with these cycles, they cannot be statistically dismissed as stochastically forced variations. In Figure 1.9 (*inset E*), the sum of 3 Gaussian band-pass filters is compared to the DSRa* record of Core MD02-2519. It shows that the combination of the periodical events every ~ 5.3, 4.2 and 2.9 ka can explain most of the changes in the records from the ETNP during the last glacial.
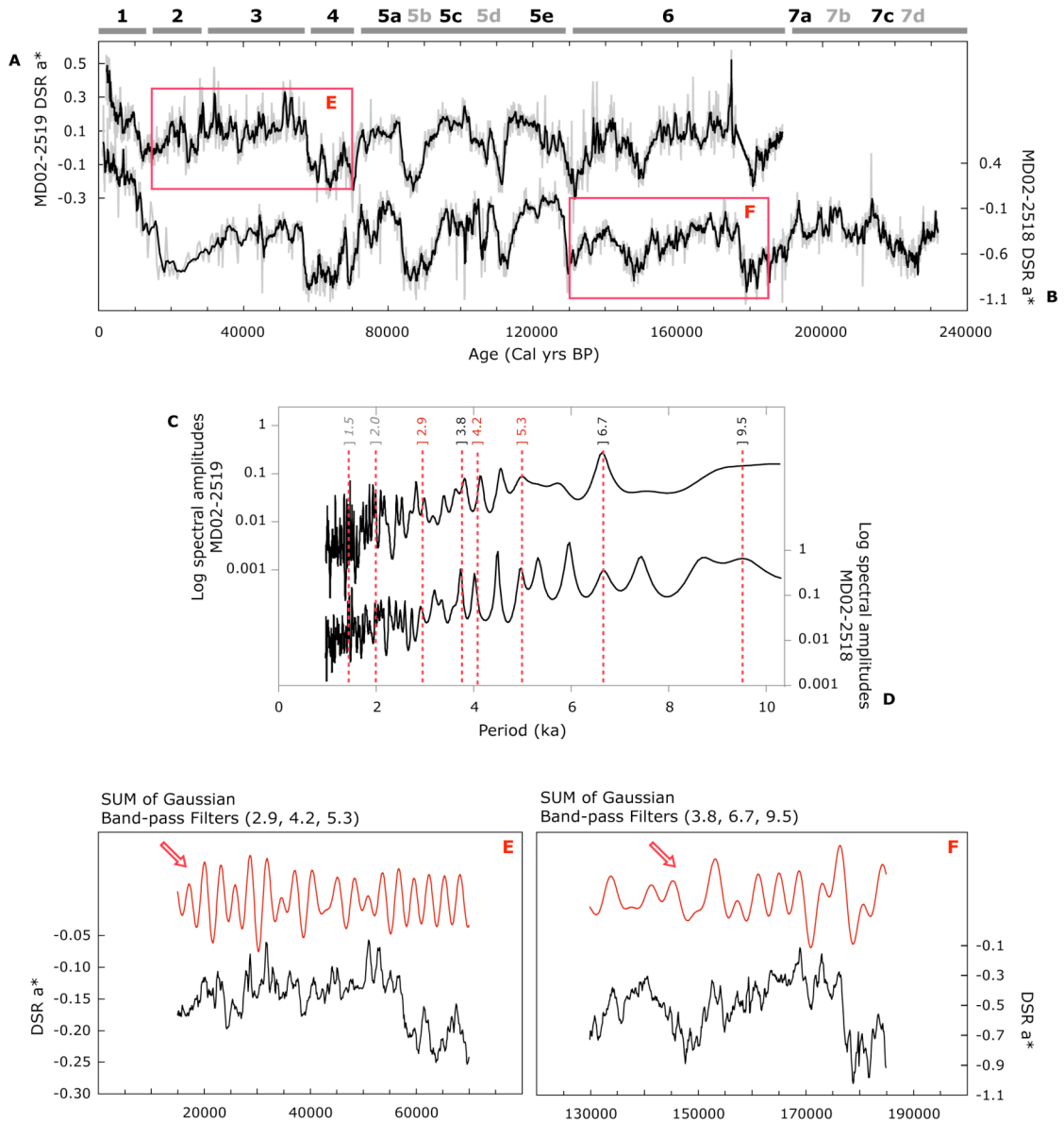
Figure 1-9 Spectral Analyses applied to the DSRa* records of cores (A) MD02-2519 and (B) MD02-2518; inset E spans from 15-70 ka and inset F spans 130-185 ka. The spectral results are shown in (C) and (D). The dotted red lines indicate the common and most prominent periodicities of the two glacial intervals. Red and black numbers are the predominant periodicities identified during MIS-2 to 4 and MIS-6 respectively, confirmed by the results of wavelets analyses (see Figure 1.10). Grey numbers in italics indicate the frequency of the "1-2 ka cycle". (E) Combined red line is the SUM of Gaussian band-pass filters (bandwidth = 0.2 x10^{-4}) between 15-70 ka with periodicities centred at 2.9, 4.2 and 5.3 ka (frequencies of 3.44 x10^{-4}, 2.40 x10^{-4} and 1.90 x10^{-4} cycles/yr, respectively). (F) Combined line is the SUM of the periodicities between 130-185 ka centred at 3.8, 6.7 and 9.5 ka (frequencies = 2.60 x10^{-4}, 1.48 x10^{-4} and 1.05 x10^{-4} cycles/yr, respectively). The comparison shows that most of the variability seen in the records of Mazatlan (black lines in E and F) can be explained by the sum of these cycles (red lines in E and F).
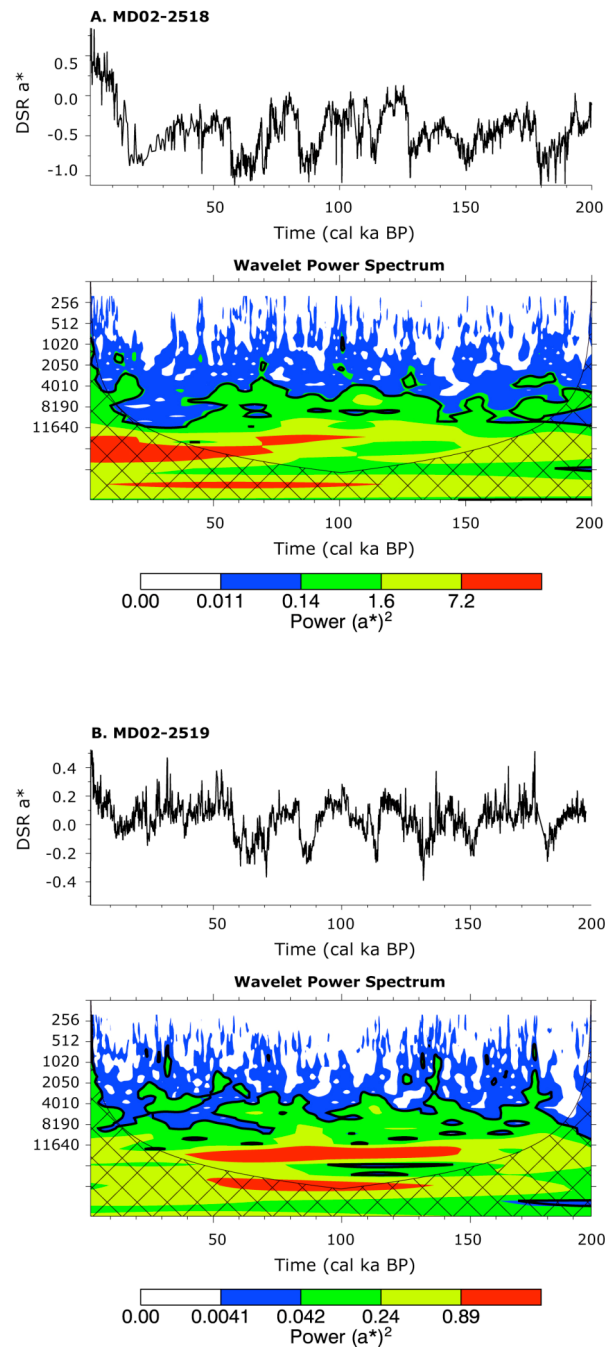
Figure 1-10 Wavelet Analyses applied to DSRa* records of cores (A) MD02-2518 and (B) MD02-2519. The wavelet power spectra analyses use the Morlet method (non-dimensional frequency = 6). Contour levels are chosen so that 75%, 50%, 25%, and 5% of the wavelet power is above each level. Black contour is the 10% significance level, using a white-noise background spectrum. The crosshatched region is the cone of influence (COI), where zero padding reduced the variance. The COI is the region of the wavelet spectrum defined as the e-folding time for the autocorrelation at each scale of the wavelet power. The e-folding time is chosen such that the wavelet power for a discontinuity at the edge, drops by a factor of e^{-2} and ensures that edge effects are negligible beyond that point (Torrence and Compo, 1998).

The diminished significance of the "1-2 ka cycle" documented in our records during the last glacial interval, in comparison to the North Atlantic, could be caused by the "symmetric pattern" displayed in the %OC and DSRa* records. In other words, the symmetrical shape could 'smooth' two smaller periods into 'one' more significant period. Although this explanation would require further investigation, we consider that the presence of such longer periodicities cannot be considered a complete artefact of the combined effect of two "1-2 ka cycles".

Periodicities of "1-2 ka cycle" are shown to be prominent in the glacial North Atlantic records, as well as periodicities > 5 ka. For instance, studies by Bond et al. (1993) argued that the H-events occurred broadly every 5 to 10 ka, with a more precise mean of ~ 7.0 ± 2.4 ka, which has been related to the internal dynamics of ice sheets during MIS-3 (MacAyeal, 1993; McManus et al., 1999). However, controversy remains on the origin of the millennial scale variations in the climate system, frequently considered as a response to an external forcing rather than an internal fluctuation. The regular pacing of the "1-2 ka cycle" has been reported not only during the last glacial but also durig the penultimate interglacial period. Various authors even propose that it is a response from outside the Earth climatic system (Bond et al., 1997; Isono et al., 2009; Rahmstorf, 2003). Although the origin of the "1-2 ka cycle" remains unknown and few is known about its Holocene climatic impacts, it seems well coupled to the internal variability of the mid-latitudes and polar region, finding less expression in the lower latitudes.

Studies from mid-latitude records off California and Oregon during the last glacial period have reported equivalent results to those found off NW Mexico, where longer periodicities than 3 ka are prominent over shorter ones (Pisias et al., 2001). Although these observations were originally interpreted as changes in the northward flow of the California Countercurrent (Pisias, 1978), of further significance was the suggestion that they reflect the response of NE Pacific to the variability in the tropical Pacific (Pisias et al., 2001). Spectral and wavelets analyses from tropical records worldwide clearly denote the dominance of longer periodicities during the last glacial. Data from stalagmites in South Africa report the strongest variability centred on quasi-periodicities between 2.5 and 4 ka (Holmgrena, 2003). Lake records from Tanzania (S Africa) indicate dominant periodicities at 3.6, 7.55 and 11.3 ka (Garcin, 2006), similar to terrestrial reconstructions of surface moisture in NE Australia (Turney, 2004). Furthermore, results of spectral and wavelet analyses from Cariaco Basin

(Venezuela) and the SE Pacific (off Chile) show main periodicity bands centred at 4.5 and 3.1 ka, although weaker periodicities (1-2 ka) are also evident (Kaiser et al., 2007). In the cores MD02-2518 and MD02-2519, the predominance of longer periodicity bands (5.3, 4.2 and 2.9 ka) over shorter could be an essential character of low latitude rapid climate variability, besides heat transport. The dominance of the low frequency events in the tropical climate system suggests that the mechanism behind millennial timescale events derives from periodic external forcings (e.g. variations in the luminosity of the sun), and not only from ice sheet dynamics. Although the expression of the low frequency band is not fully documented in Holocene records (i.e. due to the reduced climatic variability relative to the glacial), in the next section we corroborate the influence that the tropical circulation exerts during glacial periods, as reinforced by the examination of the penultimate glacial.

1.3.4   MIS 6 – MIS 7: patterns and periodicities

The documentation of millennial-scale events in the earth system beyond the last glacial period is rare, due to the scarcity of available high-resolution records. Therefore, of special value is the comparison done between the NW Mexican records (MD02-2518 and MD02-2519 DSRa*) and those mid-latitude records from the Iberian margin (ODP-977A δ^{18}O-PF and Uk'^{37}), to confirm the relationship between the NE Pacific upwelling and the North Atlantic SST over the penultimate glacial period (i.e. MIS-6).

In Figure 1.7, the interstadial (stadial) events show correspondence to the maxima (minima) surface temperatures in the Core ODP-977A and comparatively, to maxima (minima) productivity events in the cores MD02-2518 and MD02-2519. As noted for the last glacial period, the DSRa* maxima or interstadials have more symmetric shapes. However, the amplitude variations of the sediment DSRa* seems to be lower during the penultimate glacial (relative to the last glacial) showing a consistent trend towards the bottom of the core. This might be an artefact of the reduction in the "red/green" attributes due to gradual organic decomposition (e.g. photosynthetic pigments) and/or compaction. Although this represents a disadvantage for using the sediment colour properties to quantifying %OC down-core, it does not obscure the existence of millennial-scale events during MIS-6.

The results of the spectral and wavelets analysis show differences when compared to the previous glacial time. In general, it can be said that the millennial events are less

frequent. The most coherent periodicities occur every 9.5, 6.7 and 3.8 ka (Figure 1.9 - *inset F*). The frequency centred at 3.8 ka could be similar to the last glacial frequencies centred at 2.9 or 4.2 ka/cycle, but the absence of that at ~1.5 ka is significant in the wavelet analyses in the penultimate glacial (Figure 1.10).

The lack of evidence of the "1-2 ka cycle" and the less frequent millennial-scale variability over MIS-6 relative to MIS-2-4 has been previously noted in both, the Northern and Southern Hemispheres. Martrat *et al*. (2004, 2007) documented the absence of "1-2 ka cycle" in North Atlantic mid-latitude records (i.e. Iberian margin), suggesting that this frequency cycle is not a persistent characteristic of the climatic system during MIS-6 and beyond. Indeed, IRD-events also report to be less frequent during MIS-6 in North Atlantic high-latitudes (McManus et al., 1999), indicating less frequent variability in the internal dynamics of the ice-sheets (relative to MIS-2-4) in agreement with δ^{18}O-PF records (i.e. ODP-980 (McManus et al., 1999). Furthermore, this finding extends to records from Antarctica. Studies have reported time series analyses in records from Vostok (δD, and also CH_4) with frequencies correspondent to periods of ~ 10.0, 6.0 and 3.3 ka during MIS-6 (Siddall et al., 2006). The dominance of the frequencies both in SH polar temperatures and methane, which is sourced in NH landmasses, suggest intimate interhemispheric coupling. The dominant periodicities in Antarctica and North Atlantic records match those of the Mexican margin DSRa* records (i.e. 9.5, 6.7 and 3.9 ka/cycle; Figure 1.9 *C and D – inset F*), indicating their prevalence in the low-latitudes. Therefore, the time series analyses reveal the intimate inter-hemispheric relationship within the climate system, linking tropical and polar-regions. As well as the key role that the lower latitudes play in the transmission and modulation of millennial scale climate cycles.

1.3.5   Global implications linked to the ETNP climate variability

The ETNP is an integral part of the low latitude large-scale climate system. As part of the tropical region, it is affected by seasonal variations according to the migration of the Intertropical Convergence Zone (ITCZ), which controls seasonal and regional patterns of rainfall, surface currents and winds-shifts between hemispheres (Ivanochko et al., 2005; Marret et al., 2001; Peterson et al., 2000; Wang et al., 2001). Concurrently, the region is also affected by atmospheric pressure systems of the North Pacific (the Pacific-High and the Aleutian-Low) and western North America (Low), which control the shore-parallel winds

and the upwelling along much of the coast (Bakun and Nelson, 1991).

During the *boreal winter*, the ITCZ is located in its southernmost position at ~15°S over South America (Barry and Chorley, 2003). In consequence, the atmospheric and surface ocean circulation over the ETNP shift to the south. The continental Low-pressure system is developed over NW Mexico, whereas a weaker North Pacific-High is positioned south of ~28°N when the Aleutian-Low domains. This differential heating between the warmer continent and the cooler ocean creates the perfect atmospheric gradient required to fuel and sustain the seasonal upwelling (Bakun and Nelson, 1991; Ganeshram and Pedersen, 1998).

During the *boreal summer*, when the ITCZ reaches its northernmost position at ~10°N over South America, the Mexican mainland becomes influenced by the moisture-laden air masses brought by the SE trade winds, increasing tropical rainfalls and hurricanes in the region. The upwelling along the Mexican margin is suppressed due to the onshore flowing of the westerly winds, caused by the establishment of the Mexican-Low at ~30°N and the northernmost position of the strengthened North Pacific-High at ~38°N (Bakun and Nelson, 1991; Ganeshram and Pedersen, 1998).

During the *Last Glacial Maximum* (LGM), various circulation models have emphasised the role of the large Laurentide ice sheet in reducing the land-ocean thermal gradients and the atmospheric pressure gradient between the continent and the ocean (CLIMAP Project Members, 1984; COHMAP Members, 1988; Lunkeit et al., 1998; Romanova et al., 2006). The establishment of the semi-permanent high-pressure cell overlying the ice sheet, the blocking effect of the increased ice sheet elevation, and the enhancement of the Aleutian Low, may caused a modified splitting of the westerly jet over North America. With the substantial weakening of the North Pacific High and the continental Low, the coastal winds along the western margin could be substantially reduced suppressing regional upwelling and productivity along the margin (Ganeshram and Pedersen, 1998; Lyle et al., 1992). Hence, the regulation of the North American atmospheric circulation patterns during LGM, seamed to be strongly influenced by the elevated topography, affecting the reduction of the zonal (latitudinal) pressure gradients.
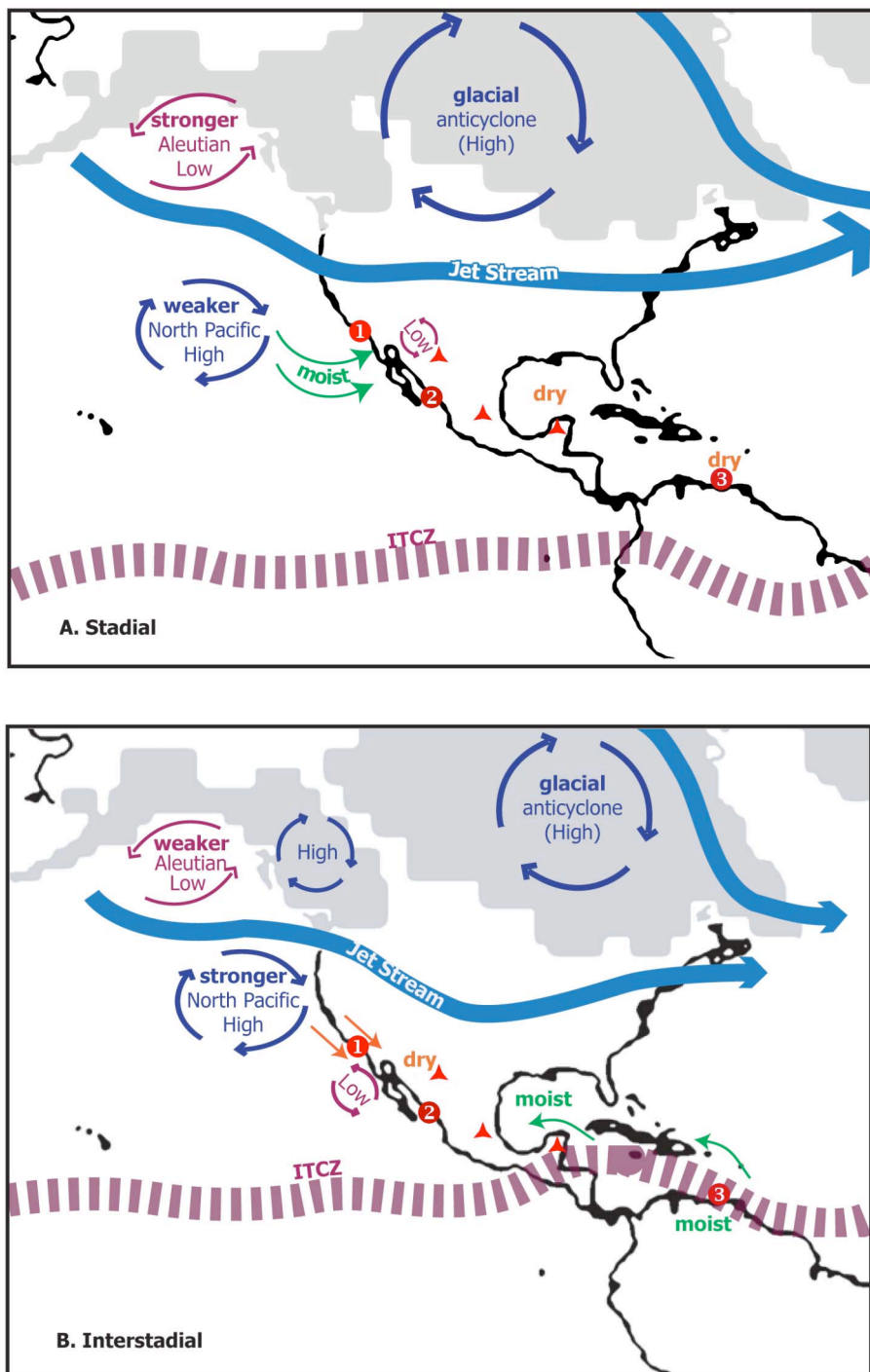
Figure 1-11 Schematic model of the proposed atmospheric circulation pattern occurred during (A) stadials and (B) interstadials over the last glacial. Red numbers are marine records from (1) Santa Barbara Basin (Hendy and Kennett, 2003), (2) Mazatlan (this study), (3) Cariaco Basin (Peterson et al., 2000). Red triangles are lake records from Northern, Central and SE Mexico – i.e. Chihuahua and Sonora Deserts (Metcalfe et al., 2002; Ortega-Guerrero et al., 1999), Central Mexico and the Yucatan Peninsula (Metcalfe et al., 2000).

On the other hand, reconstructions based on paleo-proxy data and models in the tropical Pacific, emphasise the climatic impact of tropical cooling during LGM (CLIMAP Project Members, 1984; Kim et al., 2008; Koutavas and Lynch-Stieglitz, 2003; Lohmann and Lorenz, 2000; Romanova et al., 2006). According to them, the reduction of the Hadley circulation and the southward shift of the ITCZ were caused by reduced energy release from the atmosphere and meridional pressure gradients, favouring pronounced seasonality on land. The increase in southerly flow over western North America possibly led to a poleward atmospheric heat transport greater than the present, causing large enough perturbations to alter regional precipitation. For instance, modelling reconstructions during LGM have shown an incidence of precipitation over western US and Mexico, but a decrease over Canada and large parts of the North Atlantic, including the Gulf of Mexico (Kim et al., 2008). However, model simulations have found that the southward displacement of the ITCZ, and the resulting decrease in oceanic heat transport to the NH, might cause greater influences on climate during LGM than the Laurentide Ice sheet (Lohmann and Lorenz, 2000; Romanova et al., 2006).

As previously discussed in *section 1.3.2*, stadial and interstadial events are clearly represented in the proxy records of productivity during glacial (e.g. MIS-3 and MIS-6), and interglacials intervals (e.g. MIS-5). Therefore, the anchoring of the semi-permanent high pressure over the large ice sheet, envisioned in previous studies (CLIMAP Project Members, 1984; COHMAP Members, 1988; Ganeshram and Pedersen, 1998), is not entirely adequate to explain rapid changes persistent throughout the last glacial and beyond. Instead, we propose a scenario where the position of the ITCZ plays a key role (Figure 1.11).

A. Stadial events.- In the records collected off NW Mexico, low %OC coincide with colder events suggesting that reduced productivity and upwelling were typical during stadials (*section 1.3.2*). Reduced productivity along the NE Pacific has been previously reported during these periods and explained through atmospheric instabilities (Hendy and Kennett, 1999, 2000). As shown in Figure 1.11-A, reduced shore-parallel NW surface-winds could provoke weaker zonal and meridional pressure gradients, which ultimately reduced the upwelling intensity and modified the continental environment of NW Mexico towards a more humid scenario (Metcalfe et al., 2002; Ortega-Guerrero et al., 1999; van Meerbeeck et al., 2009). Drier conditions also prevailed over most of SE Mexico (Metcalfe et al., 2002) and Central America (Peterson et al., 2000), hence suggesting that the trade winds were

located south of its modern summer position. A stronger surface-flow in the Pacific was probably intensified as the North Pacific-High weakened and retained in a semi-permanent southernmost position, along with the ITCZ. As discussed by studies in tropical regions worldwide, the ITCZ was preferentially located southward, relative to interstadials (Ivanochko et al., 2005; Peterson et al., 2000; Wang et al., 2001). Therefore, the southward position of the ITCZ could reduce the ocean heat transport to higher latitudes, favouring colder conditions in the NH. Over the Laurentide Ice Sheet, however, a semi-permanent anticyclone circulation (Peltier, 1994; van Meerbeeck et al., 2009) could favour the strengthening of the Aleutian-Low (Hendy and Kennett, 2000) and the polar circulation. Although with some reduction relative to LGM (van Meerbeeck et al., 2009), the enhanced polar atmospheric circulation during stadials could sustain the ice expansion over MIS 2 - 4, the split of the jet stream into two, and the southward extension of sea-ice cover restricted to the winter season (van Meerbeeck et al., 2009) due to the varying glacial insolation.

B. Interstadial events.- Off NW Mexico, the interstadial warm events can be identified as rapid increases in concentrations of OC, suggesting enhanced productivity and upwelling (*see section 1.3.2*). The northward shift of the stronger subtropical-High and the establishment of a low-pressure cell off NW Mexico could favour intense wind-flow parallel to the coast, fuelling the upwelling and reducing the moisture transport to the continent. The reduction of the ice cap could weaken the Aleutian-Low but contribute to the NE migration of the North Pacific-High (as it is today during spring and early summer) (Stott et al., 2002). The path of the jet stream possibly recovered a meandering shape between an oncoming front and a high-pressure cell (Figure 1.11-B). In the Arctic region, model simulations suggest that under interstadial conditions, the development of convection sites and sea-ice extent was more similar to present-day climate (van Meerbeeck et al., 2009). As conditions warmed, the rainfall increased slightly over S Mexico and Central America toward wetter conditions than during stadials; perhaps caused by enhanced NH seasonality relative to LGM and the latitudinal shift of the ITCZ (Metcalfe et al., 2002; Peterson et al., 2000). A relative northward migration of the ITCZ during interstadials has been proposed by a variety of studies in tropical regions (Ivanochko et al., 2005; Peterson et al., 2000; Wang et al., 2001). The relative warm conditions could enhance the ocean heat transport to polar regions, and reduce both, the size of the Laurentide ice-sheet and the development of the glacial-anticyclone over North America. This could make stronger temperature gradients along the

western margin relative to the course of stadials. Simultaneously, the northward position of the ITCZ could impose humid conditions over most of Central America (Metcalfe et al., 2002; Peterson et al., 2000), as the trade winds migrated north.

In general, the proposed climatic scenario during stadial and interstadial episodes in the ETNP is consistent with paleoclimate records showing that: (1) marine productivity and upwelling decreased during stadials and increased during interstadials, as suggested by the %OC and DSRa* records from this study. (2) Wetter conditions prevailed during most of the last glacial period, but enhanced during LGM in the Chihuahua and the Sonora deserts (NW Mexico) based on paleo-lake reconstructions (Metcalfe et al., 2002; Ortega-Guerrero et al., 1999). Although it is unclear whether changes in lake levels and the marine productivity variations are coeval on millennial-scale due to the poor age control of lake records, it is worth noting that in San Felipe Basin, Sonora (NW Mexico), the periods of high humidity (~45 ka) and high lake productivity (~34 – 28 ka) coincide with stadials. (3) Finally, climatic reconstructions in cores from tropical regions from South America (Cariaco basin), Asia (Somali Margin, Hulu Cave) and Central Africa (Benguela) have attributed changes in rainfall, riverine discharge and marine productivity, to the re-arrangement in the ITCZ position (Hughen et al., 1996; Ivanochko et al., 2005; Marret et al., 2001; Peterson et al., 2000; Wang et al., 2001). This suggests that the position of the ITCZ shifted globally over stadials and interstadials, irrespectively of glacial-interglacial periods. Therefore, the periods of more intense upwelling and productivity in the western coasts of North America, coincide with periods when the ITCZ shifted northwards, positioned north of the equator (Figure 1.12). This supports the notion that rapid and well established teleconnections have existed between lower and higher latitudes, at least over the last 240 ka.

The tropical regions have also the potential to modulate terrestrial and marine emissions of greenhouse-gasses (GHG), which in turn provide a positive feedback (i.e. amplify) on the climate system by altering the energy balance (Flückiger et al., 2004; Ivanochko et al., 2005). In Figure 1.13, we show the close similarity that the ETNP records displays relative to methane (CH_4) records from both hemispheres. As documented in ice core records from Greenland and Antarctica, the CH_4 variations are closely coupled to timing and processes in the NH, with most of its sources in the tropics (Blunier et al., 1998; Brook et al., 1996; Chappellaz et al., 1993). Consequently, the CH_4 records have been identified as a close proxy for NH temperature and tropical rainfall over the continent. Thus when the

ETNP productivity proxy records presented in this chapter are compared to other records from tropical regions, we provide evidence to suggest that climate interactions between marine productivity, continental wetness, temperature, large-scale atmospheric circulation, and GHG emissions were modified in parallel at millennial timescales.
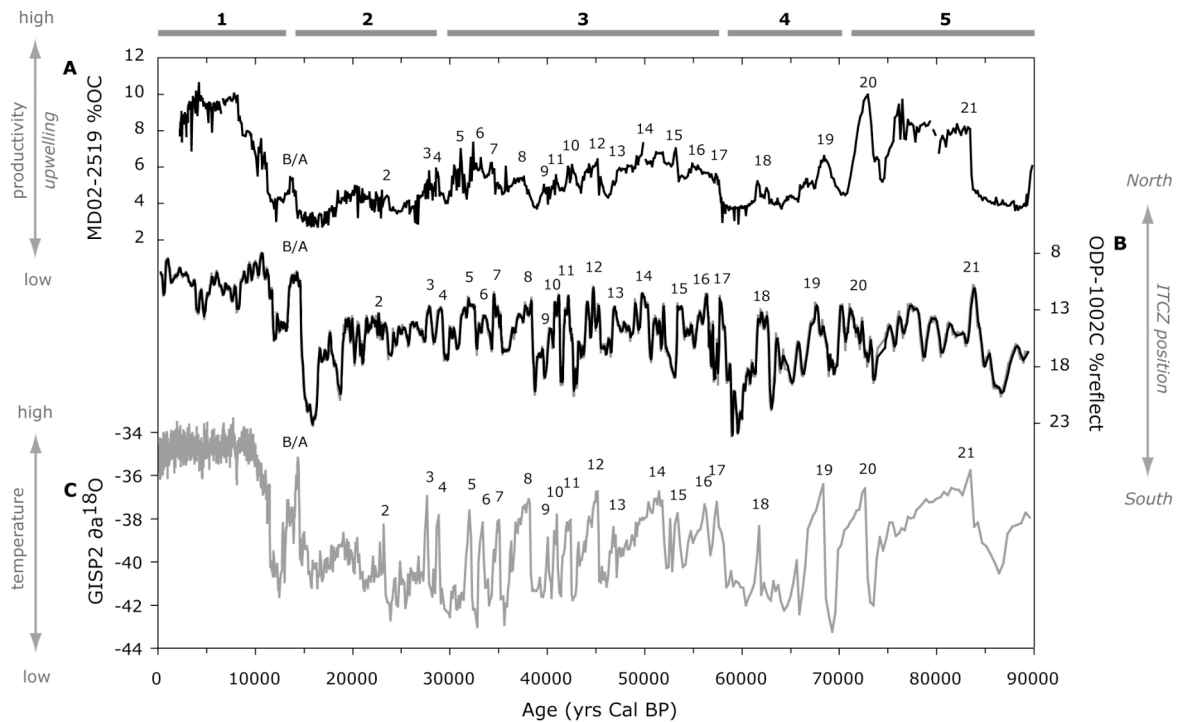
Figure 1-12 Comparison of reconstructed proxy records of upwelling and productivity in lower latitudes, and temperature over Greenland. (A) %OC of Core MD02-2519; (B) Colour reflectance (550 nm) of Cariaco Basin sediments of Core ODP-1002C (5-point moving average) (Peterson et al., 2000); and (C) δ18O GISP2 (Grootes and Stuiver, 1997). Sediment OC variations (Core MD02-2519) are controlled by changes in export productivity driven by upwelling (left arrow). Colour variations of the sediments (Core ODP-1002C) are driven by changes in surface productivity that increase the organic rain, leading to darker sediments (anoxic conditions) (right arrow); they also match to the increase in terrigenous and nutrients inputs from rivers (i.e. increased precipitation) associated to the northward displacement of the ITCZ (Ti record not shown). The δ18O record is associated to temperature variations, which increase during interstadials and decrease during stadials (left arrow).
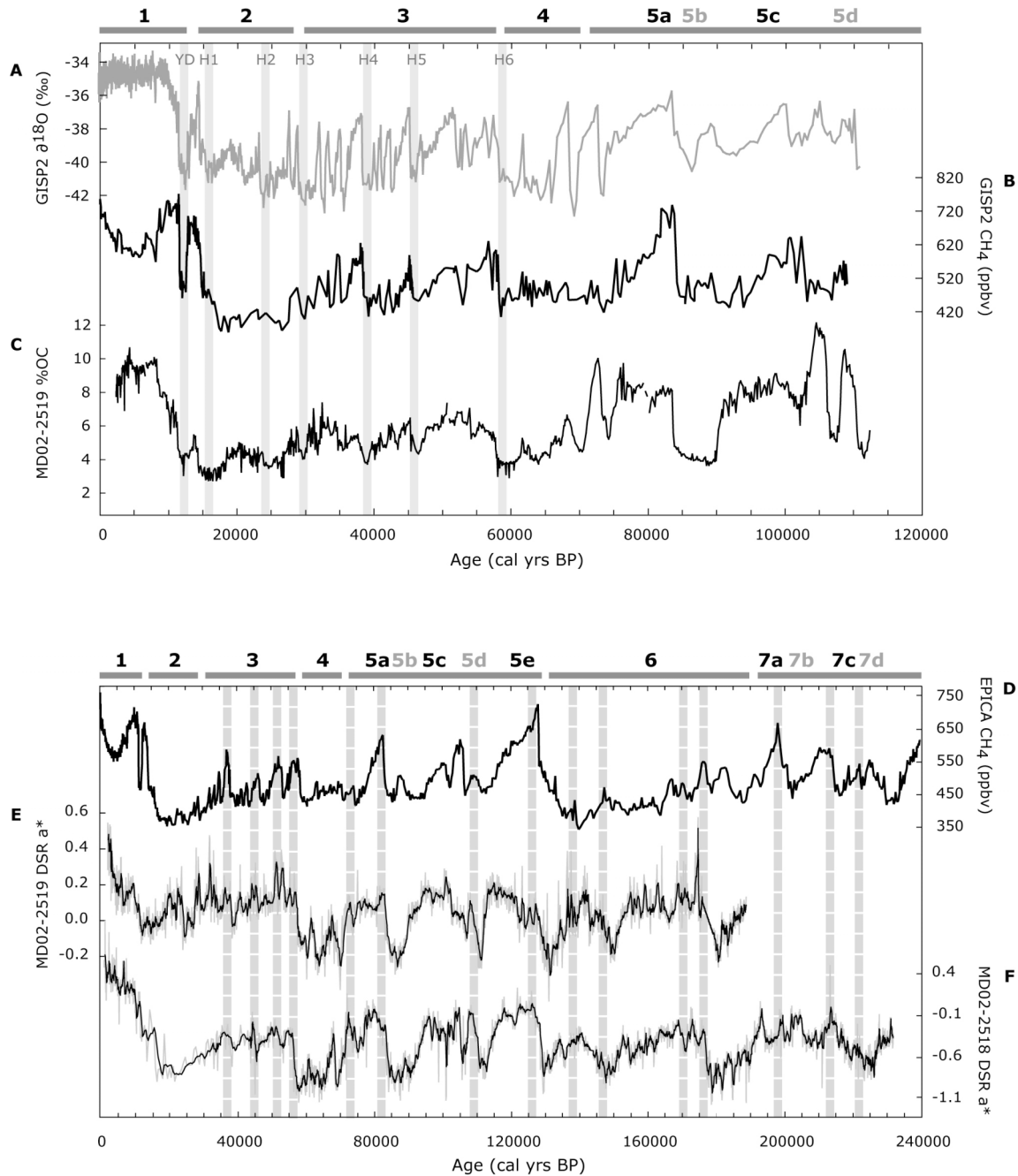
Figure 1-13 Comparison between productivity records in the ETNP and greenhouse gas concentration records from Greenland and Antarctica. Graphs on top span 120 ka. (A) δ¹⁸O GISP2 data (Blunier and Brook, 2001). (B) CH₄ data from GISP2, NGRIP and GRIP (Blunier and Brook, 2001; Flückiger, et al., 2004); (C) %OC data of Core MD02-2519. Vertical grey lines correspond to YD and H-events. Graphs below span 240 ka. (D) CH₄ from EPICA (using gas age EDC3 (Loulergue, et al., 2008)). (E) DSRa* data of the Core MD02-2519. (F) DSRa* data of the Core MD02-2518. Harsh dotted lines show related maxima events between records.

Therefore, the association between 'tropical – northern latitudes' record involves not only the high latitude circulation, but also aspects of the tropical hydrologic cycle, monsoon circulation and the location of the ITCZ. The millennial scale cycles of productivity reconstructed here are linked to tropical processes through variations in the position of the ITCZ and the wind patterns. The presence of Southern Ocean influence during major interstadials is revealed through the observation of gradual and more symmetric patterns in the major interstadial events. The dominance of longer over shorter periodicities in the records of the ETNP is shown by time series and wavelet analyses, indicating the influence of external forcing at millennial timescales. The global occurrence of the > 2.9 ka/cycle in the climatic records reinforces the control that the tropical regions exerted on the atmospheric teleconnections over the last two glacial cycles.

1.4   Conclusions

In this chapter, we have constructed the age model for the Core MD02-2519 that will subsequently be applied to all other chapters, being the central core of this thesis. It is based on radiocarbon dating and tuning to $\delta^{18}O$ records from Greenland (GISP2) and North Atlantic mid-latitudes (ODP-977A).

In addition to the Core MD02-2519, the marine sediment Core MD02-2518 is the first high-resolution record of the ETNP documenting 240 ka of changes in productivity and upwelling at millennial timescales. We confirm that records of organic carbon and reflectivity from the ETNP can be tuned to Greenland and North Atlantic records during the last and penultimate glacial periods. In the ETNP, productivity increases are typically high during interstadials, but the opposite during stadials. This suggests an intimate link between upwelling in the tropics and high latitude temperatures variability in the NH.

The time series analyses applied to the ETNP records reveal subtle differences between high and low latitude records. The character of the rapid climatic events tends to be more abrupt in higher latitudes and more gradual in lower latitudes. Asymmetric 'saw-tooth' shapes are typical of the D/O events recorded in Greenland and the North Atlantic, whereas symmetric shapes are characteristic in the ETNP records. Two major implications are: (1) that tuning to major interstadial events from Antarctica is also possible; and (2) that the low

latitude upwelling responds sensitively to interhemispheric teleconnections transmitted both by the atmosphere and by the ocean.

Although the most prominent temperature minima events recorded in higher latitudes marine records always coincide to H-events, the records from lower latitudes do not always have an equivalent of pronounced productivity minima relative to other stadial events suggesting that the North Atlantic cooling during H events represents a local amplification. The millennial timescale periodicities obtained with spectral analyses show that the so-called '1-2 ka cycle' might not be a dominant feature in climatic records over the last 240 ka. Less frequent millennial-scale oscillations $(2.9 - 4.2, 5.3 - 6.7$ and 9.5 ka/cycle) are more significant in marine sediments records from the ETNP. The dominance of low frequency events in the climate system suggest that the mechanism behind millennial timescale events also derives from external forcing and changes in heat transport, not only from ice sheet dynamics.

The reconstructed records of productivity off NW Mexico support the notion that the latitudinal migration of the ITCZ is fundamental for the regulation of the wind driven upwelling in the NE Pacific margin. At millennial timescales, the impact of the northward (southward) displacement of the ITCZ, the reduction (enhancement) of the zonal pressure gradients and the reduced (elevated) ice cap topography over North America, favoured a complete reorganisation of the atmospheric circulation in the course of interstadials (stadials), increasing (reducing) the wind intensity, and ultimately the productivity. The inference is further supported by the close correspondence between records of upwelling, tropical rainfall in the Northern Hemisphere and CH_4 concentrations in ice cores. The correlation between records of productivity, rainfall, temperature and GHG concentrations, which overall show the dominance of less frequent and more amplified millennial scale events, reinforces that the tropical regions are key regulators of global climate.
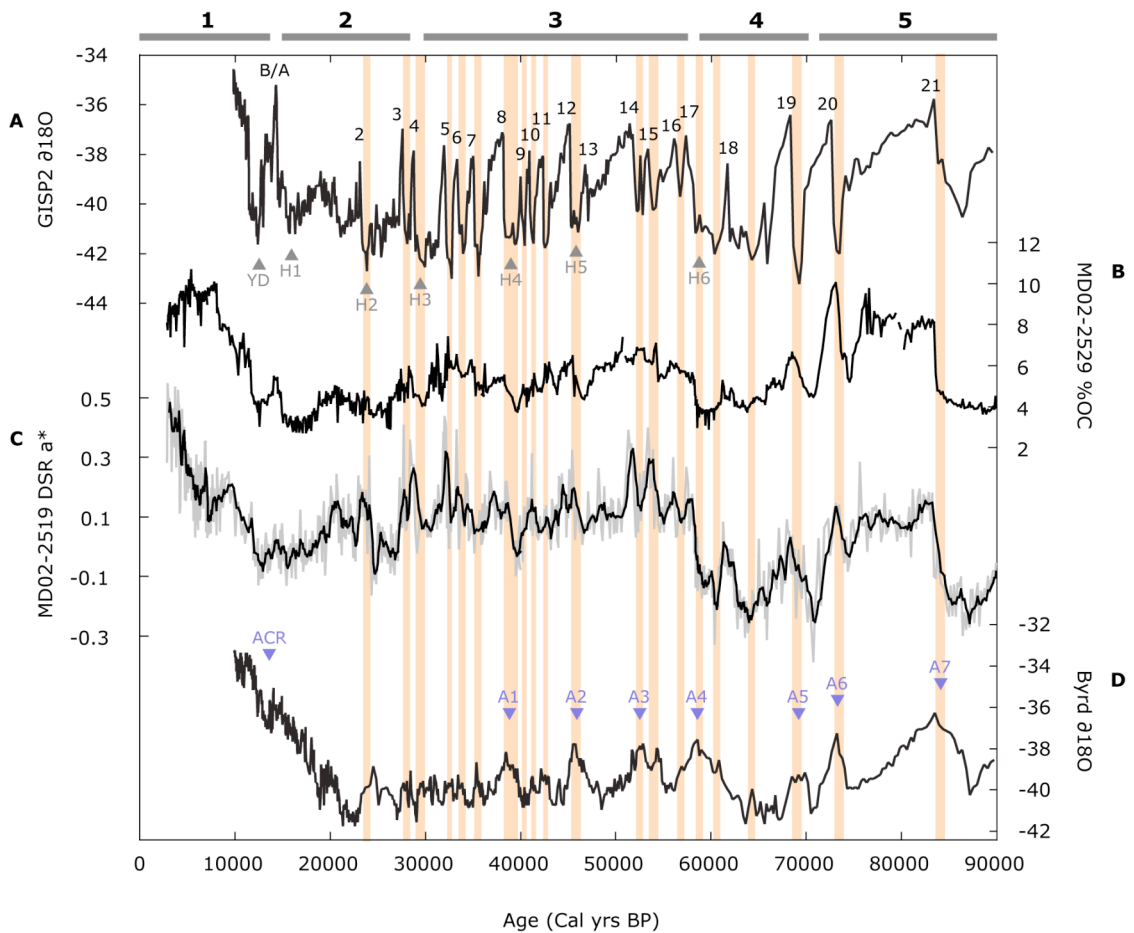
Annexed Figure 1a. Comparison between Core MD02-2519 productivity proxy records and temperature proxy records from (A) Greenland -GISP2- and (D) Antarctica -Byrd- ice cores, all ploted in the same timescale (i.e. Blunier and Brook, 2001; based on CH$_4$ synchronization). The age model construction for the (B) %OC and (C) DSRa* records is based on tuning to major interstadial events (see annexed Figure 1b and Table 1.3). Numbers are D/O events; A-events are warm episodes in Antarctica. The colour bands indicate Greenland stadial periods comparative to Antarctica temperature increases.
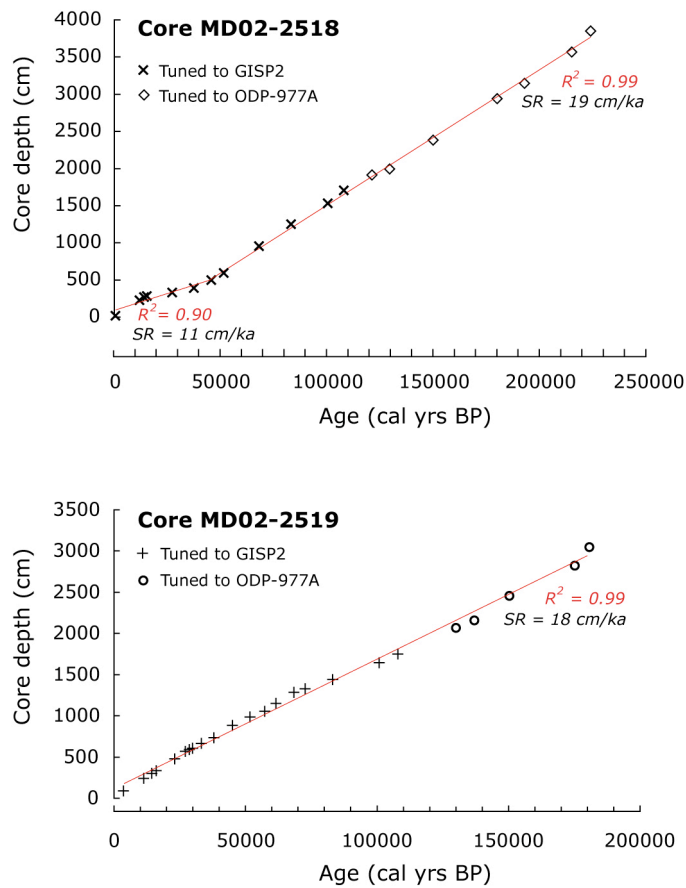
Annexed Figure 1b. Age models constructed for cores MD02-2518 and MD02-2519 based on tuning to GISP2/Byrd scale (Blunier and Brook, 2001) from 0 – 120 cal ka BP, and to ODP-977A chronology (Martrat et al., 2004) beyond the limit of GISP2 (for comparison with the "radiocarbon – tuned" age model see Figure 1.2).

🌐

Chapter 2

δ¹⁵N records in the eastern tropical North Pacific: denitrification and advection of heavy nitrate over the last 120 ka

2.1   Introduction

2.1.1   Denitrification

The marine nitrogen cycle may have played a key role in modulating past climate changes, as it is a limiting nutrient in the ocean. The bio-available nitrogen exerts an important control on ocean productivity, ocean-atmosphere fluxes of carbon with associated elements, and sediment burial (Volk and Hoffert, 1985). The bio-available or fixed nitrogen (mainly in the form of nitrate – NO_3^-) has its major source in the marine N-fixation and its major sink through water column and sediment denitrification. Thus the marine nitrogen cycle and the oceanic nitrate inventory are largely controlled by biological processes within the ocean. The N-inventory variations, associated with changes in denitrification, have been proposed as a potential driver of atmospheric greenhouse-gases (GHG) concentrations on glacial to interglacial time scales (Altabet et al., 1995; Falkowski, 1997; Ganeshram et al., 1995; Gruber and Sarmiento, 1997). For instance, glacial declines in denitrification and the resulting increase in fixed nitrogen inventory are suggested as mechanisms for lowering the atmospheric CO_2 by increasing the biological activity (Altabet et al., 1995; Galbraith et al., 2004; Ganeshram et al., 2000; Ganeshram et al., 1995) On the other hand, the nitrous oxide (N_2O) produced as a by-product of denitrification, is an important GHG that could potentially produce large-scale changes in global climate (Flückiger et al., 2004; Flückiger et al., 1999; Ivanochko et al., 2005).

Denitrification in the ocean occurs in suboxic subsurface waters (O_2 levels < 1.5 ml/L), where denitrifying bacteria use NO_3^- as the electron acceptor to degrade organic matter while releasing N_2O and N_2 to the atmosphere (Brandes et al., 1998). Given that the nitrogen cycle is largely controlled by biological processes, one of the key responses engendered by the nutrient-N cycle is the kinetic fractionation of nitrogen isotopes. In the subsurface waters of the open ocean, the typical $^{14}N/^{15}N$ ratio ($\delta^{15}N$) of dissolved nitrate is

4.5 - 5.5‰, reflecting the relative balance between nitrogen fixation and denitrification. The N-fixation produces NO_3^- isotopically similar to atmospheric N_2 (0 ‰), however, denitrification discriminates against $^{15}NO_3^-$ and preferentially converts $^{14}NO_3^-$ to gaseous products. In the oxygen minimum zones (OMZ), as denitrification continues, the residual NO_3^- becomes enriched in the heavier isotope, confering a characteristic $^{15}NO_3^-$ enriched signal in subsurface waters (~100 to 500 m depth) (Brandes et al., 1998; Cline and Kaplan, 1975). In areas of upwelling and water column denitrification, the heavy $^{15}NO_3^-$ is supplied to the surface waters resulting in $\delta^{15}N$ enrichments of the sinking particulate organic matter and in the sediments below (Ganeshram et al., 2000; Gruber and Sarmiento, 1997; Thunell and Kepple, 2004). Thus, the sedimentary $\delta^{15}N$ signatures are used as a proxy of denitrification in marginal sediments underlying denitrification zones, where processes such as diagenetic alterations have very little impact on the isotopic signatures (Altabet et al., 1995; Altabet et al., 2002; Brandes et al., 1998; Ganeshram et al., 2000).

The most important regions for water column denitrification are the Eastern Tropical North Pacific (ETNP), the Eastern Tropical South Pacific (ETSP), and the Arabian Sea (AS) (Altabet et al., 2002; Ganeshram et al., 2000; Martinez et al., 2006) (Figure 2.1). Which are productive upwelling regions that host large oxygen-deficient water masses, combination that sustains high rates of denitrification (Ganeshram et al., 1995). As a result, a nitrate deficit is developed relative to phosphate, which is measured by the calculated property 'N*' (*defined in the caption of* Figure 2.1-B). Sedimentary analyses performed in these regions suggest that past changes in the water column denitrification can be driven by two mechanisms: variations in local productivity and the advection of oxygen-supply. Hence, denitrification changes are attributed to variations in productivity (Altabet et al., 2002; Ganeshram et al., 2002; Ganeshram et al., 2000; Hendy et al., 2004) and variations in ocean circulation from higher latitudes where the subsurface waters that oxygenate the denitrification zones are formed (Behl and Kennett, 1996; Galbraith et al., 2004; Kienast et al., 2002; Martinez et al., 2006).

A.

Dissolved Oxygen [ml/L] - 250 m depth

B.

N* on σ_θ 26.5 (mmol/m^3)

C.
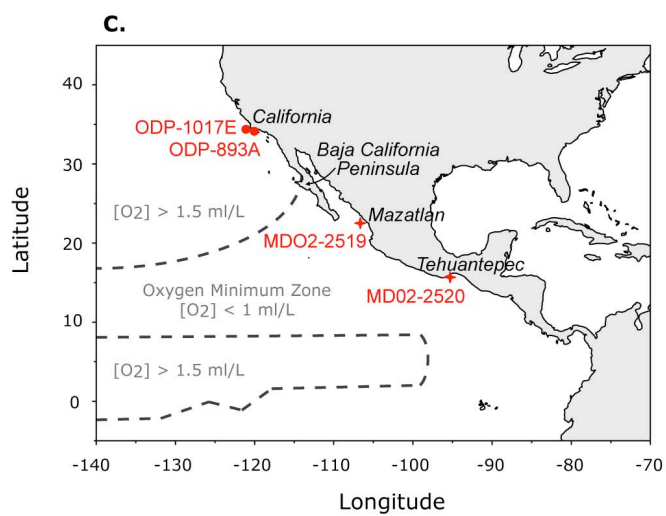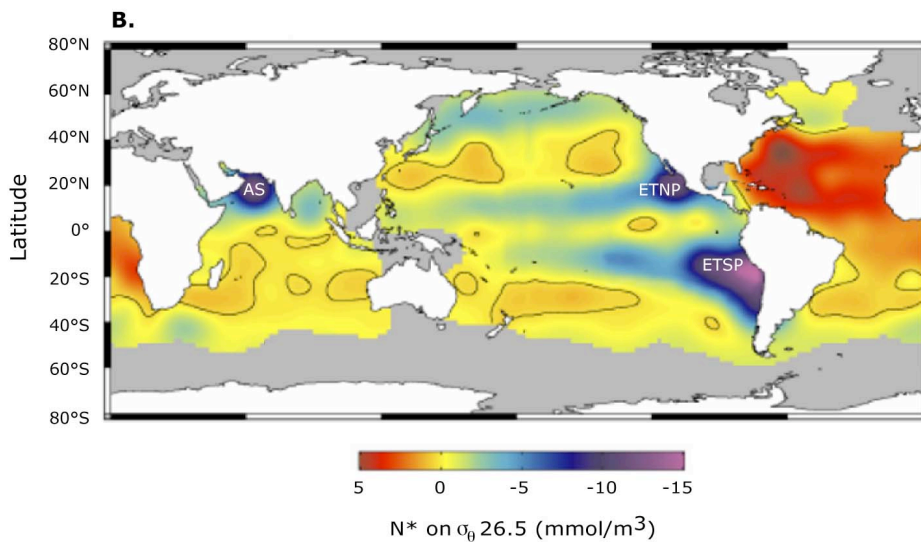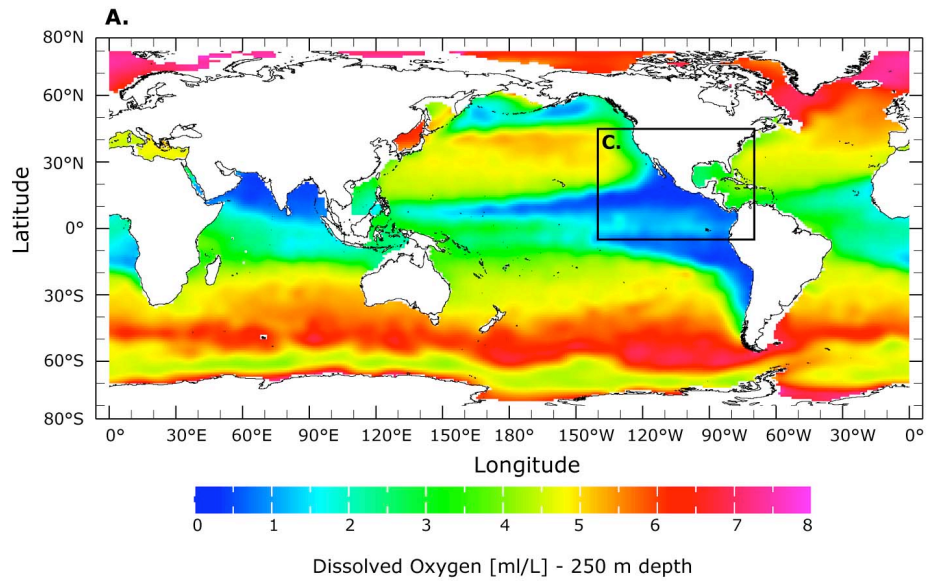
Figure 2-1 Study area. (A) Distribution of dissolved O_2 (ml/L) at 250 m water depth (Levitus and Boyer, 1994). The areas with $[O_2] < 1$ ml/L are known as Oxygen Minimum Zones (OMZ). (B) Distribution of N* on the 26.5 isopycnal (~ 250 m water depth), modified from Pennington et al. (2006). The subsurface waters of the ETNP, the ETSP and the AS, undergo substantial denitrification as indicated by negative values of N* (Gruber and Sarmiento, 1997). N* is a Redfield-based N:P index adjusted such that positive values indicate that nitrogen fixation dominates, whereas negative values indicate that denitrification dominates ($N* = 0.87 [NO_3 - 16 PO_4 + 2.9] \mu M \ kg^{-1}$). (C) $\delta^{15}N$ records used in this study from the eastern tropical North Pacific (diamonds) and off California (dots): Core MD02-2519 was collected off Mazatlan, Mexico, whereas Core MD02-2520 from the Gulf of Tehuantepec, Mexico (see text). Cores ODP-893A (lat 34°17.25'N; long 120° 02.2'W; 576.5 m water depth) (Emmer and Thunell, 2000) and ODP-1017E are located off California (lat 34°32'N; long 121° 06'W; 955 m water depth) (Hendy and Pedersen, 2005). Dotted line indicated the edges of the OMZ at 250 m water depth (see inset C in map A).

Most studies in the NE Pacific show temporal agreement between periods of intensified denitrification and enhanced productivity (e.g. based on proxy records of %organic-carbon, opal and bio-barium (Ba/Al) ratios) both on glacial-interglacial and millennial time scales. This suggests that the water column denitrification in the ETNP could respond to past changes in upwelling, and fluxes of organic material to the sediments (Ganeshram et al., 2000; Ganeshram et al., 1995). In addition, studies from Santa Barbara Basin (SBB) (Emmer and Thunell, 2000) show that periods of intensified denitrification match periods of low oxygenation in bottom waters, previously reported by Behl and Kennett (1996). Hence it represents a strong regional coupling between upwelling, denitrification and oxygenation in the basin. Later, Ortiz et al. (2004) and Hendy et al. (2004) suggested that changes in the bottom water oxygenation off California were produced by the changes in the organic matter decay and the consumption of oxygen in a broad regional scale.

Based on these studies, it is inferred that: (1) productivity and oxygenation changes seem to be coeval across the NE Pacific margin; (2) the advection of denitrified nitrate to the NE Pacific had to be transported northward from the ETNP; (3) the ETNP denitrification zone is the most feasible source of the heavy $\delta^{15}N$ signatures down the margin during interstadial events (Behl and Kennett, 1996; Emmer and Thunell, 2000; Hendy and Pedersen, 2005). However, this coherent picture has been recently questioned:

First, Thunell and Kepple (2004) showed that in the Gulf of Tehuantepec, the $\delta^{15}N$ changes exhibited different timing relative to the records in the north. Here, the $\delta^{15}N$ record show enriched values during the deglaciation (~ 23 to 17 cal ka BP), followed by a

continuous $\delta^{15}N$ decline during the last 10 ka of the Holocene, which is as depleted as the glacial period. In general, because there is no clear pattern to link the millennial scale events of this record to Northern Hemisphere (NH) climate change, the authors argued in favour of a localized weakening of the OMZ during the mid- to late Holocene. This pattern suggests that the history of denitrification in the southern part of the ETNP is different from what is expected in the NE Pacific $\delta^{15}N$ records, which shows a clear glacial-interglacial transition with high Holocene values relative to the glacial, punctuated by declines in $\delta^{15}N$ during Younger Dryas (YD) and Heinrich (H)1 events. Importantly, these findings question whether the millennial scale denitrification variations in the NE Pacific are originated in the ETNP. Additionally, the study by Hendy and Pedersen (2006) suggest that the exiting data from Tehuantepec reinforces that the OMZ in the ETNP has a clearly different history relative to the records in the NE Pacific, and cannot be any significant exchange of subsurface waters between the ETNP and California during the last deglaciation and the last glacial period.

Second, some studies have focussed on the last deglaciation (Hendy and Pedersen, 2005; Kienast et al., 2002) showing time differences between denitrification ($\delta^{15}N$) and paleo-productivity (OC-MAR and trace metals Cd and Ag) proxy records from Oregon and California, respecto to the ETNP. Specifically, the OC-MAR records suggested that the productivity off Oregon led by several thousand years the productivity off Mazatlan. Kienast et al. (2002) hypothesized that the decoupling of local surface production and denitrification rates originated from circulation changes in the equatorial Pacific during the last deglaciation. During the Last Glacial Maximum (LGM), a stronger Equatorial Undercurrent (EUC) could supply more oxygen to the southern parts of ETNP, therefore reducing denitrification and a consequent decoupling from primary productivity. The idea of a stronger EUC is based on the assumption that stronger trade winds occurred during the glacial, as suggested by paleoceanographic and modelling based results (e.g. Anderson et al., 2006; Parkin and Shackleton, 1973; Paytan et al., 1996).

In this chapter, we revisit the issue of timing the $\delta^{15}N$ changes in the ETNP by presenting two well-dated millennial scale resolution records spanning the last 120 ka, from cores located in the northern (Mazatlan) and southern (Gulf of Tehuantepec) parts of the ETNP denitrification zone (Figure 2.1-C). We will compare the timing of denitrification changes between N and S, in relation to published records along the eastern Pacific margin to assess their relative differences and their causes. Moreover, the record from the northern

part of the ETNP (Mazatlan) is reported for fist time at millennial scale resolution; whereas the record from the southern part of the ETNP (Tehuantepec) is extended up to MIS-3.

2.2   Study area

2.2.1   Upwelling

In the NW Mexican margin (off Mazatlan) and the Gulf of Tehuantepec, upwelling and high biological productivity occur during winter and early spring, resulting from southward flowing winds controlled by the southern position of the Intertropical Convergence Zone (ITCZ), and variations in the positions of the pressure systems. For instance, the winds flowing off Mazatlan travel parallel to the coast as a result of air-pressure differences between the North Pacific-High and the thermal Low centred on the continent (Badan-Dangon, 1998; Reyes and Lavin, 1997). The winds flowing in the Gulf of Tehuantepec, travel perpendicular to the coast from the North American-High towards the tropical Low-pressure system in the Pacific Ocean (Lavin et al., 1992; Trasviña et al., 1995).

2.2.2   Hydrology

In the ETNP, the ocean circulation is characterized by the California Current (CC)-system in the north, and waters from the eastern Equatorial Pacific (EEP) in the south. The CC-system is the eastern boundary current of the large North Pacific Gyre, which includes three principal currents: (1) the shallow California Current (CC) (0-300 m); (2) the sub-superficial California Undercurrent (CUC) (200-500 m); and (3) the seasonal Davidson Current (DC), which is formed in the region during fall-winter flowing northward as a coastal surface current (0-200 m) (Badan-Dangon, 1998; Takesue et al., 2004).

The southernmost flow of the surface CC varies seasonally to finally merge into the North Equatorial Current (NEC) (Figure 2.2). During winter to early spring, the CC strengthens and extends south of the Baja California Peninsula at ~ 20°N (Kessler, 2006; Lavin et al., 1995; Wyrtki, 1965). During boreal summer and fall, the CC moves north by 10° controlled by the migration of the ITCZ, the intensification of the equatorial countercurrents, and the northward expansion of the Costa Rica Coastal Current (CRCC) up to the tip of the Baja California Peninsula (Badan-Dangon, 1998; Kessler, 2006). At subsurface depths, the Equatorial Undercurrent (EUC) transports large amounts of water

from the far W Pacific with eastward direction. Together, the EUC and two parallel thermocline-depth currents (125-400 m depth) called Tsuchiya jets or Subsurface Countercurrents, control most of the water mass balance in the E Pacific and contribute to the flow of subsurface waters in the ETNP (i.e. the Northern and Southern Subsurface Countercurrent, NSSCC and SSSCC, respectively) (Figure 2.2).
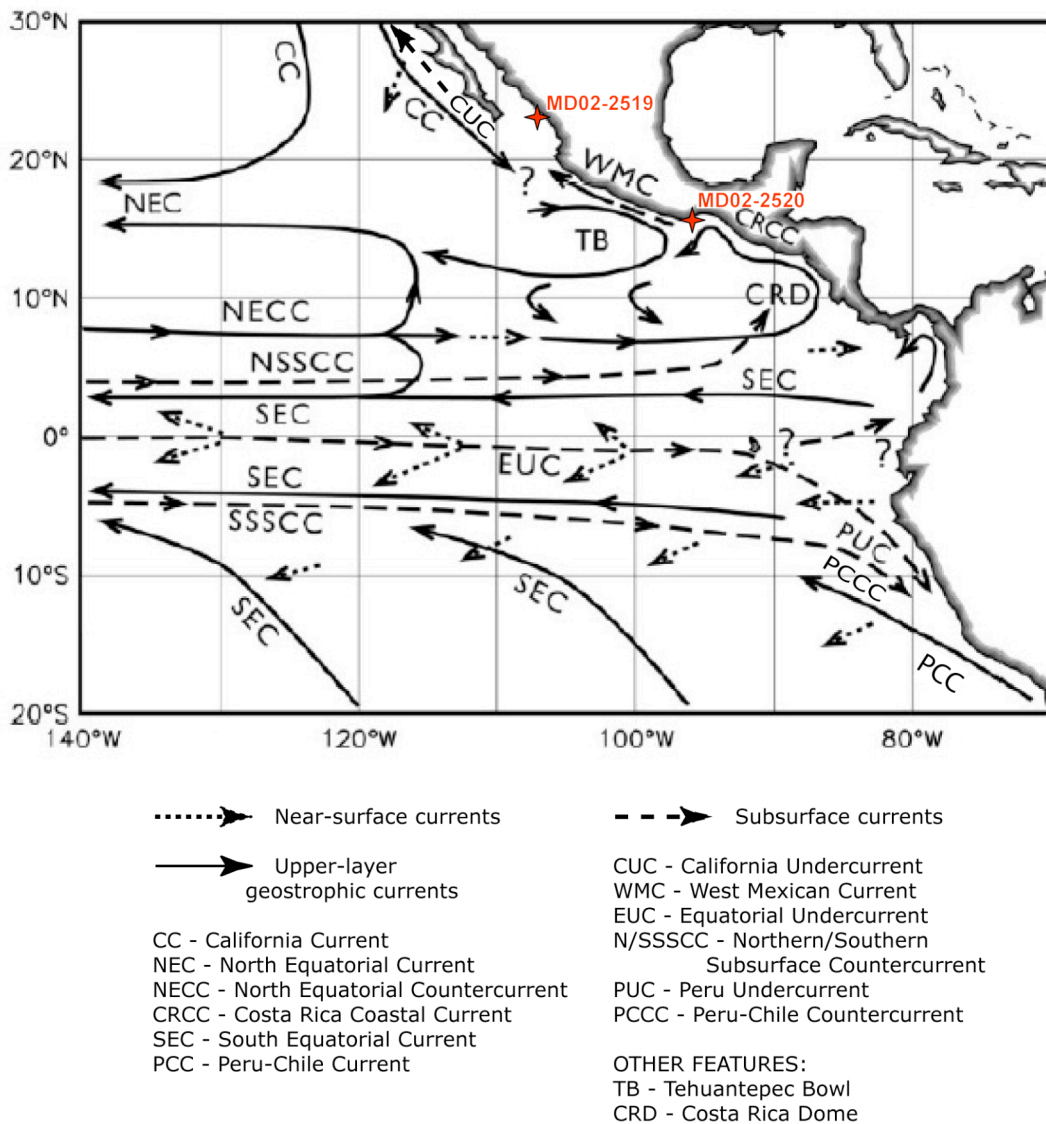
Figure 2-2 Schematic map of the annual surface and subsurface circulation influencing the ETNP (modified from Kessler, 2006). The legend at the bottom lists names and features mentioned in this chapter. The question marks (?) indicate regions where the interconnections among currents remain unknown. Red stars show the locations of cores MD02-2519–Mazatlan and MD02-2520–Tehuantepec.

2.2.3 Oxygen Minimum Zone

In the ETNP, the presence of an OMZ ($[O_2] < 1$ mL/L) is well defined and uniform that sometimes it is considered a water mass in its own, even when the T-S relationship overlap different water masses (Badan-Dangon, 1998; Lavın et al., 1997; Lavin et al., 1995). The thickness of the OMZ varies with latitude. For example, being less than 300 m thick in the equatorial region and more than 1200 m in the NE Pacific (Figure 2.1-A). The overlapped water masses within the OMZ are the Subsurface Subtropical Water (SSW) and the North Pacific Intermediate Water (NPIW) (Fiedler and Talley, 2006; Kessler, 2006). The SSW originates from equatorial undercurrents which reside in the eastern tropical Pacific at ~ 150 – 600 m depth (Badan-Dangon, 1998). The NPIW origins in the North Pacific (Bering Sea and Okhostk Sea) and travels equatorward at water depths between ~ 500 – 1200 m (Talley, 1999).

2.3 Materials and Methods

2.3.1 Sediment cores: collection, sampling and analytical techniques

Two marine sediment cores were retrieved from the ETNP with a Calypso piston corer during the oceanographic campaign MONA 2002. The Core MD02-2519 was collected off Mazatlan (lat 22° 30.89'N; long 106° 39.00'W) from 955 m depth; and the Core MD02-2520 from the Gulf of Tehuantepec (lat 15° 40.14'N; long 95° 18.00'W) from 712 m depth (Figure 2.1-C). The core sites were chosen because of their high sedimentation rate and location within the modern OMZ, and underneath an area of active subsurface denitrification were sediment reworking is minimal. Careful inspections of the cores do not reveal turbidity flow deposits nor apparent evidence of down-slope transport (*see information provided in Appendix A*).

In general, the sediments in the Core MD02-2519 vary between laminated to massive and bioturbated intervals. The dominant sediment is very dark in colour, indicative of high amounts of deposited organic matter. The sediments in the Core MD02-2520 are mostly laminated with fine to thick banding and few light sandy layers present during the deglaciation interval. The dominant sediment is silt-clay with colours grading from olive-grey to dark-grey.

The sampling of the cores was at 1-2 cm intervals. Organic carbon (wt %) and nitrogen isotopes ($\delta^{15}N$) analyses were undertaken at the Wolfson Laboratory of the School of Geosciences, the University of Edinburgh. The $\delta^{15}N$ and %OC data of Core MD02-2520 were analysed as part of the PhD Thesis of Steven Francavilla, and used in this study to improve the comparison of the existing records in the Gulf of Tehuantepec (Hendy and Pedersen, 2006; Thunell and Kepple, 2004). The analytical methodology used for both cores is similar.

The sediments samples selected for C-N analyses were freeze-dried and a portion of each was ground with an agate mortar into a fine powder. The bulk sample was acidified with HCl (5%) and heated at 70°C to remove all traces of carbonates. The %OC and $\delta^{15}N$ were determined using a C-N Elemental Analyser (CE Instruments NA2500) coupled to a CG PRISMII Mass Spectrometer. The $\delta^{13}C$ and $\delta^{15}N$ values were determined relative to CO_2 and N_2 reference gases, whose mean values are derived from the average value of a sediment standard (PACS-2: $\delta^{15}N$ = 5.215$_{air}$; $\delta^{13}C$ = -22.228 $_{PDB}$). The Craig-correction was used to calculate the carbon isotope values. The precision of the determinations is better than 0.09 ‰ and 0.10 ‰ for $\delta^{13}C$ and $\delta^{15}N$, respectively. Based on the $\delta^{13}C$-OC analyses, we confirmed that the sediments of the cores MD02-2519 and MD02-2520 are from marine origin (i.e. the range of $\delta^{13}C$ of marine organic matter = -22 to -19 ‰ (Ganeshram et al., 2000).

Organic Carbon Mass Accumulation Rates (OC-MAR, mg/cm^2/ka) were calculated using the formula suggested by Ganeshram *et al.* (1995):

$$OC\text{-}MAR = 2400\ (mg/cm^3) * [1 - porosity] * [SR\ (cm/ka)] * [fraction\ OC]$$

where, 2400 is the assumed grain density and *SR* is the sedimentation rate. Porosity data were obtained from the measurements taken on board the ship (Beaufort, 2002). Unfortunately, the OC-MAR of the Core MD02-2520 is not entirely reliable to be discussed in detail (i.e. at millennial timescale resolution) because spurious measurements were found in the fractional porosity dataset.

2.3.2   Age Models and Sedimentation Rates

The age models for the cores from the ETNP include the AMS ^{14}C dating of 19 planktonic-foraminifera and organic-carbon samples from the Core MD02-2519 collected off

Mazatlan, and 28 organic-carbon samples of the Core MD02-2520 collected from the Gulf of Tehuantepec (Table 2.1). The age model for Core MD02-2520 is entirely based on radiocarbon dates (Pichevin et al., 2010). However, the Core MD02-2519 extends beyond the radiocarbon limits (> 45 cal ka BP) and requires age control points derived from the tuning between the %OC record and the GISP2 chronology (*annexed Figure 2a*). We verified the validity of this approach in the radiocarbon dated intervals, where the AMS ^{14}C-based chronology show abrupt %OC changes coeval to millennial scale variations recorded in Greenland ice cores *(Chapter 1)*. Previous studies in the region have successfully used this approach, suggesting that a tight correlation exists between NE Pacific surface waters and Greenland air temperatures, indicating a close hemispheric climate relationship at millennial timescales (Hendy and Kennett, 2000; Hendy et al., 2002; Ortiz et al., 2004).

To extend the timescale of Core MD02-2519 beyond 40 ka, the age control points were obtained from correlation between the OC record and the major δ^{18}O GISP2 maxima events (*annexed Figure 2a*). The strategy followed is described in detail in the methods of *Chapter 1*. The AMS ^{14}C dates based on OC samples suggest that the timing of the millennial timescale events identified, correspond to the temperature proxy records from Greenland (i.e. GISP2). This is coherent with studies done in the NE Pacific (Hendy et al., 2002; Ortiz et al., 2004) showing a consistent timing between the GISP2 events (stadials and interstadials) and those seen in the younger parts of the cores (< 45 ka). This relationship thus permits temporal correlation in older intervals. The final chronology of cores MD02-2519 and MD02-2520 were constructed by linear interpolation between tie-points, producing a composite chronology spanning ∼ 120 cal ka and ∼ 50 cal ka BP, respectively.

All radiocarbon samples were analysed at the NERC Radiocarbon Laboratory (RCL), East Kilbride, UK. The AMS ^{14}C dates were converted to calendar years BP using the online version CALIB 5.0.2 for marine samples (MARINE-04) (Stuiver and Reimer, 1993). Dates older than 21,800 ^{14}C years were calibrated using the *equation 2* by Bard *et al*. (2004). The reservoir radiocarbon corrections are $\Delta R = 203 \pm 48$ (MD02-2519) and 162 ± 50 (MD02-2520), as suggested in the Marine Calibration Database (Reimer and Reimer, 2001).

Linear sedimentation rates (SR) were calculated for both cores (Figure 2.3). The average SR of Core MD02-2519 (Mazatlan) is ∼ 19 cm/ka, an indication of the stable conditions in which the sediments have been deposited. However, the SRs of Core MD02-

2520 (Gulf of Tehuantepec; average SR ~ 91 cm/ka) are higher and more variable than Core MD02-2519. As suggested by previous studies (Thunell and Kepple, 2004), some factors that may influence the SR in the Gulf of Tehuantepec include: high surface productivity, input of terrigenous sediments from adjacent areas, and past changes in sea level.

Table 2.1

AMS ^{14}C dates: Core MD02-2519

Core depth	Raw 14C Age	error	Calibrated Age	error 1σ		Notes:	
(cm)	(yrs)	±	(yrs BP)*	-	+	material	Calib source
1	2865	73	2365	116	94	OC	1
74	4049	61	3802	79	93	OC	1
140	6050	61	6266	54	72	OC	1
194	8689	64	9114	79	101	OC	1
216	9555	73	10198	82	84	PF	1
230	10272	62	11082	134	94	PF	1
284	12664	53	13911	86	75	OC	1
290	12831	64	14084	84	76	PF	1
332	14173	65	16139	205	193	PF	1
370	15717	84	18475	184	296	OC	1
424	18667	109	21417	278	272	OC	1
466	20091	173	23191	316	346	OC	1
500	21920	153	25713	208	145	OC	1
558	24147	154	28226	399	399	OC	2
576	24690	169	28831	369	369	OC	2
606	26239	216	30548	364	364	OC	2
636	27987	281	32471	349	349	OC	2
676	29852	367	34507	342	342	OC	2
758	35012	749	39522	1015	1015	OC	2

* ΔR = 203 ± 48

AMS ^{14}C dates: Core MD02-2520

Core depth	Raw 14C Age	error	Calibrated Age	error 1σ		Notes:	
(cm)	(yrs)	±	(yrs BP)*	-	+	material	Calib source
1	1063	24	515	48	38	OC	1
129	1658	37	1048	80	70	OC	1
309	3048	36	2645	78	91	OC	1
404	4084	38	3907	92	87	OC	1
534	5246	41	5442	108	91	OC	1
669	6295	43	6564	82	79	OC	1
844	8233	55	8535	109	72	OC	1
969	9480	63	10155	118	94	OC	1
1073	10764	82	11865	184	235	OC	1
1123	11648	86	13007	90	74	OC	1
1173	12662	99	13954	131	105	OC	1
1222	13279	108	14976	206	219	OC	1
1387	14750	133	16947	304	273	OC	1
1442	15588	149	18310	218	253	OC	1
1492	16046	158	18795	108	114	OC	1
1571	16652	172	19255	160	175	OC	1
1797	18589	224	21394	364	430	OC	1
2112	21177	316	24551	482	482	OC	2
2277	21957	349	25422	667	667	OC	2
2475	24387	480	28088	634	634	OC	2
2670	26767	268	30626	343	343	OC	2
2881	28392	803	32319	739	739	OC	2
2981	29807	392	33766	371	371	OC	2
3150	32199	527	36154	964	964	OC	2
3284	32557	1363	37100	1836	1836	OC	2
3329	34607	712	38300	975	975	OC	2
3438	37450	1016	41146	716	716	OC	2
3493	39587	1326	42700	990	990	OC	2

* ΔR = 162 ± 50
OC - organic carbon; PF - mixed planktonic species
(1) Stuiver *et al.*, 2005; (2) Bard *et al.*, 2004

Table 2-1 Radiocarbon dates used in the construction of the timescale for cores MD02-2519 (see Chapter 1) and MD02-2520 (Pichevin et al., 2010).
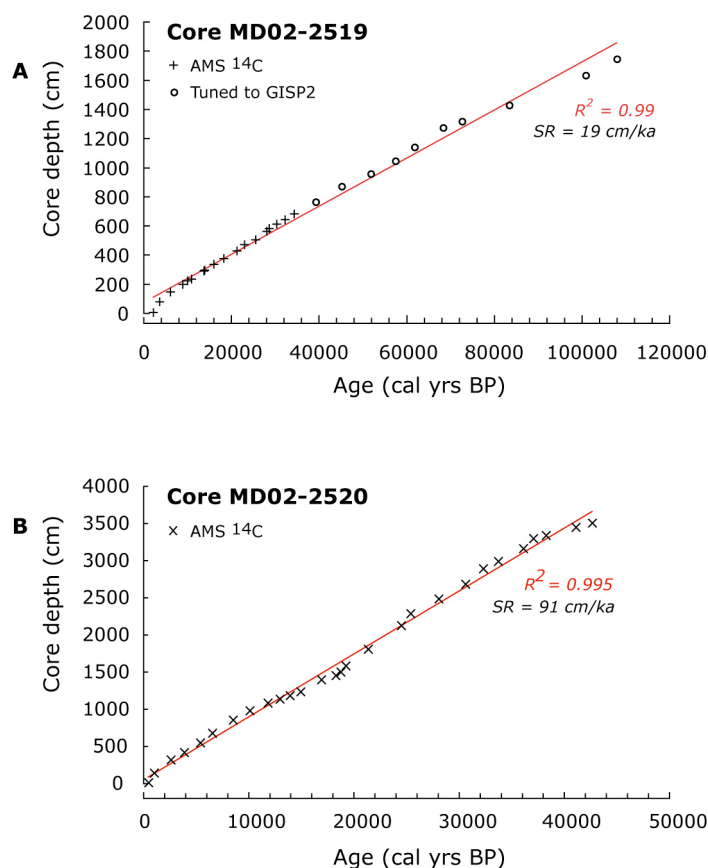
Figure 2-3 Depth vs age plots of the cores (A) MD02-2519 and (B) MD02-2520. Red line shows the average sedimentation rate.

2.4 Results and Discussion

2.4.1 Regional differences of δ^{15}N in the ETNP

In the *Core MD02-2519* collected off Mazatlan, the isotopic analyses of the sedimentary material yielded δ^{15}N values ranging from 5.3 – 11.5‰ (average value $\simeq$ 8‰) for the last 120 ka. At glacial-interglacial timescales, δ^{15}N values are heavier (7.3 - 11.5‰) during interstadials like the Marine Isotope Stage (MIS) 5, MIS-3 and the Holocene; but 2 – 3‰ lighter (5.3 - 7.6‰) during stadials like MIS-4 and MIS-2 (Figure 2.4). According to previous studies (Ganeshram et al., 2000; Ganeshram et al., 1995), the δ^{15}N values suggest that denitrification increased in the region during interglacial relative to glacial periods.
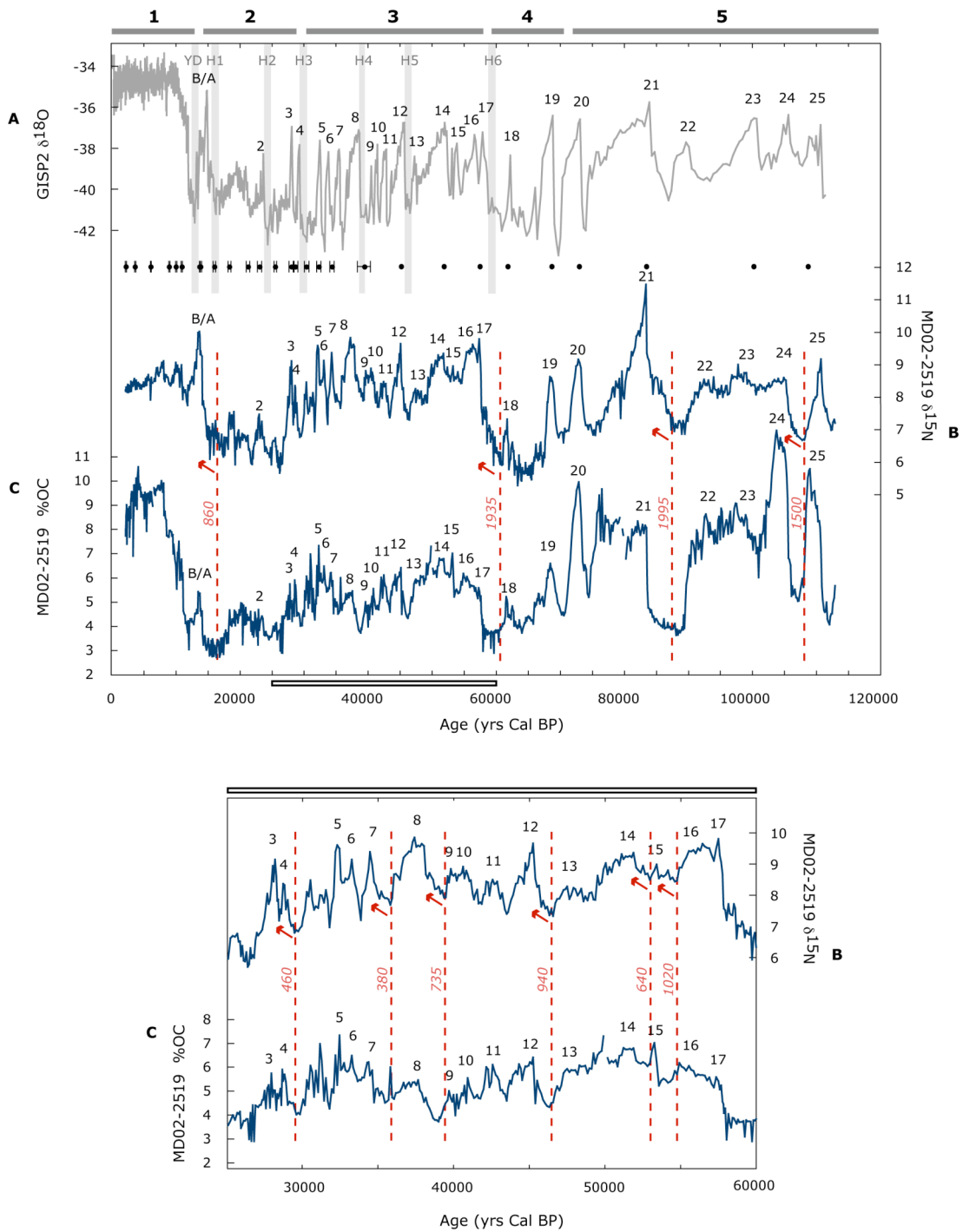
Figure 2-4 $\delta^{15}N$ and %OC records of Core MD02-2519 spanning the last 120 ka. The band on top show marine isotope stages (MIS) 1 –5. (A) $\delta^{18}O$ GISP2 record (Blunier and Brook, 2001); (B) $\delta^{15}N$ and (C) %OC records. The double-line marks the interval between 25 – 60 ka, zoomed out in the plot below. The age control points are displayed across the top of $\delta^{15}N$ record, including error bars of AMS ^{14}C dates (see Table 2.1 for details). Red arrows and vertical dotted lines mark the onset of the $\delta^{15}N$ rise over the OC record; red numbers are the years the denitrification record leads the productivity record. Numbers are D/O interstadials and B/A - Bølling/Ållerød. Grey lines mark YD – Younger Dryas and Heinrich (H) events.

Distinctively, rapid shifts of 2 – 4‰ are seen in the δ^{15}N record during MIS-2, 3 and 4 (~ 71 to 14 ka BP). The δ^{15}N values show a general increase (> 7.8‰) coincident with interstadials and a decrease during stadials. Overall, the δ^{15}N record shows the highest variability during MIS-3 and the highest amplitude change during MIS-5 (e.g. D/O-20 and 21) relative to other isotope stages (e.g. MIS-4, MIS-2 and the Holocene). During the the deglaciation, the average δ^{15}N values of Core MD02-2519 increase from 6.5 – 10‰ between 17 - 14.5 ka BP. The maximum value (~ 10‰) coincides to the B/A (~ 14.8 – 12.8 ka), which is subsequently reduced by 2.3‰ during the YD (~ 12.8 – 11.5 ka). Then, the values are recovered by ~ 1‰ during the Holocene (average values $\simeq$ 8.5‰). At millennial timescales, the δ^{15}N record of Core MD02-2519 resembles Greenland timing (Figure 2.4 and 2.5), which is furthermore supported by ^{14}C-dating as shown in the *annexed Figure 2a*. However, differences also exist as we will discuss in following sections. The sequence of abrupt changes during the glacial and the last deglaciation is moreover analogous to a variety of δ^{15}N records along the NE Pacific margin (e.g. Crusius et al., 2004; Emmer and Thunell, 2000; Hendy and Pedersen, 2005; Pride et al., 1999). Specifically, the high δ^{15}N value during the B/A is notorious, possibly attributed to a greater level of denitrification in the ETNP and an increase in the intensity of the OMZ (Crusius et al., 2004; Emmer and Thunell, 2000). The time correspondences among records collected off Mexico, California and those from Greenland, suggest an hemispheric relationship between the NH climate patterns, along with regional factors controlling the δ^{15}N record in the northern edge of ETNP.

The δ^{15}N record of the *Core MD02-2520* collected from the Gulf of Tehuantepec shows average values of ~7.6‰ over the last 50 ka BP (Figure 2.5). The δ^{15}N values are generally lower between 30 - 18 ka (~ 5.9 – 8.0‰), but relatively higher in the intervals between 32 - 45 ka (5.9 - 9.5‰) and 18 - 7 ka (7.5 - 9.6‰). Moreover, a distinct and gradual depletion (from ~ 9.0 to 6.1‰) is seen in the δ^{15}N values from ~ 11 ka up to the top of the core. At millennial timescales, rapid changes in the δ^{15}N-MD02-2520 record are recognized with greater and more frequent variability than the Core MD02-2519. Higher values (> 7.6‰) in general coincide with interstadials, and lower values during stadials. The comparison of the δ^{15}N record to the δ^{18}O records GISP2 and Byrd (Figure 2.5) shows characteristics of both, Northern and Southern Hemisphere stadial - interstadial variabilities.
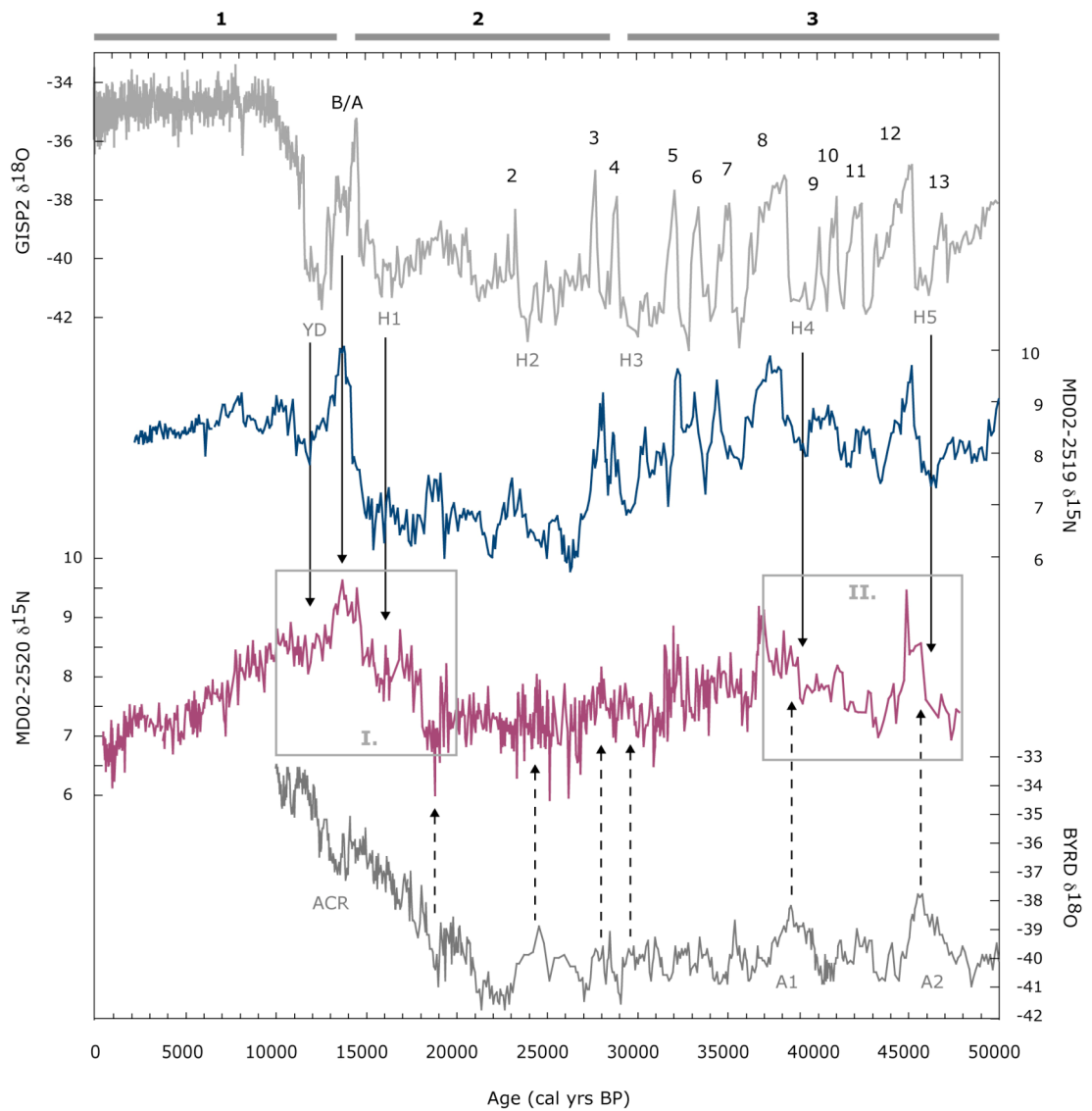
Figure 2-5 δ¹⁵N records of cores from the ETNP compared to GISP2 and Byrd δ¹⁸O records (Blunier and Brook, 2001) for the last 50 ka. The band on top shows the glacial and interglacial marine isotope stages (MIS) 1 – 3. Vertical solid arrows are intervals resembling GISP2 events, while the vertical broken lines are intervals similar to Byrd. The grey boxes I and II are zoomed out in Figure 2.6. Numbers are D/O interstadials 1 to 13. The ACR – Antarctic Cold Reversal and the warm events A1 and A2 are also indicated.
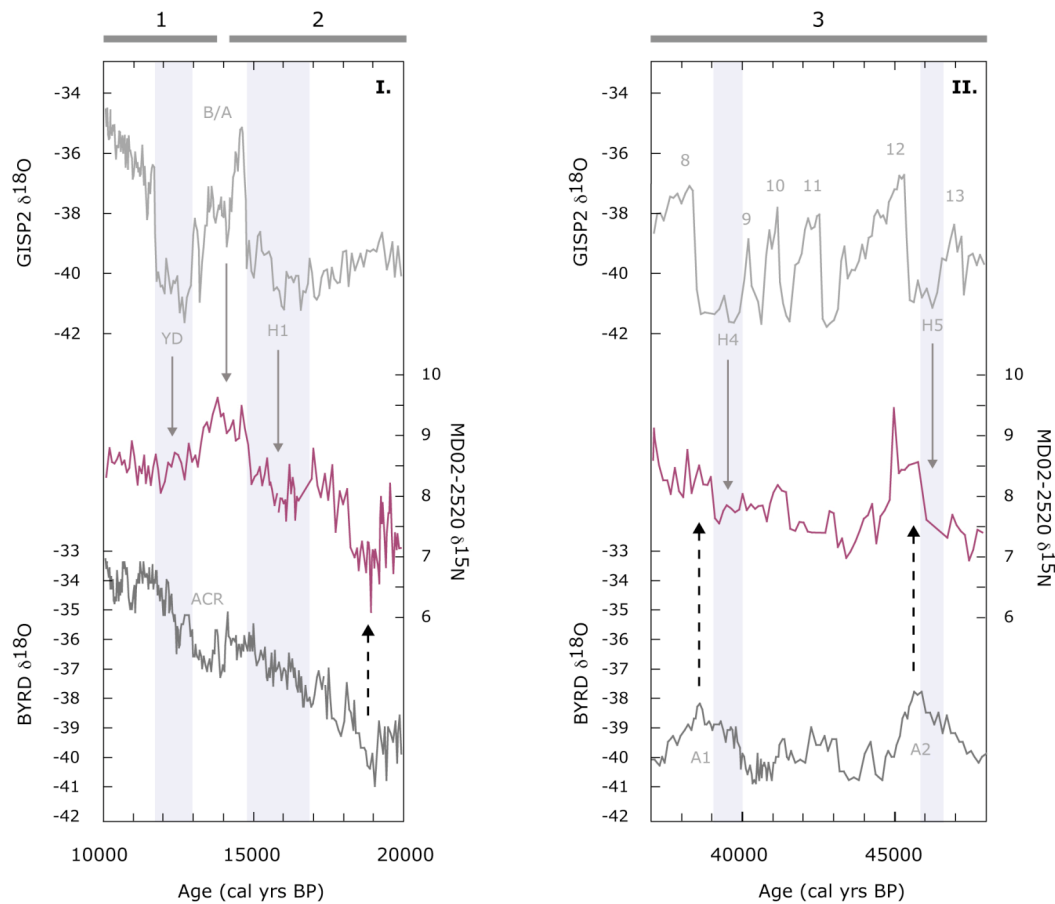
Figure 2-6 Transitional intervals in Core MD02-2520 matching GISP2 (purple bands) and Byrd timing (dotted arrows) (see Figure 2.5 for details).

In Core MD02-2520, the $\delta^{15}N$ record resembles the pattern an low amplitude variability of Antarctica during MIS-3 and MIS-2. For instance, the gradual $\delta^{15}N$ enrichments between ~ 48 and 37 ka (Figure 2.6 – *II*) are similar to Antarctica warm events A2 and A1, than to Greenland interstadials D/O-12 and 8. However, the increase in $\delta^{15}N$ appears to be briefly interrupted by the cold events H5 and H4 (at ~47.5 and ~40 ka, respectively), with relatively high values matching GISP2 interstadials 12 and 8. The combined inter-hemispheric pattern is seen all through the glacial period up to the onset of the last deglaciation. During the deglaciation, the nitrogen isotope values of Core MD02-2520 increased by 1.7‰ (from ~ 7.7‰ to 9.8‰) between H1 and the B/A (~13.8 ka). At the initial stage of the deglaciation (Figure 2.6 – *I*), the increase in $\delta^{15}N$ values is synchronic with Antarctica (onset at ~ 19 ka), although interrupted by the H1 (~16 ka) and the YD (~12 ka) events.

Overall, the $\delta^{15}N$ changes in Core MD02-2520 can be related to changes in denitrification intensity, being minimal during most of the glacial and the late Holocene, but larger during the deglaciation and the early Holocene. Moreover, these variations at glacial-interglacial timescales are comparable to records previously published in the area (Hendy and Pedersen, 2006; Thunell and Kepple, 2004), including the last part of the record (<10 ka) that shows a gradual decrease in $\delta^{15}N$ towards the top of the core. The $\delta^{15}N$ values from 5 to 1 ka are somehow comparable to the glacial values (7‰), although previous investigations attribute the Holocene decline in organic $\delta^{15}N$ to a dilution effect with depleted $\delta^{15}N$ values, perhaps due to an increase in nitrogen fixation in oligotrophic regions of the Pacific Ocean (Thunell and Kepple, 2004).

In summary, regional differences are found within the ETNP between the northern and southern denitrification zones as shown by the $\delta^{15}N$ records collected off Mazatlan and Tehuantepec. The $\delta^{15}N$ record from Mazatlan exhibits timing and features that are similar to temperature changes in Greenland ($\delta^{18}O$-GISP2), whereas the record from Tehuantepec has a mixed signature from north and south high-latitude records (GISP2 and Byrd). Broadly, the northern record MD02-2519 (Mazatlan) shows more a NH millennial scale variability; while the southern record MD02-2510 (Tehuantepec), shows a mixture of both NH and SH signals (Figure 2.5). To understand the underlying reasons of such differing trends, we consider next: (1) the relationship between denitrification variations and local surface productivity within the ETNP (Emmer and Thunell, 2000; Ganeshram et al., 2000; Ganeshram et al., 1995); and (2) the influence of oxygen advection and/or heavy nitrate from outside the ETNP denitrification zone (Meissner et al., 2005; Robinson et al., 2007).

2.4.2 Denitrification changes and local productivity

In the northern part of the ETNP off NW Mexico, although the %OC and $\delta^{15}N$ records of Core MD02-2519 show a similar pattern, differences also exist (Figure 2.4). The highest percentages of OC (> 8%) in Core MD02-2519 correspond to and the major D/O events (D/O-20 to 25) and the Holocene. The lowest percentages (< 5%) are related to glacial MIS-2, MIS-4 and the stadial periods, including H events. Moreover, this pattern is seen after calculating the OC-MAR (*annexed Figure 2b*) (average = 418 mg/cm2/ka; min = 200; max = 816), which confirms that the OC accumulation is not biased by abrupt changes in sedimentation rates, therefore, the %OC record is used for comparison instead of the OC-MAR record. However, even when the peak values of the $\delta^{15}N$ and %OC records are

synchronous, the first leads the former by several hundred to few thousand years at the onset of major interstadial excursions (e.g. D/O – 24, 21, 17, 15, 12, 10, 8 or 4), (*see red numbers in* Figure 2.4). Additionally, at the initial stage of the deglaciation, the δ^{15}N record leads by ~860 yrs the %OC record (*see dotted line at 17 ka in* Figure 2.4).

The apparent lead in δ^{15}N over %OC during excursions indicates clearly that local change in upwelling-induced productivity (i.e. elevated export production to the sediments) (Ganeshram and Pedersen, 1998; Ganeshram et al., 1995) is not the only factor that modulates δ^{15}N changes off Mazatlan. For instance, in *section 2.4.3*, we provide evidence to support that the earlier change in δ^{15}N values over OC values during interstadials in the ETNP could be explained by advection of heavy nitrate from southern regions.

In the Core MD02-2520 from the Gulf of Tehuantepec, the δ^{15}N and %OC records are largely decoupled (Figure 2.7). In general, higher %OC values (> 5.0%) are only present in some intervals of MIS-3, the deglaciation and the late Holocene. Meanwhile, lower %OC values (< 5%) are mostly present during MIS-2 and the early Holocene. This pattern, however, is not entirely confirmed by the calculated OC-MAR (*annexed Figure 2b*), which shows relatively higher values between 37.5 – 27.5 ka and 25 – 18.5 ka (~ 833 mg/cm^2/ka; min = 140, max = 1730), and for the last 6 ka (> 1000 mg/cm^2/ka). Relatively lower values are identified between 47 – 37 ka (< 340 mg/cm^2/ka) and 18.5 – 6.5 ka (~ 550 mg/cm^2/ka; min = 223, max = 880). As mentioned in the *methods* section, the porosity data show anomalies that make the dataset of Core MD02-2520 unreliable to discuss at millennial scale resolution. However, at glacial-interglacial timescales, the overall increase during late MIS-3 and early MIS-2 (relative to the interglacial) could be caused by elevated nutrient supply from equatorial Pacific waters, as will be discussed in the next chapter.

Therefore, it is clear that no simple relationship exists between the OC and δ^{15}N records of the Core MD02-2520 at millennial timescales (Figure 2.7). The OC accumulation record is neither in agreement to the δ^{15}N record, nor to other productivity proxies reported in previous studies (e.g. Hendy and Pedersen, 2006; Thunell and Kepple, 2004).
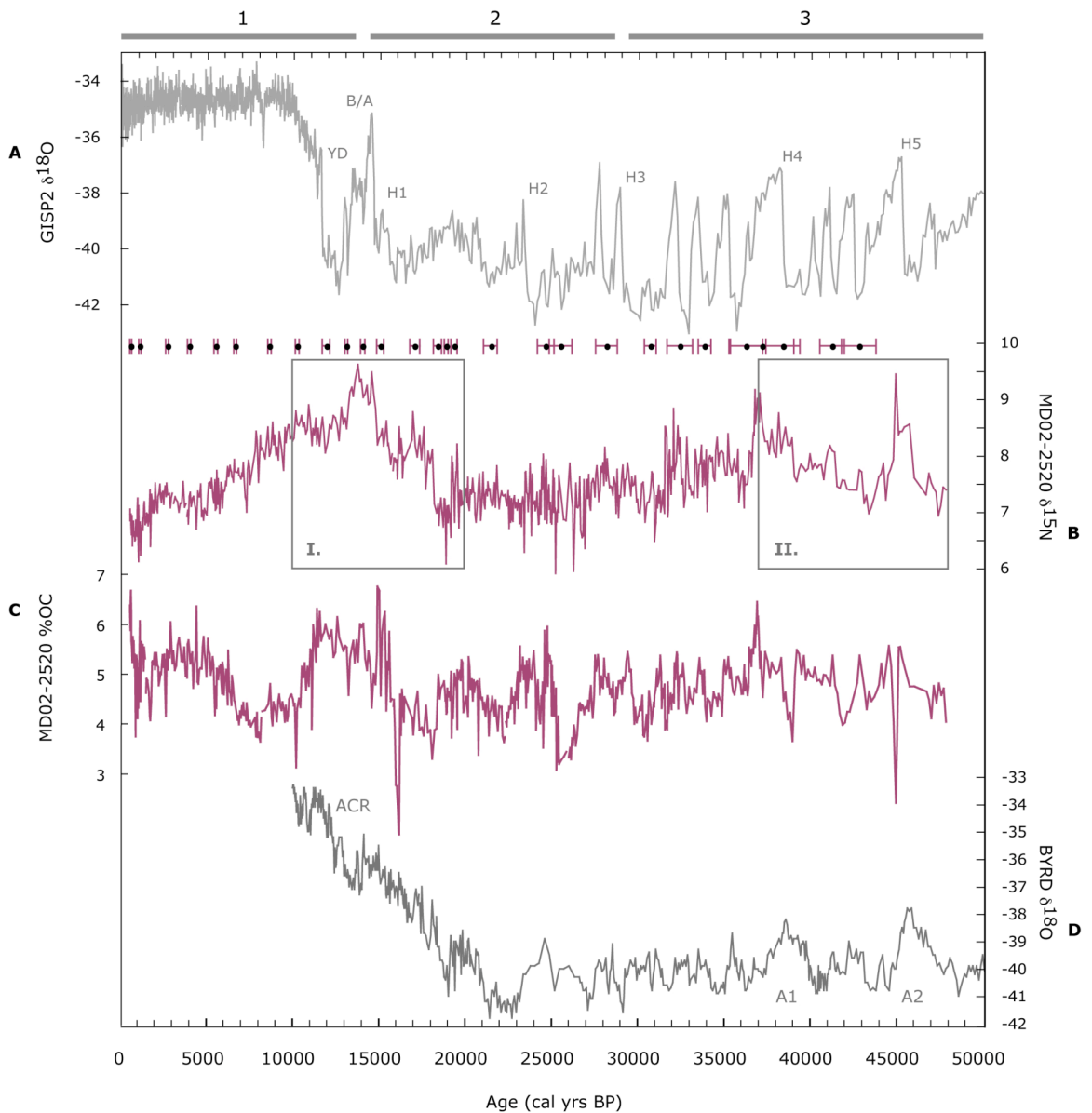
Figure 2-7 High-resolution δ¹⁵N and OC records of Core MD02-2520 spanning 50 ka BP. Band on top shows MIS 1 - 3. (A) GISP2 δ¹⁸O record; (B) δ¹⁵N and (C) %OC of Core MD02-252; (D) Byrd δ¹⁸O record (Blunier and Brook, 2001). The age control points are displayed across the top of the δ¹⁵N record, which correspond to the calendar corrected AMS ¹⁴C-dates (dots) with error bars (see Table 2.1 for detailed information). Vertical dotted lines highlight the pattern of denitrification in the Gulf of Tehuantepec, similar to the temporal variability in Antarctica. Grey boxes I and II are zoomed out in Figure 2.6.

2.4.3   Source of advective δ¹⁵N signal influencing the ETNP

The lack of relationship between δ¹⁵N and OC records off Tehuantepec and the lead/lag differences in the records from Mazatlan could indicate an advective δ¹⁵N signal from the denitrification zone of the eastern tropical South Pacific (ETSP), where

denitrification records exhibit patterns different to Greenland timing. The δ^{15}N records from the ETSP denitrification zone off Peru and Chile show patterns similar to records from Antarctica (De Pol-Holz et al., 2006; Martinez et al., 2006; Robinson et al., 2007), where the δ^{15}N enrichments match Antarctica warm events (e.g. A1 and A2), whereas δ^{15}N depletions match the cold events (e.g. Antarctic Cold Reversal). Therefore, we can suggest that the ETNP denitrification zone has a counterpart in the ETSP, where δ^{15}N variations follow SH timing. This relationship is analogous to the inter-hemispheric asynchrony recorded by Greenland and Antarctica records (Blunier and Brook, 2001), hence meaning that the onset of increased denitrification started earlier in the ETSP relative to the ETNP.

The advection of partially denitrified heavy δ^{15}N nitrate across the equator up to the ETNP could influence the δ^{15}N record from the Gulf of Tehuantepec, producing a mixture of NH and SH timing. This could have a more subtle influence in the Mazatlan margin, producing the apparent lead in δ^{15}N excursions over the organic carbon record.

In previous studies, the SH character of the ETSP δ^{15}N records has been attributed to a change in the supply of oxygen through enhanced ventilation rates and cooling of the high-latitude surface, both proposed as critical factors to reduce suboxia and denitrification (Galbraith et al., 2004; Meissner et al., 2005; Robinson et al., 2007). In the SE Pacific, the changes of the δ^{15}N greatly depend on the supply of oxygen by the Peru Undercurrent (PUC) and the preformed nutrient content of the Sub-Antarctic Mode Water (SAMW); which are fed into the Equatorial Undercurrent (EUC) (Tsuchiya and Talley, 1996, 1998). Hence, following the modern description of equatorial Pacific circulation, and assuming that the oceanic circulation in the glacial Pacific transported water from the South Pacific up north, we can explain why a leading δ^{15}N signal of heavy nitrate is found in the cores from Mazatlan and Tehuantepec.

In the modern ocean, as the EUC approaches Galapagos ($\sim$ 90°W), it splits into two main branches (Figure 2.2): (1) one that approaches South America as an undercurrent and turns south to become part of both the PUC and the PCCC (Peru-Chile Countercurrent) (Strub et al., 1998). (2) The second branch, however, breaks into many filaments whose structure and timescales remain poorly understood, but essentially feed the South Equatorial Current (SEC) (Kessler, 2006; Wyrtki, 1966) and probably the Tsuchiya jets (i.e. NSSCC and SSSCC).

Off Peru and Chile, the poleward flow of the PUC and PCCC has an equatorward counterpart, the Peru-Chile Current (PCC) (Wyrtki, 1966). The nutritive PCC is occasionally divided into an oceanic and a coastal branch, separated by the PCCC when the equatorward flow is intensified by the surface coastal jet (upwelling) in summer (austral winter) (Strub et al., 1998). When the equatorward flow of the PCC is intensified, it can extend as deep as 900 m, and be found 40-100 km offshore (Strub et al., 1998). As moving north, the PCC merges into the SEC and the large-scale circulation of the equatorial Pacific (Figure 2.2).
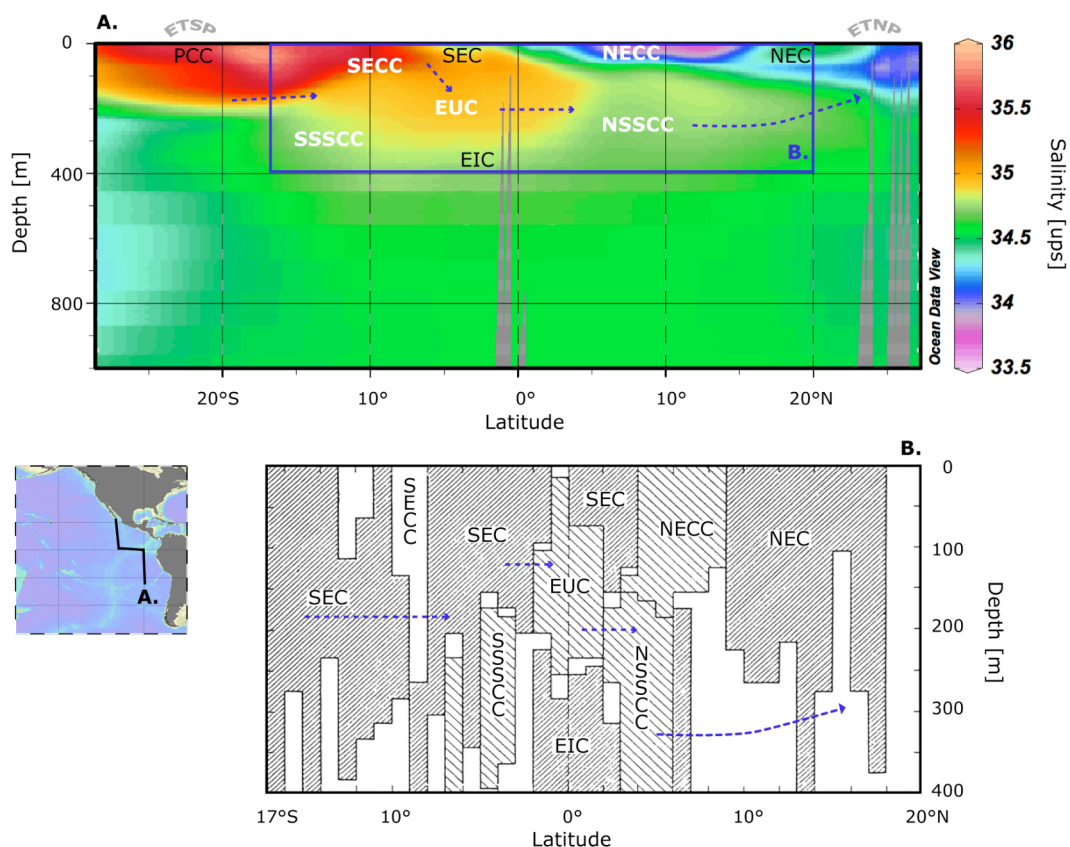
Figure 2-8 Schematic pathway proposed to explained the advection of heavy δ¹⁵N signal from the ETSP (eastern tropical North Pacific) to the ETNP (eastern tropical South Pacific) (blue dotted arrows). (A) Salinity [ups] in the water column of the eastern tropical Pacific, from 30°S to 28°N (see map inset – lower panel) (Key et al., 2004; Schlitzer, 2004). The abbreviated names are surface and subsurface currents in the study area, identified from their salinity values. Name abbreviations in black (white) are currents moving to the west (east). The full names are listed in Figure 2.2 and explained in the main text. (B) Schematic of meridional circulation in the central Pacific (Wyrtki and Kilonsky, 1984) for the first 400 m water depth. The equatorial circulation is described by a set of zonal flows: shaded boxes are currents moving westward, while lined boxes are currents moving eastward.

Therefore, we suggest that the during the glacial period, the *glacial EUC system* could transport partially denitrified nitrate and low oxygen waters form the ETSP into the ETNP at the onset of the major interstadials. This scenario would have both: the effect of elevating the source of heavy $\delta^{15}N$ signatures, and the potential to fuel local denitrification. Moreover, we propose that the potential pathway for the advection of heavy $\delta^{15}N$ signal from the ETSP to the ETNP was through subsurface waters. As shown in Figure 2.8, the gradual mixing between SEC and EUC is a continuous feeding and draining of the outgoing and incoming zonal currents. Thus similar to the modern ocean circulation, the *glacial EUC and SEC* could exchange water in the past, not only with the South Pacific waters, but also with the system of countercurrents travelling north along the ETNP (called NECC and NSSCC).

If a similar system of subsurface currents existed in the past, then the Gulf of Tehuantepec could be particularly sensitive to the influence of advective signals, given its proximity to the southern denitrification zone. Although in a smaller scale, it is also possible that local oceanographic features like the Costa Rica Dome (CRD) and/or the Tehuantepec Bowl (TB) (Figure 2.2) could affect the redistribution and recycling of nutrients and oxygen in the southern part of the ETNP. The study of nitrogen isotope records in the Core MD02-2519 hence suggest two possible mechanisms to explain the relationship between %OC and $\delta^{15}N$: (1) One associated to local changes in denitrification, possibly driven by local productivity and oxygen consumption as shown by the relationship between %OC and $\delta^{15}N$ records. (2) While a second could be associated to the advection of low oxygen and heavy nitrate from the South Pacific, identified by the early transitions in the $\delta^{15}N$ record. The influence of the advective component off Mazatlan is much more subtle relative to the Gulf of Tehuantepec, which could diminished as it was transported north along the coast of Mexico via subsurface countercurrents, in some way, similar to the modern Western Mexican Current (WMC) and the California Undercurrent (CUC) (Kessler, 2006; Tsuchiya and Talley, 1998) (Figure 2.2). Moreover, the decrease of the influence of the SH signal (reduced as it propagates through the CUC) could explain the distinctive NH $\delta^{15}N$ signal recorded in the northernmost regions outside the denitrification zone. As shown in Figure 2.9, the comparison between $\delta^{15}N$ records from localities off California, SBB and Mazatlan shows great similarity and almost synchronous NH pattern over the last 50 ka. Therefore, the record from Mazatlan fits within the picture previously suggested by studies in the NE Pacific (Chang et al., 2008; Emmer and Thunell, 2000; Hendy and Pedersen, 2005; Kienast

et al., 2002), where the ETNP is the source region of the $\delta^{15}N$ signal found off Oregon, California, and as far north as Vancouver.
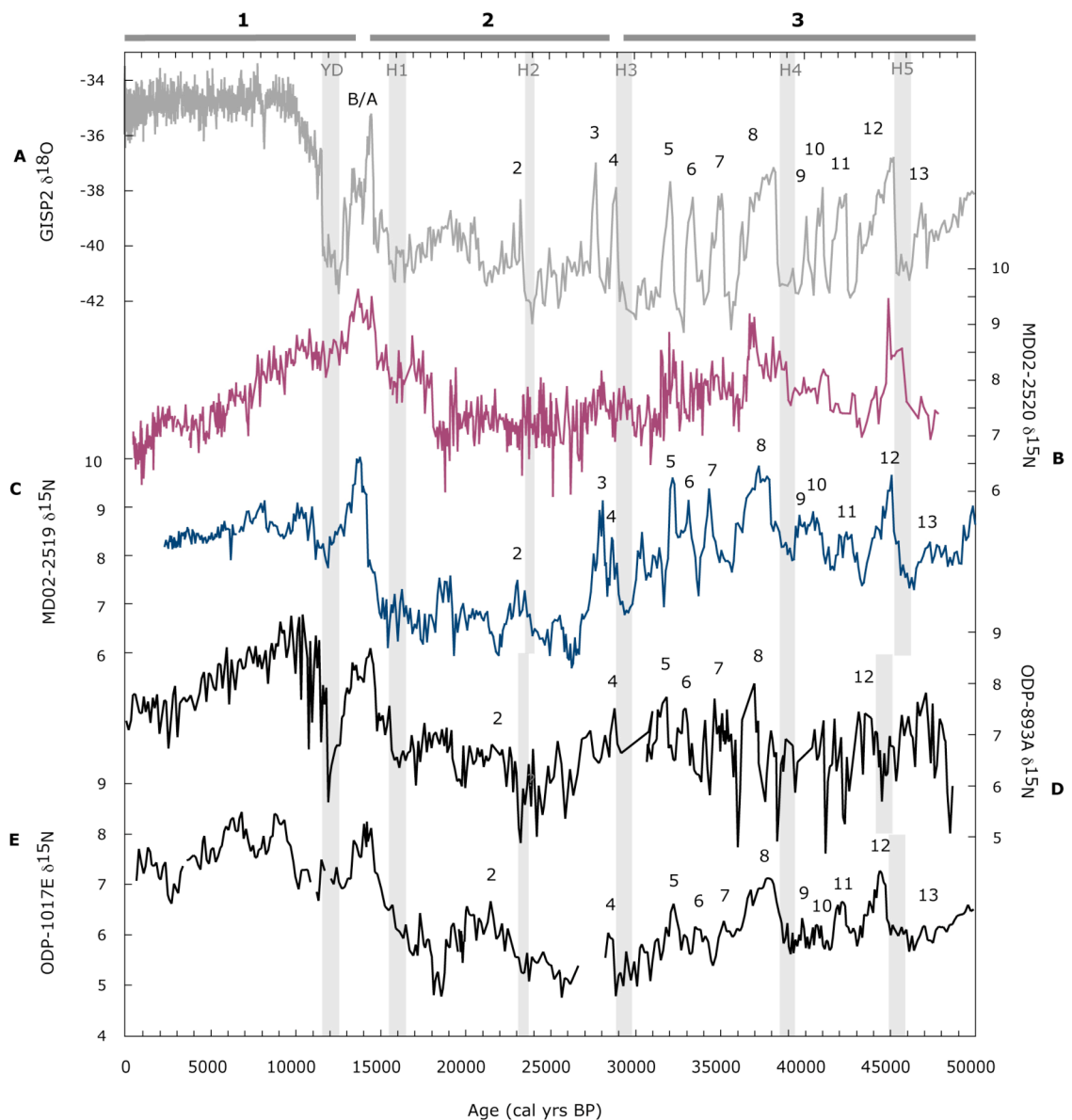
Figure 2-9 Comparison between $\delta^{15}N$ records of cores from the NE Pacific and (A) GISP2 $\delta^{18}O$ record, as reference of NH rapid temperature variability. The band on top shows MIS 1 – 3. The $\delta^{15}N$ records from the ETNP are: (B) MD02-2520 and (C) MD02-2519. The $\delta^{15}N$ records from the northern NE Pacific regions are: (D) Site ODP-893A (Emmer and Thunell, 2000), (E) Site ODP-1017E (Hendy and Pedersen, 2005).

In summary, the reconstruction of $\delta^{15}N$ records from the ETNP document changes in denitrification, in addition to advection of heavy nitrate by subsurface waters at the onset of insterstadials. This is suggested by the $\delta^{15}N$ leading signal over the productivity proxy record

(%OC) found in Core MD02-2519, probably transmitted from the ETSP denitrification zone. This signal could be diluted as they displaced geographically up north and become gradually transformed in the typical NH climatic signal displaying D/O stadial and interstadial events. The δ^{15}N data from the Gulf of Tehuantepec, although different to other records in the NE Pacific, testifies the time differences of denitrification changes between hemispheres, and highlights that the δ^{15}N variations in the southern edge of the ETNP are not solely controlled by productivity, but also sensible to the oceanic advection of oxygen and nitrate.

2.5 Conclusions

The nitrogen isotope records from the ETNP show sedimentary δ^{15}N variations at glacial-interglacial and millennial timescale resolution. Lower δ^{15}N values are generally observed during glacial and stadial periods, but higher during interglacials and interstadials. The δ^{15}N record from the northern part of the ETNP (Mazatlan) exhibits timing and features similar to temperature variations in Greenland, with characteristic of NH timing. Conversely, the core from the southern part of the ETNP (Tehuantepec) shows mixed signatures between NH and SH timing, with amplitude variations more similar to Antarctica than to Greenland δ^{18}O records.

The Core MD02-2519 from Mazatlan reflects the influence of two mechanisms. One related to changes in paleoproductivity, based on the relationship between the %OC and the δ^{15}N records, suggesting reduction in upwelling and denitrification off NW Mexico during the colder climatic periods, but an increase during warm periods. The second is linked to the advection of heavy nitrate from the south, possibly from the ETSP, as the δ^{15}N record leads the interstadial onsets over the productivity proxy. The Core MD02-2520 from the Gulf of Tehuantepec was particularly sensitive to the influence of such an advective signal given its proximity to the southern denitrification zone, and because the heavy δ^{15}N signal is stronger in Tehuantepec than Mazatlan. The potential pathway for the advection of heavy nitrate was through equatorial subsurface-currents. The heavy δ^{15}N signal was diluted northward and transformed into the typical NH signal, as documented by the δ^{15}N records outside the denitrification zone (e.g. California, Oregon and Vancouver). Thus, we support the hypothesis that the ETNP is the source of the sedimentary δ^{15}N signal in the NE Pacific; and highlight the role played by the subsurface waters to transmit rapid climatic signals between high and low latitudes.
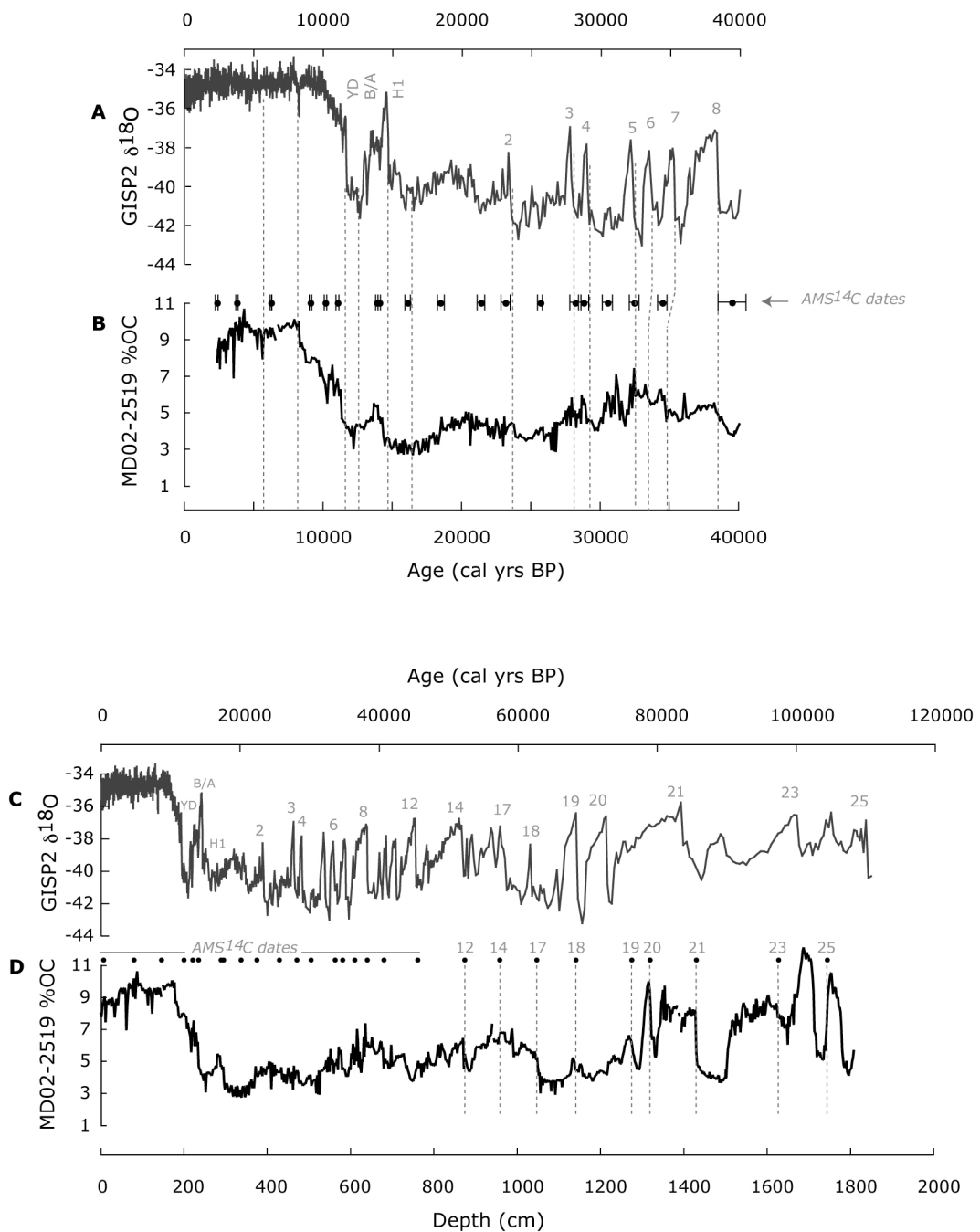
Annexed Figure 2a – Age model construction of the Core MD02-2519 (see Chapter 1). Upper plot spans the last 40 ka BP: (A) δ¹⁸O GISP2 record (Grootes and Stuiver, 1997) is shown for reference to compare with (B) %OC record of MD02-2519. Dots with error bars are the AMS ¹⁴C dates listed on Table 2.1. Lower plot span the last 120 ka BP: (C) GISP2 δ¹⁸O record vs. time. (D) %OC record MD02-2519 (Mazatlan) vs. depth; dotted lines show the position of the age control points used to construct the final chronology.
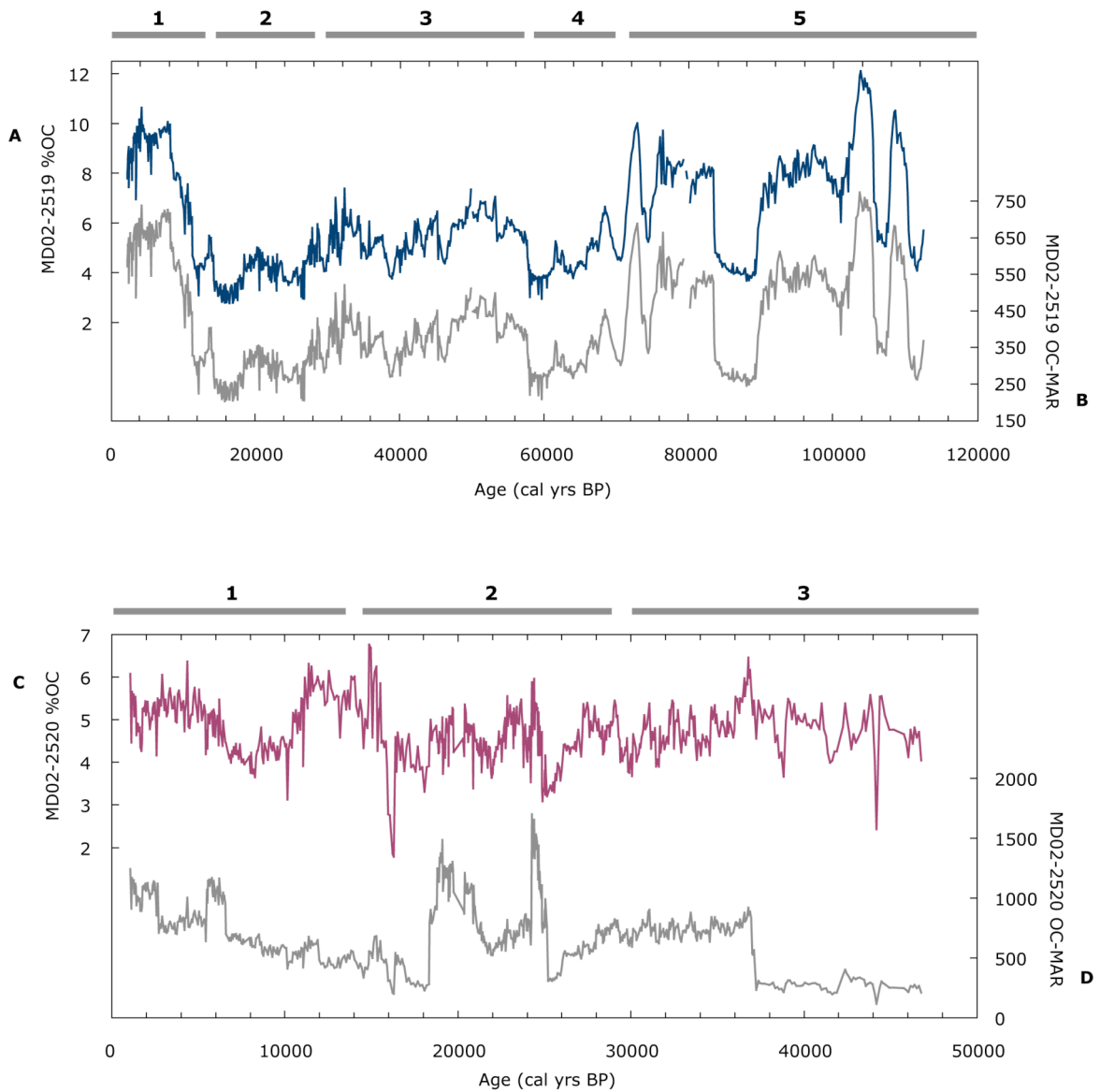
Annexed Figure 2b - Comparison of %OC records to the calculated OC-MAR of cores MD02-2519 (A and B) for the last 120 ka; and MD02-2520 (C and D) for the last 50 ka.

Chapter 3

Influences of circulation and iron input in the opal production of the Eastern Tropical Pacific

3.1   Introduction

The analyses of ancient air-bubbles trapped in ice-cores reveal that the atmospheric CO_2 (pCO_2) concentration rose from ~ 180 to 280 ppmv during the last glacial – interglacial (G-IG) transition (Archer et al., 2000a; Archer et al., 2000b; Petit et al., 1999). The cause of these changes in CO_2 concentration, however, remains unresolved. Variations in the magnitude and nature of the marine productivity have the capability to control pCO_2 at G-IG timescales through the *biological pump* of carbon (Berger and Wefer, 1991; Broecker et al., 1992). The removal of dissolved carbon from the surface ocean by photosynthetic organisms and its transport to the deep layers by settling particles might contribute to the marine uptake of CO_2 from the atmosphere, resulting in the atmospheric drawdown of CO_2 by storing C in the ocean. Ocean productivity controls the partitioning of CO_2 between the deep sea and the mixed layer by means of sinking particulate organic carbon (POC) (dead tissues and fecal pellets) and inorganic material (such as calcium carbonate), which are isolated from the atmosphere (Archer et al., 2000b; Fasham, 2003).

Modelling works indicate that a 40% increase in the *rain rate ratio* of carbon (the flux of POC/$CaCO_3$ to the ocean interior) could explain the ~80 ppmv decrease in pCO_2 during the Last Glacial Maximum (LGM) (Archer and Maierreimer, 1994; Ridgwell et al., 2002). Although such a severe change would require a drastic ecological shift in favour of non-calcareous phytoplankton during glacial periods (Archer et al., 2000a). The s*ilicate switch hypothesis* (Ridgwell et al., 2002) explains that an increase in the silicic acid availability ($Si(OH)_4$) could permit siliceous diatoms to further "out compete" smaller and more tightly grazing-controlled phytoplankton species (coccolithophorids) for limiting nutrients such as nitrate (NO_3^-) and iron (Fe). This hypothesis stems from the modern observation that in large parts of the ocean the production of siliceous phytoplankton is limited by the availability of silicic acid (Brzezinski and Nelson, 1996). Decreasing the population of coccolithophorids by increasing $Si(OH)_4$ availability to diatoms would reduce

the deep ocean flux of $CaCO_3$ relative to organic carbon (OC), increasing the rain rate ratio. Hence, the reduced alkalinity gradient between surface and deep ocean (resulting from the increase in rain rate ratio), would have the potential to lower PCO_2 in the surface ocean and ultimately, the atmospheric pCO_2 (Dymond and Lyle, 1985; Sigman and Boyle, 2000). Moreover, the model of silica dominated primary production is attractive because the diatom frustules can transfer carbon to the deep ocean more efficiently than pico- and nanoplankton which are more prone to grazing pressure (Ganeshram, 2002). Several mechanisms have been proposed to increase the glacial availability of $Si(OH)_4$ for biological uptake in the surface ocean: changes in dust flux (Harrison, 2000), continental rock weathering (Dymond and Lyle, 1985), and/or a decrease in the rates of Si removal by opal burial on continental shelves (Ridgwell et al., 2002).

Alternatively, the *Silicic Acid Leakage Hypothesis* (SALH) (Brzezinski et al., 2002) put forward the possibility that rather than a whole-ocean change in $Si(OH)_4$ inventory, a meridional redistribution of nutrients could have promoted diatom production in the low latitudes. The so-called High Nitrate Low Chlorophyll (HNLC) regions, where biological production is subject to severe Fe limitation, are also important areas of opal burial and Si sink in the ocean (e.g. the Southern Ocean). The latter is at least partly attributed to the production of heavily silicified diatom frustules under the constraint of Fe limitation. The SALH therefore suggests, that enhanced dust deposition over the Southern Ocean during the glacial might decrease the relative utilisation of $Si(OH)_4$ compared to NO_3^- by diatoms, and result in an equator-ward transport of *unutilised* $Si(OH)_4$. This may benefit the subtropics, which today receive insufficient supply of silicic acid and limits diatom growth.

Modern Fe-enrichment experiments and modelling studies support the SALH (Mosseri et al., 2008; Takeda et al., 2006). Under Fe-replete conditions during the glacial, the diatom uptake of Si:N could be significantly reduced south of the Polar Front from Si:N ratios of ~ 4 to Si:N of ~ 1 (Takeda, 1998) due to reduced silicification of diatom frustules. The outcome of Fe fertilisation would be the relative depletion of NO_3 leaving a surplus of $Si(OH)_4$ in the surface waters that could be transported to the tropics (Brzezinski et al., 2002). Modelling of the SALH predicts that diatom production in the entire equatorial Pacific would benefit from additional silicic acid supply transported by intermediate waters sourced in the Southern Ocean (Matsumoto et al., 2002). Owing to this $Si(OH)_4$ supply, it is expected that opal burial should have been greater during the glacial than during the

Holocene. In this way, the SALH links the "glacial source of nutritive waters" (i.e. the Southern Ocean) with the most feasible "glacial sink" of carbon, the equatorial Pacific.

However, data from the Pacific Ocean are sparse and equivocal. Evidence is lacking for a uniform increase in opal production and burial in the tropical oceans during the last glacial period as predicted by SALH (Kienast et al., 2006; Moore et al., 2004; Richaud et al., 2007). The reconstruction of biogenic fluxes from cores in the eastern equatorial Pacific (EEP) (Bradtmiller et al., 2006; Higginson and Altabet, 2004; Kienast et al., 2006; Richaud et al., 2007) has not confirmed the predictions of high opal accumulation in the EEP during the last glacial period (i.e. Marine Isotope Stages (MIS) 2 to 4). In fact, opal contents and accumulation declined in the EEP during glacial periods (Bradtmiller et al., 2006), which has raised questions about the enhanced equator-ward silicic acid supply from the Southern Ocean (Brzezinski et al., 2002). On the other hand, the pattern predicted by the SALH can be seen along the coastal upwelling off Peru and Chile (24°S and 33°S) (Mohtadi and Hebbeln, 2004), where opal accumulation is higher during the last glacial than during the Holocene.

A recent study has provided an explanation for the apparent lack of response in the EEP to silicic acid leakage during the last glacial period (Pichevin et al., 2009). Like the Southern Ocean, the modern EEP is HNLC. Therefore enhanced glacial Fe inputs (McGee et al., 2007; Winckler et al., 2008) can reduce Si-utilisation and silicification of diatoms in the EEP, resulting in reduced opal production and burial despite any potential increase in $Si(OH)_4$ availability through leakage from higher latitudes. Such inference is consistent with Si-isotopes signatures held in diatom frustules during glacial periods, showing the presence of excess silicic acid in the glacial EEP (Pichevin et al., 2009). Importantly, this study broadens the silicic acid leakage hypothesis, where modern HNLC regions of both high and low latitudes conserve silicic acid during diatom growth under increased Fe availability, and act as a net additional source of silicic acid to adjoining regions (Pichevin et al., 2009). Therefore, it is important to evaluate such a scenario during the glacial period because this additional source of silicic acid could have effectively reduced the limitation of Si during diatom growth, increasing the rain rate ratios and pCO_2 drawdown.

In this chapter, we explore the possibility of increased silicic acid supply in the eastern tropical North Pacific (ETNP) through the reconstruction of opal contents and Si:C and Si:N ratios during the last glacial-interglacial cycle. The reconstructions of 3 opal (wt %)

records from the ETNP are presented at glacial-interglacial timescale and, for first time, at millennial timescales over the last 120 ka.

3.2   Materials and Methods

3.2.1   Core location

Three marine sediment cores retrieved with a Calypso piston corer during the MONA Cruise 2002 (Beaufort, 2002) are studied in this chapter. They were collected from the eastern tropical North Pacific (ETNP) (Figure 3.1), a region with intense seasonal upwelling and high productivity, very much influenced by nutritive waters from equatorial origin (Kessler, 2006). The cores are located within an area of denitrification (N-deficit at the subsurface of 26.5 isopycnal), and general conditions of insufficient supply of silicate (SiO_2) (i.e. Si-limited) (Moore et al., 2004; Pennington et al., 2006) (Figure 3.1). The Core MD02-2519 was collected off Mazatlan, NW Mexico (Lat. 22° 30.89'N; Long. 106° 39.00'W; 955 m water depth); the Core MD02-2520 from the Gulf of Tehuantepec, Mexico (Lat. 15° 40.14'N; Long. 95° 18.00'W; 712 m water depth); and the Core MD02-2524 from the Nicaragua Basin (Lat. 12° 00. 55'N; Long. 87° 54. 83'W; 863 m water depth). The sediments of the cores are silty-clays, olive-grey to dark olive-grey in colour. They are mostly laminated but interrupted by few bioturbated intervals (*see* Appendix A). Minor lithologic components in these cores include layers and lenses of volcanic ashes. In addition, the sediments of Core MD02-2524 show oblique stratification and sandy layers with graded bedding in the interval between 320 – 645 cm core depth, possibly caused by a slump. Thus a depth correction of 325 cm was applied to this interval.

3.2.2   Analytical methods

All geochemical analyses were performed in specialised laboratories in the School of Geosciences, the University of Edinburgh. After sub-sampling the sediments, the samples were freeze-died and ground in an agate mortar to homogenize them prior to processing. The samples selected for C-N analyses were decalcified with HCl (5%) on a hot plate at 70°C. The percentage of organic C and N were determined using a C-N Elemental Analyser (CE Instruments NA2500) coupled to a CG PRISMII Mass Spectrometer. Elemental %C and %N were determined at 1-2 cm resolution, but in this chapter we only present the C-N samples associated with opal data.
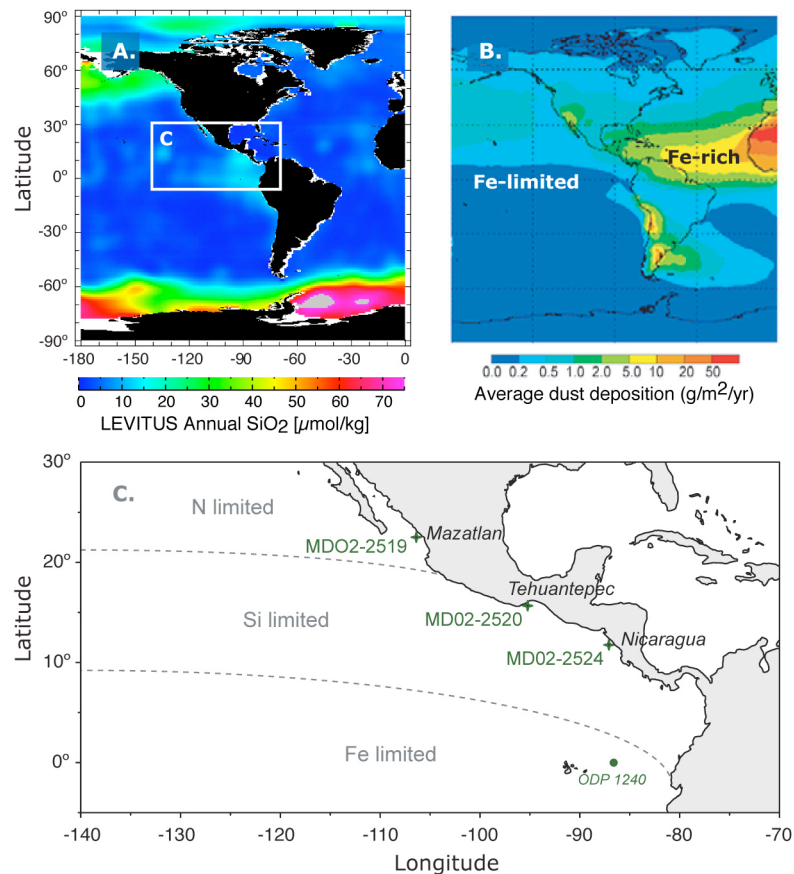
Figure 3-1 Study area and location of the cores. (A) [SiO$_2$] at 50 m water depth (Levitus et al., 1994). (B) Average dust deposition in the modern ocean showing areas of Fe-limitation and Fe-rich conditions (Baker and Jickells, 2006). (C) Location of ETNP cores from Mazatlan (MD02-2519), the Gulf of Tehuantepec (MD02-2520) and Nicaragua (MD02-2524). The EEP Core ODP-1240 (Pichevin et al., 2009) is located north of the Cornegie Ridge, Panama Basin (0° 01.31'N; 86° 27.76'W; 2921 m water depth). Dotted lines show areas of surface N, Si and Fe limitation in the eastern Pacific (Moore et al., 2004).

Biogenic Silica (Si$_{OPAL}$) determinations were done at 5 to 10 cm resolution using molybdate-blue spectrophotometry after alkaline extraction (i.e using a 2N Na$_2$CO$_3$ solution at 85° C for 3 hours) following the method by Mortlock and Froelich (1989). The opal (wt %) was calculated with the equation: *% opal = Si$_{OPAL}$ X 2.4*; where 2.4 is the conversion factor assuming that most of the diatomaceous silica (younger than 30 Ma) displays a relatively constant water mass of about 10% (formula: SiO$_2$ · 0.4 H$_2$O) (Mortlock and Froelich, 1989). Replicate opal measurements confirm the reproducibility and accuracy of these determinations. Two internal sediment standards (*a* and *b*) from two sediment cores (collected off Mazatlan and the Gulf of California) were routinely analysed to determine precision and accuracy between runs. *Standard a* is the sample 0 – 1 cm of the Core MD02-

2519 (n = 35; max = 4.39%, min = 3.10%; 1σ std dev. = 0.35%). *Standard b* is a diatom-mud sample from the Gulf of California (n = 35; max = 40.14%, min = 32.10%; 1σ std dev. = 2.33%).

To verify that the opal records of the cores MD02-2420 and MD02-2524 have not being biased by dilution of Si terrigenous, the opal/Aluminium ratios were calculated from existing Al data (by S. Francavilla (*unpublished data*) and Pichevin *et al.* (2010), respectively). The normalisation of the opal (wt %) to Al (wt %) is shown in Figure 3.2, which confirms that the silica present in the sediments is of biogenic origin and above crustal ratios of Si/Al (i.e. assuming that the aluminium is entirely associated with the terrigenous fraction). To calculate the Si_{OPAL}:C and Si_{OPAL}:N ratios (hereinafter Si:C and Si:N), the elemental composition of organic C and N (wt %) was transformed to molar ratios.

3.2.3 Age Controls

The age models of the cores are mostly based on accelerator mass spectrometry (AMS) ^{14}C dates (< 42 cal ka BP). In older sections (> 45 cal ka BP), the timescale of well-known δ^{18}O ice-core records was used. The final chronologies were completed by linear interpolation between the age control points.

The AMS ^{14}C dates were determined at the NERC Radiocarbon Laboratory, East Kilbride, UK. The AMS ^{14}C dates were obtained from samples of ~ 5 mg of organic carbon (present in ~ 15 – 25 mg of bulk sediment). The chronologies of the cores MD02-2519, MD02-2520 and MD02-2524 are based on 19, 28 and 17 AMS ^{14}C dates respectively listed in Table 3.1. All AMS ^{14}C were converted to calendar years BP using the online version CALIB 5.0.2 for marine samples (Stuiver, 2005). The local reservoir corrections (ΔR) correspond to 203 ± 48 yrs (MD02-2519), 162 ± 50 yrs (Core MD02-2520) and 281 ± 50 (Core MD02-2524) as reported in the Marine Reservoir Correction Database (Reimer and Reimer, 2001). Samples older than 21,800 ^{14}C yrs were calibrated with the polynomial *equation 2* by Bard *et al.* (2004).

The chronology of the older part of the Core MD02-2519 (> 45 ka) was completed by tuning to the Greenland ice-core record GISP2 (Blunier and Brook, 2001; Grootes and Stuiver, 1997). The age control points were obtained from the correlation between the OC record and the major δ^{18}O GISP2 maxima events. A full description of the age model is

described in *Chapter 1*. The age model for the Core MD02-2520 is entirely based on AMS ^{14}C dates, but the age model of the Core MD02-2524 includes two anchor points tuned to the δ^{18}O-EPICA record, based on the match between records (Pichevin et al., 2010). This approach is similar to that used in *Chapter 1* for the Core MD02-2519, however, the difference resides in the fact that the δ^{15}N record of Core MD02-2524 clearly reflects "Antarctica timing" (Pichevin et al., 2010).

3.2.4   Accumulation Rates

The mass accumulation rates (mg/cm^2/ka) of the biogenic opal were calculated with the formula below (Ganeshram et al., 1995):

*MAR = 2400 (mg/cm^3) * [1 − porosity] * [SR (cm/ka)] * [fraction of OC or Opal]*

 where, 2400 is the assumed grain density and SR is the sedimentation rate between control points. Porosity data were measured on board the ship (Beaufort, 2002). In Figures 3.2 and 3.3, we show the position of the age control points, the average SR and the comparison between %opal and opal-MAR. To avoid SR-artefacts caused by the proximity between age control points (AMS ^{14}C dates) in cores MD02-2520 and MD02-2524, some of the dates listed in Table 3.1 were omitted to calculate the OC- and opal-MAR. As previously noted (on page 68), the sediments of Core MD02-2524 include intervals of rapid sedimentation, interpreted as slumping. These result in spikes of high sedimentation rate that could introduce artefacts into our mass accumulation rate calculations. To avoid this, we omitted one of two AMS ^{14}C control points at each place where ^{14}C dates were spaced by less than 800 years (*see red arrows in* Figure 3.2). Additionally, the last 3000 years of MAR-estimates of the Core MD02-2520 (and the corresponding ^{14}C dates) were intentionally omitted because spurious fractional porosity measurements were found in the dataset. Therefore, the opal-MARs are only used to describe patterns at glacial-interglacial timescale, as they are not adequate for discussions at shorter timescales (i.e. millennial).

Table 3.1

AMS ^{14}C dates: Core MD02-2519

Core depth (cm)	Raw 14C Age (yrs)	error ±	Calibrated Age (yrs BP)*	error 1σ −	+	Notes: material	Calib source
1	2865	73	2365	116	94	OC	1
74	4049	61	3802	79	93	OC	1
140	6050	61	6266	54	72	OC	1
194	8689	64	9114	79	101	OC	1
216	9555	73	10198	82	84	PF	1
230	10272	62	11082	134	94	PF	1
284	12664	53	13911	86	75	OC	1
290	12831	64	14084	84	76	PF	1
332	14173	65	16139	205	193	PF	1
370	15717	84	18475	184	296	OC	1
424	18667	109	21417	278	272	OC	1
466	20091	173	23191	316	346	OC	1
500	21920	153	25713	208	145	OC	1
558	24147	154	28226	399	399	OC	2
576	24690	169	28831	369	369	OC	2
606	26239	216	30548	364	364	OC	2
636	27987	281	32471	349	349	OC	2
676	29852	367	34507	342	342	OC	2
758	35012	749	39522	1015	1015	OC	2

* ΔR = 203 ± 48

AMS ^{14}C dates: Core MD02-2520

Core depth (cm)	Raw 14C Age (yrs)	error ±	Calibrated Age (yrs BP)*	error 1σ −	+	Notes: material	Calib source
1	1063	24	515	48	38	OC	1
129	1658	37	1048	80	70	OC	1
309	3048	36	2645	78	91	OC	1
404	4084	38	3907	92	87	OC	1
534	5246	41	5442	108	91	OC	1
669	6295	43	6564	82	79	OC	1
844	8233	55	8535	109	72	OC	1
969	9480	63	10155	118	94	OC	1
1073	10764	82	11865	184	235	OC	1
1123	11648	86	13007	90	74	OC	1
1173	12662	99	13954	131	105	OC	1
1222	13279	108	14976	206	219	OC	1
1387	14750	133	16947	304	273	OC	1
1442	15588	149	18310	218	253	OC	1
1492	16046	158	18795	108	114	OC	1
1571	16652	172	19255	160	175	OC	1
1797	18589	224	21394	364	430	OC	1
2112	21177	316	24551	482	482	OC	2
2277	21957	349	25422	667	667	OC	2
2475	24387	480	28088	634	634	OC	2
2670	26767	268	30626	343	343	OC	2
2881	28392	803	32319	739	739	OC	2
2981	29807	392	33766	371	371	OC	2
3150	32199	527	36154	964	964	OC	2
3284	32557	1363	37100	1836	1836	OC	2
3329	34607	712	38300	975	975	OC	2
3438	37450	1016	41146	716	716	OC	2
3493	39587	1326	42700	990	990	OC	2

* ΔR = 162 ± 50

AMS ^{14}C dates: Core MD02-2524

Core depth (cm)	Raw 14C Age (yrs)	error ±	Calibrated Age (yrs BP)*	error 1σ −	+	Notes: material	data source
10	3796	37	3679	74	74	OC	1
136	8245	37	8681	124	124	OC	1
175	10051	43	11579	103	103	OC	1
225	11677	50	13027	59	59	OC	1
280	13238	107	15090	176	176	OC	1
371	17588	86	20255	171	171	OC	1
455	18049	208	20757	285	285	OC	1
601	20375	121	23876	252	252	OC	1
641	21270	135	24662	367	367	OC	2
731	23001	167	26583	289	289	OC	2
771	23069	168	26658	285	285	OC	2
821	24707	227	28440	368	368	OC	2
876	25472	227	29260	250	250	OC	2
971	28104	316	32028	739	739	OC	2
990	28756	347	32700	815	815	OC	2
1016	29081	357	33033	621	621	OC	2
1041	29441	373	33400	539	539	OC	2
1166	32106	521	36069	932	932	OC	2
1410	40164	1426	43596	1426	1426	OC	2

* ΔR = 281 ± 50

OC - organic carbon; PF - mixed planktonic species
(1) Stuiver *et al.*, 2005; (2) Bard *et al.*, 2004

Table 3-1 Radiocarbon dates of the cores MD02-2519, MD02-2520 and MD02-2524.
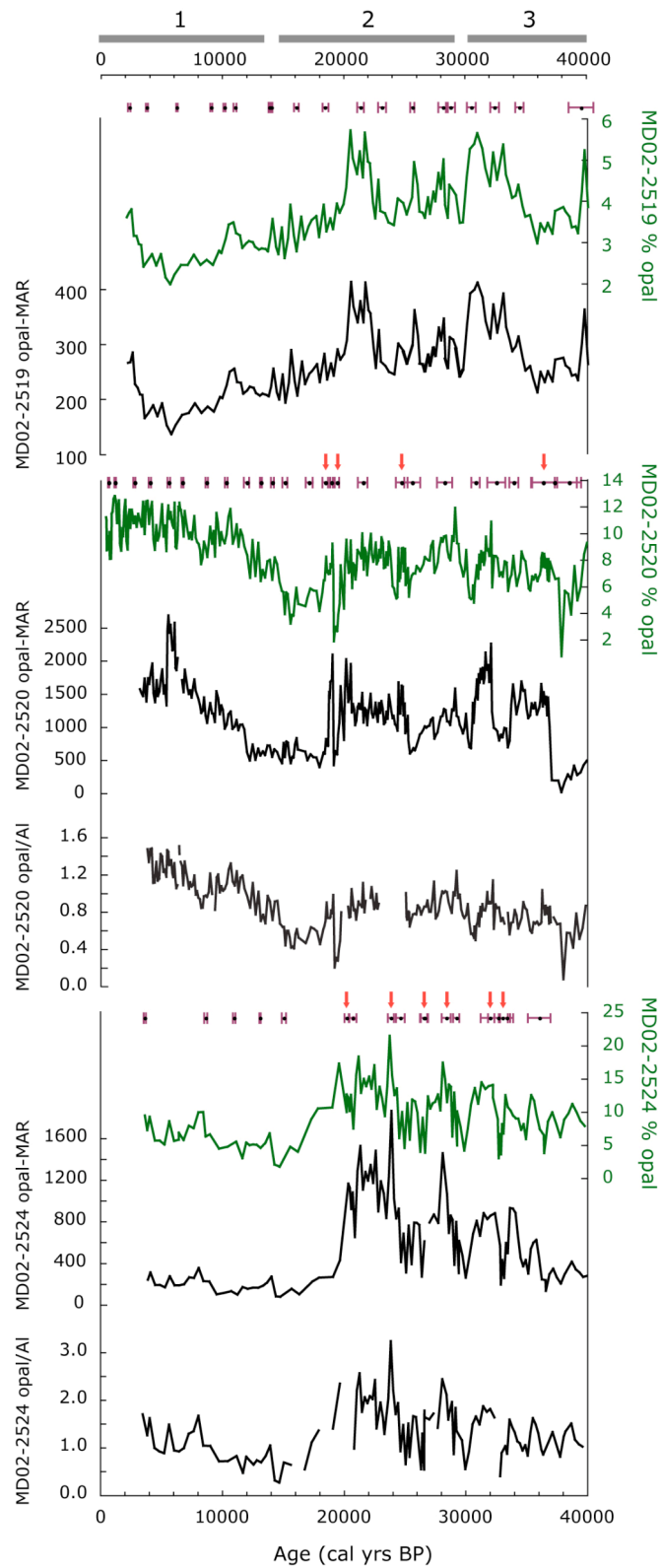
Figure 3-2 Comparisons between opal (wt %), opal-MAR (mg/cm²/ka) and opal/Al ratios for each core from the ETNP. Dots with error bars mark the position of the AMS ¹⁴C dates; the red arrows show ¹⁴C dates that have been omitted to calculate opal-MAR (see methods).

3.3　Results

3.3.1　Opal variations at glacial - interglacial timescales

The opal records (%opal and opal-MAR) from the ETNP show in general, consistent patterns of temporal variability (Figures 3.2 and 3.4). At glacial-interglacial (G-IG) timescales, the opal (wt % and MAR) is higher between 33 – 18 ka, being maximum during LGM (24 – 18 ka). The opal (wt % and MAR) values are relatively lower during interglacials like MIS-5d (120 – 105 ka), MIS-5b (91 – 83 ka) and most of MIS-1 (from 12 to 5 ka). Moderate to low opal values are found during the interglacial MIS-5c (100 – 90 ka), MIS-5a (83 – 74 ka), the glacial MIS-4 and the first half of MIS-3 (71 – 35 ka).

The most pronounced change in %opal and opal-MAR of the cores from the ETNP is the drastic decline at about 18 ka (Figure 3.2 and 3.4). At the end of the LGM and over Termination I (T1: 17 – 11 ka) the Core MD02-2519 collected off Mazatlan declined from maximum values of 5.7% to minimum values of 2.7% (from 411 to 204 mg/cm^2/ka). In the Core MD02-2520 collected from Tehuantepec, the opal changed from 9.2% to 3.2% (from 2100 to 400 mg/cm^2/ka); whereas the Core MD02-2524 from Nicaragua changed from 18% to 1.8% (from 20500 to 100 mg/cm^2/ka). During the Holocene, the cores from Nicaragua and Mazatlan (MD02-2519 and MD02-2524) record low %opal (i.e. < 3.5% and < 9%, respectively). Such low Holocene values have been also reported in the Gulf of California (Douglas et al., 2007), thus the trend towards low opal contents during the Holocene relative to the glacial seems to be common in this area. However, the core collected from the Gulf of Tehuantepec (MD02-2520) is an exception to this general assessment. It will be discussed separately in *section 3.4.3* (page 83) and so it is not shown in Figure 3.5.

In Figure 3.5 we shown G-IG comparisons between opal records in the ETNP and the EEP. In general, the record closer to the equatorial region (i.e. Nicaragua) has higher opal values during LGM (interval around 21 ka) than the record farther north (i.e. Mazatlan). In contrast to records from the ETNP, the Core ODP-1240 from the EEP (Pichevin et al., 2009) exhibits opal minimum during LGM and a gradual increase towards TI. Published records of opal-MARs and opal fluxes in other sites from the EEP support this observation, whereas those in the ETSP show a similar trend than ETNP opal records (Bradtmiller et al., 2006; Kienast et al., 2006; Mohtadi and Hebbeln, 2004).

The pattern of the Si:C and Si:N molar ratios is also largely consistent between 33 and 11 ka in the records from the ETNP, and comparable to the variations in %opal (Figure 3.6 and Table 3.2). Cores MD02-2519 and MD-2524 display lower Si:C and Si:N molar ratios during the Holocene and relatively high values at 33 - 18 ka. Core MD02-2520 is a slight exception because it records lower Si:C and Si:N during TI, and shows higher ratios during the Holocene than during the glacial. All the records, however, show moderate Si:C and Si:N molar ratios during older intervals of MIS-3 and MIS-4 (*not shown*); along with Si:C and Si:N molar ratios with 2.4 to 2.8–folds change from LGM to TI.
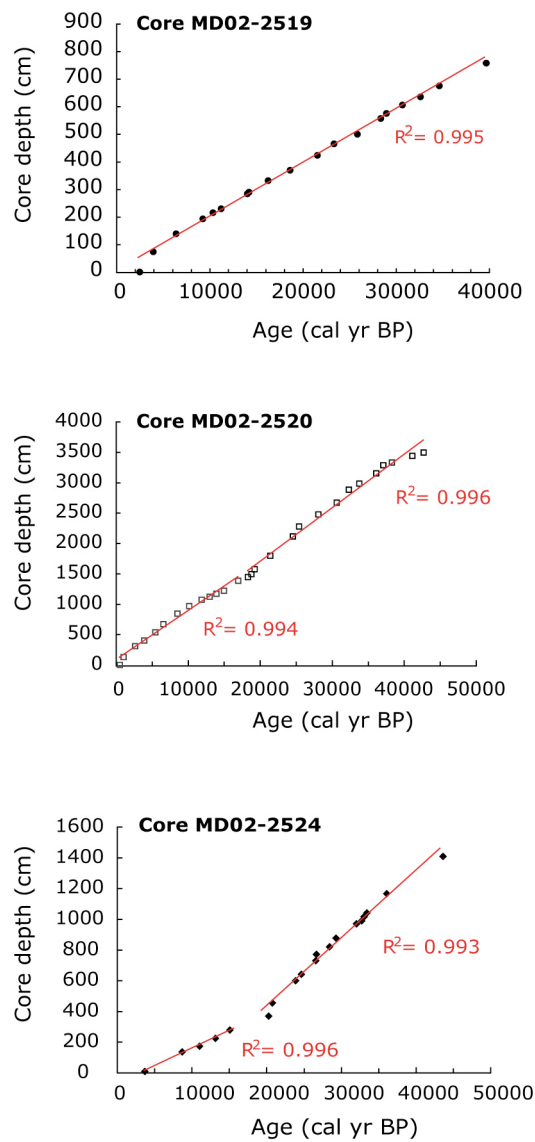
Figure 3-3 Depth vs. AMS ^{14}C dates for each core from the ETNP (see Table 3.1 for full list of radiocarbon dates).
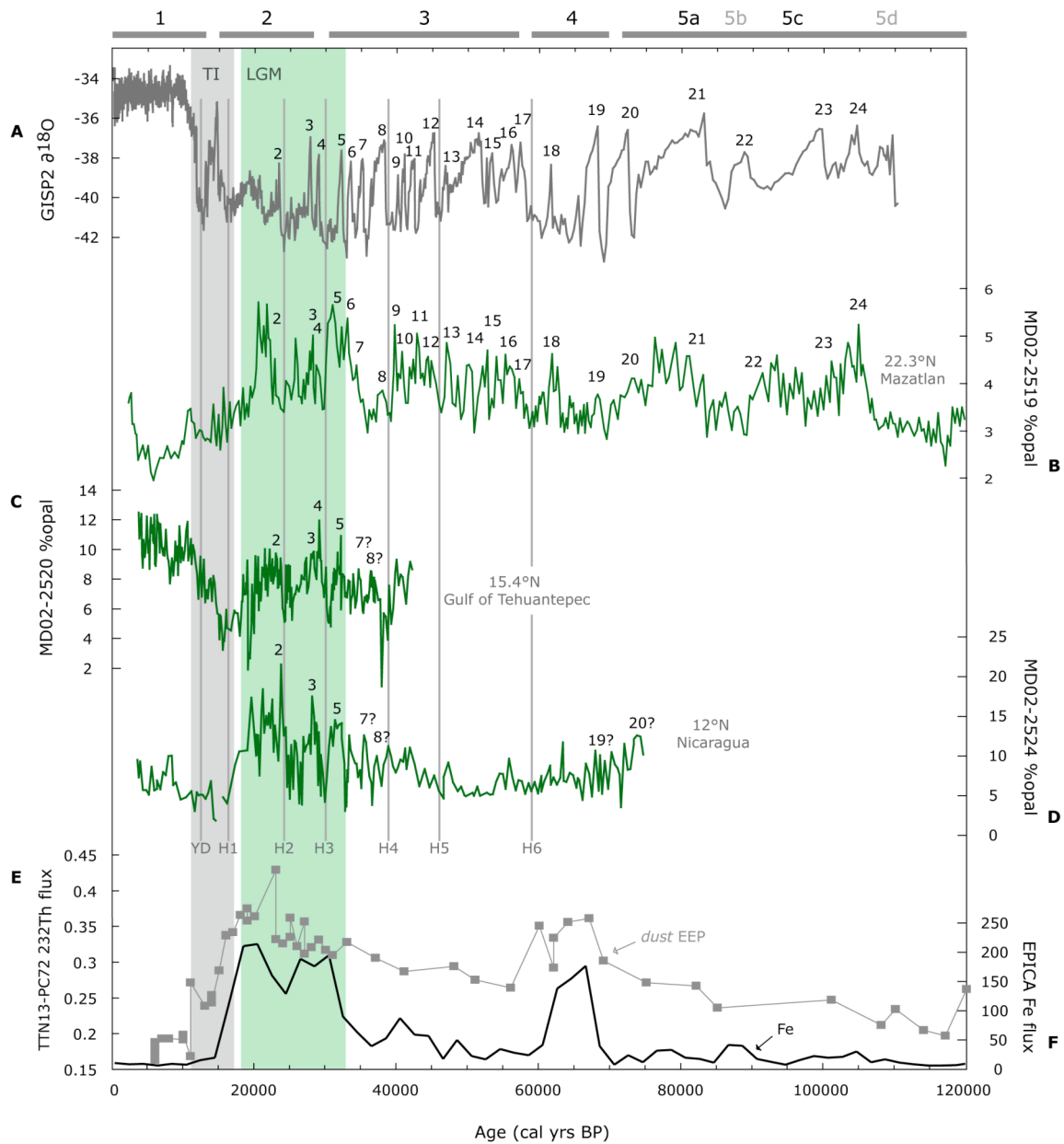
Figure 3-4 ETNP Opal (wt %) records between 0 - 120 cal ka BP. (A) δ¹⁸O GISP2 record (Grootes and Stuiver, 1997) - interstadial warm events (D/O) are marked with numbers. (B) Core MD02-2519 collected off Mazatlan; (C) Core MD02-2520 collected off Tehuantepec; (D) Core MD02-2524 collected from Nicaragua. (E) ²³²Thorium flux (µg/cm²/ka) of Core TTN13-PC72 from the central equatorial Pacific, used as a proxy of dust flux (Winckler et al., 2008); (F) EPICA Fe flux (µg/m²/yr; EDC2 timescale) (Wolff, 2006). Numbers on top show MIS-1 to 5; The pale-green band highlight the period of opal maximum between 33 – 18 ka, while the grey band the period of opal minimum between 17 – 11 ka. T1 and LGM stand for Termination 1 and Last Glacial Maximum, respectively. YD – Younger Dryas and Heinrich events 1 - 6 are also shown with grey vertical lines.
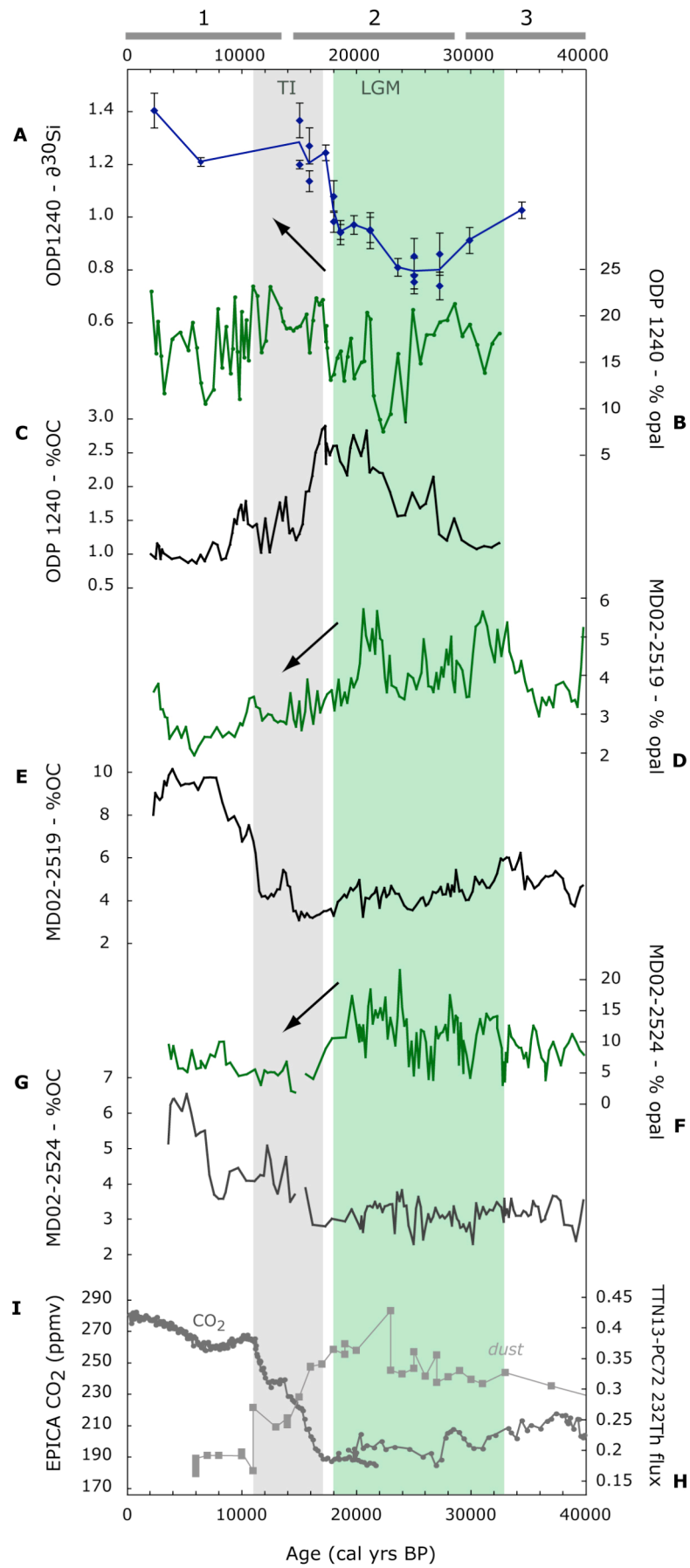
Figure 3-5 Opal (green) and organic carbon (black) records from cores in the EEP and ETNP plotted versus calendar ages BP. Numbers on top are MIS 1 to 3. Core ODP 1240 records of (A) $\delta^{30}Si$ of diatoms, (B) % opal and (C) % organic carbon (Pichevin et al., 2009). Core MD02-2519 records of (D) % opal and (E) % organic carbon. Core MD02-2524 records of (F) % opal; (G) % organic carbon. Record from EPICA Dome C of (H) ^{232}Th flux ($\mu g/cm^2/ka$) in the equatorial Pacific used as a proxy of dust (Winckler et al., 2008); (I) atmospheric CO_2 concentration (ppmv) (Ahn and Brook, 2008; Monnin et al., 2001). The pale-green band highlights the period of opal maximum between 33 – 18 ka, while the grey band the period of opal minimum between 17 – 11 ka. Black arrows show the trend of the glacial to interglacial opal change.

3.3.2   Opal variations at millennial time scale

The reconstruction of 3 opal (wt %) records is shown at millennial scale resolution in Figure 3.4, spanning 120 ka BP. In general, the ETNP records show rapid changes during the glacial period that resembles some of the stadial-interstadial events like in ice-core records from Greenland. Lower %opal values are identified over stadial events, but relatively higher values during most of the major interstadial events. In addition, the longest record (i.e. Core MD02-2519) shows an abrupt change between MIS-5d and MIS-5c (Figure 3.4). On the other hand, such millennial scale variability disappears in the Si:C and Si:N records (Figure 3.6). The quick variations in the ratios make difficult to establish clear patterns and correlations between records during interstadials, however, during some of the major stadials (e.g. Heinrich events) the ratios remain lower.

3.4   Discussion

3.4.1   The Opal proxy record

The biogenic silica is measured in this study as the opal concentration (wt %) in the sediments, and represents the relative contribution of opal producing organisms (mainly diatoms, but to a lesser extent radiolarians and possibly sponge spicules) to the total sediment (Egge and Aksnes, 1992; Ragueneau et al., 2000). In the continental margins, the opal content in sediments can be influenced by redistribution processes, opal preservation during settling burial and dilution by terrigenous components (DeMaster, 2002; Nelson et al., 2002; Nelson et al., 2001; Ragueneau et al., 2000). Therefore, we should be cautious while interpreting sedimentary opal contents as records of opal production. In this study, we interpret the opal contents in marine records as mainly reflecting water production and fluxes, based on the following observations. In sediments from the continental margin with

shallow water column, the opal dissolution mainly occurs at the sediment surface and during burial, thus the opal preservation normally increases with higher sediment accumulation rates. However, we do not observe such systematic relationship between opal contents and sedimentation rate in our records (Figure 3.2), where the broad glacial-interglacial variations are largely independent of sedimentation rates changes. We observe that in the ETNP opal records, the sedimentation rates are linear (Figure 3.3), thus we exclude opal preservation as a factor of change for the opal content. The Si:C and Si:N ratios broadly follow the pattern of %opal, indicating that dilution by terrigenous inputs is not the key factor influencing these records. This is also supported by the broad agreements between opal-MAR and %opal records with a few exceptions. For instance, the regional increase if opal contents during the last glacial period and its decline starting at ~ 18 ka is evidenced by our 3 records (Figure 3.4). Thus the pattern cannot be simply explained by site specific processes, such as sediment redistribution and focussing, given that these processes are expected to vary with sites. Through this chapter, we then consider the %opal changes in a qualitative sense, as reflecting variations in opal supply to the sediments from the upper water column.

3.4.2 Evidence of excess silicic acid leakage from the EEP during the last glacial

Biogenic records from the EEP show increases in organic carbon burial rates during glacial intervals (*see* Figure 3.5) indicating a more efficient biological pump during glacial periods in contrast to the HNLC condition prevailing today. However, glacial opal accumulation rates are lower, which present a paradox because $Si(OH)_4$ leakage from the Southern Ocean is expected to result in an increase in opal accumulation in the low latitudes (Brzezinski et al., 2002; Matsumoto et al., 2002). The Si-isotope ($\delta^{30}Si$) measurements provide an explanation for the paradoxical decline in opal accumulation during glacial period. The presence of excess unutilised $Si(OH)_4$ is indicated by the lighter $\delta^{30}Si$ values of ~0.95‰ during the glacial intervals (Pichevin et al., 2009). In contrast to Holocene values of ~1.3‰, which indicates more or less complete utilisation of silicic acid and conditions of Si-limitation that prevail in the modern EEP (Dugdale et al., 2002; Moore et al., 2004), The transition from light to heavy values occur at ~18 ka matching the decline in dust accumulation and pCO$_2$. This suggests excess silicic acid in the glacial EEP remained unutilised by siliceous organisms explaining the decline in opal accumulation rates during these periods despite the proposed increase in silicic acid supply (Pichevin et al., 2009). This should have resulted from the decrease in Si:C uptake ratio of diatoms under conditions of

increased Fe availability from enhanced dust inputs. Export of this excess unutilised silicic acid through tropical surface and subsurface circulation, should have enhanced opal production and rain rate ratios in adjoining subtropical regions where $Si(OH)_4$ is a limiting nutrient for diatom growth.
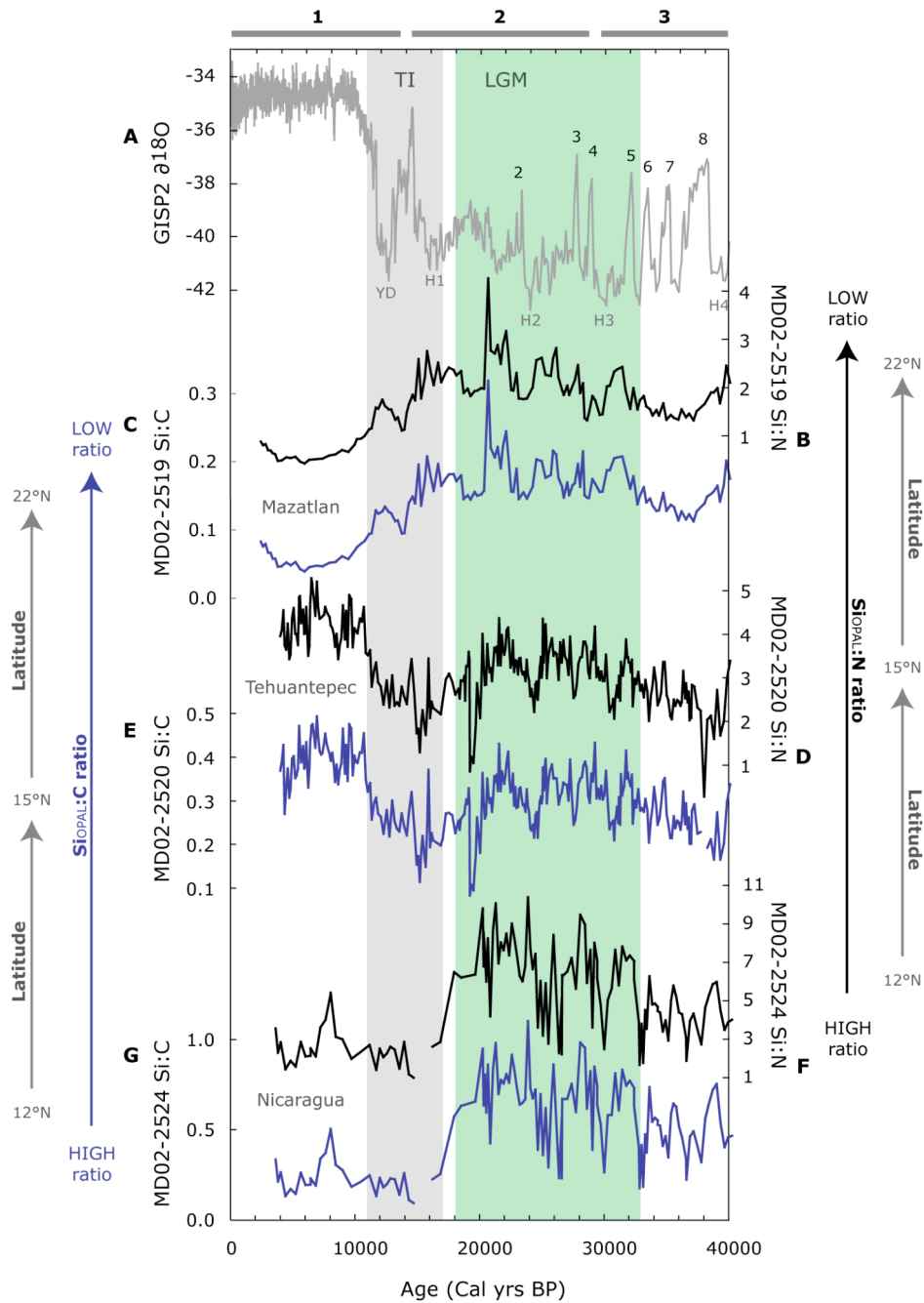
Figure 3-6 Molar Si_{OPAL}:C and Si_{OPAL}:N ratios. (A) $\delta^{18}O$ GISP2 record (used for reference); (B and C) MD02-2519; (D and E) MD02-2520; (F and G) MD02-2524. Arrows indicate the decrease in Si_{OPAL}:C and Si_{OPAL}:N ratio with increase in latitude.

3.4.3   Glacial-interglacial opal variations

The prominent feature of high opal content and accumulation rate during the glacial interval at about 33 - 18 ka, and the pronounced decline in opal content and accumulation rate during TI about 17 - 11 ka (Figure 3.4), are consistently observed in the opal records along the ETNP margin. This feature cannot be explained by local changes in upwelling, since organic carbon and other productivity proxies show low values during the last glacial period (*see Chapter 1*), along with a pronounced increase during interglacials equivalent to warm events recorded in Greenland (Ganeshram and Pedersen, 1998; Hendy and Kennett, 2000; Ortiz et al., 2004). Therefore, the decoupling between opal and the productivity proxy records during the last glacial requires an alternative explanation. The Si:C and Si:N ratios generally follow opal contents with high values during the last glacial and LGM, indicating that opal production (as a proportion of total productivity) increased during this period and subsequently declined during the deglaciation (TI). The organic carbon records show lower levels of C during LGM relative to the Holocene (Figure 3.5), also coincident with lower levels of N (*not shown*). Reduced export of carbon to the sediments has been linked to reduced upwelling during glacials, but the opposite during integlacials (Ganeshram and Pedersen, 1998; Hendy and Kennett, 2000; Ortiz et al., 2004). Hence, because lower C and N contents are consistently found in the cores from the ETNP during glacial times, the high Si:C and Si:N ratios (Table 3.4) cannot be explained by a reduction in total productivity. Instead, the high Si:C and Si:N ratios can be a shift in the type of production between climatic stages, toward the dominance of siliceous producers during the glacial. This could be attributed to higher supply of silicic acid relative to other macro-nutrients to the eastern tropical Pacific (ETP) during the last glacial period, which would also explain the elevated opal contents and sedimentation rates present in these cores (Figure 3.2). In this way, the apparent increase in relative opal production can be linked to enhanced silicic acid supply form the EEP, as suggested by Pichevin et al. (2009).

Continental margins bordering the ETNP are particularly sensitive to additional export of silicic acid during glacial periods. Biological productivity in these margins are Si and/or N limited today (Figure 3.1) although not severely Fe-limited. Fe limitation occurs only transiently at the end of upwelling episodes (Moore et al., 2004; Pennington et al., 2006). This is evident from the rapid depletion of macronutrients by biological utilisation in upwelled waters along the coast. Thus, the supply of additional $Si(OH)_4$ during glacial is expected to increase opal production in this area. The nutrient budgets of the ETP and EEP

are intimately connected by surface and subsurface circulation, hence a change in the nutrient status in one of these regions is expected to impact the other (Toggweiler and Carson, 1995). Thus, we propose that the potential pathway to supply additional $Si(OH)_4$ to the ETNP from the south during the glacial can be through subsurface waters.

Table 3.2
Si:C and Si:N molar ratios

	Si/C	Si/N
MIS-1		
MD02-2519	0.07	0.87
MD02-2520	0.36	3.87
MD02-2524	0.23	2.49
MIS-2		
MD02-2519	0.17	2.20
MD02-2520	0.28	3.02
MD02-2524	0.64	6.38
MIS-3		
MD02-2519	0.14	1.69
MD02-2520	0.28	2.79
MD02-2524	0.48	4.56
MIS-4		
MD02-2519	0.14	1.73
MD02-2524	0.42	4.56
MIS-5		
MD02-2519	0.10	1.30

Table 3-2 Average Si:C and Si:N molar ratios in the cores MD02-2519, MD02-2520 and MD02-2524 during the marine isotope stages (MIS) 1 – 5.

When waters from the South Pacific (South Equatorial Current (SEC) and Peru-Chile Current (PCC)) join the large-scale circulation of the equatorial region (Kessler, 2006; Wyrtki, 1966), they mix gradually with the Equatorial Undercurrent (EUC) and the Tsuchiya jets (i.e. NSSCC and SSSCC) (Tsuchiya and Talley, 1996, 1998). The gradual mixing between the SEC and the EUC is a continuous feeding and draining of outgoing and incoming zonal currents. In this way, the EUC exchanges water with South Pacific and North Pacific currents like the North Equatorial Countercurrent (NECC) and the NSSCC (Tsuchiya and Talley, 1996; Wyrtki, 1966). Thus, the mixing of zonal currents within the EUC can transfer excess nutrients to the surface waters as they travel north via Costa Rica Coastal Current (CRCC) and Western Mexican Current (WMC) (Fiedler and Talley, 2006; Kessler, 2006). In this way, the ETNP margins could be influenced by silicic acid supply from the Southern Ocean as well as the EEP. As a result, the nutrient budgets of the ETP and EEP are intimately connected with each other through surface and subsurface circulation. Hence a change in the nutrient status in one of these regions is expected to impact the other

(Toggweiler and Carson, 1995), where the Mode Waters furnish a pathway for meridional transport of nutrients from the South Pacific to the tropics (Matsumoto et al., 2002).

Additional evidence to support the northward transfer of nutrients from the EEP to the ETNP is found in the Si:C and Si:N ratios as they tend to lower as the latitudinal location of the cores increases. The core from Nicaragua show the highest average of Si:C and Si:N values during the glacial (0.6 and 6.0, respectively), followed by the core from Gulf of Tehuantepec (0.3 and 3.0, respectively) and the northernmost core collected off Mazatlan (0.15 and 2.0, respectively) (Figure 3.6). This suggest that the Si:C and Si:N ratios trace the northward pathway followed by the CRCC, WMC and SSW and the gradual decline in Si export towards the north. Furthermore, this is not restricted to the last glacial period. The longest opal record spanning the last 120 ka (Core MD02-2519) shows that the lowest opal content occurs during the last interglacial (MIS-5d and 5b) are similar to the Holocene. The values recover slightly during intervals younger than 105 ka (Figure 3.4) also followed by the Si:C and Si:N ratios (Table 3.2). Thus, the decrease in silicic acid supply to the ETNP at the end of the glaciations, such as those predicted for last glacial-interglacial transition, may have been a persistent feature during former glacial-interglacial transitions.

Holocene differences between Opal records

During the mid- to late Holocene (< 11 ka), the Core MD02-2520 collected from the Gulf of Tehuantepec shows high opal contents, which differ from the lower values seen in the cores taken off Mazatlan (MD02-2519) and Nicaragua (MD02-2524) (*compare* Figures 3.2 and 3.6). Such difference does not undermine the interpretation that decline excess $Si(OH)_4$ was supplied from HNLC regions during the Holocene. We attribute this unique Holocene feature to local factors that lead to elevated mid- to late Holocene opal contents in the sediments of the Gulf of Tehuantepec. Also note that the elevated Holocene opal (wt %) content match the higher Si:C and Si:N ratios (Figure 3.6) indicating that this may have been the result of increased opal as a proportion of total production, perhaps linked to an additional source of $Si(OH)_4$ established after ~11 ka BP.

Today, the Gulf of Tehuantepec is unique as it experiences extremely high biological production, where two important wind-forcing events of mesoscale variability (i.e. length scale of ~ 10^2 km) occur annually. The most significant wind-driven events (called

Tehuanos) occur during winter-spring, resulting in intense upwelling that supplies large amounts of nutrients to the euphotic zone (Barton et al., 2009; Trasviña et al., 1995), a condition that is common in the eastern boundary currents regimes of the ETP margins. The second event occurs during summer when the cross-isthmus wind-jet induces dipole eddy formation (Trasviña and Barton, 2008) leading nutritive waters from ~100 m depth to reach the photic zone as a result of the cyclonic circulation (Barton et al., 2009; Farber-Lorda et al., 2004). As a consequence, the Gulf of Tehuantepec experiences the highest annual average supply of silicic acid to the euphotic zone (i.e. $[SiO_2] \simeq 42.5 \, \mu M$; mean concentrations between 0-100 m water depth) which is more than double of what other areas in the ETNP receive on annual basis. For example, the annual average $[SiO_2]$ in the coastal boundary current regions are $\simeq 19.7 \, \mu M$ off Mazatlan and $\simeq 16.8 \, \mu M$ in the Gulf of Papagayo (Pennington et al., 2006). In contrast, the annual average of nitrate concentration in the euphotic zone does not show such an anomaly in the Gulf of Tehuantepec. Along the ETNP margin, the nitrate is gradually exhausted northward of the equator as a consequence of denitrification, which consumes nitrate in the upwelling source waters (Moore et al., 2004; Pennington et al., 2006). For example, the annual average $[NO_3^-] \simeq 20.3 \, \mu M$ in the Gulf of Papagayo, $\simeq 18.3 \, \mu M$ in the Gulf of Tehuantepec and $\simeq 14.0 \, \mu M$ off Mazatlan. Thus in the Gulf of Tehuantepec the $[SiO_2]$ to $[NO_3^-]$ ratios of upwelled waters are at least twice as high as other areas in the ETNP, which is attributed to persistent upwelling, resulting in the tapping of water from deeper subsurface layers. This should in turn elevate opal production over total production in this area during the Holocene.

Further, the increase in Si:C and Si:N occur after ~11 ka in the Gulf of Tehuantepec core (Figure 3.6), when the ITCZ was established in its northern-most position (Haug et al., 2001), could be also a factor in the establishment of the modern cyclonic circulation in the Gulf of Tehuantepec favouring the supply of waters with relatively elevated levels of silicic acid during the mid- to late Holocene.

3.4.4 Opal variations at millennial timescales

The reconstructions of 3 opal wt% records are presented at millennial scale resolution in Figure 3.4 spanning ~120 ka. In general, the ETNP records show millennial scale variability during the glacial period that resembles some of the stadial-interstadial events seen in the temperature and greenhouse-gas records from Greenland. Low %opal values are identified during stadial events (in particular H events), and higher values can be

identified during some of the major interstadials. In addition, the longest record (Core MD02-2519) shows abrupt changes between MIS-5d and 5a. Thus, unlike the glacial-interglacial trends, the millennial timescale changes in opal largely follow the variability of the temperature proxy (Figure 3.4). However, these clear millennial scale patterns largely disappear in the Si:C and Si:N records. Hence it appears that the variability in opal records on these time scales is not governed by changes in opal production relative to total production influenced by the leakage of silicic acid from adjacent or distant regions. Instead, this points to changes in upwelling and total production as a cause for the millennial scale productivity pattern. Increase in upwelling induced productivity during interstadials relative to stadial have been previously suggested by several studies using a range of proxies like organic carbon (Hendy et al., 2002; Ortiz et al., 2004). Thus the opal records from the ETNP reflect both, the surplus of silicic acid supply from adjoining regions during glacial periods, and regional upwelling at millennial timescales during the last glacial period.

3.4.5 Implications

The observed trends in opal accumulation/production at glacial-interglacial timescales are consistent with the hypothesis of a leakage of surplus silicic acid from the EEP to the tropical regions (ETSP and ETNP) during the last glacial, due to increased iron supply to the equatorial HNLC region. The glacial increase in diatom accumulation relative to the Holocene in the equatorial Pacific suggest that Si leakage from the EEP (Pichevin et al., 2009) could explain the increase in %opal found in the records from the ETNP. This mechanism has the potential to explain the glacial pattern found in records from the Peru-Chile margin (Mohtadi and Hebbeln, 2004), which resembles the trends we observe off Mexico and Nicaragua. The similarities between both regions suggest that a similar increase in opal production and burial affected occurred through equatorial undercurrents (e.g. EUC system). This is relevant because the combination of more invigorated biological pump in the EEP and the increase in silicic acid supply to the continental margin of the ETP could exert a key role to drawdown pCO2 to glacial levels as previously predicted by the SALH (Brzezinski et al., 2002). Assuming that the biological productivity in the regions was not limited by the availability of iron, silicon or nitrogen, the combined effect of C uptake from the EEP and ETP could help reduce the CO_2 evasion from the ocean by increasing C storage.

3.5   Conclusions

Opal reconstructions in 3 cores from the ETNP show increased opal content and high Si:C and Si:N ratios during LGM, while lower values during the Holocene. The G-IG trend in the opal records from the ETNP is similar to existing records in the ETSP. Both of these regions show high opal accumulation between 33 and 18 ka, including the LGM. This study provides an explanation for this variable pattern by suggesting that the productivity response was different in the severely Fe-limited areas (both HNLC and non-HNLC regions) during the glacial. In the HNLC regions, like the EEP, the $Si(OH)_4$ usage declined during glacials due to reduced $Si(OH)_4$ uptake (relative to N) during diatom growth, as suggested by a recent study (Pichevin et al., 2009) and therefore did not witness a net increase in opal fluxes. However, it was exported to adjoining areas such as the ETNP (this study) and the ETSP benefiting siliceous production during glacial periods, evident by the increase in opal contents and fluxes. If this glacial export of $Si(OH)_4$ and the consequent increase in siliceous production documented in the ETP were to occur more widely, this could have increased the rain rate ratios in the low-latitude ocean contributing to lower the pCO_2 of this period. Currently, the records are too sparse in coverage to fully evaluate this scenario.

More broadly, our study illustrates the complexity in interpreting opal records. Traditionally, the variability in opal records were linked to changes in productivity and upwelling history (e.g. Charles et al., 1991; Rathburn et al., 2001). Millennial time scales changes in the opal records in the ETNP appears to follow such a pattern. However, our study also illustrates that three other factors can affect opal records. First, changes in Si:N uptake ratios of diatoms in response to variability in Fe-availability in HNLC regions, as illustrated by the EEP where opal fluxes were reduced during the glacials in response to increased Fe availability and resulting Si:N uptake by diatoms. Second, changes in the availability of silicic acid relative to other macronutrients, which explains the increase in opal fluxes in the ETNP margins during glacial periods, despite the relative decline in upwelling during this period. Finally, opal burial can also vary with the nature of upwelling tapping waters from various depths resulting in changes in the levels of $Si(OH)_4$ relative to nitrate responding to local climatological factors, as discussed in the case of Gulf of Tehuantepec. All these factors need to be considered in interpreting opal records.

<div align="center">🌍</div>

Chapter 4

Reconstructing water masses variations in the ETNP: evaluating northern and southern components of intermediate circulation

4.1   Introduction

The intermediate waters are prominent features in the subtropical regions of the world ocean roughly centred at depths between 500 - 1000 m. They originate in subpolar regions, well defined in the Pacific Ocean by their salinity minimum (~34.3 - 34.5), namely the North Pacific Intermediate Water (NPIW) and the Antarctic Intermediate Water (AAIW) (Talley, 1999). They have major importance in the global climate as they convey salt, heat and oxygen from poles to tropics (Talley, 1999; You, 2003). But in spite of their global relevance, they remain as intriguing elements of the vast Pacific Ocean. The examination of past intermediate water variability has been limited by the lack of suitable localities with sediments at these depths. Nevertheless, it is recognised that substantial changes in the configuration of Pacific intermediate water masses could act as a significant modulator of atmospheric CO_2 in the Pleistocene (Keigwin, 1998; Lynch-Stieglitz et al., 1994; Marchitto et al., 2007; Mix et al., 1999; Ninnemann and Charles, 1997; van Geen et al., 1996).

Based on evidences from marine cores from the Pacific and the Atlantic, it has been hypothesised that the Southern Ocean (SO) intermediate waters could play a major role in determining the onset of the last deglaciation in the tropics (Ninnemann and Charles, 1997; Spero and Lea, 2002). Given their role as a conveyor of fresher and nutritive waters to the tropical thermocline, the intermediate circulation could gradually promote the breakdown of vertical stratification, increase the surface nutrient content and activate the biological pump (Loubere and Bennett, 2008; Ninnemann and Charles, 1997; Spero and Lea, 2002). Modelling and paleoclimatic studies suggest that waters formed off Antarctica (e.g. intermediate and/or bottom waters) could be more wide spread in the North Pacific during glacial and deglacial periods, possibly exerting a much larger influence relative to the present (Campin, 1999; Keeling, 2007; Ninnemann and Charles, 1997). For instance, evidence is found in the foraminiferal carbon isotope records from subsurface and mid-depths in the equatorial Pacific (Koutavas and Lynch-Stieglitz, 2004; Mix et al., 1991; Pena

et al., 2008; Spero and Lea, 2002), which show a distinct signal of depleted $\delta^{13}C$ values during glacial and deglacial periods. This chemical feature is attributed to SO source waters since such a $\delta^{13}C$ minimum has been found only in areas of the tropical Indo-Pacific, the South Atlantic and the Subantarctic (Loubere and Bennett, 2008; Lynch-Stieglitz et al., 1994; Mix et al., 1991; Ninnemann and Charles, 1997; Spero and Lea, 2002). Although a recent study advocates that incursion of SO waters could occur at intermediate depths in the NE Pacific as far as 23°N off NW Mexico during the deglaciation (Marchitto et al., 2007).

Intermediate water reconstructions in the glacial NE Pacific along the California margin also invoke changes in the formation extent of the NPIW. These studies link the increased ventilation of the Oxygen Minimum Zone (OMZ) during the last glacial (between 60 - 14 ka BP) to enhanced formation of northern sourced intermediate waters (Cannariato et al., 1999; Keigwin, 2002; Stott et al., 2002). In contrast, some studies suggest the northward advection of southern component intermediate waters from subtropical areas during the deglaciation (Keigwin, 2002; Mix et al., 1999) and the major interstadial events (Hendy and Kennett, 2003). As a result, the Late Quaternary history of intermediate water circulation in eastern tropical North Pacific (ETNP) remains poorly understood. Therefore, the key focus of this work is to document intermediate water mass changes in the tropical Pacific at glacial-interglacial and millennial timescales

Here, we present a reconstruction of changes in intermediate ocean circulation in the ETNP over the last 200 ka using benthic foraminifera carbon isotopes ($\delta^{13}C_b$) from a core collected off NW Mexico. The Core MD02-2519 is strategically located at 955 m water depth where the modern NPIW impinges the continental slope off Mazatlan (Figure 4.1). In this study, the use of the $\delta^{13}C_b$ record is used as a fingerprint of intermediate water change in the study area. Furthermore, we present a spatial comparison of $\delta^{13}C$ records from the Pacific Ocean (NE, NW, Equatorial and SW Pacific) to obtain a synoptic picture of intermediate water variations at glacial-interglacial (G-IG) and millennial timescales during ~200 ka BP.

To accomplish this, we first investigate different factors that could influence the carbon isotope ratios of benthic foraminifera ($\delta^{13}C_b$), such as productivity and vital effects. Microhabitat preferences of the benthic species and their effect in the $\delta^{13}C$ values are examined by reconstructing multi-species $\delta^{13}C$ records with foraminifera preferring shallow-infaunal and deep-infaunal habitats. Second, we calibrate the $\delta^{13}C_b$ results of *Uvigerina spp.*

with the dissolved inorganic carbon of bottom waters ($\delta^{13}C_{DIC}$). Third, we investigate temporal variations in $\delta^{13}C$ within different water depths by comparing $\delta^{13}C_b$ records from three piston-cores collected along a depth transect off NW Mexico (Figure 4.1). The Core NH15P, collected from shallow depths (420 m), is bathed by Subsurface Subtropical Water (SSW); while the cores PC08 and MD02-2519 (705 and 955 m, respectively) are bathed by the upper and lower layer of the modern NPIW. The $\delta^{13}C_b$ values along the depth transect are used to assess local productivity changes that could influence $\delta^{13}C$ variations over time. Finally, down-core comparisons with records from the North and South Pacific are used to evaluate possible sources of intermediate water influencing the $\delta^{13}C$ benthic records.
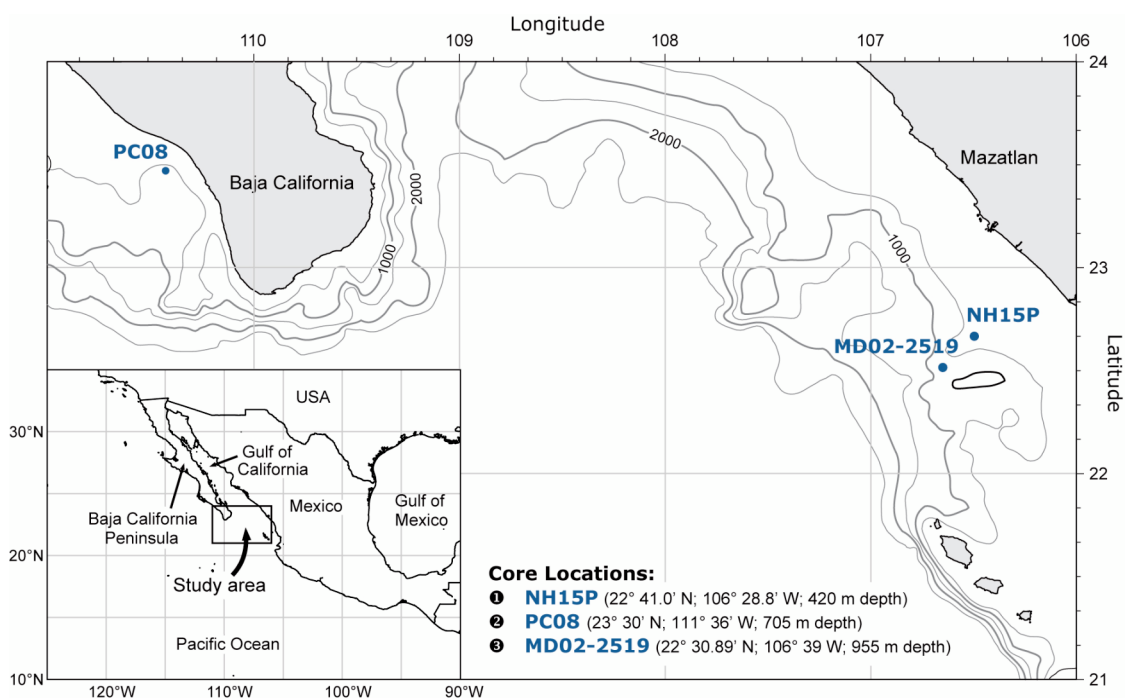
Figure 4-1 Map of the study area including the location of cores NH15 and MD02-2519 collected off Mazatlan, and Core PC08 from Southern Baja California.

4.1.1 Intermediate water masses in the Pacific Ocean

Traditionally, two water masses are considered to be dominant at intermediate depths in the Pacific Ocean defined in terms of their salinity minimum (Reid, 1997; Schmitz, 1996; Talley, 1999): the North Pacific Intermediate Water (NPIW) and the Antarctic Intermediate Water (AAIW) (Figure 4.2). However, geochemical tracers (i.e. salinity, oxygen, phosphate, nitrate, silicate, and carbon species: $\delta^{13}C$, $\Delta^{14}C$, TIC and alkalinity)

suggest the existence of a third intermediate water mass located in the tropics: the Equatorial Intermediate Water (EqIW) (Bostock, 2005; Firing et al., 1998; Wijffels, 1993).
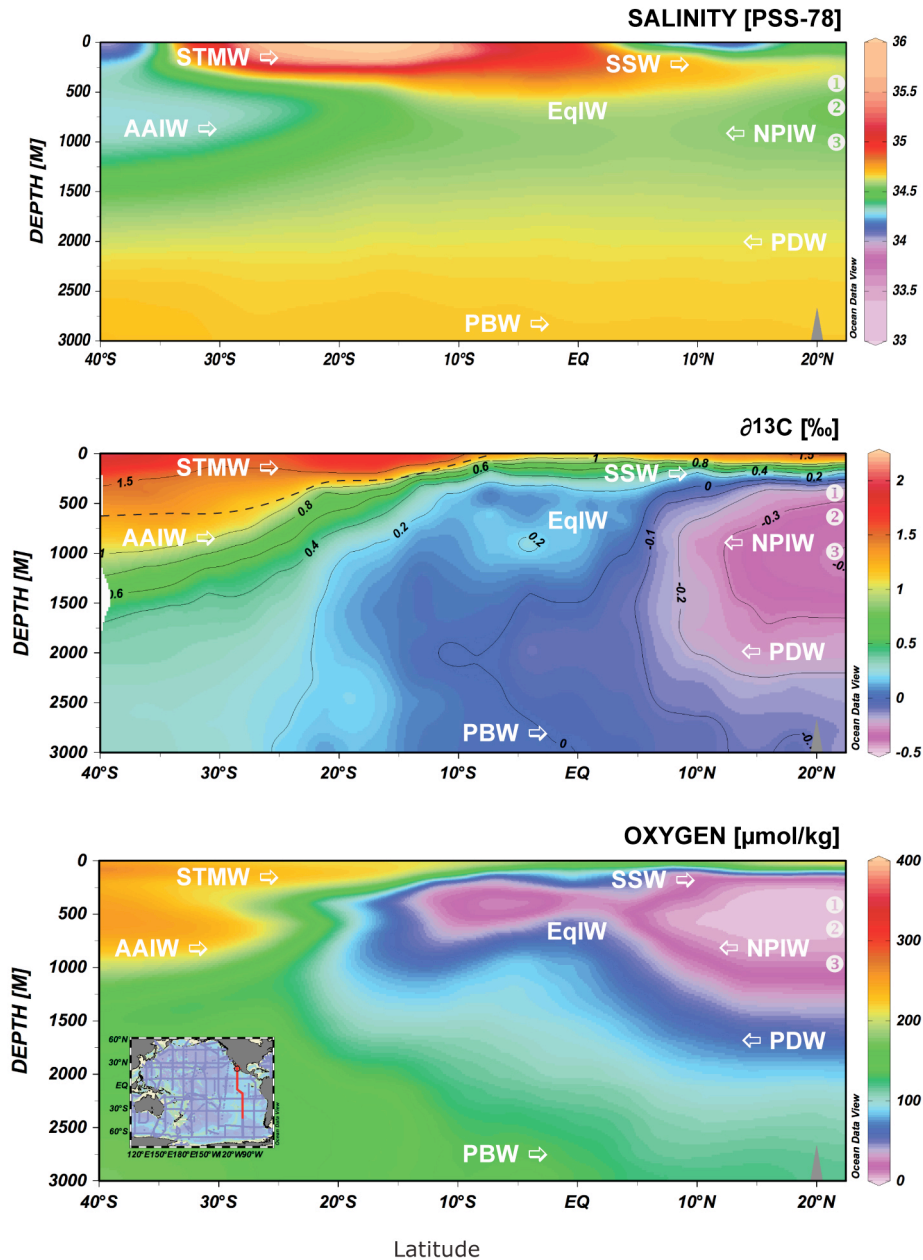
Figure 4-2 Salinity (PSS78 - Practical Salinity Scale 1978), δ ^{13}C content (‰) and Oxygen concentration (µmol/kg) in the water column along the GLODAP Cruise-18 (see map inset in the lower panel) (Key et al., 2004; Schlitzer, 2004). White circles with numbers to the right, show the water depth positions of the cores (1) NH15P, (2) PC08 and (3) MD02-2519 (see Figure 4.1). SSW – Subsurface Subtropical Water; STMW – Subtropical Mode Water; NPIW – North Pacific Intermediate Water; AAIW – Antarctic Intermediate Water; EqIW – Equatorial Intermediate Water; PDW – Pacific Deep Water; PBW – Pacific Bottom Water.

The area of formation of the modern NPIW is located in the eastern segment of the North Pacific subtropical gyre (You, 2003), greatly influenced by water exported from the Okhotsk Sea and Gulf of Alaska (You et al., 2000). The NPIW, is found where fresh sub-Arctic waters spread southward, forming a well-defined salinity minimum at σ_θ 26.8 with low oxygen concentrations (50 – 150 μmol/kg) (Reid, 1997; Talley, 1999; You, 2003). The AAIW forming in the SE Pacific to the west of Chile (Molinelli, 1981), is the most extensive and important water mass at intermediate depths in the Pacific Ocean. The AAIW is a distinctive body of water due to its unique characteristics of relatively high oxygen (200-250 μmoles/kg), low salinity (34.3 - 34.5), cold temperature (3.5 – 10º C) and average density of 27.1 (σ_θ) (Molinelli, 1981; Talley, 1999) (Figure 4.2).

Unlike the NPIW and the AAIW, which have distinct sources in the sub polar regions, the EqIW is a complex mixture of intermediate and deep water masses from the north and south (Bostock, 2005; Firing et al., 1998; Wijffels, 1993). The carbon isotope tracers ($\delta^{13}C_{air-sea}$) allude to the AAIW as the parent water of the EqIW, whilst direct tracer data (O_2, nutrients, TIC) emphasize on the importance of its mixing with upwelled waters from deep layers rich in nutrients, low in oxygen, and high in salinity (Bostock, 2005). Defining this water mass is further complicated by the differences in the oxygen and nutrient content of the waters on either sides of the equator, allowing distinction to be made between EqIW into a northern (NEqIW) and a southern section (SEqIW). Despite the mixed origin, given the distinct physical and geochemical properties, many authors suggest that the EqIWs should be considered independent of the AAIW and the NPIW (Firing et al., 1998; Wijffels, 1993). However, other authors assume that most of the water in the equatorial Pacific region derives from the AAIW (Talley, 1999).

In this study, we follow the traditional classification because the NPIW and the AAIW show substantial difference in the preformed $\delta^{13}C_{DIC}$ due to source conditions. The AAIW is formed as a thick, outcropping mixed layer, enriched in $\delta^{13}C_{DIC}$ as much as 1‰ (relative to NPIW) due to high gas exchange rate which allows partial equilibration with the atmosphere at relatively cold temperatures (Charles et al., 1993; Kroopnick, 1985). On the other hand, the NPIW is formed with little equilibration with the atmosphere at relatively low salinities and warmer temperatures (compared with AAIW), limiting water formation and leading to lighter preformed $\delta^{13}C_{DIC}$ values (Kroopnick, 1985). Therefore, the temporal

and regional difference of the $\delta^{13}C_{DIC}$ values of the two Pacific intermediate water will be used to trace past variations by means of the analysis of $\delta^{13}C$ in shells of foraminifera.

4.2   Carbon Isotopes

Carbon isotope ratios ($\delta^{13}C$) in calcite shells of foraminifera have been used as tracers of ocean circulation, ventilation (e.g. of the NPIW) (Mix et al., 1999; Stott et al., 2000; van Geen et al., 1996), and tracers of changes in surface productivity (Berelson and Stott, 2003; Zahn et al., 1986). However, the difficulty of interpreting carbon isotope data stems from additional potential influences like biological or microhabitat effects. Although some foraminifera (e.g. *Cibicidoides* spp.) secrete their tests incorporating the dissolved inorganic carbon (DIC) in near equilibrium with the environment, a slight depletion in the isotopic composition is caused by biological fractionation. Moreover, the isotopic signal of ambient DIC recorded by calcite can be influenced by factors such as gas exchange, temperature and/or carbon remineralisation, which requires evaluation before using the $\delta^{13}C$ of foraminifera as a tracer of changes in ocean circulation (Bostock et al., 2004; Charles et al., 1993; Rohling and Cooke, 1999). Some of the most important physical and biological factors are described next:

Gas exchange influence

The isotopic fractionation during gas exchange of CO_2 at the water-atmosphere interface increases with decreasing temperatures (Mook et al., 1974), which in polar regions leads the colder waters to display a larger temperature dependent fractionation relative to the atmosphere and higher $\delta^{13}C$-DIC values (Charles et al., 1993). Gas exchange rates also depend on sea ice thawing and wind mixing on the surface in high latitudes, where less ice and stronger winds allow the $\delta^{13}C_{DIC}$ in seawater to equilibrate with the atmosphere. For instance, the cold surface water and circumpolar circulation in the formation regions of AAIW, leads to substantial air-sea exchange of CO_2 conferring the characteristic enrichment in $\delta^{13}C$ values (i.e. AAIW $\delta^{13}C_{DIC} \simeq 1‰$) (Charles and Fairbanks, 1990; Ninnemann and Charles, 1997). Therefore, temperature, stratification and sea ice variability in high latitude source areas can impact the preformed $\delta^{13}C$ of the intermediate water masses.

Organic carbon remineralisation

Primary production of organic carbon preferentially fractionates in favour of the lighter isotope (^{12}C) within the photic zone, leaving surface waters enriched in ^{13}C (Kroopnick, 1985). Respiration of sinking particulate carbon then leads to a progressive ^{12}C-enrichment as the water masses flow through the ocean, producing a negative δ^{13}C gradient between the surface and the deep waters (Charles et al., 1993; Rohling and Cooke, 1999). Thus in regions of intense local upwelling and productivity, the δ^{13}C of bottom waters are affected in favour of lighter values due to decomposition of isotopically light phytodetrital organic matter (Berger and Vincent, 1986; Shackleton et al., 1983). When the organic matter sinks into the deep ocean, the remineralisation consumes O_2 from the water and releases CO_2 by respiration process imparting a lighter isotopic signature in the δ^{13}C of bottom and sediment pore-waters.

Ocean circulation

Horizontal and vertical mixing or advection of waters with different δ^{13}C values from a range of depths and regions can reduce the δ^{13}C gradient formed by carbon remineralisation (Bostock et al., 2004). An example is the upwelling of deeper ^{12}C-enriched deeper waters in the eastern equatorial Pacific (EEP) (Spero and Lea, 2002), which produces surface ^{12}C depletion during equatorial divergence.

Vital effects

The vital effects, as they are broadly called, cause each foraminifera species to fractionate carbon and oxygen isotopes differently. These isotopic offsets are thought to reflect the combination of different habitats, physiologies, and feeding habits during the life cycles of individual species of foraminifera (Jorissen, 1999). Various planktonic foraminifera species show significant differences in δ^{13}C according to their size and symbiotic relationships (Oppo and Fairbanks, 1989; Spero et al., 2003). Conversely, benthic foraminifera δ^{13}C values are influenced by the oxygen content, the quality of the organic matter available and the biological interactions with other organisms (Bernhard and Sen Gupta, 1999; Jorissen, 1999).

One of the most relevant aspects to consider for studies based on benthic foraminifera is the depth habitat, because at depths below the bio-irrigation zone the pore water DIC exhibits pronounced gradients depleted in ^{13}C due to contributions from respired carbon. As a result, lighter δ^{13}C values are recorded by deep dwelling species reflecting lighter pore water DIC signatures. Therefore, most studies suggest the use of epifaunal over infaunal species, as those organisms living on the surface of the sediments correlate better with the bottom water δ^{13}C (Keigwin, 2002; Stott et al., 2000; van Geen et al., 1996). For this reason, the use of the epifaunal foraminifer *Cibicidoides* is commonly selected to reconstruct δ^{13}C stratigraphies (Duplessy et al., 1984; Stott et al., 2000; Zahn et al., 1986). Unfortunately, these species are scarce in the marginal settings of the eastern Pacific due to prevalent anoxic conditions ([O2] < 1.5 ml/L). It has been shown in previous studies (Cannariato et al., 1999; Kaiho, 1994; Sen Gupta and Machain-Castillo, 1993) that the decrease in oxygen content limits the distribution of *Cibicidoides* on the sediments. As a result, taxa more abundant and more tolerant to poor oxygen environments are used instead of *Cibicidoides*. That is the case of the shallow-infaunal foraminifera *Uvigerina*, which dwells in the top-most sediment layer (McCorkle et al., 1997). Previous studies, however, highlight potential factors that could influence the δ^{13}C signal based on infaunal species. Among the factors are: variations in O_2 content of the sediment and bottom waters (Bernhard and Sen Gupta, 1999; Bernhard et al., 1997; Cannariato et al., 1999); productivity and carbon fluxes, organic carbon (OC) oxidation-rates (Berelson and Stott, 2003; Holsten et al., 2004; McCorkle et al., 1997); and ventilation in the NPIW (Keigwin, 2002; Stott et al., 2002; van Geen et al., 1996). Therefore, before reconstructing the history of bottom water δ^{13}C in the ETNP, we first evaluate two aspects: (1) the influence of OC accumulation and (2) the microhabitat effect in the shallow-infaunal species, by comparing with OC records and δ^{13}C in a suite of benthic foraminifera species from different depth habitats.

It has been suggested (Keigwin and Jones, 1990; McCorkle et al., 1997; Zahn et al., 1986) that the δ^{13}C values of the *Uvigerina* group can be controlled by local habitat effects rather than bottom water signatures, because the signal can be influenced by the accumulation rate of organic carbon. In this way, the release of respired carbon (^{12}C-rich) to the pore-water DIC pool could engender lighter δ^{13}C signatures in the shells of benthic foraminifera. Hence, the degree to which this is recorded by foraminiferal calcite can be function of the microhabitat depth of the species, as well as the rate of carbon flux to the sediments. However, if such influence is significant for a given species, the δ^{13}C record

should show a relationship with the productivity proxy records of the same core MD02-2519. This effect is evaluated in Core MD02-2519 by comparing the $\delta^{13}C_b$ to the organic carbon record (%OC), which has been extensively used a productivity proxy along the margin (Ganeshram et al., 2000; Hendy and Pedersen, 2005; Ortiz et al., 2004). Additionally, the evaluation of the offset between bottom waters and infaunal species is used to assess specific vital effects resulting from the depth habitat. We then present a comparison between $\delta^{13}C$ records of four benthic foraminifera species from different sediment depths. Here, *Bolivina argentea* is identified as the shallow infaunal species that closely reflect bottom water $\delta^{13}C$ values, as suggested by Holstein *et al.* (2004). Thus, by comparing the *B. argentea* values with those of *Uvigerina* spp., we assess whether the latter are able to record large-scale variations linked to bottom water DIC concentrations, and discuss the potential implications of such finding.

In addition, comparisons of the $\delta^{13}C$ record from Core MD02-2519 to Core NH15P collected at 420 m (Ganeshram, *unpublished results*) and Core PC08 collected at 705 m (Carriquiry, *unpublished results*) are used to constrain depth-dependent changes in $\delta^{13}C$. The influence of local changes in productivity is expected to produce uniform temporal changes at all depths, while variations linked to water masses are expected to decouple from productivity. Finally, comparisons between $\delta^{13}C$ records from distant regions in the Pacific are made to evaluate the areas of water mass formation of the $\delta^{13}C$ signal found in the ETNP.

4.3   Materials and Methods

4.3.1   Sediment sampling and analyses

Marine sediment samples were obtained from the 36 m calypso piston Core MD02-2519 located off Mazatlan, NW Mexico (Figure 4.1) during the MONA Expedition 2002 (Beaufort, 2002). The *working* half of the core was evenly sampled every cm, stored in plastic bags, and kept in a cold room at 4ºC. The samples for carbon and oxygen isotope analyses were selected every 5-10 cm in the first 18 m of the core, and every 20 cm in the second half. All selected samples were disaggregated in distilled water and washed over a 63-μm sieve. Benthic foraminifera species were handpicked from the > 63 μm fraction at regular intervals, except where foraminiferal calcite were scarce. Radiocarbon ages were determined for 19 intervals with accelerator mass spectrometry (AMS ^{14}C) at the NERC

Radiocarbon Laboratory (RCL) East Kilbride, UK. The samples are based on mixed planktonic foraminifera (15 mg) or organic carbon (~100 mg of bulk sediments after decarbonating).

4.3.2 Interspecies comparison of benthic foraminifera records

Benthic foraminifera samples were analysed for both $\delta^{13}C$ and $\delta^{18}O$ on 0.03 - 0.2 mg sub-samples (about 10 to 25 organisms). The tests were cleaned ultrasonically in distilled water for few seconds prior to the analyses. The hand-picked carbonate samples were reacted with 100% orthophosphoric acid at 75°C in a "Kiel Carbonate III" preparation device, and the resulting CO_2 analysed on a "Thermo Electron Delta$^+$ Advantage" stable isotope ratio mass spectrometer at the Wolfson Laboratory, the University of Edinburgh, UK. The standard deviation for 56 analyses of a marble powder (MAB2B) run as a sample over the same period as the study samples was ± 0.06‰ for $\delta^{13}C$ and ± 0.07‰ for $\delta^{18}O$. All carbonate isotope values are quoted relative to Peedee Belemnite (PDB).

Carbon and oxygen isotope measurements were performed in four of the most common species present in Core MD02-2519: *Buliminella tenuata*, *Bolivina argentea s.l.*, *Bolivina seminuda s.l.* and *Uvigerina* spp. mainly *U. peregrina* (see Supplement at the end of this chapter). The species were selected according to their habitat within the sediments as shallow-infaunal and deep-infaunal. *B. argentea* is a shallow infaunal species that lives with maxima abundances within the first mm of sediment (Holsten et al., 2004). *Uvigerina* spp. and *B. subadvena* are shallow-infaunal species living within 1– 3 mm depth. *B. tenuata* is considered a deep-infaunal species with preferential habitat within 5 – 6 mm depth (Holsten et al., 2004; McCorkle et al., 1997).

4.3.3 Age model

The age models for the upper 40 ka were derived from 19 AMS ^{14}C dates of either planktonic foraminifera or organic carbon samples (Table 4.1). The use of interchangeably planktonic foraminifera (PF) and organic carbon (OC) dates in intervals where planktonics were scarce, is justified by the fact that the OC-based ages do not show significant offsets from the PF-dates in the nearby samples. This is consistent with previous studies which have constructed chronologies based on bulk OC in other cores of the area (Ganeshram et al.,

1999), showing that the sediments underlying this upwelling region are overwhelmingly algal derived (Ganeshram et al., 2000).

Table 4.1
AMS ^{14}C dates: Core MD02-2519

Core depth (cm)	Raw ^{14}C Age (ka)	error ±	Calibrated Age (ka BP)*	error 1σ -	+	Notes: Material	Calib source
1	2865	73	2365	116	94	OC	1
74	4049	61	3802	79	93	OC	1
140	6050	61	6266	54	72	OC	1
194	8689	64	9114	79	101	OC	1
216	9555	73	10198	82	84	PF	1
230	10272	62	11082	134	94	PF	1
284	12664	53	13911	86	75	OC	1
290	12831	64	14084	84	76	PF	1
332	14173	65	16139	205	193	PF	1
370	15717	84	18475	184	296	OC	1
424	18667	109	21417	278	272	OC	1
466	20091	173	23191	316	346	OC	1
500	21920	153	25713	208	145	OC	1
558	24147	154	28226	399	399	OC	2
576	24690	169	28831	369	369	OC	2
606	26239	216	30548	364	364	OC	2
636	27987	281	32471	349	349	OC	2
676	29852	367	34507	342	342	OC	2
758	35012	749	39522	1015	1015	OC	2

* ΔR = 203 ± 48
OC - organic carbon; PF - mixed planktonic foraminifera
(1) Stuiver *et al.*, 2005; (2) Bard *et al.*, 2004

Table 4-1 Radiocarbon dates of Core MD02-2519.

The ^{14}C dates were calibrated with Calib 5.0.2 (Stuiver and Reimer, 1993) using a reservoir correction (ΔR) of 203 ± 50, as reported in the Marine Reservoir Correction Dataset (Reimer et al., 2004). Radiocarbon ages older than 22 ka were transformed to calendar years BP using the polynomial *equation 2* of Bard *et al*. (2004). Ages between 40 - 120 ka are based on tuning between major events found in the %OC record and the D/O events of the δ^{18}O-GISP2 record (Grootes and Stuiver, 1997) following previous studies in the margin (Ortiz et al., 2004). Beyond 120 ka, the OC record was tuned to the ODP-977A δ^{18}O record from the Iberian Margin (Martrat et al., 2004), as described in *Chapter 1*. The final chronology of the Core MD02-2519 was calculated by linear interpolation between the tie points listed in Table 4.2. To name the events we use the classification from GISP2 (Grootes and Stuiver, 1997) and LR04 (Lisiecki and Raymo, 2005) δ^{18}O records.

4.3.4   Carbon isotope records used in this study

Carbon isotope records of the Core MD02-2519 (955 m water depth) were compared with two other $\delta^{13}C_b$ records from NW Mexico: Core NH15P (420 m water depth) and Core PC08 (705 m water depth) collected from the upper slope off Mazatlan and the mid-slope off Southern Baja California, respectively. The comparisons were used to evaluate the depth dependence of the $\delta^{13}C_b$ records and to constrain changes within water masses.

Table 1.1

AGE MODEL: Core MD02-2518

Source	MD02-2518 depth (cm)	Age (Cal ka BP)	Source (symbol)
AMS ^{14}C	10	1.2	×
AMS ^{14}C	140	6.7	×
AMS ^{14}C	230	11.2	×
AMS ^{14}C	260	13.8	×
AMS ^{14}C	284	18.9	×
AMS ^{14}C	340	33.2	×
AMS ^{14}C	372	36.2	×
AMS ^{14}C	422	44.0	×
D/O 12	490	45.3	◇
D/O 14	590	51.9	◇
D/O 17	664	57.5	◇
D/O 19	954	68.4	◇
D/O 21	1250	83.6	◇
D/O 23	1534	101.0	◇
D/O 25	1712	108.1	◇
(MIS 5e) 26	1906	121.6	◇
(MIS 6.0) S1'	1990	130.0	◇
(MIS 6.4) S4'	2376	150.3	◇
(MIS 6.6) 9'	2930	180.8	◇
(MIS 7a) 11'	3146	193.4	◇
(MIS 7c) 12'	3560	215.5	◇
(MIS 7d) 13'	3836	224.5	◇

AGE MODEL: Core MD02-2519

Source	MD02-2519 depth (cm)	Age (Cal ka BP)	Source (symbol)
AMS ^{14}C	1	2.4	+
AMS ^{14}C	74	3.8	+
AMS ^{14}C	140	6.3	+
AMS ^{14}C	194	9.1	+
AMS ^{14}C	216	10.2	+
AMS ^{14}C	230	11.1	+
AMS ^{14}C	284	13.9	+
AMS ^{14}C	290	14.1	+
AMS ^{14}C	332	16.1	+
AMS ^{14}C	370	18.5	+
AMS ^{14}C	424	21.4	+
AMS ^{14}C	466	23.2	+
AMS ^{14}C	500	25.7	+
AMS ^{14}C	558	28.2	+
AMS ^{14}C	576	28.8	+
AMS ^{14}C	606	30.5	+
AMS ^{14}C	636	32.5	+
AMS ^{14}C	676	34.5	+
AMS ^{14}C	758	39.5	+
D/O 12	870	45.3	○
D/O 14	956	51.9	○
D/O 17	1044	57.5	○
D/O 18	1138	61.9	○
D/O 19	1272	68.4	○
D/O 20	1316	72.8	○
D/O 21	1428	83.6	○
D/O 23	1630	101.0	○
D/O 25	1744	108.1	○
(MIS 6.0) S1'	2070	130.0	○
(MIS 6.2) 1'	2156	137.0	○
(MIS 6.4) S4'	2458	151.3	○
(MIS 6.5) 8'	2824	175.1	○
(MIS 6.6) 9'	3040	180.8	○

Table 4-2 Age model of Core MD02-2519 listing the 33 tie points derived from AMS ^{14}C dates and tuning. Marine Isotope Stages (MIS) are given for reference (see Chapter 1).

The age model construction of Core NH15 (based on AMS ^{14}C-dates) and the isotopic determinations based on *Bolivina* spp. samples are described in a paper by Ganeshram *et al.* (2000). The δ^{13}C measurements (Ganeshram, *unpublished data*) are reported to the PDB standard with 1σ precision of replicate samples better than 0.1‰. For the Core PC08, the age model is described in a paper by Marchitto *et al.* (2007); whereas the δ^{13}C analyses of *Uvigerina peregrina* (Carriquiry, *unpublished data*) were undertaken at the Instituto de Investigaciones Oceanológicas de la Universidad Autónoma de Baja California (UABC) Mexico, using an isotope ratio mass spectrometer (OPTIMA) interfaced to an automated common acid bath (ISOCARB). About 5 to 11 *U. peregrina* tests were manually picked from the 125 – 250 μm fraction, oven-dried and stored in vials. Before analyses, foraminifera samples were heated at 350°C to eliminate potential organic traces. The external precision of the isotopic measurements of δ^{18}O and δ^{13}C (‰ vs. PDB) is < 0.04 ‰ (Carriquiry, *pers. comm.*).

4.4   Results

The constructed chronology for the Core MD02-2519 indicates that the δ^{18}O and δ^{13}C records span ~ 200 cal ka BP (Figure 4.3), with an average sedimentation rate of ~ 20 cm/ka. The δ^{13}C and δ^{18}O records based on samples of *Uvigerina* spp. are of the highest resolution (i.e. centennial to millennial scale) and the most evenly sampled (i.e. every 5 - 20 cm) of the four species analysed due to the ubiquitous preservation in the Core MD02-2519.

As shown in Figures 4.3 and 4.4, the δ^{13}C-*Uvigerina* records show the most depleted values during glacials and the subsequent terminations, relative to interglacials. The average δ^{13}C values during interglacials MIS-3 and MIS-5 are ~ -0.6‰, whereas average δ^{13}C values during glacials MIS-2, MIS-4 and MIS-6 are ~ -0.9‰, -0.8‰ and -1.25‰ (respectively). This shows a difference in δ^{13}C shifts of 0.44‰, 0.35‰ and 0.75‰ lower than each succeeding interglacial. These glacial-interglacial (G-IG) changes are clearly larger than the -0.3‰ glacial shift attributed to terrestrial biomass changes (Curry et al., 1988; Shackleton, 1977). Smaller amplitudes of millennial timescale variability are also seen when the sampling resolution is high, although no clear pattern can be described nor correlated, to the temperature variability recorded in ice cores from Greenland or Antarctica.
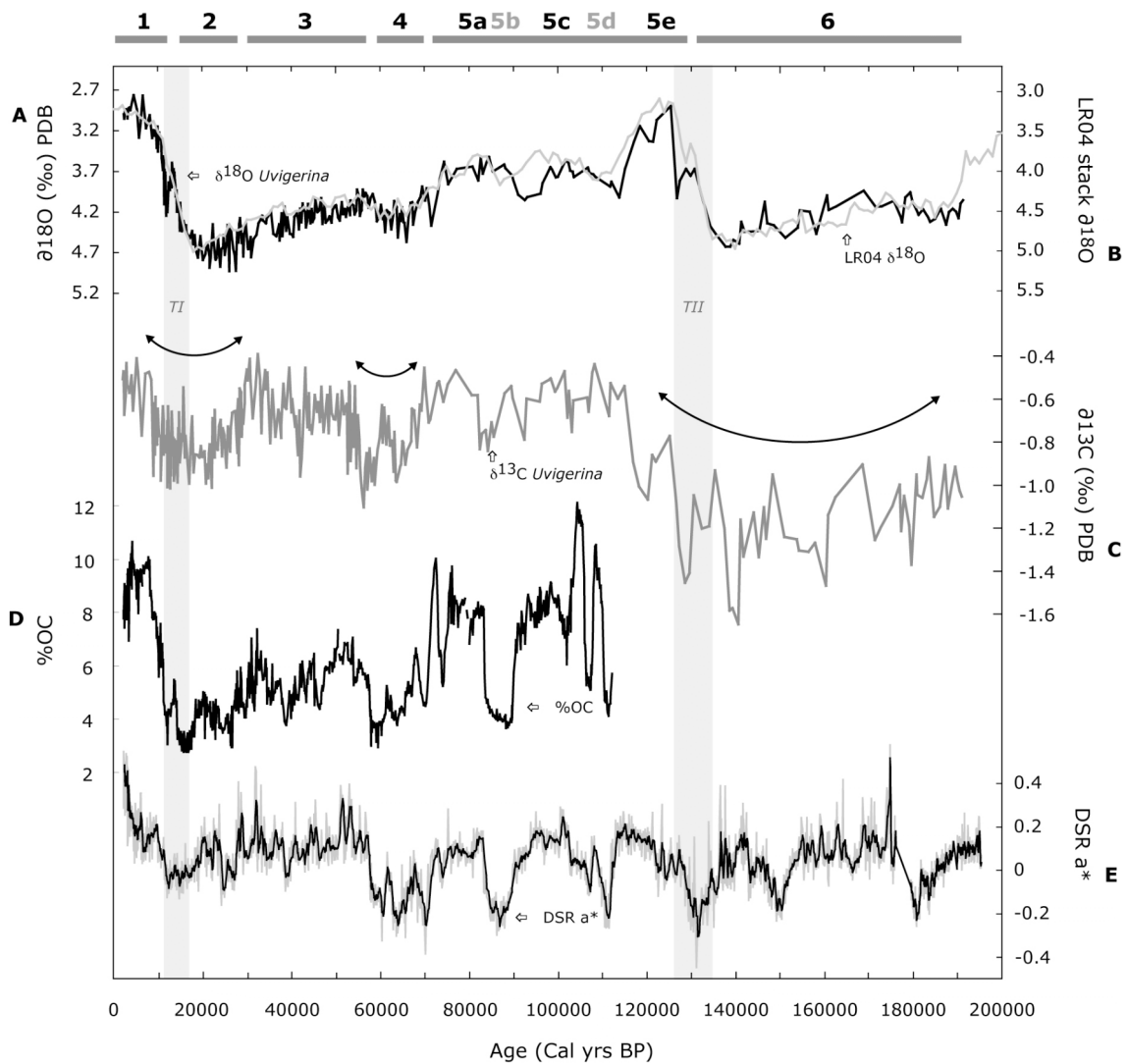
Figure 4-3 Records of Core MD02-2519 spanning the last 200 ka. (A) δ^{18}O based on Uvigerina spp.; (B) LR04 δ^{18}O stack record (Lisiecki and Raymo, 2005); (C) δ^{13}C – Uvigerina spp. (D) Organic carbon record (%OC); (E) Diffuse Spectral Reflectivity (DSRa*) (black line – 5 point moving average). Curved arrows mark the position of the δ^{13}C$_b$ minima events; numbers on top are marine isotope stages; vertical grey bands mark the last (Termination I) and the penultimate (Termination II) deglaciations.

The δ^{13}C records of 4 benthic foraminifera analysed in Core MD02-2519 are presented in Figure 4.5. The comparison between the benthic foraminifera species shows that the overall pattern in all four δ^{13}C$_b$ records is similar although the amplitudes are different. The species *B. tenuata* shows the highest amplitude change and the most depleted δ^{13}C values of all four species, followed by *B. subadvena*. The species *B. argentea* has comparable δ^{13}C values and amplitudes to *Uvigerina* spp. (i.e. < 0.1‰ change) during the MIS-1 to 4. The biggest difference between shallower dwelling species and deep-infaunal

species (*B. tenuata*) also occurs during glacials (i.e. MIS 2, 4 and 6). A common feature between benthic species is the broad δ^{13}C minimum that extends over glacial periods and terminations. The recovery to relatively enriched and stable interglacial values is gradual between 10 and 5 ka. Additionally, the core-top sample of δ^{13}C-*Uvigerina* only shows a 0.05‰ difference between the top value (-0.5‰) and the mean δ^{13}C$_{DIC}$ (-0.45‰) from the nearest GLODAP station at 990 m water depth (station 17190 – cruise 18, 22° N / 110°W (Key et al., 2004); marked as an *open circle* in Figure 4.5).

The relationship between the δ^{13}C-*Uvigerina* spp. and the %OC records is evaluated at glacial-interglacial and millennial timescales (Figures 4.3 and 4.4). It shows that the lower δ^{13}C values tend to occur mostly in intervals of low %OC during glacial periods; however, no clear correspondence exists in shorter millennial scale events (e.g. interstadials or Dansgaard/Oeschger events (D/O) 5, 6, 9, 10, 15 or 16).

The comparison between the Mazatlan and Baja California δ^{13}C-BF records over the last 40 ka is shown in Figure 4.6. In the Core NH15P, the δ^{13}C – *Bolivina* record shows a gradual decrease of ~0.7‰ (from -0.7 to -1.4‰) between 30 and 11 ka, followed by a variable enrichment of ~0.8‰ between 11 and 2 ka. In the Core PC08, the δ^{13}C – *Uvigerina* record also shows a gradual decrease of 0.8‰ (from -0.5 to -1.3‰) between 30 - 11 ka, followed by a rapid and variable enrichment of ~1.0‰ (from -1.3 to -0.3‰) between 11 – 6 ka. On the other hand, the Core MD02-2519 show a broader δ^{13}C minimum that spans approximately 22 ka (from 30 to 8 ka). It shows a gradual decrease of 0.5‰ (from -0.45 to -0.95‰) between ~30 to 18 ka and a gradual 0.3‰ rise (from -1.0 to -0.7‰) during T1 (~17 – 11 ka) and up to -0.6‰ during the last 8 ka of the Holocene.

4.5   Discussion

4.5.1   Proxy evaluation

In this chapter, we attempt to reconstruct the temporal pattern of intermediate water circulation in the ETNP during the Late Pleistocene. During glacial times, the δ^{13}C$_b$ record in the Core MD02-2519 shows depleted values consistently over MIS-2, MIS-4 and MIS-6, but the opposite during interglacials MIS-3 and MIS-5. However, before considering the δ^{13}C$_b$ record as a proxy of bottom water DIC, we must evaluate the effect of microhabitat depth in

the species-specific isotopic fractionation, and the relationship with the organic carbon accumulation in this site, since both factors tend to deplete the δ^{13}C values.
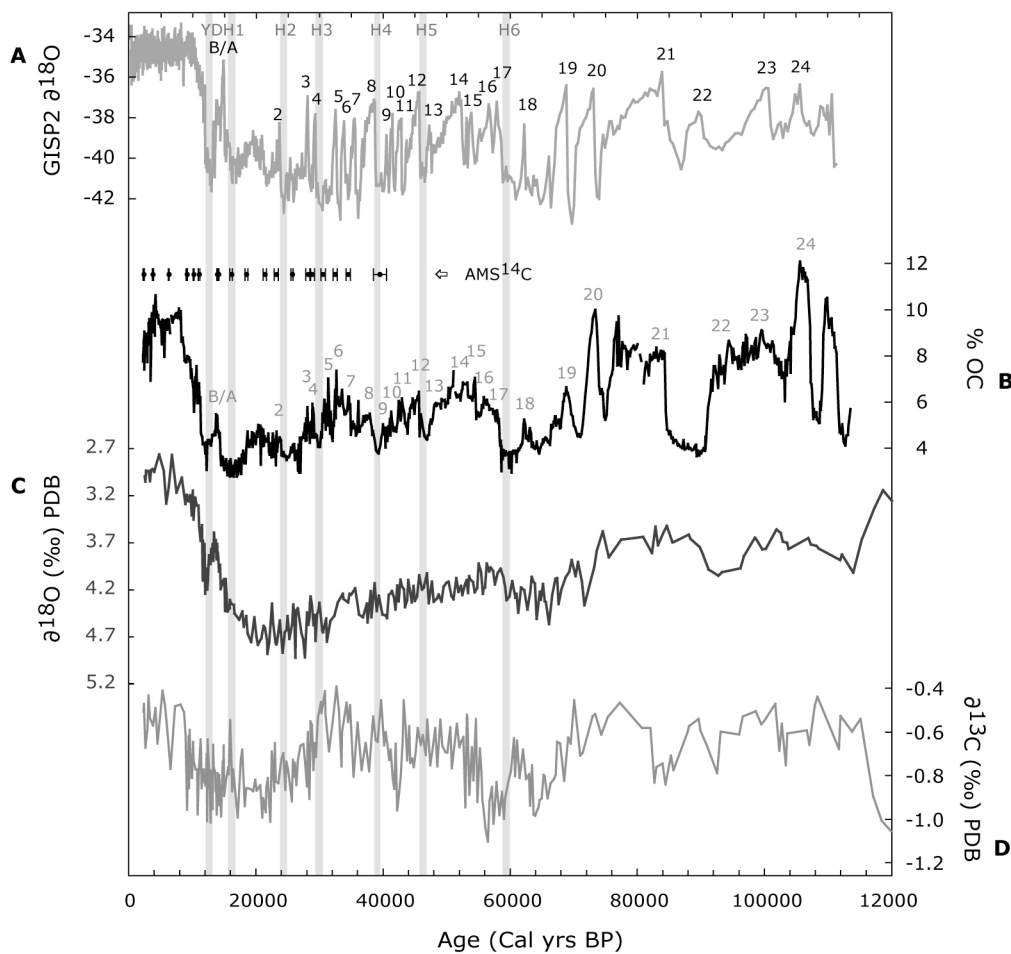
Figure 4-4 Records of Core MD02-2519 spanning the last 120 ka. (A) δ^{18}O GISP2 (Grootes and Stuiver, 1997) shown for reference; (B) % Organic carbon; (C) δ^{18}O – Uvigerina spp.; (D) δ^{13}C – Uvigerina spp. Numbers are interstadial events D/O, B/A - Bølling/Allerød, and vertical grey lines mark the Younger Dryas (YD) and Heinrich events (H1 to H6).

Microhabitat depth effects

The δ^{13}C records of benthic foraminifera in the Core MD02-2519 suggest that the increase in habitat depth leads to depleted δ^{13}C values. As shown in Figure 4.5, the core top values of the infaunal species *B. tenuata, B. subadvena* and *Uvigerina* have lower δ^{13}C values relative to *B. argentea*, whereas the deep-infaunal dwellers (*B. tenuata*) are more strongly depleted than the shallow-infaunal (*B. argentea* and *Uvigerina*) species. This trend is in agreement with the microhabitat preferences of the species, as reported in modern

studies of surface sediments along the NE Pacific (Berelson and Stott, 2003; Holsten et al., 2004; McCorkle et al., 1997; McCorkle et al., 1990; Stott et al., 2002).

During the most of the Holocene (~ 12 to 2.5 ka), the $\delta^{13}C$ average values of the shallow infaunal *B. argentea* (-0.55‰) and *Uvigerina* spp. (-0.57‰) are almost identical, whereas the deep-infaunal *B. subadvena* (-0.74‰) and *B. tenuata* (-1.24‰) show the most negative $\delta^{13}C$ values. Overall, this trend is consistent along the entire core length and suggests that the species maintained a similar depth dependence over the last ~ 200 ka. Another feature displayed in the foraminiferal $\delta^{13}C$ data is the small intra-core variability observed by *B. argentea* and *Uvigerina* spp. relative to *B. tenuata*, which may reflect the restricted and stable depth habitat of these species (Bernhard 1992). In modern studies, even similarities between top core $\delta^{13}C$ values of shallow-infaunal and epifaunal species (e.g. *Cibicidoides*) have been observed (Holsten et al., 2004; McCorkle et al., 1997; McCorkle and Keigwin, 1994; Silva et al., 1996). In contrast, the deep-infaunal species *B. tenuata* shows large amplitude variations in the carbon isotope record ($\delta^{13}C_{max}$ = -0.9‰; $\delta^{13}C_{min}$ = -2.9‰), with almost a 1.8‰ change from glacial to interglacial values. This may reflect the ability of the species to migrate vertically within the sediments, because the deeper the habitat, the more ^{12}C-enriched values are registered. This is consistent with field observations documenting that the vital effect variations of these species commonly shift the $\delta^{13}C$ toward lighter values, where an offset from equilibrium with bottom waters is generally smaller than 2‰ (Berelson and Stott, 2003; Grossman, 1987; Holsten et al., 2004).

In the Core MD02-2519, we observe that the core-top $\delta^{13}C$ values of *B. argentea* and *Uvigerina* records are very similar to the bottom water $\delta^{13}C$ (marked as open circles in Figure 4.5) with a small difference of ~ 0.05‰. This could indicate that the sediment pore waters, where *B. argentea* and *Uvigerina* spp. calcify, are in a very narrow and geochemically homogeneous zone that matches the bottom water $\delta^{13}C_{DIC}$ values. As a result, the $\delta^{13}C$ of shallow-infaunal species like *Uvigerina* yield an approximate record of variations in intermediate waters. This observation is supported by field studies in modern sediments, which document relatively small $\delta^{13}C$ differences between bottom water DIC and calcite shells of *U. peregrina* (Holsten et al., 2004; McCorkle et al., 1997). The constant depth habitat in which *Uvigerina* calcifies hence supports its utility in reconstructions of bottom waters, being particularly useful where epifaunal species are lacking. However, before considering the $\delta^{13}C$-*Uvigerina* record as a proxy to reconstruct bottom waters, we must rule

out the potential effect of OC decomposition within the sediments (McCorkle and Emerson, 1988; McCorkle et al., 1985; Zahn et al., 1986). This will be evaluated in the next section.
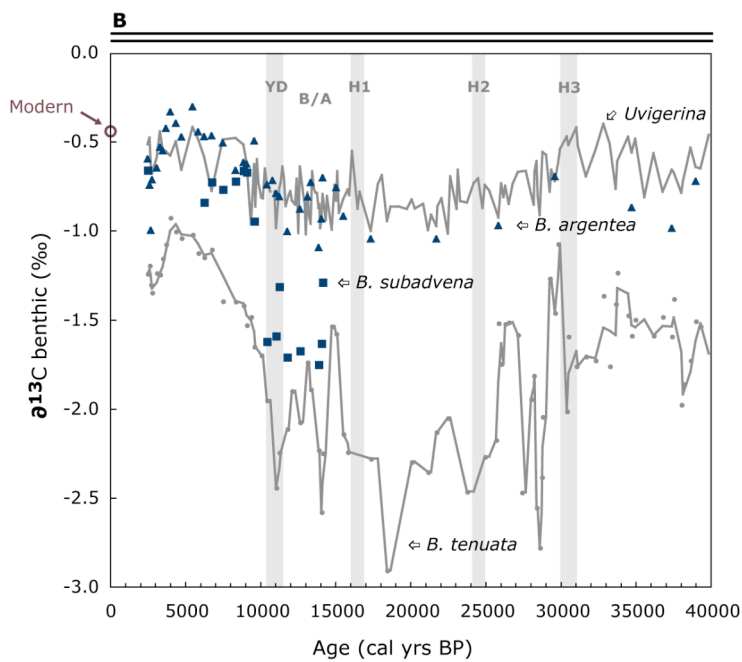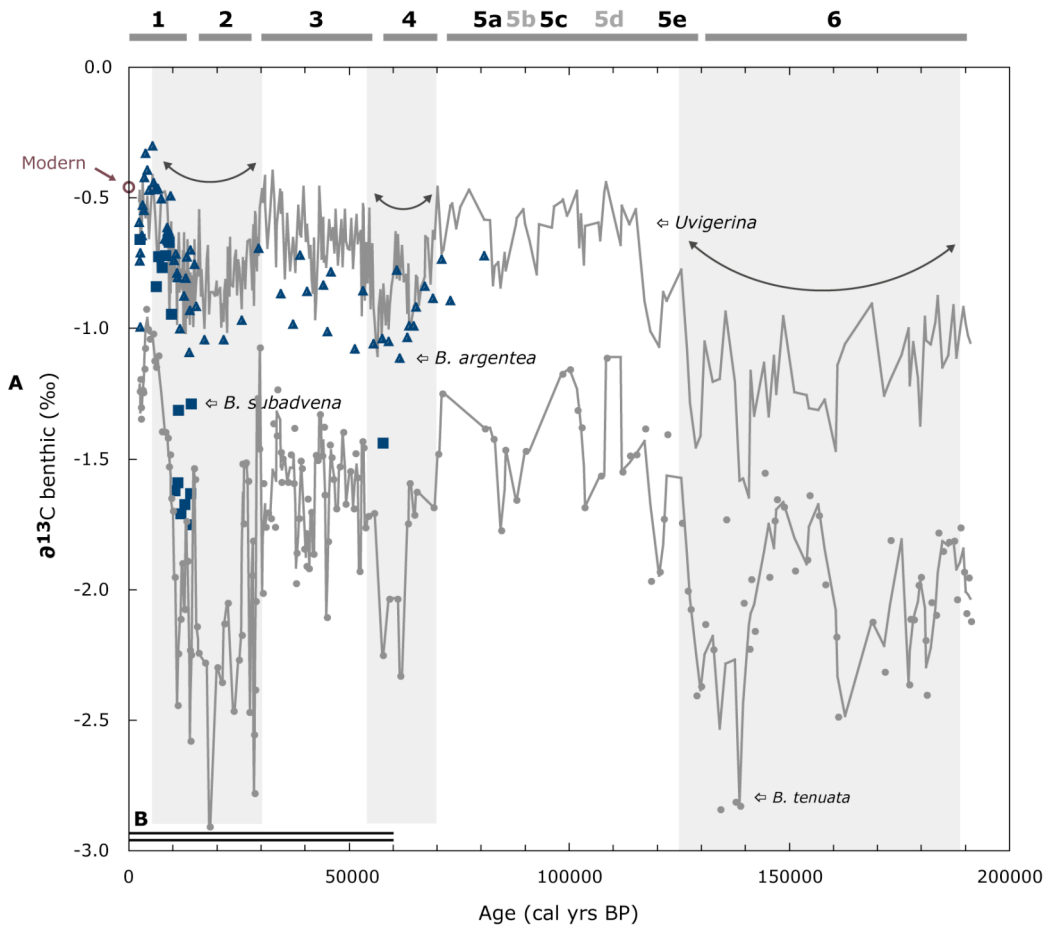
Figure 4-5 Benthic foraminifera carbon isotope records of Core MD02-2519. (A) Records spanning the last 200 ka; arrows and shaded bands show the $\delta^{13}C_b$ minima events. (B) $\delta^{13}C_b$ records spanning the last 40 ka; Uvigerina spp. – solid grey line; Bolivina argentea – triangles; Bolivina subadvena – squares; Buliminella tenuata – solid grey line with dots (the line is a 2 point moving average). The open circle shows the modern $\delta^{13}C_{DIC}$ value (-0.45‰) of bottom waters at 990 m from the GLODAP cruise 18, station 17190 (Key et al., 2004). Vertical grey lines mark the events YD and H1 to H3.

Organic carbon effects

Modern studies claim a spatial relationship between OC-rain and negative $\delta^{13}C$ values of benthic foraminifera in the NE Pacific (Berelson and Stott, 2003), where a causal relationship between high OC (^{12}C-rich) fluxes and a negative deviation in $\delta^{13}C$ values from bottom waters has been reported in species like *Uvigerina* (McCorkle et al., 1997; Zahn et al., 1986). Hence, we now compare the $\delta^{13}C_b$ of Core MD02-2519 with records of productivity and organic carbon accumulation, reconstructed in *Chapter 1* (Figure 4.3). Overall, the %OC and the diffuse spectral reflectivity (DSRa*) records display a pattern that does not match with the $\delta^{13}C_b$ variability. For instance, depleted glacial $\delta^{13}C_b$ values are present when OC contents are lower, thus indicative of substantial reductions in productivity and carbon fluxes (Ganeshram and Pedersen, 1998; Hendy et al., 2002; Ortiz et al., 2004). Therefore, because the $\delta^{13}C_b$ values are not high when OC is low, the carbon isotope signal does not seem to be forced by changes in productivity or remineralised carbon exported to the seafloor. Moreover, the timing between the $\delta^{13}C_b$ and the organic carbon (%OC) curve is also different. The %OC records exhibit millennial timescale variability matching temperature variations in Greenland ($\delta^{18}O$-GISP2), which is not recognized in the $\delta^{13}C_b$ record (Figure 4.4). As a result, these observations suggests that: (a) the $\delta^{13}C$-*Uvigerina* do not yield a useful productivity record in this location; and (b) the organic carbon do not exert a critical control on the $\delta^{13}C_b$. Therefore, it is possible that the $\delta^{13}C$ composition of pore waters where *Uvigerina* calcify, was essentially reproducing the $\delta^{13}C$-DIC signal of bottom waters during glacial stages, as a consequence of the narrow depth interval in which the species dwell.

On the other hand, although little correlation exists between the $\delta^{13}C$-*Uvigerina* and the OC record, it is possible that a poorly-known relationship between the primarily flux of organic matter to the sea-floor and organic carbon accumulation rates (McCorkle et al., 1997; Zahn et al., 1986), even redox gradients within the sediments or ecological parameters

(van der Zwaan et al., 1999), may affect the isotopic signal of the infaunal species. These factors are not considered here, as further studies are required to rule out such influences. However, even given the limitations of using shallow infaunal species, the δ^{13}C -*Uvigerina* record seems to be the best strategy available to investigate intemediate water variations in the ETNP. As we will discuss next, this assumption is based on: (1) the narrow depth range in which the *Uvigerina* spp. calcifies; (2) the small intra-core variability that is similar to the epifaunal species; (3) the lack of correspondence with OC and productivity records over longer timescales; (4) the core-top values that are close to bottom water DIC; and (5) the pattern exhibited by the $\delta^{13}C_b$ records that shows not to be local, but regional in extent.

4.5.2 Comparison between cores from the ETNP

From the observations discussed in the previous sections and assuming that the δ^{13}C-*Uvigerina* record could be useful to study changes in the bottom waters of the ETNP, the next question centres on finding the origin of the $\delta^{13}C_b$ variability, and more importantly, to assess whether the signal not driven by local processes. For this, the $\delta^{13}C_b$ record of Core MD02-2519 is compared with nearby records (i.e. NH15P and PC08) collected from relative shallower depths (Figure 4.2) to create a picture of subsurface to intermediate water mass variation in the ETNP over the last 40 ka.

As shown in Figure 4.6, a better correspondence exists between the cores NH15 (δ^{13}C-*Bolivina* spp.) and PC08 (δ^{13}C-*Uvigerina* spp.), as they document more similar patterns and timing (within dating errors). The Core MD02-2519 collected off Mazatlan from 955 mbsl shows a broad δ^{13}C minimum spanning from ~ 30 – 8 ka. This interval includes the Last Glacial Maximum (24 – 18 ka), Termination I (17 – 11 ka), and up to the mid-Holocene (~ 8 ka). This contrasts with the Core NH15 collected from 420 mbsl and the Core PC08 from 705 mbsl, where the δ^{13}C minimum is centred between ~12 - 8 ka, with relatively enriched values between ~ 40 - 15 ka (including LGM).

In the modern ocean, the cores MD02-2519 and PC08 are located within the influence of the North Pacific Intermediate Water (NPIW, depth range: ~500 – 1200 m). However, the Core NH15P is located within the influence of the Subsurface Water (SSW, depth range: ~150 - 500 m; 34.5 ≥ S ≤ 35) (Talley, 1999) (see Figure 4.2). The SSW exhibits seasonal variability: travelling shallower during the winter (~150 m depth) but deeper during summer (300-350 m depth) (Badan-Dangon, 1998; Lavin et al., 1997). The boundary

between NPIW and SSW oscillates in response to the seasonal expansion and contraction of the SSW, which is displaced southward during the winter, but northward during the summer (Lavín et al., 1997; Sverdrup et al., 1946).
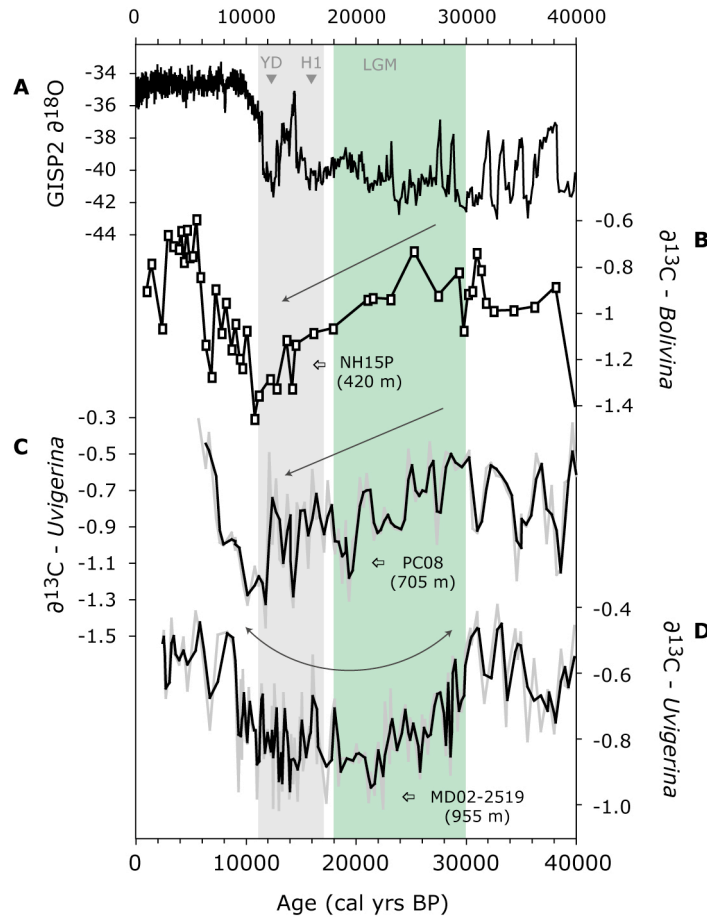
Figure 4-6 $\delta^{13}C_b$ records of cores from the ETNP spanning the last 40 ka. (A) $\delta^{18}O$ GISP2 record; (B) Core NH15P from Mazatlan (Ganeshram, unpublished results); (C) Core PC08 from Baja California (Carriquiry, unpublished results) (black line - 2-point moving average); (D) Core MDO2-2519 from Mazatlan (black line - 2-point moving average);. Pale-green shade between 30 – 18 ka marks the onset of the $\delta^{13}C$ minimum in Core MD02-2519 up to the end of LGM. Termination I is shaded in grey, which includes YD and H1.

Thus in the course of the last glacial, between 30 – 18 ka, the difference between the $\delta^{13}C_b$ records of cores MD02-2519 and PC08 suggest that the intermediate water boundaries were different from today. This could mean that the 3 cores (NH15, PC08 and MD02-2519) were influenced by similar bottom water conditions (i.e. ^{13}C-depleted) with smaller vertical gradients in the Core MD02-2519, because it could be bathed by a deeper and more stable water mass. However, during T1, the changes in bottom water conditions could affect

differentially the Core MD02-2519, relative to cores NH15P and PC08. In addition, the changes in organic carbon fluxes and local productivity at G-IG timescale, do not seem an adequate explanation to the variations found in these $\delta^{13}C_b$ records. This is because the %OC records are consistently elevated during interglacials and reduced during glacials, being decoupled frorm $\delta^{13}C_b$. In the following two sections, we extend the comparison of the $\delta^{13}C$ foraminiferal records to other regions in the Pacific Ocean (Figure 4.7) to track the sources of preformed-$\delta^{13}C$ found in the ETNP during LGM and TI.
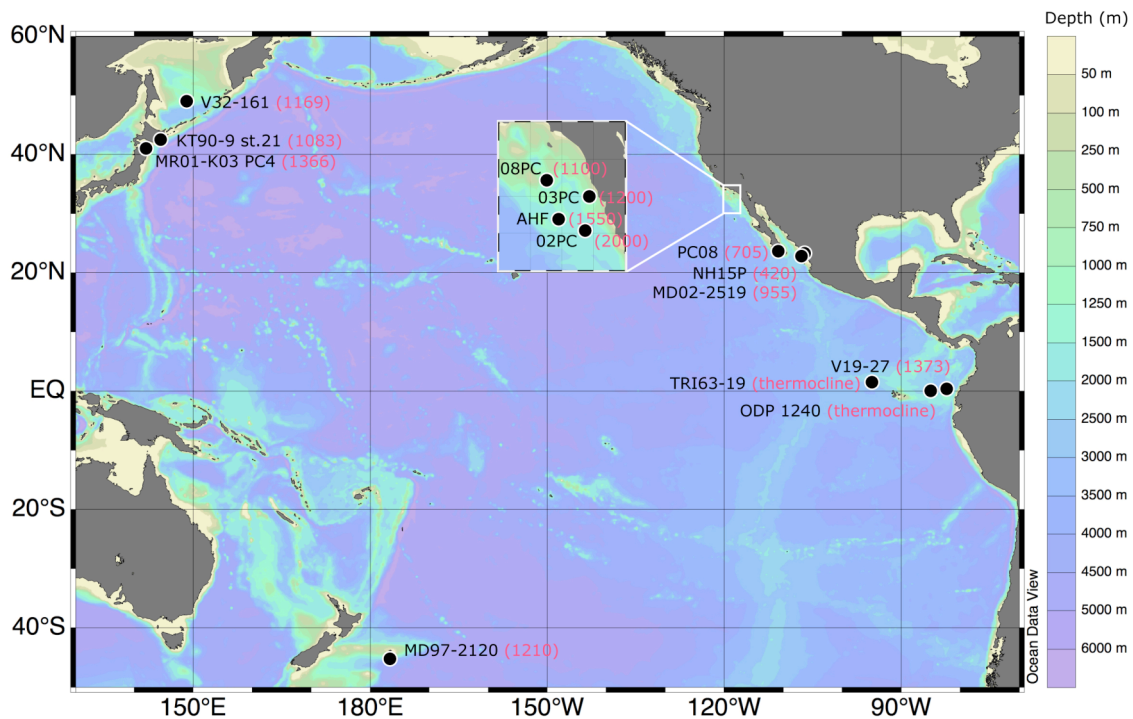
Figure 4-7. Location map of the $\delta^{13}C$ records discussed in this chapter (water depth (m) is shown in red brackets). **NE Pacific:** *MD02-2519 and NH15P - $\delta^{13}C_b$ from Mazatlan; PC08 - $\delta^{13}C_b$ from Baja California; 02PC - $\delta^{13}C_b$ from Animal Basin; AHF - $\delta^{13}C_b$ from No Name Basin; 03PC - $\delta^{13}C_b$ from Descanso Plain; 08PC – $\delta^{13}C_b$ from San Nicolas Basin.* **E Eq. Pacific:** *TR163-19 - $\delta^{13}C_p$ from Coccos Ridge; V19-27 - $\delta^{13}C_b$ and ODP 1240 - $\delta^{13}C_p$ from Panama Basin.* **SW Pacific:** *MD97-2120 - $\delta^{13}C_b$ from New Zealand.* **NW Pacific:** *V32-161- $\delta^{13}C_b$ from the Okhotsk Sea; KT90-9 st. 21- $\delta^{13}C_b$ and MR01-K03 PC4 - $\delta^{13}C_b$ from Northern Japan Sea. See full details in the main text and captions of Figures 4.8 to 4.10.*
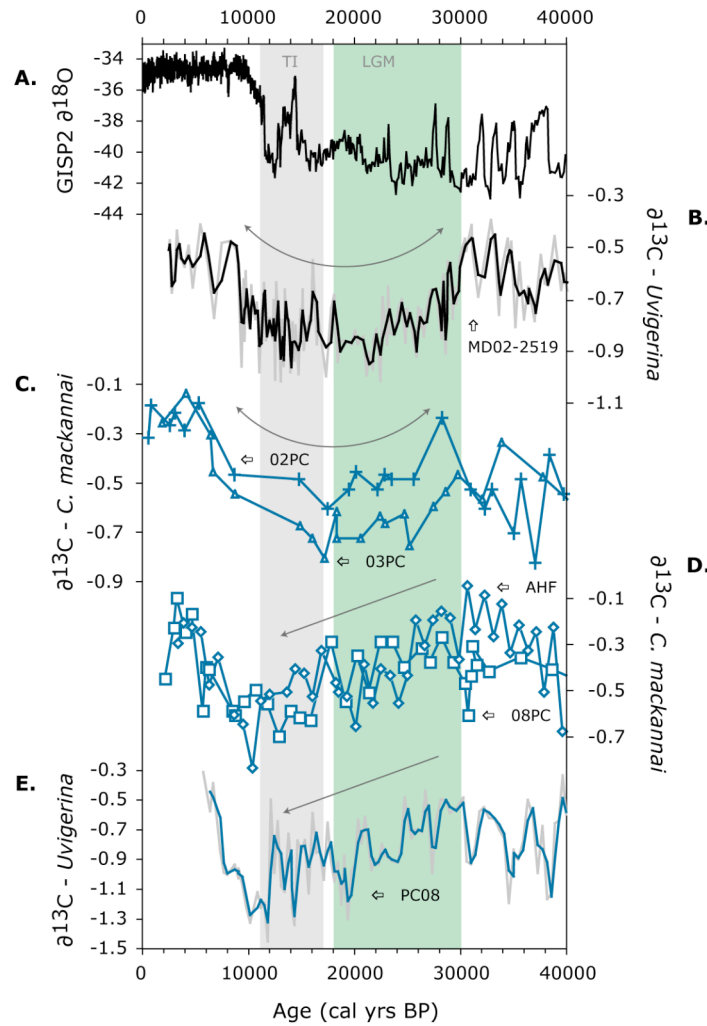
Figure 4-8 δ¹³C_b records from the northeastern Pacific spanning the last 40 ka. (A) δ¹⁸O GISP2 record shown for reference; (B) Core MD02-2519 (Mazatlan; 955 m water depth) (2 point moving average; this study); (C) EW9504-02PC (Animal Basin; 2000 m) and EW9504-03PC (Descanso Plain; 1200 m) (Stott et al., 2000); (D) EW9504-08PC (San Nicolas Basin; 1100 m) and AHF16832 (No Name Basin; 1550 m) (Stott et al., 2000); (E) PC08 (Baja California; 705 m) (2 point moving average).

4.5.3 Sources of δ¹³C signatures off NW Mexico

In Figure 4.8, we present a comparison of δ¹³C_b records retrieved from intermediate waters in the NE Pacific at depths shallower than 2000 m. Here, we observe that although the cores are from similar depths and locations, they show two different patterns. One that shows a broad δ¹³C minimum from ~ 30 to 8 ka; while the other shows relatively depleted δ¹³C values during LGM and the last deglaciation followed by an abrupt rise in δ¹³C values at ~10 ka. The first pattern is found in the Core MD02-2519 (955 mbsl) and the cores 02PC (2000 mbsl) and 03PC (1200 mbsl) from Animal basin and Descanso plain (Figure 4.8 B and

C). The second pattern is found in the $\delta^{13}C$ records of cores NH15P (420 mbsl) and PC08 (705 mbsl) from Mazatlan and Baja California and cores 08PC (1100 mbsl) and AHF (1550 mbsl) from San Nicolas and No Name basins (Figure 4.8 D and E). Thus, the broad deglacial $\delta^{13}C$ minima found in the Core MD02-2519 is found in both shallow and deep sites, and as we will see further, in both northern and southern Pacific. Overall, it is therefore difficult to constrain the regional and depth influence of each pattern, but previous studies attribute some of the differences to the complex glacial circulation of the NE Pacific (Stott et al., 2000; van Geen et al., 1996) influenced by a mixture of northern and southern source waters (Hendy and Kennett, 2003; Keigwin, 2002; Mix et al., 1999). Next, we evaluate the broad $\delta^{13}C_b$ minima event in the Core MD02-2519, which spans two important climatic periods (TI and LGM), by comparing the $\delta^{13}C$ records of the NE Pacific to other cores from intermediate depths in the Pacific Ocean.

The last deglaciation (TI)

Along the ETNP, the lighter deglacial $\delta^{13}C$ minimum seems to be an ubiquitous signature in the $\delta^{13}C_b$ records: NH15P (450 m), PC08 (705 m), MD02-2519 (955 m) and those from the adjacent basins off California (Figure 4.6 and 4.8). Based on previous reconstructions, this typical deglacial $\delta^{13}C$ minimum has only been reported in planktonic and benthic foraminifera $\delta^{13}C$ records linked to the Southern Ocean (SO) (Ninnemann and Charles, 1997; Spero and Lea, 2002). However, the $\delta^{13}C_b$ pattern found in the cores collected from the ETNP seem comparable to $\delta^{13}C_p$ records of planktonic foraminifera from the equatorial Pacific (Figure 4.9), suggesting an oceanic relationship between the ETNP and the EEP over the last deglaciation.

From previous studies (Loubere and Bennett, 2008; Ninnemann and Charles, 1997; Pena et al., 2008; Spero and Lea, 2002), the extensive distribution of the deglacial $\delta^{13}C$ minimum and the rate at which the full signal appears in different basins (i.e. the South Atlantic, the Indo-Pacific, the South and the Equatorial Pacific) points at the subantarctic as the source region. In the subantarctic region, the $\delta^{13}C$ depletion has been explained as the effect of the gradual resumption of the upwelling system. Previous reconstructions suggest, that an increase in productivity could be stimulated by the combination of the southward displacement of the westerlies, and the reinforcement of the Antarctic Circumpolar Current (ACC) (Toggweiler et al., 2006). This process might activate the northward advection of

$\delta^{13}C$-depleted waters from the Subantarctic Front, the source of Subantarctic Mode Water (SAMW), which is closely associated to AAIW (Bostock et al., 2004).
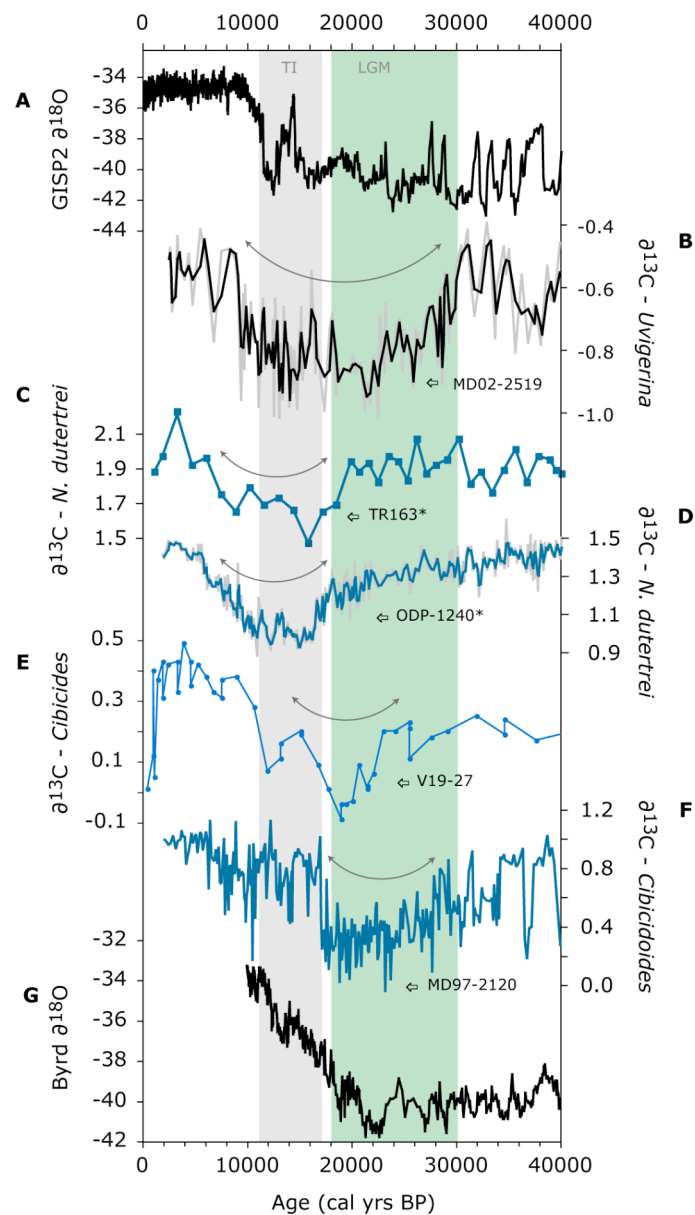
Figure 4-9 $\delta^{13}C$ foraminifera records from the eastern equatorial and southwest Pacific spanning the last 40 ka (marked with a symbol * are $\delta^{13}C$ records based on thermocline dwellers planktonic foraminifera). (A) GISP2 and (G) Byrd $\delta^{18}O$ records (Blunier et al., 1998). (B) Uvigerina spp. record of Core MDO2-2519 (2 point moving average); (C) Neogloboquadrina dutertrei record of Core TR163-19 (Coccos Ridge; 2348 m water depth) (Spero and Lea, 2002);(D) Neogloboquadrina dutertrei record of Core ODP-1240 (Panama Basin; 2921m) (Pena et al., 2008); (E) Cibicides spp. record of Core V19-27 (Panama Basin; 1373 m) (Mix et al., 1991); (F) Cibicidoides spp. record of Core MD97-2120 (New Zealand; 1210 m) (Pahnke and Zahn, 2005).

However, the $\delta^{13}C_b$ records from intermediate and subsurface waters in the ETNP appear to be uniformly affected during T1, suggesting a southern source with mixing of overlying waters. For instance, just above the AAIW and the SAMW are the Thermocline Waters (TW) (Wyrtki, 1966), whose exact location of formation is uncertain, but in the modern ocean receive large influence of Pacific Deep Waters (DW) (Tomczak, 2007). Thus, the direct contribution of DW to the TW-layer could explain the $\delta^{13}C$-depleted values found in the thermocline dwellers $\delta^{13}C$ records from the equatorial Pacific. As a result of advection and transformation of the SAMW properties (in the eastern subtropical gyre) with the mixture with Subtropical Mode Waters (STMW) (Hanawa and Talley, 2001), the remineralised carbon could be incorporated in the Equatorial Undercurrent (EUC). Then, after crossing the zonal equatorial circulation, the depleted $\delta^{13}C$ signal could encounter the subsurface and intermediate waters of the ETNP. In this way, the pathway of subthermocline and mode water circulation during the deglaciation (*see* Figure 4.2) could transfer chemical signatures from the Subantarctic region to northern latitudes (Curry et al., 1988; Lynch-Stieglitz et al., 1994; Pena et al., 2008; Spero and Lea, 2002).

The Last Glacial Maximum (LGM)

Although the general pattern of the $\delta^{13}C$ records of cores MD02-2519 and PC08 is different during the last glacial (24 – 18 ka), they converge to a similar value of -0.9‰, which is ~0.6‰ lower than modern values (Figure 4.6). When such a trend is compared to glacial records from the NW Pacific (source region of NPIW), this pattern is not identified (*see* Figure 4.10 C and E). Thus setting the idea that the intermediate water circulation could be different during the glacial, relative to the modern ocean.

Today, the cores PC08 and MD02-2519 are bathed by intermediate waters formed in the North Pacific, being the NW Pacific a region that contributes to North Pacific ventilation through production of NPIW (Talley, 1991, 1999; You et al., 2000). However, during the last glacial and LGM (i.e. interval between 30 and 18 ka), the $\delta^{13}C_b$ records from the NW Pacific mostly document $\delta^{13}C$ values either enriched or less than 0.2‰ depleted, relative to the Holocene (e.g. Figure 4.10 C and E). This pattern during the glacial has been interpreted, on one hand, as the result of better ventilated and nutrient depleted subsurface waters (i.e. less carbon remineralisation) (Broecker and Maier-Reimer, 1992; Herguera, 1992; Keigwin, 1998; Mix et al., 1991). On the other hand, ^{13}C enrichments could be attributed to

thermodynamic effects of enhanced air-sea gas exchange and high productivity in the source area (Keigwin, 1998; Morley et al., 1991; Shibahara et al., 2007). Reconstructions of records in the NE Pacific have suggested increased formation of intermediate water (akin to NPIW) in the NW Pacific and marginal seas during glacial periods (Gorbarenko, 1996). Well-ventilated upper intermediate waters during LGM have been inferred from benthic foraminifera assemblages, sediment laminations and enriched δ^{13}C-records of benthic foraminifera in NE Pacific basins like Santa Barbara, San Nicolas, East Cortez or San Clemente (Cannariato et al., 1999; Hendy and Kennett, 2003; Stott et al., 2000). However, the cores MD02-2519 and PC08 do not fit in this interpretation. Instead, the carbon isotopic signatures suggest that southern component waters (i.e. akin to AAIW) could have influenced northern regions as far as Mazatlan and Baja California.

Depleted $\delta^{13}C_b$ values during LGM have only been reported in the eastern equatorial and the South Pacific (Bostock et al., 2004; Lynch-Stieglitz et al., 1994; Mix et al., 1991; Pahnke and Zahn, 2005). In Figure 4.9, we present a comparison between the $\delta^{13}C_b$ records from Mazatlan, the EEP and the SW Pacific (i.e. Figure 4.9 B, E-F). Although the absolute $\delta^{13}C_b$ values are not equivalent because the records from the EEP and SW Pacific remain ~ 0.8 to 1.0‰ higher than the Core MD02-2519, the 3 records show a similar δ^{13}C minimum trend between 30 – 18 ka. Where the absolute $\delta^{13}C_b$ values could be attributed to a δ^{13}C decline in the intermediate water as it flows north from its southern source. On the other hand, this trend is different to that seen in records from the NW Pacific (Figure 4.10 C to E), which suggests that the cause of glacial δ^{13}C-depletion off Mazatlan and Baja California did not originate in the North Pacific. Therefore, the glacial δ^{13}C minimum could be associated either (1) to changes in the climate and water mass formation in the South Pacific, or (2) to changes in the deep water circulation.

In the first case, the substantial atmospheric and ocean cooling, the intensification of winds and upwelling, expansion of the sea-ice coverage and increased salinity, are among the local factors in the Antarctic region related to the low δ^{13}C values found in intermediate waters (Gersonde et al., 2003; Sigman and Boyle, 2000). Slower circulation and enhanced stratification at surface during the glacial (i.e. increased density) are viewed as favourable conditions for δ^{13}C gradients to develop (Bostock et al., 2004). Thus an extensive and more substantial glacial Antarctic IW (glacial-AAIW) could extend northward, transferring a preformed δ^{13}C signal to the equatorial Pacific, as evidenced in the intermediate water Core

V19-27 (Figure 4.9 E). Such a signal could then be transported via subthermocline and intermediate currents (Firing et al., 1998; Tsuchiya and Talley, 1998) up to the ETNP. The possibility that a modified glacial-AAIW could be much stronger and more extensive in the past, crossing the equator and ventilating the North Pacific, has been previously proposed (Loubere and Bennett, 2008; Ninnemann and Charles, 1997; Spero and Lea, 2002).
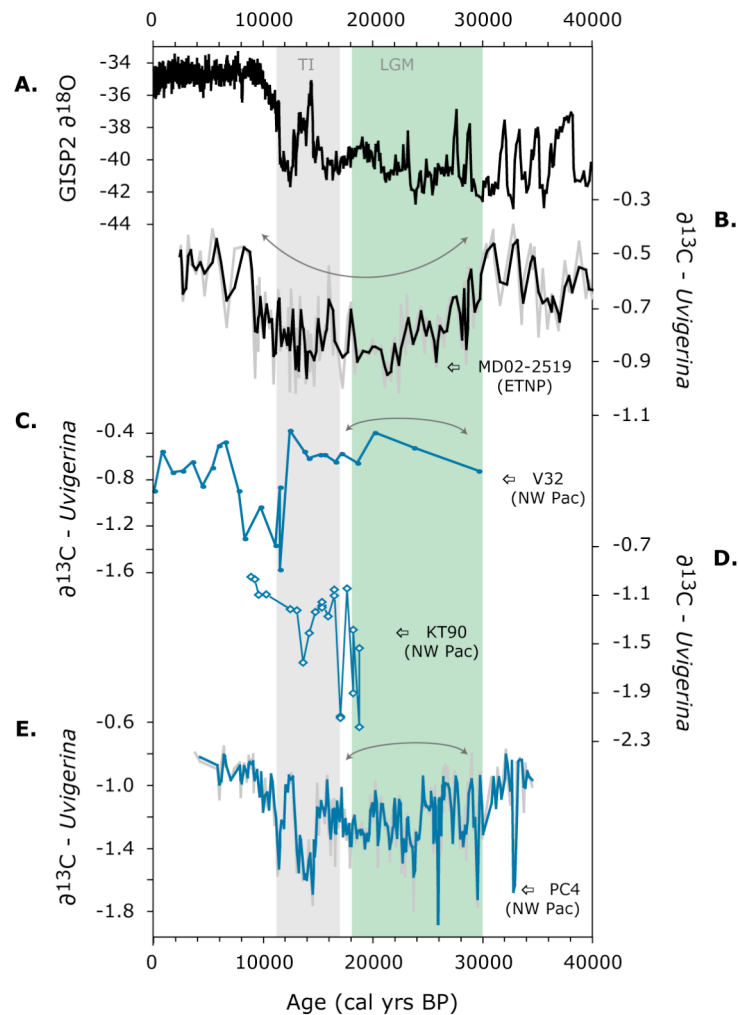
Figure 4-10 $\delta^{13}C_b$ records from the northwest Pacific spanning the last 40 ka. (A) $\delta^{18}O$ GISP2 record shown for reference; (B) Core MD02-2519 (Mazatlan; 955 m) (this study); (C) V32-161 Okhotsk Sea; 1169 m) (Morley et al., 1991); (D) KT90-9 station 21 (Hokkaido; 1083 m) (Oba and Murayama, 2004); (E) MR01-K03 PC4 (N Japan Sea; 1366 m; 2 point moving average) (Hoshiba et al., 2006).

Secondly, the glacial depletion of the $\delta^{13}C_b$ records from Southern Ocean intermediate waters has been associated to changes in deep water circulation (Bostock et al., 2004; Pahnke and Zahn, 2005). It is suggested that under thermally stratified conditions,

slower vertical mixing could lead to greater storage of CO_2 in the deep ocean producing ^{13}C-depleted bottom waters (Lynch-Stieglitz et al., 1994; Ninnemann and Charles, 1997; Sigman and Boyle, 2000). However, it is unknown whether such situation may apply to other regions of the deep Pacific Ocean. Although absolute $\delta^{13}C_b$ values are not comparable between distant regions because the data have not been normalized either to *Cibicidoides* or *Uvigerina* glacial values (due to lack of references), the pattern displayed by NE and NW Pacific records from deep waters (below 2000 m) seems to be in agreement with this glacial scenario. It suggests that the δ^{13}C minimum recorded in these regions was maybe influenced by ^{13}C-depleted deep water masses (Lund and Mix, 1998; Matsumoto et al., 2002; Mix et al., 1999). In the NW Pacific, the glacial distribution of the lowest δ^{13}C values suggests that the boundary of the oldest and more nutrient-rich water mass shifted to 2500 - 3000 m water depth, in contrast to the Holocene penetration that today is centred about 2000 m (Matsumoto and Lynch-Stieglitz, 1999; Matsumoto et al., 2002). In the NE Pacific, the effect of ^{13}C depleted waters could be produced by the change in the northward flow rate of the Pacific Bottom Water (PBW), which then returns with southward and shallower flowing along the margin in the form of Pacific Deep Water (PDW) (Lund and Mix, 1998).

In this regard, the depleted $\delta^{13}C_b$ signal found in the Core MD02-2519 suggests that the intermediate waters from the ETNP could be influenced either by a modified glacial-AAIW, or by glacial-PDW (*see* Figure 4.2). In the first case, the implication is that the preformed δ^{13}C signal is directly linked to South Pacific intermediate water circulation, which transported a depleted δ^{13}C signal to the ETNP during LGM. The second case suggests that the lower layer of the intermediate water mass was more closely linked to the deep water circulation of the Pacific. To differentiate between both hypotheses is difficult at this point because additional studies with broader geographical coverage are required. However, the record of intermediate water radiocarbon activity (Δ^{14}C) (discussed in detail in *Chapter 5)* support the assumption that aged waters from the deep Pacific invaded the lower intermediate waters of the ETNP during LGM (today bathed by the NPIW).

In Figure 4.11 we show the reconstruction of intermediate water Δ^{14}C from Mazatlan (i.e. Δ^{14}C benthic foraminifera record of Core MD02-2519). It shows that during the last glacial, the bottom waters declined by ~ 200‰, which represents, waters older than 1000 – 1500 yrs relative to Holocene values. This means that during LGM, the vertical $\Delta^{14}C_b$ gradient was stronger between the bottom waters at 955 m and the atmosphere, if compared

to modern conditions (Reimer et al., 2004). The combination of depleted $\delta^{13}C$ and low $\Delta^{14}C$ values could be the result of more stratified conditions and very isolated Pacific waters (i.e. rich in remineralised 'old carbon'). Two additional lines of evidence support this suggestion. 1) That sedimentary geochemical records from the North Pacific abyss (3.2 km water depth) document deeper waters much older and isolated during the LGM than today (Galbraith et al., 2007); and 2) the suggestion that SO waters were relatively poorly ventilated and older than 2000 years during LGM, as shown by the presence of depleted $\delta^{13}C$ waters in the deep SW Pacific (Pahnke and Zahn, 2005; Sikes et al., 2000).
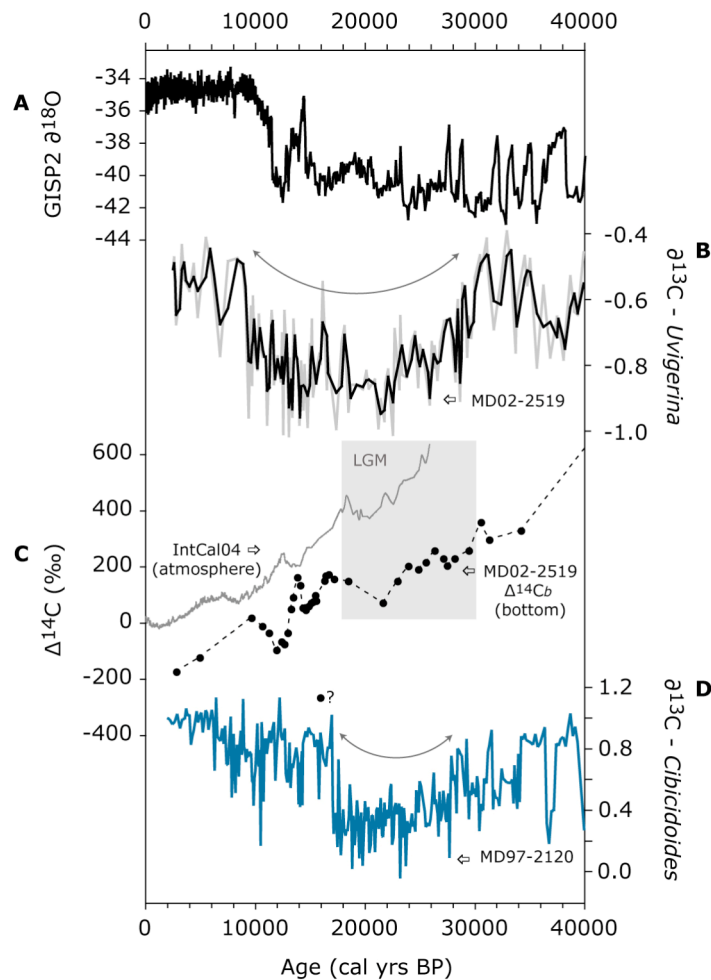
Figure 4-11 Comparison between $\delta^{13}C_b$ and $\Delta^{14}C_b$ records from intermediate depths. (A) GISP2 record shown for reference (Grootes and Stuiver, 1997); Core MD02-2519: (B) $\delta^{13}C_b$ record and (C) radiocarbon activity ($\Delta^{14}C_b$) reconstruction of bottom water at 955 m water depth (see Chapter 5), relative to changes in atmospheric $\Delta^{14}C$ through time provided by the IntCal04 compilation (Reimer et al., 2004); (D) intermediate depth $\delta^{13}C_b$record from Core MD97-2120 from the SW Pacific (Pahnke and Zahn, 2005).

The last and penultimate glacial periods

In Figure 4.12. we show a down-core comparison between $\delta^{13}C$ records of Core MD02-2519 from the ETNP (i.e. $\delta^{13}C_b$ – *Uvigerina*), cores ODP-1240 and V19-27 from the EEP (i.e. $\delta^{13}C_p$ – *N. dutertrei* and $\delta^{13}C_b$ – *Cibicides*), and Core MD97-2120 from the SW Pacific (i.e. $\delta^{13}C_b$ - *Cibicidoides*). Overall, it suggests that the $\delta^{13}C_b$ record MD02-2519 reflects a composite pattern of SW Pacific and EEP signals over the last 90 ka. For instance, since depleted $\delta^{13}C$ values are seen in records of intermediate waters from the SW Pacific, the EEP and the ETNP between 75 - 60 ka and 30 – 18 ka, relative to the Holocene (Figure 4.12 D - E). As well as the deglacial $\delta^{13}C$ minima seen in the thermocline record from the EEP (Figure 4.12 C), which is similar to that of Core MD02-2519 between 17 – 8 ka. These trends, which are common to the SW Pacific, EEP and ETNP, set up the idea that ^{13}C depleted waters could be transmitted from the SO to lower latitudes (Pena et al., 2008; Spero and Lea, 2002). Through subthermocline and mode water circulation, the waters transporting depleted $\delta^{13}C$ values could travel along the equatorial Pacific via the EUC system. Consequently, the ETNP could be influenced by southern source intermediate waters during glacial and deglacial intervals, although from different water depths, alternating between subsurface and intermediate water influences. This also suggests that the present configuration of the study area, where northern component waters (e.g. NPIW) are dominant, only occurred during interglacial periods. As we will discuss next, this idea seems consistent with older intervals like the penultimate deglaciation and the glacial MIS-6.

In Figure 4.3, we identify the presence of depleted $\delta^{13}C$ values during MIS-6 and Termination II in the Core MD02-2519 (i.e interval between 190 to 132 ka), relative to the penultimate interglacial (MIS-5). During the penultimate glacial (MIS-6), the $\delta^{13}C_b$ values were more depleted and sustained than the last glacial period. For instance, the $\delta^{13}C$ values during MIS-6 are depleted by more than ~0.5‰ relative to MIS-2 and MIS-4. Similarly, during TII (~ 132 to 125 ka) the $\delta^{13}C_b$ values are more depleted relative to TI (~17 to 11 ka) (i.e. TII $_{change} \simeq 1‰$; TI $_{change} \simeq 0.5‰$) (grey bands in Figure 4.3). Although very few studies have focused on this time period, this pattern is a consistent signal worldwide, not only recorded in the deep-sea (Hodell et al., 2003; Yamane, 2003), but also at mid- to shallow depths (Pahnke and Zahn, 2005; Pena et al., 2008).
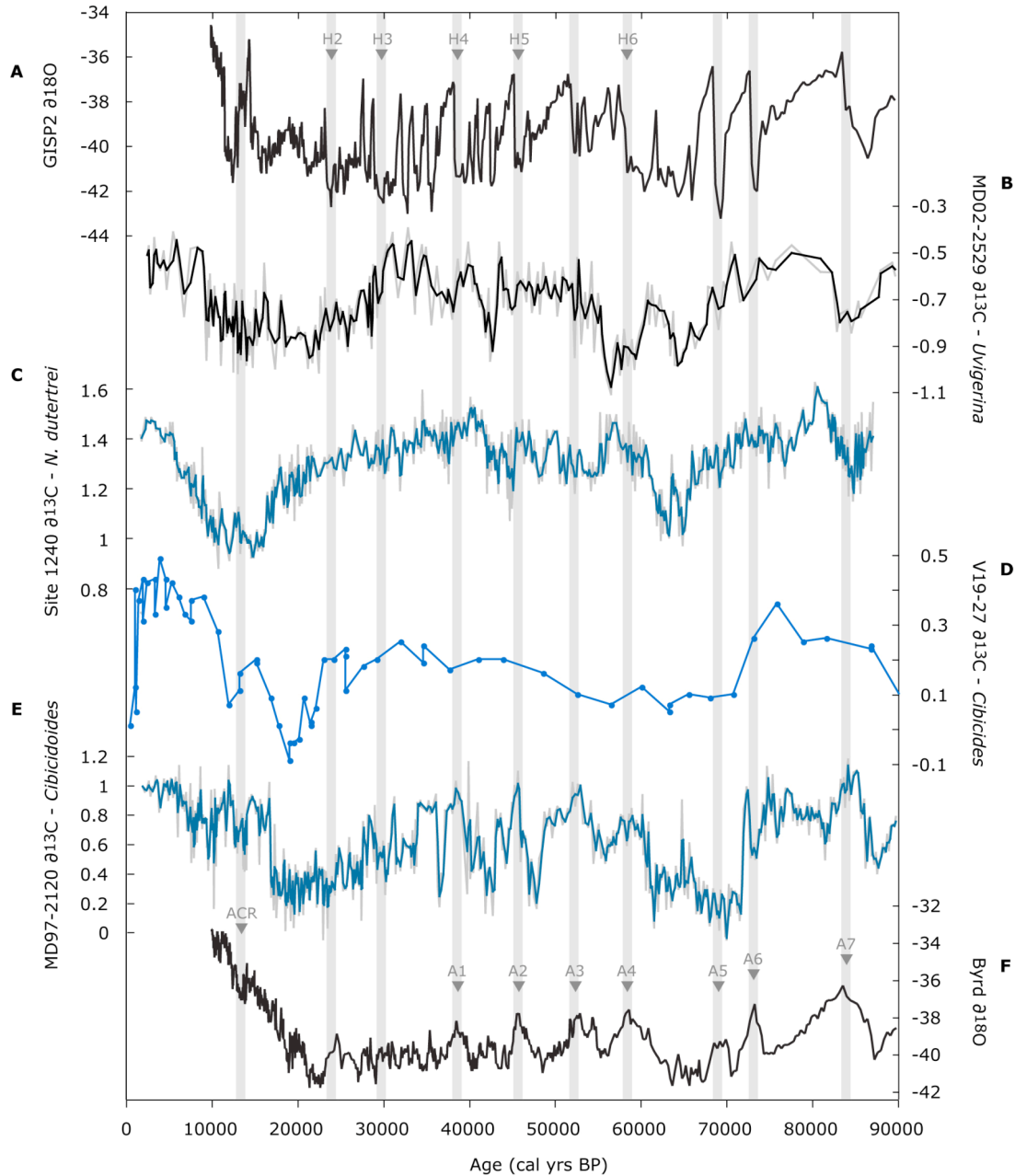
Figure 4-12 Benthic and planktonic foraminifera $\delta^{13}C$ records of the cores in the ETP, EEP and SW Pacific, spanning the last 90 ka. (A) GISP2 and (F) Byrd $\delta^{18}O$ records (Blunier and Brook, 2001) shown for reference. (B) Core MD02-2519 $\delta^{13}C_b$ Uvigerina (2 point moving average; this study); (C) ODP Core Site 1240 $\delta^{13}C_p$ N. dutertrei (Pena et al., 2008); (D) Core V19-27 $\delta^{13}C_b$ Cibicides spp. (Mix et al., 1991); (E) Core MD97-2120 $\delta^{13}C_b$ Cibicidoides spp. (Pahnke and Zahn, 2005).

The so-called TII $\delta^{13}C$-shift has been reported as an inherent feature of the ocean displaying an average glacial-integlacial shift of 0.5 - 0.7‰ with time offsets (Banakar, 2005; Duplessy et al., 1984). Two leading hypotheses are suggested to explain such large

shift. One suggests that this shift represents a fundamental change in the deep ocean circulation (Duplessy et al., 1984; Spero and Lea, 2002). The other explains that it represents a major transfer of terrestrial light-carbon to the ocean-reservoir caused by changes in the global wind patterns (Banakar, 2005).

The idea involving ocean dynamics attributes the large negative shift to diminished production of North Atlantic Deep Water (NADW), assuming that the global ocean was mostly filled with ^{13}C-depleted deep water formed by slow mixing of Pacific re-circulated water and Antarctic Bottom Water (AABW). However, even the complete shut down of NADW could not account to explain the ~ 0.5-$0.7‰$ depletion during TII, because the estimated whole-ocean change (due to increased nutrient inventories from G to IG times) is $\sim 0.3‰$ (i.e. calculated from the last glaciation to Holocene) (Boyle, 1992; Hodell et al., 2003). In consequence, an alternative explanation suggests that during TII, a drastic alteration in global climate and wind pattern may lead to a net transfer of terrestrial light-carbon to the oceans (both inorganic and organic) (Banakar, 2005). For instance, it can be through small variations in equatorial Pacific sea surface temperatures (SST) that large-scale changes in the Walker Circulation may affect the global wind patterns (Cane, 1998). However, such hypothesis has not been quantified yet by calculations of the transfer and burial of calcite to the sediments or within the terrestrial carbon reservoir.

Although it is possible that both mechanisms acted together over the penultimate glacial, another important component is still unclear in this picture: the intermediate waters. The intermediate waters are essential components of the ocean system as they convey climatic signals (e.g. heat, nutrients, oxygen) between high and low latitudes. Similar to the last glacial and TI, the intermediate waters of the SO and the equatorial regions may have played an important role in transferring and sustaining a depleted δ^{13}C signal worldwide during the penultimate glacial and TII. Hence, the intermediate circulation of the Pacific Ocean might be crucial in the reorganisation of the carbon cycle also during glacial periods.

4.6   Conclusions

In the Core MD02-2519, the isotopic analyses of multi-species of benthic foraminifera suggest that the microhabitat is largely responsible for depleting the $\delta^{13}C_b$ values of shallow-infaunal species like *B. argentea* and *Uvigerina* spp. However, a small $\delta^{13}C$ offset between bottom waters $\delta^{13}C_{DIC}$ and shallow-infaunal species, is documented in the $\delta^{13}C$ *Uvigerina* record of Core MD02-2519, which seems to limit the effect of the species-specific isotopic fractionation. Such an effect could be caused by the narrow and geochemically homogenous zone where the species calcify. In consequence, the reconstructed $\delta^{13}C$-*Uvigerina* record yields an indirect but approximate indicator of the $\delta^{13}C$ signal of intermediate waters in the ETNP. However, further studies of $\delta^{13}C_b$ are required to completely rule-out that artifacts of the vital effects are not misleading the assumption that $\delta^{13}C$ – *Uvigerina* is a good approximate proxy of bottom water DIC conditions.

Depth dependent isotopic variations in $\delta^{13}C$ were investigated in 3 different cores: NH15P (420 m water depth), PC08 (705 m) and MD02-2519 (955 m). The local productivity does not seem to have an important influence on these $\delta^{13}C_b$ records at G-IG scales, as inferred from the clear decoupling between the productivity proxies (i.e. OC and DSRa* records) and the $\delta^{13}C_b$ records. Moreover, the consistent $\delta^{13}C$-depleted values during LGM and TI seem to be regional in extent.

We suggest that the depleted $\delta^{13}C$ values found in the ETNP records between 30 - 8 ka are related to Southern Components Waters (SCW), since only the regions influenced by SO waters document depleted $\delta^{13}C$ values throughout the last glacial and deglaciation. During TI, the $\delta^{13}C$ minimum found off NE Mexico is attributed to the influence of thermocline and possibly mode waters travelling northward via the EUC system, up to the ETNP; whereas the $\delta^{13}C$ values during LGM are attributed to the incursion of deep waters from South Pacific origin.

The oceanic link between high and low latitudes is documented by the transmission of preformed low-$\delta^{13}C$ from the South Pacific as far north as ~ 23°N. The intermediate water flowing from the SO to the tropics was possibly a lot more extensive during glacials than interglacials, where Northern Component Waters (NCW) domain. This scenario is also

registred during the penultimate glacial-interglacial cycle, where a broad $\delta^{13}C$ minimum is seen in the Core MD02-2519 during MIS-6 and TII. Although the cause of the pre-TII low-$\delta^{13}C$ values remains unknown, we suggest that such depleted $\delta^{13}C$ signal could be influenced and transmitted worldwide by intermediate waters, highlighting their role in propagating climatic signals from poles to tropics at different timescales.

Additional studies are still required to better constrain the intermediate water $\delta^{13}C$ records of the ETNP, where epifaunal species of benthic foraminifera are scarce. In addition, to evaluate changes ocean circulation at G-IG and millennial timescales, it is required to study present and past patterns of $\delta^{13}C$ in several intermediate water sites, through the Pacific and the world oceans.

4.7   Supplement: Benthic Foraminifera Taxa.

Bolivina argentea s.l. Cushman=*Bolivina argentea* Walton, 1955 (p. 1001, pl. 101, Figures. 26–27)=*Bolivina argentea* var. *monicana* Zalensy 1959.

Remark. In this study, we applied a broader species concept to include the wide range of morphologic variability observed and make the results comparable with other locations along the Pacific margin (e.g. Holsten *et al.*, 2004). Hence, all morphotypes that have elongate, twisted to slightly twisted tests with acute and keeled edges were grouped in the samples. The number of chambers is not considered in the identification.

Bolivina subadvena s.l. Cushman 1935=*Bolivina subadvena* Cushman var. *sulphurensis* Cushman and Adams 1935 (p. 20, pl. 3, Figures. 8–9).

Buliminella tenuata Cushman=*Buliminella subfusiformis* Cushman var. *tenuata* Cushman 1927 (p. 149, pl. 2, Figure 9).

Uvigerina var. *peregrina* Cushman 1923.

🌐

Chapter 5

Evaluating the redistribution and the release of glacial 'old-Carbon' during the last deglaciation

5.1   Introduction

At the last glacial termination, the carbon content of the atmosphere increased from ~ 360 to 560 gigatons (Gt) (IPCC, 2001) representing ~ 80 ppmv increase in atmospheric CO_2 levels (Barnola et al., 1987; Monnin et al., 2001; Smith et al., 1999). Oceanic carbon sequestration during the Last Glacial Maximum (LGM; ~ 20 cal ka BP) and it subsequent release during the deglacial is thought to have played a major role in such increase in atmospheric CO_2 concentrations (Ahn and Brook, 2008; Broecker and Peng, 1982; Sigman and Boyle, 2000). Such a perturbation in the C cycle is expected to imprint a signal on the radiocarbon activity ($\Delta^{14}C$) of the carbon reservoirs of the deep and near surface ocean, and the atmosphere (Broecker et al., 2008).

During the period between ~18 – 12.8 cal ka BP, the atmospheric radiocarbon activity ($\Delta^{14}C$) exhibited a drop of 200‰ $\pm$ 20 (see *red square* in Figure 5.1), which cannot be fully accounted by changes in atmospheric ^{14}C production rates of this period (Broecker and Barker, 2007; Hughen et al., 2006; Hughen et al., 2004). However, dilution by the relocation of ^{14}C-depleted 'old carbon' isolated from the atmosphere in the deep ocean may explain such a drop. The location of the 'old carbon' pool in the deep ocean during LGM and the pathway of its release through the upper layers are important questions that remain to be fully addressed (Broecker and Barker, 2007).

Two recent studies have reported evidence of transient 'old carbon' signatures during the last deglaciation suggesting redistribution via intermediate waters in the Pacific low latitudes. First, a study based on benthic foraminiferal ^{14}C measurements from a core collected off Baja California (Marchitto et al., 2007), documented a drop of ~ 350 ‰ in $\Delta^{14}C$ activity in the intermediate water of the Pacific (705 m water depth) (Figure 5.1). Importantly, this drop occurred in two stages spanning the Heinrich 1 (H1; 17.8 - 16 ka) and

the Younger Dryas (YD; 12.8 - 11.5 ka). These events also coincide with two periods of accelerated CO_2 increase, as recorded in ice cores from Antarctica (Figure 5.1). A second study (Stott et al., 2009), based on planktonic and benthic foraminifera $\Delta^{14}C$ records, documented a much larger deglacial drop (up to 500 ‰) in a core collected underneath the equatorial divergence region off Galapagos (617 m water depth). The documentation of ^{14}C-depletion in the near surface dwelling planktonic foraminifera during the last deglaciation is relevant as it suggests upwelling and degassing of 'old carbon' in the eastern equatorial Pacific (EEP). Although both studies strongly support that intermediate waters in the eastern Pacific acted as a conduit for the redistribution and release of 'old carbon' from the ocean, the extent of this signal and its source remains unclear. In fact, the proposed routing of "old carbon" release via Southern Ocean (SO) intemediate waters has been recently questioned, as no $\Delta^{14}C$ signal of "old carbon" is documented in the eastern South Pacific (ESP) waters off Chile (De Pol-Holz et al., 2010). Therefore, constraining the depth and the geographical range of the waters bearing depleted ^{14}C signatures is essential to identify the location of the isolated deep carbon pool and its pathway of release from the glacial ocean.

In this chapter, we reconstruct $\Delta^{14}C$ records of surface (planktonic foraminifera and organic carbon) and intermediate (benthic foraminifera) waters in the eastern tropical North Pacific (ETNP), to evaluate the extent of ^{14}C-depleted waters during the last deglaciation. Using the Core MD02-2519, retrieved from the continental slope off Mazatlan, NW Mexico (Figure 5.2), we attempt to constrain the depths of the intermediate water mass carrying 'old carbon'. For this, we compare the benthic $\Delta^{14}C$ record of the Core MD02-2519 (995 m) with two records previously published (Figure 5.2): the Core PC08 retrieved from 705 m water depth off Baja California (Marchitto et al., 2007), and the Core VM21-30 retrieved from 617 m water depth in the eastern equatorial Pacific (EEP) (Stott et al., 2009). The $\Delta^{14}C$ signatures of planktonic foraminifera and organic matter are additionally used to evaluate the surface ocean response to the abrupt release of 'old carbon'. In addition, we compare the $\delta^{13}C_b$ record of Core MD02-2519 to previously publised $\delta^{13}C_b$ records from the SO, to evaluate if a ^{13}C-depletion signal is consistent with the ocean release of remineralised 'old carbon' during the deglaciation.
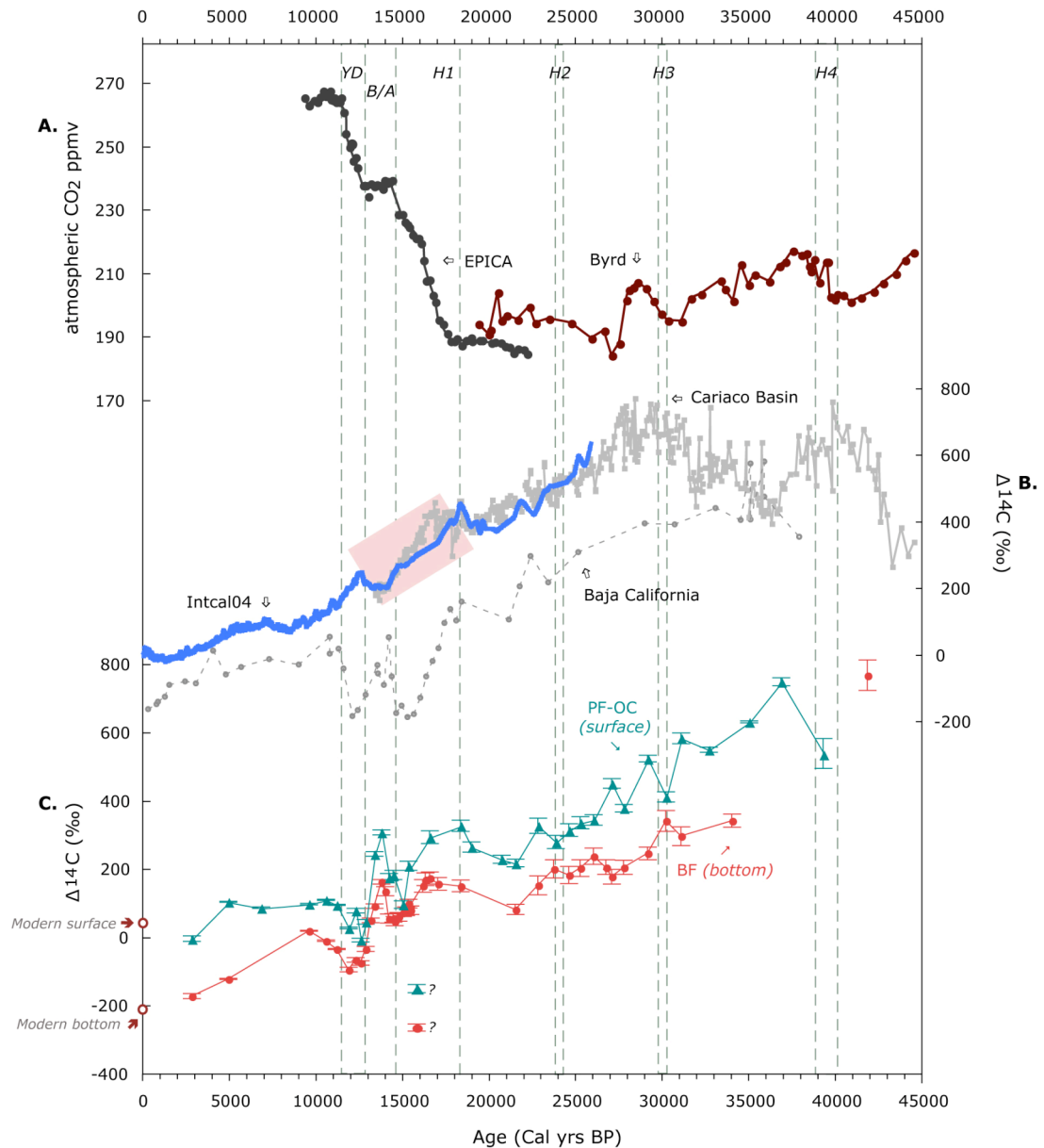
Figure 5-1 Atmospheric and oceanic radiocarbon activity ($\Delta^{14}C$) records spanning the last 45 ka. (A) $CO_{2\ atm}$ ice core records from Antarctica: Byrd – brown dots (Ahn and Brook, 2008) and EPICA – black dots (Monnin et al., 2001). (B) Atmospheric $\Delta^{14}C$ records from Cariaco Basin (based on planktonic foraminifera (Hughen et al., 2006), on Hulu timescale) and Intcal04 (based on tree rings, varve sediments and corals (Reimer et al., 2004)); intermediate water $\Delta^{14}C$ record from Baja California - open grey circles (Marchitto et al., 2007). Red rectangle over the $\Delta^{14}C_{atm}$ records marks the deglacial 200‰ change. (C) $\Delta^{14}C$ records of Core MD02-2519 (955 m depth) based on benthic foraminifera (red circles) and planktonic foraminifera-organic carbon (green triangles). $\Delta^{14}C$ error bars are obtained by combining radiocarbon age errors with estimated calendar uncertainty (see methods*), both listed in Table 5.2. Open dark-red circles at 52‰ and -209.8‰ are $\Delta^{14}C$ modern values of surface and intermediate waters at 955 m, based on local measurements from the nearest GEOSECS profile (ISTA 343) (Key et al., 2004; Ostlund and Stuiver, 1980). Limits of the YD, B/A (Bølling/Ållerød) and H events are also indicated (vertical dotted lines).*
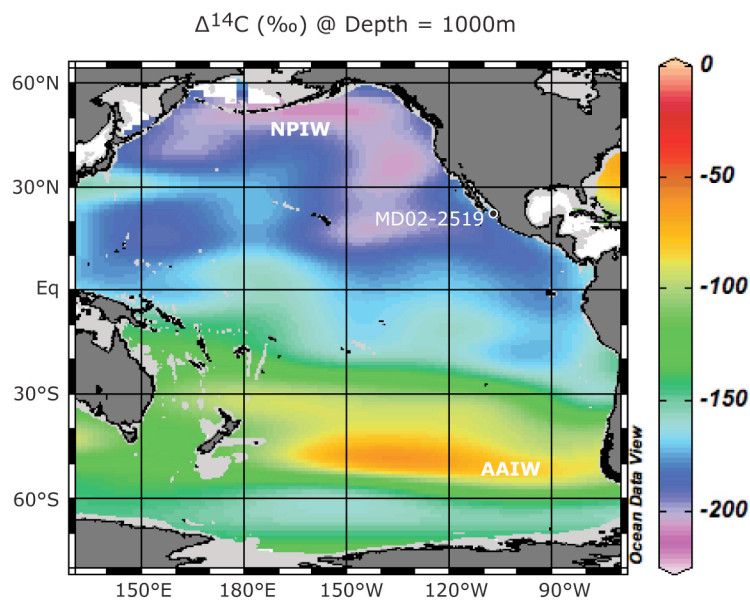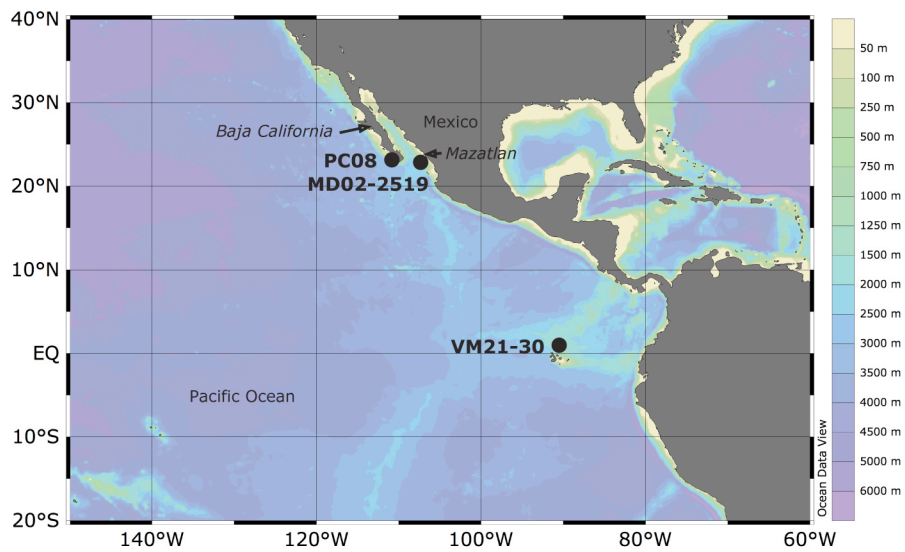
Figure 5-2 Location map of the marine sediment cores described in the text. Core MD02-2519 retrieved off Mazatlan (lat 22°30.89N; long 106°39.00W; 955 m water depth) (Beaufort, 2002); Core PC08 (i.e. core triplet MC19/GC31/PC08) from southern Baja California (lat 23.47°N; long 111.43°W; 705 m water depth) (Marchitto et al., 2007); and Core VM21-30 from Galapagos (lat. 1°13' S; long. 89° 41'W; 617 m water depth) (Stott et al., 2009). The bottom picture is the GLODAP iso-surface at 1000 m water depth (Key et al., 2004) showing the location of Core MD02-2519 retrieved from 955 mbsl, and the $\Delta^{14}C$ content of the two main Pacific intermediate waters: NPIW (North Pacific Intermediate Water) and AAIW (Antarctic Intermediate Water).

5.2   Material and Methods

5.2.1   Sediment samples and isotopic analyses

Sediment samples from the Core MD02-2519 were selected to analyse (*a*) radiocarbon (^{14}C) in samples of benthic foraminifera (BF), planktonic foraminifera (PF) and organic carbon (OC); and (*b*) stable isotopes in BF. To obtain the foraminifera samples, we sub-sampled ~ 5 cm^3 of dried sediments. Subsequently, the samples were disaggregated in distilled water and washed with running tap water though a mesh size of 63 μm. Benthic and planktonic foraminifera shells were handpicked from the size fraction > 63 and > 250 μm, respectively. Prior the analyses, the calcite samples were sonified for few seconds with double distilled water and dried overnight in an oven at 50° C.

Radiocarbon

Radiocarbon analyses were performed on 41 samples of mixed benthic foraminifera, 11 of mixed planktonic and 25 of organic carbon (i.e. decalcified bulk sediment samples). Such a number of ^{14}C dates was necessary to compare to existing Δ^{14}C records. However, not all data points were adequate to be included in the age model construction described in *Chapter 1*, because the ^{14}C calibration output anomalous ages (i.e. older or younger than expected based on correlation to GISP2 records). On the other hand, the evaluation of such anomalies is the goal of the present chapter.

Obtaining enough calcite material from the same sediment sample to perform species-specific ^{14}C analyses was not possible for this study. Thus, the strategy of using mixed benthic or mixed planktonic foraminifera was chosen over joining several adjacent intervals with single species (e.g. between 5 - 10 samples). Even though the benthic foraminifera inhabit a wide range of sediment depths, the majority of the species do not live deeper than $2 - 4$ cm. For instance, infaunal species like *Brizalina*, *Bolivina* and *Uvigerina* (the most abundant along the margin) preferably dwell in the first 1 mm $- 2$ cm (Holsten et al., 2004; McCorkle et al., 1997; McCorkle et al., 1990). Therefore, this approach was undertaken to obtain an adequate sample size without compromising the precision of each ^{14}C-date, given that the estimated age in each cm of sediment $\sim 50 - 100$ yrs.

In this way, approximately $15 - 20$ mg of foraminiferal CaCO$_3$ and 120 mg of bulk sediment samples were used to perform the ^{14}C analyses. The ^{14}C content was determined by

Accelerator Mass Spectrometry (AMS) at the NERC Radiocarbon Laboratory, East Kilbride, United Kingdom (through allocations 1183-0406 and 1259.1007.001 - 005). As part of the standard pre-treatment, the raw samples (n= 77) were hydrolysed to CO_2 using 85% ortophosphoric acid at 25°C, and the gas converted to graphite by Fe/Zn reduction. The CO_2 sub-samples were measured for ^{13}C, normalised to a $\delta^{13}C$ of –25‰, and the results expressed as %modern (Stuiver and Polach, 1977).

Stable isotopes

The $\delta^{18}O$ and $\delta^{13}C$ analyses in shells of the benthic foraminifera *Uvigerina* spp. were determined on a Thermo Electron Delta$^+$ Advantage mass spectrometer at the Wolfson Laboratory, the University of Edinburgh. The standard deviation for 56 analyses of a marble powder (MAB2B) run as a sample over the same period as the studied samples was ± 0.06‰ for $\delta^{13}C$ and ± 0.07‰ for $\delta^{18}O$. The sampling intervals varied between 2-10 cm in 800 cm core length, which means a sampling resolution of 100 - 500 years. To obtain an even distribution of samples every 250 years, linear interpolation between data points was applied to the $\delta^{18}O$ and $\delta^{13}C$ series. The *new sampling* of the series was performed using the Mac OS X software *AnalySeries* 2.0.4.2 (Paillard et al., 1996).

5.2.2 Radiocarbon activity ($\Delta^{14}C$)

By convention, the radiocarbon to carbon ratio ($^{14}C/^{12}C$) is expressed as the ^{13}C-normalized difference from that of pre-industrial atmospheric CO_2 (Stuiver and Polach, 1977). Hence, the atmospheric radiocarbon concentration ($\Delta^{14}C$) is expressed as the difference in ^{14}C activity (measured in ‰) between the sample and the standard, after corrections for fractionation and sample age. The $\Delta^{14}C$ determinations are based on the work by Stuiver and Polach (1977) using the calculation scheme developed by Adkins and Boyle (1997), which considers the effect of a changing atmospheric environment and provides an independent way to choose the best initial atmospheric value for the deep water mass:

$$\Delta^{14}C = (\frac{e^{-^{14}C\ age/8033}}{e^{-cal\ age/8266}} - 1) * 1000$$

where, the ^{14}C age (years BP) is the *conventional radiocarbon date* (i.e. the reported ^{14}C ages); *8033* is the Libby mean life for radiocarbon (in years); *cal age* is the calendar age (i.e.

the independent age based on GISP2-Hulu timescale); *8266* is the true ^{14}C decay constant or *λ mean life* (in years).

The Δ^{14}C uncertainties (error bars in Figure 5.1) were obtained by compounding the *conventional ^{14}C age error* with the estimated *calendar error*, which is the estimated precision of our tuning with respect to the independent chronology but not any error in the GISP2-Hulu chronology itself (Marchitto, *pers. comm.*).

5.2.3   Age model

The calculation of the Δ^{14}C essentially requires a radiocarbon independent chronology (i.e. supplementary to that based on ^{14}C calibration). Such a chronology is obtained by tuning the %OC MD02-2519 record with the records of δ^{18}O GISP2 (Grootes and Stuiver, 1997) and Hulu Cave (Wang et al., 2001) following the method suggested by Marchitto *et al.* (2007). The strategy of using such chronology is to truthfully compare to existing Δ^{14}C$_{atm}$ records (i.e. Intcal04 and Cariaco Basin), which are conventionally reported on Hulu Cave timescale (Hughen et al., 2006; Reimer et al., 2004). Consequently, the tuning between the *%OC MD02-2519* record and the δ^{18}O GISP2 record (*Chapter 1*) requires to be consistent to the Hulu Cave chronology. However, because the GISP2 scale is parallel over the last ~25 ka to Hulu Cave and coral chronologies, the dates younger than 25 ka were tuned to δ^{18}O GISP2 record (Figure 5.3) taking advantage of the close similarity between the records of %OC MD02-2519 and δ^{18}O GISP2 (*see Chapter 1*). Dates older than 25 ka were tuned to Hulu-Cave to derive calendar ages, where the tie-points were taken at or between stadial–interstadial events (Figure 5.3). The final chronology (Figure 5.3-D) was obtained by linear interpolation between 21 control-points (Table 5.1).
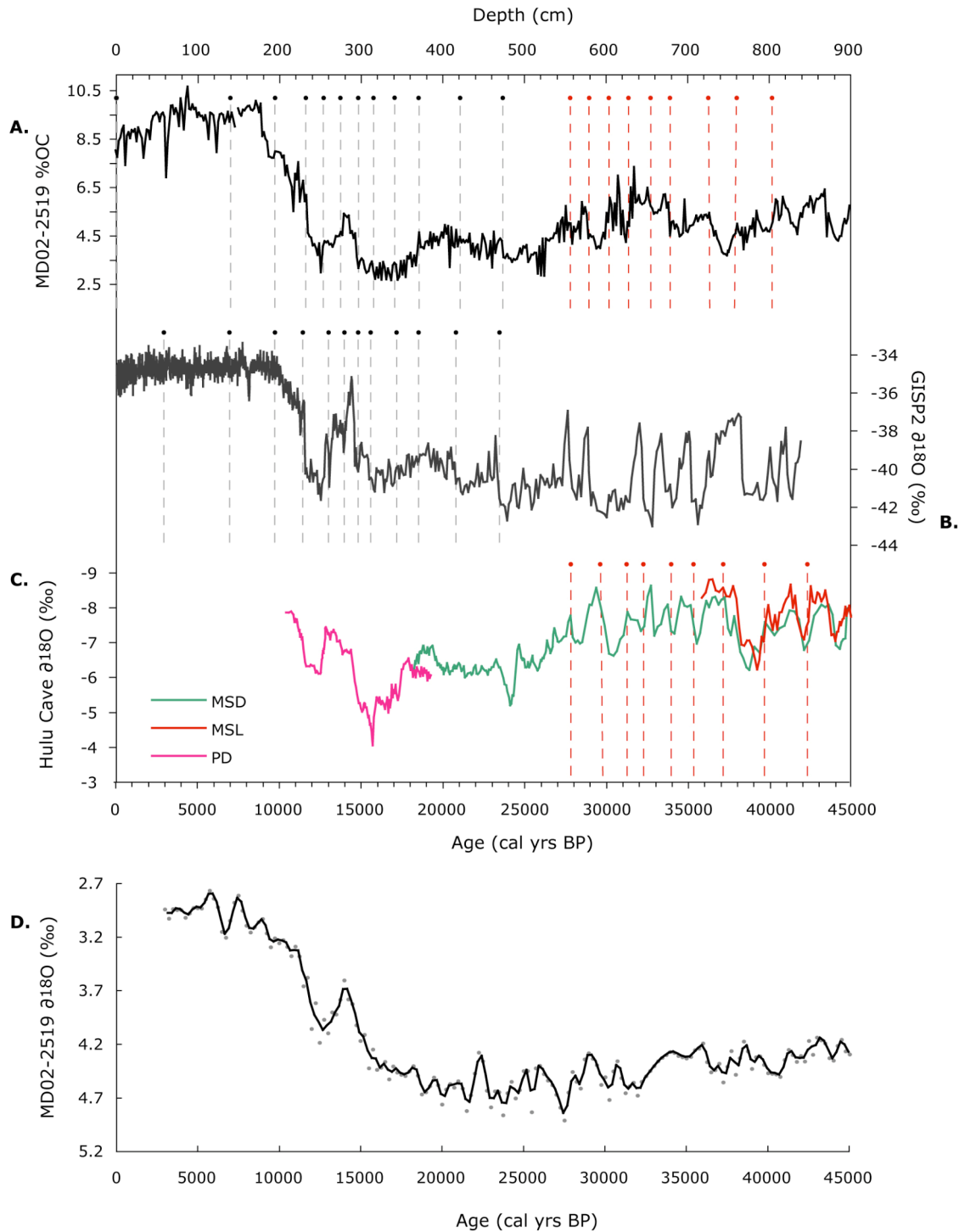
Figure 5-3 Core MD02-2519 composite age model. (A) %OC plotted vs. depth. (B) GISP2 δ¹⁸O record (Grootes and Stuiver, 1997). (C) Hulu Cave δ¹⁸O record from three different stalagmites (Wang et al., 2001). (D) Core MD02-2519 δ¹⁸O-Uvigerina (grey dots) record vs. age (black line – 2 point moving average). Black dotted lines mark tie-points based on GISP2 scale, whereas the red dotted lines are tie-points based on Hulu Cave scale (see Table 5.1 for full list of tie points).

Table 5.1. Age Model Core MD02-2519

	Core depth (cm)	GISP2 - Hulu [*] (cal yrs BP)
1	0	2900
2	140	6900
3	194	9700
4	232	11400
5	254	13000
6	274	13992
7	296	14800
8	314	15800
9	340	17200
10	370	18500
11	422	20800
12	476	23500
13	556	27844
14	580	29694
15	606	31300
16	626	32375
17	656	33995
18	678	35388
19	725	37166
20	760	39730
21	804	42402

[*] Tuned to ∂18O-GISP2 ice core (Grootes et al,. 1993)
and ∂18O-Hulu Cave speleothem (Wang et al., 2001)

Table 5-1 Age Model of Core MD02-2519 listing the 21 tie points from GISP2 (black) and Hulu Cave (red) chronologies.

In Figure 5.4, we show the age vs. depth relationship of the AMS ^{14}C samples in the Core MD02-2519 based on benthic foraminifera (BF), and planktonic foraminifera – organic carbon samples (hereinafter PF-OC) (Table 5.2). The use of interchangeably planktonic foraminifera and organic carbon based ^{14}C-dates in intervals where planktonics were scarce, is justified by the fact that the OC-based ages do not show significant offsets from the PF-based ages in those nearby samples where measurements were collected (see *black squares* in Figure 5.4-A). Such similarity allowed us to construct a combined record that represents the ocean surface Δ^{14}C (Figure 5.1). Published records of δ^{13}C-OC data (Ganeshram et al., 2000) also confirm that the organic-rich sediments underlying this upwelling region (6-10 wt %OC) preserve overwhelmingly algal derived organic carbon (Ganeshram et al., 1999).

The ^{14}C age differences between benthic foraminifera (BF) (i.e. bottom conditions) and PF-OC dates (i.e. surface conditions) show an average age difference of 990 yrs, which reliably indicate that the BF ^{14}C ages are always older, relative to the PF-OC ages (Figure 5.4

and Table 5.2). The average surface – bottom age difference is ~785 years between 17.8 – 11.5 ka BP (ca. deglaciation period), and ~1085 years between 18 – 30 ka BP (ca. last glacial period). Two broad intervals showing older ages are found amid 250-340 cm depth in both, planktonic and benthic samples (see Figure 5.4), which correspond to the deglacial events H1 and YD. With the exception of this interval, the relationship between ^{14}C ages and depth is fairly linear (*top plot in* Figure 5.4).

In the Figure 5.1, we show the calculated Δ^{14}C values of the Core MD02-2519 plotted on independent chronology tuned to GISP2 – Hulu Cave scale (Figure 5.3). Also, plotted for comparison are the Δ^{14}C atmospheric records from Intcal04 (Reimer et al., 2004) and Cariaco Basin (Hughen et al., 2006), and the benthic record of Core PC08 from Baja California (Marchitto et al., 2007). For reference: the modern atmospheric Δ^{14}C value is 0‰, the warm surface waters have average values of -40‰, deep waters formed in the North Atlantic have values close to -70‰, and the deep waters formed in the Southern Ocean values of -160 ‰. In the Pacific, the average value of the deep waters has a preformed value of -105‰ because they are a mixture of waters sourced in the North Atlantic and the Southern Ocean. In the ETNP, the Δ^{14}C from intermediate waters at 1000 mbsl is close to -200‰ (dark-red circle in Figure 5.1), whereas the deep NE Pacific (> 3500 m water depth) has the most negative Δ^{14}C value of the whole ocean of -250‰ (Matsumoto and Key, 2004; Peacock et al., 1999). In Figure 5.1, it is shown that the most recent intervals of the Core MD02-2519 collected off Mazatlan document benthic Δ^{14}C values of -200‰ and PF-OC values of 52‰, consistent with modern observations at intermediate and surface depths (Matsumoto and Key, 2004).
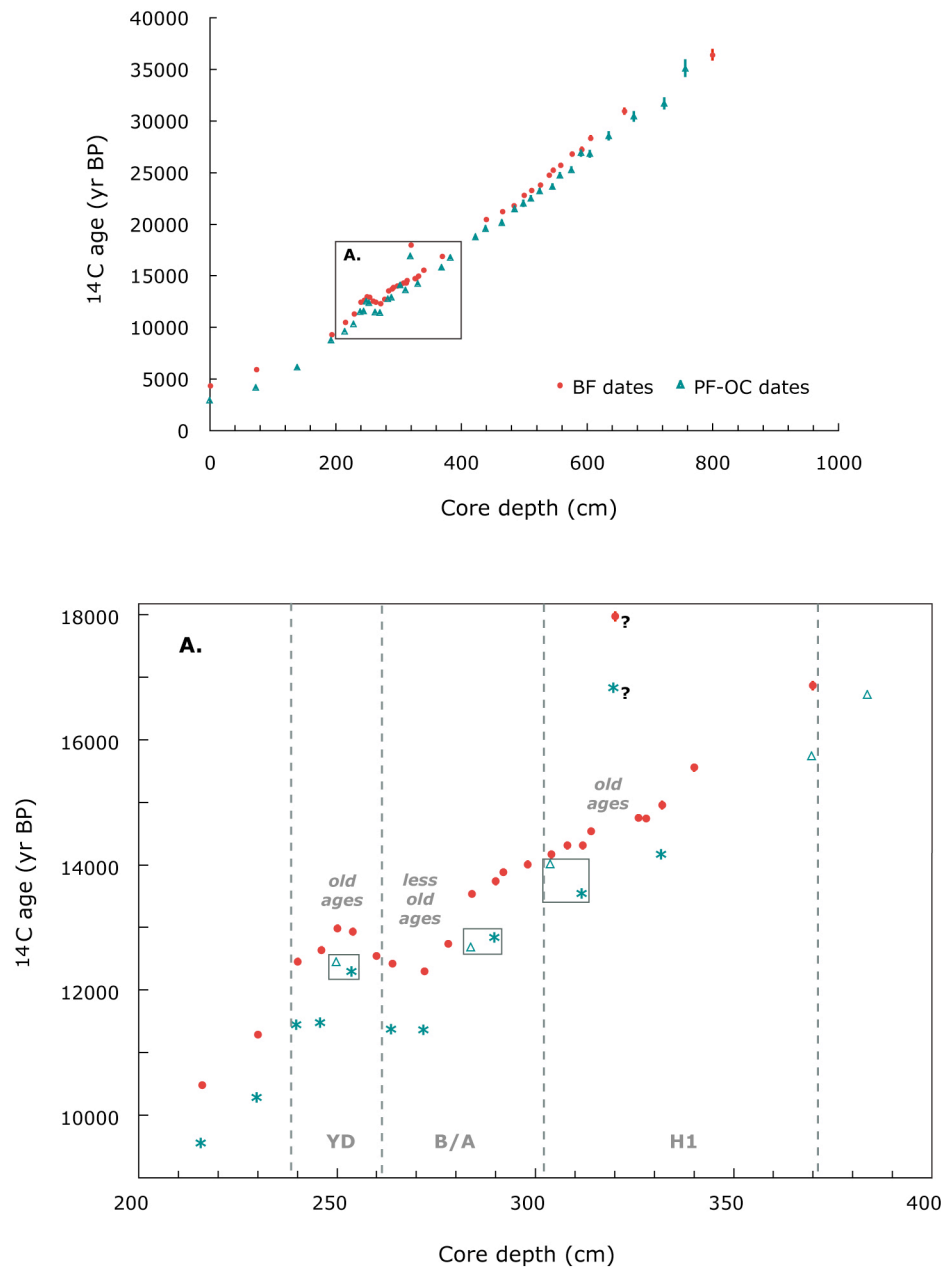
Figure 5-4 Radiocarbon ages (non calibrated) vs. depth of Core MD02-2519, based on benthic foraminifera (red circles) and planktonic foraminifera - organic carbon (green trianges) samples. - Inset A - shows the AMS ^{14}C dates based on planktonic foraminifera with asterisks, while those based on organic carbon with triangles (see Table 5.2). Data points enclosed in black-squares validate the age consistency between PF and OC AMS ^{14}C dates. Vertical dashed-grey lines show the boundaries of H1, the B/A and the YD in the Core MD02-2519, based on tuning to GISP2 scale.

Table 5.2. Core MD02-2519 - AMS ¹⁴C dates

Depth (cm)	Nature of sample	¹⁴C Enrich. (% modern ± 1s)			Convent. ¹⁴C age (years BP ± 1σ)			Carbon cont. (% wt.)	∂¹³C VPDB ‰ ± 0.1	GISP2 - Hulu age (Cal yrs BP)*			Δ¹⁴C ‰		
1	mixed BF	58.13	+/-	0.25	4357	+/-	35	12.2	-0.8	2900	+/-	100	-174	+/-	8
74	mixed BF	47.78	+/-	0.21	5933	+/-	35	11.9	-1.0	5014	+/-	25	-124	+/-	1
194	mixed BF	31.47	+/-	0.14	9286	+/-	35	12.2	-0.9	9700	+/-	25	18	+/-	1
216	mixed BF	27.14	+/-	0.13	10477	+/-	39	10.7	-1.0	10684	+/-	25	-12	+/-	2
230	mixed BF	24.54	+/-	0.12	11284	+/-	40	11.4	1.0	11311	+/-	25	-36	+/-	2
240	mixed BF	21.21	+/-	0.11	12456	+/-	41	10.1	-0.9	11982	+/-	100	-96	+/-	7
246	mixed BF	20.75	+/-	0.11	12632	+/-	41	9.9	-0.4	12418	+/-	100	-68	+/-	7
250	mixed BF	19.85	+/-	0.11	12987	+/-	43	11.4	-1.2	12709	+/-	100	-76	+/-	7
254	mixed BF	20.00	+/-	0.1	12929	+/-	42	10.1	-0.6	13000	+/-	100	-36	+/-	7
260	mixed BF	20.98	+/-	0.11	12544	+/-	41	10.7	-0.8	13298	+/-	100	48	+/-	7
264	mixed BF	21.30	+/-	0.11	12423	+/-	41	10.1	-0.8	13496	+/-	100	90	+/-	7
272	mixed BF	21.62	+/-	0.11	12302	+/-	41	11	-0.7	13893	+/-	100	161	+/-	7
278	mixed BF	20.48	+/-	0.11	12737	+/-	41	11.1	-0.8	14139	+/-	150	133	+/-	13
284	mixed BF	18.53	+/-	0.08	13540	+/-	36	10.8	-1.7	14359	+/-	150	53	+/-	14
290	mixed BF	18.09	+/-	0.1	13737	+/-	44	11.2	-1.6	14580	+/-	150	55	+/-	13
292	mixed BF	17.76	+/-	0.09	13882	+/-	43	11.1	-0.8	14653	+/-	150	46	+/-	13
298	mixed BF	17.48	+/-	0.09	14009	+/-	43	10.8	-0.7	14887	+/-	150	59	+/-	13
304	mixed BF	17.14	+/-	0.1	14169	+/-	46	11	-1.1	15147	+/-	150	71	+/-	12
308	mixed BF	16.84	+/-	0.09	14308	+/-	43	9.8	-1.1	15320	+/-	150	75	+/-	13
312	mixed BF	16.84	+/-	0.1	14308	+/-	46	9.9	-0.9	15493	+/-	150	98	+/-	12
314	mixed BF	16.37	+/-	0.09	14536	+/-	43	9.5	-0.6	15580	+/-	150	78	+/-	13
320	mixed BF	10.65	+/-	0.08	17991	+/-	60	10.4	-1.5	15954	+/-	150	-266	+/-	11
326	mixed BF	15.94	+/-	0.09	14750	+/-	44	9.7	-0.8	16328	+/-	200	149	+/-	19
328	mixed BF	15.96	+/-	0.09	14742	+/-	45	9.9	-4.6	16452	+/-	200	168	+/-	19
332	mixed BF	15.54	+/-	0.09	14954	+/-	48	9.7	-0.8	16702	+/-	200	172	+/-	18
340	mixed BF	14.42	+/-	0.09	15554	+/-	48	9.4	-0.9	17200	+/-	200	156	+/-	18
370	mixed BF	12.26	+/-	0.09	16863	+/-	57	10	-2.5	18500	+/-	200	149	+/-	17
440	mixed BF	7.82	+/-	0.07	20472	+/-	73	10.9	-1.6	21631	+/-	200	71	+/-	15
466	mixed BF	7.12	+/-	0.07	21222	+/-	76	10.4	-2.0	22981	+/-	300	148	+/-	27
484	mixed BF	6.63	+/-	0.07	21800	+/-	82	10.6	-0.7	23956	+/-	300	202	+/-	26
500	mixed BF	5.88	+/-	0.07	22766	+/-	90	10.4	-1.2	24867	+/-	300	190	+/-	25
512	mixed BF	5.52	+/-	0.06	23263	+/-	94	10.6	-1.0	25551	+/-	300	216	+/-	25
526	mixed BF	5.18	+/-	0.06	23774	+/-	100	10.1	-1.0	26349	+/-	300	256	+/-	24
540	mixed BF	4.61	+/-	0.07	24724	+/-	118	10.3	-1.2	27147	+/-	300	229	+/-	22
546	mixed BF	4.32	+/-	0.06	25230	+/-	119	10.5	-1.5	27488	+/-	300	203	+/-	22
558	mixed BF	4.07	+/-	0.06	25721	+/-	124	10.2	-1.2	28172	+/-	300	229	+/-	21
576	mixed BF	3.56	+/-	0.06	26801	+/-	141	9.4	-2.0	29465	+/-	300	256	+/-	19
592	mixed BF	3.37	+/-	0.06	27229	+/-	147	10.2	-0.8	30548	+/-	400	358	+/-	31
606	mixed BF	2.94	+/-	0.06	28340	+/-	171	10.3	-1.8	31300	+/-	400	295	+/-	27
660	mixed BF	2.12	+/-	0.06	30948	+/-	240	10.7	-0.9	34187	+/-	400	327	+/-	19
801	mixed BF	1.08	+/-	0.06	36399	+/-	461	9.6	-1.0	41911	+/-	400	714	+/-	44
1	organic matter	70.01	+/-	0.31	2865	+/-	35	14.3	-21.9	2900	+/-	100	-6	+/-	8
74	organic matter	60.10	+/-	0.28	4090	+/-	37	16.9	-23.2	5014	+/-	25	102	+/-	2
140	organic matter	47.09	+/-	0.23	6050	+/-	38	15.8	-21.4	6900	+/-	25	85	+/-	2
194	organic matter	33.90	+/-	0.18	8689	+/-	42	14.5	-21.2	9700	+/-	25	96	+/-	2
216	mixed PF	30.44	+/-	0.14	9555	+/-	38	11.1	0.8	10684	+/-	25	109	+/-	2
230	mixed PF	27.84	+/-	0.13	10272	+/-	39	10.9	1.2	11311	+/-	25	94	+/-	2
240	mixed PF	24.07	+/-	0.11	11441	+/-	38	10.6	1.5	11982	+/-	25	26	+/-	2
246	mixed PF	23.96	+/-	0.12	11477	+/-	41	10.7	1.4	12418	+/-	100	76	+/-	7
250	organic matter	21.28	+/-	0.14	12429	+/-	52	6.5	-21.9	12709	+/-	100	-10	+/-	6
254	mixed PF	21.66	+/-	0.11	12287	+/-	42	10.9	1.4	13000	+/-	100	44	+/-	7
264	mixed PF	24.28	+/-	0.12	11372	+/-	40	10.8	1.8	13496	+/-	100	242	+/-	7
272	mixed PF	24.32	+/-	0.11	11359	+/-	38	10.7	1.4	13893	+/-	100	306	+/-	7
284	organic matter	20.67	+/-	0.14	12664	+/-	53	8.7	-22.6	14359	+/-	150	174	+/-	12
290	mixed PF	20.25	+/-	0.1	12831	+/-	42	11.1	1.3	14580	+/-	150	181	+/-	13
304	organic matter	17.52	+/-	0.13	13994	+/-	59	5	-21.9	15147	+/-	150	95	+/-	11
312	mixed PF	18.53	+/-	0.1	13540	+/-	43	8.4	1.7	15493	+/-	150	208	+/-	13
320	mixed PF	12.32	+/-	0.08	16822	+/-	52	10.7	1.9	15954	+/-	150	-151	+/-	12
332	mixed PF	17.13	+/-	0.09	14173	+/-	44	9.6	1.6	16702	+/-	200	292	+/-	19
370	organic matter	14.13	+/-	0.12	15717	+/-	69	6.4	-21.1	18500	+/-	200	325	+/-	16
384	organic matter	12.50	+/-	0.12	16705	+/-	78	6.8	-20.9	19096	+/-	200	259	+/-	15
424	organic matter	9.79	+/-	0.12	18667	+/-	98	6.2	-20.8	20800	+/-	200	212	+/-	12
440	organic matter	8.80	+/-	0.12	19520	+/-	108	7.1	-21	21631	+/-	200	205	+/-	11
466	organic matter	8.20	+/-	0.12	20091	+/-	116	6.3	-21	22981	+/-	300	322	+/-	22
486	organic matter	6.97	+/-	0.12	21399	+/-	139	4.8	-21.1	24070	+/-	300	281	+/-	19
500	organic matter	6.53	+/-	0.12	21920	+/-	145	6.3	-20.9	24867	+/-	300	323	+/-	18
512	organic matter	6.13	+/-	0.12	22422	+/-	155	5.3	-20.9	25551	+/-	300	350	+/-	17
526	organic matter	5.63	+/-	0.12	23109	+/-	168	5.6	-20.8	26349	+/-	300	365	+/-	15
546	organic matter	5.33	+/-	0.12	23553	+/-	180	7.5	-21.2	27488	+/-	300	482	+/-	14
558	organic matter	4.65	+/-	0.12	24641	+/-	203	6.8	-21.3	28172	+/-	300	406	+/-	11
576	organic matter	4.35	+/-	0.12	25184	+/-	218	9.1	-21.2	29465	+/-	300	536	+/-	9
592	organic matter	3.55	+/-	0.12	26819	+/-	269	5.5	-21.2	30548	+/-	400	429	+/-	15
606	organic matter	3.59	+/-	0.12	26733	+/-	265	8.6	-20.6	31300	+/-	400	582	+/-	16
636	organic matter	2.89	+/-	0.12	28481	+/-	330	10	-21.1	32908	+/-	400	546	+/-	7
676	organic matter	2.29	+/-	0.12	30346	+/-	416	8.6	-21	35180	+/-	400	613	+/-	3
724	organic matter	1.96	+/-	0.12	31601	+/-	487	5.6	-21.2	37129	+/-	400	747	+/-	12
758	organic matter	1.28	+/-	0.12	35012	+/-	749	5.6	-21.1	39583	+/-	400	538	+/-	44

Table 5-2 List of radiocarbon data of Core MD02-2519, including derived GISP2-Hulu ages with errors (*) (based on estimated precision of tie-points), and the calculated Δ¹⁴C for each date (see methods and Figure 5.1 for details).

5.3 Results and Discussion

5.3.1 Radiocarbon age structure of shallow and intermediate depth in the ETNP

In Figure 5.1-C are shown surface (PF-OC) and 995 m water depth (BF) radiocarbon activity reconstructions of the Core MD02-2519 collected off Mazatlan, spanning the last ~ 40 ka BP. Remarkable features in these records are two prominent deglacial minima events between 17.8 – 14.5 ka BP and 12.8 - 11.5 ka BP. The onset of these Δ^{14}C decreases is similar in time to H1 and YD, although the first minimum is reached ~ 2 ka after H1 (Figure 5.5). Such trends largely agree with a previously published Δ^{14}C record (Core PC08) from Baja California (Marchitto et al., 2007) showing similar incursions during these periods, which indicate the presence of 'old carbon' in the ETNP.

In the Δ^{14}C records of the Core MD02-2519, these deglacial minima are seen not only in the BF, but also in the PF-OC record (Figure 5.5). The first transient event (close to the H1 event) began at ~ 16.5 ka BP in the benthic record, but ~1800 years earlier in the PF-OC record. Both records show minima Δ^{14}C values of about 95‰ and 46‰ (respectively) between 15.2 – 14.8 cal ka BP. The second event (coincident with YD) began in both records at ~ 13.5 ka, but they show the lowest values between 12.7 and 12 cal ka BP (i.e. –96‰ in the BF-based record and –10‰ in the PF-OC record). To determine changes in *ventilation ages*, we applied the *projection-age method* developed by Adkins and Boyle (1997). Although subject to uncertainties, the decay projections of the deglacial Δ^{14}C values of the Core MD02-2519 take us back to the atmospheric values from that time, resulting in apparent ventilation ages of 1200 - 1750 yrs for bottom waters (BF), and 550 - 1000 yrs for surface waters (PF-OC) during the YD and the interval surrounding H1 (respectively).

5.3.2 Comparison between existing Δ^{14}C records

The comparison of 3 benthic foraminiferal records (Figure 5.6-C) from the eastern tropical Pacific (ETP) evidence strong depth-dependent gradients in Δ^{14}C during the deglaciation. The Core MD02-2519 (retrieved from 955 m) show benthic Δ^{14}C values depleted as low as -96‰ during YD, and 46‰ close to the H1 event; whereas the Core PC08 (retrieved from 705 m) is as depleted as -200‰. However, the benthic record of Core VM21-30 (retrieved from 617m) shows the most depleted Δ^{14}C signatures (up to – 600‰) during the deglaciation. On the other hand, published Δ^{14}C records from other regions in the Pacific

do not show any evidence for significant aging during the deglacial, such as the western equatorial Pacific (WEP; at 2800 m water depth) (Broecker et al., 2008) and the eastern South Pacific off central Chile (ESP; at 1000 m water depth) (De Pol-Holz et al., 2010). Therefore, the ^{14}C age of the water masses appears to be aging while depth decreases, indicating that the strongest signature of 'old carbon' could be centred at even shallower depths. This proposition is supported by the record in the EEP (Core VM21-30), which shows even older ages than those in the record from Baja California (Core PC08). This suggests that the transient deglacial 'old carbon' signatures were restricted to the intermediate water masses of the ETP (~400 - 1200 m water depth), and the strongest signal may have plied at water depths shallower than ~ 600 m during the deglacial. Although published Δ^{14}C benthic records shallower than 600 m are currently lacking, such an inference is based on the geographical distribution of 'old carbon' in the surface waters of the ETP (Figure 5.6-B). As well as evidence from unpublished data in the SW Pacific, off New Zealand (Sikes et al., 2006), which record reservoir ages of shallow subthermocline waters appearing older relative to intermediate waters than in modern profiles.

5.3.3   Old carbon source and redistribution during the last deglaciation

The source of the 'old carbon' signal has been examined in previous studies (Broecker et al., 2008; Keeling, 2007; Marchitto et al., 2007), by means of a range of current evidence in the Pacific Ocean. Available data in the Gulf of Alaska indicates that the deep waters (3647 mbsl) of the glacial North Pacific are only 1000 yrs older than the subsequent deglacial (Galbraith et al., 2007). Even when evidence of old water masses has not been reported in the WEP (Broecker et al., 2008), the waters from the EEP show the most ^{14}C-depleted values of the deglaciation, with an age difference relative to LGM older than 6000 yrs (Stott et al., 2009). Whereas, the oldest apparent ventilation ages (> 5040 yrs) in the glacial deep ocean (2700 mbsl) are only documented in the SW Pacific, off New Zealand (Sikes et al., 2000). Although the extent of water masses bearing 'old carbon' in the SO is currently uncertain (Broecker and Barker, 2007), the evidence indicates that the conditions in the glacial SO were conducive for isolated deep water masses of many thousand yrs old to exist (Keeling, 2007; Marchitto et al., 2007; Stott et al., 2009). For instance, the upper layers of the SO in the Pacific sector were possibly well stratified during the last glacial, isolating some of the highest density deep waters of the ocean (Adkins et al., 2002a, b). However, there remains the question of how the deglacial 'old carbon' signatures reached the ETP from southern sources, and why is this signal registered in benthic and planktonic Δ^{14}C.
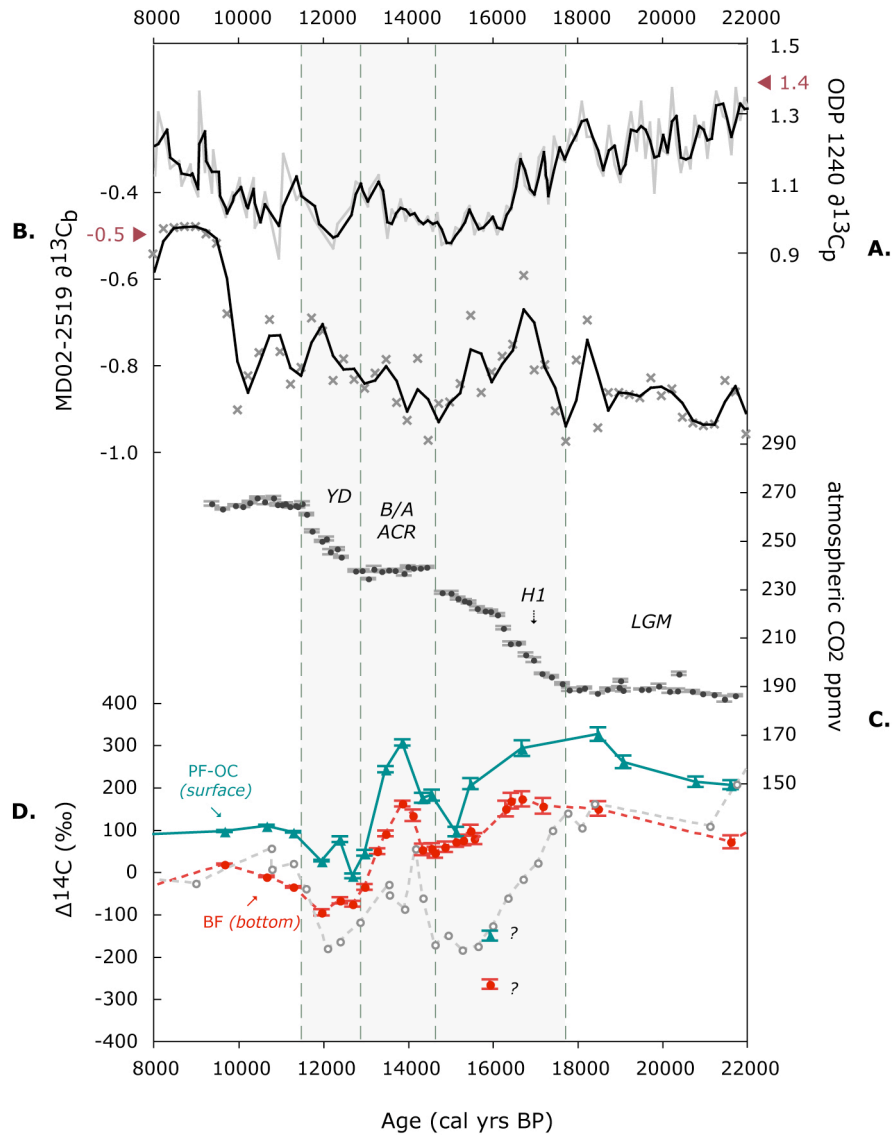
Figure 5-5 Records of stable carbon isotopes and radiocarbon activities between 22 - 8 ka. (A) δ^{13}C record of planktonic foraminifera (N. dutertrei) of Core ODP-1240 from the EEP (Pena et al., 2008); curve in black – 2 point moving average; left arrow with number marks the core top value. (B) δ^{13}C-Uvigerina record (‰) (grey crosses) of Core MD02-2519 curve in black – 2 point moving average; right arrow with number marks the core top value. (C) atmospheric CO$_2$ record of EPICA Dome C (Monnin et al., 2001) placed on the GISP2 timescale (black circles). (D) Δ^{14}C records of Core MD02-2519 from intermediate (red circles) and surface waters (green triangles), compared to the Δ^{14}C record of PC08 from Baja California (open grey circles) (Marchitto et al., 2007). Vertical dashed grey lines show the boundaries of H1, B/A and YD based on the GISP2 δ^{18}O scale (Grootes and Stuiver, 1997). LGM and ACR stand for Last Glacial Maximum and Antarctic Cold Reversal, respectively.
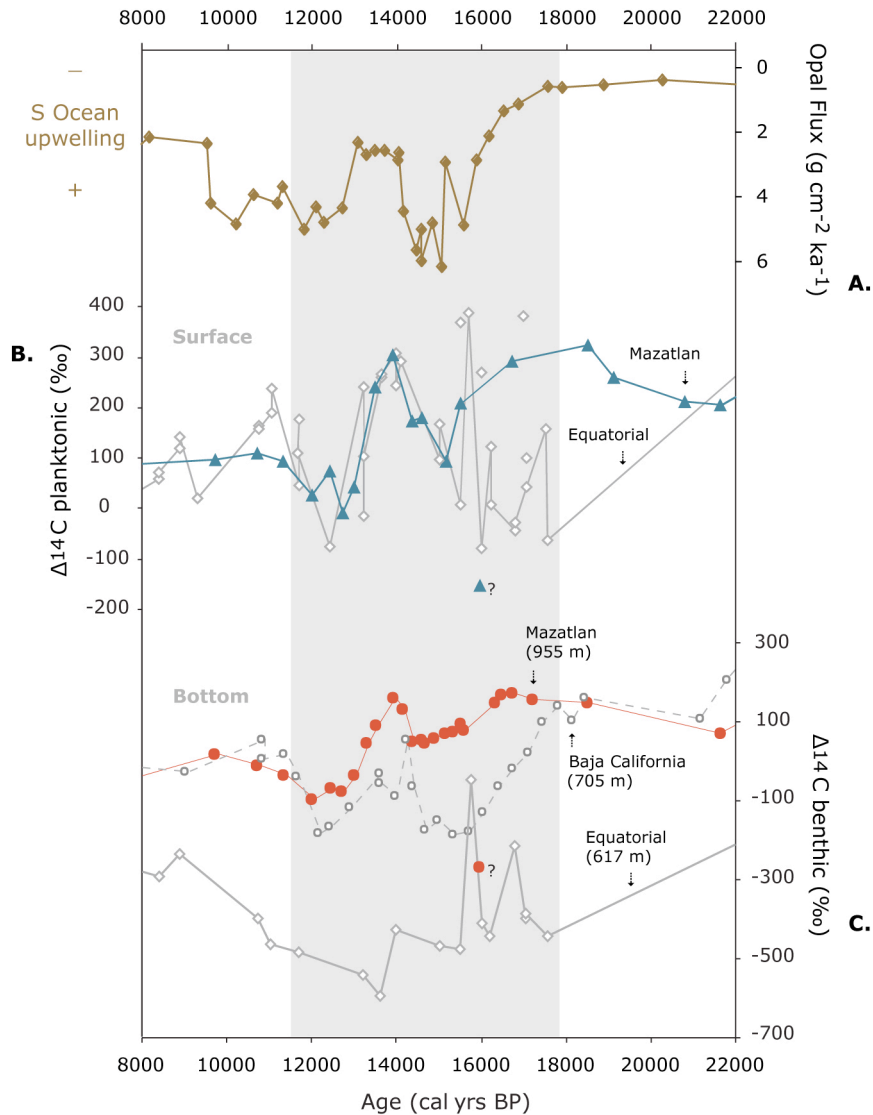
Figure 5-6 Comparison of records from surface and intermediate water between 22 – 8 ka. (A) Opal flux data from the South Atlantic sector, a proxy for Southern Ocean upwelling (Anderson et al., 2009). (B) Δ^{14}C surface records from Mazatlan (green triangles) and Galapagos in the EEP (open grey diamonds), as proxies of 'old carbon' release to the sea surface linked to Southern Ocean overturning. (C) Δ^{14}C bottom records from Mazatlan (red circles), Baja California (open grey circles) and Galapagos (open grey diamonds) as proxies for Southern Ocean overturning strength. Grey band delimits the interval between H1, B/A and YD (similar to Figure 5.5).

     In the modern equatorial Pacific, the water masses underlying the equatorial divergence at depths > 500 m are mainly sourced from AAIW and NPIW, which originate in the S and N Pacific, respectively (Talley, 1999). Today, the AAIW is barely traceable north of the equator (Fiedler and Talley, 2006), but several studies suggest that the SO intermediate waters could be more extensive in the past, and penetrate further north than

today (Marchitto et al., 2007; Schulte et al., 1999; Spero and Lea, 2002). As a result, a primary interpretation (Marchitto et al., 2007) to the deglacial excursions of 'old carbon' found off Baja California is that they represent changes in the preformed ^{14}C content of AAIW, acquired by mixing with upwelled old deep-waters south of the subantarctic zone. This interpretation, however, was recently questioned by a study in the coast of central Chile (De Pol-Holz et al., 2010), which lacks evidence of any incursion of old water during the deglacial. Importantly, the eastern South Pacific is the main region of formation of AAIW (Talley, 1999). Therefore, the conection of the ETP to the SO overturning strength via AAIW requires an alternative explanation.

Based on the Δ^{14}C records of Core MD02-2519, we could argue that the deglacial changes in the ETP were not restricted to intermediate water (IW) circulation, but extended to the subthermocline and surface circulation as well. On one hand, any change in the Δ^{14}C signal incorporated in the organic matter (produced at surface) could be transported to the seafloor. Thus the organic carbon signal incorporated in the tests of infaunal foraminifera species, could affect the BF-isotopic signal from above. As discussed in *Chapter 4*, previous studies (Keigwin and Jones, 1990; McCorkle et al., 1997; Zahn et al., 1986) indicate that the isotopic fractionation of infaunal species can be greatly controlled by changes in OC accumulation and microhabitat effects. As a result, the isotopic signal could reflect surface conditions rather than bottom water signatures, being a disadvantage to reconstruct circulation processes. However, given that the organic carbon production in the ETNP was very low during stadial events like the H1 and the YD (*see Chapters 1 and 2*), we believe that the influence of 'old carbon' from surface waters being transported to the sea-floor can not solely account for our observed patterns. In adition, if the organic carbon production would have affected the Δ^{14}C signal, ages should appear younger, not older. Instead, we suggest that the advection of waters from the equatorial Pacific could transport the ^{14}C-depleted signal to Baja California and Mazatlan, via subthermocline currents across the equator (Firing et al., 1998). This is supported by the fact that the oldest deglacial signal is found in the records of Core VM21-30 with respect to the Core MD02-2519. Furthermore, this may explain why the deglacial 'old carbon' signatures, centred at water masses shallower than 600 m, vanish with depth (Figure 5.6).

In addition, the Δ^{14}C PF-OC of Core MD02-2519 suggests that the deglacial 'old carbon' signatures in the ETP could reach the surface ocean by means of increased

upwelling, indicating degassing and atmospheric release of CO_2. Correspondence between CO_2 rises surrounding the H1 and the YD, and increased opal production linked to changes in upwelling (driven by the southward shift of Southern Hemisphere westerlies) has been documented in the in the SO Polar Front (Anderson et al., 2009) (Figure 5.6-A), also coinciding with Antarctica warmings. Thus in similar way, the activation of the upwelling areas in the eastern Pacific (along with the SO) could be an important locus of 'old carbon' release to the atmosphere during the deglaciation. The idea of atmospheric 'old carbon' release is supported by a recent work (Lourantou et al., in press), which documents depleted $\delta^{13}CO_2$ values in ice-core records from Antarctica during these events. Such a signal is consistent to the integrate signal of oceanic and biospheric processes, which could be triggered by the activation of the major upwelling systems, akin to the SO and the E Pacific.

To trace the routing of 'old carbon' linking the SO overturning to the surface waters of the Pacific sector is still difficult due to the poor geographical coverage of $\Delta^{14}C$ records. But assuming that the general circulation of the modern ocean could be applicable to the past, we propose an alternative redistribution pathway to that proposed by Marchitto et al. (2007). In addition to the results from the eastern South Pacific (De Pol-Holz et al., 2010), we seek an alternative to the influence of AAIW as the path for mixing and propagating 'old carbon' because its overall circulation is zonal (not meridional) (Reid, 1997; Tomczak, 2007; van Aken, 2007). This means that the AAIW hardly travels along the coast of South America as it flows westward (not northward), thus preventing a direct connection to the ETNP. Moreover, studies in the SO (Sloyan and Rintoul, 2001; van Aken, 2007) also document a very small influence of Pacific deep water (DW) in the intermediate water (IW) in the modern ocean. The studies suggest that, at least in the Pacific, there is more DW contribution to the thermocline water (TW)-layer than the IW-layer. As the upper deep water (UDW) is sufficiently light to outcrop at high latitudes (but not in low latitudes), the TW, IW and DW circulations are largely isolated from each other in the subtropics. Therefore, the UDW outcropping in high latitude can travel to lower latitudes mostly through TW, and to a less extent through IW. Once the TW and IW reach the equator, the complex zonal circulation and mixing of the equatorial system could redistribute the 'old carbon' signal to the ETNP.

Therefore, our study supports a north-south link between the ocean and the atmosphere during the last deglaciation. When deep waters carrying 'old carbon' were incorporated in the South Pacific TW by SO overturning and reached the ETNP trough

subthermocline currents of equatorial origin (Firing et al., 1998; Tsuchiya and Talley, 1996, 1998). In addition, through ocean upwelling, subsurface waters were tapped along the equatorial divergence and the ETNP, and substantially contribute to the transient $\Delta^{14}C$ signal left on the surface records. The absence of the depleted deglacial signal in surface waters outside the strong regional upwelling, like the western-most Pacific (Broecker et al., 2008) supports this suggestion.

5.3.4 $\delta^{13}C$ trends throughout the deglaciation

During the last glacial, the isolated 'old carbon' pool stored in the deep ocean would have depleted $\delta^{13}C$ signatures (enriched in ^{12}C) of deep waters due to the continual accumulation of remineralised carbon. Thus the transient 'old carbon' signature of the last deglaciation should be accompanied by lighter $\delta^{13}C$ signatures.

In Figure 5.5-A, we compare the general structure of two $\delta^{13}C$ records from the eastern Pacific relative to the transient signal of deglacial 'old carbon'. The benthic $\delta^{13}C$ record of Core MD02-2519 shows a broad $\delta^{13}C$ minimum during the deglaciation (Figure 5.5-B), which we find difficult to interpret as palaeo-productivity (disussed in *Chapter 4*). Instead, we find a connection to the $\delta^{13}C$ minimum seen in equatorial Pacific (Figure 5.5-A) and SO records (Loubere and Bennett, 2008; Pena et al., 2008; Spero and Lea, 2002; Stott et al., 2009). The information obtained from different $\delta^{13}C$ records in the Pacific, also discussed in the previous chapter (*see* Chapter 4), points at the South Pacific as the most plausible source of such a low $\delta^{13}C_b$ signal registered in the records from Mazatlan.

Previous studies (Charles et al., 1996; Franke et al., 2008; Ninnemann and Charles, 1997) agree that during the last glacial period, the SO contained the lowest $\delta^{13}C$ and $\Delta^{14}C$ values of the whole ocean, as a response of local accumulation of remineralised carbon and poor water ventilation. During the deglaciation, sea-ice retreat and reduction in brine formation around Antarctica could reduce the density of these poorly ventilated waters and favour their transport to lower latitudes (Keeling, 2007). Furthermore, the SO waters could impart the transient low $\delta^{13}C$ values to subthermocline and mode waters (Charles et al., 1996; Keeling and Stephens, 2001; Lynch-Stieglitz et al., 1994) and finally, to the subsurface waters in the ETNP. In this regard, the low transient $\Delta^{14}C$ and $\delta^{13}C$ signatures found in the cores collected off Mexico and the equatorial Pacific coincide with this scenario; where the

enhanced northward flow of Southern Ocean waters could be an important source of variation for the Pacific low latitudes.

5.4 Conclusions

In this study, using Δ^{14}C reconstructions of surface and intermediate waters, we document that the eastern Pacific acted as a conduit for the release and redistribution of glacial 'old carbon' to the atmosphere during the deglaciation. The Mazatlan intermediate Δ^{14}C record is in agreement two previous publication from Baja California and Galapagos (Marchitto *et al.*, 2007; Stott *et al.*, 2009, respectively), suggesting the occurrence two transient events of ^{14}C-depleted (aged) waters in the eastern Pacific surrounding the events H1 and YD.

Given that the depleted Δ^{14}C signal is only weakly registered at ~955 m water depth in the ETNP, the "old water mass" transporting such a signal was possibly centred at depths shallower than 600 m as its influence is seen in records from surface waters (i.e. PF-OC record). This depth distribution strongly suggests a SO source for the deglacial old ^{14}C signatures in the ETNP, possibly transported by equatorial undercurrents and subthermocline waters but not by AAIW, as originally proposed. During the last deglaciation, the documentation of depleted Δ^{14}C signatures in the surface record additionally suggests that the upwelling of the eastern Pacific could be an important mechanism through which CO_2 evaded from the ocean into the atmosphere. Therefore, a key aspect is that the old ages are being registered when the ocean is degassing and atmospheric CO_2 is rising.

These interpretations greatly rely on the assumption that the benthic fauna record bottom waters. Although we are aware that mixing species of infaunal foraminifera has limitations, at present this is the only method available to study the cores of the ETNP. Future developments should target the possibility of identifying and measuring more appropriate species.

🌍

Chapter 6

Concluding Remarks

In this study, the paleoceanographic history of the eastern tropical North Pacific (ETNP) was analyzed over the last two glacial cycles of the Late Quaternary. The aim of this work was to unravel the nature of millennial (sub-orbital) timescale variations in the same core MD02-2519. Further comparisons with records from distant regions were made to reconstruct: (1) inter-hemispheric links between tropical and polar regions, (2) biogeochemical impacts and (3) the potential of the low latitudes to regulate Greenhouse Gas (GHG) concentrations on these timescales. A summary of the principal contributions, their implications and suggestions for future research are presented in this chapter.

The study was focussed on the marine sediment Core MD02-2519 although other cores from the ETNP were also included (i.e. MD02-2518, MD02-2520, MD02-2524, NH15P, PC08). Most of the cores were retrieved during the IMAGES VIII (MONA) cruise on board the R/V Marion Dufresne (*June 2002*). These cores were selected to broaden the geographical and depth coverage of oceanographic features, allowing two perspectives of the same climatic system to be developed: surface and intermediate circulation. The ETNP is a region that experiences intense winter upwelling and productivity, which greatly influences water column denitrification. At intermediate depths, the region is bathed by the North Pacific Intermediate Water and within an extended Oxygen Minimum Zone. However, in the study site we document variable conditions throughout the Late Quaternary, as suggested by multi-proxy geochemical analyses in marine sediment samples, which allowed the reconstruction of several high-resolution records spanning 200-240 ka of history of environmental changes.

Upwelling-induced productivity changes following Greenland timing were documented by means of organic carbon records (*%OC* and *DSRa**) (*Chapter 1*) and confirmed by opal records (*Chapter 3*). An increased accumulation of OC was present during warm interstadial periods (Dansgaard Oeschger - D/O), while a decrease occurred during cold stadial and Heinrich (H) events (Figure 6.1 A and C). During the isotope stages MIS-2-4 and MIS-6, the productivity changes in the ETNP occurred with longer periodicities

than the temperature changes in high latitudes of the Northern Hemisphere (NH) (Figure 6.1 B and D). The dominance of low frequency events in the tropical climate system suggests that millennial timescale cycles derive not only from ice sheet dynamics, but also from external forcing and meridional heat transport variations. A scenario describing the regional atmospheric circulation during stadial – interstadial episodes was assembled from existing circulation models, terrestrial paleoclimatic evidence and upwelling proxy records from this thesis. The similarity between NH records suggests that a strong atmospheric coupling between high and low latitudes could affect the position of the Intertropical Convergence Zone (ITCZ) and influence the local upwelling in the ETNP.
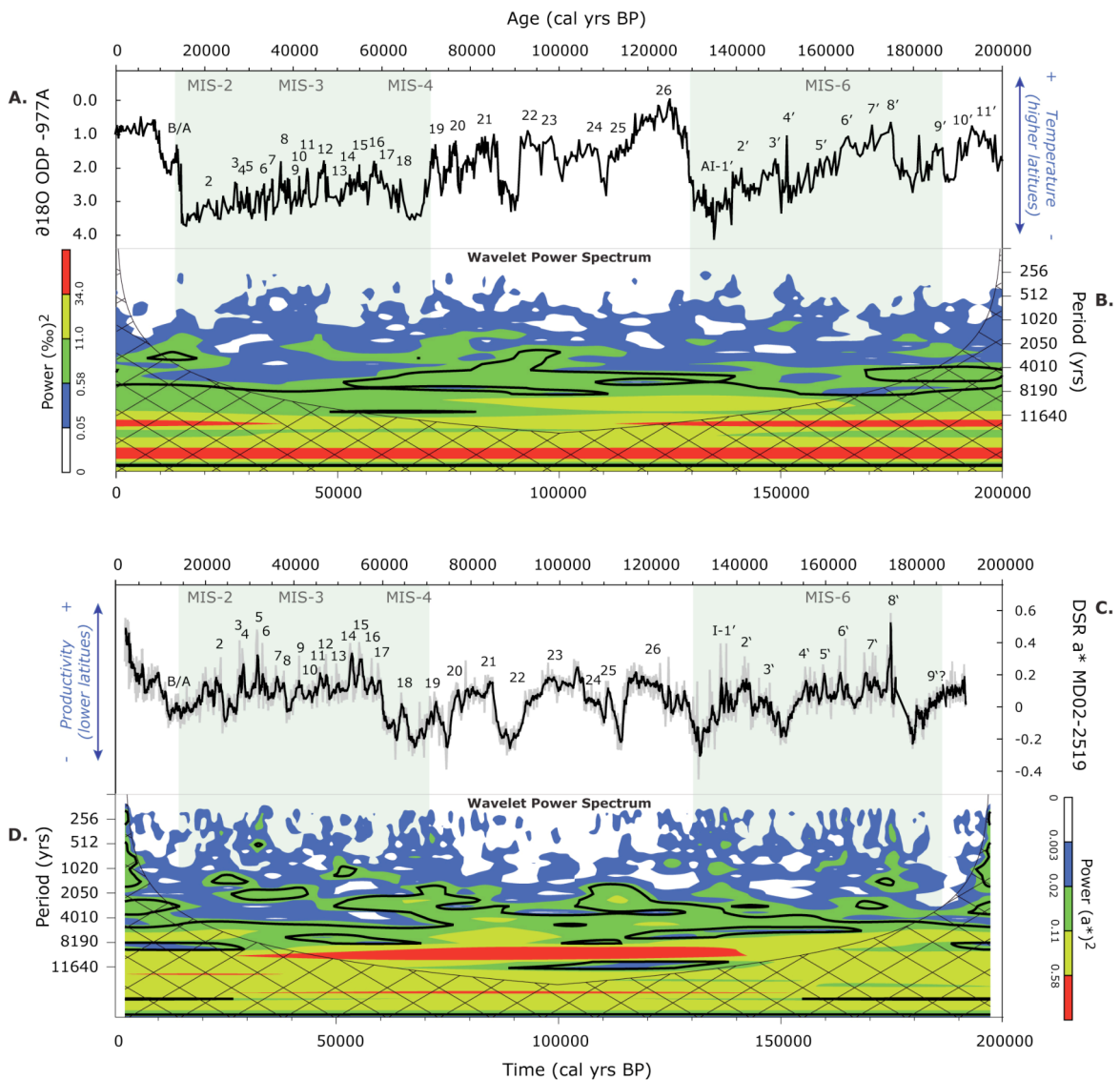
Figure 6-1 The comparing of the NW Mexican proxy record of productivity with a North Atlantic proxy record of sea surface temperature during the last 200 ka (calendar age BP). (A) δ^{18}O planktonic foraminifera record of Core ODP-977A from the Iberian Margin; (Martrat et al., 2004). (B) Wavelet analyses of Core ODP-977A using the online resource by (Torrence and Compo, 1998). Contour levels were chosen so that 75%, 50%, 25%, and 5% of the wavelet power is above each level, respectively. Black contour is the 10% significance level using a white-noise background spectrum. The crosshatched region is the cone of influence (COI). (C) DSRa* (Diffuse Spectral Reflectivity) productivity proxy record of Core MD02-2519 (full details in Chapter 1), black line - 5 point moving average. (D) Wavelet analyses of Core MD02-2519. The shaded areas show the penultimate (MIS)-6) and the last (MIS 2-4) glacial periods. Notice the time period (years/cycle) differences between both glacial periods and between records ODP-977A and MD02-2519.

Changes in the opal accumulation in cores collected from the ETNP (*Chapter 3*) reflect variations in the biogenic supply of opal to the sediments from the upper water column. Although opal seems to be controlled by upwelling at millennial timescales, it is significantly affected by changes in the supply of unutilized nutrients advected from regions like the eastern equatorial Pacific (EEP) or the Southern Ocean (SO). In the ETNP, the records of %opal, opal-MAR, Si_{OPAL}:C and Si_{OPAL}:N ratios evidence higher values during LGM (Last Glacial Maximum) with a subsequent decline during TI (Termination 1); thus indicative of opal production decrease as a portion of total productivity at the end of the last glacial period (Figure 6.2-D). Glacial increases in opal accumulation are consistently found along the ETP (eastern tropical Pacific) on both sides of the equator (ETNP and ETSP). This pattern can be seen as the response of increased silicic acid ($Si(OH)_4$) supply from the EEP under Fe-replete glacial conditions. Together, the high diatom production of the EEP and ETP during LGM, could have profound implications in global climate. An ecological shift favouring siliceous over calcareous organisms and the consequent increase in export productivity may have been implicated in the deglacial drawdown of pCO$_2$. By linking the glacial source of nutritive waters (i.e. SO) to the glacial sink of carbon (i.e. ETP and EEP), the ETNP opal records and the Si_{OPAL}:C and Si_{OPAL}:N ratios support such a hypothesis.

Using benthic foraminifera δ^{13}C records of cores collected from the ETNP, we document the occurrence of intermediate water variations over the last 200 ka (*Chapter 4*). Unfortunately, the construction of carbon isotope records based on epifaunal species (e.g. *Cibicidoides*) was not possible due to the limiting anoxic conditions of the intermediate waters off NW Mexico. As an alternative, and despite the limitations, we evaluated the use of shallow-infaunal species (*Uvigerina* spp.) as an approximate indicator of δ^{13}C-DIC with positive results. *Uvigerina* is an abundant species in oxygen minimum zones, which lives

within a narrow depth range of calcification (i.e. maxima abundances at $\sim$ 1–3 mm depth in the sediments). *Uvigerina* spp. have a small intra-core $\delta^{13}C$ variability very similar to that of epifaunal species, which we assume is comparable to the $\delta^{13}C$-DIC of bottom waters. The present study suggest that $\delta^{13}C_b$ is not controlled by variations in productivity or organic matter accumulation because there is no correspondence with OC records. At glacial-interglacial timescales, the changes recorded by $\delta^{13}C$-*Uvigerina* resemble those of nearby records in the NE Pacific, noticeable by the broad $\delta^{13}C$ minima across LGM and T1, which is unlikely to be attributed to SO effects. After comparing to records from intermediate depths in the NW and SW Pacific, the depleted $\delta^{13}C$ intervals suggest the influence of southern component waters (SCW) during the last and penultimate glacial (Figure 6.2-E), different to the influence of northern component waters (NCW) prevailing in the modern ocean.

The final chapter (*Chapter 5*) is centred on the deglaciation (surrounding the events H1 and YD), and documents the oceanic release of aged carbon as a transient signal in the ETNP intermediate waters. This effect is attributed to the injection of "old carbon" isolated from the atmosphere in the glacial deep ocean. Although our interpretations rely on the assumption that the benthic fauna record bottom water conditions, at present this is the best strategy available. Future developments should target the identification and measuring of more appropriate species. Our reconstructions suggest that the glacial bottom waters in the ETNP were older than 1200 - 1750 yrs, whereas the surface waters were older than 550 - 1000 yrs, relative to the Holocene. The documentation of low radiocarbon activity ($\Delta^{14}C$) in intermediate waters, as well as the prominent $\delta^{13}C$ minimum found in records of foraminifera (*Chapter 4*), suggest the Southern Ocean as its source. The 'old carbon' signal was possibly travelling at depths shallower than $\sim$ 600 m (Figure 6.2-F), transported north through South Pacific subthermocline waters, then incorporated within the equatorial undercurrent circulation to finally reach the circulation of the ETNP. The detection of ^{14}C-depletion in surface samples suggest that the upwelling was an important locus of CO_2 release from the ocean during the last deglaciation. Therefore, a substantial reorganization of the Pacific subthermocline waters was perhaps related to southern sources of circulation. It was only after $\sim$ 6 ka that the modern conditions (driven by NCW) were established (Figure 6.2-E).

Implications

The use of geochemical tracers (mainly stable and radioactive isotopes of C, O and N) allowed us to investigate at millennial to glacial timescales the paleoceanography of the ETNP during the Late Quaternary (i.e. changes in productivity, denitrification and intermediate water circulation). The reconstruction of proxy records spanning ~ 200 – 240 ka identifies a tight connection between variations in climate, changes in surface, subsurface and intermediate water depths. It is appreciable that the lower latitudes are fundamental in controlling interhemispheric links with higher latitudes through latitudinal displacements of the ITCZ, the rearrangement of the wind systems, and oceanic circulation.

Variations found on the surface ocean, although coupled to upwelling and productivity, show evidence of the bipolar operation of the atmosphere, as registered in the tropical regions like the combined response of temperature shifts in both hemispheres (i.e. evidenced by the tuning either to Greenland or Antarctica chronologies shown in *Chapter 1*). Although linking NH-related processes (e.g. upwelling in the ETNP) to Antarctica timing is difficult, this can be useful to develop new approaches to explain past climate from a southern hemisphere or tropical perspective, moreover improving our understanding of rapid climate changes. At subsurface and intermediate water depths, oceanic influences from the South Pacific to the ETNP are identified in a variety of records, mostly evident during climatic transitions (e.g. glacial terminations and stadial-interstadials shifts). This is evidenced through the advection of isotopically heavy nitrate from the ETSP, the transport of unutilized silica, and the influence of southern component intermediate waters left in $\delta^{13}C$ records of benthic foraminifera. The contribution of the SO in the ETNP records determines that the present state of circulation of the Pacific Ocean has been variable over the last two glacial cycles. Additionally, the processes described here could have worked in tandem during glacial terminations, accelerating the oceanic release of "old carbon" and air-sea gas exchange of GHG, with positive effects in global warming.

Future work

Although this thesis was focussed on the study of the strong coupling between physical and biological processes and the key role that the eastern tropical Pacific exerts on climate, more work on the modern oceanography and paleoceanography is still essential for

a complete understanding of this tropical region. In the past, not many records in the tropical Pacific have studied variations in productivity at millennial timescales, neither have they been extended beyond the last glacial cycle, nor they have identified the periodicities of the rapid climatic events. A broad distribution of high resolution records from the tropical regions could confirm some of the hypotheses proposed in this thesis to explain the mechanism behind rapid climate changes. This would also require improvements to accurate the chronologies of the different paleo-data sets and expand their comparison. However, multi-proxy studies in the same core are visibly more suitable to reduce time uncertainties.

In the ETNP denitrification zone, additional OC and $\delta^{15}N$ reconstructions in cores between 25 and 33° N would be required to delimit the northern influence of the ETSP signal, and to differentiate between productivity controls on $\delta^{15}N$ and the advection of heavy nitrate. On the other hand, better geographical coverage of opal records and overall information from the tropical regions is still required over the Late Quaternary. Further reconstructions of opal records along the ETP, could resolve the influence that the unutilized silica exerted in diatom populations during the last glacial, re-evaluate their contribution to the oceanic silica budget, and quantify their contribution to reducing CO_2 to glacial levels.

Studies on carbon isotopes distributions at the present and in the past are required to accurately model the intermediate circulation of the Pacific Ocean. For instance, analysis of shallow-infaunal benthic foraminifera species and the geochemistry of sediment pore-water are essential to know the effects of remineralization or OC fluxes, which could potentially influence the isotopic composition of foraminifera shells. Also, it is important to verify that the $\delta^{13}C$-*Uvigerina* is an accurate tracer of intermediate water masses, specially in areas where epifaunal species are unavailable or rare.

Finally, to improve our understand of the oceanic release of 'old-carbon' via subsurface and intermediate waters, potential targets are those cores retrieved at depths between 400 – 1000 mbsl in the Pacific and Indian oceans. Tracking the pathway of 'old carbon' release from the SO to the equatorial and coastal upwelling regions is an important issue to address in future studies. To broaden the geographical distribution of proxy records of ocean circulation is essential to understand the role of intermediate waters in climate, allowing a suite of records from tropics, subtropics and template regions to be correlated with those from high latitudes.
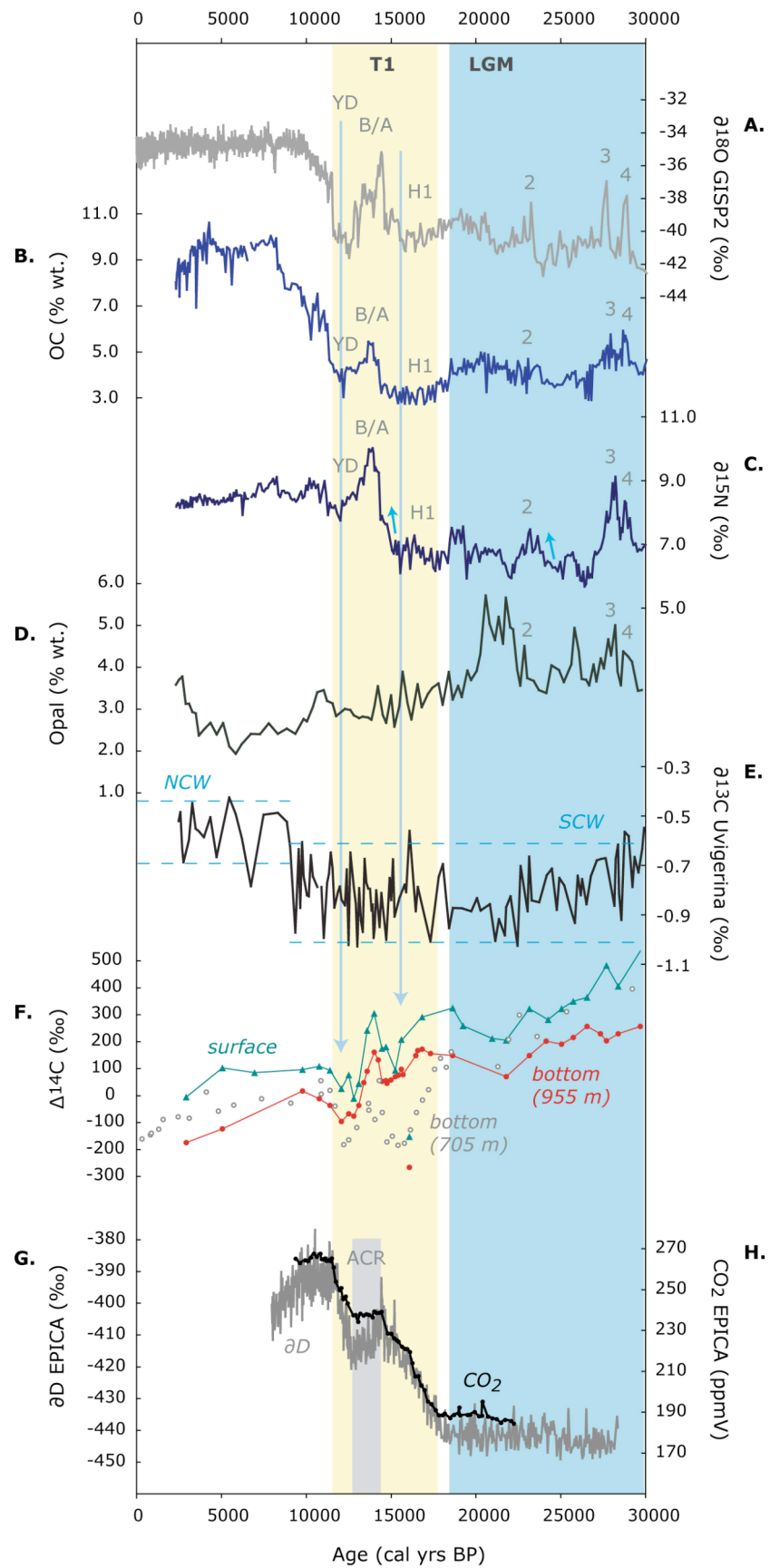
Figure 6-2 The relationship between reconstructed records of Core MD02-2519 spanning 0-30 ka (calendar age BP). (A) GISP2 $\delta^{18}O$ record of temperature. (B – F): Core MD02-2519 records of (B) productivity (i.e. organic carbon - OC % wt.); (C) denitrification ($\delta^{15}N$); (D) opal (% wt.) seen as a fraction of total productivity; (E) intermediate water ($\delta^{13}C$-Uvigerina); and (F) radiocarbon activity ($\Delta^{14}C$) from surface (green triangles: planktonic foraminifera - organic carbon samples) and bottom waters (red circles: benthic foraminifera samples). Grey dots is the $\Delta^{14}C$ benthic foraminifera record of Core PC08 (Marchitto et al., 2007). (G) δD Antarctic records of temperature and (H) CO_2 records of EPICA in GISP2 timescale (Monnin et al., 2001). Blue shaded area limits the time period when Southern Component intermediate Waters (SCW) influenced the study site. The light cream shaded area marks the two spites of old radiocarbon ages surrounding the events YD and H1 (see long blue arrows). The small blue arrows (i.e. placed at H1 and D/O 2) on the $\delta^{15}N$ record highlight the decoupling with the OC proxy record of productivity, caused by advection of heavy $^{15}NO_3^-$. The B/A and D/O warm phases are shown in ice cores from Greenland, whereas the ACR is indicated by shading on the Antarctica ice core.

🌐

References

Adkins, J.F., and Boyle, E.A., 1997, Changing atmospheric D14C and the record of deep water paleo-ventilation ages: Paleoceanography, v. 12, p. 337-344.

Adkins, J.F., McIntyre, K., and Schrag, D.P., 2002a, The salinity, temperature, and delta O-18 of the glacial deep ocean: Science, v. 298, p. 1769-1773.

—, 2002b, The temperature, salinity and delta O-18 of the LGM deep ocean: Geochimica Et Cosmochimica Acta, v. 66, p. A7-A7.

Ahn, J., and Brook, E.J., 2008, Atmospheric CO2 and climate on millennial time scales during the last glacial period: Science, v. 322, p. 83-85.

Alley, R.B., Clark, P.U., Keigwin, L.D., and Webb, R.S., 1999, Making Sense of Millennial-Scale Climate Change, *in* Clark, P.U., Webb, R.S., and Keigwin, L.D., eds., Mechanisms of Global Climate Change at Millennial Time Scales, Volume 112: Geophysical Monograph: Washington, American Geophysical Union, p. 385-394.

Altabet, M.A., Francois, R., Murray, D.W., and Prell, W.L., 1995, Climate-Related Variations in Denitrification in the Arabian Sea from Sediment N-15/N-14 Ratios: Nature, v. 373, p. 506-509.

Altabet, M.A., Higginson, M.J., and Murray, D.W., 2002, The effect of millennial-scale changes in Arabian Sea denitrification on atmospheric CO2: Nature, v. 415, p. 159-162.

Anderson, R.F., Ali, S., Bradtmiller, L.I., Nielsen, S.H.H., Fleisher, M.Q., Anderson, B.E., and Burckle, L.H., 2009, Wind-Driven Upwelling in the Southern Ocean and the Deglacial Rise in Atmospheric CO2: Science, v. 323, p. 1443-1448.

Anderson, R.F., Fleisher, M.Q., and Lao, Y., 2006, Glacial-interglacial variability in the delivery of dust to the central equatorial Pacific Ocean: Earth and Planetary Science Letters, v. 242, p. 406-414.

Archer, D., and Maierreimer, E., 1994, Effect of Deep-Sea Sedimentary Calcite Preservation on Atmospheric CO2 Concentration: Nature, v. 367, p. 260-263.

Archer, D., Winguth, A., Lea, D., and Mahowald, N., 2000a, What caused the glacial/interglacial atmospheric pCO(2) cycles?: Reviews of Geophysics, v. 38, p. 159-189.

Archer, D.E., Eshel, G., Winguth, A., Broecker, W., Pierrehumbert, R., Tobis, M., and Jacob, R., 2000b, Atmospheric pCO(2) sensitivity to the biological pump in the ocean: Global Biogeochemical Cycles, v. 14, p. 1219-1230.

Badan-Dangon, A., 1998, Coastal circulation from the Galápagos to the Gulf of California, *in* Robinson, A.R., and Brink, K.H., eds., The Sea, vol 11: New York J. Wiley and Sons, p. 315–344.

Baker, A.R., and Jickells, T.D., 2006, Mineral particle size as a control on aerosol iron solubility: Geophysical Research Letters, v. 33, p. 1706-1719.

Bakun, A., and Nelson, C.S., 1991, The seasonal cycle of wind stress curl in subtropical eastern boundary current regions: Journal of Physical Oceanography, v. 21, p. 1815-1834.

Banakar, V.K., 2005, d13C depleted oceans before the Termination 2: More nutrient-rich

deep-water formation or light-carbon transfer?: Indian Journal of Marine Sciences, v. 34, p. 249-258.

Bard, E., Rostek, F., and Menot-Combes, G., 2004, Radiocarbon calibration beyond 20,000 C-14 yr BP by means of planktonic foraminifera of the Iberian Margin: Quaternary Research, v. 61, p. 204-214.

Barker, S., and Knorr, G., 2007, Antarctic climate signature in the Greenland ice core record: Proc Natl Acad Sci, v. 104, p. 17278 - 17282.

Barnola, J.M., Raynaud, D., Korotkevich, Y.S., and Lorius, C., 1987, Vostok Ice Core Provides 160,000-Year Record of Atmospheric Co2: Nature, v. 329, p. 408-414.

Barry, R.G., and Chorley, R., 2003, Atmosphere, Weather and Climate: London, Routhledge, 421 p.

Barton, E.D., Lavín, M.F., and Trasviña, A., 2009, Coastal circulation and hydrography in the Gulf of Tehuantepec, Mexico, during winter: Continental Shelf Research, v. 29, p. 485-500.

Beaufort, L., 2002, IMAGES VIII MONA Cruise Report, Institut Polaire Francais Paul-Émile Victor (IPEV), les rapports de campagnes à la mer, Volume OCE/2002/03: http://www.images-pages.org/ftp/pub/MONA/MONA_cruise_report.pdf, PANGAEA, p. 452.

Behl, R.J., and Kennett, J.P., 1996, Brief interstadial events in the Santa Barbara basin, NE Pacific, during the past 60 kyr: Nature, v. 379, p. 243-246.

Berelson, W.M., and Stott, L.D., 2003, Productivity and organic carbon rain to the California margin seafloor: Modern and paleoceanographic perspectives: Paleoceanography, v. 18, p. DOI: 10.1029/2001PA000672.

Berger, A.L., 1984, Accuracy and frequency stability of the Earth's orbital elements during the Quaternary, in Berger, A.L., Imbrie, J., Hays, J., Kukla, G., and Saltzman, B., eds., Milankovitch & Climate: Dordrecht, Netherlands, D. Reidal, p. 3 - 39.

Berger, W.H., and Vincent, E., 1986, Deep-Sea Carbonates - Reading the Carbon-Isotope Signal: Geologische Rundschau, v. 75, p. 249-269.

Berger, W.H., and Wefer, G., 1991, Productivity of the Glacial Ocean - Discussion of the Iron Hypothesis: Limnology and Oceanography, v. 36, p. 1899-1918.

Bernhard, J.M., and Sen Gupta, B.K., 1999, Foraminifera of oxygen-depleted environments, in Sen Gupta, B.K., ed., Modern foraminifera: Dordrecht, Kluwer, p. 201-216.

Bernhard, J.M., Sen Gupta, B.K., and Borne, P.F., 1997, Benthic foraminiferal proxy to estimate dysoxic bottom-water oxygen concentrations: Santa Barbara Basin, U.S. Pacific continental margin: Journal of Foraminiferal Research, v. 27, p. 301-310.

Blunier, T., and Brook, E.J., 2001, Timing of millennial-scale climate change in Antarctica and Greenland during the last glacial period: Science, v. 291, p. 109-112.

Blunier, T., Chappellaz, J., Schwander, J., Dallenbach, A., Stauffer, B., Stocker, T.F., Raynaud, D., Jouzel, J., Clausen, H.B., Hammer, C.U., and Johnsen, S.J., 1998, Asynchrony of Antarctic and Greenland climate change during the last glacial period: Nature, v. 394, p. 739-743.

Bond, G., Broecker, W., Johnsen, S., McManus, J., Labeyrie, L., Jouzel, J., and Bonani, G., 1993, Correlations between Climate Records from North-Atlantic Sediments and

Greenland Ice: Nature, v. 365, p. 143-147.

Bond, G., Showers, W., Cheseby, M., Lotti, R., Allmasi, P., deMenocal, P., Priore, P., Cullen, H., Hajdas, I., and Bonani, G., 1997, A pervasive millennial-scale cycle in North Atlantic Holocene and glacial climates: Science, v. 278, p. 1257 - 1266.

Bond, G.C., Showers, W., Elliot, M., Evans, M., Lotti, R., Hajdas, I., Bonani, G., and Johnson, S., 1999, The North Atlantic's 1–2 kyr climate rhythm: relation to Heinrich events, Dansgaard/Oeschger cycles and the little ice age, *in* Clark, P.U., Webb, R.S., Keigwin, L.D., ed., Mechanisms of Global Change at Millennial Time Scales: Geophysical Monograph: Washington DC, American Geophysical Union, p. 59–76.

Bostock, H.C., 2005, Geochemically tracing the intermediate and surface waters in the Tasman Sea, southwest Pacific [Ph. D. thesis], The Australian National University.

Bostock, H.C., Opdyke, B.N., Gagan, M.K., and Fifield, L.K., 2004, Carbon isotope evidence for changes in Antarctic Intermediate Water circulation and ocean ventilation in the southwest Pacific during the last deglaciation: Paleoceanography, v. 19, p. DOI: 10.1029/2004PA001047.

Boyle, E.A., 1992, Cadmium and Delta-C-13 Paleochemical Ocean Distributions During the Stage-2 Glacial Maximum: Annual Review of Earth and Planetary Sciences, v. 20, p. 245-287.

Bradtmiller, L.I., Anderson, R.F., Fleisher, M.Q., and Burckle, L.H., 2006, Diatom productivity in the equatorial Pacific Ocean from the last glacial period to the present: A test of the silicic acid leakage hypothesis: Paleoceanography, v. 21, p. DOI: 10.1029/2006PA001282.

Brandes, J.A., Devol, A.H., Yoshinari, T., Jayakumar, D.A., and Naqvi, S.W.A., 1998, Isotopic composition of nitrate in the central Arabian Sea and eastern tropical North Pacific: A tracer for mixing and nitrogen cycles: Limnology and Oceanography, v. 43, p. 1680-1689.

Broecker, W., and Barker, S., 2007, A 190[per mille sign] drop in atmosphere's [Delta]14C during the "Mystery Interval" (17.5 to 14.5 kyr): Earth and Planetary Science Letters, v. 256, p. 90-99.

Broecker, W., Clark, E., and Barker, S., 2008, Near constancy of the Pacific Ocean surface to mid-depth radiocarbon-age difference over the last 20 kyr: Earth and Planetary Science Letters, v. 274, p. 322-326.

Broecker, W.S., 1992, The Great Ocean Conveyor: Global Warming : Physics and Facts, v. 247, p. 129-161.

—, 2000, Abrupt climate change: causal constraints provided by the paleoclimate record: Earth-Science Reviews, v. 51, p. 137-154.

Broecker, W.S., Bond, G.C., Klas, M., Clark, E., and McManus, J., 1992, Origin of the Northern Atlantic Heinrich Events: Climate Dynamics v. 6, p. 265-273.

Broecker, W.S., and Maier-Reimer, E., 1992, The influence of air and sea exchange on the carbon isotope distribution in the sea: Global Biogeochemical Cycles, v. 6, p. 315-320.

Broecker, W.S., and Peng, T.H., 1982, Tracers in the sea, Eldigio Press Lamont Doherty Geological Observatory, 690 p.

Brook, E.J., Sowers, T., and Orchardo, J., 1996, Rapid variations in atmospheric methane

concentration during the past 110,000 years: Science, v. 273, p. 1087-1091.

Brzezinski, M.A., and Nelson, D.M., 1996, Chronic substrate limitation of silicic acid uptake rates in the western Sargasso Sea: Deep-Sea Research Part Ii-Topical Studies in Oceanography, v. 43, p. 437-453.

Brzezinski, M.A., Pride, C.J., Franck, V.M., Sigman, D.M., Sarmiento, J.L., Matsumoto, K., Gruber, N., Rau, G.H., and Coale, K.H., 2002, A switch from Si(OH)(4) to NO3-depletion in the glacial Southern Ocean: Geophysical Research Letters, v. 29, p. DOI: 10.1029/2001GL014349.

Campin, J.-M., Fichefet, T., and Duplessy, J.-C., 1999, Problems with using radiocarbon to infer ocean ventilation rates for past and present climates: Earth Planet. Sci. Lett., v. 165, p. 17-24.

Cane, M.A., 1998, A role for tropical Pacific: Science, v. 282, p. 59-61.

Cannariato, K.G., Kennett, J.P., and Behl, R.J., 1999, Biotic response to late Quaternary rapid climate switches in Santa Barbara Basin:Ecological and evolutionary implications: Geology, v. 27, p. 63–66.

Chang, A.S., Pedersen, T.F., and Hendy, I.L., 2008, Late Quaternary paleoproductivity history on the Vancouver Island margin, western Canada: a multiproxy geochemical study: Canadian Journal of Earth Sciences, v. 45, p. 1283-1297.

Chappellaz, J.A., Fung, I.Y., and Thompson, A.M., 1993, The atmospheric CH4 increase since the Last Glacial Maximum: Tellus, v. 45B, p. 228 - 241.

Charles, C.D., and Fairbanks, R.G., 1990, Glacial to interglacial changes in the isotopic gradients of Southern Ocean surface water, *in* Bleil, and Theide, eds., Geologic History of Polar Oceans: Arctic versus Antarctic, Volume 308: NATO ASI Series: Boston, Mass, Kluwer Academic Publishers, p. 519-538.

Charles, C.D., Froehlich, P.N., Zibello, M.A., Mortlock, R.A., and Morely, J.J., 1991, Biogenic opal in southern ocean sediment over the past 450,000 years: Implications for surface water chemistry and circulation: Paleoceanography, v. 6, p. 697-728.

Charles, C.D., LynchStieglitz, J., Ninnemann, U.S., and Fairbanks, R.G., 1996, Climate connections between the hemisphere revealed by deep sea sediment core ice core correlations: Earth and Planetary Science Letters, v. 142, p. 19-27.

Charles, C.D., Wright, J.D., and Fairanks, R.G., 1993, Thermodynamic influences of the marine carbon isotope record: Paleoceanography, v. 8, p. 691-697.

Clark, P.U., Alley, R.B., and Pollard, D., 1999a, Climatology - Northern hemisphere ice-sheet influences on global climate change: Science, v. 286, p. 1104-1111.

Clark, P.U., Dyke, A.S., Shakun, J.D., Carlson, A.E., Clark, J., Wohlfarth, B., Mitrovica, J.X., Hostetler, S.W., and McCabe, A.M., 2009, The Last Glacial Maximum: Science, v. 325, p. 710-714.

Clark, P.U., Webb, R.S., and Keigwin, L.D., 1999b, Mechanisms of Millennial-Scale Global Climate Change: Washington D.C., AGU Geophysical Monograph 112.

CLIMAP Project Members, 1984, The last interglacial ocean: Quaternary Research, v. 21, p. 123-224.

Cline, J.D., and Kaplan, I.R., 1975, Isotopic fractionation of dissolved nitrate during denitrification in the eastern tropical North Pacific Ocean. : Mar. Chem, v. 3, p. 271–

299.

COHMAP Members, 1988, Climate changes of the last 18,000 years: observations and model simulations: Science, v. 271, p. 1043-1052.

Crusius, J., Pedersen, T.F., Kienast, S., Keigwin, L., and Labeyrie, L., 2004, Influence of northwest Pacific productivity on North Pacific Intermediate Water oxygen concentrations during the Boiling-Allerod interval (14.7-12.9 ka): Geology, v. 32, p. 633-636.

Curry, W., and Oppo, D.W., 1997, Synchronous, high frequency oscillations in the tropical sea surface temperature and North Atlantic deep-water production during the last glacial cycle: Paleoceanography, v. 12, p. 1-14.

Curry, W.B., Duplessy, J.-C., Labeyrie, L.D., and Shackleton, N.J., 1988, Changes in the distrubution of d13C of deep water ΣCO2 between the last delaciation and the Holocene: Paleoceanography, v. 3, p. 317-342.

Dansgaard, W., Johnsen, S.J., Clausen, H.B., Dahl-Jensen, D., Gundestrup, N., Hammer, C.U., and Oeschger, H., 1984, North Atlantic climatic oscillations revealed by deep Greenland ice cores, in Hansen, J.E., and Takahashi, T., eds., Climatic Processes and Climate Sensitivity, Volume 29: Washington D.C., Geophys. Monogr. Series AGU, p. 288-298.

Dansgaard, W., Johnsen, S.J., Clausen, H.B., Dahl-Jensen, D., Gundestrup, N.S., Hammer, C.U., Hvidberg, C.S., Steffensen, J.P., Sveinbørnsdottir, A.E., Jouzel, J., and Bond, G., 1993, Evidence for general instability of past climate from a 250-kyr ice-core record. : Nature, v. 364, p. 218-220.

De Pol-Holz, R., Keigwin, L., Southon, J., Hebbeln, D., and Mohtadi, M., 2010, No signature of abyssal carbon in intermediate waters off Chile during deglaciation: Nature Geoscience, v. 3, p. 192-195.

De Pol-Holz, R., Ulloa, O., Dezileau, L., Kaiser, J., Lamy, F., and Hebbeln, D., 2006, Melting of the Patagonian Ice Sheet and deglacial perturbations of the nitrogen cycle in the eastern South Pacific: Geophysical Research Letters, v. 33, p. DOI: 10.1029/2005GL024477.

DeMaster, D.J., 2002, The accumulation and cycling of biogenic silica in the Southern Ocean: revisiting the marine silica budget: Deep-Sea Research Part II-Topical Studies in Oceanography, v. 49, p. 3155-3167.

Douglas, R., Gonzalez-Yajimovich, O., Ledesma-Vazquez, J., and Staines-Urias, F., 2007, Climate forcing, primary production and the distribution of Holocene biogenic sediments in the Gulf of California: Quaternary Science Reviews, v. 26, p. 115-129.

Dugdale, R.C., Barber, R.T., Chai, F., Peng, T.H., and Wilkerson, F.P., 2002, One-dimensional ecosystem model of the equatorial Pacific upwelling system. Part II: sensitivity analysis and comparison with JGOFS EqPac data: Deep-Sea Research Part Ii-Topical Studies in Oceanography, v. 49, p. 2747-2768.

Duplessy, J.-C., Shackleton, N.J., Matthews, R.K., Prell, W.L., Ruddiman, W.F., Caralp, M., and Hendy, C.H., 1984, 13C Record of benthic foraminifera in the last interglacial ocean: Implications for the carbon cycle and the global deep water circulation: Quaternary Research, v. 21, p. 225-243.

Dymond, J., and Lyle, M., 1985, Flux comparisons between sediments and sediment traps in the eastern tropical Pacific: Implications for atmospheric CO2 variations during the

Pleistocene: Limnology and Oceanography, v. 30, p. 699–712.

Egge, J.K., and Aksnes, D.L., 1992, Silicate as Regulating Nutrient in Phytoplankton Competition: Marine Ecology-Progress Series, v. 83, p. 281-289.

Emmer, E., and Thunell, R.C., 2000, Nitrogen isotope variations in Santa Barbara Basin sediments: Implications for denitrification in the eastern tropical North Pacific during the last 50,000 years. : Paleoceanography, v. 15, p. 377-387.

EPICA, Augustin, L., Barbante, C., Barnes, P.R.F., Barnola, J.M., Bigler, M., Castellano, E., Cattani, O., Chappellaz, J., DahlJensen, D., Delmonte, B., Dreyfus, G., Durand, G., Falourd, S., Fischer, H., Fluckiger, J., Hansson, M.E., Huybrechts, P., Jugie, R., Johnsen, S.J., Jouzel, J., Kaufmann, P., Kipfstuhl, J., Lambert, F., Lipenkov, V.Y., Littot, G.V.C., Longinelli, A., Lorrain, R., Maggi, V., Masson-Delmotte, V., Miller, H., Mulvaney, R., Oerlemans, J., Oerter, H., Orombelli, G., Parrenin, F., Peel, D.A., Petit, J.R., Raynaud, D., Ritz, C., Ruth, U., Schwander, J., Siegenthaler, U., Souchez, R., Stauffer, B., Steffensen, J.P., Stenni, B., Stocker, T.F., Tabacco, I.E., Udisti, R., van de Wal, R.S.W., van den Broeke, M., Weiss, J., Wilhelms, F., Winther, J.G., Wolff, E.W., and Zucchelli, M., 2004, Eight glacial cycles from an Antarctic ice core: Nature, v. 429, p. 623-628.

Falkowski, P.G., 1997, Evolution of the nitrogen cycle and its influence on the biological sequestration of CO2 in the ocean: Nature, v. 387, p. 272-275.

Farber-Lorda, J., Lavín, M.F., and Guerrero-Ruiz, M.A., 2004, Effects of wind forcing on the trophic conditions, zooplankton biomass and krill biochemical composition in the Gulf of Tehuantepec: Deep Sea Research Part II: Topical Studies in Oceanography, v. 51, p. 601-614.

Fasham, M.J.R., 2003, Ocean biogeochemistry: the role of the ocean carbon cycle in global change, Springer-Verlag.

Fiedler, P.C., and Talley, L.D., 2006, Hydrography of the eastern tropical Pacific: A review: Progress in Oceanography, v. 69, p. 143-180.

Firing, E., Wijffels, S.E., and Hacker, P., 1998, Equatorial subthermocline currents across the Pacific: Journal of Geophysical Research, v. 103, p. 21413–21423.

Flückiger, J., Blunier, T., Stauffer, B., Chappellaz, J., Spahni, R., Kawamura, K., Schwander, J., Stocker, T.F., and Dahl-Jensen, D., 2004, N2O and CH4 Variations during the last glacial epoch: insight into global processes: Glob. Biogeochem. Cycles v. 18, p. DOI: 10.1029/2003GB002122.

Flückiger, J., Dallenbach, A., Blunier, T., Stauffer, B., Stocker, T.F., Raynaud, J.M., and Barnola, J.M., 1999, Variations in atmospheric N2O concentration during abrupt climatic changes: Science, v. 285, p. 227 – 230.

Franke, J., Paul, A., and Schulz, M., 2008, Modeling variations of marine reservoir ages during the last 45 000 years: Climate of the Past, v. 4, p. 125-136.

Galbraith, E.D., Jaccard, S.L., Pedersen, T.F., Sigman, D.M., Haug, G.H., Cook, M., Southon, J.R., and Francois, R., 2007, Carbon dioxide release from the North Pacific abyss during the last deglaciation: Nature, v. 449, p. 890-U9.

Galbraith, E.D., Kienast, M., Pedersen, T.F., and Calvert, S.E., 2004, Glacial-interglacial modulation of the marine nitrogen cycle by high-latitude O-2 supply to the global thermocline: Paleoceanography, v. 19, p. DOI: 10.1029/2003PA001000.

Ganeshram, R.S., 2002, Global change - Oceanic action at a distance: Nature, v. 419, p. 123-125.

Ganeshram, R.S., Calvert, S.E., Pedersen, T.F., and Cowie, G.L., 1999, Factors controlling the burial of organic carbon in laminated and bioturbated sediments off NW Mexico: Implications for hydrocarbon preservation: Geochimica Et Cosmochimica Acta, v. 63, p. 1723-1734.

Ganeshram, R.S., and Pedersen, T.F., 1998, Glacial-interglacial variability in upwelling and bioproductivity off NW Mexico: Implications for quaternary paleoclimate: Paleoceanography, v. 13, p. 634-645.

Ganeshram, R.S., Pedersen, T.F., Calvert, S.E., and Francois, R., 2002, Reduced nitrogen fixation in the glacial ocean inferred from changes in marine nitrogen and phosphorus inventories: Nature, v. 415, p. 156-159.

Ganeshram, R.S., Pedersen, T.F., Calvert, S.E., McNeill, G.W., and Fontugne, M.R., 2000, Glacial-interglacial variability in denitrification in the world's oceans: Causes and consequences: Paleoceanography, v. 15, p. 361-376.

Ganeshram, R.S., Pedersen, T.F., Calvert, S.E., and Murray, J.W., 1995, Large Changes in Oceanic Nutrient Inventories from Glacial to Interglacial Periods: Nature, v. 376, p. 755-758.

Ganopolski, A., and Ramstorf, S., 2001, Rapid changes of glacial climate simulated in a coupled modelsphere climate extending into the last interglacial period. : Nature, v. 409, p. 153-158.

Garcin, Y., Williamson D., Taieb M., Vincens A., Mathé P.E., Majule A. , 2006, Centennial to millennial changes in maar-lake deposition during the last 45,000 years in tropical Southern Africa (Lake Masoko, Tanzania): Palaeo, v. 239, p. 334-354.

Gersonde, R., Abelmann, A., Brathauer, U., Becquey, S., Bianchi, C., Cortese, G., Grobe, H., Kuhn, G., Niebler, H.S., Segl, M., Sieger, R., Zielinski, U., and Futterer, D.K., 2003, Last glacial sea surface temperatures and sea-ice extent in the Southern Ocean (Atlantic-Indian sector): A multiproxy approach: Paleoceanography, v. 18, p. DOI: 10.1029/2002PA000809.

Gorbarenko, S.A., 1996, Stable isotope and lithologic evidence of late-glacial and Holocene oceanography of the northwestern Pacific and its marginal seas: Quaternary Research, v. 46, p. 230-250.

Grootes, P.M., and Stuiver, M., 1997, Oxygen 18/16 variability in Greenland snow and ice with 10(-3)- to 10(5)-year time resolution: Journal of Geophysical Research-Oceans, v. 102, p. 26455-26470.

Grossman, E.L., 1987, Stable Isotopes in Modern Benthic Foraminifera - a Study of Vital Effect: Journal of Foraminiferal Research, v. 17, p. 48-61.

Gruber, N., and Sarmiento, J.L., 1997, Global patterns of marine nitrogen fixation and denitrification: Global Biogeochemical Cycles, v. 11, p. 235-266.

Hanawa, K., and Talley, L.D., 2001, Mode Waters, in Siedler, G., and Church, J., eds., Ocean Circulation and Climate, International Geophysics Series, Academic Press., p. 373-386.

Harrison, K.G., 2000, Role of increased marine silica input on paleo-pCO(2) levels: Paleoceanography, v. 15, p. 292-298.

Haug, G.H., Hughen, K.A., Sigman, D.M., Peterson, L.C., and Röhl, U., 2001, Southward Migration of the Intertropical Convergence Zone Through the Holocene: Science, v. 293, p. 1304 - 1308.

Hays, J.D., Imbrie, J., and Shackleton, N.J., 1976, Variations in the Earth's Orbit: Pacemaker of the Ice Ages: Science, v. 194, p. 1121-1132.

Heinrich, H., 1988, Origin and consequences of cycling ice rafting in the Northeast Atlantic Ocean during the past 130,000 years: Quaternary Research v. 29, p. 142-152

Hemming, S.R., 2004, Heinrich Events: Massive Late Pleistocene detritus layers of the North Atlantic and their global climate imprint: Review of Geophysics, v. 42, p. 20032003RG000128.

Hendy, I.L., and Kennett, J.P., 1999, Latest Quaternary North Pacific surface-water responses imply atmosphere-driven climate instability: Geology, v. 27, p. 291-294.

—, 2000, Dansgaard-Oeschger cycles and the California Current System: Planktonic foraminiferal response to rapid climate change in Santa Barbara Basin, Ocean Drilling Program hole 893A: Paleoceanography, v. 15, p. 30-42.

—, 2003, Tropical forcing of North Pacific intermediate water distribution during Late Quaternary rapid climate change?: Quaternary Science Reviews, v. 22, p. 673-689.

Hendy, I.L., Kennett, J.P., Roark, E.B., and Ingram, B.L., 2002, Apparent synchroneity of submillennial scale climate events between Greenland and Santa Barbara Basin, California from 30-10 ka: Quaternary Science Reviews, v. 21, p. 1167-1184.

Hendy, I.L., and Pedersen, T.F., 2005, Is pore water oxygen content decoupled from productivity on the California Margin? Trace element results from Ocean Drilling Program Hole 1017E, San Lucia slope, California: Paleoceanography, v. 20, p. DOI: 10.1029/2004PA001123.

—, 2006, Oxygen minimum zone expansion in the eastern tropical North Pacific during deglaciation: Geophysical Research Letters, v. 33, p. DOI: 10.1029/2006GL025975.

Hendy, I.L., Pedersen, T.F., Kennett, J.P., and Tada, R., 2004, Intermittent existence of a southern Californian upwelling cell during submillennial climate change of the last 60 kyr: Paleoceanography, v. 19, p. DOI: 10.1029/2003PA000965.

Herguera, J.C., 1992, Deep-Sea Benthic Foraminifera and Biogenic Opal - Glacial to Postglacial Productivity Changes in the Western Equatorial Pacific: Marine Micropaleontology, v. 19, p. 79-98.

Higginson, M.J., and Altabet, M.A., 2004, Initial test of the silicic acid leakage hypothesis using sedimentary biomarkers: Geophysical Research Letters, v. 31, p. DOI: 10.1029/2004GL020511.

Hodell, D.A., Venz, K.A., Charles, C.D., and Ninnemann, U.S., 2003, Pleistocene vertical carbon isotope and carbonate gradients in the South Atlantic sector of the Southern Ocean: Geochemistry Geophysics Geosystems, v. 4, p. DOI:10.1029/2002GC000367.

Holmgrena, K., Lee-Thorpb, J.A., Cooperc, G.R.J, Lundblada, K., Partridged, T.C., Scotte, L., Sithaldeenb, R., Talmaf, A. S., Tyson, P.D., 2003, Persistent millennial-scale climatic variability over the past 25,000 years in Southern Africa: Quaternary Science Reviews, v. 22, p. 2311–2326.

Holsten, J., Stott, L.D., and Berelson, W., 2004, Reconstructing benthic carbon oxidation

rates using delta C-13 of benthic foraminifers: Marine Micropaleontology, v. 53, p. 117-132.

Hoshiba, M., Ahagon, N., Ohkushi, K., Uchida, M., Motoyama, I., and Nishimura, A., 2006, Foraminiferal oxygen and carbon isotopes during the last 34 kyr off northern Japan, northwestern Pacific: Marine Micropaleontology, v. 61, p. 196-208.

Hughen, K., Southon, J., Lehman, S., Bertrand, C., and Turnbull, J., 2006, Marine-derived C-14 calibration and activity record for the past 50,000 years updated from the Cariaco Basin: Quaternary Science Reviews, v. 25, p. 3216-3227.

Hughen, K.A., Baillie, M.G.L., Bard, E., Beck, J.W., Bertrand, C.J.H., Blackwell, P.G., Buck, C.E., Burr, G.S., Cutler, K.B., Damon, P.E., Edwards, R.L., Fairbanks, R.G., Friedrich, M., Guilderson, T.P., Kromer, B., McCormac, G., Manning, S., Ramsey, C.B., Reimer, P.J., Reimer, R.W., Remmele, S., Southon, J.R., Stuiver, M., Talamo, S., Taylor, F.W., van der Plicht, J., and Weyhenmeyer, C.E., 2004, Marine04 marine radiocarbon age calibration, 0-26 cal kyr BP: Radiocarbon, v. 46, p. 1059-1086.

Hughen, K.A., Overpeck, J.T., Peterson, L.C., and Trumbore, S., 1996, Rapid climate changes in the tropical Atlantic region during the last deglaciation: Nature, v. 380, p. 51-54.

Imbrie, J., Hays, J.D., Martinson, D.G., McIntyre, A., Mix, A.C., Morley, J.J., Pisias, N.G., Prell, W.L., and Shackleton, N.J., 1984, The orbital theory of Pleistocene climate: Support from a revised chronology of the marine d18O record, *in* Berger, A., ed., Milankovitch and Climate, Volume Part 1: New York, Springer, p. 269–305.

IPCC, 2001, Climate Change 2001: The Scientific Basis. Contribution of Working Group I to the Third Assessment Report of the Intergovernmental Panel on Climate Change: Cambridge, United Kingdom and New York, USA, Cambridge University Press, 881 p.

Isono, D., Yamamoto, M., Irino, T., Oba, T., Murayama, M., Toshio, N., and Kawahata, H., 2009, The 1500-year climate oscillation in the midlatitude NorthPacific during the Holocene: Geology, v. 37, p. 591-594.

Ivanochko, T.S., Ganeshram, R.S., Brummer, G.J.A., Ganssen, G., Jung, S.J.A., Moreton, S.G., and Kroon, D., 2005, Variations in tropical convection as an amplifier of global climate change at the millennial scale: Earth and Planetary Science Letters, v. 235, p. 302-314.

Jorissen, F.J., 1999, Benthic foraminiferal microhabitats below the sediment-water interface, *in* Sen Gupta, B.K., ed., Ecology of recent foraminifera: Dordrecht, The Netherlands, Kluwer Academic Publishers, p. 161-179.

Kaiho, K., 1994, Benthic foraminiferal dissolved-oxygen index and dissolved-oxygen levels in the modern ocean: Geology, v. 22, p. 719-722.

Kaiser, J., Lamy, F., Arz, H.W., and Hebbeln, D., 2007, Dynamics of the millennial-scale sea surface temperature and Patagonian Ice Sheet fluctuations in southern Chile during the last 70 kyr (ODP Site 1233). Quaternary International v. 161, p. 77-89.

Keeling, R.F., 2007, Deglaciation mysteries: Science, v. 316, p. 1440-1441.

Keeling, R.F., and Stephens, B.B., 2001, Antarctic sea ice and the control of Pleistocene climate instability: Paleoceanography, v. 16, p. 112-131.

Keigwin, L.D., 1998, Glacial-Age Hydrography of the Far Northwest Pacific Ocean:

Paleoceanography, v. 13, p. 323–339.

—, 2002, Late Pleistocene-Holocene paleoceanography and ventilation of the Gulf of California: Journal of Oceanography, v. 58, p. 421-432.

Keigwin, L.D., and Jones, G.A., 1990, Deglacial climatic oscillations in the Gulf of California: Paleoceanography, v. 5, p. 1009–1023.

—, 1994, Western North-Atlantic Evidence for Millennial-Scale Changes in Ocean Circulation and Climate: Journal of Geophysical Research-Oceans, v. 99, p. 12397-12410.

Kennett, J.P., and Ingram, B.L., 1995, A 20,000-year record of ocean circulation and climate change from the Santa Barbara Basin: Nature, v. 377, p. 510-512.

Kessler, W.S., 2006, The circulation of the eastern tropical Pacific: A review: Progress in Oceanography, v. 69, p. 181-217.

Key, R.M., Kozyr, A., Sabine, C.L., Lee, K., Wanninkhof, R., Bullister, J.L., Feely, R.A., Millero, F.J., Mordy, C., and Peng, T.H., 2004, A global ocean carbon climatology: Results from Global Data Analysis Project (GLODAP): Global Biogeochemical Cycles, v. 18, p. DOI: 10.1029/2004GB002247.

Kienast, S.S., Calvert, S.E., and Pedersen, T.F., 2002, Nitrogen isotope and productivity variations along the northeast Pacific margin over the last 120 kyr: Surface and subsurface paleoceanography: Paleoceanography, v. 17, p. DOI: 10.1029/2001PA000650.

Kienast, S.S., Kienast, M., Jaccard, S., Calvert, S.E., and Francois, R., 2006, Testing the silica leakage hypothesis with sedimentary opal records from the eastern equatorial Pacific over the last 150 kyrs: Geophysical Research Letters, v. 33, p. DOI: 10.1029/2006GL026651.

Kim, S.J., Crowley, T.J., Erickson, D.J., Govindasamy, B., Duffy, P.B., and Lee, B.Y., 2008, High-resolution climate simulation of the last glacial maximum: Climate Dynamics, v. 31, p. 1-16.

Koutavas, A., and Lynch-Stieglitz, J., 2003, Glacial-interglacial dynamics of the eastern equatorial Pacific cold tongue Intertropical Convergence Zone system reconstructed from oxygen isotope records: Paleoceanography, v. 18, p. DOI: 10.1029/2003PA000894.

—, 2004, Variability of the marine ITCZ over the eastern Pacific during the past 30,000 years - Regional perspective and global context: Hadley Circulation: Present, Past and Future, v. 21, p. 347-369.

Kroopnick, P., 1985, The distribution of carbon-13 in the world oceans: Deep Sea Research, v. 32, p. 57-84.

Lavın, M.F., Beier, E., and Badan, A., 1997, Estructura Hidrografica y Circulacion del Golfo de California: Escalas estacional e interanual, in UGM, ed., Contribuciones a la Oceanografıa Fısica en Mexico: Monografıa No. 3, Union Geofısica Mexicana, p. 141-171.

Lavin, M.F., Gaxiolacastro, G., Robles, J.M., and Richter, K., 1995, Winter Water Masses and Nutrients in the Northern Gulf of California: Journal of Geophysical Research-Oceans, v. 100, p. 8587-8605.

Lavin, M.F., Robles, J.M., Argote, M.L., Barton, E.D., Smith, R., Brown, J., Kosro, M.,

Trasviña, A., Vevez, H.S., and Garcia, J., 1992, Física del Golfo de Tehuantepec: Ciencia y Desarrollo, v. 18, p. 97-107.

Levitus, S., and Boyer, T.P., 1994, World Ocean Atlas 1994, v. 2: Oxygen.

Levitus, S., Burgett, R., and Boyer, T.P., 1994, World Ocean Atlas 1994, v. 3: Nutrients.

Lisiecki, L.E., and Raymo, M.E., 2005, A Pliocene-Pleistocene stack of 57 globally distributed benthic d18O records: Paleoceanography, v. 20, p. PA1003.

Lohmann, G., and Lorenz, S., 2000, On the hydrological cycle under paleoclimatic conditions as derived from AGCM simulations: Journal of Geophysical Research-Atmospheres, v. 105, p. 17417-17436.

Loubere, P., and Bennett, S., 2008, Southern Ocean biogeochemical impact on the tropical ocean: Stable isotope records from the Pacific for the past 25,000 years: Global and Planetary Change, v. 63, p. 333-340.

Lourantou, A., Lavric, J.V., Köhler, P., Barnola, J.-M., Paillard, D., Michel, E., Raynaud, D., and Chappellaz, J.A., in press, New atmospheric carbon isotopic measurements constrain the CO_2 rise during the last deglaciation: Global Biogeochemical Cycles, p. doi:10.1029/2009GB003545.

Lund, D.C., and Mix, A.C., 1998, Millennial-scale deep water oscillations: Reflections of the North Atlantic in the deep Pacific from 10 to 60 ka: Paleoceanography, v. 13, p. 10-19.

Lunkeit, F., Fraedrich, K., and Bauer, S.E., 1998, Storm tracks in a warmer climate: sensitivity studies with a simplified global circulation model: Climate Dynamics, v. 14, p. 813-826.

Lyle, M.W., Prahl, F.G., and Sparrow, M.A., 1992, Upwelling and Productivity Changes Inferred from a Temperature Record in the Central Equatorial Pacific: Nature, v. 355, p. 812-815.

Lynch-Stieglitz, J., Fairbanks, R.G., and Charles, C.D., 1994, Glacial-interglacial history of Antarctic Intermediate Water: Relative strengths of Antarctic vs. Indian Ocean sources: Paleoceanography, v. 9, p. 7-29.

MacAyeal, D.R., 1993, Binge/purge oscillations of the Laurentide ice sheet as a cause of the North Atlantic's Heinrich events: Paleoceanography, v. 8, p. 775-784.

Marchitto, T.M., Lehman, S.J., Ortiz, J.D., Fluckiger, J., and van Geen, A., 2007, Marine radiocarbon evidence for the mechanism of deglacial atmospheric CO_2 rise: Science, v. 316, p. 1456-1459.

Marret, F., Scourse, J.D., Versteegh, G., Jansen, J.H.F., and Schneider, R., 2001, Integrated marine and terrestrial evidence for abrupt Congo River palaeodischarge fluctuations during the last deglaciation: Journal of Quaternary Science, v. 16, p. 761-766.

Martinez, P., Lamy, F., Robinson, R.R., Pichevin, L., and Billy, I., 2006, Atypical delta N-15 variations at the southern boundary of the East Pacific oxygen minimum zone over the last 50 ka: Quaternary Science Reviews, v. 25, p. 3017-3028.

Martinson, D.G., Pisias, N.G., Hays, J.D., Imbrie, J., Moore, T.C., and Shackleton, N.J., 1987, Age dating and the orbital theory of the Ice Ages: development of a high resolution 0 to 30,000 year chronostratigraphy: Quat. Res. , v. 27, p. 1-29.

Martrat, B., Grimalt, J.O., Lopez-Martinez, C., Cacho, I., Sierro, F.J., Flores, J.A., Zahn, R.,

Canals, M., Curtis, J.H., and Hodell, D.A., 2004, Abrupt temperature changes in the Western Mediterranean over the past 250,000 years: Science, v. 306, p. 1762-1765.

Martrat, B., Grimalt, J.O., Shackleton, N.J., de Abreu, L., Hutterli, M.A., and Stocker, T.F., 2007, Four climate cycles of recurring deep and surface water destabilizations on the Iberian margin: Science, v. 317, p. 502-507.

Matsumoto, K., and Key, R.M., 2004, Natural radiocarbon distribution in the deep ocean, *in* Shiyomi, M., Kawahata, H., Koizumi, H., Tsuda, A., and Awaya, Y., eds., Global Environmental Change in the Ocean and on Land: Tokyo, TERRAPUB, p. 45-58.

Matsumoto, K., and Lynch-Stieglitz, J., 1999, Similar glacial and Holocene deep water circulation inferred from southeast Pacific benthic foraminiferal carbon isotope composition: Paleoceanography, v. 14, p. 149-163.

Matsumoto, K., Sarmiento, J.L., and Brzezinski, M.A., 2002, Silicic acid leakage from the Southern Ocean: A possible explanation for glacial atmospheric pCO(2): Global Biogeochemical Cycles, v. 16, p. DOI: 10.1029/2001GB001442.

McCorkle, D.C., Corliss, B.H., and Farnham, C.A., 1997, Vertical distributions and stable isotopic compositions of live (stained) benthic foraminifera from the North Carolina and California continental margin: Deep-Sea Research II, v. 44, p. 983-1024.

McCorkle, D.C., and Emerson, S.R., 1988, The Relationship between Pore Water Carbon Isotopic Composition and Bottom Water Oxygen Concentration: Geochimica Et Cosmochimica Acta, v. 52, p. 1169-1178.

McCorkle, D.C., Emerson, S.R., and Quay, P.D., 1985, Stable Carbon Isotopes in Marine Porewaters: Earth and Planetary Science Letters, v. 74, p. 13-26.

McCorkle, D.C., and Keigwin, L.D., 1994, Depth Profiles of Delta-C-13 in Bottom Water and Core Top C-Wuellerstorfi on the Ontong Java Plateau and Emperor Seamounts: Paleoceanography, v. 9, p. 197-208.

McCorkle, D.C., Keigwin. L.D., Corliss, B.H., and Emerson, S.R., 1990, The influence of microhabitats on the carbon isotopic composition of deep-sea benthic foraminifera: Paleoceanography, v. 5, p. 161 - 185.

McGee, D., Marcantonio, F., and Lynch-Stieglitz, J., 2007, Deglacial changes in dust flux in the eastern equatorial Pacific: Earth and Planetary Science Letters, v. 257, p. 215-230.

McIntyre, A., and Ruddiman, W.F., 1972, Northeast Atlantic post-Eemian paleooceanography: a predictive analog of the future: Quaternary Research, v. 2, p. 350-354.

McManus, J.F., Bond, G.C., Broecker, W.S., Johnsen, S., Labeyrie, L., and Higgins, S., 1994, High-Resolution Climate Records from the North-Atlantic During the Last Interglacial: Nature, v. 371, p. 326-329.

McManus, J.F., Oppo, D.W., and Cullen, J.L., 1999, A 0.5-million-year record of millennial scale climate variability in the North Atlantic: Science, v. 283, p. 971-975.

Meissner, K.J., Galbraith, E.D., and Volker, C., 2005, Denitrification under glacial and interglacial conditions: A physical approach: Paleoceanography, v. 20, p. DOI: 10.1029/2004PA001083.

Metcalfe, S., Say, A., Black, S., McCulloch, R., and O'Hara, S., 2002, Wet Conditions during the Last Glaciation in the Chihuahuan Desert, Alta Babicora Basin, Mexico:

Quaternary Research v. 57, p. 91-101.

Metcalfe, S.E., O'Hara, S.L., Caballero, M., and Davies, S.J., 2000, Records of Late Pleistocene-Holocene climatic change in Mexico - a review: Quaternary Science Reviews, v. 19, p. 699-721.

Milankovitch, M.M., 1941, Canon of Insolation and the Ice Age Problem: Washington DC, United States Department of Commerce and the National Science Foundation.

Mix, A.C., Bard, E., and Schneider, R., 2001, Environmental processes of the ice age: land, oceans, glaciers (EPILOG): Quaternary Science Reviews, v. 20, p. 627-657.

Mix, A.C., Lund, D.C., Pisias, N.G., Boden, P., Bornmalm, L., Lyle, M., and Pike, J., 1999, Rapid climate oscillations in the North Pacific during the Last Deglaciation reflect Northern and Southern Hemisphere sources, *in* Clark, P.U., Webb, R.S., and Keigwin, L.D., eds., Mechanisms of Global Climate Change at Millennial Time Scales.: Geophysical Monograph 112: Washington, DC, American Geophysics Union.

Mix, A.C., Pisias, N.G., Zahn, R., Rugh, W., Lopez, C., and Nelson, K., 1991, Carbon 13 in Pacific deep and intermediate waters, 0-370 ka: Implications for ocean circulation and Pleistocene CO_2: Paleoceanography, v. 6, p. 205-227.

Mix, A.C., Rugh, W., Pisias, N.G., and Veirs, S., 1992, Leg 138 Shipboard sedimentologists, and the led 138 Scientific Party. Color reflectance spectroscopy: a tool for rapid characterization of deep sea sediments, Volume 138, Proc. Ocean Drill. Program, Init. Rep., p. 67-77.

Mohtadi, M., and Hebbeln, D., 2004, Mechanisms and variations of the paleoproductivity off northern Chile (24 degrees S-33 degrees S) during the last 40,000 years: Paleoceanography, v. 19, p. DOI: 10.1029/2004PA001003.

Molinelli, E.J., 1981, The Antarctic influence on Antarctic Intermediate Water: J. Mar. Res., v. 39, p. 267-292.

Monnin, E., Indermuhle, A., Dallenbach, A., Fluckiger, J., Stauffer, B., Stocker, T.F., Raynaud, D., and Barnola, J.-M., 2001, Atmospheric CO_2 Concentrations over the Last Glacial Termination: Science, v. 291, p. 112-114.

Mook, W.G., Bommerso, J., and Staverma, W., 1974, Carbon Isotope Fractionation between Dissolved Bicarbonate and Gaseous Carbon-Dioxide: Earth and Planetary Science Letters, v. 22, p. 169-176.

Moore, J.K., Doney, S.C., and Lindsay, K., 2004, Upper ocean ecosystem dynamics and iron cycling in a global three-dimensional model: Global Biogeochemical Cycles, v. 18, p. DOI: 10.1029/2004GB002220.

Morley, J.J., Heusser, L.E., and Shackleton, N.J., 1991, Late Pleistocene/Holocene radiolarian and pollen records from sediments in the sea of Okhotsk: Paleoceanography, v. 6, p. 121-131.

Mortlock, R.A., and Froelich, P.N., 1989, A Simple Method for the Rapid-Determination of Biogenic Opal in Pelagic Marine-Sediments: Deep-Sea Research Part a-Oceanographic Research Papers, v. 36, p. 1415-1426.

Mosseri, J., QuÈguiner, B., Armand, L., and Cornet-Barthaux, V., 2008, Impact of iron on silicon utilization by diatoms in the Southern Ocean: A case study of Si/N cycle decoupling in a naturally iron-enriched area: Deep Sea Research Part II: Topical

Studies in Oceanography, v. 55, p. 801-819.

Nelson, D.M., Anderson, R.F., Barber, R.T., Brzezinski, M.A., Buesseler, K.O., Chase, Z., Collier, R.W., Dickson, M.L., Francois, R., Hiscock, M.R., Honjo, S., Marra, J., Martin, W.R., Sambrotto, R.N., Sayles, F.L., and Sigmon, D.E., 2002, Vertical budgets for organic carbon and biogenic silica in the Pacific sector of the Southern Ocean, 1996-1998: Deep-Sea Research Part II-Topical Studies in Oceanography, v. 49, p. 1645-1674.

Nelson, D.M., Brzezinski, M.A., Sigmon, D.E., and Franck, V.M., 2001, A seasonal progression of Si limitation in the Pacific sector of the Southern Ocean: Deep-Sea Research Part Ii-Topical Studies in Oceanography, v. 48, p. 3973-3995.

Ninnemann, U., and Charles, C.D., 1997, Regional differences in quaternary Subantarctic nutrient cycling: link to intermediate and deep water ventilation: Paleoceanography, v. 12, p. 560–567.

Ninnemann, U.S., and Charles, C.D., 2002, Changes in the mode of Southern Ocean circulation over the last glacial cycle revealed by foraminiferal stable isotopic variability: Earth and Planetary Science Letters, v. 201, p. 383-396.

Oba, T., and Murayama, M., 2004, Sea-surface temperature and salinity changes in the northwest Pacific since the Last Glacial Maximum: Journal of Quaternary Science, v. 19, p. 335-346.

Ono, A., Takahashi, K., Katsuki, K., Okazaki, Y., and Sakamoto, T., 2005, The Dansgaard-Oeschger cycles discovered in the up stream source region of the North Pacific Intermediate Water formation: Geophysical Research Letters, v. 32, p. DOI: 10.1029/2004GL022260.

Oppo, D.W., and Fairbanks, R.G., 1989, Carbon isotope composition of phosphate-free surface water of the past 22,000 years: Paleoceanography, v. 4, p. 333-351.

Ortega-Guerrero, B., Caballero-Miranda, M., Lozano-Garcia, S., and O., V.M.d.l., 1999, Paleoenviromental record of the last 70,000 yr in San Felipe Basin, Sonora desert, Mexico: preliminary results: Geofisica Internacional v. 38, p. 1-11.

Ortiz, J., Mix, A., Harris, S., and O'Connell, S., 1999, Diffuse spectral reflectance as a proxy for percent carbonate content in North Atlantic sediments: Paleoceanography, v. 14, p. 171-186.

Ortiz, J.D., O'Connell, S.B., DelViscio, J., Dean, W., Carriquiry, J.D., Marchitto, T., Zheng, Y., and van Geen, A., 2004, Enhanced marine productivity off western North America during warm climate intervals of the past 52 ky: Geology, v. 32, p. 521-524.

Ostlund, H.G., and Stuiver, M., 1980, Geosecs Pacific Radiocarbon: Radiocarbon, v. 22, p. 25-53.

Pahnke, K., and Zahn, R., 2005, Southern hemisphere water mass conversion linked with North Atlantic climate variability: Science, v. 307, p. 1741-1746.

Paillard, D., Labeyrie, L., and Yiou, P., 1996, Macintosh program performs time-series analysis: EOS Trans AGU, v. 77, p. 379.

Parkin, D.W., and Shackleton, N., 1973, rade wind and temperature correlations down a deep-sea core off the Sahara coast: Nature, v. 245, p. 455–457.

Paytan, A., Kastner, M., and Chavez, F.P., 1996, Glacial to interglacial fluctuations in

productivity in the equatorial Pacific as indicated by marine barite: Science, v. 274, p. 1355-1357.

Peacock, S., Visbeck, M., and Broecker, W.S., 1999, Deep water formation rates inferred from global tracer distributions: an inverse approach, *in* Kasibhatla, P., Heimann, M., Rayner, P., Mahowald, N., Prinn, R., and Hartley, G., eds., Inverse Methods in Global Biogeochemical Cycles: Geophysical Monograph Series 114: Washington D.C., AGU, p. 185 – 194.

Pedersen, T.F., François, R., François, L., Alverson, K., and McManus, J., 2003, The Late Quaternary History of Biogeochemical Cycling of Carbon, *in* Alverson, K.D., Bradley, R.S., and Pedersen, T.S., eds., Paleoclimate, Global Change and the Future: Berlin Heidelberg, Springer-Verlag, p. 63-79.

Peltier, W.R., 1994, Ice Age Paleotopography: Science, v. 265, p. 195-201.

Pena, L.D., Cacho, I., Ferretti, P., and Hall, M.A., 2008, El Nino-Southern Oscillation-like variability during glacial terminations and interlatitudinal teleconnections: Paleoceanography, v. 23, p. DOI: 10.1029/2008PA001620.

Pennington, J.T., Mahoney, K.L., Kuwahara, V.S., Kolber, D.D., Calienes, R., and Chavez, F.P., 2006, Primary production in the eastern tropical Pacific: A review: Progress in Oceanography, v. 69, p. 285-317.

Peterson, L.C., Haug, G.H., Hughen, K.A., and Rohl, U., 2000, Rapid changes in the hydrologic cycle of the tropical Atlantic during the last glacial: Science, v. 290, p. 1947 – 1951.

Petit, J.R., Jouzel, J., Raynaud, D., Barkov, N.I., Barnola, J.M., Basile, I., Bender, M., Chappellaz, J., Davis, M., Delaygue, G., Delmotte, M., Kotlyakov, V.M., Legrand, M., Lipenkov, V.Y., Lorius, C., Pepin, L., Ritz, C., Saltzman, E., and Stievenard, M., 1999, Climate and atmospheric history of the past 420,000 years from the Vostok ice core, Antarctica: Nature, v. 399, p. 429-436.

Pichevin, L.E., Ganeshram, R.S., Francavilla, S., Arellano-Torres, E., Pedersen, T.F., and Beaufort, L., 2010, Inter-hemispheric leakage of isotopically heavy nitrate in the Eastern Tropical Pacific during the last glacial period: Paleoceanography, v. 25, p. DOI: 10.1029/2009PA001754.

Pichevin, L.E., Reynolds, B.C., Ganeshram, R.S., Cacho, I., Pena, L.D., Keefe, K., and Ellam, R.M., 2009, Enhanced carbon pump inferred from relaxation of nutrient limitation in the glacial ocean: Nature, v. 459, p. 1114-1117.

Pisias, N.G., 1978, Paleoceanography of the Santa Barbara Basin during the last 8000 years: Quaternary Research, v. 10, p. 366–384.

Pisias, N.G., Mix, A.C., and Heusser, L., 2001, Millennial scale climate variability of the northeast Pacific Ocean and northwest North America based on radiolaria and Polen: Quaternary Science Reviews, v. 20, p. 1561-1576.

Pride, C., Thunell, R., Sigman, D., Keigwin, L., Altabet, M., and Tappa, E., 1999, Nitrogen isotopic variations in the Gulf of California since the last deglaciation: Response to global climate change: Paleoceanography, v. 14, p. 397-409.

Ragueneau, O., Treguer, P., Leynaert, A., Anderson, R.F., Brzezinski, M.A., DeMaster, D.J., Dugdale, R.C., Dymond, J., Fischer, G., Francois, R., Heinze, C., Maier-Reimer, E., Martin-Jezequel, V., Nelson, D.M., and Queguiner, B., 2000, A review of the Si cycle in the modem ocean: recent progress and missing gaps in the application of

biogenic opal as a paleoproductivity proxy: Global and Planetary Change, v. 26, p. 317-365.

Rahmstorf, S., 2003, Timing of abrupt climate chage: A precise clock: Geophysical Research Letters, v. 30, p. 1510.

Rathburn, A.E., Perez, M.E., and Lange, C.B., 2001, Benthicepelagic coupling in the Southern California Bight: relationships between sinking organic material, diatoms, benthic foraminifera: Marine Micropaleontology, v. 43, p. 261-271.

Reid, J.L., 1997, On the total geostrophic circulation of the Pacific Ocean. Flow patterns, tracers and transports: Progress in Oceanography, v. 39, p. 263-352.

Reimer, P.J., Baillie, M.G.L., Bard, E., Bayliss, A., Beck, J.W., Bertrand, C.J.H., Blackwell, P.G., Buck, C.E., Burr, G.S., Cutler, K.B., Damon, P.E., Edwards, R.L., Fairbanks, R.G., Friedrich, M., Guilderson, T.P., Hogg, A.G., Hughen, K.A., Kromer, B., McCormac, G., Manning, S., Ramsey, C.B., Reimer, R.W., Remmele, S., Southon, J.R., Stuiver, M., Talamo, S., Taylor, F.W., van der Plicht, J., and Weyhenmeyer, C.E., 2004, IntCal04 terrestrial radiocarbon age calibration, 0-26 cal kyr BP: Radiocarbon, v. 46, p. 1029-1058.

Reimer, P.J., and Reimer, R.W., 2001, A marine reservoir correction database and on-line interface (supplemental material URL:http://www.calib.org): Radiocarbon, v. 43, p. 461-463.

Reyes, A.C., and Lavin, M.F., 1997, Effects of the autumn-winter meteorology upon the surface heat loss in the Northern Gulf of California: Atmosfera, v. 10, p. 101-123.

Richaud, M., Loubere, P., Pichat, S., and Francois, R., 2007, Changes in opal flux and the rain ratio during the last 50,000 years in the equatorial Pacific: Deep-Sea Research Part Ii-Topical Studies in Oceanography, v. 54, p. 762-771.

Ridgwell, A.J., Watson, A.J., and Archer, D.E., 2002, Modeling the response of the oceanic Si inventory to perturbation, and consequences for atmospheric CO2: Global Biogeochemical Cycles, v. 16.

Robinson, R.S., Mix, A., and Martinez, P., 2007, Southern Ocean control on the extent of denitrification in the southeastern Pacific: Quaternary Science Reviews, v. 26, p. 201-212.

Roden, G.I., 1962, Oceanographic aspects of the eastern equatorial Pacific: Geophysica Internacional v. 2, p. 77–92.

Rohling, E.J., and Cooke, S., 1999, Stable oxygen and carbon isotope ratios in foraminiferal carbonate, in Sen Gupta, B.K., ed., Modern Foraminifera: Dordrecht, The Netherlands, Kluwer Academic, p. 239-258.

Romanova, V., Lohmann, G., and Grosfeld, K., 2006, Effect of land albedo, CO2, orography, and oceanic heat transport on extreme climates: Climate of the Past, v. 2, p. 31-42.

Schlitzer, R., 2004, Ocean Data View, http://odv.awi-bremerhaven.de.

Schmitz, W.J., Jr.,, 1996, On the world ocean circulation: Volume I, Some global features / North Atlantic circulation, Woods Hole Océanographie Institution Technical Report WHOI-96-03, 150 p.

Schulte, S., Rostek, F., Bard, E., Rullkötter, J., and Marchal, O., 1999, Variations of oxygen-minimum and primary productivity recorded in sediments of the Arabian Sea: Earth

and Planetary Science Letters, v. 173, p. 205-221.

Schulz, M., and Stattegger, K., 1997, SPECTRUM: Spectral analysis of unevenly spaced paleoclimatic time series: Computers & Geosciences v. 23, p. 929-945.

Sen Gupta, B.K., and Machain-Castillo, M.L., 1993, Benthic foraminifera in oxygen-poor habitats: Marine Micropaleontology, v. 20, p. 3 - 4.

Shackleton, N.J., 1977, 13C in Uvigerina: Tropical rainforest history and the equatorial Pacific carbonate dissolution cycles, *in* Anderson, N., and Malahof, A., eds., Fate of Fossil Fuel CO2 in the Oceans: New York, Plenum, p. 401-427.

Shackleton, N.J., Hall, M.A., Line, J., and Shuxi, C., 1983, Carbon Isotope Data in Core V19-30 Confirm Reduced Carbon-Dioxide Concentration in the Ice-Age Atmosphere: Nature, v. 306, p. 319-322.

Shibahara, A., Ohkushi, K., Kennett, J.P., and Ikehara, K., 2007, Late Quaternary changes in intermediate water oxygenation and oxygen minimum zone, northern Japan: A benthic foraminiferal perspective: Paleoceanography, v. 22, p. DOI: 10.1029/2005PA001234.

Siddall, M., Stocker, T.F., Spahni, R., and Blunier, T., 2006, Using a maximum simplicity paleoclimate model to simulate millenial variability during the last four glacial cycles: Quaternary Science Reviews, v. 25, p. 3185-3197.

Sigman, D.M., and Boyle, E.A., 2000, Glacial/interglacial variations in atmospheric carbon dioxide: Nature, v. 407, p. 859-869.

Sikes, E.L., Guilderson, T.P., Rose, K.A., and Shane, P.A., 2006, Deep Water Ages in the Southwest Pacific and Southern Ocean Since the Last Glacial Maximum, AGU Fall Meeting Abstracts: San Francisco, American Geophysical Union.

Sikes, E.L., Samson, C.R., Guilderson, T.P., and Howard, W.R., 2000, Old radiocarbon ages in the southwest Pacific Ocean during the last glacial period and deglaciation: Nature, v. 405, p. 555-559.

Silva, K.A., Corliss, B.H., Rathburn, A.E., and Thunell, R.C., 1996, Seasonality of living benthic foraminifera from the San Pedro Basin, California borderland: Journal of Foraminiferal Research, v. 26, p. 71-93.

Sloyan, B.M., and Rintoul, S.R., 2001, The Southern Ocean Limb of the Global Deep Overturning Circulation: Journal of Physical Oceanography, v. 31, p. 143-173.

Smith, H.J., Fischer, H., Wahlen, M., Mastroianni, D., and Deck, B., 1999, Dual modes of the carbon cycle since the Last Glacial Maximum: Nature, v. 400, p. 248-250.

Spahni, R., Chappellaz, J., Stocker, T.F., Loulergue, L., Hausammann, G., Kawamura, K., Fluckiger, J., Schwander, J., Raynaud, D., Masson-Delmotte, V., and Jouzel, J., 2005, Atmospheric methane and nitrous oxide of the late Pleistocene from Antarctic ice cores: Science, v. 310, p. 1317-1321.

Spero, H.J., and Lea, D.W., 2002, The cause of carbon isotope minimum events on glacial terminations: Science, v. 296, p. 522-525.

Spero, H.J., Mielke, K.M., Kalve, E.M., Lea, D.W., and Pak, D.K., 2003, Multispecies approach to reconstructing eastern equatorial Pacific thermocline hydrography during the past 360 kyr: Paleoceanography, v. 18, p. DOI: 10.1029/2002PA000814.

Stott, L.D., Neumann, M., and Hammond, D., 2000, Intermediate water ventilation on the

northeasthern Pacific margin during the late Pleistocene inferred from benthic foraminiferal d13C: Paleoceanography, v. 15, p. 161-169.

Stott, L.D., Poulsen, C., Lund, S., and Thunell, R., 2002, Super ENSO and global climate oscillations at millennial time scales: Science, v. 297, p. 222-226.

Stott, L.D., Southon, J., Timmermann, A., and Koutavas, A., 2009, Radiocarbon age anomaly at intermediate water depth in the Pacific Ocean during the last deglaciation: Paleoceanography, v. 24, p. DOI:10.1029/2008PA001690.

Strub, P.T., Mesias, J.M., Montecino, V., Rutlant, J., and Salinas, S., 1998, Coastal ocean circulation off Western South America, *in* Robinson, A.R., and Brink, K.H., eds., The Global Coastal Ocean. The Sea: New York, Wiley, p. 273-314.

Stuiver, M., and Polach, H.A., 1977, Discussion: Reporting of 14C Data: Radiocarbon, v. 19, p. 355-363.

Stuiver, M., and Reimer, P.J., 1993, Extended 14C database and revised CALIB radiocarbon calibration program: Radiocarbon, v. 35, p. 215-230.

Stuiver, M., Reimer, P. J., and Reimer, R. W. , 2005, CALIB 5.0. [WWW program and documentation].

Sverdrup, H.U., Johnson, M.W., and Fleming, R.H., 1946, The Oceans: New York.

Takeda, S., 1998, Influence of iron availability on nutrient consumption ratio of diatoms in oceanic waters: Nature, v. 393, p. 774-777.

Takeda, S., Yoshie, N., Boyd, P.W., and Yamanaka, Y., 2006, Modeling studies investigating the causes of preferential depletion of silicic acid relative to nitrate during SERIES, a mesoscale iron enrichment in the NE subarctic Pacific: Deep Sea Research Part II: Topical Studies in Oceanography, v. 53, p. 2297-2326.

Takesue, R.K., van Geen, A., Carriquiry, J.D., Ortiz, E., Godinez-Orta, L., Granados, I., Saldivar, M., Ortlieb, L., Escribano, R., Guzman, N., Castilla, J.C., Varas, M., Salamanca, M., and Figueroa, C., 2004, Influence of coastal upwelling and El Nino-Southern Oscillation on nearshore water along Baja California and Chile: Shore-based monitoring during 1997-2000: Journal of Geophysical Research-Oceans, v. 109.

Talley, L.D., 1991, An Okhotsk Sea-Water Anomaly - Implications for Ventilation in the North Pacific: Deep-Sea Research Part a-Oceanographic Research Papers, v. 38, p. S171-S190.

—, 1999, Some aspects of ocean heat transport by the shallow, intermediate and deep overturning circulations, *in* Clark, E., Webb, R.S., and Keigwin, L., eds., Mechanisms of Global Climate Change at Millenial Time Scales, Volume 112: Geophys. Mono. Ser., 112, American Geophysical Union, p. 1-22.

Thunell, R.C., and Kepple, A.B., 2004, Glacial-Holocene δ15N record from the Gulf of Tehuantepec, Mexico: Implications for denitrification in the eastern equatorial Pacific and changes in atmospheric N2O: Global Biogeochem. Cycles, v. 18, p. DOI: 10.1029/2002GB002028.

Toggweiler, J.R., and Carson, S., 1995, What are upwelling systems contributing to the ocean's carbon and nutrient budgets?: Upwelling in the Ocean, v. 18, p. 337-360.

Toggweiler, J.R., Russell, J.L., and Carson, S.R., 2006, Midlatitude westerlies, atmospheric CO2, and climate change during the ice ages: Paleoceanography, v. 21, p. DOI:

10.1029/2005PA001154.

Tomczak, M., 2007, Variability of Antarctic intermediateWater properties in the South Pacific Ocean: Ocean Science, v. 3, p. 363-377.

Torrence, C., and Compo, G.P., 1998, A practical guide to wavelet analysis: Bulletin of the American Meteorological Society, v. 79, p. 61-78.

Trasviña, A., and Barton, E.D., 2008, Summer circulation in the Mexican tropical Pacific: Deep Sea Research Part I: Oceanographic Research Papers, v. 55, p. 587-607.

Trasviña, A., Barton, E.D., Brown, J., Velez, H.S., Kosro, P.M., and Smith, R.L., 1995, Offshore Wind Forcing in the Gulf of Tehuantepec, Mexico - the Asymmetric Circulation: Journal of Geophysical Research-Oceans, v. 100, p. 20649-20663.

Tsuchiya, M., and Talley, L.D., 1996, Water-property distributions along an eastern Pacific hydrographic section at 135W: Journal of Marine Research, v. 54, p. 541-564.

—, 1998, A Pacific hydrographic section at 88 degrees W: Water-property distribution: Journal of Geophysical Research-Oceans, v. 103, p. 12899-12918.

Turney, C.S.M., Kershaw A.P., Clemens S.C., Branch N., Moss P. T., Fifield L. K. , 2004, Millennial and orbital variations of El Niño/Southern Oscillation and high-latitude climate in the last glacial period: Nature, v. 428, p. 306 – 310.

van Aken, H.M., 2007, The Oceanic Thermohaline Circulation: An Introduction: New York, Springer, 326 p.

van der Zwaan, G.J., Duijnstee, I.A.P., den Dulk, M., Ernst, S.R., Jannink, N.T., and Kouwenhoven, T.J., 1999, Benthic foraminifers: proxies or problems? A review of paleoecological concepts.: Earth-Science Reviews, v. 46, p. 213 - 236.

van Geen, A., Fairbanks, R.G., Dartnell, P., McGann, M., Gardner, J.V., and Kashgarian, M., 1996, Ventilation changes in the northeast Pacific during the last deglaciation: Paleoceanography, v. 11, p. 519-528.

van Geen, A., Zheng, Y., Bernhard, J.M., Cannariato, K.G., Carriquiry, J., Dean, W.E., Eakins, B.W., Ortiz, J.D., and Pike, J., 2003, On the preservation of laminated sediments along the western margin of North America: Paleoceanography, v. 18, p. DOI: 10.1029/2003PA000911.

van Kreveld, S., Sarnthein, M., Erlenkeuser, H., Grootes, P., Jung, S., Nadeau, M. J., Pflaumann, U., and Voelker, 2000, A. Potential links between surging ice sheets, circulation changes, and the Dansgaard-Oeschger cycles in the Irminger Sea, 60-18 kyr: Paleoceanography, v. 15, p. 425-442.

van Meerbeeck, C.J., Renssen, H., and Roche, D.M., 2009, How did Marine Isotope Stage 3 and Last Glacial Maximum climates differ? - Perspectives from equilibrium simulations: Climate of the Past, v. 5, p. 33-51.

Volk, T., and Hoffert, M.I., 1985, Ocean carbon pumps: analysis of relative strengths and efficiencies in ocean-driven atmospheric CO2 changes, in The Carbon Cycle and Atmospheric CO2, *in* Sundquist, E.T., and Broecker, W.S., eds., Natural Variations Archean to Present: Geophysical Monograph 32: Washington D.C., American Geophysical Union, p. 99-110.

Wang, Y.J., Cheng, H., Edwards, R.L., An, Z.S., Wu, J.Y., Shen, C.C., and Dorale, J.A., 2001, A high-resolution absolute-dated Late Pleistocene monsoon record from Hulu Cave, China: Science, v. 294, p. 2345-2348.

Wijffels, S.E., 1993, Exchanges between hemispheres and gyres: A direct approach to the mean circulation of the Equatorial Pacific: WHOI-93-42, Woods Hole Oceanographic Institution.

Winckler, G., Anderson, R.F., Fleisher, M.Q., McGee, D., and Mahowald, N., 2008, Covariant glacial-interglacial dust fluxes in the equatorial Pacific and Antarctica: Science, v. 320, p. 93-96.

Wolff, E.W., H. Fischer, F. Fundel, U. Ruth, B. Twarloh, G.C. Littot, R. Mulvaney, R. Rothlisberger, M. de Angelis, C.F. Boutron, M. Hansson, U. Jonsell, M.A. Hutterli, F. Lambert, P. Kaufmann, B. Stauffer, T.F. Stocker, J.P. Steffensen, M. Bigler, M.L. Siggaard-Andersen, R. Udisti, S. Becagli, E. Castellano, M. Severi, D. Wagenbach, C. Barbante, P. Gabrielli, and V. Gaspari, 2006, Ocean sea-ice extent, productivity and iron flux over the past eight glacial cycles: Nature, v. 440, p. 491-496.

Wyrtki, K., 1965, The Annual and Semi-annual Variation of Sea Surface Temperature in the North Pacific Ocean: Limnology and Oceanography, v. 10, p. 307-313.

—, 1966, Intermediate Waters of Pacific Ocean: Limnology and Oceanography, v. 11, p. 313-317.

Wyrtki, K., and Kilonsky, B., 1984, Mean water and current structure during the Hawaii-to-Tahiti shuttle experiment: J. Phys. Oceanogr., v. 14, p. 242-254.

Yamane, M., 2003, Late Quaternary variations in water mass in the Shatsky Rise area, northwest Pacific Ocean: Marine Micropaleontology, v. 48, p. 205-223.

You, Y., 2003, The pathway and circulation of North Pacific Intermediate Water: Geoph. Res. Letters, v. 30, p. 2291.

You, Y., Suginohara, N., Fukasawa, M., Yasuda, I., Kaneko, I., Yoritaka, H., and Kawamiya, M., 2000, Roles of the Okhotsk Sea and Gulf of Alaska in forming the North Pacific Intermediate Water: J. Geophys. Res., v. 105, p. 3253–3280.

Zahn, R., Winn, K., and Sarnthein, M., 1986, Benthic foraminiferal 13C and accumulation rates of organic carbon: Uvigerina peregrina group and Cibicidoides wuellerstorfi: Paleoceanography, v. 1, p. 27-42.

List of Figures

Tables

Appendix A

Marine Sediment Cores

This study is focussed on the marine sediment Core MD02-2519 collected off Mazatlan (NW Mexico) with a Calypso Piston Corer on board the R/V Marion Dufresne, during the IMAGES VIII (International Marine Past Global Change Study) MONA Cruise (Marges Ouest Nord Américaines) in June 2002 (Beaufort, 2002). However, other MONA cores were additionally used. Their lithology, structures and drilling information are presented in this section (see *legend* at the end of this section).

Core MD02-2519

(Lat. 22° 30.89' N; Long. 106° 39.00' W; 955 m water depth) (Figure I).

The core comprises ~ 3600 cm (after correction of VOID intervals) of continuous massive, laminated and mildly bioturbated sequences. The dominant sediment mostly consists of terrigenous components, with various amounts of biogenic components: silty clay, foraminifer-nannofossil silty clay, nannofossil silty clay, nannofossil clay, clayey foraminifer-nannofossil ooze, clayey nannofossil ooze, and nannofossil ooze. The colours range from olive grey and dark olive grey to very dark grey and black. From 220 cm to 630 cm, distinct laminations and colour bands alternate with bioturbated intervals. Bioturbation is common in the lower part of the core, from 2000 - 2320 cm, 3130 - 3360 cm, and 3900 cm - to the bottom of the core. Faintly laminated intervals are also present. Minor lithologies include tephra layers at 2160 cm, 2440 cm and 2855 cm.

Core MD02-2518

(Lat. 22° 40.39' N; Long. 106° 29.19' W; 450 m water depth) (Figure II).

This core comprises ~ 4000 cm of silty clay sediments, with minor amounts of diatoms and/or nannofossils. The colours range from olive grey and dark olive grey to very dark grey. Massive intervals, sometimes bioturbated alternate with laminated intervals throughout the core. Minor lithologies include foraminifer clayey silt, olive grey; grey layers of clayey silt (0.5 cm to 1 cm thick); and tephra layers olive brown and white at 1220 cm, 2780 cm and 3340 cm. A few shell fragments, fish scales, wood fragments, and a large angular cobble of limestone occurs at 3580 cm are locally present.

Core MD02-2520

(Lat. 15° 40.14' N; Long. 95° 18.00' W; 712 m water depth) (Figure III).

The core comprises 3676 cm (after correction of VOID intervals) of dominantly silty clay sediment. The colours vary from olive grey and olive green to dark olive grey in the upper part of the core, but grades to very dark grey and black from 1200 cm to 3000 cm, and to dark olive and dark olive grey in the lower part of the core. The sediment is mostly laminated throughout the core. Laminations are very fine, and sometimes a thicker banding is superposed. Rare slightly bioturbated intervals are present. Minor lithologies include a few fine light sandy layers present from 300 cm to 1200 cm; and grey to brown coarse tephra layers throughout the core.

Core MD02-2524

(Lat. 12° 00.55' N; Long. 87° 54.83' W; 863 m water depth) (Figure IV).

This core dominantly consists of 3026 cm of silty clay sediments olive and olive grey to dark olive grey and very dark grey in colour. The upper part of the core, down to 600 cm is mostly bioturbated. The sediments show oblique stratification and sandy layers with graded bedding in the interval between 320 – 645 cm core depth, possibly caused by a slump. Thus a depth correction of 325 cm was applied to this interval. From 600 cm to 1750 cm the sediment is mostly laminated, interrupted by few bioturbated intervals. Sandy layers with graded bedding also occur. The lower part of the core below 1750 cm is mostly massive, with some faintly laminated intervals and minor bioturbation. Minor lithology includes layers and lenses of volcanic ash, grey to black, throughout the core.

Core: MD02-2519
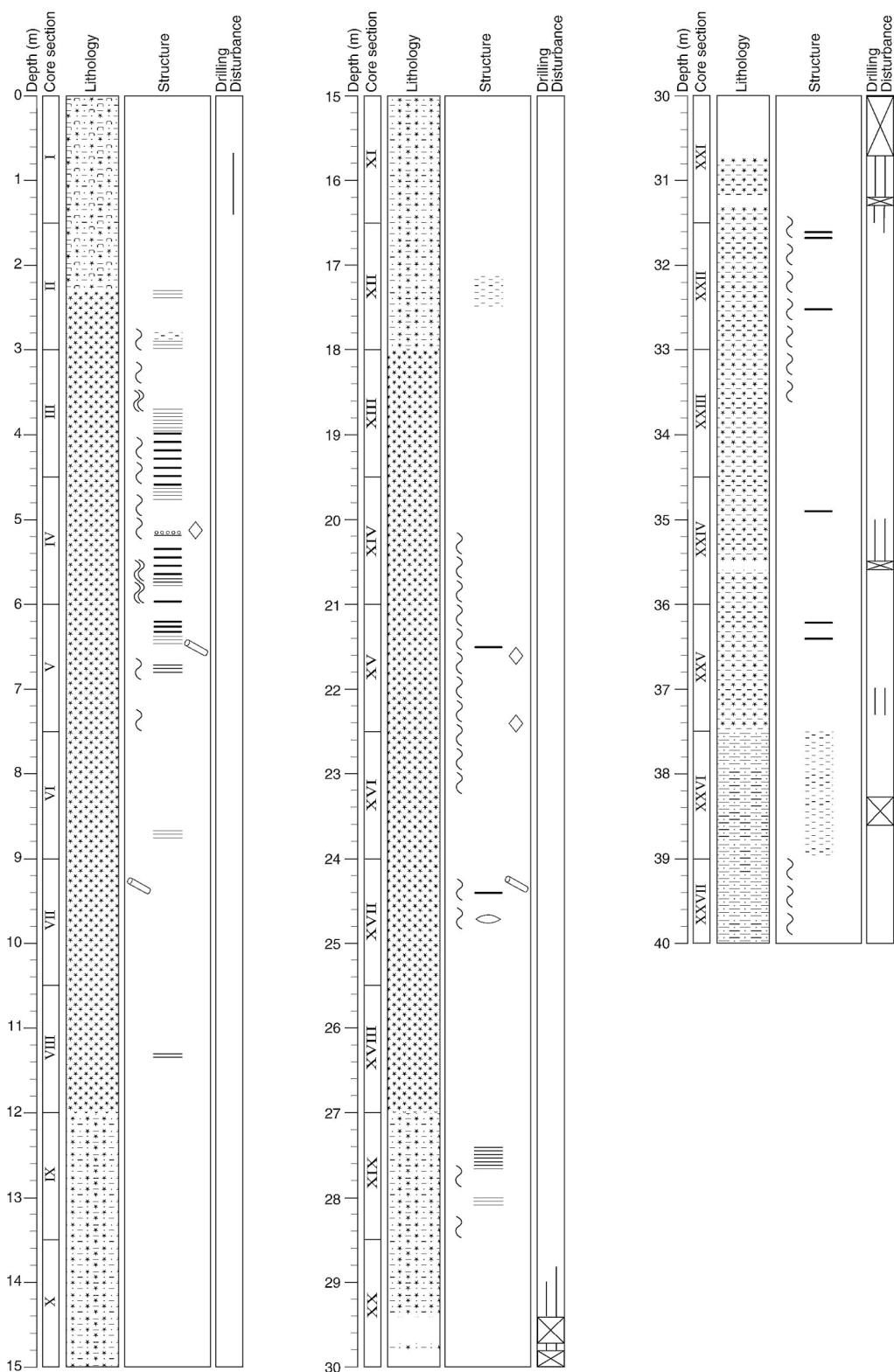
Figure I. Lithology, sediment structures and drilling information of Core MD02-2519.

Core: MD02-2518

Figure II. Lithology, sediment structures and drilling information of Core MD02-2518.

Core: MD02-2520
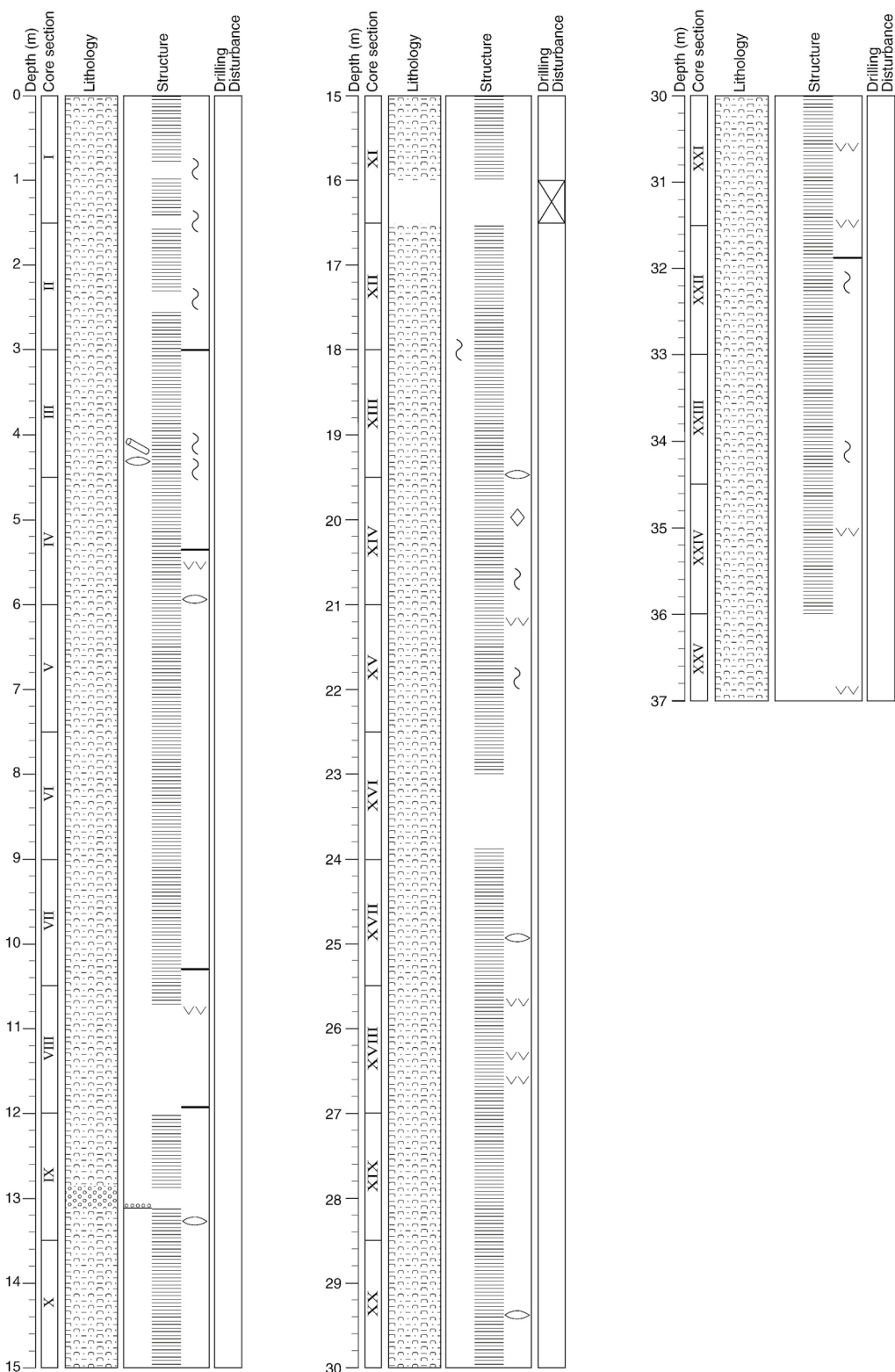
Figure III. Lithology, sediment structures and drilling information of Core MD02-2520.

Core: MD02-2524
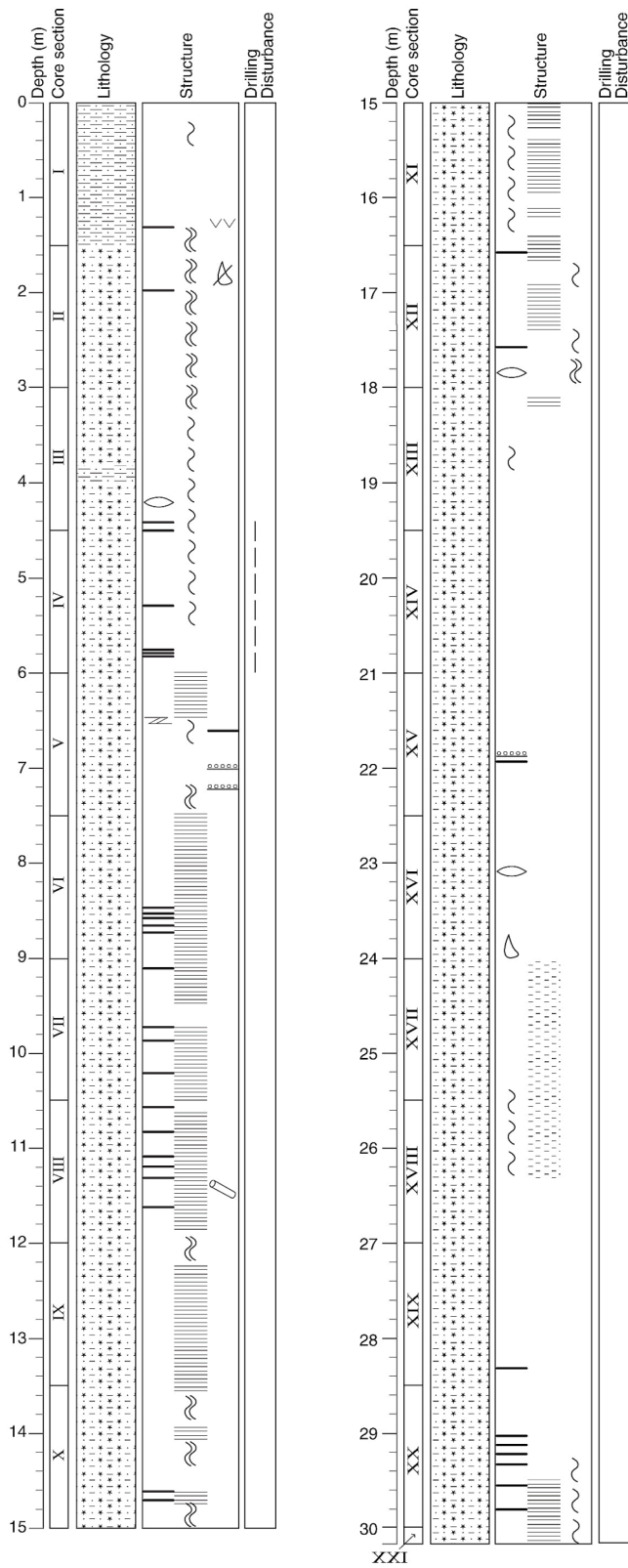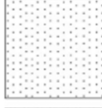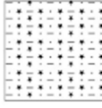
Figure IV. Lithology, sediment structures and drilling information of Core MD02-2524.

Legend for Core Description

Lithology

Silty clay

Silt

Sand

Nannofossil ooze

Nannofossil clay

Nannofossil silty clay

Diatom-nannofossil silty clay

Diatom silty clay

Structure and Drilling Disturbance

Slight bioturbation

Heavy bioturbation

Fish debris

Shell

Shell fragment

Wood fragment

Ash layer

Black oxide/sulphide layer

Isolated pebble/granule

Sand lens or pocket

Normal graded bedding

Isolated layer

Lamination or thin layer

Oblique stratification

Slightly disturbed

Heavily disturbed

Void

Appendix B

Data from Core MD02-2519

Carbon and Nitrogen Isotopes

Biogenic Silica (Opal)

Stable Carbon and Oxygen Isotopes

Note: Physical Parameters and Diffuse Spectral Reflectivity data have been already published by Beaufort (2002) @ http://www.pangaea.de/

CARBON AND NITROGEN ISOTOPES

Core MD02-2519 Depth cm	Age cal years BP	Elemental % Comp (C)	Isotopic delta (C13)	Elemental % Comp (N)	Isotopic delta (N15)	% C/N	molar atomic C/N	OC MAR mg/cm2/kyr
0	2365	7.987	-21.226	0.870	8.185	9.180	10.711	589.22
2	2385	7.721	-20.968	0.832	8.222	9.280	10.827	569.59
4	2424	8.382	-20.796	0.924	8.265	9.071	10.583	618.36
6	2463	8.525	-20.869	0.940	8.298	9.069	10.581	628.91
8	2503	8.83	-20.795	0.977	8.234	9.038	10.544	630.85
10	2542	8.997	-20.828	0.978	8.216	9.199	10.733	646.31
12	2582	7.377	-20.987	0.783	8.151	9.421	10.992	523.97
14	2621	8.582	-20.776	0.946	8.257	9.072	10.584	614.68
16	2660	8.726	-20.697	0.966	8.321	9.033	10.539	634.04
18	2700	8.476	-20.784	0.930	8.382	9.114	10.633	624.25
20	2739	8.81	-20.909	0.973	8.282	9.054	10.564	660.00
22	2778	8.752	-20.826	0.956	8.378	9.155	10.681	635.36
24	2818	8.848	-20.83	0.987	8.144	8.965	10.459	634.52
26	2857	8.367	-20.982	0.876	8.309	9.551	11.143	611.17
28	2896	8.931	-20.726	0.978	8.168	9.132	10.654	632.31
30	2936	8.668	-20.786	0.959	8.344	9.039	10.545	626.78
32	2975	8.49	-20.72	0.930	8.308	9.129	10.651	595.68
34	3015	7.677	-20.433	0.828	8.239	9.272	10.817	544.65
36	3054	8.322	-20.722	0.915	8.168	9.095	10.611	595.37
38	3093	8.832	-20.746	0.982	8.269	8.994	10.493	632.58
40	3133	8.797	-20.642	0.975	8.189	9.023	10.526	617.36
42	3172	8.455	-20.724	0.907	8.326	9.322	10.876	588.73
44	3211	9.163	-20.755	1.014	8.477	9.036	10.543	644.24
46	3251	9.379	-20.784	1.032	8.223	9.088	10.603	651.62
48	3290	9.431	-20.79	1.028	8.179	9.174	10.703	661.31
50	3330	9.544	-20.9	0.986	8.397	9.680	11.293	675.86
52	3369	9.454	-20.762	1.046	8.448	9.038	10.545	667.64
54	3408	9.169	-20.804	0.990	8.415	9.262	10.805	643.99
56	3448	9.464	-20.733	1.026	8.408	9.224	10.762	672.83
58	3487	9.523	-20.787	1.023	8.44	9.309	10.860	682.54
60	3526	9.347	-20.789	1.017	8.459	9.191	10.723	664.28
62	3566	6.888	-21.088	0.727	8.338	9.475	11.054	484.18
64	3605	8.321	-20.88	0.895	8.397	9.297	10.847	578.52
66	3645	9.068	-20.967	0.994	8.476	9.123	10.643	640.08
68	3684	9.811	-20.888	1.042	8.503	9.416	10.985	685.56
70	3723	9.822	-20.802	1.064	8.561	9.231	10.770	683.44
72	3763	9.475	-20.786	1.019	8.519	9.298	10.848	661.61
74	3802	9.711	-20.904	1.018	8.456	9.539	11.129	686.90
76	3877	9.51	-20.744	1.018	8.349	9.342	10.899	674.15
78	3951	8.973	-20.847	0.941	8.24	9.536	11.125	625.46
80	4026	10.116	-20.856	1.100	8.516	9.196	10.729	699.43
82	4101	9.624	-20.79	1.045	8.45	9.210	10.744	662.35
84	4175	8.832	-20.686	0.946	8.253	9.336	10.892	600.48
86	4250	10.118	-20.817	1.102	8.435	9.181	10.712	693.46
88	4325	10.582	-20.641	1.153	8.442	9.178	10.707	736.06
90	4399	9.684	-20.657	1.048	8.397	9.240	10.781	680.40
92	4474	9.647	-20.789	1.044	8.332	9.240	10.780	659.36
94	4549	9.869	-20.79	1.076	8.398	9.172	10.701	667.85
96	4623	9.671	-20.806	1.054	8.26	9.176	10.705	647.73
98	4698	9.721	-20.523	1.057	8.338	9.197	10.730	666.96
100	4773	9.345	-20.838	0.961	8.358	9.724	11.345	655.44
102	4847	9.519	-20.614	1.031	8.254	9.233	10.772	665.23
104	4922	9.379	-20.584	1.024	8.306	9.159	10.686	642.50
106	4997	9.409	-20.672	1.035	8.377	9.091	10.606	664.38
108	5071	9.203	-20.557	0.984	8.342	9.353	10.911	653.29
110	5146	9.426	-20.754	1.023	8.452	9.214	10.750	675.36
112	5221	9.115	-20.666	0.976	8.323	9.339	10.896	669.90
114	5295	8.447	-20.773	0.895	8.344	9.438	11.011	617.43
116	5370	9.523	-20.809	0.990	8.425	9.619	11.222	686.27
118	5445	9.49	-20.901	0.969	8.385	9.794	11.426	688.55
120	5519	9.415	-20.758	0.981	8.564	9.597	11.197	679.72
122	5594	8.936	-20.702	0.926	8.365	9.650	11.258	626.53
124	5669	7.91	-20.628	0.799	8.376	9.900	11.550	543.16
126	5743	9.162	-20.876	0.947	8.614	9.675	11.287	652.78
128	5818	9.451	-20.787	0.964	8.51	9.804	11.438	682.55
130	5893	9.49	-20.77	0.976	8.684	9.723	11.344	666.38
132	5967	9.442	-20.837	0.984	8.533	9.596	11.195	667.64
134	6042	9.09	-20.886	0.950	8.535	9.568	11.163	625.08
136	6117	9.287	-20.771	0.973	8.537	9.545	11.135	654.33
138	6191	9.555	-20.955	0.983	8.522	9.720	11.340	654.56
140	6266	9.149	-20.735	0.925	7.916	9.891	11.539	638.63
142	6371	9.529	-20.805	0.983	8.607	9.694	11.309	693.40
144	6477	9.269	-20.92	0.957	8.431	9.685	11.300	671.53
146	6582	8.954	-20.923	0.923	8.428	9.701	11.318	647.76
	6688							
150	6793	9.705	-20.867	1.006	8.481	9.647	11.255	687.74
152	6899	9.483	-20.861	0.971	8.571	9.766	11.394	652.80

154	7004	9.401	-20.812	0.964	8.5	9.752	11.377	676.41
156	7110	9.653	-20.812	0.991	8.713	9.741	11.364	705.10
158	7215	9.609	-20.9	0.975	8.892	9.855	11.498	714.21
160	7321	9.721	-20.775	0.984	8.9	9.879	11.526	705.15
162	7426	9.786	-20.653	0.999	8.702	9.796	11.428	707.55
164	7532	9.806	-20.778	0.983	8.656	9.976	11.638	722.13
166	7637	9.648	-20.629	1.009	8.75	9.562	11.156	710.88
168	7743	9.612	-20.726	0.973	8.773	9.879	11.525	692.37
170	7848	9.712	-21.02	0.979	8.892	9.920	11.574	698.15
172	7954	10.003	-21.068	1.011	8.964	9.894	11.543	724.38
174	8059	9.802	-21.185	0.975	9.055	10.053	11.729	715.51
176	8165	9.542	-21.164	0.950	8.892	10.044	11.718	690.06
178	8270	9.9	-21.122	0.980	9.111	10.102	11.786	714.82
180	8376	8.564	-21.025	0.848	8.568	10.099	11.782	619.26
182	8481	8.738	-21.011	0.866	8.481	10.090	11.772	634.63
184	8587	8.466	-20.898	0.856	8.682	9.890	11.539	612.38
186	8692	8.359	-20.853	0.833	8.677	10.035	11.707	620.21
188	8798	7.733	-20.939	0.766	8.61	10.095	11.778	571.99
190	8903	7.714	-20.903	0.767	8.616	10.057	11.734	563.66
192	9009	7.686	-20.919	0.779	8.585	9.866	11.511	566.38
194	9114	7.677	-20.711	0.757	8.441	10.141	11.832	557.57
196	9213	7.946	-20.769	0.787	8.393	10.097	11.779	573.08
198	9311	7.936	-20.783	0.785	8.417	10.110	11.794	578.78
200	9410	7.912	-20.672	0.783	8.344	10.105	11.789	578.38
202	9508	7.874	-20.873	0.784	8.405	10.043	11.717	586.09
204	9607	7.711	-20.783	0.779	8.538	9.899	11.548	563.12
206	9705	7.774	-20.94	0.787	8.659	9.878	11.524	569.50
208	9804	6.979	-20.851	0.682	8.448	10.233	11.939	517.99
210	9902	7.368	-20.786	0.728	8.508	10.121	11.808	541.69
212	10001	6.959	-21.121	0.685	8.838	10.159	11.852	513.09
214	10099	6.734	-21.484	0.621	8.712	10.844	12.651	498.59
216	10198	6.492	-21.493	0.629	9.061	10.321	12.041	484.49
218	10324	5.513	-21.646	0.520	8.77	10.602	12.369	402.65
220	10451	7.033	-21.726	0.688	8.976	10.222	11.926	517.52
222	10577	6.796	-21.771	0.652	8.769	10.423	12.161	498.63
224	10703	7.501	-21.792	0.729	8.868	10.289	12.004	546.38
226	10829	5.891	-21.508	0.562	8.313	10.482	12.229	434.01
228	10956	6.411	-21.563	0.615	8.664	10.424	12.162	467.66
230	11082	6.751	-21.78	0.649	8.986	10.402	12.136	497.92
232	11187	5.909	-21.52	0.558	8.558	10.590	12.355	438.77
234	11292	6.169	-21.227	0.584	7.924	10.563	12.324	444.17
236	11396	4.617	-21.173	0.432	8.296	10.688	12.469	325.48
238	11501	4.484	-21.21	0.418	8.161	10.727	12.515	323.69
240	11606	4.424	-21.228	0.417	8.146	10.609	12.377	322.86
242	11711	4.103	-21.332	0.378	8.219	10.854	12.664	299.80
244	11815	4.158	-21.195	0.383	7.991	10.856	12.666	306.54
246	11920	4.001	-20.856	0.371	7.866	10.784	12.582	297.32
248	12025	3.716	-21.09	0.355	7.746	10.468	12.212	273.56
250	12130	4.198	-21.098	0.390	8.364	10.764	12.558	307.67
252	12235	3.005	-21.323	0.267	8.221	11.255	13.130	220.75
254	12339	4.069	-21.099	0.391	8.27	10.407	12.141	300.41
256	12444	4.289	-21.171	0.419	8.478	10.236	11.942	321.98
258	12549	4.237	-20.988	0.399	8.428	10.619	12.389	312.99
260	12654	4.285	-21.217	0.406	8.547	10.554	12.313	316.57
262	12758	4.148	-21.233	0.395	8.624	10.501	12.251	313.87
264	12863	4.173	-21.213	0.390	8.536	10.700	12.483	308.33
266	12968	4.055	-21.392	0.383	8.401	10.587	12.352	296.43
268	13073	4.219	-21.072	0.408	8.798	10.341	12.064	306.59
270	13178	4.507	-20.711	0.440	9.046	10.243	11.950	333.01
272	13282	4.484	-21.235	0.428	9.071	10.477	12.223	333.32
274	13387	4.498	-21.116	0.430	8.885	10.460	12.204	333.81
276	13492	4.665	-21.338	0.463	9.442	10.076	11.755	339.76
278	13597	4.529	-21.161	0.435	9.478	10.411	12.147	342.66
280	13701	5.411	-21.693	0.534	9.976	10.133	11.822	399.40
282	13806	5.325	-21.708	0.518	9.915	10.280	11.993	387.14
284	13911	5.265	-21.63	0.515	10.012	10.223	11.927	392.11
286	13969	5.339	-21.907	0.510	9.878	10.469	12.213	400.58
288	14026	4.622	-21.745	0.427	9.308	10.824	12.628	340.33
290	14084	4.699	-21.847	0.442	9.412	10.631	12.403	338.21
292	14182	4.414		0.420	9.304	10.510	12.261	319.32
294	14280	4.609	-21.681	0.453	9.247	10.174	11.870	331.32
296	14378	3.651	-21.178	0.351	7.771	10.402	12.135	269.34
298	14475	3.197	-21.387	0.300	7.883	10.657	12.433	235.93
300	14573	3.482	-21.275	0.326	7.72	10.681	12.461	257.39
302	14671	3.573	-21.073	0.328	7.638	10.893	12.709	260.49
304	14769	3.499	-21.18	0.326	7.636	10.733	12.522	259.10
306	14867	3.167	-20.933	0.301	7.377	10.522	12.275	236.07
308	14965	2.989	-20.908	0.273	7.088	10.949	12.774	221.75
310	15063	3.065	-21.095	0.270	6.808	11.352	13.244	224.88
312	15160	3.326	-20.925	0.292	6.709	11.390	13.289	244.55
314	15258	3.454	-21.054	0.307	7.108	11.251	13.126	258.25
316	15356	3.071	-20.853	0.266	6.685	11.545	13.469	229.79

318	15454	2.753	-21.118	0.233	7.067	11.815	13.785	205.99
320	15552	3.21	-20.909	0.291	6.097	11.031	12.869	239.56
322	15650	2.806	-20.907	0.252	6.601	11.135	12.991	210.37
324	15748	3.38	-21.11	0.297	6.963	11.380	13.277	250.43
326	15845	2.715	-20.937	0.239	6.822	11.360	13.253	199.51
328	15943	3.44	-21.124	0.310	7.18	11.097	12.946	253.35
330	16041	3.205	-21.072	0.287	6.817	11.167	13.028	237.46
332	16139	2.737	-20.857	0.239	6.231	11.452	13.361	204.82
334	16262	3.173	-20.664	0.283	7.004	11.212	13.081	237.63
336	16385	2.95	-20.694	0.247	7.275	11.943	13.934	222.01
338	16508	2.698	-20.628	0.238	6.739	11.336	13.225	204.66
340	16631	3.291	-20.719	0.301	6.938	10.934	12.756	245.23
342	16754	3.405	-20.53	0.310	6.599	10.984	12.815	249.83
344	16877	3.339	-20.559	0.304	6.889	10.984	12.814	248.67
346	17000	2.71	-20.41	0.232	6.389	11.681	13.628	202.05
348	17123	2.834	-20.404	0.250	6.556	11.336	13.225	210.25
350	17246	3.473	-20.366	0.306	6.492	11.350	13.241	252.61
352	17368	2.922	-20.172	0.258	6.853	11.326	13.213	217.42
354	17491	3.493	-20.393	0.306	6.264	11.415	13.318	249.10
356	17614	2.821	-20.227	0.242	6.166	11.657	13.600	204.49
358	17737	3.66	-20.406	0.329	6.766	11.125	12.979	269.14
360	17860	3.585	-20.165	0.322	6.217	11.134	12.989	260.37
362	17983	3.815	-20.672	0.340	6.761	11.221	13.091	276.39
364	18106	3.269	-20.54	0.290	6.756	11.272	13.151	242.33
366	18229	3.709	-20.41	0.320	6.6	11.591	13.522	271.65
368	18352	3.292	-20.614	0.280	6.413	11.757	13.717	236.43
370	18475	3.911	-20.654	0.350	7.178	11.174	13.037	282.90
372	18584	4.65	-20.408	0.436	7.516	10.665	12.443	335.56
374	18693	4.035	-20.725	0.361	7.246	11.177	13.040	292.53
376	18802	4.047	-20.7	0.359	7.028	11.273	13.152	291.18
378	18911	3.988	-20.461	0.358	7.447	11.140	12.996	289.90
380	19020	4.26	-20.661	0.380	7.438	11.211	13.079	316.01
382	19129	4.28	-20.221	0.397	7.045	10.781	12.578	311.48
384	19238	4.128	-20.496	0.379	7.56	10.892	12.707	303.79
386	19347	4.642	-20.513	0.423	6.927	10.974	12.803	340.67
388	19456	4.012	-20.372	0.445	5.93	9.016	10.518	293.94
390	19565	4.57	-20.446	0.429	6.769	10.653	12.428	337.66
392	19674	4.296	-20.494	0.373	6.411	11.517	13.437	315.80
394	19783	4.456	-20.514	0.403	6.667	11.057	12.900	326.47
396	19892	4.123	-20.441	0.378	6.891	10.907	12.725	295.64
398	20000	4.429	-20.572	0.421	6.99	10.520	12.274	319.72
400	20109	4.649	-20.511	0.416	6.728	11.175	13.038	334.73
402	20218	4.435	-20.321	0.397	6.46	11.171	13.033	321.13
404	20327	4.939	-20.23	0.461	6.754	10.714	12.499	350.20
406	20436	4.588	-20.624	0.423	6.718	10.846	12.654	328.01
408	20545	4.909	-20.285	0.452	6.877	10.861	12.671	353.05
410	20654	3.219	-20.583	0.281	6.683	11.456	13.365	232.06
412	20763	4.846	-20.34	0.430	6.844	11.270	13.148	349.50
414	20872	4.115	-20.473	0.383	6.768	10.744	12.535	300.01
416	20981	4.037	-20.604	0.389	6.825	10.378	12.108	294.78
418	21090	4.746	-20.523	0.435	6.706	10.910	12.729	345.12
420	21199	4.07	-20.343	0.362	6.648	11.243	13.117	295.90
422	21308	4.459	-20.047	0.397	6.778	11.232	13.104	324.83
424	21417	4.227	-20.344	0.379	6.821	11.153	13.012	306.17
426	21501	4.344	-20.462	0.400	6.536	10.860	12.670	310.57
428	21586	4.234	-19.916	0.382	6.388	11.084	12.931	303.22
430	21670	4.33	-19.947	0.385	6.41	11.247	13.121	321.24
432	21755	4.255	-19.949	0.396	6.318	10.745	12.536	318.17
434	21839	4.582	-19.885	0.412	6.148	11.121	12.975	331.77
436	21924	3.776	-20.403	0.337	6.008	11.205	13.072	273.97
438	22008	4.185	-20.071	0.376	5.961	11.130	12.985	305.59
440	22093	3.644	-20.391	0.328	5.938	11.110	12.961	264.72
442	22177	4.038	-20.132	0.373	6.354	10.826	12.630	298.32
444	22262	4.148	-20.281	0.373	6.118	11.121	12.974	299.74
446	22346	3.545	-20.12	0.317	6.446	11.183	13.047	256.57
448	22431	3.927	-20.268	0.349	6.57	11.252	13.128	288.39
450	22515	4.562	-20.169	0.428	6.581	10.659	12.435	339.57
452	22600	4.409	-20.056	0.407	6.698	10.833	12.638	318.38
454	22684	4.149	-20.618	0.388	6.875	10.693	12.476	297.88
456	22769	3.578	-20.359	0.332	6.986	10.777	12.573	263.93
458	22853	3.717	-20.192	0.333	6.689	11.162	13.023	272.27
460	22938	4.292	-20.612	0.412	6.741	10.417	12.154	308.99
462	23022	3.2	-20.511	0.281	7.06	11.388	13.286	224.88
464	23107	4.669	-20.507	0.444	7.356	10.516	12.268	332.73
466	23191	3.808	-20.771	0.354	7.468	10.757	12.550	267.99
468	23339	4.15	-20.484	0.421	6.75	9.857	11.500	295.34
470	23488	4.3	-20.681	0.441	6.872	9.751	11.376	302.43
472	23636	4.394	-20.283	0.394	7.252	11.152	13.011	308.94
474	23784	4.297	-20.405	0.412	6.73	10.430	12.168	308.89
476	23933	3.629	-20.378	0.343	6.768	10.580	12.344	261.32
478	24081	3.59	-20.447	0.329	6.338	10.912	12.730	259.56
480	24229	3.757	-20.406	0.356	6.472	10.553	12.312	270.35

482	24378	3.603	-20.423	0.333	6.41	10.820	12.623	265.51
484	24526	3.585	-20.554	0.331	6.272	10.831	12.636	265.73
486	24675	3.432	-20.259	0.304	6.278	11.289	13.171	253.04
488	24823	3.557	-20.227	0.323	6.153	11.012	12.848	260.43
490	24971	3.534	-20.557	0.316	6.449	11.184	13.047	257.30
492	25120	3.556	-20.439	0.398	5.931	8.935	10.424	258.88
494	25268	3.735	-20.335	0.339	6.595	11.018	12.854	269.71
496	25416	3.978	-20.14	0.359	6.662	11.081	12.928	292.65
498	25565	3.78	-20.221	0.352	6.645	10.739	12.528	280.15
500	25713	4.073	-20.43	0.384	6.744	10.607	12.375	296.02
502	25800	4.028	-20.364	0.390	6.479	10.328	12.050	291.03
504	25886	4.125	-19.95	0.400	6.494	10.313	12.031	301.18
506	25973	3.433	-20.617	0.315	6.014	10.898	12.715	249.87
508	26060	3.568	-20.434	0.330	6.355	10.812	12.614	254.80
510	26146	3.746	-19.919	0.327	5.876	11.456	13.365	268.15
512	26233	3.739	-20.191	0.332	5.846	11.262	13.139	263.25
514	26320	3.816	-20.062	0.354	6.148	10.780	12.576	269.89
516	26406	3.813	-20.134	0.382	5.675	9.982	11.645	266.75
518	26493	2.961	-20.236	0.269	5.757	11.007	12.842	208.67
520	26579	4.08	-20.228	0.398	6.275	10.251	11.960	289.03
522	26666	2.89	-20.187	0.259	5.945	11.158	13.018	203.45
524	26753	4.393	-20.019	0.407	6.047	10.794	12.593	307.79
526	26839	2.873	-20.112	0.247	5.964	11.632	13.570	202.65
528	26926	4.388	-20.047	0.407	6.523	10.781	12.578	310.27
530	27013	4.344	-19.805	0.421	6.769	10.318	12.038	298.58
532	27099	4.31	-19.824	0.408	6.684	10.564	12.324	302.86
534	27186	4.401	-19.987	0.417	6.735	10.554	12.313	313.02
536	27273	4.413	-19.952	0.417	6.798	10.583	12.347	308.69
538	27359	4.607	-20.175	0.427	6.866	10.789	12.587	323.99
540	27446	4.613	-20.153	0.436	7.043	10.580	12.344	320.34
542	27533	5.005	-20.364	0.469	7.242	10.672	12.450	347.81
544	27619	4.26	-20.426	0.388	7.618	10.979	12.809	297.60
546	27706	5.094	-20.411	0.485	8.016	10.503	12.254	351.58
548	27792	5.237	-20.457	0.480	7.689	10.910	12.729	365.30
550	27879	4.279	-20.706	0.398	7.828	10.751	12.543	301.38
552	27966	5.728	-20.666	0.586	8.284	9.775	11.404	395.53
554	28052	4.744	-20.778	0.480	8.911	9.883	11.531	338.47
556	28139	5.03	-20.784	0.530	8.407	9.491	11.072	349.38
558	28226	5.014	-20.69	0.537	9.114	9.337	10.893	348.11
560	28293	4.184	-20.746	0.506	8.581	8.269	9.647	288.13
562	28360	4.866	-20.829	0.614	7.799	7.925	9.246	344.15
564	28427	4.681	-20.815	0.604	7.832	7.750	9.042	328.39
566	28495	4.798	-20.837	0.606	7.157	7.917	9.237	342.28
568	28562	5.084	-20.777	0.637	7.512	7.981	9.311	365.76
570	28629	4.396	-20.542	0.572	7.388	7.685	8.966	315.47
572	28696	5.883	-20.351	0.679	7.925	8.664	10.108	426.65
574	28763	5.406	-20.535	0.627	8.345	8.622	10.059	385.12
576	28831	5.673	-20.563	0.619	8.291	9.165	10.692	401.97
578	28945	5.386	-20.421	0.601	7.516	8.962	10.455	388.01
580	29060	4.409	-20.334	0.493	7.818	8.943	10.434	318.20
582	29174	4.545	-20.268	0.514	7.185	8.842	10.316	331.51
584	29289	4.465	-20.236	0.503	6.984	8.877	10.356	315.46
586	29403	4.491	-20.287	0.550	7.031	8.165	9.526	318.77
588	29518	4.262	-20.277	0.530	6.774	8.042	9.382	298.20
590	29632	3.995	-20.232	0.508	6.85	7.864	9.175	279.32
592	29747	4.076	-20.157	0.520	6.812	7.838	9.145	290.04
594	29861	4.007	-20.308	0.503	6.914	7.966	9.294	292.63
596	29975	4.372	-20.294	0.493	6.986	8.868	10.346	325.28
598	30090	4.626	-20.374	0.485	7.256	9.538	11.128	339.19
600	30204	4.397	-20.356	0.477	7.495	9.218	10.754	321.65
602	30319	5.443	-20.367	0.601	8.074	9.057	10.566	403.36
604	30433	5.075	-20.426	0.543	7.938	9.346	10.904	376.88
606	30548	6.051	-20.188	0.629	8.454	9.620	11.223	426.43
608	30676	5.774	-20.185	0.567	7.803	10.183	11.881	407.00
610	30804	4.738	-20.188	0.486	7.498	9.749	11.374	350.54
612	30933	5.836	-20.185	0.556	7.626	10.496	12.246	421.33
614	31061	4.934	-20.063	0.501	7.563	9.848	11.490	357.91
616	31189	6.962	-19.903	0.683	7.983	10.193	11.892	496.26
618	31317	6.232	-19.954	0.602	7.962	10.352	12.078	436.49
620	31446	4.579	-19.982	0.458	7.736	9.998	11.664	332.79
622	31574	5.532	-19.969	0.607	8.136	9.114	10.633	399.30
624	31702	4.573	-19.994	0.519	7.812	8.811	10.280	325.11
626	31830	4.245	-20.499	0.412	6.94	10.303	12.021	302.69
628	31958	5.064	-20.069	0.495	7.68	10.230	11.935	367.29
630	32087	4.909	-20.268	0.587	7.925	8.363	9.757	349.20
632	32215	6.484	-20.384	0.682	9.361	9.507	11.092	473.57
634	32343	5.24	-20.438	0.551	9.58	9.510	11.095	374.92
636	32471	7.316	-20.389	0.709	9.466	10.319	12.039	518.09
638	32573	5.86	-20.461	0.634	8.462	9.243	10.783	416.51
640	32675	5.939	-20.274	0.618	8.368	9.610	11.212	420.62
642	32777	6.156	-20.424	0.616	8.376	9.994	11.659	433.53
644	32878	5.866	-20.279	0.593	8.506	9.892	11.541	419.67

646	32980	5.794	-20.315	0.591	8.465	9.804	11.438	414.75
648	33082	5.839	-20.254	0.598	8.513	9.764	11.392	423.93
650	33184	5.988	-20.266	0.621	8.666	9.643	11.250	435.24
652	33285	6.463	-20.295	0.653	9.122	9.897	11.547	466.49
654	33387	5.973	-20.189	0.606	8.706	9.856	11.499	426.25
656	33489	5.725	-20.186	0.639	8.344	8.959	10.453	408.69
658	33591	5.61	-20.321	0.605	8.178	9.273	10.818	398.33
660	33693	5.4	-20.125	0.594	7.947	9.091	10.606	381.74
662	33794	5.46	-20.113	0.605	7.5	9.025	10.529	386.43
664	33896	5.434	-20.128	0.603	7.171	9.012	10.514	382.55
666	33998	5.559	-20.173	0.553	7.945	10.052	11.728	390.71
668	34100	5.542	-20.232	0.604	8.068	9.175	10.705	382.91
670	34201	5.84	-20.061	0.567	8.17	10.300	12.016	418.52
672	34303	6.174	-20.076	0.627	8.543	9.847	11.488	439.43
674	34405	6.2	-20.162	0.649	8.808	9.553	11.145	442.40
676	34507	5.647	-20.237	0.563	9.36	10.030	11.702	397.04
678	34629	5.854	-20.24	0.601	8.942	9.740	11.364	415.61
680	34751	4.51	-20.387	0.486	8.39	9.280	10.826	319.93
682	34874	5.058	-20.402	0.559	8.278	9.048	10.556	350.34
684	34996	5.104	-20.344	0.573	8.037	8.908	10.392	356.77
686	35118	4.803	-20.526	0.551	7.86	8.717	10.170	341.58
688	35241	4.966	-20.325	0.553	8.088	8.980	10.477	361.32
690	35363	4.825	-20.507	0.538	7.943	8.968	10.463	343.02
692	35485	4.489	-20.31	0.498	7.876	9.014	10.516	321.41
694	35608	4.544	-20.32	0.512	7.873	8.875	10.354	323.01
696	35730	4.622	-20.443	0.507	7.841	9.116	10.636	329.42
698	35852	5.99	-20.14	0.587	7.662	10.204	11.905	430.98
700	35975	4.712	-20.31	0.467	7.877	10.090	11.772	337.42
702	36097	4.654	-20.322	0.459	8.636	10.139	11.829	333.38
704	36219	4.903	-20.187	0.466	8.653	10.521	12.275	355.26
706	36342	4.924	-20.418	0.467	8.566	10.544	12.301	349.62
708	36464	4.963	-20.295	0.478	8.474	10.383	12.113	356.04
710	36586	5.117	-20.369	0.495	8.881	10.337	12.060	362.91
712	36708	5.33	-20.447	0.519	9.172	10.270	11.981	377.79
714	36831	5.101	-20.508	0.497	9.242	10.264	11.974	370.31
716	36953	5.261	-20.498	0.503	9.3	10.459	12.202	376.13
718	37075	5.341	-20.457	0.518	9.371	10.311	12.029	378.31
720	37198	5.169	-20.463	0.508	9.355	10.175	11.871	374.91
722	37320	5.35	-20.575	0.521	9.678	10.269	11.980	380.26
724	37442	5.362	-20.592	0.523	9.825	10.252	11.961	386.94
726	37565	5.237	-20.641	0.518	9.514	10.110	11.795	377.83
728	37687	5.441	-20.749	0.538	9.562	10.113	11.799	390.42
730	37809	5.009	-20.676	0.487	9.53	10.285	12.000	357.95
732	37932	4.898	-20.892	0.472	9.618	10.377	12.107	343.97
734	38054	4.525	-20.634	0.449	9.556	10.078	11.758	316.97
736	38176	4.698	-20.686	0.448	8.638	10.487	12.234	335.03
738	38299	4.402	-20.809	0.422	8.506	10.431	12.170	314.21
740	38421	4.255	-20.649	0.400	8.68	10.638	12.410	300.97
742	38543	4.069	-20.653	0.390	8.576	10.433	12.172	299.61
744	38666	3.852	-20.552	0.370	8.475	10.411	12.146	279.51
746	38788	3.774	-20.773	0.372	8.171	10.145	11.836	267.63
748	38910	3.763	-20.63	0.366	8.177	10.281	11.995	269.92
750	39033	3.699	-20.615	0.357	8.252	10.361	12.088	267.87
751	39094	3.895	-20.583	0.361	8.198	10.789	12.588	283.13
752	39155	3.851	-20.417	0.371	8.025	10.380	12.110	280.98
754	39277	4.075	-20.467	0.404	8.126	10.087	11.768	298.72
756	39400	4.33	-20.499	0.417	7.897	10.384	12.114	312.50
758	39522	4.496	-20.533	0.424	7.914	10.604	12.371	327.42
760	39625	4.601	-20.556	0.436	8.587	10.553	12.312	327.46
762	39728	4.989	-20.432	0.473	8.379	10.548	12.305	346.82
764	39831	4.68	-20.461	0.449	8.81	10.423	12.160	323.58
766	39934	4.542	-20.39	0.432	8.625	10.514	12.266	313.11
768	40036	4.828	-20.36	0.464	8.592	10.405	12.139	330.03
770	40139	3.957	-20.376	0.385	8.662	10.278	11.991	270.91
772	40242	4.837	-20.275	0.467	8.44	10.358	12.084	335.50
774	40345	4.258	-20.326	0.404	8.622	10.540	12.296	300.56
776	40448	4.588	-20.485	0.444	8.616	10.333	12.056	317.97
778	40551	4.891	-20.308	0.472	8.69	10.362	12.089	344.88
780	40654	4.801	-20.468	0.459	8.88	10.460	12.203	343.55
782	40757	5.216	-20.627	0.482	8.517	10.822	12.625	374.10
784	40859	4.48	-20.195	0.436	8.757	10.275	11.988	322.41
786	40962	5.529	-20.289	0.541	8.641	10.220	11.923	390.95
788	41065	5.176	-20.314	0.491	8.427	10.542	12.299	364.47
790	41168	5.026	-20.377	0.472	8.449	10.648	12.423	353.74
792	41271	4.84	-20.337	0.463	8.021	10.454	12.196	341.96
794	41374	4.695	-20.318	0.449	7.835	10.457	12.199	328.57
796	41477	4.732	-20.421	0.449	8.008	10.539	12.295	329.61
798	41580	4.821	-20.35	0.475	8.158	10.149	11.841	334.87
800	41682	4.696	-20.319	0.446	7.701	10.529	12.284	327.68
802	41785	4.672	-20.293	0.459	7.754	10.179	11.875	334.25
804	41888	4.857	-20.163	0.471	7.694	10.312	12.031	354.46
806	41991	5.064	-20.274	0.476	7.988	10.639	12.412	366.30

808	42094	5.441	-20.379	0.506	8.009	10.753	12.545	379.35
810	42197	5.992	-20.339	0.567	8.414	10.568	12.329	425.40
812	42300	5.891	-20.342	0.557	8.376	10.576	12.339	415.06
814	42403	5.149	-20.374	0.509	7.96	10.116	11.802	360.42
816	42505	5.364	-20.398	0.497	8.356	10.793	12.592	367.59
818	42608	6.09	-20.465	0.563	8.464	10.817	12.620	414.60
820	42711	5.83	-20.414	0.554	8.331	10.523	12.277	397.05
822	42814	5.656	-20.333	0.546	8.356	10.359	12.085	383.72
824	42917	5.596	-20.332	0.522	8.412	10.720	12.507	381.34
826	43020	5.428	-20.337	0.490	8.053	11.078	12.924	379.11
828	43123	5.011	-20.305	0.480	7.868	10.440	12.180	347.82
830	43226	5.039	-20.312	0.481	8.04	10.476	12.222	350.05
832	43328	4.887	-20.312	0.462	7.76	10.578	12.341	338.57
834	43431	4.86	-20.273	0.451	7.512	10.776	12.572	334.76
836	43534	4.575	-20.287	0.445	7.379	10.281	11.994	321.10
838	43637	5.116	-20.411	0.495	7.433	10.335	12.058	354.60
840	43740	5.422	-20.384	0.514	7.679	10.549	12.307	378.82
842	43843	5.279	-20.395	0.512	7.838	10.311	12.029	363.23
844	43946	5.662	-20.399	0.535	7.986	10.583	12.347	387.78
846	44049	5.734	-20.464	0.528	8.161	10.860	12.670	390.79
848	44151	5.825	-20.465	0.551	8.335	10.572	12.334	398.47
850	44254	5.694	-20.596	0.516	8.363	11.035	12.874	386.81
852	44357	6.108	-20.552	0.575	8.585	10.623	12.393	413.19
854	44460	5.925	-20.599	0.559	8.557	10.599	12.366	397.85
856	44563	5.447	-20.665	0.486	8.516	11.208	13.076	362.55
858	44666	5.826	-20.818	0.568	8.337	10.257	11.967	398.82
860	44769	6.023	-20.689	0.566	8.997	10.641	12.415	417.37
862	44872	6.008	-20.801	0.579	8.775	10.377	12.106	412.06
864	44974	6.049	-20.854	0.575	8.935	10.520	12.273	422.68
866	45077	6.201	-20.883	0.590	9.326	10.510	12.262	430.87
868	45180	6.128	-20.811	0.581	9.328	10.547	12.305	428.15
870	45283	6.4	-21.302	0.576	9.64	11.111	12.963	448.67
872	45438	4.474	-20.742	0.429	8.494	10.429	12.167	312.88
874	45592	5.414	-20.6	0.511	8.239	10.595	12.361	377.38
876	45747	5.1	-20.582	0.486	8.277	10.494	12.243	355.04
878	45902	4.876		0.477	7.599	10.222	11.926	345.22
880	46056	4.617	-20.511	0.451	7.785	10.237	11.943	323.83
882	46211	4.458	-20.163	0.433	7.549	10.296	12.012	319.15
884	46366	4.36	-20.507	0.414	7.611	10.531	12.287	316.55
886	46520	4.306	-20.563	0.435	7.331	9.899	11.549	309.26
888	46675	4.476	-20.459	0.436	7.518	10.266	11.977	323.77
890	46830	4.505	-20.379	0.434	7.299	10.380	12.110	327.41
892	46984	4.946	-20.394	0.474	7.721	10.435	12.174	360.15
894	47139	5.186	-20.521	0.486	7.851	10.671	12.449	376.52
896	47293	5.011	-20.271	0.484	7.861	10.353	12.079	361.20
898	47448	5.207	-20.349	0.486	7.973	10.714	12.500	382.85
900	47603	5.732	-20.312	0.529	8.133	10.836	12.641	414.57
902	47757	5.841	-20.351	0.533	8.165	10.959	12.785	424.84
904	47912	5.913	-20.21	0.532	8.256	11.115	12.967	423.61
906	48067	5.779	-20.076	0.531	7.848	10.883	12.697	418.96
908	48221	5.869	-20.149	0.517	7.983	11.352	13.244	422.76
910	48376	5.858	-20.138	0.545	8.205	10.749	12.540	422.01
912	48531	5.861	-20.148	0.545	8.171	10.754	12.546	414.45
914	48685	5.68	-20.305	0.514	7.968	11.051	12.892	394.11
916	48840	6.059	-20.199	0.557	8.046	10.878	12.691	424.52
918	48995	6.012	-19.842	0.553	8.183	10.872	12.684	424.66
920	49149	6.024	-20.217	0.578	7.776	10.422	12.159	433.18
922	49304	6.05	-20.158	0.573	7.937	10.558	12.318	430.21
924	49459	5.728	-20.283	0.532	7.808	10.767	12.561	417.37
926	49613	5.942	-20.056	0.532	8.041	11.169	13.031	432.48
928	49768	5.913	-19.982	0.513	8.064	11.526	13.447	426.46
930	49923	6.571	-20.044	0.618	7.829	10.633	12.405	488.51
932	50077	6.13	-20.125	0.563	7.826	10.888	12.703	451.77
934	50232	6.495	-20.179	0.573	8.599	11.335	13.224	478.19
936	50386	6.587	-20.112	0.552	8.309	11.933	13.922	476.20
938	50541	6.661	-19.989	0.560	8.386	11.895	13.877	481.77
940	50696	7.285	-19.665	0.579	8.802	12.582	14.679	509.41
942	50850		-19.429	0.605	9.002			
944	51005	6.365	-20.237	0.566	8.646	11.246	13.120	446.58
946	51160	6.151	-20.445	0.571	8.878	10.772	12.568	445.48
948	51314	6.248	-20.5	0.578	8.717	10.810	12.611	450.01
950	51469	6.191	-20.566	0.571	8.993	10.842	12.649	444.28
952	51624	6.28	-20.521	0.572	9.119	10.979	12.809	456.93
954	51778	6.017	-20.557	0.529	9.085	11.374	13.270	427.91
956	51933	6.456	-20.554	0.593	8.934	10.887	12.702	453.18
958	52060	6.497	-20.657	0.579	9.291	11.221	13.091	464.44
960	52188	6.791	-20.474	0.606	9.134	11.206	13.074	487.78
962	52315	6.726	-20.469	0.582	9.221	11.557	13.483	482.90
964	52443	6.727	-20.558	0.596	9.201	11.287	13.168	484.40
966	52570	6.747	-20.39	0.600	9.238	11.245	13.119	481.21
968	52698	6.712	-20.558	0.572	9.188	11.734	13.690	479.15
970	52825	6.778	-20.596	0.608	9.332	11.148	13.006	478.16

972	52952	6.257	-20.385	0.557	8.853	11.233	13.106	432.97
974	53080	6.171	-20.448	0.540	8.772	11.428	13.332	432.82
976	53207	6.133	-20.345	0.528	8.702	11.616	13.551	437.07
978	53335	6.195	-20.497	0.550	8.912	11.264	13.141	445.23
980	53462	6.139	-20.328	0.540	8.644	11.369	13.263	435.69
982	53590	6.023	-20.285	0.539	8.665	11.174	13.037	432.67
984	53717	6.149	-20.314	0.534	8.476	11.515	13.434	434.79
986	53844	6.702	-20.243	0.592	8.642	11.321	13.208	471.43
988	53972	6.995	-20.336	0.589	8.765	11.876	13.855	495.64
990	54099	6.208	-20.307	0.553	8.954	11.226	13.097	428.16
992	54227	5.204	-20.413	0.463	8.512	11.240	13.113	361.47
994	54354	5.424	-20.372	0.477	8.618	11.371	13.266	387.51
996	54482	5.502	-20.411	0.499	8.565	11.026	12.864	385.94
998	54609	5.445	-20.379	0.494	8.624	11.022	12.859	374.03
1000	54737	5.335	-20.478	0.462	8.776	11.548	13.472	375.75
1002	54864	5.38	-20.328	0.464	8.489	11.595	13.527	375.93
1004	54991	5.495	-20.258	0.479	8.543	11.472	13.384	384.01
1006	55119	5.827	-20.233	0.520	8.416	11.206	13.073	412.12
1008	55246	5.693	-20.392	0.504	8.437	11.296	13.178	401.57
1010	55374	6.157	-20.353	0.547	8.861	11.256	13.132	440.64
1012	55501	6.016	-20.394	0.547	8.859	10.998	12.831	436.54
1014	55629	5.955	-20.305	0.541	9.049	11.007	12.842	427.30
1016	55756	5.839	-20.514	0.523	9.174	11.164	13.025	419.31
1018	55883	6.039	-20.68	0.543	9.385	11.122	12.975	437.91
1020	56011	5.882	-20.632	0.544	9.378	10.813	12.615	429.99
1022	56138	5.825	-20.773	0.543	9.424	10.727	12.515	419.30
1024	56266	5.602	-20.717	0.520	9.323	10.773	12.569	399.54
1026	56393	5.676	-20.694	0.526	9.481	10.791	12.589	398.70
1028	56521	5.653	-20.8	0.523	9.403	10.809	12.610	409.14
1030	56648	5.651	-20.771	0.521	9.619	10.846	12.654	409.96
1032	56775	5.634	-20.751	0.506	9.537	11.134	12.990	402.20
1034	56903	5.435	-20.667	0.512	9.485	10.615	12.384	390.65
1036	57030	5.56	-20.85	0.525	9.472	10.590	12.356	403.68
1038	57158	5.279	-20.862	0.491	9.255	10.752	12.543	383.58
1040	57285	5.134	-20.673	0.481	9.078	10.674	12.453	367.42
1042	57413	5.574	-20.601	0.518	9.461	10.761	12.554	397.00
1044	57540	5.4	-20.73	0.501	9.779	10.778	12.575	392.99
1046	57632	5.044	-20.878	0.449	9.251	11.234	13.106	368.03
1048	57724	5.223	-21.039	0.490	9.034	10.659	12.436	381.77
1050	57816	4.542	-21.279	0.403	8.661	13.149	13.149	333.81
1051	57862	4.432	-21.31	0.440	7.67	10.073	11.752	323.10
1052	57909	4.058	-20.959	0.416	7.546	9.755	11.381	293.43
1054	58001	4.254	-21.008	0.428	7.494	9.939	11.596	312.33
1056	58093	2.948	-20.951	0.312	7.166	9.449	11.024	217.65
1058	58185	4.025	-20.944	0.402	7.687	10.012	11.681	291.05
1060	58277	3.656	-20.826	0.377	7.394	9.698	11.314	256.30
1062	58369	3.46	-20.945	0.340	7.351	10.176	11.873	242.53
1064	58461	3.863	-20.867	0.394	7.329	9.805	11.439	274.62
1066	58553	3.837	-20.847	0.365	7.686	10.512	12.264	272.77
1068	58646	3.723	-20.76	0.365	7.548	10.200	11.900	268.36
1070	58738	3.618	-20.905	0.397	6.576	9.113	10.632	255.91
1072	58830	3.785	-20.87	0.421	7.019	8.990	10.489	278.52
1074	58922	3.676	-20.726	0.376	6.989	9.777	11.406	264.88
1076	59014	3.69	-20.813	0.369	6.965	10.000	11.667	268.75
1078	59106	3.691	-20.769	0.342	7.128	10.792	12.591	267.62
1080	59198	3.725	-20.671	0.363	7.019	10.262	11.972	271.33
1082	59290	3.07	-20.563	0.306	6.624	10.033	11.705	216.85
1084	59383	3.765	-20.805	0.375	6.838	10.040	11.713	270.00
1086	59475	3.719	-20.51	0.375	6.759	9.917	11.570	267.65
1088	59567	3.719	-20.457	0.361	6.717	10.302	12.019	270.99
1090	59659	3.706	-20.412	0.361	6.946	10.266	11.977	266.56
1092	59751	2.873	-20.652	0.277	5.91	10.372	12.100	206.20
1094	59843	3.763	-20.283	0.374	6.598	10.061	11.738	267.12
1096	59935	3.752	-20.452	0.364	6.769	10.308	12.026	267.63
1098	60027	3.82	-20.267	0.393	6.307	9.720	11.340	275.60
1100	60120	3.723	-20.479	0.366	6.429	10.172	11.867	270.24
1102	60212	3.721	-20.428	0.375	6.44	9.923	11.576	272.56
1104	60304	3.778	-20.456	0.383	6.278	9.864	11.508	270.78
1106	60396	3.815	-20.535	0.362	6.311	10.539	12.295	270.01
1108	60488	3.329	-20.418	0.327	6.176	10.180	11.877	238.08
1110	60580	3.811	-20.405	0.349	6.31	10.920	12.740	271.62
1112	60672	3.808	-20.274	0.377	6.061	10.101	11.784	269.42
1114	60764	3.908	-20.47	0.394	5.939	9.919	11.572	283.16
1116	60857	3.867	-20.267	0.383	6.298	10.097	11.779	277.35
1118	60949	3.954	-20.459	0.406	6.008	9.739	11.362	284.01
1120	61041	3.976	-20.321	0.373	5.913	10.660	12.436	285.75
1122	61133	4.096	-20.301	0.385	5.966	10.639	12.412	292.33
1124	61225	4.054	-20.315	0.373	5.938	10.869	12.680	286.52
1126	61317	4.081	-20.279	0.402	6.792	10.152	11.844	285.63
1128	61409	4.158	-20.372	0.387	6.643	10.744	12.535	295.13
1130	61501	4.396	-20.257	0.419	6.893	10.492	12.240	312.49
1132	61594	4.947	-20.375	0.440	6.961	11.243	13.117	351.41

CARBON AND NITROGEN ISOTOPES

1134	61686	5.191	-20.394	0.442	6.872	11.744	13.702	364.64
1136	61778	5.0575	-19.898	0.450	6.99		13.112	356.79
1138	61870	4.924	-20.372	0.446	7.324	11.040	12.880	338.40
1140	61968	4.376	-20.51	0.447	6.764	9.790	11.421	298.52
1142	62066	4.459	-20.582	0.447	6.551	9.975	11.638	305.82
1144	62164	4.349	-20.395	0.447	5.785	9.729	11.351	298.88
1146	62262	4.404	-20.294	0.398	6.038	11.065	12.910	301.55
1148	62360	4.268	-20.339	0.397	6.106	10.751	12.542	294.36
1150	62458	4.639	-20.217	0.431	6.418	10.763	12.557	320.14
1152	62556	4.81	-20.017	0.427	6.567	11.265	13.142	322.24
1154	62654	4.698	-20.058	0.400	6.613	11.745	13.703	327.32
1156	62752	4.571	-20.615	0.425	6.328	10.755	12.548	323.14
1158	62850	3.986	-20.266	0.372	6.351	10.715	12.501	283.87
1160	62948	4.144	-20.249	0.390	5.611	10.626	12.397	290.58
1162	63046	4.176	-20.331	0.390	6.047	10.708	12.492	293.41
1164	63144	3.976	-20.522	0.377	5.785	10.546	12.304	283.35
1166	63242	3.944	-20.35	0.374	5.88	10.545	12.303	282.07
1168	63340	3.901	-20.335	0.384	5.86	10.159	11.852	280.68
1170	63438	4.003	-20.392	0.383	5.288	10.452	12.194	287.59
1172	63536	3.953	-20.473	0.367	5.575	10.771	12.566	280.06
1174	63634	4.23	-21.013	0.384	6.219	11.016	12.852	295.85
1176	63732	3.951	-20.52	0.372	5.701	10.621	12.391	274.24
1178	63830	3.966	-20.465	0.371	5.94	10.690	12.472	279.20
1180	63928	3.784	-20.355	0.387	5.452	9.778	11.407	265.80
1182	64026	3.702	-20.345	0.376	5.434	9.846	11.487	263.64
1184	64124	3.864	-20.422	0.386	5.828	10.010	11.679	273.88
1186	64222	3.932	-20.459	0.382	5.692	10.293	12.009	280.15
1188	64320	4.039	-20.354	0.390	5.711	10.356	12.082	281.24
1190	64418	4.121	-20.25	0.400	5.65	10.303	12.020	282.68
1192	64516	4.128	-20.149	0.406	5.698	10.167	11.862	284.81
1194	64614	4.329	-20.38	0.416	5.983	10.406	12.141	303.17
1196	64712	4.193	-20.386	0.409	5.666	10.252	11.960	293.30
1198	64810	4.327	-20.651	0.413	5.811	10.477	12.223	303.66
1200	64908	4.38	-20.378	0.419	5.62	10.453	12.196	304.34
1202	65006	4.395	-20.31	0.405	5.732	10.852	12.660	311.92
1204	65104	4.308	-20.292	0.414	5.875	10.406	12.140	303.14
1206	65203	4.347	-20.353	0.409	5.613	10.628	12.400	302.69
1208	65301	4.273	-20.369	0.410	5.909	10.422	12.159	300.22
1210	65399	4.213	-20.375	0.403	5.546	10.454	12.196	299.31
1212	65497	4.223	-20.315	0.403	5.468	10.479	12.225	293.12
1214	65595	4.228	-20.28	0.401	5.97	10.544	12.301	291.91
1216	65693	4.072	-20.306	0.369	5.645	11.035	12.874	280.28
1218	65791	4.404	-20.277	0.401	5.904	10.983	12.813	301.89
1220	65889	4.961	-20.341	0.437	6.151	11.352	13.244	338.67
1222	65987	4.797	-20.329	0.434	6.052	11.053	12.895	330.06
1224	66085	4.875	-20.365	0.417	6.357	11.691	13.639	346.78
1226	66183	4.871	-20.288	0.435	6.559	11.198	13.064	348.88
1228	66281	5.107	-20.288	0.465	6.141	10.983	12.813	364.62
1230	66379	5.059	-20.233	0.453	6.143	11.168	13.029	359.99
1232	66477	5.32	-20.307	0.492	6.059	10.813	12.615	379.95
1234	66575	5.317	-20.413	0.496	6.279	10.720	12.506	374.35
1236	66673	4.909	-20.304	0.441	6.098	11.132	12.987	344.43
1238	66771	5.034	-20.492	0.476	6.479	10.576	12.338	354.59
1240	66869	5.062	-20.375	0.458	6.615	11.052	12.894	356.40
1242	66967	5.097	-20.302	0.476	6.213	10.708	12.493	365.73
1244	67065	5.192	-20.37	0.478	6.195	10.862	12.672	357.62
1246	67163	5.002	-20.409	0.478	5.868	10.464	12.209	343.68
1248	67261	4.807	-20.318	0.459	6.04	10.473	12.218	331.07
1250	67359	4.842	-20.406	0.458	6.292	10.572	12.334	340.48
1252	67457	5.189	-20.339	0.495	6.15	10.483	12.230	365.72
1254	67555	5.386	-20.374	0.489	6.657	11.014	12.850	375.30
1256	67653	5.605	-20.299	0.526	6.939	10.656	12.432	385.52
1258	67751	5.965	-20.357	0.545	7.242	10.945	12.769	409.89
1260	67849	5.988	-20.315	0.557	7.848	10.750	12.542	408.30
1262	67947	6.307	-20.367	0.568	7.845	11.104	12.955	431.18
1264	68045	6.249	-20.419	0.565	8.148	11.060	12.904	424.05
1266	68143	6.357	-20.449	0.574	8.333	11.075	12.921	434.96
1268	68241	6.582	-20.508	0.591	8.625	11.137	12.993	450.52
1270	68339	6.328	-20.623	0.584	8.492	10.836	12.642	429.67
1272	68437	6.347	-20.548	0.586	8.596	10.831	12.636	433.14
1274	68633	6.172	-20.605	0.562	8.473	10.982	12.813	422.40
1276	68829	5.858	-20.682	0.529	8.148	11.074	12.919	399.43
1278	69025	5.421	-20.655	0.513	7.476	10.567	12.328	375.79
1280	69221	5.311	-20.612	0.484	7.158	10.973	12.802	360.75
1282	69417	4.933	-20.512	0.466	6.89	10.586	12.350	347.12
1284	69613	4.827	-20.585	0.453	6.763	10.656	12.432	336.15
1286	69809	4.639	-20.706	0.446	6.886	10.401	12.135	316.46
1288	70005	4.454	-20.646	0.422	6.929	10.555	12.314	310.57
1290	70201	4.551	-20.537	0.430	6.912	10.584	12.348	311.43
1292	70397	4.421	-20.585	0.419	6.599	10.551	12.310	299.39
1294	70594	4.559	-20.628	0.431	7.042	10.578	12.341	310.71
1296	70790	4.941	-20.362	0.460	6.945	10.741	12.532	338.72

1298	70986	5.529	-20.265	0.499	6.975	11.080	12.927	378.53
1300	71182	6.222	-20.188	0.568	6.96	10.954	12.780	423.08
1302	71378	6.76	-20.156	0.586	7.28	11.536	13.458	457.18
1304	71574	7.432	-20.219	0.659	7.691	11.278	13.157	515.80
1306	71770	8.215	-20.318	0.717	8.083	11.457	13.367	574.97
1308	71966	8.733	-20.244	0.730	8.352	11.963	13.957	601.88
1310	72162	8.99	-20.37	0.734	8.587	12.248	14.289	626.87
1312	72358	9.597	-20.618	0.773	8.95	12.415	14.484	655.48
1314	72554	9.792	-20.549	0.786	8.982	12.458	14.534	672.23
1316	72750	9.958	-20.722	0.802	9.157	12.416	14.486	686.96
1318	72943	9.395	-20.603	0.757	9.058	12.411	14.479	634.93
1320	73136	8.327	-20.697	0.720	8.894	11.565	13.493	559.01
1322	73329	6.661	-20.598	0.588	8.044	11.328	13.216	439.99
1324	73522	6.297	-20.572	0.585	7.609	10.764	12.558	414.55
1326	73715	6.512	-20.383	0.585	7.361	11.132	12.987	434.82
1328	73908	6.343	-20.4	0.574	7.131	11.051	12.892	418.98
1330	74101	5.334	-20.247	0.484	7.141	11.021	12.857	348.11
1332	74294	5.173	-20.431	0.482	7.011	10.732	12.521	331.90
1334	74487	5.383	-20.326	0.494	7.143	10.897	12.713	349.50
1336	74680	6.459	-20.187	0.588	7.155	10.985	12.815	431.07
1338	74873	6.628	-19.974	0.584	6.986	11.349	13.241	449.44
1340	75066	7.005	-20.019	0.640	6.838	10.945	12.770	477.24
1342	75259	7.141	-19.932	0.629	6.982	11.353	13.245	491.40
1344	75452	7.405	-19.797	0.666	6.829	11.119	12.972	500.92
1346	75645	8.671	-19.831	0.762	7.231	11.379	13.276	572.76
1348	75838	8.829	-19.788	0.770	7.174	11.466	13.377	590.33
1350	76031	9.404	-19.519	0.815	7.279	11.539	13.462	623.17
1352	76224	7.534	-19.771	0.661	6.934	11.398	13.298	512.54
1354	76417	9.665	-19.573	0.840	7.272	11.506	13.424	662.25
1356	76610	7.554	-19.592	0.657	7.298	11.498	13.414	516.93
1358	76803	7.5	-19.684	0.652	7.325	11.503	13.420	506.31
1360	76996	8.557	-19.446	0.781	7.612	10.956	12.783	589.47
1362	77189	8.302	-19.876	0.760	7.684	10.924	12.744	594.62
1364	77382	8.384	-19.693	0.752	7.545	11.149	13.007	585.77
1366	77575	8.238	-19.728	0.753	7.876	10.940	12.764	553.77
1368	77768	7.383	-19.919	0.659	7.889	11.203	13.071	482.97
1370	77961	8.156	-19.809	0.736	7.975	11.082	12.928	531.54
1372	78154	7.929	-19.88	0.695	8.251	11.409	13.310	514.81
1374	78346	8.244	-19.914	0.727	8.306	11.340	13.230	520.04
1376	78539	8.313	-19.941	0.717	8.011	11.594	13.526	556.64
1378	78732	8.398	-19.894	0.720	8.476	11.664	13.608	571.11
1380	78925	8.227	-19.876	0.709	8.338	11.604	13.538	578.30
1382	79118	8.285	-20.071	0.689	8.292	12.025	14.029	573.92
1384	79311	8.472	-19.93	0.716	8.571	11.832	13.804	588.67
1386	79504			0.365	7.348			
1388	79697	7.997	-20.126	0.697	8.794	11.473	13.386	546.26
1390	79890	7.745666667	-20.049	0.416	8.089			
1392	80083		-19.924	0.285	7.957			
1394	80276	6.768	-20.232	0.571	8.48	11.853	13.828	456.51
1396	80469	7.403	-20.054	0.641	8.74	11.549	13.474	509.43
1398	80662	7.671	-20.199	0.648	8.875	11.838	13.811	516.29
1400	80855	7.449	-20.168	0.644	8.829	11.567	13.495	506.70
1402	81048	7.107	-20.252	0.621	8.949	11.444	13.352	482.45
1404	81241	7.988	-20.291	0.700	9.382	11.411	13.313	536.71
1406	81434	7.759	-20.289	0.668	9.28	11.615	13.551	527.47
1408	81627	7.838	-20.373	0.673	9.4	11.646	13.587	532.39
1410	81820	8.088	-20.42	0.689	9.531	11.739	13.695	528.90
1412	82013	7.877	-20.549	0.683	9.863	11.533	13.455	523.65
1414	82206	8.324	-20.599	0.738	9.899	11.279	13.159	555.41
1416	82399	8.004	-20.718	0.714	10.029	11.210	13.078	531.77
1418	82592	7.752	-20.712	0.690	9.881	11.235	13.107	514.90
1420	82785	8	-20.805	0.729	10.259	10.974	12.803	532.61
1422	82978	8.186	-20.721	0.727	10.197	11.260	13.137	543.19
1424	83171	7.834	-20.864	0.695	10.641	11.272	13.151	525.59
1426	83364	8.156	-20.888	0.713	10.955	11.439	13.345	543.93
1428	83557	8.052	-20.919	0.720	11.452	11.183	13.047	526.94
1430	83730	5.537	-20.986	0.493	9.355	11.231	13.103	359.91
1432	83902	4.744	-20.801	0.417	9.221	11.376	13.273	311.89
1434	84075	4.701	-20.88	0.426	9.119	11.035	12.874	307.53
1436	84248	4.561	-20.713	0.396	8.927	11.518	13.437	301.31
1438	84421	4.656	-20.736	0.410	8.612	11.356	13.249	306.14
1440	84593	4.366	-20.863	0.388	8.677	11.253	13.128	290.07
1442	84766	4.391	-20.767	0.409	8.098	10.736	12.525	292.77
1444	84939	4.159	-20.619	0.370	8.535	11.241	13.114	269.42
1446	85111	4.281	-20.728	0.385	8.59	11.119	12.973	272.11
1448	85284	4.28	-20.739	0.381	8.612	11.234	13.106	276.52
1450	85457	4.161	-20.622	0.374	8.584	11.126	12.980	273.19
1452	85629	4.071	-20.651	0.364	8.369	11.184	13.048	272.43
1454	85802	4.079	-20.778	0.361	8.109	11.299	13.182	276.30
1456	85975	3.993	-20.711	0.360	8.159	11.092	12.940	261.08
1458	86148	4.006	-20.472	0.362	8.5	11.066	12.911	263.21
1460	86320	3.932	-20.576	0.362	8.102	10.862	12.672	261.07

1462	86493	4.278	-20.64	0.398	8.103	10.749	12.540	288.94
1464	86666	3.884	-20.579	0.347	8.03	11.193	13.059	255.10
1466	86838	3.91	-20.669	0.356	8.043	10.983	12.814	261.72
1468	87011	3.935	-20.662	0.369	7.554	10.664	12.441	264.07
1470	87184	4.126	-20.656	0.384	7.505	10.745	12.536	279.89
1472	87356	3.926	-20.625	0.358	7.612	10.966	12.794	264.33
1474	87529	3.952	-20.574	0.358	7.49	11.039	12.879	264.89
1476	87702	3.855	-20.582	0.347	7.454	11.110	12.961	258.29
1478	87875	3.858	-20.6	0.348	6.995	11.086	12.934	255.56
1480	88047	3.876	-20.564	0.364	7.379	10.648	12.423	261.09
1482	88220	4.02	-20.682	0.365	7.156	11.014	12.849	272.27
1484	88393	4.093	-20.661	0.364	6.957	11.245	13.119	273.37
1486	88565	3.608	-20.634	0.331	7.176	10.900	12.717	242.63
1488	88738	3.841	-20.789	0.363	7.081	10.581	12.345	262.12
1490	88911	3.621	-20.54	0.344	7.057	10.526	12.281	246.19
1492	89083	3.8	-20.839	0.369	7.263	10.298	12.014	258.11
1494	89256	3.724	-20.759	0.353	7.278	10.550	12.308	255.78
1496	89429	3.815	-20.587	0.366	7.179	10.423	12.161	259.66
1498	89602	3.937	-20.579	0.376	6.868	10.471	12.216	267.19
1500	89774	3.838	-20.535	0.381	7.152	10.073	11.752	261.07
1501	89861	4.435	-20.633	0.424	7.273	10.460	12.203	300.76
1502	89947	3.901	-20.474	0.365	7.174	10.688	12.469	263.73
1504	90120	4.813	-20.571	0.450	6.872	10.696	12.478	326.45
1506	90292	5.698	-20.502	0.529	7.164	10.771	12.566	378.14
1508	90465	6.03	-20.373	0.558	7.457	10.806	12.608	404.31
1510	90638	6.377	-20.35	0.566	7.262	11.267	13.145	433.26
1512	90811	6.92	-20.296	0.634	7.624	10.915	12.734	473.14
1514	90983	6.456	-20.432	0.598	7.56	10.796	12.595	439.10
1516	91156	7.518	-20.345	0.678	7.707	11.088	12.937	506.36
1518	91329	7.505	-20.319	0.683	7.882	10.988	12.820	505.05
1520	91501	7.338	-20.253	0.695	7.787	10.558	12.318	513.41
1522	91674	7.068	-20.302	0.641	7.861	11.027	12.864	498.21
1524	91847	6.572	-20.288	0.593	8.143	11.083	12.930	453.64
1526	92019	7.958	-20.34	0.712	8.091	11.177	13.040	537.68
1528	92192	7.829	-20.499	0.729	8.143	10.739	12.529	559.15
1530	92365	7.169	-20.378	0.653	7.983	10.979	12.808	513.71
1532	92538	7.36	-20.445	0.669	8.195	11.001	12.835	528.29
1534	92710	7.524	-20.393	0.681	8.446	11.048	12.890	525.99
1536	92883	6.752	-20.424	0.615	8.259	10.979	12.809	480.08
1538	93056	7.545	-20.324	0.696	8.324	10.841	12.647	533.50
1540	93228	8.065	-20.233	0.719	8.428	11.217	13.086	578.83
1542	93401	8.502	-20.296	0.784	8.539	10.844	12.652	599.50
1544	93574	8.618	-20.539	0.783	8.379	11.006	12.841	609.72
1546	93746	8.439	-20.426	0.779	8.409	10.833	12.639	592.99
1548	93919	8.32	-20.31	0.754	8.363	11.034	12.874	580.69
1550	94092	7.667	-20.327	0.679	8.521	11.292	13.174	532.67
1552	94265	8.258	-20.316	0.751	8.387	10.996	12.829	564.49
1554	94437	7.802	-20.419	0.722	8.165	10.806	12.607	527.65
1556	94610	7.883	-20.382	0.704	8.189	11.197	13.064	525.66
1558	94783	7.897	-20.361	0.726	8.143	10.877	12.690	533.56
1560	94955	7.399	-20.26	0.674	8.61	10.978	12.807	500.46
1562	95128	7.956	-20.396	0.736	8.271	10.810	12.611	541.32
1564	95301	7.48	-20.423	0.681	8.226	10.984	12.814	514.37
1566	95474	7.408	-20.385	0.676	8.214	10.959	12.785	501.07
1568	95646	8.351	-20.446	0.753	7.978	11.090	12.939	553.39
1570	95819	8.519	-20.43	0.787	8.249	10.825	12.629	565.98
1572	95992	7.571	-20.379	0.687	8.101	11.020	12.857	499.85
1574	96164	8.853	-20.342	0.782	8.197	11.321	13.208	579.07
1576	96337	8.712	-20.327	0.763	8.355	11.418	13.321	570.48
1578	96510	7.687	-20.572	0.677	7.997	11.355	13.247	507.44
1580	96682	7.911	-20.523	0.708	8.174	11.174	13.036	530.05
1582	96855	8.124	-20.62	0.705	8.147	11.523	13.444	535.03
1584	97028	8.374	-20.642	0.727	8.35	11.519	13.438	551.91
1586	97201	8.221	-20.614	0.736	8.353	11.170	13.031	549.54
1588	97373	7.792	-20.654	0.708	8.07	11.006	12.840	518.45
1590	97546	8.53	-20.675	0.768	8.095	11.107	12.958	553.48
1592	97719	8.724	-20.564	0.780	8.157	11.185	13.049	570.98
1594	97891	7.843	-20.591	0.692	8.445	11.334	13.223	513.96
1596	98064	7.914	-20.575	0.679	8.677	11.655	13.598	527.86
1598	98237	8.396	-20.605	0.752	8.578	11.165	13.026	553.42
1600	98409	8.852	-20.613	0.784	8.622	11.291	13.173	585.07
1602	98582	9.063	-20.653	0.797	8.628	11.371	13.267	592.58
1604	98755	9.047	-20.659	0.804	8.613	11.252	13.128	597.81
1606	98928	8.645	-20.608	0.765	8.565	11.301	13.184	585.16
1608	99100	8.503	-20.552	0.785	9.006	10.832	12.637	559.16
1610	99273	8.394	-20.653	0.749	8.655	11.207	13.075	555.28
1612	99446	8.317	-20.642	0.745	8.619	11.164	13.024	549.17
1614	99618	8.472	-20.645	0.753	8.701	11.251	13.126	555.74
1616	99791	8.409	-20.662	0.752	8.602	11.182	13.046	557.03
1618	99964	8.153	-20.577	0.730	8.487	11.168	13.030	530.55
1620	100136	8.354	-20.629	0.750	8.744	11.139	12.995	540.49
1622	100309	8.586	-20.62	0.769	8.737	11.165	13.026	563.00

1624	100482	8.397	-20.632	0.758	8.748	11.078	12.924	544.16
1626	100655	7.654	-20.601	0.732	8.407	10.456	12.199	508.02
1628	100827	7.937		0.717	8.524	11.070	12.915	518.24
1630	101000	7.653	-20.416	0.705	8.488	10.855	12.665	500.82
1632	101125	7.597	-20.52	0.693	8.411	10.962	12.790	501.19
1634	101250	7.819	-20.54	0.728	8.354	10.740	12.530	510.41
1636	101375	7.136	-20.584	0.685	8.384	10.418	12.154	475.03
1638	101500	7.679	-20.586	0.700	8.375	10.970	12.798	506.16
1640	101625	7.687	-20.509	0.704	8.38	10.919	12.739	497.02
1642	101751	7.003	-20.497	0.654	8.195	10.708	12.493	461.32
1644	101876	6.993	-20.526	0.620	8.067	11.279	13.159	458.72
1646	102001	7.231	-20.433	0.670	8.203	10.793	12.591	472.62
1648	102126	7.235	-20.492	0.675	8.291	10.719	12.505	479.56
1650	102251	5.996	-20.56	0.568	8.211	10.556	12.316	402.72
1652	102376	7.76	-20.579	0.719	8.368	10.793	12.592	524.87
1654	102501	7.11	-20.626	0.648	8.354	10.972	12.801	486.72
1656	102626	7.77	-20.592	0.719	8.328	10.807	12.608	518.82
1658	102751	7.804	-20.593	0.712	8.244	10.961	12.787	532.95
1660	102876	7.971	-20.57	0.734	8.277	10.860	12.670	532.51
1662	103001	8.554	-20.538	0.776	8.286	11.023	12.860	570.34
1664	103126	7.234	-20.546	0.651	8.166	11.112	12.964	479.61
1666	103252	9.171	-20.828	0.768	8.267	11.941	13.932	611.55
1668	103377	9.004	-20.519	0.800	8.338	11.255	13.131	588.87
1670	103502	9.098	-20.551	0.811	8.318	11.218	13.088	608.76
1672	103627	8.913	-20.58	0.795	8.42	11.211	13.080	589.47
1674	103752	9.223	-20.486	0.816	8.293	11.303	13.186	607.79
1676	103877	9.625	-20.487	0.818	8.332	11.767	13.728	638.60
1678	104002	10.273	-20.326	0.864	8.352	11.890	13.872	686.21
1680	104127	10.606	-20.327	0.889	8.459	11.930	13.919	739.98
1682	104252	10.927	-20.341	0.913	8.472	11.968	13.963	749.26
1684	104377	11.313	-20.324	0.931	8.522	12.151	14.177	772.03
1686	104502	11.855	-20.244	0.937	8.476	12.652	14.761	815.51
1688	104628	12.07	-20.348	0.987	8.464	12.229	14.267	797.77
1690	104753	11.806	-20.48	0.978	8.478	12.072	14.084	785.52
1692	104878	11.576	-20.46	0.952	8.556	12.160	14.186	761.90
1694	105003	11.317	-20.537	0.944	8.466	11.988	13.986	765.37
1696	105128	11.764	-20.452	0.966	8.45	12.178	14.208	799.73
1698	105253	11.451	-20.394	0.961	8.403	11.916	13.902	772.85
1700	105378	11.572	-20.363	0.980	8.451	11.808	13.776	792.26
1702	105503	11.191	-20.547	0.943	8.475	11.867	13.845	762.88
1704	105628	11.367	-20.652	0.952	8.582	11.940	13.930	770.52
1706	105753	11.263	-20.731	0.970	8.535	11.611	13.547	769.17
1708	105878	10.739	-20.775	0.932	8.507	11.523	13.443	734.61
1710	106004	10.164	-20.637	0.873	8.12	11.643	13.583	687.73
1712	106129	9.255	-20.626	0.807	7.972	11.468	13.380	619.42
1714	106254	6.804	-20.562	0.611	7.567	11.136	12.992	454.38
1716	106379	6.735	-20.588	0.612	7.454	11.005	12.839	446.08
1718	106504	6.501	-20.56	0.585	7.446	11.113	12.965	425.12
1720	106629	5.218	-20.542	0.474	7.058	11.008	12.843	347.01
1722	106754	5.641	-20.488	0.519	7.214	10.869	12.680	382.06
1724	106879	5.295	-20.463	0.490	6.979	10.806	12.607	366.49
1726	107004	5.392	-20.457	0.504	7.029	10.698	12.481	376.82
1728	107129	5.507	-20.448	0.499	6.869	11.036	12.875	376.85
1730	107254	5.169	-20.578	0.479	6.979	10.791	12.590	352.20
1732	107379	5.152	-20.451	0.481	6.785	10.711	12.496	357.44
1734	107505	5.023	-20.505	0.474	6.791	10.597	12.363	347.83
1736	107630	5.027	-20.407	0.478	6.763	10.517	12.270	341.46
1738	107755	5.944	-20.255	0.543	6.656	10.947	12.771	409.47
1740	107880	5.599	-20.325	0.516	6.686	10.851	12.659	395.22
1742	108005	6.455	-20.119	0.586	6.67	11.015	12.851	469.55
1744	108130	7.312	-20.001	0.656	6.759	11.146	13.004	521.50
1746	108264	8.859	-19.992	0.791	6.955	11.200	13.066	626.63
1748	108398	9.397	-20.034	0.821	6.983	11.446	13.353	643.66
1750	108533	10.101	-19.886	0.878	7.034	11.505	13.422	698.15
1752	108667	10.411	-19.973	0.904	7.258	11.517	13.436	716.94
1754	108801	10.477	-20.059	0.904	7.353	11.590	13.521	714.98
1756	108935	9.893	-20.176	0.858	7.456	11.530	13.452	672.38
1758	109069	9.179	-20.122	0.788	7.565	11.648	13.590	617.56
1760	109203	9.483	-20.154	0.820	7.731	11.565	13.492	654.97
1762	109338	9.519	-20.265	0.841	7.897	11.319	13.205	656.52
1764	109472	9.573	-20.259	0.842	7.894	11.369	13.264	665.25
1766	109606	9.028	-20.447	0.786	7.986	11.486	13.400	609.09
1768	109740	8.872	-20.475	0.786	7.984	11.288	13.169	607.77
1770	109874	8.95	-20.444	0.780	8.052	11.474	13.387	628.97
1772	110008	8.305	-20.843	0.756	8.751	10.985	12.816	563.50
1774	110143	8.335	-20.874	0.761	8.752	10.953	12.778	562.20
1776	110277	8.044	-20.98	0.726	8.908	11.080	12.927	533.51
1778	110411	7.172	-21.292	0.662	9.154	10.834	12.639	468.76
1780	110545	5.634	-21.213	0.541	8.472	10.414	12.150	363.96
1782	110679	5.085	-21.09	0.504	8.086	10.089	11.771	335.14
1784	110813	4.646	-21.033	0.438	7.739	10.607	12.375	307.42
1786	110948	4.562	-21.036	0.450	7.672	10.138	11.827	301.71

CARBON AND NITROGEN ISOTOPES

1788	111082	4.585	-21.078	0.456	7.539	10.055	11.731	312.82
1790	111216	4.979	-20.897	0.470	7.621	10.594	12.359	336.81
1792	111350	4.286	-21.105	0.419	7.411	10.229	11.934	281.85
1794	111484	4.169	-21.048	0.418	7.269	9.974	11.636	274.09
1796	111618	4.049	-21.109	0.400	7.171	10.123	11.810	271.29
1798	111753	4.381	-21.426	0.440	7.115	9.957	11.616	282.41
1800	111887	4.483	-21.272	0.431	6.97	10.401	12.135	298.50
1802	112021	4.508	-21.049	0.457	6.987	9.864	11.508	303.33
1804	112155	4.945	-20.98	0.495	7.21	9.990	11.655	329.06
1806	112289	5.159	-20.965	0.490	7.294	10.529	12.283	350.25
1808	112423	5.65	-20.784	0.530	7.19	10.660	12.437	383.63

BIOGENIC SILICA (OPAL)

Core MD02-2519

Depth cm	Age cal years BP	Opal % wt.	Si %	molar BSi/C	molar BSi/N	Opal MAR mg/cm2/kyr
0	2365	3.573	1.489	0.080	0.856	263.568
10	2542	3.686	1.536	0.073	0.785	264.778
20	2739	3.770	1.571	0.076	0.807	282.451
30	2936	3.115	1.298	0.064	0.677	225.215
40	3133	3.117	1.299	0.063	0.666	218.768
50	3330	2.922	1.217	0.055	0.617	206.917
60	3526	2.890	1.204	0.055	0.592	205.375
70	3723	2.355	0.981	0.043	0.461	163.848
80	4026	2.501	1.042	0.044	0.474	172.919
90	4399	2.661	1.109	0.049	0.529	186.965
100	4773	2.382	0.993	0.046	0.516	167.071
110	5146	2.658	1.108	0.050	0.541	190.473
120	5519	2.099	0.874	0.040	0.446	151.519
130	5893	1.923	0.801	0.036	0.411	135.046
140	6266	2.160	0.900	0.042	0.487	150.804
150	6793	2.400	1.000	0.044	0.497	170.085
160	7321	2.394	0.997	0.044	0.507	173.635
170	7848	2.650	1.104	0.049	0.564	190.478
180	8376	2.396	0.998	0.050	0.589	173.239
190	8903	2.524	1.052	0.058	0.686	184.446
200	9410	2.399	0.999	0.054	0.638	175.353
210	9902	2.755	1.148	0.067	0.788	202.515
214	10099	2.695	1.123	0.071	0.904	199.562
220	10451	3.037	1.265	0.077	0.920	223.467
224	10703	3.394	1.414	0.081	0.970	247.213
230	11082	3.443	1.434	0.091	1.105	253.925
234	11292	3.185	1.327	0.092	1.136	229.320
240	11606	3.126	1.303	0.126	1.562	228.139
244	11815	2.821	1.175	0.121	1.534	207.958
250	12130	2.924	1.218	0.124	1.716	214.291
254	12339	2.990	1.246	0.131	1.593	220.769
260	12654	2.965	1.235	0.124	1.521	219.049
264	12863	2.840	1.183	0.122	1.517	209.831
270	13178	2.773	1.155	0.110	1.313	204.865
274	13387	2.809	1.170	0.112	1.361	208.467
280	13701	2.787	1.161	0.092	1.087	205.697
284	13911	2.733	1.139	0.093	1.106	203.542
290	14084	3.067	1.278	0.117	1.446	220.760
294	14280	3.534	1.472	0.137	1.625	254.031
300	14573	2.850	1.187	0.146	1.821	210.635
304	14769	2.665	1.110	0.136	1.703	197.356
310	15063	3.315	1.381	0.193	2.558	243.221
314	15258	2.572	1.072	0.133	1.745	192.311
320	15552	3.056	1.273	0.170	2.188	228.091
324	15748	3.883	1.618	0.205	2.724	287.696
330	16041	3.126	1.302	0.174	2.269	231.591
334	16262	2.740	1.142	0.154	2.017	205.213
340	16631	3.580	1.492	0.194	2.478	266.785
344	16877	3.033	1.264	0.162	2.078	225.855
350	17246	3.352	1.397	0.172	2.282	243.789
354	17491	3.500	1.458	0.179	2.383	249.581
360	17860	3.604	1.502	0.180	2.332	261.742
364	18106	3.090	1.287	0.169	2.220	229.045
370	18475	3.876	1.615	0.177	2.307	280.388
374	18693	3.220	1.342	0.143	1.858	233.444
380	19020	3.542	1.476	0.148	1.942	262.736
384	19238	3.278	1.366	0.142	1.802	241.216
390	19565	3.910	1.629	0.153	1.899	288.923
394	19783	3.685	1.535	0.148	1.905	269.985
400	20109	3.900	1.625	0.150	1.953	280.773
404	20327	4.297	1.790	0.155	1.942	304.674
410	20654	5.700	2.375	0.316	4.226	410.910
414	20872	5.024	2.093	0.218	2.733	366.265
420	21199	4.636	1.932	0.203	2.668	337.051
424	21417	5.190	2.163	0.219	2.853	375.941
430	21670	4.549	1.895	0.188	2.462	337.477
434	21839	5.652	2.355	0.220	2.858	409.266
440	22093	4.943	2.060	0.242	3.140	359.097

BIOGENIC SILICA (OPAL)

444	22262	4.892	2.038	0.211	2.732	353.480
450	22515	3.934	1.639	0.154	1.915	292.813
454	22684	3.549	1.479	0.153	1.906	254.816
460	22938	4.495	1.873	0.187	2.273	323.595
464	23107	3.730	1.554	0.143	1.750	265.831
470	23488	3.665	1.527	0.152	1.731	257.773
474	23784	3.447	1.436	0.143	1.743	247.781
480	24229	3.374	1.406	0.160	1.975	242.799
484	24526	4.032	1.680	0.201	2.538	298.877
490	24971	3.918	1.632	0.198	2.583	285.260
494	25268	3.635	1.515	0.174	2.234	262.490
500	25713	4.060	1.691	0.178	2.202	295.037
504	25886	4.928	2.053	0.213	2.567	359.804
510	26146	4.362	1.818	0.208	2.779	312.248
514	26320	3.709	1.545	0.174	2.183	262.327
520	26579	3.688	1.537	0.161	1.931	261.266
524	26753	3.556	1.482	0.145	1.820	249.167
530	27013	4.054	1.689	0.167	2.006	278.644
534	27186	3.650	1.521	0.148	1.824	259.603
540	27446	4.196	1.748	0.162	2.005	291.390
544	27619	3.960	1.650	0.166	2.126	276.645
550	27879	4.654	1.939	0.194	2.436	327.771
554	28052	4.273	1.781	0.161	1.855	304.888
560	28293	4.993	2.080	0.213	2.056	343.810
564	28427	3.885	1.619	0.148	1.340	272.555
570	28629	3.555	1.481	0.144	1.295	255.151
574	28763	4.365	1.819	0.144	1.450	310.942
580	29060	4.242	1.767	0.172	1.793	306.144
584	29289	4.120	1.717	0.165	1.707	291.120
590	29632	3.427	1.428	0.153	1.405	239.591
594	29861	3.443	1.435	0.153	1.426	251.424
600	30204	4.559	1.900	0.185	1.991	333.489
604	30433	5.250	2.188	0.185	2.014	389.897
610	30804	5.365	2.236	0.202	2.300	396.955
614	31061	5.637	2.349	0.204	2.344	408.898
620	31446	5.261	2.192	0.205	2.393	382.348
624	31702	4.778	1.991	0.187	1.918	339.659
630	32087	4.333	1.805	0.158	1.538	308.210
634	32343	5.169	2.154	0.176	1.955	369.872
640	32675	4.494	1.873	0.135	1.515	318.286
644	32878	4.849	2.020	0.148	1.704	346.906
650	33184	5.360	2.233	0.160	1.798	389.595
654	33387	4.613	1.922	0.138	1.586	329.173
660	33693	4.324	1.802	0.143	1.517	305.684
664	33896	4.051	1.688	0.133	1.400	285.194
670	34201	4.098	1.708	0.125	1.506	293.702
674	34405	4.362	1.818	0.126	1.400	311.278
680	34751	3.835	1.598	0.152	1.644	272.016
684	34996	3.582	1.493	0.125	1.302	250.404
690	35363	3.634	1.514	0.135	1.407	258.370
694	35608	3.319	1.383	0.130	1.350	235.927
700	35975	2.937	1.224	0.111	1.310	210.320
704	36219	3.414	1.422	0.124	1.526	247.338
710	36586	3.226	1.344	0.113	1.358	228.774
714	36831	3.428	1.428	0.120	1.437	248.860
720	37198	3.172	1.322	0.110	1.301	230.038
724	37442	3.732	1.555	0.124	1.487	269.310
730	38082	3.824	1.593	0.136	1.636	273.236
734	38288	3.708	1.545	0.146	1.721	259.762
740	38596	3.584	1.493	0.150	1.867	253.530
744	38802	3.316	1.382	0.154	1.867	240.597
750	39111	3.354	1.398	0.162	1.957	242.885
754	39316	3.180	1.325	0.139	1.640	233.122
760	39625	4.194	1.748	0.163	2.004	298.501
764	39831	5.218	2.174	0.199	2.421	360.784
770	40139	3.824	1.593	0.173	2.069	261.819
774	40345	4.181	1.742	0.175	2.156	295.130
780	40654	4.091	1.705	0.152	1.857	292.749
784	40859	4.647	1.936	0.185	2.220	334.400
790	41168	3.900	1.625	0.139	1.721	274.480
794	41374	3.561	1.484	0.135	1.652	249.192
800	41682	3.561	1.484	0.135	1.663	248.465
804	41888	4.319	1.799	0.159	1.910	315.171

810	42197	4.086	1.703	0.122	1.501	290.087
814	42385	4.483	1.868	0.155	1.835	313.829
820	42711	3.982	1.659	0.122	1.497	271.188
824	42917	5.034	2.097	0.161	2.009	343.033
830	43226	4.737	1.974	0.168	2.052	329.057
834	43431	4.087	1.703	0.150	1.888	281.535
840	43740	4.190	1.746	0.138	1.698	292.758
844	43946	3.949	1.645	0.125	1.538	270.472
850	44254	4.475	1.864	0.140	1.807	303.983
854	44460	4.546	1.894	0.137	1.694	305.236
860	44769	3.900	1.625	0.116	1.435	270.229
864	44974	4.449	1.854	0.131	1.612	310.913
870	45283	4.172	1.738	0.116	1.509	292.448
874	45592	3.975	1.656	0.131	1.620	277.047
880	46056	3.538	1.474	0.137	1.634	248.118
884	46366	3.368	1.403	0.138	1.695	244.508
890	46830	3.689	1.537	0.146	1.771	268.112
894	47139	4.836	2.015	0.167	2.073	351.088
900	47603	4.391	1.830	0.137	1.729	317.613
904	47912	3.559	1.483	0.107	1.394	254.937
910	48376	3.493	1.455	0.106	1.335	251.615
914	48685	4.133	1.722	0.130	1.675	286.768
920	49149	3.225	1.344	0.096	1.162	231.897
924	49459	3.393	1.414	0.106	1.329	247.266
930	49923	4.355	1.814	0.118	1.468	323.740
934	50232	4.380	1.825	0.120	1.592	322.458
940	50696	4.224	1.760	0.104	1.520	295.395
944	51005	2.933	1.222	0.082	1.080	205.795
950	51469	3.689	1.537	0.106	1.346	264.708
954	51778	3.922	1.634	0.116	1.545	278.911
960	52188	4.341	1.809	0.114	1.492	311.824
964	52443	3.910	1.629	0.104	1.367	281.538
970	52825	4.683	1.951	0.123	1.605	330.347
974	53080	3.225	1.344	0.093	1.244	226.220
980	53462	3.654	1.523	0.106	1.410	259.345
984	53717	3.473	1.447	0.101	1.355	245.549
990	54099	4.543	1.893	0.131	1.712	313.355
994	54354	4.056	1.690	0.134	1.772	289.806
1000	54737	4.046	1.686	0.135	1.824	284.939
1004	54991	3.565	1.485	0.116	1.551	249.147
1010	55374	4.588	1.912	0.133	1.747	328.325
1014	55629	4.174	1.739	0.125	1.607	299.509
1020	56011	4.339	1.808	0.132	1.662	317.155
1024	56266	4.276	1.782	0.136	1.713	304.994
1030	56648	4.103	1.709	0.130	1.640	297.628
1034	56903	3.455	1.440	0.114	1.406	248.356
1040	57285	4.066	1.694	0.141	1.761	290.963
1044	57540	3.766	1.569	0.125	1.566	274.095
1050	57816	3.799	1.583	0.149	1.964	279.235
1054	58001	3.245	1.352	0.136	1.580	238.252
1060	58277	3.529	1.471	0.172	1.950	247.433
1064	58461	3.472	1.447	0.161	1.836	246.847
1070	58738	3.032	1.263	0.150	1.591	214.492
1074	58922	3.182	1.326	0.155	1.763	229.307
1080	59198	3.376	1.407	0.163	1.937	245.902
1084	59383	3.061	1.275	0.145	1.701	219.513
1090	59659	3.493	1.455	0.168	2.016	251.235
1094	59843	3.177	1.324	0.151	1.770	225.503
1100	60120	3.698	1.541	0.177	2.105	268.437
1104	60304	3.546	1.478	0.168	1.929	254.181
1110	60580	3.785	1.577	0.177	2.259	269.773
1114	60764	3.784	1.577	0.173	2.001	274.166
1120	61041	3.299	1.375	0.148	1.843	237.090
1124	61225	3.119	1.299	0.137	1.742	220.423
1130	61501	3.905	1.627	0.159	1.941	277.551
1134	61686	4.170	1.737	0.143	1.965	292.906
1140	61968	4.603	1.918	0.188	2.145	313.985
1144	62164	3.812	1.588	0.157	1.777	261.995
1150	62458	3.844	1.602	0.148	1.858	265.304
1154	62654	4.321	1.801	0.164	2.251	301.079
1160	62948	3.700	1.542	0.159	1.976	259.421
1164	63144	3.053	1.272	0.137	1.687	217.578
1170	63438	3.340	1.392	0.149	1.817	239.944

BIOGENIC SILICA (OPAL)

1174	63634	2.953	1.231	0.125	1.602	206.565
1180	63928	3.239	1.350	0.153	1.744	227.538
1184	64124	3.027	1.261	0.140	1.634	214.563
1190	64418	3.705	1.544	0.161	1.929	254.109
1194	64614	3.472	1.447	0.143	1.739	243.175
1200	64908	3.564	1.485	0.145	1.772	247.661
1204	65104	3.133	1.306	0.130	1.577	220.472
1210	65399	3.318	1.382	0.141	1.715	235.699
1214	65595	2.923	1.218	0.123	1.519	201.809
1220	65889	3.399	1.416	0.122	1.620	232.047
1224	66085	3.086	1.286	0.113	1.542	219.490
1230	66379	3.528	1.470	0.125	1.623	251.063
1234	66575	2.931	1.221	0.098	1.231	206.395
1240	66869	3.563	1.485	0.126	1.621	250.874
1244	67065	3.188	1.328	0.110	1.390	219.596
1250	67359	3.048	1.270	0.112	1.386	214.325
1254	67555	3.279	1.366	0.109	1.397	228.502
1260	67849	3.332	1.388	0.099	1.246	227.205
1264	68045	3.656	1.523	0.104	1.348	248.083
1270	68339	3.741	1.559	0.106	1.334	253.982
1274	68633	3.637	1.516	0.105	1.348	248.935
1280	69221	3.008	1.253	0.101	1.295	204.301
1284	69613	2.799	1.166	0.104	1.287	194.902
1290	70201	3.521	1.467	0.138	1.706	240.965
1294	70594	3.623	1.510	0.142	1.751	246.947
1300	71182	3.220	1.342	0.092	1.181	218.962
1304	71574	3.732	1.555	0.090	1.180	258.984
1310	72162	3.683	1.534	0.073	1.045	256.797
1314	72554	3.794	1.581	0.069	1.006	260.476
1320	73136	4.081	1.700	0.088	1.181	273.952
1324	73522	4.086	1.702	0.116	1.455	268.984
1330	74101	3.785	1.577	0.127	1.629	247.021
1334	74487	4.049	1.687	0.134	1.708	262.898
1340	75066	3.518	1.466	0.090	1.145	239.701
1344	75452	3.947	1.644	0.095	1.235	266.974
1350	76031	3.920	1.633	0.074	1.002	259.763
1354	76417	4.951	2.063	0.091	1.228	339.237
1360	76996	4.211	1.754	0.088	1.123	290.054
1364	77382	4.693	1.955	0.100	1.300	327.863
1370	77961	3.350	1.661	0.087	1.129	218.301
1374	78346	4.104	1.710	0.089	1.176	258.888
1380	78925	4.571	1.905	0.099	1.343	321.337
1384	79311	4.839	2.016	0.102	1.408	336.229
1390	79890	3.836	1.598	0.088	1.921	268.129
1394	80276	3.906	1.627	0.103	1.425	263.440
1400	80855	4.556	1.898	0.109	1.474	309.904
1404	81241	4.560	1.900	0.102	1.357	306.416
1410	81820	3.884	1.618	0.086	1.174	253.967
1414	82206	3.495	1.456	0.075	0.987	233.220
1420	82785	3.958	1.649	0.088	1.131	263.482
1424	83171	4.160	1.733	0.095	1.247	279.074
1430	83730	2.848	1.187	0.092	1.204	185.149
1434	84075	3.399	1.416	0.129	1.662	222.361
1440	84593	2.517	1.508	0.148	1.943	167.250
1444	84939	2.999	1.250	0.129	1.689	194.264
1450	85457	3.591	1.496	0.154	2.001	235.790
1454	85802	3.489	1.454	0.153	2.014	236.341
1460	86320	3.780	1.575	0.172	2.175	250.969
1464	86666	3.404	1.418	0.157	2.044	223.565
1470	87184	2.989	1.246	0.129	1.622	202.784
1474	87529	3.377	1.407	0.153	1.965	226.328
1480	88047	3.487	1.453	0.161	1.996	234.860
1484	88393	3.331	1.388	0.145	1.907	222.485
1490	88911	2.898	1.208	0.143	1.755	197.043
1494	89256	2.884	1.202	0.138	1.702	198.085
1500	89774	3.723	1.551	0.173	2.036	253.252
1504	90120	3.635	1.515	0.135	1.683	246.560
1510	90638	3.076	1.601	0.108	1.414	208.988
1514	90983	3.989	1.662	0.110	1.390	271.278
1520	91501	2.981	1.748	0.102	1.257	208.571
1524	91847	3.952	1.647	0.107	1.388	272.771
1530	92365	3.604	1.502	0.090	1.150	258.223
1534	92710	4.411	1.838	0.105	1.349	308.360

1540	93228	4.257	1.774	0.094	1.234	305.546
1544	93574	4.571	1.905	0.095	1.216	323.396
1550	94092	3.490	1.454	0.081	1.071	242.501
1554	94437	4.181	1.742	0.096	1.206	282.775
1560	94955	3.320	1.383	0.080	1.026	224.526
1564	95301	3.973	1.656	0.095	1.216	273.229
1570	95819	3.660	1.525	0.077	0.969	243.174
1574	96164	4.308	1.795	0.087	1.148	281.799
1580	96682	3.770	1.571	0.085	1.109	252.571
1584	97028	4.195	1.748	0.089	1.202	276.449
1590	97546	3.078	1.282	0.064	0.835	199.710
1594	97891	3.671	1.529	0.084	1.105	240.541
1600	98409	3.442	1.434	0.069	0.915	227.524
1604	98755	3.809	1.587	0.075	0.987	251.702
1610	99273	3.293	1.372	0.070	0.916	217.821
1614	99618	3.871	1.613	0.082	1.071	253.957
1620	100136	3.428	1.428	0.073	0.952	221.779
1624	100482	4.138	1.724	0.088	1.137	268.182
1630	101000	3.584	1.493	0.084	1.059	234.527
1634	101250	4.444	1.852	0.102	1.272	290.128
1640	101625	4.115	1.715	0.096	1.218	266.091
1644	101876	4.096	1.707	0.105	1.376	268.674
1650	102251	3.304	1.377	0.098	1.212	221.927
1654	102501	4.388	1.828	0.110	1.411	300.389
1660	102876	3.763	1.568	0.084	1.068	251.410
1664	103126	4.482	1.867	0.111	1.434	297.147
1670	103502	4.837	2.015	0.095	1.243	323.654
1674	103752	4.743	1.976	0.092	1.211	312.545
1680	104127	4.329	1.804	0.073	1.014	302.026
1684	104377	4.349	1.812	0.069	0.973	296.794
1690	104753	4.014	1.673	0.061	0.855	267.097
1694	105003	5.219	2.175	0.082	1.152	352.968
1700	105378	4.149	1.729	0.064	0.882	284.064
1704	105628	4.367	1.820	0.069	0.956	296.030
1710	106004	4.056	1.690	0.071	0.968	274.415
1714	106254	3.785	1.577	0.099	1.291	252.771
1720	106629	3.361	1.400	0.115	1.477	223.506
1724	106879	3.650	1.521	0.123	1.552	252.646
1730	107254	3.208	1.336	0.111	1.395	218.552
1734	107505	3.212	1.339	0.114	1.412	222.455
1740	107880	3.004	1.252	0.096	1.213	212.076
1744	108130	3.048	1.270	0.074	0.968	217.398
1750	108533	3.096	1.290	0.055	0.735	213.987
1754	108801	3.248	1.353	0.055	0.749	221.660
1760	109203	3.023	1.260	0.057	0.768	208.809
1764	109472	3.368	1.404	0.063	0.833	234.079
1770	109874	3.134	1.306	0.063	0.837	220.273
1774	110143	3.120	1.300	0.067	0.854	210.426
1780	110545	2.844	1.185	0.090	1.095	183.735
1784	110813	3.239	1.350	0.125	1.541	214.340
1790	111216	2.954	1.231	0.106	1.309	199.798
1794	111484	3.054	1.272	0.131	1.522	200.755
1800	111887	3.172	1.322	0.126	1.533	211.203
1804	112155	3.107	1.294	0.112	1.307	206.723
1810	112558	2.666	1.237			180.076
1814	112826	4.723	1.196			313.098
1820	113229	2.555	1.246			170.743
1824	113497	3.254	1.356			217.524
1830	113899	2.587	1.240			164.043
1834	114168	3.009	1.254			208.195
1840	114570	2.743	1.143			185.997
1844	114839	3.172	1.322			216.602
1850	115241	2.223	1.106			151.238
1854	115509	3.001	1.250			200.764
1860	115912	2.735	1.139			182.854
1864	116180	3.350	1.396			225.280
1870	116583	1.997	1.141			129.935
1874	116851	2.651	1.105			173.061
1880	117254	2.234	0.931			145.638
1884	117522	2.867	1.195			188.184
1890	117925	2.659	1.108			174.113
1894	118193	3.469	1.445			224.792
1900	118595	3.141	1.309			193.036

BIOGENIC SILICA (OPAL)

1904	118864	3.443	1.434	216.548
1910	119266	3.083	1.285	197.149
1914	119535	3.474	1.447	222.395
1920	119937	3.220	1.342	207.034
1924	120205	3.697	1.540	240.044
1930	120608	3.568	1.486	231.399
1934	120876	3.501	1.459	231.341
1940	121279	3.112	1.297	200.235
1944	121547	3.442	1.434	219.292
1950	121950	3.303	1.376	214.052
1954	122218	3.842	1.601	249.740
1960	122621	2.721	1.134	181.983
1964	122889	3.422	1.426	225.849
1970	123291	2.672	1.114	176.573
1974	123560		1.155	
1980	123962	2.784	1.160	188.367
1984	124231		1.269	
1990	124633	2.459	1.163	160.711
1994	124901		1.281	
2000	125304	2.771	1.154	186.179
2004	125572		1.280	
2010	125975	3.090	1.287	198.527
2014	126243		1.212	
2020	126646	2.653	1.105	170.625
2024	126914		1.223	
2030	127317	2.567	1.069	162.772
2034	127585		1.271	
2040	127987	2.634	1.098	167.242
2044	128256		1.265	
2050	128658	2.819	1.174	178.741
2054	128927		1.477	
2060	129329	3.406	1.419	225.831
2064	129597		1.348	
2070	130000	2.998	1.249	193.115
2074	130326		1.351	
2080	130814	3.132	1.305	203.967
2084	131140		1.657	
2090	131628	3.489	1.456	228.246
2094	131953		1.720	

STABLE CARBON and OXYGEN ISOTOPES

Core MD02-2519

Depth (cm) non corrected	Depth (cm) corrected	Age cal years BP	Uvigerina spp		B. tenuata		B. subadvena		B. argentea	
			d13C	d18O	d13C	d18O	d13C	d18O	d13C	d18O
0	0	2365								
9	9	2522	-0.51	3.00	-1.24	2.95	-0.66	2.90	-0.60	3.00
15	15	2641	-0.48	3.06	-1.20	2.28			-0.74	3.13
20	20	2739	-0.63	2.94	-1.30	3.00			-1.00	2.96
24	24	2818	-0.68	2.95	-1.35	2.85			-0.71	3.01
40	40	3133	-0.59	2.95	-1.24	2.81			-0.65	2.99
50	50	3330	-0.44	3.05	-1.24	2.95			-0.53	2.97
60	60	3526	-0.54	2.94	-1.16	2.94			-0.55	3.03
70	70	3723	-0.55	2.92	-1.08	2.88			-0.43	3.03
80	80	4026	-0.58	2.96	-0.93	2.89			-0.33	3.00
90	90	4399	-0.50	2.86	-1.00	2.81			-0.40	3.07
100	100	4773	-0.66	2.77	-1.04	2.81			-0.47	3.13
120	120	5519	-0.42	2.95	-1.02	2.82			-0.30	3.01
130	130	5893	-0.48	3.29	-1.12	2.93			-0.45	3.05
140	140	6266	-0.58	3.12	-1.15	3.04	-0.84	3.25	-0.47	3.04
150	150	6793	-0.78	2.77	-1.10	2.96	-0.73	3.14	-0.47	3.13
164	164	7532	-0.49	3.18	-1.40	2.95	-0.77	3.12	-0.51	3.09
180	180	8376	-0.48	3.02	-1.40	3.11	-0.72	3.27	-0.66	3.13
190	190	8903	-0.52	3.30	-1.42	3.10	-0.66	3.33	-0.62	3.35
194	194	9114	-0.62	3.20	-1.53	3.04	-0.67	3.26	-0.63	3.25
200	200	9410	-0.96	3.27	-1.48	3.15				
204	204	9607	-0.63	3.21	-1.65	3.25	-0.95	3.45	-0.50	3.36
206	206	9705	-0.86	3.22						
208	208	9804	-0.60	3.29						
210	210	9902	-0.73	3.42						
214	214	10099	-0.81	3.15	-1.70	3.24				
216	216	10198	-0.82	3.46						
218	218	10324	-0.65	3.35						
220	220	10451	-0.74	3.23	-1.95	3.41	-1.62	3.41	-0.74	3.42
224	224	10703	-0.78	3.31						
226	226	10829		3.29					-0.72	3.29
228	228	10956	-0.78	3.31						
230	230	11082	-0.99	3.54	-2.44	3.26	-1.59	3.53	-0.79	3.43
234	234	11292	-0.76	3.69	-2.25	3.53	-1.31	3.57	-0.81	3.52
236	236	11396	-0.73	3.62						
238	238	11501	-0.64	3.52						
240	240	11606	-0.70	4.11						
242	242	11711	-0.86	3.69						
244	244	11815	-0.83	3.84	-2.11	3.94	-1.71	4.13	-1.00	3.71
246	246	11920	-0.80	3.72						
248	248	12025	-0.78	4.18						
250	250	12130	-0.83	3.98	-1.90	3.73				
254	254	12339	-0.85	3.92						
256	256	12444	-0.71	4.10						
258	258	12549	-1.01	3.97						
260	260	12654	-0.64	3.84	-2.08	4.00	-1.68	4.04	-0.88	3.73
264	264	12863	-0.79	3.93						
266	266	12968	-0.85	3.78						
268	268	13073	-1.02	3.87						
270	270	13178	-0.78	3.72	-1.74	3.68			-0.81	3.80
272	272	13282	-0.92	3.65						
274	274	13387	-0.96	3.60	-1.89	3.80			-0.73	3.80
276	276	13492	-0.67	3.66						
278	278	13597	-0.76	3.80						
280	280	13701	-0.79	3.68						
282	282	13806	-0.79	3.88						
284	284	13911	-0.87	3.72	-2.23	3.91	-1.75	3.93	-1.10	4.04
286	286	13969	-0.85	3.89						
288	288	14026	-0.99	3.82						
290	290	14084	-0.94	3.87	-2.58	3.92	-1.63	3.94	-0.93	3.98
292	292	14182	-0.79	4.01	-2.25	3.93	-1.29	4.16	-0.70	4.05
296	296	14378	-0.94	3.94						
298	298	14475	-0.80	4.20						
304	304	14769	-0.99	4.13	-1.54	4.00				
308	308	14965	-0.74	4.10						
310	310	15063	-0.83	4.19	-1.58	4.06			-0.76	4.08
312	312	15160	-0.67	4.43						
314	314	15258	-0.90	4.09						
320	320	15552	-0.82	4.44	-2.14	4.46			-0.92	4.40
326	326	15845	-0.77	4.41	-2.24	4.04				
328	328	15943	-0.80	4.32						
332	332	16139	-0.55	4.55						
338	338	16508	-0.88	4.37						
340	340	16631	-0.78	4.46						
352	352	17368	-1.00	4.50	-2.28	4.58			-1.05	4.59
360	360	17860	-0.74	4.44						
364	364	18106	-0.69	4.40						
370	370	18475	-0.95	4.49	-2.91	4.33				
374	374	18693	-0.86	4.67						
384	384	19238	-0.87	4.64						
394	394	19783	-0.88	4.50						
400	400	20109	-0.82	4.59	-2.30	4.42				

404	404	20327	-0.87	4.79				
414	414	20872	-0.85	4.55				
420	420	21199	-1.00	4.59	-2.36	4.40		
424	424	21417	-0.91	4.61				
432	432	21755	-0.97	4.47	-2.13	4.55	-1.05	4.49
434	434	21839	-0.86	4.89				
440	440	22093	-0.82	4.77				
450	450	22515	-1.02	4.35	-2.05	4.32		
454	454	22684	-0.69	4.20				
464	464	23107	-0.88	4.77				
466	466	23191	-0.66	4.79				
468	468	23339	-0.83	4.77				
474	474	23784	-0.84	4.53	-2.47	4.49		
480	480	24229	-0.73	4.88				
484	484	24526	-0.70	4.66				
488	488	24823	-0.87	4.63				
490	490	24971	-0.74	4.49	-2.27	4.34		
494	494	25268	-0.77	4.73				
500	500	25713	-0.88	4.57	-2.18	4.32		
504	504	25886	-0.93	4.36	-1.52	4.44	-0.97	4.54
508	508	26060	-0.73	4.49	-1.75	4.54		
512	512	26233	-0.81	4.93				
514	514	26320	-0.75	4.43	-1.52	4.44		
520	520	26579	-0.85	4.40	-1.51	4.30		
526	526	26839	-0.74	4.51				
534	534	27186	-0.67	4.59	-1.59	4.39		
540	540	27446	-0.67	4.73	-2.47	4.44		
546	546	27706	-0.66	4.92				
554	554	28052	-0.79	4.45	-1.95	4.47		
558	558	28226	-0.85	4.48	-1.81	4.36		
560	560	28293	-0.67	4.58				
564	564	28427	-0.61	4.62	-2.56	4.10		
566	566	28495	-0.80	4.35				
570	570	28629	-0.91	4.28	-2.78	4.09		
574	574	28763	-0.65	4.35	-2.39	4.29		
576	576	28831	-0.56	4.37	-2.05	4.40		
580	580	29060	-0.57	4.59				
584	584	29289	-0.78	4.48	-1.27	4.38		
586	586	29403	-0.66	4.75				
590	590	29632	-0.72	4.47	-1.46	4.24	-0.70	4.28
594	594	29861	-0.62	4.40	-1.07	4.43		
596	596	29975	-0.54	4.35				
604	604	30433	-0.47	4.65	-2.01	4.35		
606	606	30548	-0.52	4.66	-1.59	4.48		
614	614	31061	-0.42	4.51	-1.76	4.28		
616	616	31189	-0.52	4.76				
624	624	31702	-0.69	4.54	-1.71	4.37		
634	634	32343	-0.55	4.44	-1.73	4.35		
644	644	32878	-0.40	4.34	-1.36	4.29		
652	652	33285	-0.51	4.30	-1.76	4.39		
660	660	33693	-0.76	4.25	-1.41	4.23		
662	662	33794	-0.61	4.30	-1.23	4.30		
676	676	34507	-0.47	4.34	-1.47	4.23		
680	680	34751	-0.56	4.25	-1.59	4.24	-0.87	4.29
684	684	34996	-0.48	4.26	-1.50	4.25		
694	694	35608	-0.81	4.19				
704	704	36219	-0.56	4.47	-1.59	4.33		
714	714	36831	-0.78	4.44	-1.48	4.26		
724	724	37442	-0.66	4.35	-1.59	4.07	-0.99	4.13
726	726	37565	-0.67	4.56	-1.38	4.30		
734	734	38054	-0.79	4.22	-1.98	4.04		
736	736	38176	-0.72	4.50	-1.86	3.99		4.06
744	744	38666	-0.53	4.14	-1.73	4.06		
750	750	39033	-0.64	4.43	-1.51	4.20	-0.72	4.10
755	755	39339	-0.65	4.27	-1.54	4.04		
765	765	39882	-0.46	4.47	-1.85	3.99		
775	775	40396	-0.67	4.48	-1.91	4.02		
780	780	40654	-0.61	4.51	-1.65	4.17	-0.86	4.26
785	785	40911	-0.67	4.26	-1.92	3.94		
791	791	41219	-0.73	4.24				
795	795	41425	-0.69	4.40	-1.70	4.05		
801	801	41734	-0.82	4.29				
805	805	41940	-0.87	4.41	-1.86	4.15		
811	811	42248	-0.66	4.16				
815	815	42454	-0.97	4.31	-1.49	4.14		
821	821	42763	-0.88	4.10				
825	825	42968	-0.81	4.17	-1.51	4.13		
831	831	43277	-0.65	4.20				
835	835	43483	-0.46	4.39	-1.33	4.04		
841	841	43791	-0.59	4.32				
845	845	43997	-0.74	4.10	-1.49	4.13		
851	851	44306	-0.58	4.24	-1.38	4.04	-0.84	4.22
855	855	44511	-0.75	4.34	-1.64	4.03		
861	861	44820	-0.73	4.17				
865	865	45026	-0.77	4.33	-2.11	4.01		
871	871	45360	-0.70	4.28	-1.82	4.00	-1.02	4.08
875	875	45670	-0.59	4.29	-1.45	3.86		

881	881	46134	-0.66	4.21	-1.49	4.03			-0.79	4.05
885	885	46443	-0.62	4.22	-1.58	3.87				
891	891	46907	-0.71	4.04						
895	895	47216	-0.55	4.39	-1.69	4.01				
901	901	47680	-0.76	4.12						
905	905	47989	-0.70	4.33	-1.53	4.19				
911	911	48453	-0.59	4.30						
915	915	48763	-0.77	4.26	-1.40	4.05				
921	921	49227	-0.55	4.33	-1.67	3.92				
925	925	49536	-0.67	4.17						
931	931	50000	-0.70	4.13						
935	935	50309	-0.70	4.12	-1.55	4.05				
941	941	50773	-0.59	4.27						
945	945	51082	-0.77	4.31	-1.69	4.14				
951	951	51546	-0.65	4.08	-1.48	4.06			-1.08	4.14
955	955	51856	-0.57	4.37	-1.57	4.18				
961	961	52252	-0.68	4.17						
965	965	52506	-0.65	4.29	-1.93	3.81				
971	971	52889	-0.63	4.16						
975	975	53144	-0.95	4.10	-1.43	3.85				
979	979	53398	-0.53	4.24	-1.46	3.94			-0.86	3.96
981	981	53526	-0.54	4.06						
985	985	53781	-0.89	4.10	-1.76	3.74				
991	991	54163	-0.68	4.12						
995	995	54418	-0.83	4.23	-1.72	3.97				
1001	1001	54800	-0.55	4.19						
1005	1005	55055	-0.93	3.93						
1011	1011	55437	-0.68	4.02						
1015	1015	55692	-0.79	4.25						
1017	1017	55820	-0.92	4.20	-1.71	4.05			-1.06	4.12
1021	1021	56075	-0.98	4.19						
1025	1025	56329	-1.05	3.93						
1031	1031	56712	-1.11	4.01						
1035	1035	56967	-0.92	3.97						
1041	1041	57349	-0.86	4.01						
1045	1045	57586	-1.03	4.04						
1049	1049	57770	-0.98	4.10	-2.25	3.97	-1.44	4.04	-1.04	4.07
1055	1055	58047	-0.83	4.03						
1065	1065	58507	-0.99	3.98						
1075	1075	58968	-0.88	4.07						
1081	1081	59244	-1.00	4.18	-2.04	4.07			-1.05	3.96
1085	1085	59429	-0.91	4.32						
1095	1095	59889	-0.84	4.28						
1105	1105	60350	-0.78	4.12						
1115	1115	60811	-0.63	4.29						
1119	1119	60995	-0.81	4.25	-2.04	4.15			-0.78	4.37
1125	1125	61271	-0.65	4.45						
1135	1135	61732	-0.82	4.18	-2.33	4.09			-1.12	4.23
1145	1145	62213	-0.69	4.21						
1155	1155	62703	-0.82	4.42						
1165	1165	63193	-0.80	4.23						
1169	1169	63389	-0.94	4.07	-1.75	3.98			-1.04	4.19
1175	1175	63683	-0.76	4.12						
1179	1179	63879	-0.98	4.14	-1.59	3.99			-0.99	4.20
1185	1185	64173	-0.99	4.52						
1195	1195	64663	-0.95	4.23						
1199	1199	64859	-0.92	4.31	-1.72	4.22			-1.00	4.31
1205	1205	65154	-0.91	4.15						
1211	1211	65448	-0.80	4.33	-1.63	4.16			-0.92	4.28
1215	1215	65644	-0.81	4.34						
1225	1225	66134	-0.91	4.57						
1235	1235	66624	-0.84	4.26						
1245	1245	67114	-0.82	4.09						
1251	1251	67408	-0.80	4.08					-0.84	4.23
1255	1255	67604	-0.65	4.21						
1265	1265	68094	-0.66	4.30						
1275	1275	68731	-0.83	4.07						
1281	1281	69319	-0.63	4.02	-1.69	3.89			-0.89	3.88
1285	1285	69711	-0.66	3.89						
1291	1291	70299	-0.46	4.10	-1.48	3.76				
1295	1295	70692	-0.56	3.91						
1301	1301	71280	-0.71	4.12	-1.25	3.78			-0.74	3.80
1305	1305	71672	-0.70	4.37						
1321	1321	73232	-0.53	3.96					-0.90	3.79
1325	1325	73618	-0.52	3.79						
1335	1335	74583	-0.62	3.59						
1345	1345	75548	-0.54	3.86						
1365	1365	77478	-0.47	3.68						
1401	1401	80952	-0.59	3.65	-1.38	3.45			-0.72	3.77
1415	1415	82303	-0.59	3.85						
1421	1421	82882	-0.84	3.54	-1.42	3.49				
1425	1425	83268	-0.77	3.73						
1435	1435	84161	-0.75	3.60						
1441	1441	84680	-0.85	3.53	-1.77	3.39				
1451	1451	85543	-0.71	3.71	-1.46	3.41				
1455	1455	85888	-0.78	3.70						
1481	1481	88134	-0.61	3.62	-1.66	3.64				

1484	1484	88393	-0.58	3.66			
1501	1501	89861	-0.55	3.75			
1505	1505	90206	-0.60	3.81	-1.47	3.62	
1517	1517	91242	-0.67	3.99			
1535	1535	92797	-0.79	4.06			
1541	1541	93315	-0.60	4.02			
1575	1575	96251	-0.62	3.98			
1581	1581	96769	-0.53	3.85			
1601	1601	98496	-0.52	3.65	-1.17	3.58	
1605	1605	98841	-0.51	3.68			
1615	1615	99705	-0.57	3.78			
1621	1621	100223	-0.55	3.77	-1.16	3.55	
1645	1645	101938	-0.48	3.57	-1.31	3.55	
1655	1655	102564	-0.69	3.60			
1661	1661	102939	-0.57	3.69	-1.38	3.47	
1671	1671	103564	-0.76	3.71	-1.69	3.44	
1675	1675	103814	-0.61	3.77			
1725	1725	106942	-0.60	3.66			
1731	1731	107317	-0.67	3.73	-1.57	3.43	
1745	1745	108197	-0.48	3.74			
1751	1751	108600	-0.44	3.77	-1.11	3.65	
1801	1801	111954	-0.68	3.89			
1805	1805	112222	-0.53	3.83	-1.55	3.70	
1831	1831	113966	-0.60	4.02	-1.49	3.58	
1851	1851	115308	-0.55	3.67	-1.48	3.42	
1881	1881	117321	-0.90	3.34	-1.38	3.12	
1901	1901	118662	-1.01	3.15	-1.97	3.09	
1931	1931	120675	-1.07	3.33	-1.93	3.09	
1945	1945	121614	-0.87	3.34	-1.73	3.19	
1957	1957	122419	-0.90	3.08	-1.41	2.85	
2005	2005	125639	-0.78	2.90	-1.75	3.07	
2025	2025	126981	-1.09	4.03	-2.01	3.33	
2035	2035	127652	-1.29	3.82	-2.08	3.38	
2055	2055	128994	-1.46	3.68	-2.41	3.88	
2071	2071	130067	-1.41	3.76	-2.37	3.72	
2085	2085	131006	-1.05	3.68	-2.13	3.81	
2105	2105	132849	-1.21	4.06	-2.23	4.24	
2125	2125	134477	-1.20	4.38	-2.84	4.01	
2141	2141	135779	-0.94	4.48	-1.73	4.35	
2201	2177	137923	-1.21	4.63	-2.82	4.49	
2225	2201	138978	-1.59	4.63	-2.83	4.36	
2241	2217	139681	-1.58	4.55	-2.05	4.43	
2271	2247	140999	-1.65	4.59	-2.23	4.37	
2281	2257	141439	-1.17	4.33	-1.96	4.43	
2301	2275	142230	-1.34	4.44	-2.16	4.39	
2351	2327	144515	-1.13	4.44	-1.55	4.35	
2375	2351	145570	-1.34	4.43	-1.95	4.22	
2401	2377	146712	-1.11	4.08	-1.74	4.25	
2415	2391	147328	-1.25	4.34	-1.66	4.33	
2451	2425	148822	-0.96	4.37	-1.68	4.22	
2501	2475	151423	-1.25	4.52	-1.93	4.30	
2541	2515	154131	-1.26	4.40	-1.89	4.28	
2549	2523	154672	-1.31	4.18	-1.64	4.31	
2581	2555	156839	-1.32	4.20	-1.72	4.11	
2603	2577	158328	-1.28	4.47	-1.98	4.16	
2639	2613	160765	-1.47	4.00	-2.18	3.92	
2645	2619	161172	-1.14	4.18	-2.49	4.16	
2671	2645	162932	-1.06	4.13			
2761	2735	169025	-0.91	3.94	-2.12	3.94	
2801	2775	171733	-1.26	4.14	-2.32	3.96	
2821	2795	173087	-1.20	4.14	-1.81	3.90	
2881	2851	175766	-1.10	4.07		3.97	
2975	2911	177356	-1.00	4.27	-2.37	3.95	
2990	2921	177621	-1.22	4.33	-2.11	4.02	
3091	2949	178363	-1.06	4.03	-2.12	4.00	
3141	2991	179476	-1.19	3.96	-1.98	3.72	
3161	3011	180006	-1.38	4.07	-1.95	3.87	
3201	3051	181067	-0.96	4.20	-2.20	4.23	
3211	3061	181332	-1.05	4.24	-2.41	4.19	
3251	3101	182392	-1.06	4.17	-2.05	4.24	
3291	3141	183452	-0.98	4.27	-2.10	4.20	
3311	3161	183982	-0.88	4.32	-1.78	4.16	
3351	3201	185042	-1.15	4.29	-1.85	4.24	
3401	3251	186367	-1.11	4.16	-1.82	4.05	
3445	3295	187534	-0.91	4.36	-1.81	4.06	
3471	3321	188223	-1.11	4.20	-2.04	3.90	
3501	3351	189018	-1.01	4.16	-1.76	3.97	
3531	3381	189813	-0.92	4.20	-1.93	4.01	
3551	3401	190343	-0.98	4.28	-2.09	4.04	
3581	3419	190820	-1.03	4.10	-1.96	3.97	
3601	3439	191350	-1.06	4.06	-2.12	4.00	
3641	*3479*	*192411*	*-1.04*	*4.22*	*-1.83*	*3.98*	*
3671	*3509*	*193206*	*-0.77*	*4.31*	*-1.75*	*3.98*	*
3691	*3529*	*193736*	*-0.85*	*4.31*	*-1.78*	*3.94*	*
3741	*3579*	*195061*	*-0.92*	*4.29*	*-1.81*	*3.90*	*
3751	*3589*	*195326*	*-0.93*	*4.24*	*-1.75*	*3.82*	*
3761	*3599*	*195591*	*-1.12*	*4.10*	*-1.90*	*3.91*	*

3791	3629	196386	-0.98	4.38	-1.66	3.97	*
3801	3639	196651	-1.04	4.34	-1.81	3.90	*
3811	3649	196916	-0.89	4.30	-1.77	3.89	*
3831	3669	197446	-0.79	4.43	-1.80	3.99	*
3871	3695	198136	-0.97	4.30	-1.73	4.05	*
3891	3715	198666	-0.98	4.29	-1.74	4.08	*
3901	3725	198931	-0.90	4.35	-1.62	4.01	*
3931	3755	199726	-1.07	4.37	-1.85	3.98	*
3941	3765	199991	-1.01	4.43	-1.77	3.96	*
3961	3785	200521	-0.86	4.43	-1.64	3.99	*
3981	3805	201051	-0.85	4.43	-1.73	3.75	*
3991	3815	201316	-0.99	4.24	-1.74	3.87	*

* data not used

Appendix C

Data from other Cores

Core MD02-2518

Core MD02-2520

Core MD02-2524

Core PC08

Core NH15P

Note: Physical Parameters and Diffuse Spectral Reflectivity data of the cores collected during the MONA Cruise, have been already published by Beaufort (2002) @ http://www.pangaea.de/

Core MD02-2518

Depth (cm) (corrected)	Age cal yrs BP	Elemental Comp (% C)	Depth (cm) (corrected)	Age cal yrs BP	DSR a* (red/green)
9	1200	7.256	10	1242	0.475
10	1242	7.424	12	1326	0.553
11	1284	7.536	14	1410	0.520
12	1326	7.758	16	1493	0.512
13	1368	7.097	18	1577	1.023
14	1410	7.300	20	1661	0.372
15	1452	7.312	22	1745	0.176
16	1493	7.158	24	1829	0.452
17	1535	7.522	26	1912	0.082
18	1577	7.332	28	1996	0.375
19	1619	7.501	30	2080	0.418
20	1661	6.893	32	2164	0.363
21	1703	7.312	34	2248	0.506
22	1745	7.263	36	2331	0.385
23	1787	7.709	38	2415	0.371
24	1829	7.764	40	2499	0.383
25	1871	7.511	42	2583	0.321
26	1912	7.597	44	2667	0.883
27	1954	7.628	46	2750	0.748
28	1996	7.508	48	2834	0.275
29	2038	7.873	50	2918	0.311
30	2080	7.850	52	3002	0.302
31	2122	7.731	54	3086	0.357
32	2164	7.850	56	3169	0.371
33	2206	7.220	58	3253	0.179
34	2248	6.986	60	3337	0.316
35	2290	7.916	62	3421	0.268
36	2331	8.136	64	3505	0.322
37	2373	8.006	66	3588	0.396
38	2415	7.453	68	3672	0.616
39	2457	7.446	70	3756	0.187
40	2499	8.117	72	3840	0.254
41	2541	8.675	74	3924	0.261
42	2583	8.162	76	4007	0.520
43	2625	7.419	78	4091	0.353
44	2667	7.754	80	4175	0.582
45	2709	8.347	82	4259	0.423
46	2750	8.751	84	4343	0.560
47	2792	8.647	86	4426	0.328
48	2834	8.306	88	4510	0.254
49	2876	7.815	90	4594	0.265
50	2918	7.768	92	4678	0.293
51	2960	8.277	94	4762	0.276
52	3002	7.642	96	4845	0.702
53	3044	8.138	98	4929	0.222
54	3086	7.920	100	5013	0.192
55	3128	8.018	102	5097	0.241
56	3169	7.380	104	5181	0.261
57	3211	7.614	106	5264	0.135
58	3253	7.548	108	5348	0.259
59	3295	8.091	110	5432	0.160
60	3337		112	5516	0.345
61	3379	7.319	114	5600	0.280
62	3421	7.273	116	5683	-0.203
63	3463	6.459	118	5767	0.210
64	3505	8.715	120	5851	0.283
65	3547	7.336	122	5935	0.192
66	3588	6.743	124	6019	0.215
67	3630	7.032	126	6102	0.174
68	3672	7.225	128	6186	0.318
69	3714	7.997	130	6270	0.244
70	3756	7.756	132	6354	0.261
71	3798	7.805	134	6438	0.246
72	3840	7.895	136	6521	0.230
73	3882	7.546	138	6605	0.257
74	3924	7.450	140	6689	0.541
75	3966	7.355	142	6789	
76	4007	7.364	144	6890	

77	4049	7.128	146	6990	
78	4091	7.001	148	7091	
79	4133	7.059	150	7191	
80	4175	7.053	152	7291	0.154
81	4217	7.053	154	7392	0.209
82	4259	7.043	156	7492	0.226
83	4301	7.190	158	7593	0.039
84	4343	7.030	160	7693	0.156
85	4385	7.301	162	7793	0.573
86	4426	7.416	164	7894	0.276
87	4468	7.572	166	7994	0.181
88	4510	6.953	168	8095	0.223
89	4552	7.307	170	8195	0.227
90	4594	7.200	172	8295	0.277
91	4636	7.326	174	8396	0.118
92	4678	7.284	176	8496	0.129
93	4720	7.452	178	8597	0.255
94	4762	7.324	180	8697	0.043
95	4804	7.200	182	8797	0.300
96	4845	8.527	184	8898	0.315
97	4887	7.440	186	8998	0.200
98	4929	7.496	188	9099	0.276
99	4971	7.651	190	9199	0.251
100	5013	7.671	192	9299	0.218
101	5055	7.785	194	9400	0.135
102	5097	8.176	196	9500	0.224
103	5139	7.422	198	9601	0.150
104	5181	7.716	200	9701	0.338
105	5223	7.582	202	9801	0.040
106	5264	7.298	204	9902	0.295
107	5306	7.175	206	10002	0.227
108	5348	7.164	208	10103	0.061
109	5390	7.234	210	10203	0.120
110	5432	7.193	212	10303	0.306
111	5474	6.907	214	10404	-0.064
112	5516	6.759	216	10504	-0.070
113	5558	6.096	218	10605	-0.120
114	5600	5.156	220	10705	-0.316
115	5642	3.748	222	10805	-0.099
116	5683	8.242	224	10906	0.035
117	5725	8.296	226	11006	-0.086
118	5767	7.903	228	11107	-0.027
120	5851	8.249	230	11207	0.006
121	5893	8.225	232	11378	0.172
122	5935	8.010	234	11548	-0.011
123	5977	8.325	236	11719	0.174
124	6019	8.265	238	11890	-0.365
125	6061	8.494	240	12061	-0.331
126	6102	8.503	242	12231	-0.409
127	6144	8.325	244	12402	-0.352
128	6186	7.977	246	12573	-0.301
129	6228	7.482	248	12744	-0.295
130	6270	8.158	250	12914	-0.283
134	6438	8.101	252	13085	-0.226
135	6480	8.058	254	13256	-0.323
136	6521	8.234	256	13427	-0.265
137	6563	8.724	258	13597	-0.343
138	6605	7.597	260	13768	-0.646
139	6647	7.554	262	14193	-0.417
140	6689	7.891	264	14619	-0.040
141	6739	7.778	266	15044	-0.143
142	6789	7.589	268	15469	-0.316
143	6840	8.264	270	15894	-0.345
144	6890	8.067	272	16320	-0.726
145	6940	8.446	274	16745	-0.887
146	6990	8.200	276	17170	-0.751
147	7040	8.386	278	17595	-0.737
148	7091	8.464	280	18021	-0.806
149	7141	8.437	282	18446	-0.851
150	7191	6.889	284	18871	-0.326
152	7291	7.166	286	19384	-0.728
154	7392	7.879	288	19898	-0.852
156	7492	7.573	290	20411	-0.733

158	7593	7.613	292	20924	-0.837
160	7693	7.302	294	21438	-0.712
162	7793	6.889	296	21951	-0.884
164	7894	6.882	298	22464	-0.808
166	7994	7.000	300	22978	-0.799
168	8095	7.560	302	23491	-0.783
170	8195	7.293	304	24004	-0.743
172	8295	6.808	306	24518	-0.657
174	8396	6.771	308	25031	-0.603
176	8496	6.942	310	25544	-0.699
178	8597		312	26058	-0.693
180	8697	6.659	314	26571	-0.692
182	8797	6.618	316	27084	-0.686
184	8898	6.467	318	27597	-0.509
186	8998	6.729	320	28111	-0.480
188	9099	6.838	322	28624	-0.588
190	9199	6.742	324	29137	-0.682
192	9299	6.594	326	29651	-0.542
194	9400	6.577	328	30164	-0.555
196	9500	6.506	330	30677	-0.701
198	9601	6.724	332	31191	-0.439
200	9701	6.667	334	31704	-0.393
202	9801	6.583	336	32217	-0.579
204	9902	6.432	338	32731	-0.384
206	10002	6.317	340	33244	-0.387
208	10103	3.055	342	33428	-0.735
210	10203	5.607	344	33611	-0.432
211	10253	5.832	346	33795	-0.574
212	10303	4.616	348	33979	-0.548
213	10354	1.567	350	34162	-0.339
214	10404	4.367	352	34346	-0.294
215	10454	4.243	354	34530	-0.755
216	10504	4.405	356	34713	-0.425
217	10554	4.228	358	34897	-0.371
218	10605	3.829	360	35081	-0.347
219	10655	1.553	362	35264	-0.372
220	10705	1.101	364	35448	-0.306
221	10755	2.143	366	35632	-0.373
222	10805	4.173	368	35815	-0.226
224	10906	4.986	370	35999	-0.294
226	11006	4.893	372	36183	-0.347
228	11107	4.974	374	36496	-0.288
230	11207	5.047	376	36809	-0.504
232	11378	4.869	378	37122	-0.318
234	11548	4.457	380	37436	-0.213
236	11719	4.622	382	37749	-0.452
238	11890	3.275	384	38062	-0.306
240	12061	1.955	386	38375	-0.555
242	12231	2.230	388	38689	-0.708
244	12402	3.126	390	39002	-0.430
246	12573	3.417	392	39315	-0.422
248	12744	3.738	394	39628	-0.479
250	12914	3.535	396	39941	-0.507
252	13085	3.752	398	40255	-0.463
254	13256	3.377	400	40568	-0.411
256	13427	3.015	402	40881	-0.406
258	13597	3.414	404	41194	-0.221
260	13768	2.403	406	41508	-0.303
261	13981	2.976	408	41821	-0.340
262	14193	2.421	410	42134	-0.368
263	14406	1.506	412	42447	-0.458
264	14619	2.978	414	42760	-0.393
265	14831	2.152	416	43074	-0.381
266	15044	3.160	418	43387	-0.288
267	15256	3.003	420	43700	-0.509
268	15469	2.700	422	44013	-0.307
269	15682	1.858	424	44051	-0.368
272	16320	2.213	426	44088	-0.329
274	16745	1.051	428	44125	-0.618
276	17170	1.200	430	44163	-0.307
278	17595	1.197	432	44200	-0.667
280	18021	2.292	434	44237	-0.470
282	18446	1.203	436	44275	-0.386

284	18871	1.206	438	44312	-0.389
286	19384	1.156	440	44349	-0.397
288	19898	1.212	442	44387	-0.417
290	20411	1.144	444	44424	-0.286
292	20924	1.173	446	44461	-0.463
294	21438	1.127	448	44499	-0.418
296	21951	1.182	450	44536	-0.342
298	22464	1.130	452	44574	-0.208
300	22978	1.207	454	44611	-0.066
302	23491	1.231	456	44648	-0.298
304	24004	1.227	458	44686	-0.118
306	24518	1.189	460	44723	-0.250
308	25031	1.205	462	44760	-0.192
310	25544	0.999	464	44798	-0.296
312	26058	1.161	466	44835	-0.196
314	26571	1.137	468	44872	-0.328
316	27084	1.450	470	44910	-0.139
318	27597	1.290	472	44947	-0.356
320	28111	1.476	474	44984	-0.269
322	28624	1.525	476	45022	-0.161
324	29137	1.397	478	45059	-0.333
326	29651	1.462	480	45096	-0.250
328	30164	1.604	482	45134	-0.323
330	30677	1.724	484	45171	-0.281
332	31191	1.807	486	45208	-0.309
334	31704	1.769	488	45246	-0.184
336	32217	1.837	490	45283	-0.392
338	32731	1.896	492	45416	-1.040
340	33244	1.886	494	45549	-0.344
342	33428	1.501	496	45682	-0.589
344	33611	2.022	498	45815	-0.590
346	33795	1.939	500	45948	-0.690
348	33979	1.812	502	46081	-0.444
350	34162	1.762	504	46214	-0.420
352	34346	2.223	506	46347	-0.517
354	34530	1.464	508	46480	-0.516
356	34713	1.978	510	46613	-0.316
358	34897	2.085	512	46746	-0.485
360	35081	2.192	514	46879	-0.398
362	35264	2.148	516	47012	-0.453
364	35448	2.660	518	47145	-0.473
366	35632	2.354	520	47278	-0.349
368	35815	2.299	522	47411	-0.387
370	35999	2.914	524	47544	-0.411
372	36183	3.159	526	47677	-0.456
374	36496	2.503	528	47810	-0.428
376	36809	2.702	530	47943	-0.402
378	37122	2.545	532	48076	-0.349
380	37436	2.546	534	48209	-0.479
382	37749	2.343	536	48342	-0.366
384	38062	2.179	538	48475	-0.400
386	38375	1.771	540	48608	-0.390
388	38689	1.926	542	48741	-0.416
390	39002	2.030	544	48874	-0.390
392	39315	1.770	546	49007	-0.357
394	39628	1.797	548	49140	-0.238
396	39941	1.806	550	49273	-0.258
398	40255	1.658	552	49406	-0.481
400	40568	2.114	554	49539	-0.239
402	40881	2.214	556	49672	-0.415
404	41194	2.002	558	49805	-0.253
406	41508	2.541	560	49938	-0.244
408	41821	1.973	562	50071	-0.188
410	42134	2.049	564	50204	-0.310
412	42447	2.136	566	50337	-0.234
414	42760	2.233	568	50470	-0.266
416	43074	2.165	570	50603	-0.295
418	43387	2.105	572	50736	-0.488
420	43700	2.347	574	50869	-0.396
422	44013	3.072	576	51002	-0.282
424	44051	2.593	578	51135	-0.193
426	44088	2.676	580	51268	-0.154
428	44125	2.109	582	51401	-0.328

430	44163	2.206	584	51534	-0.286
432	44200	2.078	586	51667	-0.222
434	44237	2.094	588	51800	-0.319
436	44275	2.242	590	51933	-0.321
438	44312	2.334	592	52085	-0.352
440	44349	2.406	594	52236	-0.413
442	44387	2.290	596	52388	-0.354
444	44424	2.203	598	52539	-0.454
446	44461	2.283	600	52691	
448	44499	2.486	602	52842	-0.590
450	44536	3.125	604	52994	-0.416
452	44574	3.230	606	53145	-0.348
454	44611	4.043	608	53297	-0.451
456	44648	3.453	610	53448	-0.551
458	44686	4.132	612	53600	-0.421
460	44723	3.723	614	53751	-0.666
462	44760	3.470	616	53903	-0.294
464	44798	3.417	618	54055	-0.359
466	44835	3.730	620	54206	-0.281
468	44872	3.628	622	54358	-0.313
470	44910	4.204	624	54509	-0.314
472	44947	3.544	626	54661	-0.288
474	44984	3.522	628	54812	-0.276
476	45022	3.649	630	54964	-0.294
478	45059	3.761	632	55115	-0.253
480	45096	3.799	634	55267	-0.329
482	45134	3.359	636	55418	-0.456
484	45171	3.392	638	55570	-0.339
486	45208	3.776	640	55722	-0.250
488	45246	3.854	642	55873	-0.315
490	45283	3.644	644	56025	-0.420
492	45416	2.648	646	56176	-0.329
494	45549	2.229	648	56328	-0.261
496	45682	2.163	650	56479	-0.486
498	45815	1.925	652	56631	-0.443
500	45948	1.827	654	56782	-1.009
502	46081	2.143	656	56934	-0.968
504	46214	2.025	658	57085	-0.745
506	46347	2.205	660	57237	-0.654
508	46480	2.351	662	57388	-0.740
510	46613	2.569	664	57540	-1.021
512	46746	2.910	666	57615	-1.048
514	46879	2.926	668	57690	-0.964
516	47012	2.865	670	57765	-0.873
518	47145	2.114	672	57841	-0.952
520	47278	2.785	674	57916	-1.009
522	47411	3.225	676	57991	-0.954
524	47544	2.857	678	58066	-0.905
526	47677	3.223	680	58141	-0.931
528	47810	3.162	682	58216	-1.135
530	47943	3.017	684	58292	-1.070
532	48076	3.076	686	58367	-0.971
534	48209		688	58442	-0.910
536	48342	2.854	690	58517	-0.928
538	48475	3.195	692	58592	-0.978
540	48608	3.472	694	58667	-0.968
542	48741	3.258	696	58742	-1.006
544	48874	3.464	698	58818	-0.854
546	49007	3.378	700	58893	-0.904
548	49140	3.070	702	58968	-0.992
550	49273	3.410	704	59043	-1.037
552	49406	3.852	706	59118	-0.879
554	49539	3.326	708	59193	-0.743
556	49672	3.674	710	59268	-0.945
558	49805	3.669	712	59344	-0.843
559	49872	4.139	714	59419	-0.875
560	49938	6.344	716	59494	-0.903
562	50071	5.574	718	59569	-0.687
564	50204	3.634	720	59644	-0.828
566	50337	3.661	722	59719	-0.865
568	50470	4.108	724	59795	-0.823
570	50603	3.866	726	59870	-0.911
572	50736	4.388	728	59945	-0.923

574	50869	4.357	730	60020	-0.931
576	51002	3.992	732	60095	-0.770
578	51135	3.775	734	60170	-0.996
580	51268	4.079	736	60245	-1.051
582	51401	4.286	738	60321	-0.896
584	51534	4.284	740	60396	-0.857
586	51667	4.345	742	60471	-0.784
588	51800	3.680	744	60546	-1.011
590	51933	3.780	746	60621	-0.916
592	52085	3.394	748	60696	-0.734
594	52236	2.946	750	60772	-0.680
596	52388	2.903	752	60847	-0.612
598	52539	2.259	754	60922	-0.594
600	52691	2.022	756	60997	-0.569
602	52842	2.568	758	61072	-0.695
604	52994	3.390	760	61147	-0.658
606	53145	2.944	762	61222	-0.629
608	53297	3.829	764	61298	-0.567
610	53448	3.641	766	61373	-1.069
612	53600	3.737	768	61448	-0.729
614	53751	2.287	770	61523	-0.638
616	53903	2.895	772	61598	-0.860
618	54055	3.714	774	61673	-0.878
620	54206	3.594	776	61748	-0.885
622	54358	3.605	778	61824	-0.819
624	54509	3.918	780	61899	-0.911
626	54661	4.586	782	61974	-0.773
628	54812	3.887	784	62049	-0.637
630	54964	3.369	786	62124	-0.938
632	55115	3.806	788	62199	-0.697
634	55267	4.548	790	62275	-1.021
636	55418	4.387	792	62350	-0.745
638	55570	3.471	794	62425	-0.811
640	55722	4.345	796	62500	-0.945
642	55873	3.654	798	62575	-0.726
644	56025	3.582	800	62650	-0.910
646	56176	3.794	802	62725	-1.075
648	56328	3.726	804	62801	-0.945
650	56479	2.938	806	62876	-0.705
652	56631	3.249	808	62951	-0.965
653	56707	2.333	810	63026	-0.869
654	56782	2.626	812	63101	-0.713
656	56934	1.308	814	63176	-0.868
658	57085	1.506	816	63252	-0.776
660	57237	1.669	818	63327	-0.936
662	57388	2.141	820	63402	-0.712
664	57540	2.192	822	63477	-0.815
666	57615	1.281	824	63552	-0.753
668	57690	1.330	826	63627	-0.749
670	57765	1.177	828	63702	-0.750
672	57841	1.279	830	63778	-0.826
674	57916	1.249	832	63853	-0.773
676	57991	1.224	834	63928	-0.775
678	58066	1.171	836	64003	-0.918
680	58141	1.184	838	64078	-0.858
682	58216	1.165	840	64153	-0.765
684	58292	1.249	842	64229	-1.131
686	58367	1.452	844	64304	-1.096
688	58442	1.364	846	64379	-0.656
690	58517	1.256	848	64454	-0.800
692	58592	1.363	850	64529	-0.887
694	58667	1.339	852	64604	-1.024
696	58742	1.285	854	64679	-0.924
698	58818	1.391	856	64755	-0.943
700	58893	1.379	858	64830	-0.927
702	58968	1.343	860	64905	-1.100
704	59043	1.365	862	64980	-0.867
706	59118	1.435	864	65055	-0.839
708	59193	1.401	866	65130	-1.001
710	59268	1.443	868	65205	-0.908
712	59344	1.411	870	65281	-0.807
714	59419		872	65356	-0.736
716	59494	1.441	874	65431	-0.824

718	59569	1.548	876	65506	-0.846
720	59644	1.452	878	65581	-0.789
722	59719	1.468	880	65656	-0.866
724	59795	1.480	882	65732	-1.001
726	59870	1.484	884	65807	-0.893
728	59945	1.532	886	65882	-0.790
730	60020	1.471	888	65957	-0.956
732	60095	1.453	890	66032	-0.956
734	60170	1.452	892	66107	-0.794
736	60245	1.482	894	66182	-0.821
738	60321	1.466	896	66258	-0.729
740	60396		898	66333	-0.833
742	60471	1.616	900	66408	
744	60546	1.499	902	66483	-0.579
746	60621	1.560	904	66558	-0.670
748	60696	1.694	906	66633	-0.623
750	60772	1.872	908	66709	-0.560
752	60847	1.843	910	66784	-0.891
754	60922	1.820	912	66859	-0.649
756	60997	1.921	914	66934	-0.786
758	61072	1.670	916	67009	-0.714
760	61147	2.082	918	67084	-0.541
762	61222	1.883	920	67159	-0.651
764	61298	2.184	922	67235	-0.442
766	61373	1.848	924	67310	-0.651
768	61448	1.722	926	67385	-0.465
770	61523	1.749	928	67460	-0.494
772	61598	1.643	930	67535	-0.667
774	61673	1.701	932	67610	-0.631
776	61748	1.629	934	67685	-0.682
778	61824	1.596	936	67761	-0.455
780	61899	1.623	938	67836	-0.581
782	61974	1.636	940	67911	-0.253
784	62049	1.568	942	67986	-0.580
786	62124	1.477	944	68061	-0.415
788	62199	1.563	946	68136	-0.361
790	62275	1.530	948	68212	-0.275
792	62350	1.552	950	68287	-0.411
794	62425	1.590	952	68362	-0.391
796	62500	1.727	954	68437	-0.179
798	62575	1.748	956	68539	-0.410
800	62650	1.509	958	68641	-0.653
802	62725	1.630	960	68743	-0.667
804	62801	1.650	962	68846	-0.834
806	62876	1.698	964	68948	-0.926
808	62951	1.702	966	69050	-0.899
810	63026	1.728	968	69152	-0.937
812	63101	1.681	970	69254	-0.990
814	63176	1.794	972	69356	-0.874
816	63252	1.731	974	69459	-0.960
818	63327	1.771	976	69561	-0.992
820	63402	1.759	978	69663	-0.911
822	63477	1.916	980	69765	-0.891
824	63552	1.846	982	69867	-0.739
826	63627	1.836	984	69969	-0.783
828	63702	1.865	986	70072	-0.791
830	63778	1.985	988	70174	-0.631
832	63853	1.893	990	70276	-0.799
834	63928	1.881	992	70378	-0.744
836	64003	1.889	994	70480	-0.923
838	64078	1.922	996	70582	-0.643
840	64153	1.886	998	70685	-0.798
842	64229	1.849	1000	70787	-0.377
844	64304	1.819	1002	70889	-0.564
846	64379	1.791	1004	70991	-0.648
848	64454	1.736	1006	71093	-0.705
850	64529	1.750	1008	71195	-0.475
852	64604	1.862	1010	71298	-0.459
854	64679	1.796	1012	71400	-0.591
856	64755	1.718	1014	71502	-0.614
858	64830	1.668	1016	71604	-0.665
860	64905	1.636	1018	71706	-0.679
866	65130	1.627	1020	71808	-0.236

868	65205	1.734	1022	71911	-0.234
870	65281	1.614	1024	72013	-0.071
872	65356	1.654	1026	72115	-0.165
874	65431	1.606	1028	72217	-0.867
876	65506	1.498	1030	72319	-0.236
878	65581	1.568	1032	72421	0.149
880	65656	1.711	1034	72523	-0.207
882	65732	1.738	1036	72626	-0.073
884	65807	1.857	1038	72728	-0.126
886	65882	1.869	1040	72830	-0.074
888	65957	1.935	1042	72932	-0.162
890	66032	1.845	1044	73034	-0.285
892	66107	1.900	1046	73136	-0.287
894	66182	1.772	1048	73239	
896	66258	1.990	1050	73341	
898	66333	2.155	1052	73443	-0.138
900	66408	2.480	1054	73545	-0.359
902	66483	2.311	1056	73647	-0.409
904	66558	2.447	1058	73749	-0.430
906	66633	2.154	1060	73852	-0.243
908	66709	2.436	1062	73954	-0.359
910	66784	1.698	1064	74056	-0.541
912	66859	2.060	1066	74158	-0.216
914	66934	2.066	1068	74260	-0.135
916	67009	1.810	1070	74362	-0.147
918	67084	1.899	1072	74465	-0.208
920	67159	2.402	1074	74567	-0.485
922	67235	2.401	1076	74669	-0.290
924	67310	2.232	1078	74771	-0.370
926	67385	2.548	1080	74873	-0.466
928	67460	2.616	1082	74975	-0.395
930	67535	1.872	1084	75078	-0.533
932	67610	2.882	1086	75180	-0.499
934	67685	2.949	1088	75282	-0.548
936	67761	2.658	1090	75384	-0.529
938	67836	3.105	1092	75486	-0.506
940	67911	3.578	1094	75588	-0.608
942	67986	2.981	1096	75691	-0.493
944	68061	3.702	1098	75793	-0.436
945	68099	3.546	1100	75895	-0.395
946	68136	3.553	1102	75997	-0.366
948	68212	3.118	1104	76099	-0.353
950	68287	3.632	1106	76201	-0.459
952	68362	4.138	1108	76303	-0.242
954	68437	4.115	1110	76406	-0.449
956	68539	3.514	1112	76508	-0.344
958	68641	2.832	1114	76610	-0.430
960	68743	2.688	1116	76712	-0.419
962	68846	2.091	1118	76814	-0.503
964	68948	2.150	1120	76916	-0.467
966	69050	2.074	1122	77019	-0.426
968	69152	2.127	1124	77121	-0.514
970	69254	2.028	1126	77223	-0.204
972	69356	1.991	1128	77325	-0.201
974	69459	2.019	1130	77427	-0.245
976	69561	1.948	1132	77529	-0.065
978	69663	1.973	1134	77632	-0.125
980	69765	2.115	1136	77734	-0.022
982	69867	2.114	1138	77836	-0.180
984	69969	2.141	1140	77938	-0.124
986	70072	2.137	1142	78040	-0.717
988	70174	2.264	1144	78142	0.068
990	70276	2.172	1146	78245	-0.352
992	70378	2.275	1148	78347	0.008
994	70480	2.292	1150	78449	-0.087
996	70582	2.671	1152	78551	-0.117
998	70685	2.687	1154	78653	0.007
1000	70787	2.704	1156	78755	-0.002
1002	70889	2.600	1158	78858	-0.160
1004	70991		1160	78960	-0.158
1006	71093	2.624	1162	79062	-0.245
1008	71195	2.786	1164	79164	-0.128
1010	71298	2.652	1166	79266	-0.137

1012	71400	2.806	1168	79368	-0.093
1014	71502	2.873	1170	79471	-0.247
1016	71604	3.523	1172	79573	-0.049
1018	71706	3.009	1174	79675	-0.141
1020	71808	3.876	1176	79777	-0.129
1022	71911	4.807	1178	79879	-0.051
1024	72013	4.569	1180	79981	0.081
1026	72115	6.363	1182	80083	-0.093
1028	72217	5.187	1184	80186	0.032
1030	72319	3.963	1186	80288	-0.121
1032	72421	5.883	1188	80390	-0.052
1034	72523	6.033	1190	80492	-0.093
1036	72626	5.603	1192	80594	0.004
1038	72728	6.149	1194	80696	-0.052
1040	72830	5.219	1196	80799	-0.125
1042	72932	6.408	1198	80901	-0.086
1044	73034	7.935	1200	81003	-0.179
1046	73136	4.452	1202	81105	-0.191
1047	73188	4.759	1204	81207	-0.179
1048	73239	4.914	1206	81309	-0.175
1049	73290	3.973	1208	81412	
1050	73341	4.624	1210	81514	-0.161
1052	73443	4.244	1212	81616	-0.174
1054	73545	4.811	1214	81718	-0.065
1056	73647	4.431	1216	81820	-0.215
1058	73749	4.965	1218	81922	-0.243
1060	73852	3.287	1220	82025	-0.227
1062	73954		1222	82127	-0.357
1064	74056	3.751	1224	82229	-0.197
1066	74158	3.870	1226	82331	-0.339
1068	74260	4.322	1228	82433	-0.254
1070	74362	4.377	1230	82535	-0.208
1072	74465	4.312	1232	82638	-0.241
1074	74567	3.389	1234	82740	-0.219
1076	74669	3.307	1236	82842	-0.458
1078	74771	3.025	1238	82944	-0.233
1080	74873	2.919	1240	83046	-0.283
1082	74975	2.932	1242	83148	-0.235
1084	75078	2.610	1244	83251	-0.174
1086	75180	2.648	1246	83353	-0.239
1088	75282	2.457	1248	83455	-0.289
1090	75384	2.425	1250	83557	-0.157
1092	75486	2.391	1252	83680	-0.286
1094	75588	3.196	1254	83803	-0.674
1096	75691	2.741	1256	83926	-0.812
1098	75793	2.586	1258	84048	-0.661
1100	75895	2.779	1260	84171	-0.473
1102	75997	2.902	1262	84294	-0.434
1104	76099	2.850	1264	84417	-0.829
1106	76201	2.771	1266	84540	-1.010
1108	76303	3.005	1268	84663	-0.908
1110	76406	3.034	1270	84785	-0.780
1112	76508	2.845	1272	84908	-0.648
1114	76610	2.610	1274	85031	-0.779
1116	76712	2.595	1276	85154	-0.545
1118	76814	2.849	1278	85277	-0.814
1120	76916	2.982	1280	85400	-0.716
1122	77019	3.093	1282	85522	-0.911
1124	77121	3.665	1284	85645	-0.830
1126	77223	3.608	1286	85768	-0.884
1128	77325	5.098	1288	85891	-0.862
1130	77427	5.419	1290	86014	-0.831
1131	77478	5.968	1292	86137	-0.903
1132	77529	1.398	1294	86259	-0.981
1134	77632	5.734	1296	86382	-0.795
1136	77734	4.713	1298	86505	-1.005
1138	77836	5.346	1300	86628	-0.780
1140	77938	5.950	1302	86751	-0.776
1142	78040	6.480	1304	86874	-0.779
1144	78142	6.636	1306	86996	-0.712
1146	78245	6.426	1308	87119	-0.877
1148	78347	8.466	1310	87242	-0.677
1150	78449	6.326	1312	87365	-0.792

1152	78551	5.830	1314	87488	-0.712
1154	78653	5.304	1316	87611	-0.889
1156	78755	5.817	1318	87733	-1.052
1158	78858	5.379	1320	87856	-0.749
1160	78960	4.733	1322	87979	-1.112
1161	79011	3.250	1324	88102	-0.692
1162	79062	4.383	1326	88225	-0.907
1164	79164	4.922	1328	88348	-0.739
1166	79266	4.882	1330	88471	-0.721
1167	79317	3.499	1332	88593	-0.812
1168	79368	4.995	1334	88716	-0.990
1170	79471	4.442	1336	88839	-0.650
1172	79573	7.065	1338	88962	-0.555
1174	79675	6.079	1340	89085	-0.661
1176	79777	5.889	1342	89208	-0.632
1178	79879	5.442	1344	89330	-0.678
1180	79981	6.245	1346	89453	-0.528
1182	80083	5.656	1348	89576	-0.698
1184	80186	5.723	1350	89699	
1186	80288	5.906	1352	89822	-0.856
1188	80390	5.480	1354	89945	-0.705
1190	80492	6.337	1356	90067	-0.826
1192	80594	5.443	1358	90190	-0.595
1194	80696	6.246	1360	90313	-0.593
1196	80799	5.604	1362	90436	-1.004
1198	80901	5.582	1364	90559	-0.910
1200	81003	5.706	1366	90682	-0.571
1204	81207	5.886	1368	90804	-0.813
1206	81309	5.277	1370	90927	-0.904
1208	81412	5.772	1372	91050	-0.658
1210	81514	5.497	1374	91173	-0.868
1212	81616	4.673	1376	91296	-0.663
1214	81718	4.017	1378	91419	-0.732
1216	81820	6.035	1380	91541	-0.665
1218	81922	5.436	1382	91664	-0.769
1220	82025	5.182	1384	91787	-0.667
1222	82127	6.677	1386	91910	-0.801
1224	82229	6.935	1388	92033	-0.695
1226	82331	5.697	1390	92156	-0.684
1228	82433	5.874	1392	92279	-0.544
1230	82535	5.907	1394	92401	-0.439
1232	82638	5.853	1396	92524	-0.555
1234	82740	5.881	1398	92647	-0.671
1235	82791	3.204	1400	92770	-0.664
1236	82842	2.795	1402	92893	-0.663
1238	82944	5.566	1404	93016	-0.539
1240	83046	5.218	1406	93138	-0.462
1242	83148	5.710	1408	93261	-0.430
1244	83251	5.778	1410	93384	-0.472
1246	83353	5.225	1412	93507	-0.428
1248	83455	5.039	1414	93630	-0.601
1250	83557	5.121	1416	93753	-0.304
1252	83680	4.155	1418	93875	-0.447
1253	83741	3.959	1420	93998	-0.363
1254	83803	2.310	1422	94121	-0.362
1256	83926	2.023	1424	94244	-0.451
1258	84048	1.853	1426	94367	-0.344
1260	84171	2.844	1428	94490	-0.167
1262	84294	1.950	1430	94612	-0.432
1264	84417	1.885	1432	94735	-0.251
1266	84540	1.770	1434	94858	-0.241
1268	84663	1.682	1436	94981	-0.112
1270	84785	1.951	1438	95104	-0.185
1272	84908	1.888	1440	95227	-0.293
1274	85031	1.730	1442	95349	-0.248
1276	85154	1.837	1444	95472	-0.264
1278	85277	1.829	1446	95595	-0.163
1280	85400	1.816	1448	95718	-0.155
1282	85522	1.883	1450	95841	-0.112
1284	85645	1.743	1452	95964	-0.121
1286	85768	1.786	1454	96086	-0.185
1288	85891	1.742	1456	96209	-0.023
1290	86014	1.711	1458	96332	-0.180

1292	86137	1.735	1460	96455	-0.078
1294	86259	1.707	1462	96578	-0.242
1296	86382	1.614	1464	96701	-0.260
1298	86505	1.695	1466	96824	-0.349
1300	86628	1.742	1468	96946	-0.302
1302	86751	1.847	1470	97069	-0.513
1304	86874	1.791	1472	97192	-0.473
1306	86996	1.756	1474	97315	-0.388
1308	87119	1.694	1476	97438	-0.242
1310	87242	1.754	1478	97561	-0.074
1312	87365	1.775	1480	97683	-0.057
1314	87488	1.791	1482	97806	-0.150
1316	87611	1.801	1484	97929	-0.169
1318	87733	1.675	1486	98052	-0.196
1320	87856	1.758	1488	98175	-0.270
1322	87979	1.742	1490	98298	-0.185
1324	88102	1.754	1492	98420	-0.227
1326	88225	1.739	1494	98543	-0.368
1328	88348	1.776	1496	98666	-0.308
1330	88471	1.812	1498	98789	-0.331
1332	88593	1.830	1500	98912	
1334	88716		1502	99035	-0.059
1336	88839	1.887	1504	99157	-0.893
1338	88962	1.848	1506	99280	-0.175
1340	89085	1.909	1508	99403	-0.252
1342	89208	1.822	1510	99526	-0.388
1344	89330	1.907	1512	99649	-0.319
1346	89453	1.877	1514	99772	-0.168
1348	89576	1.859	1516	99894	-0.272
1350	89699	1.880	1518	100017	-0.403
1352	89822	1.916	1520	100140	-0.230
1354	89945	1.864	1522	100263	-0.253
1356	90067	1.897	1524	100386	-0.265
1358	90190	1.934	1526	100509	-0.232
1360	90313	1.868	1528	100631	-0.302
1362	90436	1.933	1530	100754	-0.410
1364	90559	1.956	1532	100877	-0.351
1366	90682	2.055	1534	101000	-0.294
1368	90804		1536	101080	-0.305
1370	90927	2.004	1538	101160	-0.397
1372	91050	2.014	1540	101240	-0.292
1374	91173	1.975	1542	101320	-1.111
1376	91296	1.995	1544	101401	-1.065
1378	91419	1.924	1546	101481	-0.701
1380	91541	1.941	1548	101561	-0.272
1382	91664	1.959	1550	101641	-0.309
1384	91787	2.040	1552	101721	-0.229
1386	91910	2.049	1554	101801	-0.215
1388	92033	2.227	1556	101881	-0.169
1390	92156	2.380	1558	101961	-0.169
1392	92279	2.334	1560	102041	-0.159
1394	92401	2.319	1562	102122	-0.497
1396	92524	2.382	1564	102202	-0.565
1398	92647	2.399	1566	102282	-0.283
1400	92770	2.348	1568	102362	-0.245
1402	92893	2.455	1570	102442	-0.192
1404	93016	2.553	1572	102522	-0.191
1406	93138	2.432	1574	102602	-0.263
1408	93261	2.647	1576	102682	-0.207
1410	93384	2.674	1578	102762	-0.339
1412	93507	2.808	1580	102843	-0.150
1414	93630	2.890	1582	102923	-0.161
1416	93753	2.876	1584	103003	-0.321
1418	93875	2.888	1586	103083	-0.365
1420	93998	2.784	1588	103163	-0.373
1422	94121	2.700	1590	103243	-0.249
1424	94244	2.799	1592	103323	-0.442
1426	94367	3.540	1594	103403	-0.443
1428	94490	4.323	1596	103483	-0.435
1430	94612	3.698	1598	103564	-0.268
1432	94735	3.924	1600	103644	-0.377
1434	94858	4.113	1602	103724	-0.013
1436	94981	4.164	1604	103804	-0.158

CORE MD02-2518

1438	95104	3.936	1606	103884	-0.070
1440	95227	4.188	1608	103964	-0.044
1442	95349	3.847	1610	104044	-0.096
1444	95472	4.002	1612	104124	-0.171
1446	95595	4.668	1614	104204	0.075
1448	95718	5.000	1616	104285	-0.060
1450	95841	5.003	1618	104365	-0.412
1452	95964	4.983	1620	104445	-0.079
1454	96086	4.983	1622	104525	-0.142
1456	96209	5.306	1624	104605	-0.094
1458	96332	4.906	1626	104685	-0.124
1460	96455	4.884	1628	104765	-0.059
1462	96578	4.476	1630	104845	-0.127
1464	96701	4.282	1632	104926	-0.011
1466	96824	3.694	1634	105006	
1468	96946	4.370	1636	105086	
1470	97069	4.370	1638	105166	
1472	97192	3.773	1640	105246	
1474	97315	4.380	1642	105326	
1476	97438	5.065	1644	105406	
1478	97561	6.306	1646	105486	
1480	97683	6.259	1648	105566	
1482	97806	5.952	1650	105647	
1484	97929	5.060	1652	105727	
1486	98052	5.522	1654	105807	-0.551
1488	98175	5.453	1656	105887	-0.498
1490	98298	6.000	1658	105967	-0.593
1492	98420	5.226	1660	106047	-0.865
1494	98543	4.961	1662	106127	-0.704
1496	98666	5.262	1664	106207	-0.574
1498	98789	4.824	1666	106287	-0.624
1500	98912	5.589	1668	106368	-0.508
1502	99035	6.787	1670	106448	-0.111
1504	99157	2.428	1672	106528	-0.601
1506	99280	5.991	1674	106608	-0.588
1508	99403	5.483	1676	106688	-0.533
1510	99526	5.414	1678	106768	-0.448
1512	99649	4.610	1680	106848	-0.489
1514	99772	5.224	1682	106928	-0.549
1516	99894	4.560	1684	107008	-0.804
1518	100017	4.411	1686	107089	-0.442
1520	100140	5.061	1688	107169	-0.376
1522	100263	4.289	1690	107249	-0.395
1524	100386	4.912	1692	107329	-0.412
1526	100509	4.995	1694	107409	-0.528
1528	100631	4.735	1696	107489	-0.490
1530	100754	5.732	1698	107569	-0.296
1532	100877	5.179	1700	107649	-0.162
1534	101000	5.410	1702	107729	-0.357
1536	101080	4.543	1704	107810	-0.032
1538	101160	4.688	1706	107890	-0.080
1540	101240	3.559	1708	107970	-0.052
1542	101320	1.481	1710	108050	-0.080
1544	101401	1.417	1712	108130	-0.030
1546	101481	3.019	1714	108269	-0.147
1548	101561	4.490	1716	108408	-0.088
1550	101641	4.190	1718	108548	-0.124
1552	101721	4.413	1720	108687	0.013
1554	101801	5.005	1722	108826	-0.059
1556	101881	5.681	1724	108965	-0.160
1558	101961	5.352	1726	109105	-0.105
1560	102041	4.860	1728	109244	-0.102
1562	102122	2.682	1730	109383	-0.286
1564	102202		1732	109522	-0.242
1566	102282	4.288	1734	109661	-0.358
1568	102362	4.223	1736	109801	-0.268
1570	102442	4.548	1738	109940	-0.411
1572	102522	4.908	1740	110079	-0.276
1574	102602	5.254	1742	110218	-0.358
1576	102682	5.095	1744	110357	-0.405
1578	102762	5.299	1746	110497	-0.349
1580	102843	5.250	1748	110636	-0.459
1582	102923	6.152	1750	110775	-0.760

1584	103003	5.696		1752	110914	-0.768
1586	103083	5.246		1754	111054	-0.778
1588	103163	4.948		1756	111193	-0.662
1590	103243	5.820		1758	111332	-0.687
1592	103323	5.577		1760	111471	-0.471
1594	103403	5.440		1762	111610	-0.716
1596	103483	5.284		1764	111750	-0.561
1598	103564	6.277		1766	111889	-0.647
1600	103644	6.155		1768	112028	-0.687
1602	103724	6.429		1770	112167	-0.852
1604	103804	7.299		1772	112306	-0.598
1606	103884	6.631		1774	112446	-0.616
1608	103964	8.540		1776	112585	-0.496
1610	104044	7.863		1778	112724	-0.858
1612	104124	7.508		1780	112863	-0.840
1614	104204	8.027		1782	113003	-0.775
1616	104285	8.068		1784	113142	-0.712
1618	104365	4.748		1786	113281	-0.664
1620	104445	8.174		1788	113420	-0.588
1622	104525	7.847		1790	113559	-0.607
1624	104605	8.858		1792	113699	-0.391
1626	104685	7.102		1794	113838	-0.607
1628	104765	7.597		1796	113977	-0.576
1630	104845	8.056		1798	114116	-0.410
1632	104926	7.331		1800	114256	
1656	105887	2.928		1802	114395	-0.351
1660	106047	2.340		1804	114534	-0.459
1664	106207	2.386		1806	114673	-0.378
1668	106386	2.767		1808	114812	-0.386
1672	106528	2.872		1810	114952	-0.157
1676	106688	2.347		1812	115091	-0.530
1680	106848	2.302		1814	115230	-0.245
1684	107008	2.708		1816	115369	-0.321
1688	107169	3.190		1818	115508	-0.244
1692	107329	3.024		1820	115648	-0.366
1696	107489	2.923		1822	115787	-0.176
1700	107649	3.390		1824	115926	-0.202
1704	107810	4.145		1826	116065	-0.274
1708	107970	7.718		1828	116205	-0.185
1712	108130	7.425		1830	116344	-0.190
1716	108408	6.987		1832	116483	-0.194
1720	108687	6.906		1834	116622	-0.096
1724	108965	6.937		1836	116761	-0.123
1728	109244	6.135		1838	116901	-0.185
1732	109522	5.280		1840	117040	-0.215
1736	109801	5.343		1842	117179	-0.183
1740	110079	4.990		1844	117318	-0.150
1744	110357	4.157		1846	117458	-0.162
1748	110636	2.402		1848	117597	-0.134
1752	110914	1.757		1850	117736	-0.107
1756	111193	2.456		1852	117875	0.080
1760	111471	2.963		1854	118014	-0.064
1764	111750	2.515		1856	118154	-0.142
1768	112028	2.310		1858	118293	0.113
1772	112306	2.231		1860	118432	-0.074
				1862	118571	-0.122
				1864	118710	-0.092
				1866	118850	-0.159
				1868	118989	-0.096
				1870	119128	-0.106
				1872	119267	-0.059
				1874	119407	-0.172
				1876	119546	-0.042
				1878	119685	-0.149
				1880	119824	
				1882	119963	-0.077
				1884	120103	-0.117
				1886	120242	-0.099
				1888	120381	-0.125
				1890	120520	-0.138
				1892	120659	-0.078
				1894	120799	-0.178
				1896	120938	-0.263

1898	121077	-0.206
1900	121216	-0.162
1902	121356	-0.193
1904	121495	-0.266
1906	121634	-0.223
1908	121833	-0.110
1910	122032	-0.055
1912	122232	0.220
1914	122431	-0.057
1916	122630	-0.098
1918	122829	-0.032
1920	123028	0.120
1922	123228	-0.072
1924	123427	0.017
1926	123626	-0.015
1928	123825	-0.081
1930	124024	-0.002
1932	124223	-0.078
1934	124423	-0.081
1936	124622	-0.094
1938	124821	0.064
1940	125020	-0.014
1942	125219	-0.029
1944	125419	-0.091
1946	125618	-0.131
1948	125817	0.064
1950	126016	-0.039
1952	126215	0.012
1954	126415	0.186
1956	126614	-0.046
1958	126813	-0.135
1960	127012	-0.064
1962	127211	0.002
1964	127411	-0.104
1966	127610	-0.329
1968	127809	-0.117
1970	128008	-0.108
1972	128207	-0.237
1974	128406	-0.203
1976	128606	-0.288
1978	128805	-0.201
1980	129004	-0.745
1982	129203	-0.700
1984	129402	-0.606
1986	129602	-0.784
1988	129801	-1.031
1990	130000	-1.006
1992	130105	-0.602
1994	130210	-0.544
1996	130315	-0.761
1998	130420	-0.749
2000	130525	-0.708
2002	130630	-0.640
2004	130735	-0.679
2006	130840	-0.741
2008	130945	-0.520
2010	131050	-0.575
2012	131155	-0.553
2014	131260	-0.588
2016	131365	-0.624
2018	131471	-0.780
2020	131576	-0.572
2022	131681	-0.790
2024	131786	-0.771
2026	131891	-0.787
2028	131996	-0.655
2030	132101	-0.611
2032	132206	-0.733
2034	132311	-0.762
2036	132416	-0.639
2038	132521	-0.536
2040	132626	-0.506
2042	132731	-0.655

2044	132836	-0.043
2046	132941	-0.652
2048	133046	-0.620
2050	133151	-0.514
2052	133256	-0.623
2054	133361	-0.403
2056	133466	-0.620
2058	133571	-0.406
2060	133676	-0.656
2062	133781	-0.456
2064	133886	-0.401
2066	133991	-0.459
2068	134096	-0.395
2070	134201	-0.452
2072	134306	-0.495
2074	134412	-0.324
2076	134517	-0.316
2078	134622	-0.348
2080	134727	-0.591
2082	134832	-0.395
2084	134937	-0.355
2086	135042	-0.510
2088	135147	-0.427
2090	135252	-0.557
2092	135357	-0.463
2094	135462	-0.539
2096	135567	-0.565
2098	135672	-0.628
2100	135777	-0.708
2102	135882	-0.571
2104	135987	-0.527
2106	136092	-0.588
2108	136197	-0.726
2110	136302	-0.696
2112	136407	-0.528
2114	136512	-0.492
2116	136617	-0.484
2118	136722	-0.468
2120	136827	-0.464
2122	136932	-0.461
2124	137037	-0.458
2126	137142	-0.440
2128	137248	-0.422
2130	137353	-0.425
2132	137458	-0.494
2134	137563	-0.541
2136	137668	-0.373
2138	137773	-0.520
2140	137878	-0.317
2142	137983	-0.453
2144	138088	-0.344
2146	138193	-0.440
2148	138298	-0.424
2150	138403	-0.420
2152	138508	-0.448
2154	138613	-0.395
2156	138718	-0.324
2158	138823	-0.347
2160	138928	-0.452
2162	139033	-0.613
2164	139138	-0.383
2166	139243	-0.359
2168	139348	-0.430
2170	139453	-0.379
2172	139558	-0.259
2174	139663	-0.328
2176	139768	-0.400
2178	139873	-0.431
2180	139978	-0.335
2182	140083	-0.527
2184	140189	-0.236
2186	140294	-0.285
2188	140399	-0.322

2190	140504	-0.437
2192	140609	-0.357
2194	140714	-0.247
2196	140819	-0.283
2198	140924	-0.316
2200	141029	-0.354
2202	141134	-0.365
2204	141239	-0.394
2206	141344	-0.399
2208	141449	-0.360
2210	141554	-0.465
2212	141659	-0.396
2214	141764	-0.447
2216	141869	-0.526
2218	141974	-0.513
2220	142079	-0.425
2222	142184	-0.350
2224	142289	-0.509
2226	142394	-0.520
2228	142499	-0.428
2230	142604	
2232	142709	-0.428
2234	142814	-0.418
2236	142919	-0.573
2238	143024	-0.467
2240	143130	-0.487
2242	143235	-0.517
2244	143340	
2246	143445	
2248	143550	
2250	143655	
2252	143760	
2254	143865	
2256	143970	
2258	144075	
2260	144180	
2262	144285	
2264	144390	-0.526
2266	144495	-0.607
2268	144600	-0.608
2270	144705	-0.568
2272	144810	-0.632
2274	144915	-0.597
2276	145020	-0.542
2278	145125	-0.477
2280	145230	-0.472
2282	145335	-0.480
2284	145440	-0.791
2286	145545	-0.510
2288	145650	-0.677
2290	145755	-0.779
2292	145860	-0.783
2294	145966	-0.711
2296	146071	-0.588
2298	146176	-0.818
2300	146281	-0.741
2302	146386	-0.499
2304	146491	-0.598
2306	146596	-0.551
2308	146701	-0.540
2310	146806	-0.538
2312	146911	-0.835
2314	147016	-0.725
2316	147121	-0.681
2318	147226	-0.624
2320	147331	-0.586
2322	147436	-0.682
2324	147541	-0.912
2326	147646	-0.751
2328	147751	
2330	147856	
2332	147961	
2334	148066	-0.968

2336	148171	-0.841
2338	148276	-0.630
2340	148381	-0.785
2342	148486	-0.847
2344	148591	-0.606
2346	148696	-0.849
2348	148801	-0.578
2350	148907	-0.638
2352	149012	-0.611
2354	149117	-0.842
2356	149222	-0.749
2358	149327	-0.933
2360	149432	-0.721
2362	149537	-0.785
2364	149642	-0.787
2366	149747	-0.754
2368	149852	-0.823
2370	149957	-0.561
2372	150062	-0.814
2374	150167	-0.609
2376	150272	-0.770
2378	150382	-0.820
2380	150492	-0.818
2382	150602	-0.838
2384	150712	-0.612
2386	150823	-0.783
2388	150933	-0.608
2390	151043	-0.694
2392	151153	-0.526
2394	151263	-0.632
2396	151373	-0.463
2398	151483	-0.490
2400	151593	
2402	151704	-0.494
2404	151814	-0.654
2406	151924	-0.764
2408	152034	-0.533
2410	152144	-0.537
2412	152254	-0.430
2414	152364	-0.519
2416	152474	-0.583
2418	152585	-0.440
2420	152695	-0.384
2422	152805	-0.374
2424	152915	-0.319
2426	153025	-0.382
2428	153135	-0.225
2430	153245	-0.458
2432	153355	-0.392
2434	153465	-0.475
2436	153576	-0.492
2438	153686	-0.456
2440	153796	-0.411
2442	153906	-0.508
2444	154016	-0.560
2446	154126	-0.553
2448	154236	-0.376
2450	154346	-0.327
2452	154457	-0.416
2454	154567	-0.363
2456	154677	-0.375
2458	154787	-0.664
2460	154897	-0.478
2462	155007	-0.625
2464	155117	-0.699
2466	155227	-0.708
2468	155337	-0.729
2470	155448	-0.660
2472	155558	-0.456
2474	155668	-0.506
2476	155778	-0.610
2478	155888	-0.637
2480	155998	-0.545

2482	156108	-0.663
2484	156218	-0.581
2486	156329	-0.634
2488	156439	-0.624
2490	156549	-0.420
2492	156659	-0.491
2494	156769	-0.691
2496	156879	-0.467
2498	156989	-0.460
2500	157099	-0.494
2502	157210	-0.560
2504	157320	-0.614
2506	157430	-0.308
2508	157540	-0.291
2510	157650	-0.463
2512	157760	-0.470
2514	157870	-0.533
2516	157980	-0.583
2518	158090	-0.390
2520	158201	-0.458
2522	158311	-0.613
2524	158421	-0.393
2526	158531	-0.532
2528	158641	-0.521
2530	158751	-0.447
2532	158861	-0.480
2534	158971	-0.736
2536	159082	-0.531
2538	159192	-0.488
2540	159302	-0.465
2542	159412	-0.528
2544	159522	-0.249
2546	159632	-0.382
2548	159742	
2550	159852	
2552	159962	
2554	160073	-0.563
2556	160183	-0.580
2558	160293	-0.371
2560	160403	-0.388
2562	160513	-0.446
2564	160623	-0.471
2566	160733	-0.255
2568	160843	-0.472
2570	160954	-0.344
2572	161064	-0.262
2574	161174	-0.396
2576	161284	-0.474
2578	161394	-0.390
2580	161504	-0.411
2582	161614	-0.377
2584	161724	-0.498
2586	161835	-0.395
2588	161945	-0.533
2590	162055	-0.393
2592	162165	-0.711
2594	162275	-0.644
2596	162385	-0.375
2598	162495	-0.354
2600	162605	-0.390
2602	162715	-0.543
2604	162826	-0.358
2606	162936	-0.308
2608	163046	-0.561
2610	163156	-0.464
2612	163266	-0.415
2614	163376	-0.345
2616	163486	-0.303
2618	163596	-0.334
2620	163707	-0.248
2622	163817	-0.264
2624	163927	-0.257
2626	164037	-0.259

2628	164147	-0.366
2630	164257	-0.227
2632	164367	-0.415
2634	164477	-0.227
2636	164587	-0.289
2638	164698	-0.288
2640	164808	-0.342
2642	164918	-0.369
2644	165028	-0.350
2646	165138	-0.236
2648	165248	-0.406
2650	165358	-0.362
2652	165468	-0.364
2654	165579	-0.263
2656	165689	-0.364
2658	165799	-0.307
2660	165909	-0.246
2662	166019	-0.302
2664	166129	-0.488
2666	166239	-0.413
2668	166349	-0.207
2670	166460	-0.237
2672	166570	-0.304
2674	166680	-0.328
2676	166790	-0.472
2678	166900	-0.435
2680	167010	-0.311
2682	167120	-0.320
2684	167230	-0.294
2686	167340	-0.321
2688	167451	-0.411
2690	167561	-0.348
2692	167671	-0.493
2694	167781	-0.178
2696	167891	-0.314
2698	168001	-0.303
2700	168111	-0.353
2702	168221	-0.230
2704	168332	-0.207
2706	168442	-0.256
2708	168552	-0.224
2710	168662	-0.214
2712	168772	-0.290
2714	168882	-0.159
2716	168992	
2718	169102	
2720	169212	
2722	169323	
2724	169433	
2726	169543	
2728	169653	
2730	169763	
2732	169873	
2734	169983	
2736	170093	-0.339
2738	170204	-0.314
2740	170314	-0.333
2742	170424	-0.265
2744	170534	-0.365
2746	170644	-0.500
2748	170754	-0.368
2750	170864	-0.552
2752	170974	-0.434
2754	171085	-0.461
2756	171195	-0.582
2758	171305	-0.563
2760	171415	-0.454
2762	171525	-0.572
2764	171635	-0.485
2766	171745	-0.378
2768	171855	-0.495
2770	171965	-0.234
2772	172076	-0.210

2774	172186	-0.317
2776	172296	-0.322
2778	172406	-0.409
2780	172516	-0.409
2782	172626	-0.396
2784	172736	-0.372
2786	172846	-0.149
2788	172957	-0.424
2790	173067	-0.008
2792	173177	-0.266
2794	173287	-0.284
2796	173397	-0.028
2798	173507	-0.167
2800	173617	-0.311
2802	173727	-0.304
2804	173837	-0.342
2806	173948	-0.359
2808	174058	-0.458
2810	174168	-0.167
2812	174278	-0.412
2814	174388	-0.391
2816	174498	-0.304
2818	174608	-0.608
2820	174718	-0.283
2822	174829	-0.456
2824	174939	-0.473
2826	175049	-0.390
2828	175159	-0.547
2830	175269	-0.422
2832	175379	-0.469
2834	175489	-0.383
2836	175599	-0.335
2838	175710	-0.278
2840	175820	-0.424
2842	175930	-0.500
2844	176040	-0.295
2846	176150	-0.350
2848	176260	-0.160
2850	176370	
2852	176480	-0.369
2854	176590	-0.326
2856	176701	-0.233
2858	176811	-0.313
2860	176921	-0.278
2862	177031	-0.362
2864	177141	-0.483
2866	177251	-0.667
2868	177361	-0.565
2870	177471	-0.598
2872	177582	-0.736
2874	177692	-0.800
2876	177802	-0.862
2878	177912	-0.802
2880	178022	-0.607
2882	178132	-0.841
2884	178242	-0.956
2886	178352	-0.535
2888	178462	-0.647
2890	178573	-0.522
2892	178683	-0.731
2894	178793	-0.958
2896	178903	-0.959
2898	179013	-1.160
2900	179123	-0.809
2902	179233	-1.122
2904	179343	-1.078
2906	179454	-0.864
2908	179564	-0.838
2910	179674	-0.904
2912	179784	-0.868
2914	179894	-0.676
2916	180004	
2918	180114	

2920	180224	
2922	180335	
2924	180445	-0.914
2926	180555	-0.695
2928	180665	-0.711
2930	180775	-0.614
2932	180892	
2934	181008	-0.720
2936	181125	-0.860
2938	181242	-0.849
2940	181358	-0.860
2942	181475	-0.735
2944	181592	-0.704
2946	181708	-0.794
2948	181825	-0.980
2950	181942	-1.032
2952	182058	-0.827
2954	182175	-1.108
2956	182292	-1.004
2958	182408	-0.867
2960	182525	-0.676
2962	182642	-0.645
2964	182758	-0.624
2966	182875	-0.665
2968	182992	-0.699
2970	183108	-0.713
2972	183225	-0.806
2974	183342	-0.741
2976	183458	-0.648
2978	183575	-0.538
2980	183692	-0.574
2982	183808	-0.543
2984	183925	-0.574
2986	184042	-0.583
2988	184158	-0.638
2990	184275	-0.693
2992	184392	-0.686
2994	184508	-0.631
2996	184625	-0.679
2998	184742	-0.537
3000	184858	-0.588
3002	184975	-0.957
3004	185092	-0.651
3006	185208	-1.077
3008	185325	-1.107
3010	185442	-0.830
3012	185558	-0.841
3014	185675	-0.775
3016	185792	-0.617
3018	185908	-0.659
3020	186025	-0.664
3022	186142	-0.779
3024	186258	-0.755
3026	186375	-0.678
3028	186492	-0.553
3030	186608	-0.607
3032	186725	-0.459
3034	186842	-0.447
3036	186958	-0.624
3038	187075	-0.592
3040	187192	-0.889
3042	187308	-0.615
3044	187425	-0.748
3046	187542	-0.666
3048	187658	-0.581
3050	187775	-0.567
3052	187892	-0.514
3054	188008	-0.533
3056	188125	-0.633
3058	188242	-0.536
3060	188358	-0.492
3062	188475	-0.561
3064	188592	-0.522

3066	188708	-0.459
3068	188825	-0.630
3070	188942	-0.542
3072	189058	-0.467
3074	189175	-1.139
3076	189292	-0.340
3078	189408	-0.685
3080	189525	-0.381
3082	189642	-0.700
3084	189758	-0.579
3086	189875	-0.721
3088	189992	-0.893
3090	190108	-0.584
3092	190225	-0.419
3094	190342	-0.740
3096	190458	-0.622
3098	190575	-0.480
3100	190692	-0.570
3102	190808	-0.389
3104	190925	-0.457
3106	191042	-0.420
3108	191158	-0.431
3110	191275	-0.470
3112	191392	-0.442
3114	191508	-0.360
3116	191625	-0.314
3118	191742	-0.173
3120	191858	-0.539
3122	191975	-0.457
3124	192092	-0.254
3126	192208	-0.287
3128	192325	-0.380
3130	192442	-0.374
3132	192558	-0.215
3134	192675	-0.206
3136	192792	-0.283
3138	192908	-0.367
3140	193025	-0.126
3142	193142	-0.298
3144	193258	-0.196
3146	193375	0.062
3148	193482	-0.060
3150	193589	
3152	193696	
3154	193803	-0.074
3156	193910	-0.213
3158	194017	-0.200
3160	194125	-0.218
3162	194232	-0.168
3164	194339	-0.338
3166	194446	-0.244
3168	194553	-0.377
3170	194660	-0.302
3172	194767	-0.534
3174	194874	-0.387
3176	194981	-0.500
3178	195088	-0.276
3180	195195	-0.376
3182	195302	-0.336
3184	195409	-0.455
3186	195517	-0.498
3188	195624	-0.376
3190	195731	-0.459
3192	195838	-0.349
3194	195945	-0.546
3196	196052	-0.342
3198	196159	-0.432
3200	196266	-0.401
3202	196373	-0.443
3204	196480	-0.274
3206	196587	-0.502
3208	196694	-0.304
3210	196801	-0.414

3212	196909	-0.474
3214	197016	-0.406
3216	197123	-0.379
3218	197230	-0.373
3220	197337	-0.325
3222	197444	-0.349
3224	197551	-0.431
3226	197658	-0.375
3228	197765	-0.320
3230	197872	-0.382
3232	197979	-0.373
3234	198086	-0.338
3236	198193	-0.457
3238	198301	-0.311
3240	198408	-0.307
3242	198515	-0.303
3244	198622	-0.332
3246	198729	-0.253
3248	198836	-0.258
3250	198943	-0.276
3252	199050	-0.037
3254	199157	-0.097
3256	199264	-0.090
3258	199371	-0.605
3260	199478	-0.100
3262	199585	-0.077
3264	199693	-0.117
3266	199800	-0.101
3268	199907	-0.120
3270	200014	-0.341
3272	200121	-0.398
3274	200228	-0.385
3276	200335	-0.487
3278	200442	-0.385
3280	200549	-0.399
3282	200656	-0.316
3284	200763	-0.426
3286	200870	-0.231
3288	200977	-0.284
3290	201085	-0.349
3292	201192	-0.259
3294	201299	-0.346
3296	201406	-0.341
3298	201513	-0.342
3300	201620	-0.400
3302	201727	-0.458
3304	201834	-0.461
3306	201941	-0.389
3308	202048	-0.259
3310	202155	-0.155
3312	202262	-0.140
3314	202369	-0.027
3316	202477	-0.139
3318	202584	0.009
3320	202691	-0.456
3322	202798	-0.475
3324	202905	-0.149
3326	203012	-0.124
3328	203119	-0.119
3330	203226	-0.107
3332	203333	-0.155
3334	203440	-0.139
3336	203547	-0.095
3338	203654	-0.077
3340	203761	-0.105
3342	203869	-0.103
3344	203976	-0.217
3346	204083	-0.218
3348	204190	-0.276
3350	204297	-0.143
3352	204404	-0.188
3354	204511	-0.139
3356	204618	-0.145

3358	204725	-0.063
3360	204832	-0.182
3362	204939	-0.032
3364	205046	-0.082
3366	205154	-0.185
3368	205261	-0.178
3370	205368	-0.188
3372	205475	-0.236
3374	205582	-0.297
3376	205689	-0.233
3378	205796	-0.475
3380	205903	-0.369
3382	206010	-0.283
3384	206117	-0.281
3386	206224	-0.333
3388	206331	-0.423
3390	206438	-0.444
3392	206546	-0.395
3394	206653	-0.357
3396	206760	-0.379
3398	206867	-0.532
3400	206974	-0.520
3402	207081	-0.324
3404	207188	-0.337
3406	207295	-0.391
3408	207402	-0.409
3410	207509	-0.279
3412	207616	-0.489
3414	207723	-0.337
3416	207830	-0.420
3418	207938	-0.478
3420	208045	-0.490
3422	208152	-0.487
3424	208259	-0.463
3426	208366	-0.440
3428	208473	-0.309
3430	208580	-0.366
3432	208687	-0.366
3434	208794	-0.526
3436	208901	-0.345
3438	209008	-0.411
3440	209115	-0.369
3442	209222	-0.354
3444	209330	-0.263
3446	209437	-0.256
3448	209544	-0.251
3450	209651	
3452	209758	-0.535
3454	209865	-0.622
3456	209972	-0.436
3458	210079	-0.394
3460	210186	-0.415
3462	210293	-0.430
3464	210400	-0.452
3466	210507	-0.434
3468	210614	-0.487
3470	210722	-0.388
3472	210829	-0.371
3474	210936	-0.294
3476	211043	-0.360
3478	211150	-0.276
3480	211257	-0.393
3482	211364	-0.209
3484	211471	-0.963
3486	211578	-0.574
3488	211685	-0.318
3490	211792	-0.311
3492	211899	-0.310
3494	212006	-0.275
3496	212114	-0.175
3498	212221	-0.164
3500	212328	-0.319
3502	212435	-0.280

3504	212542	-0.370
3506	212649	-0.227
3508	212756	-0.341
3510	212863	-0.249
3512	212970	-0.155
3514	213077	-0.341
3516	213184	-0.170
3518	213291	-0.119
3520	213398	-0.324
3522	213506	-0.333
3524	213613	-0.071
3526	213720	-0.167
3528	213827	0.491
3530	213934	-0.168
3532	214041	-0.119
3534	214148	-0.170
3536	214255	-0.305
3538	214362	-0.177
3540	214469	-0.185
3542	214576	-0.066
3544	214683	-0.323
3546	214790	-0.193
3548	214898	-0.143
3550	215005	-0.133
3552	215112	-0.222
3554	215219	-0.260
3556	215326	-0.295
3558	215433	-0.084
3560	215540	-0.178
3562	215605	-0.148
3564	215670	-0.416
3566	215735	-0.351
3568	215800	-0.280
3570	215865	-0.411
3572	215930	
3574	215995	
3576	216060	
3578	216125	
3580	216190	
3582	216255	-0.458
3584	216320	-0.509
3586	216385	-0.387
3588	216450	-0.514
3590	216515	-0.392
3592	216580	-0.381
3594	216645	-0.381
3596	216710	-0.455
3598	216775	-0.347
3600	216840	-0.283
3602	216905	-0.220
3604	216970	-0.187
3606	217036	-0.280
3608	217101	-0.420
3610	217166	-0.402
3612	217231	-0.485
3614	217296	-0.389
3616	217361	-0.456
3618	217426	-0.216
3620	217491	-0.385
3622	217556	-0.328
3624	217621	-0.395
3626	217686	-0.481
3628	217751	-0.427
3630	217816	-0.269
3632	217881	-0.492
3634	217946	-0.353
3636	218011	-0.666
3638	218076	-0.490
3640	218141	-0.452
3642	218206	-0.464
3644	218271	-0.500
3646	218336	-0.506
3648	218401	-0.611

3650	218466	-0.533
3652	218531	-0.628
3654	218596	-0.416
3656	218661	-0.389
3658	218726	-0.450
3660	218791	-0.420
3662	218856	-0.359
3664	218921	-0.473
3666	218986	-0.495
3668	219051	-0.517
3670	219116	-0.453
3672	219181	-0.686
3674	219246	-0.548
3676	219311	-0.510
3678	219376	-0.599
3680	219441	-0.576
3682	219506	-0.721
3684	219571	-0.539
3686	219636	-0.655
3688	219701	-0.509
3690	219766	-0.625
3692	219831	-0.628
3694	219896	-0.749
3696	219961	-0.582
3698	220027	-0.633
3700	220092	-0.514
3702	220157	-0.686
3704	220222	-0.537
3706	220287	-0.507
3708	220352	-0.440
3710	220417	-0.464
3712	220482	-0.490
3714	220547	-0.581
3716	220612	-0.504
3718	220677	-0.488
3720	220742	-0.400
3722	220807	-0.399
3724	220872	-0.502
3726	220937	-0.557
3728	221002	-0.536
3730	221067	-0.404
3732	221132	-0.428
3734	221197	-0.451
3736	221262	-0.529
3738	221327	-0.737
3740	221392	-0.593
3742	221457	-0.568
3744	221522	-0.404
3746	221587	-0.405
3748	221652	-0.606
3750	221717	-0.591
3752	221782	-0.208
3754	221847	-0.577
3756	221912	-0.539
3758	221977	-0.522
3760	222042	-0.854
3762	222107	-0.508
3764	222172	-0.592
3766	222237	-0.448
3768	222302	-0.501
3770	222367	-0.347
3772	222432	-0.653
3774	222497	-0.644
3776	222562	-0.603
3778	222627	-0.460
3780	222692	-0.443
3782	222757	-0.615
3784	222822	-0.736
3786	222887	-0.536
3788	222952	-0.535
3790	223018	-0.648
3792	223083	-0.554
3794	223148	-0.581

3796	223213	-0.583
3798	223278	-0.598
3800	223343	-0.666
3802	223408	-0.674
3804	223473	-0.735
3806	223538	-0.840
3808	223603	-0.641
3810	223668	-0.624
3812	223733	-0.846
3814	223798	-0.626
3816	223863	-0.879
3818	223928	-0.678
3820	223993	-0.746
3822	224058	-0.557
3824	224123	-0.599
3826	224188	-0.597
3828	224253	-0.522
3830	224318	-0.643
3832	224383	-0.623
3834	224448	-0.664
3836	224513	-0.556
3838	224578	-0.598
3840	224643	-0.607
3842	224708	-0.576
3844	224773	-0.841
3846	224838	-0.617
3848	224903	-0.738
3850	224968	-0.618
3852	225033	-0.462
3854	225098	-0.610
3856	225163	-0.655
3858	225228	-0.800
3860	225293	-0.592
3862	225358	-0.810
3864	225423	-0.449
3866	225488	-0.662
3868	225553	-0.637
3870	225618	-0.751
3872	225683	-0.715
3874	225748	-0.712
3876	225813	-0.862
3878	225878	-0.766
3880	225943	-0.534
3882	226009	-0.709
3884	226074	-0.602
3886	226139	
3888	226204	
3890	226269	
3892	226334	
3894	226399	
3896	226464	
3898	226529	
3900	226594	
3902	226659	-0.838
3904	226724	-0.774
3906	226789	-0.511
3908	226854	-0.413
3910	226919	-0.447
3912	226984	-0.706
3914	227049	-0.642
3916	227114	-0.405
3918	227179	-0.639
3920	227244	-0.691
3922	227309	-0.513
3924	227374	-0.584
3926	227439	-0.364
3928	227504	-0.534
3930	227569	-0.455
3932	227634	-0.523
3934	227699	-0.438
3936	227764	-0.457
3938	227829	-0.344
3940	227894	-0.550

3942	227959	-0.329
3944	228024	-0.190
3946	228089	-0.393
3948	228154	-0.095
3950	228219	-0.324
3952	228284	-0.367
3954	228349	-0.462
3956	228414	-0.540
3958	228479	-0.453
3960	228544	-0.536
3962	228609	-0.502
3964	228674	-0.405
3966	228739	-0.569
3968	228804	-0.465
3970	228869	-0.371
3972	228934	-0.373
3974	229000	-0.443
3976	229065	-0.467
3978	229130	-0.346
3980	229195	-0.256
3982	229260	-0.270
3984	229325	-0.399
3986	229390	-0.451
3988	229455	-0.502
3990	229520	-0.473
3992	229585	-0.295
3994	229650	-0.429
3996	229715	-0.484
3998	229780	-0.383
4000	229845	-0.265
4002	229910	-0.408
4004	229975	-0.490
4006	230040	-0.412
4008	230105	-0.442
4010	230170	-0.481
4012	230235	-0.478
4014	230300	-0.344
4016	230365	-0.421
4018	230430	-0.411
4020	230495	-0.363
4022	230560	-0.288
4024	230625	-0.426
4026	230690	-0.468
4028	230755	-0.354
4030	230820	-0.409
4032	230885	-0.375
4034	230950	-0.455
4036	231015	-0.472
4038	231080	-0.359
4040	231145	-0.460
4042	231210	-0.176
4044	231275	-0.450
4046	231340	-0.132
4048	231405	
4050	231470	
4052	231535	-0.174
4054	231600	-0.132
4056	231665	-0.371
4058	231730	-0.258
4060	231795	-0.425
4062	231860	-0.394
4064	231925	-0.249
4066	231991	-0.353
4068	232056	-0.254
4070	232121	-0.487
4072	232186	-0.434
4074	232251	-0.314

Core MD02-2520

Depth (cm) (non corrected)	Depth (cm) (corrected)	Age cal yrs BP	*Sed. Rate (smoothed)*	Elemental Comp (% C)	Elemental Comp (% N)	Opal (wt %)
	1	515				
	2	519				
	3	523				
11	4	527		6.243	0.767	11.22
21	14	569	*240.2*	6.651	0.803	11.03
31	24	611	*240.2*	5.647	0.658	8.69
41	34	652	*240.2*	5.223	0.609	9.16
51	44	694	*240.2*	5.728	0.646	9.77
61	54	736	*240.2*	5.636	0.639	9.04
71	64	777	*240.2*	5.112	0.565	8.79
81	74	819	*240.2*	5.048	0.565	10.08
91	84	861	*240.2*	5.227	0.582	8.04
101	94	902	*240.2*	5.359	0.598	9.71
111	104	944	*240.2*	4.911	0.544	8.07
121	114	986	*240.2*	5.010	0.382	8.89
131	124	1027	*240.2*	5.045	0.424	11.50
141	134	1092	*112.7*	6.051	0.373	11.65
151	144	1181	*112.7*	6.002	0.560	12.65
161	154	1270	*112.7*	5.571	0.565	12.85
171	164	1359	*112.7*	5.519	0.624	12.49
181	174	1447	*112.7*	4.603	0.461	10.80
191	184	1536	*112.7*	4.860	0.531	11.71
201	194	1625	*112.7*	4.636	0.492	12.53
211	204	1713	*112.7*	4.241	0.410	9.18
221	214	1802	*112.7*	5.221	0.540	8.66
231	224	1891	*112.7*	5.171	0.540	10.38
241	234	1980	*112.7*	5.084	0.516	9.77
251	244	2068	*112.7*	5.401	0.604	11.73
261	254	2157	*112.7*	5.116	0.585	12.54
271	264	2246	*112.7*	4.869	0.564	9.43
281	274	2334	*112.7*	4.979	0.544	8.76
291	284	2423	*112.7*	5.364	0.575	11.33
301	294	2512	*112.7*	5.379	0.594	11.79
311	304	2601	*112.7*	4.139	0.462	10.40
321	314	2711	*75.3*	5.071	0.561	11.81
331	324	2844	*75.3*	5.309	0.580	10.78
341	334	2977	*75.3*	5.544	0.620	11.28
351	344	3110	*75.3*	5.451	0.598	10.49
361	354	3243	*75.3*	5.153	0.586	11.48
371	364	3376	*75.3*	5.714	0.631	11.03
381	374	3508	*75.3*	5.239	0.566	10.54
391	384	3641	*75.3*	5.513	0.622	12.42
401	394	3774	*75.3*	4.908	0.515	9.94
411	404	3907	*75.3*	5.660	0.620	12.44
421	414	4025	*84.7*	5.194	0.566	10.67
431	424	4143	*84.7*	5.414	0.603	11.79
441	434	4261	*84.7*	5.171	0.568	12.34
451	444	4379	*84.7*	6.343	0.532	9.51
461	454	4497	*84.7*	4.783	0.501	8.72
471	464	4615	*84.7*	5.102	0.525	10.60
481	474	4734	*84.7*	5.529	0.578	9.43
491	484	4852	*84.7*	5.392	0.581	9.80
501	494	4970	*84.7*	4.930	0.520	10.85
511	504	5088	*84.7*	5.441	0.554	12.17
521	514	5206	*84.7*	4.964	0.509	9.73
531	524	5324	*84.7*	5.320	0.552	10.56
541	534	5442	*84.7*	4.159	0.484	8.65
551	544	5525	*120.3*	4.298	0.489	11.30
561	554	5608	*120.3*	5.049	0.520	12.08
571	564	5691	*120.3*	5.127	0.546	11.08

581	574	5774	*120.3*	5.174	0.549	11.56
591	584	5858	*120.3*	4.596	0.499	10.87
601	594	5941	*120.3*	5.077	0.552	10.55
611	604	6024	*120.3*	4.928	0.542	10.39
621	614	6107	*120.3*	5.072	0.556	12.28
631	624	6190	*120.3*	4.369	0.478	8.97
641	634	6273	*120.3*	4.820	0.530	8.85
651	644	6356	*120.3*	4.589	0.539	9.60
661	654	6439	*120.3*	4.944	0.533	11.98
661	661	6498	*120.3*			11.77
671	664	6522	*120.3*	4.671	0.486	12.27
671	671	6587	*88.8*			11.71
681	674	6620	*88.8*	4.431	0.486	11.74
691	684	6733	*88.8*			11.06
701	694	6846	*88.8*	4.147	0.462	9.73
711	704	6958	*88.8*	4.235	0.469	11.65
721	714	7071	*88.8*	4.333	0.492	10.87
731	724	7183	*88.8*	4.411	0.489	10.17
741	734	7296	*88.8*	4.238	0.458	9.58
751	744	7409	*88.8*	4.401	0.478	10.04
761	754	7521	*88.8*	3.976	0.450	9.53
771	764	7634	*88.8*	4.046	0.463	10.22
781	774	7747	*88.8*			11.28
791	784	7859	*88.8*			9.64
801	794	7972	*88.8*	4.104	0.444	9.31
811	804	8084	*88.8*	4.203	0.458	9.18
821	814	8197	*88.8*	3.808	0.441	8.69
831	824	8310	*88.8*	3.627	0.404	7.66
841	834	8422	*88.8*	4.241	0.457	8.09
851	844	8535	*88.8*	4.381	0.489	9.34
861	854	8665	*77.2*	4.788	0.550	8.99
871	864	8794	*77.2*	3.956	0.458	8.19
881	874	8924	*77.2*	4.308	0.496	9.25
891	884	9053	*77.2*	4.034	0.470	10.46
902	895	9196	*77.2*	4.571	0.497	9.20
911	904	9313	*77.2*	4.258	0.468	10.14
921	914	9442	*77.2*	4.268	0.464	8.21
931	924	9572	*77.2*	4.350	0.492	11.51
941	934	9701	*77.2*	4.159	0.470	10.77
951	944	9831	*77.2*	4.555	0.515	9.09
961	954	9961	*77.2*	4.480	0.509	10.06
971	964	10090	*77.2*	4.393	0.490	9.51
981	974	10237	*60.8*	4.287	0.481	9.22
991	984	10402	*60.8*	4.314	0.475	9.88
1001	994	10566	*60.8*	4.919	0.548	11.21
1011	1004	10730	*60.8*	4.663	0.534	11.80
1021	1014	10895	*60.8*	4.746	0.541	9.20
1031	1024	11059	*60.8*	5.448	0.580	9.71
1041	1034	11224	*60.8*	5.638	0.616	10.66
1051	1043	11372	*60.8*	6.292	0.674	8.97
1061	1053	11536	*60.8*	6.230	0.678	10.25
1071	1063	11701	*60.8*	5.759	0.615	9.82
1081	1073	11865	*60.8*	5.982	0.653	9.00
1091	1083	12093	*43.8*	5.690	0.625	8.31
1101	1093	12322	*43.8*	5.321	0.583	6.62
1111	1103	12550	*43.8*	6.125	0.676	9.47
1121	1113	12779	*43.8*	5.597	0.612	6.76
1131	1123	13007	*43.8*	5.543	0.636	9.26
1141	1133	13196	*52.8*	4.558	0.569	6.38
1151	1143	13386	*52.8*	5.513	0.625	7.22
1161	1153	13575	*52.8*	5.211	0.593	6.64
1171	1163	13765	*52.8*	5.230	0.592	7.87
1181	1173	13954	*52.8*	5.924	0.650	7.98
1191	1183	14163	*47.9*	5.293	0.567	6.46
1201	1192	14350	*47.9*	5.442	0.586	8.15

1211	1202	14559	*47.9*	4.306	0.468	7.64
1221	1212	14767	*47.9*	4.774	0.505	6.33
1231	1222	14976	*47.9*	6.655	0.687	5.65
1241	1232	15095	*83.7*	5.825	0.638	5.56
1251	1242	15215	*83.7*	6.227	0.638	3.89
1261	1252	15334	*83.7*	5.229	0.574	5.53
1271	1262	15454	*83.7*	4.437	0.503	5.39
1281	1272	15573	*83.7*	4.333	0.465	4.28
1291	1282	15693	*83.7*	3.867	0.397	3.18
1301	1292	15812	*83.7*	2.729	0.344	3.82
1311	1302	15932	*83.7*	1.824	0.230	3.77
1321	1312	16051	*83.7*	4.568	0.499	4.91
1331	1322	16171	*83.7*	4.673	0.505	5.87
1341	1332	16290	*83.7*	4.027	0.425	4.67
1351	1382	16887	*83.7*	4.098	0.434	4.48
1361	1392	17071	*56.8*	4.328	0.433	5.11
1371	1402	17319	*56.8*	3.858	0.411	5.81
1381	1412	17567	*56.8*	3.750	0.384	5.66
1391	1422	17814	*56.8*	3.812	0.406	5.64
1401	1432	18062	*56.8*	3.279	0.331	4.12
1411	1442	18310	*56.8*	3.891	0.422	5.50
1421	1452	18407	*56.8*	4.971	0.537	6.45
1431	1462	18504	*56.8*	4.494	0.461	6.45
1441	1472	18601	*56.8*			8.23
1451	1482	18698	*56.8*	4.776	0.507	7.06
1461	1492	18795	*56.8*	4.623	0.477	6.91
1471	1502	18853	*117.4*	4.485	0.606	7.15
1481	1512	18911	*117.4*	4.217	0.456	6.93
1491	1522	18970	*117.4*	4.534	0.490	7.64
1501	1541	19080	*117.4*	4.566	0.479	7.44
1511	1551	19139	*117.4*	5.025	0.535	9.19
1521	1561	19197	*117.4*	4.294	0.427	6.92
1531	1571	19255	*117.4*	4.089	0.462	1.85
1541	1581	19350	*117.4*	4.988	0.523	2.95
1551	1591	19444	*117.4*	4.714	0.499	2.68
1561	1599	19520	*117.4*	5.056	0.536	2.62
1571	1609	19615	*117.4*	4.996	0.541	3.83
1581	1619	19709	*117.4*	4.855	0.514	4.72
1591	1629	19804	*117.4*	5.211	0.554	7.57
1671	1658	20078	*117.4*	4.312	0.437	4.30
1681	1668	20173	*117.4*	5.326	0.560	7.56
1691	1678	20268	*117.4*	4.686	0.496	9.48
1701	1688	20362	*117.4*	4.877	0.514	8.08
1711	1698	20457	*117.4*	4.861	0.519	7.01
1721	1708	20552	*117.4*	4.756	0.522	7.08
1731	1718	20646	*117.4*	4.837	0.524	9.42
1741	1728	20741	*117.4*	3.367	0.362	5.83
1751	1738	20836	*117.4*	4.711	0.518	7.72
1761	1747	20921	*117.4*	4.468	0.495	7.60
1771	1757	21015	*117.4*	4.273	0.468	6.51
1781	1767	21110	*117.4*	4.209	0.460	7.23
1791	1777	21205	*117.4*	4.398	0.497	8.72
1802	1788	21309	*117.4*	4.491	0.499	8.55
1811	1797	21394	*117.4*	4.211	0.477	8.43
1821	1807	21494	*119.2*	4.527	0.518	8.11
1831	1817	21594	*119.2*	4.149	0.477	9.96
1841	1827	21695	*119.2*	4.031	0.461	7.23
1851	1837	21795	*119.2*	4.343	0.468	8.88
1861	1847	21895	*119.2*	4.324	0.488	8.51
1871	1857	21995	*119.2*	3.614	0.405	6.83
1881	1867	22096	*119.2*	4.027	0.461	8.07
1891	1877	22196	*119.2*	4.203	0.464	9.05
1901	1887	22296	*119.2*	4.328	0.502	9.94
1911	1897	22396	*119.2*	4.284	0.478	8.37
1921	1907	22497	*119.2*	4.414	0.508	7.84

1931	1917	22597	*119.2*	4.517	0.518	8.22
1941	1927	22697	*119.2*	4.614	0.506	9.30
1951	1936	22787	*119.2*	4.781	0.513	7.67
1961	1946	22887	*119.2*	4.302	0.489	7.92
1971	1956	22988	*119.2*	5.534	0.541	8.73
1981	1966	23088	*119.2*	5.136	0.556	8.16
1991	1976	23188	*119.2*	5.315	0.590	9.66
2001	1986	23288	*119.2*	5.045	0.562	9.24
2011	1996	23389	*119.2*	4.303	0.489	7.37
2021	2006	23489	*119.2*	4.614	0.505	7.42
2031	2016	23589	*119.2*	5.284	0.572	8.54
2041	2026	23689	*119.2*	4.985	0.545	7.60
2051	2036	23789	*119.2*	5.154	0.574	9.33
2061	2046	23890	*119.2*	5.446	0.600	8.75
2071	2056	23990	*119.2*	4.750	0.518	7.23
2081	2066	24090	*119.2*	4.548	0.489	6.00
2091	2076	24190	*119.2*	4.514	0.445	5.80
2101	2087	24301	*119.2*	3.997	0.453	5.44
2111	2097	24401	*119.2*	4.262	0.483	5.08
2121	2107	24501	*119.2*	3.503	0.381	5.17
2131	2117	24578	*119.2*	5.852	0.641	8.87
2141	2127	24630	*119.2*	4.607	0.526	6.39
2151	2137	24683	*119.2*	5.670	0.567	6.76
2161	2147	24736	*119.2*	4.747	0.505	6.61
2171	2157	24789	*119.2*	5.249	0.573	7.97
2181	2167	24842	*119.2*	5.349	0.571	8.85
2191	2177	24894	*119.2*	5.246	0.552	8.82
2201	2187	24947	*119.2*	5.141	0.535	8.86
2211	2197	25000	*119.2*	4.351	0.499	7.12
2221	2207	25053	*119.2*	4.148	0.468	7.11
2231	2217	25106	*119.2*	4.201	0.424	8.81
2241	2227	25158	*119.2*	3.367	0.380	6.07
2251	2236	25206	*119.2*	3.339	0.342	6.22
2261	2246	25259	*119.2*	3.314	0.365	7.00
2271	2256	25312	*119.2*	3.215	0.352	7.09
2281	2266	25364	*119.2*	3.694	0.401	7.35
2291	2276	25417	*119.2*	3.177	0.364	5.18
2301	2286	25544	*74.3*	3.336	0.380	6.38
2311	2296	25678	*74.3*	3.309	0.383	6.78
2321	2306	25813	*74.3*	3.267	0.373	6.96
2331	2316	25947	*74.3*	3.556	0.415	6.95
2341	2326	26082	*74.3*	3.845	0.440	7.52
2351	2336	26217	*74.3*	3.757	0.435	7.34
2361	2346	26351	*74.3*	4.383	0.505	7.11
2371	2356	26486	*74.3*	4.255	0.402	7.32
2381	2366	26620	*74.3*	4.333	0.480	7.67
2391	2376	26755	*74.3*	4.308	0.444	8.17
2401	2385	26876	*74.3*	4.299	0.486	8.08
2411	2395	27011	*74.3*	4.244	0.492	7.94
2421	2405	27145	*74.3*	4.742	0.543	7.93
2431	2415	27280	*74.3*	4.109	0.480	9.03
2441	2425	27415	*74.3*	5.351	0.617	9.39
2451	2435	27549	*74.3*	5.163	0.580	7.01
2461	2445	27684	*74.3*	5.212	0.597	7.39
2471	2455	27818	*74.3*	4.942	0.575	7.79
2481	2465	27953	*74.3*	4.709	0.558	8.83
2491	2475	28088	*74.3*	4.934	0.583	9.62
2501	2485	28218	*76.8*	4.731	0.563	9.34
2511	2495	28348	*76.8*	4.585	0.533	9.72
2521	2505	28478	*76.8*	4.526	0.537	9.79
2531	2515	28608	*76.8*	4.166	0.492	8.69
2541	2525	28739	*76.8*	4.711	0.543	8.15
2551	2535	28869	*76.8*	4.838	0.557	7.94
2561	2545	28999	*76.8*	4.844	0.570	9.77
2571	2555	29129	*76.8*	4.918	0.578	9.40

2581	2565	29259	*76.8*	4.941	0.597	11.90
2591	2575	29390	*76.8*	5.428	0.641	9.22
2601	2585	29520	*76.8*	5.040	0.594	9.16
2611	2595	29650	*76.8*	4.588	0.552	7.77
2621	2605	29780	*76.8*	3.983	0.492	7.39
2631	2615	29910	*76.8*	4.010	0.485	6.74
2641	2625	30041	*76.8*	4.145	0.517	7.21
2651	2635	30171	*76.8*	4.255	0.518	8.72
2661	2645	30301	*76.8*	3.761	0.466	6.08
2671	2655	30431	*76.8*	3.950	0.487	5.14
2681	2665	30561	*76.8*	3.644	0.457	5.03
2691	2675	30691	*124.7*			5.10
2701	2683	30731	*124.7*	4.299	0.507	6.07
2711	2693	30811	*124.7*	4.111	0.486	4.76
2721	2703	30891	*124.7*	4.405	0.524	6.21
2731	2713	30971	*124.7*	4.561	0.538	6.79
2741	2723	31051	*124.7*	4.741	0.563	7.55
2751	2733	31132	*124.7*	4.747	0.538	6.54
2761	2743	31212	*124.7*	4.875	0.578	8.36
2771	2753	31292	*124.7*	5.357	0.618	7.28
2781	2763	31372	*124.7*	4.293	0.537	8.62
2791	2773	31453	*124.7*	4.510	0.532	7.83
2801	2783	31533	*124.7*	4.775	0.585	8.51
2811	2793	31613	*124.7*	4.111	0.486	7.61
2821	2803	31693	*124.7*	3.874	0.476	8.00
2831	2813	31773	*124.7*	4.208	0.526	9.72
2841	2823	31854	*124.7*	4.487	0.530	8.76
2851	2833	31934	*124.7*	4.278	0.523	8.65
2861	2841	31998	*124.7*	4.539	0.551	8.79
2871	2851	32078	*124.7*	4.410	0.519	8.29
2881	2861	32158	*124.7*	4.874	0.604	9.01
2891	2871	32239	*124.7*	5.420	0.667	10.86
2901	2881	32319	*124.7*	4.291	0.530	5.90
2911	2891	32464	*69.1*	4.966	0.584	8.29
2921	2901	32608	*69.1*	5.205	0.606	8.25
2931	2911	32753	*69.1*	4.466	0.542	8.09
2941	2921	32898	*69.1*	4.397	0.526	6.77
2951	2931	33042	*69.1*	4.496	0.521	7.04
2961	2941	33187	*69.1*	4.382	0.551	6.70
2971	2951	33332	*69.1*	4.647	0.560	7.87
2981	2961	33476	*69.1*	5.017	0.610	7.78
2991	2971	33621	*69.1*	4.998	0.592	5.64
3001	2980	33751	*69.1*	4.578	0.531	6.55
3011	2990	33893	*110.6*	4.319	0.508	6.84
3021	3000	34034	*110.6*	4.486	0.536	8.27
3031	3010	34176	*110.6*	4.424	0.520	7.19
3041	3020	34317	*110.6*	4.436	0.535	6.04
3051	3030	34458	*110.6*	4.510	0.549	6.51
3061	3040	34600	*110.6*	4.336	0.557	7.07
3071	3050	34741	*110.6*	4.492	0.537	8.60
3081	3060	34882	*110.6*	4.141	0.506	8.10
3091	3070	35024	*110.6*	5.264	0.633	7.85
3101	3080	35165	*110.6*	5.130	0.596	7.05
3111	3090	35306	*110.6*	4.897	0.574	5.82
3121	3100	35448	*110.6*	4.775	0.580	5.66
3131	3110	35589	*110.6*	4.576	0.565	6.72
3141	3120	35730	*110.6*	4.929	0.579	6.50
3151	3130	35872	*110.6*	4.861	0.579	6.85
3161	3140	36013	*110.6*	4.586	0.549	6.38
3171	3150	36154	*110.6*	5.158	0.596	6.70
3181	3160	36225	*110.6*	4.909	0.592	6.86
3191	3170	36295	*110.6*			7.20
3201	3180	36366	*110.6*	4.561	0.541	8.14
3211	3190	36437	*110.6*	5.517	0.632	8.49
3221	3200	36507	*110.6*	5.467	0.620	7.46

3231	3210	36578	*110.6*	5.138	0.614	8.41
3241	3220	36648	*110.6*	5.451	0.618	7.94
3251	3230	36719	*110.6*	5.625	0.639	7.39
3261	3240	36789	*110.6*	5.532	0.632	8.05
3271	3250	36860	*110.6*	5.804	0.672	6.47
3281	3260	36931	*110.6*	5.961	0.668	8.05
3291	3270	37001	*110.6*	5.700	0.646	6.37
3301	3279	37065	*110.6*	5.101	0.582	7.84
3311	3289	37233	*22.7*	4.525	0.552	7.34
3321	3299	37500	*22.7*	5.248	0.593	6.54
3331	3309	37767	*22.7*	5.209	0.618	6.59
3341	3319	38033	*22.7*	5.003	0.577	0.72
3351	3329	38300	*22.7*	5.308	0.582	5.64
3361	3339	38561	*41.0*	4.613	0.536	5.41
3371	3349	38822	*41.0*	4.207	0.508	3.85
3381	3359	39083	*41.0*	4.943	0.582	7.52
3391	3369	39344	*41.0*	5.385	0.619	4.93
3401	3379	39606	*41.0*	5.348	0.623	5.95
3411	3389	39867	*41.0*	5.072	0.590	8.41
3421	3399	40128	*41.0*	4.922	0.574	9.26
3431	3409	40389	*41.0*	4.851	0.575	7.54
3441	3419	40650	*41.0*	4.776	0.561	8.23
3453	3430	40937	*41.0*			8.07
3461	3438	41146	*41.0*	4.757	0.547	7.33
3472	3449	41457	*28.5*	4.754	0.549	6.30
3481	3458	41711	*28.5*	4.184	0.501	8.19
3491	3468	41994	*28.5*	4.015	0.496	9.12
3501	3478	42276	*28.5*	4.231	0.497	8.59
3511	3488	42559	*35.4*			
3521	3498	42841	*35.4*	5.352	0.582	
3531	3508	43124	*35.4*	4.689	0.534	
3541	3518	43406	*35.4*	4.629	0.535	
3551	3528	43689	*35.4*	4.519	0.510	
3561	3538	43971	*35.4*	4.770	0.539	
3571	3548	44254	*35.4*	4.717	0.547	
3581	3558	44536	*35.4*	5.552	0.649	
3591	3568	44819	*35.4*	4.013	0.473	
3601	3578	45101	*35.4*	5.517	0.647	
3611	3586	45327	*35.4*	5.310	0.612	
3621	3596	45610	*35.4*			
3631	3606	45892	*35.4*			
3641	3616	46175	*35.4*			
3651	3626	46457	*35.4*			
3661	3636	46740	*35.4*	4.637	0.541	
3671	3646	47022	*35.4*	4.099	0.489	
3681	3656	47305	*35.4*	4.412	0.520	
3691	3666	47587	*35.4*	4.561	0.538	
3701	3676	47870	*35.4*	4.023	0.510	

Molar BSi/C	Molar BSi/N	Porosity [% vol]	OC MAR mg/cm2/kyr	Opal MAR mg/cm2/kyr	Al2O3 %	Al %	opal/Al
0.32	3.05	0.260			14.5	7.67	1.46
0.30	2.86	0.252	2867.94	4754.30	14.66	7.76	1.42
0.27	2.75	0.239	2477.65	3812.93	15.14	8.01	1.08
0.31	3.13	0.252	2251.73	3950.11	14.48	7.66	1.20
0.30	3.15	0.282	2372.05	4046.29	15.4	8.15	1.20
0.29	2.95	0.271	2366.60	3796.39	15.19	8.04	1.12
0.31	3.24	0.278	2127.41	3658.01	14.7	7.78	1.13
0.36	3.72	0.281	2090.89	4175.15	15.52	8.21	1.23
0.27	2.88	0.268	2203.89	3392.06	15.48	8.19	0.98
0.32	3.38	0.267	2265.26	4102.93	15.31	8.10	1.20
0.29	3.09	0.257	2102.78	3456.73	14.13	7.48	1.08
0.32	4.85	0.239	2197.66	3900.69	15.16	8.02	1.11
0.41	5.66	0.257	2161.20	4928.33	15.76	8.34	1.38
0.34	6.50	0.241	1691.92	3256.51	14.61	7.73	1.51
0.38	4.70	0.233	1245.74	2624.72	14.42	7.63	1.66
0.41	4.74	0.239	1147.19	2645.90	15.11	8.00	1.61
0.40	4.17	0.249	1121.20	2538.24	15.4	8.15	1.53
0.42	4.88	0.246	939.40	2203.62	14.21	7.52	1.44
0.43	4.59	0.237	1003.37	2416.78	15.44	8.17	1.43
0.48	5.31	0.235	959.05	2592.60	15.62	8.27	1.52
0.39	4.66	0.225	888.96	1923.83	13.79	7.30	1.26
0.30	3.34	0.227	1091.37	1811.08	15.34	8.12	1.07
0.36	4.00	0.233	1072.80	2153.05	14.31	7.57	1.37
0.34	3.95	0.228	1061.63	2040.93	14.7	7.78	1.26
0.39	4.04	0.228	1127.90	2448.68	15.51	8.21	1.43
0.44	4.47	0.229	1066.44	2614.74	15.5	8.20	1.53
0.35	3.48	0.214	1034.91	2004.67	15.5	8.20	1.15
0.31	3.35	0.226	1042.60	1834.06	15.68	8.30	1.06
0.38	4.11	0.215	1138.89	2406.40	15.65	8.28	1.37
0.39	4.13	0.225	1128.03	2471.95	13.17	6.97	1.69
0.45	4.69	0.238	853.16	2144.63	14.91	7.89	1.32
0.42	4.39	0.243	831.85	1937.62	15.57	8.24	1.43
0.36	3.87	0.230	738.60	1499.92	14.81	7.84	1.38
0.36	3.79	0.251	750.36	1527.00	15.24	8.07	1.40
0.34	3.66	0.239	749.78	1443.36	15.11	8.00	1.31
0.40	4.08	0.240	707.26	1576.24	16.17	8.56	1.34
0.34	3.64	0.239	785.91	1516.48	15.57	8.24	1.34
0.36	3.88	0.227	731.93	1472.64	14.03	7.43	1.42
0.40	4.16	0.225	771.56	1737.73	16.24	8.59	1.44
0.36	4.02	0.226	686.36	1390.41	15.76	8.34	1.19
0.39	4.18	0.226	791.52	1739.23	15.98	8.46	1.47
0.37	3.93	0.238	804.93	1654.01	15.16	8.02	1.33
0.39	4.07	0.238	838.75	1826.14	15.12	8.00	1.47
0.43	4.52	0.217	822.60	1962.25	15.77	8.35	1.48
0.27	3.72	0.217	1010.07	1514.47	16.21	8.58	1.11
0.33	3.63	0.223	755.24	1377.29	14.84	7.85	1.11
0.37	4.21	0.205	824.07	1712.51	15.02	7.95	1.33
0.30	3.40	0.231	863.87	1472.90	15.75	8.34	1.13
0.32	3.51	0.227	846.91	1538.61	16.03	8.48	1.15
0.39	4.35	0.220	781.66	1720.16	14.46	7.65	1.42
0.40	4.58	0.242	838.29	1874.98	16.48	8.72	1.40
0.35	3.98	0.238	768.94	1507.83	14.98	7.93	1.23
0.35	3.99	0.239	822.62	1633.59	15.97	8.45	1.25
0.37	3.72	0.244	639.25	1329.08	13.93	7.37	1.17
0.47	4.82	0.245	937.49	2465.62	14.61	7.73	1.46
0.43	4.84	0.229	1123.83	2688.41	15.8	8.36	1.44
0.39	4.23	0.241	1123.87	2428.05	16.08	8.51	1.30

CORE MD02-2520

0.40	4.38	0.237	1140.37	2546.83	16.68	8.83	1.31
0.42	4.54	0.256	987.69	2335.59	15.17	8.03	1.35
0.37	3.98	0.290	1040.92	2162.59	16.41	8.68	1.21
0.38	3.99	0.275	1031.58	2175.14	16.79	8.89	1.17
0.43	4.60	0.272	1065.82	2580.06	17.54	9.28	1.32
0.37	3.91	0.269	922.89	1894.40	14.9	7.89	1.14
0.33	3.48	0.270	1016.07	1864.80	15.91	8.42	1.05
0.37	3.71	0.262	978.50	2045.98	16.76	8.87	1.08
0.43	4.68	0.286	1019.36				
0.45	4.97		0.00		14.8	7.83	1.50
0.47	5.26	0.266	990.55		16.35	8.65	1.42
0.47	5.15		0.00				
0.47	5.03	0.276	683.42		16.63	8.80	1.33
0.45	4.71	0.274	0.00	1711.86	16.21	8.58	1.29
0.42	4.39	0.263	651.19	1528.50	16.98	8.99	1.08
0.49	5.17	0.246	680.35	1870.86	16.45	8.71	1.34
0.45	4.60	0.261	682.33	1711.44	16.68	8.83	1.23
0.41	4.33	0.269	686.91	1583.91	16.73	8.85	1.15
0.40	4.36	0.264	664.75	1502.09	17.3	9.16	1.05
0.41	4.37	0.272	682.44	1556.38	17	9.00	1.12
0.43	4.41	0.287	604.42	1448.93	16.84	8.91	1.07
0.45	4.60	0.256	641.36	1619.99	17.78	9.41	1.09
0.43	4.48	0.283	0.00	1722.56	17.94	9.49	1.19
0.42	4.43	0.243	0.00	1554.26	18.51	9.80	0.98
0.41	4.37	0.254	652.57	1480.66	17.22	9.11	1.02
0.39	4.18	0.270	653.53	1427.35	18.25	9.66	0.95
0.41	4.11	0.282	582.54	1329.42	17.58	9.30	0.93
0.38	3.95	0.256	575.17	1215.48	17.28	9.15	0.84
0.34	3.69	0.274	656.46	1252.71	18.16	9.61	0.84
0.38	3.98	0.271	680.65	1451.00	18.27	9.67	0.97
0.34	3.41	0.293	627.05	1177.83	17.49	9.26	0.97
0.37	3.72	0.296	515.60	1066.98	16.15	8.55	0.96
0.38	3.89	0.282	572.80	1230.46	17.3	9.16	1.01
0.46	4.64	0.296	525.76	1363.57	16.37	8.66	1.21
0.36	3.86	0.290	601.43	1210.24	17.6	9.31	0.99
0.43	4.51	0.358	505.91	1204.89			
0.34	3.69	0.290	561.56	1080.46	18.94	10.02	0.82
0.47	4.87	0.275	583.79	1544.85	18.65	9.87	1.17
0.46	4.78	0.281	553.46	1433.59	16.97	8.98	1.20
0.36	3.68	0.290	598.98	1195.43	17.09	9.04	1.01
0.40	4.12	0.286	592.27	1329.58	17.72	9.38	1.07
0.39	4.04	0.283	583.46	1263.19	17.57	9.30	1.02
0.38	4.00	0.272	455.47	979.99	16.69	8.83	1.04
0.41	4.34	0.280	453.69	1039.50	16.95	8.97	1.10
0.41	4.26	0.269	525.07	1196.94	16.91	8.95	1.25
0.45	4.60	0.282	488.42	1236.15	16.93	8.96	1.32
0.35	3.54	0.273	503.42	975.78	15.43	8.17	1.13
0.32	3.49	0.287	566.83	1010.17	16.98	8.99	1.08
0.34	3.61	0.287	586.60	1109.12	16.33	8.64	1.23
0.25	2.77	0.269	671.15	956.79	16.82	8.90	1.01
0.29	3.15	0.305	632.01	1039.32	16.62	8.80	1.16
0.30	3.32	0.273	611.12	1041.54	15.59	8.25	1.19
0.27	2.87	0.262	644.66	969.79	16.22	8.58	1.05
0.26	2.77	0.288	425.46	621.57	16.36	8.66	0.96
0.22	2.37	0.285	399.66	497.22	14.82	7.84	0.84
0.28	2.92	0.258	477.62	738.62	16.13	8.54	1.11
0.22	2.30	0.282	422.27	510.06	16.58	8.77	0.77
0.30	3.03	0.306	404.51	675.88	17.28	9.15	1.01
0.25	2.34	0.290	410.13	574.29	17.27	9.14	0.70
0.23	2.41	0.305	485.31	635.93	17.82	9.43	0.77
0.23	2.33	0.310	455.95	581.09	18.57	9.83	0.68
0.27	2.77	0.272	482.26	725.54	15.33	8.11	0.97
0.24	2.56	0.282	539.05	726.51	16.61	8.79	0.91
0.22	2.37	0.256	453.02	553.11	17.21	9.11	0.71
0.27	2.90	0.288	445.37	666.86	16.97	8.98	0.91

0.32	3.40	0.288	352.74	626.21	15.8	8.36	0.91
0.24	2.61	0.280	395.63	524.94	17.86	9.45	0.67
0.15	1.71	0.298	537.27	456.10	16.79	8.89	0.64
0.17	1.81	0.316	800.62	763.77	16.49	8.73	0.64
0.11	1.27	0.298	878.14	548.44	16.84	8.91	0.44
0.19	2.01	0.295	740.45	782.76	17.6	9.31	0.59
0.22	2.23	0.292	631.15	767.36	17.19	9.10	0.59
0.18	1.92	0.321	591.02	584.33	15.48	8.19	0.52
0.15	1.67	0.286	554.57	456.21	14.52	7.68	0.41
0.25	2.32	0.277	396.20	555.23	17.08	9.04	0.42
0.37	3.41	0.282	263.23	543.51	17.55	9.29	0.41
0.19	2.05	0.246	692.28	744.51	16.57	8.77	0.56
0.22	2.42	0.291	666.03	836.22	18.09	9.57	0.61
0.21	2.29	0.292	572.91	664.79	16.97	8.98	0.52
0.20	2.15	0.295	580.20	634.08	18.41	9.74	0.46
0.21	2.46	0.281	301.93	356.27	18.3	9.68	0.53
0.27	2.94	0.253	279.03	419.85	17.35	9.18	0.63
0.27	3.07	0.288	258.43	390.05	17.4	9.21	0.61
0.26	2.89	0.293	261.01	386.15	18.18	9.62	0.59
0.22	2.59	0.288	226.07	283.79	17.28	9.15	0.45
0.25	2.72	0.265	276.85	391.47	17.18	9.09	0.61
0.23	2.50	0.295	867.48	1125.21	18.91	10.01	0.64
0.26	2.92	0.318	758.77	1089.27	17.46	9.24	0.70
0.26	2.91	0.268	0.00	1491.18	17.34	9.18	0.90
0.26	2.90	0.250	886.74	1310.14	18.28	9.67	0.73
0.27	3.02	0.237	872.29	1303.47	17.85	9.45	0.73
0.28	2.46	0.239	866.29	1380.77	18.46	9.77	0.73
0.29	3.17	0.261	790.77	1299.51	17.69	9.36	0.74
0.30	3.25	0.217	900.71	1518.27	17.72	9.38	0.81
0.29	3.23	0.179	951.20	1549.35	17.94	9.49	0.78
0.33	3.58	0.189	1033.94	1890.10	17.71	9.37	0.98
0.29	3.37	0.235	832.99	1341.70	17.91	9.48	0.73
0.08	0.84	0.185	845.19	382.87	17.58	9.30	0.20
0.11	1.17	0.229	976.22	576.40	18.23	9.65	0.31
0.10	1.12	0.195	961.91	546.85	18.27	9.67	0.28
0.09	1.02	0.198	1028.39	533.74	18.15	9.61	0.27
0.14	1.48	0.180	1039.47	797.36	17.95	9.50	0.40
0.17	1.91	0.196	990.18	962.44	18.21	9.64	0.49
0.26	2.85	0.240	1003.99	1458.48	18.03	9.54	0.79
0.18	2.05	0.332	730.27	728.73			
0.25	2.81	0.273	981.85	1393.62			
0.36	3.98	0.241	902.13	1825.04			
0.30	3.27	0.266	907.61	1503.54	17.91	9.48	0.85
0.26	2.82	0.301	862.10	1243.94	18	9.53	0.74
0.27	2.83	0.274	875.44	1303.66	18.01	9.53	0.74
0.35	3.75	0.262	904.83	1762.50	17.07	9.03	1.04
0.31	3.36	0.255	635.90	1101.90	11.86	6.28	0.93
0.29	3.10	0.379	742.20	1215.94	17.93	9.49	0.81
0.30	3.20	0.409	670.43	1139.95	17.5	9.26	0.82
0.27	2.90	0.438	609.27	927.81	17.21	9.11	0.71
0.31	3.27	0.459	577.41	991.50	16.96	8.98	0.81
0.35	3.65	0.468	593.41	1176.44	18.14	9.60	0.91
0.34	3.57	0.438	640.35	1219.54	18.51	9.80	0.87
0.36	3.68	0.460	577.15	1155.11	18.31	9.69	0.87
0.32	3.26	0.450	595.77	1067.17	18.06	9.56	0.85
0.43	4.35	0.466	530.23	1272.27	16.96	8.98	1.11
0.32	3.27	0.482	499.71	896.61	17.23	9.12	0.79
0.37	3.95	0.492	527.88	1079.19	18.29	9.68	0.92
0.35	3.63	0.482	536.24	1055.73			
0.34	3.51	0.471	458.05	865.10			
0.36	3.65	0.481	500.85	1003.99			
0.38	4.06	0.486	517.31	1113.71	18.04	9.55	0.95
0.41	4.13	0.470	549.07	1261.32	17.68	9.36	1.06
0.35	3.65	0.493	520.61	1016.60	16.94	8.97	0.93
0.32	3.21	0.488	541.27	960.88	17.88	9.46	0.83

CORE MD02-2520

0.33	3.31	0.488	554.22	1009.10	18.4	9.74	0.84
0.36	3.83	0.484	569.99	1148.32	17.78	9.41	0.99
0.29	3.11	0.468	609.22	976.76	17.41	9.21	0.83
0.33	3.38	0.523	491.68	905.42	16.94	8.97	0.88
0.28	3.36	0.454	723.66	1141.65			
0.28	3.06	0.479	640.50	1017.73			
0.32	3.41	0.495	643.10	1169.21			
0.33	3.43	0.514	586.75	1074.90			
0.31	3.14	0.503	512.51	877.72			
0.29	3.06	0.495	558.39	898.53			
0.29	3.11	0.495	639.09	1032.94			
0.27	2.91	0.481	619.76	945.23			
0.32	3.39	0.441	690.51	1250.06			
0.29	3.04	0.450	717.76	1153.69			
0.27	2.91	0.400	682.22	1039.02			
0.24	2.56	0.336	722.69	953.18			
0.23	2.72	0.294	763.23	981.31			
0.24	2.50	0.328	642.96	874.89			
0.21	2.19	0.298	716.74	853.89			
0.26	2.83	0.359	538.10	794.68	14.59	7.72	0.67
0.27	2.88	0.338	927.63	1406.66			
0.25	2.53	0.339	729.06	1010.54			
0.21	2.48	0.363	865.77	1032.04			
0.25	2.73	0.362	725.63	1010.08			
0.27	2.90	0.389	768.80	1167.64			
0.30	3.23	0.356	824.58	1364.24			
0.30	3.33	0.377	782.56	1316.19			
0.31	3.45	0.363	784.26	1351.73			
0.29	2.97	0.419	451.01	738.45			
0.31	3.17	0.421	428.57	734.99			
0.37	4.33	0.459	404.98	848.83	16.64	8.81	1.00
0.32	3.33	0.476	314.73	567.45	15.43	8.17	0.74
0.33	3.79	0.473	314.02	584.65	16.47	8.72	0.71
0.38	3.99	0.487	303.34	640.50	16.64	8.81	0.79
0.39	4.20	0.463	307.80	678.81	16.71	8.84	0.80
0.36	3.82	0.443	367.10	730.40	17.47	9.25	0.79
0.29	2.96	0.463	304.39	496.32	15.31	8.10	0.64
0.34	3.50	0.468	316.59	605.41	16.87	8.93	0.71
0.37	3.69	0.472	311.50	638.55	16.69	8.83	0.77
0.38	3.89	0.450	320.60	682.58	16.97	8.98	0.77
0.35	3.49	0.473	333.99	652.41	17.07	9.03	0.77
0.35	3.56	0.464	367.65	718.97	16.37	8.66	0.87
0.35	3.52	0.383	413.22	807.32	16.44	8.70	0.84
0.29	2.93	0.298	548.89	889.98	17.47	9.25	0.77
0.31	3.79	0.300	530.96	913.22	16.88	8.93	0.82
0.32	3.33	0.296	543.87	962.25	17.02	9.01	0.85
0.34	3.84	0.305	533.89	1013.02	18.1	9.58	0.85
0.34	3.47	0.310	528.65	994.03	16.62	8.80	0.92
0.33	3.36	0.285	540.94	1012.61	18.83	9.97	0.80
0.30	3.04	0.276	612.53	1024.71	18.84	9.97	0.80
0.39	3.92	0.307	507.40	1114.78	18.62	9.85	0.92
0.31	3.17	0.318	650.94	1142.01	15.79	8.36	1.12
0.24	2.52	0.336	610.86	829.37	18.21	9.64	0.73
0.25	2.58	0.328	624.37	884.77	18.39	9.73	0.76
0.28	2.82	0.335	585.94	924.18	18.2	9.63	0.81
0.33	3.30	0.324	567.80	1064.91	17.84	9.44	0.94
0.35	3.44	0.324	614.41	1198.32	17.85	9.45	1.02
0.35	3.46	0.319	593.94	1172.87	17.67	9.35	1.00
0.38	3.80	0.288	601.47	1274.81	18	9.53	1.02
0.39	3.80	0.303	581.89	1258.75	18.33	9.70	1.01
0.37	3.68	0.319	522.78	1090.93	18.24	9.65	0.90
0.31	3.13	0.279	626.08	1082.92	18.45	9.76	0.83
0.29	2.97	0.292	631.45	1036.12	19.08	10.10	0.79
0.36	3.57	0.297	627.95	1267.01	18.34	9.71	1.01
0.34	3.39	0.275	656.94	1256.19	18.24	9.65	0.97

0.43	4.15	0.277	658.20	1585.44	18.17	9.62	1.24
0.30	3.00	0.311	689.75	1172.06	18.38	9.73	0.95
0.32	3.21	0.317	634.50	1153.28	17.6	9.31	0.98
0.30	2.93	0.279	610.24	1033.56	17.78	9.41	0.83
0.33	3.13	0.281	528.30	979.58	18.44	9.76	0.76
0.30	2.90	0.269	540.16	908.37	17.44	9.23	0.73
0.31	2.91	0.259	566.14	985.03	17.92	9.48	0.76
0.37	3.51	0.251	587.68	1204.71	18.69	9.89	0.88
0.29	2.72	0.250	520.35	840.53	16.47	8.72	0.70
0.23	2.20	0.259	539.73	702.45	17.33	9.17	0.56
0.25	2.29	0.262	495.56	683.82	16.93	8.96	0.56
0.25	2.39	0.260	0.00	695.82	18.65	9.87	0.52
0.25	2.49	0.246	970.23	1369.12	17.97	9.51	0.64
0.21	2.04	0.250	922.39	1067.41	18.26	9.66	0.49
0.25	2.47	0.236	1007.47	1420.29	18.05	9.55	0.65
0.27	2.63	0.270	995.79	1482.82	18.62	9.85	0.69
0.28	2.80	0.237	1081.76	1723.70	18.3	9.68	0.78
0.25	2.53	0.275	1029.30	1419.10	19.19	10.16	0.64
0.31	3.01	0.279	1051.80	1802.81	18.62	9.85	0.85
0.24	2.45	0.231	1232.25	1673.71	18.37	9.72	0.75
0.36	3.34	0.271	937.02	1881.03	18.46	9.77	0.88
0.31	3.07	0.262	995.45	1728.68	18.2	9.63	0.81
0.32	3.03	0.254	1065.66	1898.55			
0.33	3.26	0.267	901.23	1667.29	17.71	9.37	0.81
0.37	3.50	0.270	846.61	1747.35	17.57	9.30	0.86
0.41	3.85	0.268	922.12	2128.90	18.19	9.63	1.01
0.35	3.44	0.264	987.82	1927.58	18.65	9.87	0.89
0.36	3.45	0.279	922.61	1866.24	18.42	9.75	0.89
0.35	3.32	0.263	1001.16	1938.60	18.42	9.75	0.90
0.34	3.33	0.320	896.72	1685.47	17.58	9.30	0.89
0.33	3.11	0.310	1005.65	1859.85	18.46	9.77	0.92
0.36	3.39	0.304	1128.85	2260.93	18.06	9.56	1.14
0.25	2.32	0.302	896.27	1233.10	18.16	9.61	0.61
0.30	2.96	0.279	593.78	990.85	17.86	9.45	0.88
0.28	2.84	0.292	611.30	969.05	18.57	9.83	0.84
0.32	3.11	0.302	517.40	937.34	18.04	9.55	0.85
0.27	2.68	0.288	519.47	799.57	18.34	9.71	0.70
0.28	2.81	0.242	565.55	885.45	18.2	9.63	0.73
0.27	2.53	0.236	555.72	849.35	18.84	9.97	0.67
0.30	2.93	0.241	585.47	991.58			
0.28	2.66	0.240	632.17	980.27	18.69	9.89	0.79
0.20	1.98	0.253	619.08	698.55	19.13	10.12	0.56
0.26	2.57	0.265	570.45	816.12	18.27	9.67	0.68
0.28	2.81	0.267	536.16	849.10	18.75	9.92	0.69
0.33	3.22	0.250	571.23	1053.38	19.15	10.13	0.82
0.29	2.88	0.245	567.54	922.76	17.86	9.45	0.76
0.24	2.35	0.254	562.30	765.13	18.4	9.74	0.62
0.26	2.47	0.243	580.03	837.26	18.27	9.67	0.67
0.29	2.65	0.238	560.89	914.82	18.18	9.62	0.74
0.34	3.34	0.259	565.05	1081.80	18.03	9.54	0.90
0.35	3.34	0.279	506.91	992.01	18.19	9.63	0.84
0.27	2.58	0.251	669.58	998.67	18.15	9.61	0.82
0.25	2.46	0.318	594.35	816.23	18.78	9.94	0.71
0.21	2.11	0.262	614.08	729.25	18.37	9.72	0.60
0.21	2.03	0.214	637.46	755.59	18.61	9.85	0.57
0.26	2.48	0.238	592.17	870.23	18.58	9.83	0.68
0.24	2.34	0.254	624.29	823.52	18.34	9.71	0.67
0.25	2.47	0.248	620.47	874.69	18.72	9.91	0.69
0.25	2.42	0.296	548.61	763.36	18.37	9.72	0.66
0.23	2.34	0.283	628.42	815.69	18.89	10.00	0.67
0.25	2.41	0.282	1198.78	1674.07	18.79	9.94	0.69
0.28	2.77	0.264	0.00	1802.92	13.21	6.99	1.03
0.32	3.14	0.234	1187.62	2119.86	18.36	9.72	0.84
0.27	2.80	0.329	1259.26	1938.65	18.69	9.89	0.86
0.24	2.51	0.337	1233.16	1682.35	18.31	9.69	0.77

CORE MD02-2520

0.29	2.85	0.315	1197.56	1960.54	18.39	9.73	0.86
0.26	2.68	0.331	1239.37	1804.94	18.34	9.71	0.82
0.23	2.41	0.312	1316.62	1728.87	17.95	9.50	0.78
0.26	2.65	0.317	1285.82	1871.91	18.05	9.55	0.84
0.20	2.01	0.314	1353.19	1509.51	18.26	9.66	0.67
0.24	2.51	0.321	1375.80	1857.24	17.82	9.43	0.85
0.20	2.05	0.313	1332.43	1488.52	17.57	9.30	0.68
0.27	2.81	0.515	840.83	1292.83			
0.29	2.77	0.499	322.60	523.58	18.83	9.97	0.74
0.22	2.30	0.453	408.25	508.48	18.55	9.82	0.67
0.23	2.22	0.459	400.85	507.35	18.52	9.80	0.67
0.03	0.26	0.455	388.20	55.50	18.42	9.75	0.07
0.19	2.02	0.454	266.45	283.07	18.55	9.82	0.57
0.21	2.10	0.455	230.99	270.69	17.88	9.46	0.57
0.16	1.58	0.430	220.48	201.90	17.69	9.36	0.41
0.27	2.69	0.431	258.56	393.23	18.26	9.66	0.78
0.16	1.66	0.427	283.85	259.68	18.37	9.72	0.51
0.20	1.99	0.455	268.14	298.38	18.06	9.56	0.62
0.30	2.97	0.480	242.46	401.93	18.39	9.73	0.86
0.34	3.36	0.458	245.15	461.29	18.27	9.67	0.96
0.28	2.73	0.419	259.18	403.03	18.76	9.93	0.76
0.31	3.06	0.415	256.84	442.72	18.37	9.72	0.85
0.29	2.92	0.425	0.00	426.61	18.5	9.79	0.82
0.28	2.79	0.430	249.05	383.58	18.22	9.64	0.76
0.24	2.39	0.498	202.86	268.67	18.81	9.95	0.63
0.35	3.41	0.500	177.90	348.22	18.2	9.63	0.85
0.41	3.83	0.523	162.76	369.52	17.42	9.22	0.99
0.36	3.60	0.515	174.25	353.71	16.74	8.86	0.97
		0.353			16.15	8.55	
		0.263	335.09		18.75	9.92	
		0.273	289.43		18.84	9.97	
		0.302	274.68		18.90	10.00	
		0.281	276.02		18.86	9.98	
		0.280	291.84		18.93	10.02	
		0.391	243.92		18.58	9.83	
		0.450	259.36		18.03	9.54	
		0.466	181.94		18.26	9.66	
		0.551	210.48		17.28	9.15	
		0.460	243.70		17.62	9.32	
		0.477			17.22	9.11	
		0.486			17.94	9.49	
		0.472			18.03	9.54	
		0.481			18.28	9.67	
		0.480	204.68		18.12	9.59	
		0.487	178.60		18.27	9.67	
		0.427	214.69		18.59	9.84	
		0.464	207.80		18.00	9.53	
		0.487	175.29		17.68	9.36	

Core MD02-2524

Depth (cm) (uncorrected)	Depth (cm) (corrected)	Age cal yrs BP	*Sed. Rate (smoothed)*	Opal (wt %)	Elemental Comp (% C)	Isotopic ∂13C	Elemental Comp (% N)
10	10	3679		9.417	5.123	-19.977	0.557
15	15	3877	*25.2*	7.190	6.216	-20.018	0.663
20	20	4076	*25.2*	9.212	6.377	-19.966	0.682
30	30	4473	*25.2*	5.605	7.931	-19.767	0.835
40	40	4870	*25.2*	5.629	6.041	-19.906	0.637
50	50	5267	*25.2*	5.061	6.519	-19.901	0.684
60	60	5664	*25.2*	8.577	6.004	-19.862	0.633
70	70	6061	*25.2*	5.599	5.338	-20.228	0.563
80	80	6458	*25.2*	5.764	5.439	-20.006	0.571
80	80	6458	*25.2*	6.818	5.439	-20.006	0.571
90	90	6855	*25.2*	5.710	5.484	-20.073	0.576
100	100	7252	*25.2*	7.892	4.225	-20.207	0.46
110	110	7649	*25.2*	7.523	3.679	-20.313	0.394
120	120	8046	*25.2*	9.883	3.561	-20.113	0.386
120	120	8046	*25.2*	9.965	3.561	-20.113	0.386
130	130	8443	*25.2*	6.264	3.736	-20.307	0.423
140	140	8920	*16.8*	6.567	4.325	-20.114	0.461
150	150	9517	*16.8*	4.443	4.435	-20.259	0.477
160	160	10114	*16.8*	4.692	4.069	-20.289	0.425
170	170	10711	*16.8*	5.479	4.063	-20.362	0.429
180	180	11222	*23.5*	2.989	4.23	-20.39	0.454
190	190	11647	*23.5*	5.314	4.205	-20.367	0.447
200	200	12072	*23.5*	4.951	5.061	-20.264	0.507
210	210	12497	*23.5*	5.046	4.669	-20.429	0.471
220	220	12922	*23.5*	4.980	3.974	-20.001	0.403
230	230	13312	*28.1*	4.541	3.712	-20.279	0.392
240	240	13667	*28.1*	5.299	7.096	-20.162	0.763
250	250	14023	*28.1*	6.735	4.739	-20.137	0.498
260	260	14379	*28.1*	2.033	3.47	-20.198	0.371
270	270	14734	*28.1*	1.793	3.677	-20.121	0.384
290	290	15658	*17.6*				
290	290	15658	*17.6*	4.720	3.853	-20.326	0.382
301	301	16282	*17.6*	3.922	2.821	-20.161	0.289
320	320	17360	*17.6*	8.843	2.785	-19.872	0.285
650	330	17928	*17.6*	10.484	2.992	-19.99	0.354
670	350	19063	*17.6*	10.613	2.917	-20.249	0.349
680	360	19631	*17.6*	17.247	3.263	-20.14	0.368
700	380	20309	*63.5*	9.943	2.827	-20.028	0.307
700	380	20309	*63.5*	12.584	2.827	-20.028	0.307
720	400	20428	*63.5*	12.154	2.718	-19.969	0.329
740	420	20548	*63.5*	10.102	3.061	-19.782	0.353
760	440	20667	*63.5*	12.530	2.618	-20.438	0.318
780	460	20864	*63.5*	7.437	3.169	-19.835	0.372
790	470	21077	*63.5*	15.573	3.345	-19.722	0.376
800	480	21291	*63.5*	18.314	3.355	-19.855	0.38
810	490	21505	*63.5*	12.841	3.308	-19.877	0.387
820	500	21718	*63.5*	14.933	3.468	-19.81	0.389
830	510	21932	*63.5*	13.869	3.3	-19.824	0.38
840	520	22145	*63.5*	15.310	3.406	-19.795	0.377
850	530	22359	*63.5*	13.473	3.188	-19.778	0.383
860	540	22573	*63.5*	17.022	3.34	-20.052	0.395
870	550	22786	*63.5*	10.442	3.3665	-20.0235	0.393
880	560	23000	*63.5*	13.737	3.393	-19.995	0.391
890	570	23213	*63.5*	12.077	3.405	-19.931	0.402
900	580	23427	*63.5*	9.319	2.586	-19.869	0.325
910	590	23641	*63.5*	13.908	3.741	-20.101	0.428
920	600	23854	*63.5*	21.466	3.499	-20.226	0.432
930	610	24052	*48.0*	15.459	3.808	-20.103	0.418
940	620	24249	*48.0*	12.515	3.344	-19.979	0.394
950	630	24446	*48.0*	13.527	3.37	-20.061	0.381
960	640	24642	*48.0*	6.008	2.797	-20.002	0.349
970	650	24854	*48.0*	9.948	2.568	-20.128	0.345
980	660	25068	*48.0*	4.507	2.278	-20.362	0.298
990	670	25281	*48.0*	11.296	3.284	-19.996	0.401
1000	680	25495	*48.0*	5.758	3.607	-19.996	0.437
1010	690	25708	*48.0*	11.848	3.326	-19.823	0.406
1020	700	25921	*48.0*	11.542	2.41	-19.871	0.287

CORE MD02-2524

1030	710	26135	*48.0*	9.833	2.767	-19.652	0.3275
1040	720	26348	*48.0*	3.955	3.124	-19.433	0.368
1050	730	26562	*48.0*	9.091	2.912	-19.771	0.372
1060	740	26600	*48.5*	3.806	3.045	-19.897	0.364
1070	750	26618	*48.5*	12.292	3.299	-19.603	0.407
1080	760	26637	*48.5*	10.471	3.1595	-19.804	0.391
1090	770	26655	*48.5*	11.229	3.02	-20.005	0.375
1100	780	26978	*48.5*	11.506	3.093	-20.016	0.369
1110	790	27334	*48.5*	12.591	3.009	-19.856	0.365
1120	800	27691	*48.5*	10.213	3.076	-19.799	0.38
1130	810	28047	*48.5*	17.411	3.184	-19.728	0.384
1140	820	28404	*48.5*	14.873	2.802	-20.193	0.347
1150	830	28574	*41.8*	11.453	3.344	-20.017	0.405
1160	840	28723	*41.8*	14.073	3.1695	-19.85	0.3905
1170	850	28872	*41.8*	13.728	2.995	-19.683	0.376
1180	860	29022	*41.8*	6.250	2.914	-19.959	0.364
1190	870	29171	*41.8*	12.901	2.735	-19.544	0.337
1200	880	29377	*41.8*	4.888	2.783	-19.766	0.3385
1201	881	29406	*41.8*	10.053	2.831	-19.988	0.34
1210	890	29668	*41.8*	7.767	2.643	-19.842	0.342
1220	900	29959	*41.8*	4.148	2.875	-20.192	0.353
1230	910	30251	*41.8*	7.329	2.28	-19.881	0.305
1240	920	30542	*41.8*	11.065	3.429	-19.65	0.411
1250	930	30833	*41.8*	13.552	3.004	-19.44	0.371
1260	940	31125	*41.8*	11.222	3.323	-19.808	0.405
1270	950	31416	*41.8*	14.444	3.118	-19.783	0.386
1280	960	31707	*41.8*	13.418	3.247	-19.719	0.395
1290	970	31998	*41.8*	13.842	3.227	-19.629	0.394
1300	980	32346	*44.8*	14.056	3.457	-19.95	0.416
1300	980	32346	*44.8*	12.119	3.457	-19.95	0.416
1315	995	32764	*44.8*	8.913	3.3085	-19.805	0.399
1320	1000	32828	*44.8*	2.998	3.16	-19.66	0.382
1330	1010	32956	*44.8*	6.655	2.908	-19.586	0.367
1340	1020	33091	*49.4*	3.550	3.557	-19.867	0.426
1350	1030	33238	*49.4*	8.109	3.103	-19.477	0.376
1360	1040	33385	*49.4*	6.705	3.263	-19.718	0.398
1370	1050	33592	*49.4*	12.493	3.049	-20.157	0.417
1380	1060	33806	*49.4*	10.714	3.559	-19.935	0.468
1390	1070	34019	*49.4*	10.150	3.238	-19.753	0.438
1400	1080	34233	*49.4*	9.433	3.083	-19.598	0.422
1400	1080	34233	*49.4*	8.990	3.083	-19.598	0.422
1410	1090	34446	*49.4*	8.927	3.082	-19.523	0.428
1420	1100	34660	*49.4*	7.271	3.213	-20.526	0.45
1430	1110	34873	*49.4*	8.114	3.171	-19.501	0.428
1440	1120	35087	*49.4*	5.877	3.066	-19.742	0.423
1450	1130	35300	*49.4*	10.173	3.115	-20.057	0.427
1460	1140	35514	*49.4*	12.499	3.49	-19.774	0.453
1470	1150	35727	*49.4*	11.656	3.355	-23.475	0.468
1480	1160	35941	*49.4*	9.587	3.337	-19.864	0.457
1490	1170	36192	*32.4*	7.352	2.913	-19.922	0.359
1500	1180	36501	*32.4*	6.481	2.985	-19.8715	0.39
1501	1181	36531	*32.4*	3.729	3.057	-19.821	0.421
1510	1190	36809	*32.4*	8.495	3.337	-19.792	0.453
1520	1200	37118	*32.4*	9.889	3.647	-20.162	0.479
1530	1210	37426	*32.4*	8.217	3.626	-20.038	0.493
1540	1220	37735	*32.4*	6.172	3.509	-20.198	0.477
1550	1230	38043	*32.4*	8.788	2.824	-19.978	0.397
1560	1240	38352	*32.4*	9.751	2.808	-19.9765	0.398
1570	1250	38660	*32.4*	11.165	2.792	-19.975	0.399
1580	1260	38969	*32.4*	9.909	2.365	-20.514	0.347
1590	1270	39277	*32.4*	8.596	2.901	-19.62	0.404
1600	1280	39586	*32.4*	7.831	3.515	-19.46	0.471
1610	1290	39894	*32.4*	8.420	3.341	-19.579	0.457
1620	1300	40203	*32.4*	9.468	3.667	-19.709	0.496
1630	1310	40511	*32.4*	9.188	3.451	-19.768	0.476
1640	1320	40820	*32.4*	10.851	3.865	-19.567	0.444
1645	1325	40974	*32.4*	8.258	3.139	-19.722	0.358
1660	1340	41437	*32.4*	10.980	3.759	-19.79	0.41
1680	1360	42054	*32.4*	8.887	3.149	-19.459	0.371
1700	1380	42671	*32.4*	6.096	3.383	-19.636	0.378
1720	1400	43288	*32.4*	8.256	3.312	-19.649	0.383
1740	1420	43986	*25.6*	5.980	3.701	-19.664	0.409

1760	1440	44766	*25.6*	7.439	2.137	-19.79	0.238
1780	1460	45546	*25.6*	5.519	2.496	-19.643	0.279
1800	1480	46326	*25.6*	4.549	2.786	-19.8045	0.3095
1801	1481	46365	*25.6*	7.258	3.076	-19.966	0.34
1820	1500	47106	*25.6*	9.097	4.064	-20.102	0.436
1840	1520	47886	*25.6*	6.585	3.34	-20.011	0.371
1860	1540	48666	*25.6*	5.492	3.192	-19.866	0.362
1880	1560	49115	*44.6*	6.036	3.191	-19.809	0.355
1900	1580	49563	*44.6*	4.960	3.295	-19.738	0.365
1910	1590	49788	*44.6*	4.858	3.29	-19.815	0.356
1950	1630	50685	*44.6*	5.296	3.246	-20.023	0.38
1960	1640	50910	*44.6*	4.910	3.241	-19.958	0.37
1980	1660	51358	*44.6*	6.068	3.3545	-19.9645	0.3785
2000	1680	51807	*44.6*	4.899	3.468	-19.971	0.387
2020	1700	52256	*44.6*	5.089	3.475	-19.96	0.389
2040	1720	52705	*44.6*	5.291	3.139	-20.049	0.355
2060	1740	53153	*44.6*	5.047	3.182	-19.982	0.354
2080	1760	53602	*44.6*	5.091	3.207	-20.08	0.353
2100	1780	54051	*44.6*	6.696	3.228	-19.928	0.373
2120	1800	54500	*44.6*	7.683	3.145	-19.977	0.362
2140	1820	54948	*44.6*	7.662	2.241	-19.986	0.26
2160	1840	55397	*44.6*	5.778	2.576	-19.653	0.307
2180	1860	55846	*44.6*	9.546	2.805	-19.863	0.323
2200	1880	56294	*44.6*	7.279	2.736	-20.436	0.295
2220	1900	56743	*44.6*	5.595	2.667	-21.009	0.267
2240	1920	57192	*44.6*	6.894	2.858	-19.67	0.334
2260	1940	57641	*44.6*	6.748	2.98	-19.892	0.345
2280	1960	58089	*44.6*	5.124	3.173	-20.064	0.364
2300	1980	58538	*44.6*	6.477	3.326	-20.253	0.385
2320	2000	58987	*44.6*	5.477	3.095	-20.377	0.362
2340	2020	59436	*44.6*	6.645	3.185	-20.277	0.369
2360	2040	59884	*44.6*	5.171	3.206	-20.292	0.378
2380	2060	60333	*44.6*	7.416	5.217	-20.063	0.509
2380	2060	60333	*44.6*	5.449	5.217	-20.063	0.509
2401	2081	60804	*44.6*	6.685	3.149	-20.32	0.336
2420	2100	61230	*44.6*	7.681	3.486	-20.229	0.362
2435	2115	61567	*44.6*	8.717	3.824	-20.283	0.407
2440	2120	61679	*44.6*	6.302	3.951	-19.91	0.429
2460	2140	62128	*44.6*	7.203	4.128	-20.075	0.418
2480	2160	62577	*44.6*	6.300	4.742	-20.873	0.436
2500	2180	63025	*44.6*	7.177	3.404	-20.179	0.37
2515	2195	63362	*44.6*	11.657	4.249	-20.297	0.452
2520	2200	63474	*44.6*	6.777	3.592	-20.176	0.368
2540	2220	63923	*44.6*	6.627	3.544	-20.215	0.363
2560	2240	64372	*44.6*	7.796	3.813	-20.19	0.414
2580	2260	64820	*44.6*	7.479	2.375	-20.107	0.259
2600	2280	65269	*44.6*	5.901	3.085	-20.311	0.33
2610	2290	65493	*44.6*	7.118	3.692	-20.407	0.385
2620	2300	65718	*44.6*	6.860	3.334	-20.3	0.366
2640	2320	66167	*44.6*	4.360	3.04	-20.199	0.337
2660	2340	66615	*44.6*	8.952	4.588	-20.263	0.476
2680	2360	67064	*44.6*	7.661	3.571	-20.218	0.387
2700	2380	67513	*44.6*	4.816	4.153	-19.889	0.432
2720	2400	67961	*44.6*	10.596	4.378	-19.997	0.453
2740	2420	68410	*44.6*	5.530	3.836	-20.235	0.416
2750	2430	68635	*44.6*	9.992	4.15	-20.109	0.437
2760	2440	68859	*44.6*	5.151	4.25	-20.235	0.441
2780	2460	69308	*44.6*	9.271	4.579	-20.18	0.467
2800	2480	69756	*44.6*	5.793	4.522	-19.946	0.471
2820	2500	70205	*44.6*	10.372	4.316	-20.011	0.436
2840	2520	70654	*44.6*	8.824	4.145	-20.423	0.427
2860	2540	71103	*44.6*	8.375	4.104	-20.303	0.411
2870	2550	71327	*44.6*	7.534	4.011	-20.515	0.395
2880	2560	71551	*44.6*	3.461	4.822	-20.767	0.466
2900	2580	72000	*44.6*	11.437	2.979	-20.842	0.323
2920	2600	72449	*44.6*	8.166	3.177	-21.1	0.323
2940	2620	72897	*44.6*	8.291	2.117	-20.494	0.256
2960	2640	73346	*44.6*	11.356	2.028	-20.428	0.241
2960	2640	73346	*44.6*	11.978	2.028	-20.428	0.241
2980	2660	73795	*44.6*	12.478	1.818	-20.629	0.219
3000	2680	74244	*44.6*	12.290	3.825	-21.28	0.371
3020	2700	74692	*44.6*	10.116	3.171	-20.93	0.327

CORE MD02-2524

molar BSi/C	molar BSi/N	BSi MAR mg/cm2/kyr	Depth (cm) (uncorrected)	Age cal yrs BP	Opal %	Al2O3 %	Al %	opal/Al
0.33	3.52		8	3500	9.42	10.46	5.54	1.699
0.21	2.26	238.42	15	3879	7.19	10.79	5.72	1.257
0.26	2.81	306.21	20	4079	9.21	10.75	5.70	1.617
0.13	1.40	186.63	30	4479	5.60	10.67	5.66	0.991
0.17	1.84	186.66	40	4879	5.63	11.55	6.12	0.920
0.14	1.54	164.48	50	5280	5.06	10.84	5.75	0.881
0.26	2.82	269.44	60	5680	8.58	10.93	5.79	1.481
0.19	2.07	185.09	70	6080	5.60	11.28	5.98	0.937
0.19	2.10	183.95	80	6480	5.76	11.85	6.28	0.918
0.22	2.49	183.95	90	6880	5.71	10.89	5.77	0.989
0.19	2.07	192.25	100	7280	7.89	11.56	6.13	1.288
0.33	3.57	258.92	110	7681	7.52	10.58	5.61	1.342
0.37	3.98	253.92	120	8081	9.97	11.27	5.97	1.668
0.50	5.33	349.71	130	8481	6.26	11.4	6.04	1.037
0.50	5.38	349.71	140	9043	6.57	11.99	6.35	1.033
0.30	3.09	223.36	150	9768	4.44	11.79	6.25	0.711
0.27	2.97	219.95	160	10492	4.69	12.39	6.57	0.714
0.18	1.94	96.80	170	11217	5.48	12.6	6.68	0.820
0.21	2.30	111.63	180	11724	2.99	12.07	6.40	0.467
0.24	2.66	126.75	190	12013	5.31	12.42	6.58	0.807
0.13	1.37	93.93	200	12303	4.95	12.93	6.85	0.723
0.23	2.48	167.46	210	12593	5.05	14.88	7.89	0.640
0.17	2.03	151.66	220	12882	4.98	12.81	6.79	0.734
0.19	2.23	161.52	230	13215	4.54	12.45	6.60	0.688
0.22	2.57	160.64	240	13590	5.30	12.16	6.44	0.822
0.22	2.41	179.41	250	13965	6.73	12.2	6.47	1.042
0.13	1.45	208.91	260	14340	2.03	12.37	6.56	0.310
0.25	2.82	266.19	270	14715	1.79	12.82	6.79	0.264
0.10	1.14	78.33	280	15090	4.50	12.36	6.55	0.687
0.09	0.97	72.31	290	15664	4.72	13.97	7.40	0.637
		151.20	300	15951		13.49	7.15	
0.22	2.57	151.20	310	16812	3.92	13.73	7.28	0.539
0.25	2.83	96.86	640	17386	8.84	15.06	7.98	1.108
0.57	6.46	218.75	650	17959	10.48	14.56	7.72	1.359
0.63	6.17	258.49	660	18533		13.91	7.37	
0.65	6.34	263.43	670	19107	10.61	14.35	7.61	1.395
0.94	9.76	424.88	680	19681	17.25	13.9	7.37	2.341
0.63	6.75	1162.70	690	20255		15.12	8.01	
0.79	8.54	1162.70	700	20314	12.58	13.89	7.36	1.709
0.80	7.70	1122.93	710	20373	13.06		6.92	
0.59	5.96	918.77	720	20403	12.15	14.34	7.60	1.599
0.85	8.21	1078.60	730	20491		13.53	7.17	
0.42	4.16	646.53	740	20550	10.10	14.17	7.51	1.345
0.83	8.63	1282.64	750	20580		14.74	7.81	
0.97	10.04	1527.07	760	20668	12.53	13.91	7.37	1.700
0.69	6.91	1106.56	770	20727		15.06	7.98	
0.77	8.00	1274.31	780	20865	7.44	14.36	7.61	0.977
0.75	7.60	1191.97	790	21080	15.57	13.37	7.09	2.198
0.80	8.46	1341.01	800	21295	18.31	13.51	7.16	2.558
0.75	7.33	1169.01	810	21510	12.84	13.87	7.35	1.747
0.91	8.98	1478.76	820	21725	14.93	13.7	7.26	2.057
0.82	8.15	894.86	830	21940	13.87	13.54	7.18	1.933
0.72	7.32	1184.35	840	22155	15.31	13.89	7.36	2.080
0.63	6.26	1069.05	850	22370	13.47	12.59	6.67	2.019
0.64	5.97	830.19	860	22585	17.02	13.27	7.03	2.420
0.66	6.77	1233.88	870	22693	10.44	14.08	7.46	1.399
1.10	10.35	1862.90	880	23015	13.74	13.33	7.06	1.944
0.72	7.70	1017.12	890	23230	12.08	13.99	7.41	1.629
0.67	6.62	829.17	900	23338	9.32	13.67	7.25	1.286
0.72	7.40	923.36	910	23660	13.91	12.91	6.84	2.033
0.38	3.59	407.30	920	23876	21.47	12.52	6.64	3.235
0.69	6.01	681.03	930	24072	15.46	13.28	7.04	2.196
0.35	3.15	308.47	940	24269	12.51	13.89	7.36	1.700
0.61	5.87	758.32	950	24465	13.53	13.21	7.00	1.932
0.29	2.75	386.02	960	24662	6.01	12.3	6.52	0.922
0.64	6.08	789.10	970	24873	9.95	12.72	6.74	1.476
0.86	8.38	785.72	980	25084	4.51	13.08	6.93	0.650

0.54	5.31	764.26
0.23	2.24	265.63
0.56	5.09	607.68
0.22	2.18	
0.67	6.29	
0.66	6.27	
0.66	6.24	
0.66	6.50	788.89
0.75	7.19	866.08
0.59	5.60	785.81
0.98	9.45	1456.53
0.95	8.93	1057.29
0.61	5.89	689.38
0.72	6.75	856.53
0.82	7.61	813.92
0.38	3.58	380.85
0.84	7.98	794.00
0.74	7.07	300.62
0.63	6.16	611.07
0.52	4.73	469.79
0.26	2.45	256.98
0.57	5.01	460.76
0.58	5.61	676.49
0.81	7.61	805.95
0.60	5.77	660.40
0.83	7.80	879.14
0.74	7.08	822.46
0.77	7.32	856.23
0.73	7.04	878.55
0.63	6.07	878.55
0.40	3.85	565.55
0.17	1.63	189.54
0.41	3.78	427.10
0.18	1.74	252.19
0.47	4.49	589.76
0.37	3.51	494.92
0.73	6.24	927.33
0.54	4.77	921.39
0.56	4.83	882.19
0.55	4.66	652.74
0.52	4.44	652.74
0.52	4.35	449.00
0.40	3.37	365.92
0.46	3.95	426.98
0.34	2.89	297.38
0.58	4.96	532.80
0.64	5.75	594.31
0.62	5.19	621.54
0.51	4.37	458.69
0.45	4.27	241.07
0.33	3.06	235.21
0.22	1.85	131.65
0.45	3.91	292.19
0.48	4.30	342.59
0.40	3.47	260.04
0.31	2.70	201.71
0.56	4.61	288.52
0.63	5.22	329.32
0.71	5.83	410.15
0.75	5.95	337.58
0.53	4.43	306.20
0.40	3.46	262.20
0.45	3.84	273.53
0.46	3.98	311.94
0.48	4.02	296.27
0.50	5.09	355.47
0.47	4.81	263.16
0.52	5.58	343.82
0.50	4.99	293.71
0.32	3.36	195.59
0.45	4.49	285.12
0.29	3.05	191.68

990	25295	11.30	14.17	7.51	1.504
1000	25401	5.76	13.52	7.17	0.804
1010	25718	11.85	13.47	7.14	1.660
1020	25929	11.54	13.27	7.03	1.641
1040	26351	3.95	13.68	7.25	0.545
1050	26456	9.09	13.28	7.04	1.292
1060	26600	3.81	13.4	7.10	0.536
1070	26620	12.29	13.08	6.93	1.773
1080	26629	10.47	12.6	6.68	1.568
1090	26658	11.23	12.95	6.86	1.636
1100	27014	11.51	13.65	7.23	1.590
1110	27371	12.59	13.85	7.34	1.715
1110	27371		13.8	7.31	
1120	27727	10.21	13.64	7.23	1.413
1130	28083	17.41	13.5	7.16	2.433
1140	28440	14.87	13.3	7.05	2.110
1150	28589	11.45	13.63	7.22	1.585
1160	28663	14.07	15.49	8.21	1.714
1170	28887	13.73	13.25	7.02	1.955
1180	29036	6.25	13.72	7.27	0.860
1190	29186	12.90	13.28	7.04	1.833
1200	29260	10.05	14	7.42	1.355
1210	29697	7.77	12.74	6.75	1.150
1220	29988	4.15	14.26	7.56	0.549
1230	30280	7.33	15.18	8.05	0.911
1240	30571	11.07	14	7.42	1.491
1250	30862	13.55	15.49	8.21	1.651
1260	31154	11.22	14.26	7.56	1.485
1270	31445	14.44	14.59	7.73	1.868
1280	31736	13.42	14.48	7.67	1.748
1290	32028	13.84	14.42	7.64	1.811
1300	32364	12.12	14	7.42	1.633
1305	32532		14.42	7.64	
1305	32532		14.97	7.93	
1320	32833	3.00	14.25	7.55	0.397
1330	32966	6.65	14.21	7.53	0.884
1350	33253	8.11	14.83	7.86	1.032
1360	33400	6.71	14.58	7.73	0.868
1370	33613	12.49	14.88	7.89	1.584
1380	33827	10.71	14.14	7.49	1.430
1390	34040	10.15	14.53	7.70	1.318
1400	34254	8.99	15.01	7.96	1.130
1410	34467	8.93	15.45	8.19	1.090
1420	34681	7.27	14.66	7.77	0.936
1430	34894	8.11	14.58	7.73	1.050
1440	35108	5.88	13.39	7.10	0.828
1450	35321	10.17	14.6	7.74	1.315
1460	35535	12.50	14.57	7.72	1.619
1470	35748	11.66	14.75	7.82	1.491
1480	35962	9.59	13.91	7.37	1.300
1490	36222	7.35	14.49	7.68	0.957
1500	36376	6.48	14.34	7.60	0.853
1510	36837	8.50	14.14	7.49	1.134
1520	37144	9.89	14.11	7.48	1.322
1530	37451	8.22	14.43	7.65	1.074
1540	37758	6.17	14.47	7.67	0.805
1550	38066	8.79	13.48	7.14	1.230
1560	38219	9.75	13.74	7.28	1.339
1570	38680	11.16	13.98	7.41	1.507
1580	38987	9.91	16.02	8.49	1.167
1590	39295	8.60	15.16	8.03	1.070
1600	39602	7.83	14.49	7.68	1.020

0.62	6.51	193.78
0.39	4.12	146.34
0.41	4.28	129.16
0.42	4.45	198.76
0.40	4.35	225.83
0.35	3.70	159.08
0.31	3.16	140.33
0.34	3.54	169.80
0.27	2.83	227.70
0.26	2.84	234.89
0.29	2.90	243.31
0.27	2.76	206.83
0.26	2.70	292.79
0.25	2.64	235.98
0.26	2.73	244.29
0.30	3.11	254.86
0.28	2.97	246.66
0.28	3.00	248.40
0.37	3.74	321.58
0.44	4.42	294.56
0.61	6.14	307.51
0.40	3.92	274.54
0.61	6.16	341.98
0.49	5.26	256.02
0.37	4.37	195.35
0.43	4.30	276.32
0.40	4.07	264.89
0.29	2.93	200.17
0.35	3.50	256.84
0.32	3.15	216.07
0.37	3.75	263.12
0.29	2.85	211.89
0.25	3.04	236.17
0.19	2.23	236.17
0.38	4.15	340.38
0.39	4.42	394.86
0.41	4.46	462.78
0.28	3.06	326.42
0.31	3.59	377.77
0.24	3.01	338.03
0.38	4.04	374.19
0.49	5.37	601.25
0.34	3.84	368.98
0.33	3.80	341.97
0.37	3.92	397.38
0.56	6.02	406.02
0.34	3.73	322.64
0.34	3.85	380.84
0.37	3.90	368.36
0.26	2.70	233.72
0.35	3.92	471.44
0.38	4.12	391.06
0.21	2.32	250.80
0.43	4.87	524.33
0.26	2.77	300.14
0.43	4.76	569.59
0.22	2.43	285.16
0.36	4.14	513.21
0.23	2.56	310.75
0.43	4.96	611.98
0.38	4.31	496.38
0.36	4.25	453.74
0.34	3.97	400.55
0.13	1.55	180.89
0.69	7.38	625.52
0.46	5.27	436.85
0.70	6.75	633.76
1.00	9.82	671.76
1.05	10.35	671.76
1.23	11.87	729.71
0.57	6.90	698.57
0.57	6.44	575.56

Core PC08

Depth cm	Age cal yrs BP	d13C PDB ‰ Uvigerina	Depth cm	Age cal yrs BP	d13C PDB ‰ Uvigerina
181	5865	-0.317	877	29141	-0.592
201	6514	-0.582	896	29746	-0.564
210	6805	-0.393	916	30382	-0.489
231	7487	-0.861	926	30700	-0.917
241	7811	-0.992	936	31110	-0.938
251	8135	-1.008	946	31521	-0.813
271	8852	-0.94	956	31931	-0.584
281	9214	-1.032	966	32349	-0.555
281	9214	-0.968	976	32840	-0.625
291	9576	-1.076	986	33330	-0.634
301	9938	-1.227	996	33799	-0.706
311	10300	-1.332	1006	34240	-0.762
331	10981	-1.127	1016	34682	-1.199
341	11321	-1.229	1026	35123	-0.841
351	11661	-1.199	1027	35168	-0.884
361	11962	-1.458	1036	35574	-0.904
371	12268	-0.504	1046	36029	-0.785
381	12574	-0.997	1056	36485	-0.506
391	12881	-0.649	1066	36941	-0.619
401	13225	-1.083	1076	37397	-0.995
411	13566	-1.124	1086	37853	-0.682
421	13908	-0.733	1096	38309	-1.17
431	14199	-0.958	1106	38685	-1.139
432	14226	-1.227	1116	39040	-0.663
441	14468	-1.346	1126	39396	-0.647
451	14771	-0.78	1136	39752	-0.339
461	15123	-0.856	1156	40428	-1.08
471	15475	-0.774	1166	40725	-0.598
481	15828	-1.131	1176	41022	-1.004
491	16180	-0.594	1186	41315	-0.429
501	16532	-0.86	1196	41603	-0.499
511	16884	-0.849	1206	41890	-0.831
521	17236	-1.041	1216	42178	-0.992
531	17589	-0.658	1223	42379	-0.943
541	17928	-0.922	1236	42766	-0.839
551	18247	-1.051	1246	43077	-0.983
561	18567	-0.924	1256	43387	-0.657
571	18887	-1.211	1266	43698	-0.858
581	19206	-0.878	1276	44008	-0.813
582	19238	-1.062	1286	44319	-1.127
591	19526	-1.309	1296	44629	-1.232
601	19845	-0.985	1306	44940	-1.255
611	20165	-0.942	1326	45561	-0.669
621	20485	-0.64	1340	45995	-0.745
631	20804	-0.794	1349	46275	-0.667
641	21122	-0.618	1359	46585	-0.601
651	21440	-0.79	1369	46896	-0.869
661	21758	-0.975	1379	47206	-0.883
671	22076	-0.906	1389	47517	-0.988
681	22393	-0.94	1399	47827	-1.019
691	22711	-0.805	1409	48138	-1.043
701	23029	-0.876	1419	48448	-0.977
711	23346	-0.894	1429	48759	-0.977
721	23671	-0.915	1435	48945	-0.713
738	24224	-0.927	1444	49225	-0.929
748	24550	-0.807	1454	49535	-0.508
758	24876	-0.485	1464	49846	-0.787
768	25202	-0.653	1474	50156	-0.963
778	25527	-0.762	1484	50467	-0.884
788	25853	-0.707	1494	50777	-1.127
798	26179	-0.705	1504	51088	-1.115
808	26504	-0.723	1514	51398	-1.041
818	26830	-0.443	1524	51709	-0.636
828	27156	-0.646	1534	52019	-0.853
838	27482	-0.997	1544	52330	-1.028
848	27807	-0.658	1554	52640	-1.062
858	28277	-0.498	1564	52951	-0.894
868	28763	-0.512			

Core NH15P

Depth cm	Age cal yrs BP	∂18O PDB ‰ Bolivina	∂13C PDB ‰ Bolivina	Depth cm	Age cal yrs BP	∂18O PDB ‰ Bolivina	∂13C PDB ‰ Bolivina
6	1130	1.73	-0.91	927	105000	2.63	-1.38
14	1560	2.14	-0.79	937	106000	2.80	-1.33
34	2560	1.56	-1.07	947	107000	2.74	-1.41
44	3060	2.05	-0.67	957	108000	2.76	-1.48
53	3510	1.86	-0.71	967	109000	2.69	-1.64
64	4020	1.87	-0.73	977	110000	2.97	-1.51
74	4270	1.85	-0.65	987	111000	2.80	-1.05
83	4490	1.75	-0.78	997	112000	2.67	-1.05
94	4770	2.06	-0.64				
103	5000	1.75	-0.76				
114	5300	2.02	-0.76				
124	5650	1.80	-0.60				
134	6010	1.73	-0.85				
144	6470	2.03	-1.14				
150	7020	1.49	-1.28				
154	7380	1.78	-0.90				
160	7930	1.87	-1.09				
164	8290	1.86	-0.96				
170	8830	1.87	-1.16				
174	9150	2.24	-1.05				
180	9540	1.88	-1.20				
184	9810	2.32	-1.24				
190	10200	2.07	-1.08				
194	10500	1.77					
200	10900	1.97	-1.46				
204	11300	1.95	-1.36				
210	12300	1.94	-1.29				
214	12900	2.24	-1.33				
220	13800	2.42	-1.12				
224	14300	2.35	-1.33				
229	14600	2.53	-1.14				
236	16200	2.60	-1.09				
239	18000	2.89	-1.07				
248	21100	3.12	-0.95				
250	21600	3.04	-0.94				
257	23200	3.05	-0.94				
267	25300	3.28	-0.74				
277	27500	3.12	-0.93				
287	29400	2.96	-0.83				
297	29800	2.93	-1.08				
307	30200	2.99	-0.92				
317	30600	3.00	-0.91				
327	31000	3.26	-0.74				
337	31400	3.15	-0.82				
347	31800	2.58	-0.96				
357	32500	2.98	-0.99				
367	34300	2.64	-0.99				
377	36200	2.81	-0.98				
387	38100	2.68	-0.89				
397	39900	2.74	-1.42				
417	42600	2.86	-1.08				
427	43600	2.83	-1.09				
437	44500	3.23	-0.99				
497	50400	2.78	-0.93				
557	56200	2.67	-1.04				
567	57200	3.05	-0.72				
577	58200	2.69	-0.81				
587	59400	2.89	-0.82				
597	61500	2.95	-0.70				
647	72200	2.77	-1.14				
657	74200	2.46	-1.24				
727	83300	2.55	-0.87				
737	84700	2.16	-0.68				
757	87300	2.26	-1.39				
777	89900	2.77	-1.22				
787	91100	2.54	-0.88				